Second Edition

Ductile Design of STEEL STRUCTURES

Michel Bruneau Chia-Ming Uang Rafael Sabelli

Ductile Design of Steel Structures

About the Authors

Michel Bruneau, Ph.D., P.Eng., is Professor in the Department of Civil, Structural, and Environmental Engineering at the State University of New York at Buffalo, and an ASCE Fellow. He is a member of various AISC and CSA committees developing seismic design specifications for bridges and buildings. Dr. Bruneau has conducted extensive research on the evaluation and retrofit of existing steel structures subjected to large destructive forces. He has authored more than 400 technical publications and has received many awards for his work.

Chia-Ming Uang, Ph.D., is Professor in the Department of Structural Engineering at the University of California, San Diego. A member of the AISC's Committee on Specification and Committee on Research, he received the AISC Special Achievement Award in 2007. Dr. Uang has authored numerous articles on seismic behavior and design of steel structures.

Rafael Sabelli, S.E., is a Principal and Director of Seismic Design at Walter P. Moore and Associates, Inc., and was President of the Structural Engineers Association of California from 2009 to 2010. He is a member of the AISC Task Committee on the Seismic Provisions for Structural Steel Buildings and the ASCE 7 Seismic Subcommittee. Mr. Sabelli is the coauthor of *AISC Design Guide 20: Steel Plate Shear Walls* as well as of numerous research papers on conventional and buckling-restrained braced frames.

Ductile Design of Steel Structures

Michel Bruneau, Ph.D., P.Eng.
Chia-Ming Uang, Ph.D.
Rafael Sabelli, S.E.

Second Edition

New York Chicago San Francisco
Lisbon London Madrid Mexico City
Milan New Delhi San Juan
Seoul Singapore Sydney Toronto

The McGraw-Hill Companies

ISBN 978-0-07-162523-4
MHID 0-07-162395-7

The material in this eBook also appears in the print version of this title: ISBN 978-0-07-162395-7, MHID 0-07-162395-7.

Contents

This page intentionally left blank

Preface

The first edition of *Ductile Design of Steel Structures*, published in 1998, arrived at a time when the structural design practice was undergoing important changes. Most significantly, the impact of the Northridge and Kobe earthquakes was still being felt in the engineering community, and substantial shifts in philosophy for the seismic design of steel structures were underway. This led to numerous and frequent changes to the relevant seismic design and detailing provisions for steel structures in many codes and design standards—all while the United States completed the process of unifying its three major regional model design codes into the International Building Code (first published in 2000, and eventually adopted by all states and most municipalities in the country), and while the American Institute of Steel Construction (AISC) unified its Load and Resistance Factor Design (LRFD) and Allowable Stress Design (ASD) requirements into a single specifications.

Although these whirlwind changes made the first edition a timely document in 1998, they also progressively left it in need of an update sooner than expected. Even though the fundamental principles and structural behaviors emphasized throughout the first edition of this book remained valid, design principles and examples were anchored in specifications that had changed in a number of subtle ways over time (more so than is typically the case from one code cycle to another). With publication of the AISC 2010 Seismic Provisions and of the 2009 CSA S16 Standard for the Design of Steel Structures, crystallizing the knowledge developed in the prior 15 years on this topic (and becoming more similar to each other in content and design philosophy), and with the evolution of code changes foreseen to return to a more regular pace—barring another major earthquake that would challenge design wisdom—publication of a revised second edition of *Ductile Design of Steel Structures* is again timely.

Two audiences were kept in mind when writing this book: practicing engineers and graduate students. With respect to the first audience, engineers are nowadays exposed to a wide range of professional development opportunities, and day courses on seismic design of steel structures are common. Similar information is also scattered

over the World Wide Web (albeit covering the same topic with various degrees of technical rigor, depending on the source). This widely available and accessible information has been helpful to dispel the erroneous belief that the ductile nature of structural steel directly translates into inherently ductile structures, but a first introduction to the topic of ductile design usually leaves the engineer with many questions on the origin of many design requirements and strategies to achieve ductile structural behavior. With respect to the second group, although seismic design is not part of most undergraduate civil engineering curricula, substantial opportunities exist for graduate learning on this topic. Nowadays, most graduate structural engineering programs in North America offer a general seismic design course, often complemented by specialized courses on the design of ductile concrete and ductile steel structures, and textbooks that comprehensively cover design aspects related to this topic are needed.

In that perspective, the second edition of *Ductile Design of Steel Structures* is intended to serve both as a reference textbook on this topic and as a resource document providing breadth and depth in support of graduate and professional education opportunities. It aims to help senior undergraduate and graduate students, as well as professionals, design ductile steel structures in an informed manner. It summarizes the relevant existing information on this topic (often scattered in research reports, journal articles, and conference proceedings) into chapters on material, cross-section, component, and system response, providing useful guidance and design examples while presenting the concepts and key research results supporting the rationale underlying many of the current design principles. It is written starting from the assumption that the reader has background knowledge of conventional (nonseismic) steel design.

The emphasis of this book is on earthquake-resistant design because providing ductile structures is crucial to ensure seismic survival. However, there exist many other important applications of the principles and design approaches outlined in this textbook. For example, knowledge of how to design and detail steel structures to achieve ductile behavior is vital to ensure the satisfactory performance of structures exposed to other extreme events, such as blast forces, and to prevent their progressive collapse—two topics pushed to the forefront by the September 11, 2001 events. Other possible applications of ductile steel design include offshore structures subjected to extreme wave and ice loads, as well as bridges that can now be designed to carry normal traffic using an alternative bridge design procedure (the Autostress method) that relies heavily on ductile response and requires a good understanding of the shakedown theory. Likewise, for existing construction, plastic analysis can provide a much better estimate of a structure's actual strength than procedures based on elastic analysis, which in turn can be used advantageously to minimize the extent of needed rehabilitations—an important

advantage given that the rehabilitation of existing buildings is a growing market in North America, as part of the revitalization activities taking place in many city centers of seismic and nonseismic regions (as a consequence of either commuters' frustrations, the aging North American infrastructure, the projected North American population growth patterns, the goals of historical or heritage building preservation, and/or other societal trends). Thus, although the focus of this text is earthquake engineering, the information presented herein is broadly applicable to the ductile design of steel structures.

For its second edition, this book has been substantially expanded as follows:

- Three entirely new chapters have been added, to respectively address the design of buckling-restrained braced frames (Chapter 11) and steel plate shear walls (Chapter 12), and to review some hysteretic energy dissipating systems and design strategies that have been the subject of growing interest and proposed to achieve the objective of ductile design (Chapter 13). The latter chapter addresses structural fuses, hysteretic energy dissipating devices, bimetallic friction, rocking, and self-centering systems; it replaces the former Chapter 11 that only provided a cursory overview of passive energy dissipation.
- The previous chapter on braced frames has been completely rewritten, to eliminate obsolete and/or ambiguous information and, more importantly, to reflect the substantial changes and new developments that have taken place and have been implemented in the AISC and CSA design requirements since the last edition of this book. Concentrically braced frames and eccentrically braced frames are now each covered in separate chapters. Each chapter provides thorough insights into the knowledge on those topics that has led to the current design provisions and corresponding capacity design procedures.
- The chapter on moment-resisting frames has been substantially expanded, to reflect the major changes and developments in design requirements that have taken place since 1997.
- Chapter 2 has been expanded to include additional information and new knowledge on steel's high-temperature properties, strain rate effects, k-area fractures, strain aging, and stress corrosion, as well as information on fatigue and ductility of corroded shapes, yielding mechanism, new steel grades, and low-cycle fatigue modeling. It also includes a new section on hysteretic models, which provides much needed information for the nonlinear

inelastic analyses more frequently required by specific engineering projects nowadays.

- Chapter 3 (on cross-section properties) has been revised to address biaxial bending, introduce layer models (required for some nonlinear analyses), and add information on plastic strength of concrete-filled steel tube cross-sections.
- Chapter 4 (on plastic analysis) has been expanded to introduce yield line analysis, which is important for calculation of connections' ultimate strength and resistance to out-of-plane loads (such as blast loads).
- Chapter 6 (on applications of plastic analysis) has been expanded to address global versus local ductility demand and some other important code-related issues.
- To better link with Chapters 8 to 13, focused on earthquake engineering applications, Chapter 7 (formerly Chapter 9) has been entirely rewritten, focusing on the basic principles to relate seismic design forces and corresponding ductile demands in structures.
- New design examples in Chapters 8 to 12 have been developed in compliance with the AISC Seismic Provisions (ANSI/AISC 341-10) and Load and Resistance Factor Design, and from a practicing engineering perspective. Note that the examples in the first edition of this book approached seismic design as a secondary design step called "ductile design" (coupled with "drift-control design" in the special case of moment-resisting frames), which consisted of a design iteration starting with the results from a first design step accomplished using conventional steel design principles in nonseismic applications (called "strength design"). That two-step approach is still valid and the examples contained in the first edition remain instructive in many ways. However, the publication by the American Institute of Design Construction of design aids for seismic design has made seismic design more expeditious, eliminating the benefits of the two-step approach. Therefore, this second edition contains only new design examples consistent with this new context.
- Self-study problems have been provided for most chapters; these could be assigned to students by instructors using this book as a textbook—note that all of the problems are former assignment or exam questions I gave to students at the University at Buffalo or the University of Ottawa. Partial solutions to the problems will eventually be accessible to instructors via a password-protected link posted on the website www.michelbruneau.com.

- Chapter 14 is the only chapter that remains unmodified since the first edition. While interesting research has been conducted since the mid-1990s on the topics covered in this chapter, it has not resulted in changes to the seismic design provisions at the time of this writing.

The authorship of this second edition reflects these numerous changes in scope, breath, and structure. I sincerely thank my coauthors for helping to bring this project to fruition, namely Chia-Ming Uang (Professor, University of California, San Diego) for writing most of Chapters 7, 10, 11, and 14, and Rafael Sabelli (Structural Engineer, Walter P. Moore, Oakland, CA) for developing the design examples at the end of Chapters 8 to 12 and contributing parts of Chapter 11. The challenges of bringing to life a second edition that is twice the length of the first can be overwhelming, and their commitment and contributions are gratefully acknowledged.

From a graduate curriculum perspective, the resulting expanded textbook provides enough material to support two graduate courses: a first course on plastic analysis and design, using the material in Chapters 2 to 6, and a second course on the seismic design of steel structures based on Chapters 7 to 13. However, another effective approach is to use some aspects of all chapters as part of a single graduate course, covering only the essential aspects of Chapters 2 to 6 needed to understand the capacity design in support of the material presented in Chapters 7 to 12 (or 7 to 10 for shorter academic terms), leaving the rest of the material for future self-study in answer to project needs or for professional development purposes. Other combinations also are anticipated, reflecting the preferences and teaching styles of various instructors.

Finally, suggestions and general feedback on this book are always welcome (including e-mails confirming that there are people in this world reading book prefaces). A list of errors brought to the authors' attention will be compiled into an errata list eventually posted on the website www.michelbruneau.com, until fixed by the publisher in subsequent printings.

Michel Bruneau, Ph.D., P.Eng.

This page intentionally left blank

CHAPTER 7

Building Code Seismic Design Philosophy

7.1 Introduction

Plastic analysis and design methods presented in the previous chapters were mainly developed in the 1960s and 1970s. With the advent of computers, however, elastic design was soon favored over plastic design due to the emergence of computer structural analysis software able to perform linear elastic analysis of large structures. It was also about the same time that active research in earthquake engineering and seismic design started in North America. Although plastic design has not been widely accepted for routine design, the seismic design community soon realized that allowing structures to respond in the inelastic range was beneficial and most often unavoidable. When properly designed, plastic mechanisms would form and dissipate energy imparted by the earthquake ground motion to the structure.

Modern seismic design codes are based on decades of research and field observation after earthquakes. Although such codes to date do not explicitly use the plastic design method, a key fundamental concept of these codes is the need for ductility and ductile plastic mechanism. The seismic design community goes one step further by incorporating the capacity design concept in parallel with ductility design (as shown in the subsequent chapters). Those two underlying concepts form the basis for seismic design of structures.

7.2 Need for Ductility in Seismic Design

Structural design codes usually specify a set of load combinations that need to be considered in design. For example, ASCE 7 (ASCE 2010) requires the following for building design:

$$1.4(D + F)$$

$$1.2(D + F + T) + 1.6(L + H) + 0.5(L_r \text{ or } S \text{ or } R)$$

$1.2D + 1.6(L_r \text{ or } S \text{ or } R) + (L \text{ or } 0.8W)$
$1.2D + 1.6W + L + 0.5(L_r \text{ or } S \text{ or } R)$
$1.2D + 1.0E + L + 0.2S$
$0.9D + 1.6W + 1.6H$
$0.9D + 1.0E + 1.6H$

where D = dead load, L = live load, L_r = roof live load, S = snow load, W = wind load, and E = earthquake load. Of all the design loads, the earthquake load, E, is often the subject of much misunderstanding, as it is actually an inertia effect due to base excitation produced by an earthquake instead of a real load.

7.2.1 Elastic Response and Response Spectrum

To study the seismic effect on a structure, it is first assumed that a one-story frame can be idealized as a single-degree-of-freedom (SDOF) system, as shown in Figure 7.1a, where K is the lateral stiffness, and M is the lumped mass tributary to the roof level. The angular natural frequency, ω, and the natural period, T, of the structure are:

$$\omega = \sqrt{M/K} \tag{7.1a}$$

$$T = \frac{2\pi}{\omega} = 2\pi\sqrt{K/M} \tag{7.1b}$$

It is also assumed that this system has a 5% equivalent various damping ratio. With a sample earthquake ground motion like the one shown in Figure 7.1b as the input at the base of the frame, the elastic structural response in terms of lateral displacement relative to the base can be computed from structural dynamic theory (Chopra 2007). See Figure 7.1c for one sample response when the period of the structure is 1.0 s. Of particular interest from a design point of view is the maximum relative displacement of the mass relative to the base. This maximum displacement is defined as the spectral displacement, $S_d(T)$ at period T. By varying either M or K, the natural period of the system is also changed. If the above process is repeated for other period values, a displacement response spectrum like that shown in Figure 7.2a can be constructed. Once a response spectrum is constructed, time-consuming time-history analysis is no longer needed as the maximum relative displacement for a given period value can be simply read off from the spectrum.

To design the structure, it is necessary to know the maximum force in the member. From Hooke's law, the maximum structural force or base shear, V_e, in the elastic system is:

$$V_e(T) = K\Delta_{max} = KS_d(T) \tag{7.2}$$

Together with Eq. (7.1a), the above equation can be rewritten as:

$$V_e(T) = M\omega^2 S_d(T) \tag{7.3}$$

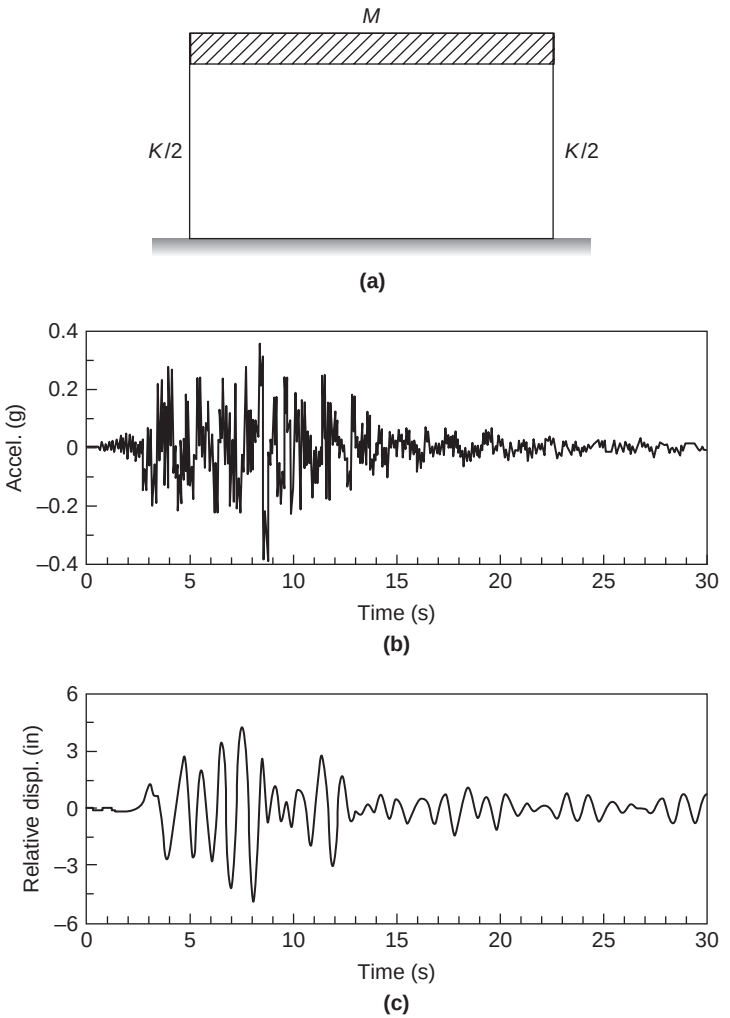

Figure 7.1 Elastic response of an SDOF system: (a) idealized one-story frame; (b) earthquake ground motion (Canoga Park, 1994 Northridge, California Earthquake); (c) relative displacement response.

Defining the pseudo-acceleration, $S_a(T)$, as the following:

$$S_a(T) = \omega^2 S_d(T) \tag{7.4}$$

then the displacement response spectrum in Figure 7.2a can be converted to a pseudo-acceleration response spectrum in Figure 7.2b, and Eq. (7.3) becomes:

$$V_e(T) = MS_a(T) = W\left(\frac{S_a(T)}{g}\right) \tag{7.5}$$

where W is the reactive weight of the system.

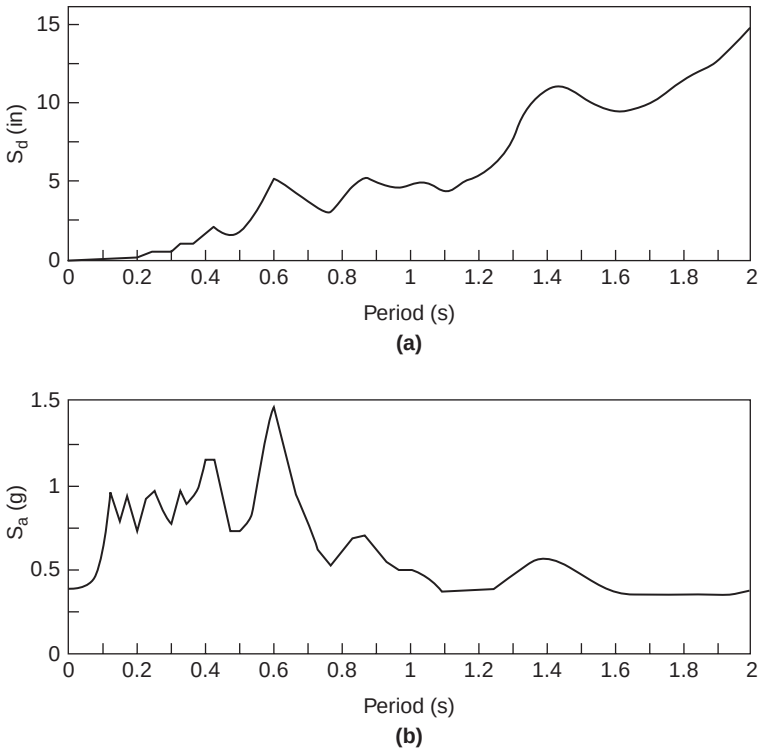

Figure 7.2 Elastic response spectra: (a) relative displacement response spectrum; (b) pseudo-acceleration response spectrum (5% damping).

7.2.2 Inelastic Response and Ductility Reduction

For the example frame to remain elastic, Figure 7.2b indicates that the structure needs to be designed for a base shear of $0.5g$:

$$V_e(T) = M(0.5g) = 0.5W \tag{7.6}$$

That is, for this structure to remain elastic, it needs to be designed for a lateral load that is equal to half of the reactive weight, which is large. Normalizing the base shear, V, by the reactive weight, W, is defined as the base shear ratio, C. Then C_e represents the elastic base shear ratio. This required force level corresponds to point A in Figure 7.3, where the elastic response is shown in dashed line O-A.

Generally, it is not economical to design a structure to remain elastic during a strong earthquake. If an effort is made to ensure that the structure possesses ductility, the required base shear force can be significantly reduced. In such a case the expected elasto-plastic

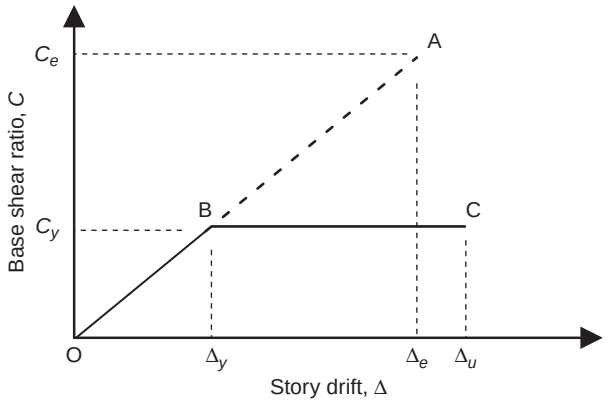

FIGURE 7.3 Definition of ductility factor and ductility reduction factor for an SDOF system.

structural response is shown as O-B-C in Figure 7.3; C_y is the yield shear ratio of the frame. This defines the ductility factor, μ, as follows:

$$\mu = \frac{\Delta_u}{\Delta_y} \tag{7.7}$$

where Δ_u and Δ_y are the maximum and yield displacements, respectively. Referring to the one-story frame in Figure 7.1a again, assume the frame has a ductility capacity of 3. As a 1-s period structure, it can be shown that the required yield base shear ratio only needs to be 35% of the elastic base shear ratio. Figures 7.4a and b show the inelastic response. The reduced yield base shear can be expressed as:

$$C_y = \frac{C_e}{R_\mu} \tag{7.8}$$

where R_μ is defined as the ductility reduction factor. In this example, the value of R_μ is 2.8 for a target μ value of 3.0.

By varying the period of the structure, the constant-ductility R_μ spectrum can be constructed. Newmark and Hall (1982) proposed a very simple ductility reduction rule for SDOF systems. In the moderate and long period range (i.e., in the velocity and displacement amplification regions of the response spectrum), it was observed that the maximum displacement of the elastic and inelastic systems are about the same. This observation leads to the following:

$$R_\mu = \mu \tag{7.9a}$$

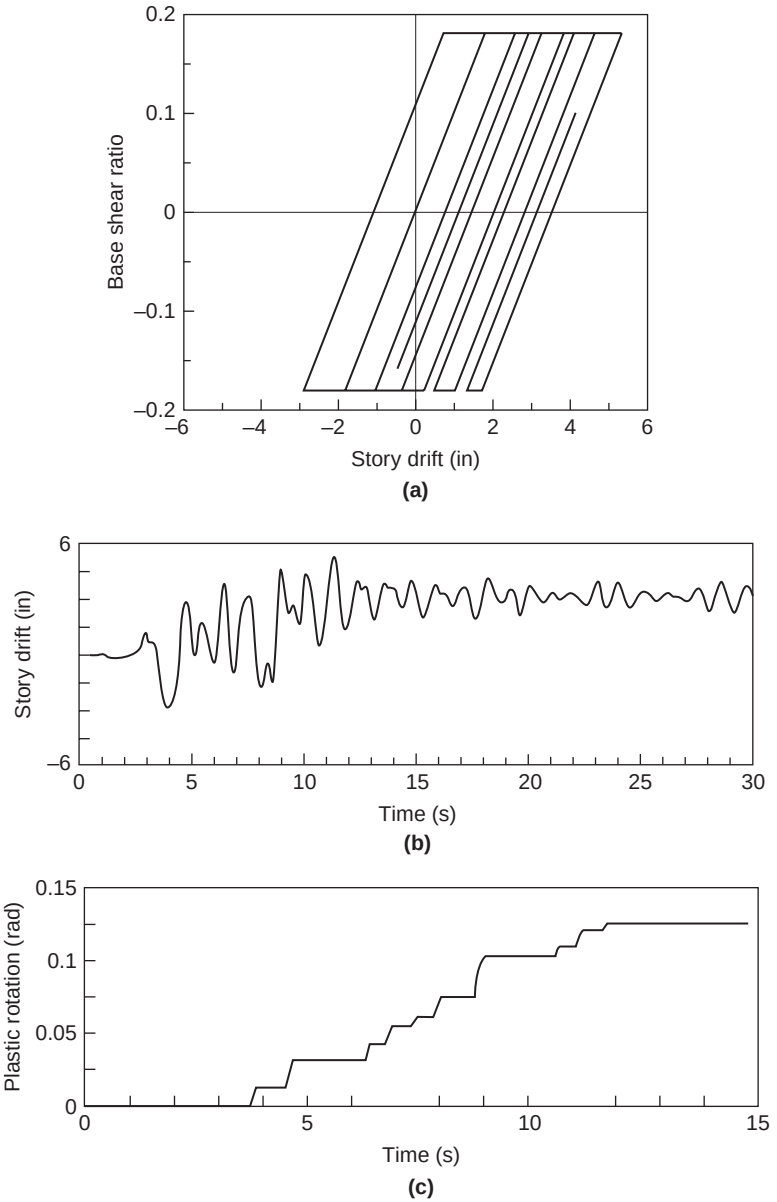

Figure 7.4 Inelastic response of an SDOF system: (a) hysteresis response; (b) relative displacement response; (c) cumulative plastic rotation.

This corresponds to the so-called equal displacement rule. The above relationship can be easily derived from Figure 7.3 by assuming the inelastic displacement, Δ_u, is equal to elastic displacement, Δ_e.

In the short period range (i.e., in the acceleration amplification region of the response spectrum), the relationship is closer to:

$$R_\mu = \sqrt{2\mu - 1} \tag{7.9b}$$

This corresponds to the so-called equal energy rule. The above equation can be derived from Figure 7.3 by equating the areas (i.e., energies) under both the O-A and O-B-C response curves. For a structure with a very short period, Newmark and Hall also observed that $R_\mu = 1$, that is, ductility is ineffective in reducing the required elastic seismic force. However, this would only be the case for structure very short in height and/or extremely stiff; the majority of building structures do not fall in this period range.

More refined ductility reduction rules have also been proposed. See, for example, Miranda and Bertero (1994) for a comparison of several force reduction rules. It should be noted that these rules were derived for SDOF systems, which cannot be applied directly to multistory building structures. See Section 7.5 for more discussion on this issue.

7.3 Collapse Mechanism versus Yield Mechanism

In plastic analysis and design, the term "collapse mechanism" is used to describe a state beyond which the structure has reached its capacity to carry monotonically increasing, static or dynamic load and becomes unstable. The term "collapse" is appropriate when the load is monotonically applied in one direction. However, this definition is not applicable for earthquake "loading" because seismic response is cyclic and transient in nature. This can be demonstrated for the inelastic response of the one-story frame presented earlier. Because the structure is designed and, thus, allowed to yield, a mechanism starts to form once plastic hinges from both ends of the columns. As shown in Figure 7.4c, plastic rotation will develop and accumulate in these hinges before the structural response is reversed in direction. Upon load reversal, the columns will respond elastically again before plastic moment is reached in the reverse direction and plastic rotation starts to accumulate again. It is through this "on" and "off" process that the earthquake energy is dissipated by plastic deformation in the structure. One major goal of seismic design is to maximize energy dissipation while controlling damage. Therefore, the term "yield" or "plastic" mechanism, rather than "collapse" mechanism, is more appropriate to describe the seismic response of structures.

7.4 Design Earthquake

The discussion so far suggests that, at least conceptually, inelastic dynamic analysis is needed for reliable seismic response prediction and design. However, this is not practical for routine design for two main reasons.

On the loading side, it is not possible to deterministically define an earthquake ground motion time history. A recorded motion like that shown in Figure 7.1b is unique by itself; it is affected by many factors like earthquake rupture mechanism, earthquake magnitude, distance from epicenter, local site (or soil) condition, duration of shaking, etc. The intensity of shaking is also dependent on the recurrence interval between large earthquakes at the site of the structure.

On the analysis side, time-history analysis is time consuming and not practical for routine design. Because in design only the maximum structural response is of concern, elastic response spectra like those shown in Figure 7.2 can be more effective. However, because the zigzag-shaped response spectra in this figure are also unique for each recorded ground motion, for design purposes, seismic codes usually provide uniform hazard, smoothed elastic pseudo-acceleration response spectra, not ground motion time histories, to represent design ground motions. A design response spectrum represents statistically an average response spectrum based on many recorded ground motions for a given recurrence interval, expressed in the form of a probability of exceedance in a number of years.

In the United States, Section 1613 of the International Building Code (ICC 2009) references to ASCE 7, *Minimum Design Loads for Buildings and Other Structures* (ASCE 2005), for the construction of elastic design spectra. ASCE 7 first specifies the spectral acceleration values for a maximum considered earthquake (MCE) with a 2475-year recurrence interval (2% probability of being exceeded in 50 years). Two thirds of these values are then used to construct the design basis earthquake (DBE) with a 475-year recurrence interval (10% probability of being exceeded in 50 years). The DBE design spectral shape is shown in Figure 7.5. A brief summary of the procedure to construct the spectrum with a direct reference to relevant sections in ASCE 7 is provided as follows.

(1) Determine site ground motion.
Use ASCE 7 Section 11.4.1 to determine mapped acceleration parameters (S_s and S_1), which are based on (a) maximum considered earthquake (MCE), a 2475-year seismic event; (b) Site class B; and (c) 5% damping. S_s is the spectral acceleration at short period (= 0.2 s), and S_1 is the spectral acceleration at T = 1 s.

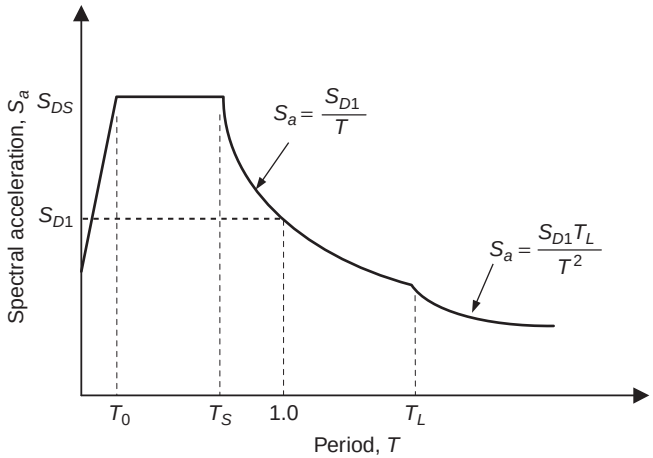

Figure 7.5 ASCE 7 design basis earthquake (DBE) elastic design spectrum.

(2) Determine site (or soil) classification.
Use Table 20.3-1 in Chapter 20 to classify the site. The default site class is D.

(3) Adjust mapped MCE spectral accelerations for the site effect (Section 11.4.3):

$$S_{MS} = F_a S_S \tag{7.10a}$$

$$S_{M1} = F_v S_1 \tag{7.10b}$$

where F_a and F_v are the site coefficients obtained from Tables 11.4-1 and 11.4-2.

(4) Determine design spectral accelerations (Section 11.4.4).
DBE spectral accelerations are two-thirds those from MCE:

$$S_{DS} = \frac{2}{3} S_{MS} \tag{7.11a}$$

$$S_{D1} = \frac{2}{3} S_{M1} \tag{7.11b}$$

The DBE elastic design spectrum in Figure 7.5 is then uniquely defined. For design purposes, ASCE 7 also requires each structure to be assigned a Seismic Design Category (SDC), which ranges from A, B, C, to D. This important category is a function of the S_{DS} value and the Occupancy Category, which depends on the level of hazard to human life in the event of structural failure. Most buildings care classified as Occupancy Category II, but essential buildings like

hospitals and fire stations are classified as Occupancy Category IV; these buildings need to be designed more conservatively.

7.5 Equivalent Lateral Force Procedure

In concept, inelastic time-history analysis is needed for seismic response prediction and design. To facilitate routine design, however, it is highly desirable to use an equivalent lateral force procedure that treats the dynamic inertia effect by equivalent loads, such that a static analysis can be used instead of a dynamic one. The Equivalent Lateral Force (ELF) procedure, which has been in use in North America for more than half a century, was developed with this intent in mind. For its simplistic nature, however, ASCE 7 limits the use of ELF procedure for certain situations. For example, more sophisticated dynamic analysis, either linear or nonlinear, will be required if the structure is highly irregular in plan or height.

Analogous to Eq. (7.8b), ASCE 7 takes into consideration of the energy dissipation capacity of the structure by introducing a Response Modification Factor, R, to reduce the required elastic design base shear:

$$C_s(T) = \frac{C_e(T)}{R} \tag{7.12}$$

where C_e, which is a function of T, is obtained from the DBE elastic design response spectrum.

$$C_e(T) = \begin{cases} \dfrac{S_{D1}}{T} \le S_{DS} & \text{for} \quad T \le T_L \\ \dfrac{S_{D1}}{T^2} \le S_{DS} & \text{for} \quad T > T_L \end{cases} \tag{7.13}$$

T_L is the long-period transition period beyond which the spectrum acceleration is inversely proportional to T^2. The relationship between C_e and C_s spectra is shown in Figure 7.6. Note that in determining the design base shear for the ELF procedure, ASCE 7 conservatively extends the horizontal plateau of the design response spectrum from T_0 to 0 second.

ASCE 7 also introduces an Importance Factor, I, to account for the importance of occupancy. The default value is 1.0. But a value of 1.5 is assigned to I for essential facilities like hospitals and fire stations. To achieve a better protection against earthquake damage for more important structures, ASCE 7 reduces the elastic base shear by R/I, which can be interpreted as the effective Response Modification Factor. For a structure whose period is not too long ($T < T_L$), ASCE 7 expresses Eq. (7.12) as follows:

$$C_s(T) = \frac{S_{D1}}{T(R/I)} \le \frac{S_{DS}}{(R/I)} \tag{7.14}$$

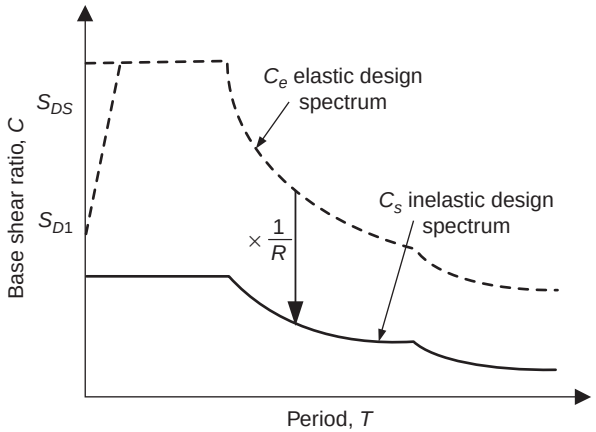

FIGURE 7.6 Relationship between ASCE 7 DBE elastic and inelastic design spectra.

The value of R ranges from 1.25 (least ductile structures) to 8.0 (most ductile structures). See Table 7.1 for the values of R for some steel seismic force-resisting systems.

The design base shear C_sW is used to define the statically applied equivalent lateral force. At this seismic design force level, a linear static structural analysis is performed and the corresponding story drift is designated as Δ_s. Because the structure is expected to respond in the inelastic range, ASCE 7 then requires Δ_s be multiplied by a Deflection Amplifications Factor, C_d, to estimate the maximum story drift. For steel structures this story drift cannot exceed the allowable value, which, based on the Occupancy Category, varies from 0.01 to 0.025 of the story height.

In addition to the two seismic performance factors, R and C_d, the third factor specified in ASCE 7 for capacity design is called the Structural Overstrength Factor, Ω_o. This factor will be discussed in the next section.

Steel Seismic Force-Resisting System	R	C_d	Ω_o
Special moment frames	8	5½	3
Ordinary moment frames	3½	3	3
Special concentrically braced frames	6	5	2
Ordinary concentrically braced frames	3¼	3¼	2
Eccentrically braced frames	8	4	2
Buckling-restrained braced frames	8	5	2½
Special steel plate shear walls	7	6	2

TABLE 7.1 ASCE 7 Sample Seismic Performance Factors

7.6 Physical Meaning of Seismic Performance Factors

Central to the ASCE 7 ELF seismic design procedure is the Response Modification Factor, R. Together with C_d and Ω_o, these three seismic performance factors greatly simplify the design process. The physical meaning of the ductility reduction factor, R_μ, for an SDOF system was discussed in Section 7.2.2. Although both R and R_μ factors are used to reduce the elastic seismic forces, the physical meaning of these two factors is somewhat different. As shown in Figure 7.3, R_μ is defined for an SDOF system where the inelastic behavior can be approximated by an elasto-perfectly plastic response. For application to seismic design of more redundant structures including multistory frames, however, the redundancy of the structure would cause the structure to yield progressively before the ultimate strength of the structure is reached. Therefore, the Newmark-Hall type of ductility reduction rule cannot be applied directly. The physical meaning of the seismic performance factors used in ASCE 7 is described in the following.

Figure 7.7 shows a typical response envelope of a structure, which can be used to explain the R-factor seismic design procedure. Based on the fundamental period of the structure, a designer first calculates the elastic design base shear, C_e (see point E in the figure). In ASCE 7, C_e is then reduced by a factor R to a design seismic force level C_s at point S [see Eq. (7.12)]. Point S is called the first significant yield point, beyond which the structure will respond inelastically. In other words, under lateral loads, a structure designed based on this reduced seismic force level first responds elastically, followed by inelastic response

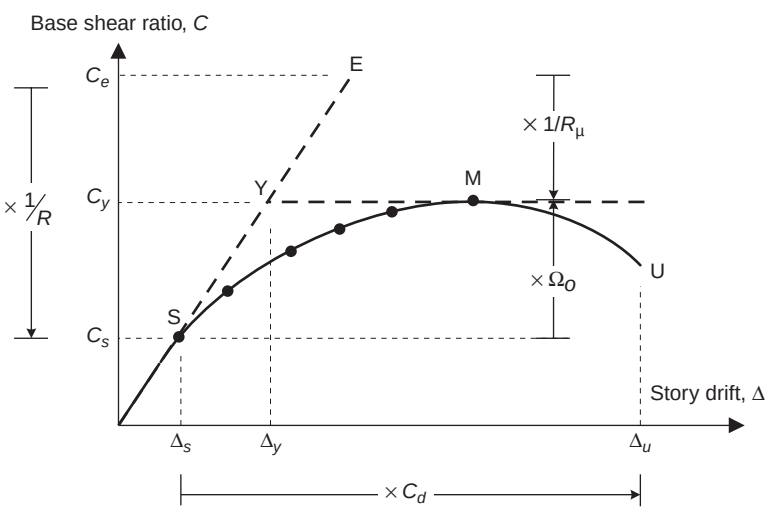

Figure 7.7 Seismic performance factors used in ASCE 7.

as the lateral forces are increased beyond that level. The redundancy that is built into the system together with ductility allows a series of plastic hinges to form in the structure, leading to a yielding mechanism at the strength level C_y.

If the actual structural response curve can be idealized by an elasto-perfectly plastic curve, the system ductility factor, μ_s, can be defined as:

$$\mu_s = \frac{\Delta_u}{\Delta_y} \tag{7.15}$$

Then the system ductility reduction factor, R_μ, can be defined like Eq. (7.8) for an SDOF system:

$$R_\mu = \frac{C_e}{C_y} \tag{7.16}$$

The reserve strength that exists between the yield level (C_y) and the first significant yield level (C_s) is defined as the system overstrength factor, Ω_o:

$$\Omega_o = \frac{C_y}{C_s} \tag{7.17}$$

System overstrength results from a number of factors including internal force redistribution, code requirements for multiple loading combinations, code minimum requirements regarding proportioning and detailing, material strength higher than that specified in the design, strain hardening, deflection constraints on system performance, member oversize, effect of nonstructural elements, and strain-rate effects.

Based on the definition of the above terms, the Response Modification Factor, R, for use with strength design can be derived as follows (Uang 1991a):

$$R = \frac{C_e}{C_s} = \frac{C_e}{C_y}\left(\frac{C_y}{C_s}\right) = R_\mu \Omega_o \tag{7.18}$$

The deflection amplification factor, C_d, is the ratio of Δ_u and Δ_s (see Figure 7.7):

$$C_d = \frac{\Delta_u}{\Delta_s} = \frac{\Delta_u}{\Delta_y}\left(\frac{\Delta_y}{\Delta_s}\right) \tag{7.19}$$

where Δ_u/Δ_y is the structural ductility factor [see Eq. (7.15)], and Δ_y/Δ_s from Figure 7.7 is equal to:

$$\frac{\Delta_y}{\Delta_s} = \frac{C_y}{C_s} = \Omega_o \tag{7.20}$$

Therefore, Eq. (7.19) can be rewritten as:

$$C_d = \mu_s \Omega_o \tag{7.21}$$

Both R and C_d factors are functions of the structural overstrength factor, structural ductility factor, and damping ratio; the effect of damping is generally included in the ductility reduction factor, R_μ. Furthermore, Eq. (7.18) shows that it is not appropriate to refer to R as a ductility reduction factor because system overstrength and ductility may contribute equally to R. Similarly, C_d is generally not equal to the system ductility factor.

7.7 Capacity Design

Ductility design and capacity design are two key concepts in seismic design. To demonstrate this concept, refer to a few commonly used lateral-load resisting systems in Figure 7.8. A thorough coverage of the design of these systems is provided in the following chapters. For the Special Moment Frame (SMF) in Figure 7.8a, energy dissipation is provided through plastic hinge formation in the beams. Therefore, only beams need to be designed to provide ductility. These members are also called the deformation-controlled element (DCE) as it is the deformation (or ductility) capacity that distinguishes these elements from the rest of the structure (ASCE 2006). To ensure that yielding will be confined to DCEs, it is essential that the remaining part of the structure, including columns and connections, have sufficient strength to remain essentially elastic. These latter elements are called force-controlled elements (FCE). Ductility is not the main concern for FCEs. Figures 7.8b and c show that diagonal braces and links are DCEs in special concentrically braced frames (Chapter 9) and eccentrically braced frames (Chapter 10), respectively.

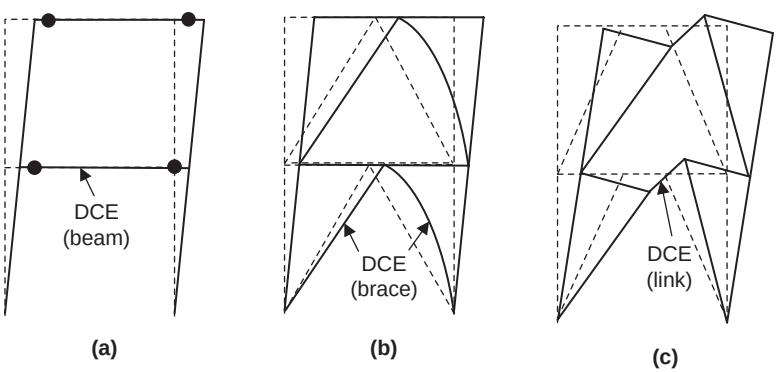

Figure 7.8 Deformation-controlled elements: (a) special moment frame; (b) special concentrically braced frame; (c) eccentrically braced frame.

Refer to Figure 7.7 again for the general response of a redundant, multistory frame. By reducing the elastic seismic force, by the *R* factor, DCEs are designed for a code-specified seismic force at the C_S base shear level. In ASCE 7, the basic load combinations for the design of DCEs are:

$$(1.2 + 0.2S_{DS})D + \rho Q_E + L + 0.2S \tag{7.22a}$$

$$(0.9 - 0.2S_{DS})D + \rho Q_E + 1.6H \tag{7.22b}$$

The value of the redundancy factor, ρ, is equal to 1.0 if certain requirements are satisfied; otherwise, the value is 1.3. The intent of the code is to encourage the use of more redundant structures.

The multiple DCEs within a structure usually will not yield at the same time. Once the most critical DCE is yielded, the ductility of this element allows more lateral load to be applied to the structure such that other DCEs will yield progressively until a full yield mechanism is formed (as shown in Chapters 2 to 6 in various examples). Therefore, the FCEs will experience and need to be designed for the higher force reached at that point. In the United States, the concept of using an amplified seismic force to design FCE was first implemented in the 1988 Uniform Building Code.

Although the concept is clear, difficulties arise when implementing it in design. Figure 7.7 shows that a structure responds elastically up to point S, beyond which nonlinear analysis is required to quantify the ultimate strength of the structure. Because in a typical design it is not practical to perform nonlinear analysis including plastic analysis, building codes provide alternate methods to overcome this obstacle. These methods can be classified as the global-level and local-level approaches.

7.7.1 Global-Level Approach

In this greatly simplified approach, ASCE 7 provides a system overstrength factor, Ω_o, to amplify the prescribed seismic design forces for the ultimate strength at point M in Figure 7.7:

$$C_y W = \Omega_o (C_s W) \tag{7.23}$$

See Table 7.1 for the values of Ω_o for a few popular structural systems. Note that these empirical values were developed mainly using engineering judgment. Although the actual system overstrength varies from one structure to the other, the code intends to provide a conservative, upper bound value for Ω_o. Because capacity design is needed for FCE, the load combinations specified in ASCE 7 are:

$$(1.2 + 0.2S_{DS})D + \Omega_o Q_E + L + 0.2S \tag{7.24a}$$

$$(0.9 - 0.2S_{DS})D + \Omega_o Q_E + 1.6H \tag{7.24b}$$

In AISC Seismic Provisions (AISC 2010), $\Omega_o Q_E$ is called the "amplified seismic loads." Taking the frame in Figure 7.8a for example, the axial load and the moment in the FCE column can be determined from an elastic analysis as shown in Figure 7.9a.

In summary, the basic seismic load combinations [Eq. (7.22)] are used to design the DCEs, whereas the basic seismic load combinations with overstrength factor [Eq. (7.24)] are used for the design of FCEs.

7.7.2 Local-Level Approach

The global approach is approximate in nature as it uses an empirical factor to amplify the prescribed seismic design forces. For many FCEs it is possible to calculate the maximum forces developed in the DCEs and are transferred to the neighboring FCEs in a rational way. This approach provides the upper bound value to the global-level approach. To demonstrate this concept, refer to the same simple moment frame shown in Figure 7.9b. The beam serves as the DCE. Plastic hinges are expected to form near the beam ends. The seismic moment diagram when the yield mechanism is reached is also shown. It is assumed that each plastic hinge is located at a distance c away from the column centerline. From Eq. (3.10), the nominal plastic moment of the beam is:

$$M_{pn} = ZF_y \tag{7.25}$$

Note that F_y is the specified minimum yield stress. Although this yield stress is used to size the member, in reality the actual yield stress is higher. The actual or the expected yield stress is:

$$F_{ye} = R_y F_y \tag{7.26}$$

where R_y is the yield stress adjustment factor. Based on a statistical evaluation of the steel material strength, AISC 341 provides values of R_y for different grades of steel (see Table 7.2[1] for some sample values). The actual beam plastic moment is then equal to the following:

$$M_{pe} = ZF_{ye} = R_y ZF_y = R_y M_{pn} \tag{7.27}$$

---

[1] R_t in Table 7.2 is used to adjust the tensile strength of the steel:

$$F_{ue} = R_t F_u$$

where F_u and F_{ue} are the specified minimum and expected tensile strengths, respectively.

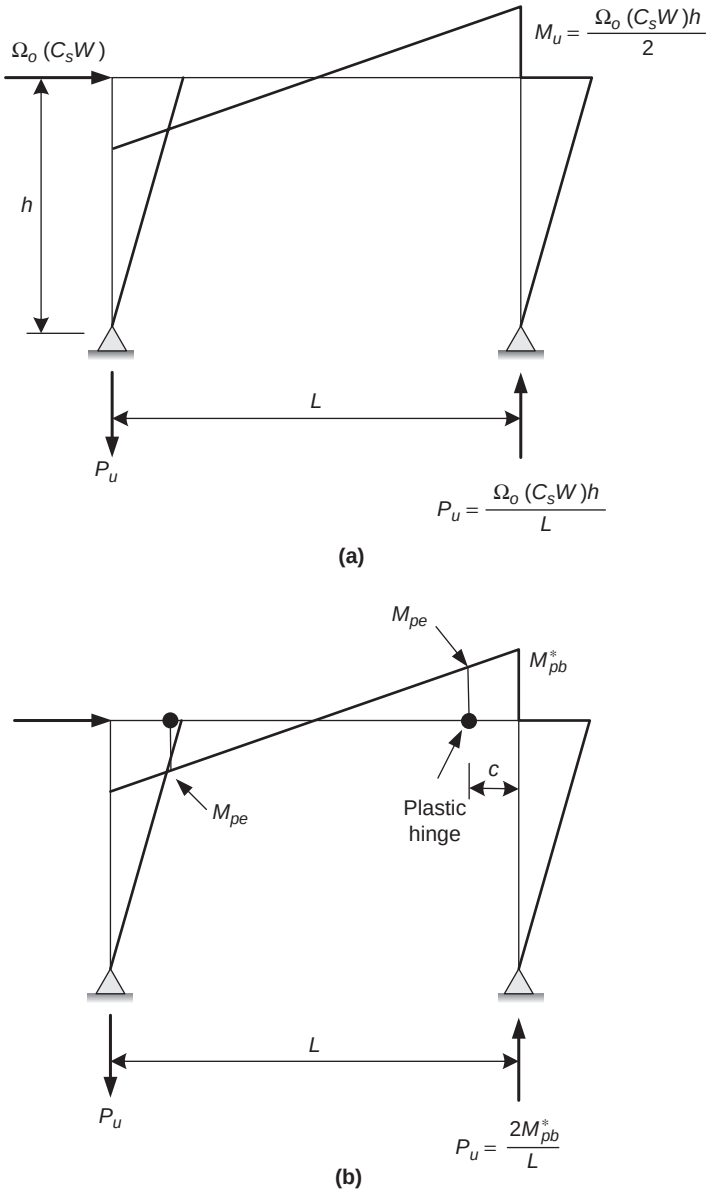

Figure 7.9 Force determination of FCE (column): (a) global-level approach; (b) local-level approach.

Application	R_y	R_t
Hot-rolled structural shapes		
• ASTM A36	1.5	1.2
• ASTM A572 Gr. 50, A992	1.1	1.1
Hollow structural sections (HSS)		
• ASTM A500 Gr. B or C	1.4	1.3
Pipes		
• ASTM A53	1.6	1.2
Plates		
• ASTM A36	1.3	1.2
• ASTM A572 Gr. 50	1.1	1.2

TABLE 7.2 ASCE 341 Sample R_y and R_t Values

Steel not only yields but also strain hardens under cyclic loading, making the beam moment at the plastic hinge even larger. So the probable maximum moment at the plastic hinge is:

$$M_{pr} = C_{pr} M_{pe} = C_{pr} R_y M_{pn} \tag{7.28}$$

where C_{pr} is the factor to account for the cyclic strain-hardening effect. This factor is assumed to be 1.1 in AISC 341. But a slightly higher value is used in AISC 358:

$$C_{pr} = \frac{F_y + F_u}{2F_y} \le 1.2 \tag{7.29}$$

It appears at first glance that a higher flexural strength developed in the beam plastic hinge is beneficial, but this is not true from the viewpoint of capacity design for the column and beam-to-column moment connections. Because the moment diagram of the beam produced by the lateral load varies linearly along the beam span, the moment at the plastic hinges extrapolated to the column is M_{pb}^*. The axial force in the column is then equal to $2M_{pb}^*/L$.

Another example to demonstrate the local-level approach is shown in Figure 9.29 for the design of beam in a Special concentrically Braced Frame (SCBF). It will be shown in Chapter 9 that an SCBF is designed to dissipate energy through brace buckling and yield. Therefore, braces are the DCEs, whereas beam and columns are the FCEs. The beam is subjected to axial force and bending moment when braces buckle and yield. When the yield mechanism is developed, the compressive brace will buckle, and its strength will drop significantly (to be discussed in Chapter 9). To design the beam, which

is a FCE, AISC 341 assumes the expected postbuckling brace strength, C, to be 30% of the expected brace compressive strength. The other brace is assumed to be yielded with an expected tensile strength, T, of $R_y F_y A_g$. Because the expected tensile strength is generally much higher than the postbuckling strength of the brace, the vertical component of these two forces will not balance, and will produce a net pull-down force at the midspan of the beam. A large moment produced by this unbalanced form, which cannot be obtained from an elastic analysis, then needs to be considered for beam design. See Chapter 9 for a more detailed discussion.

7.8 Performance-Based Seismic Design Framework

7.8.1 Seismic Performance Objective

In addition to the above summary of the US seismic design provisions based on ASCE 7, it is worthwhile to briefly summarize the performance objectives states in various similar design requirements.

The basic seismic design philosophy that appeared in the *Recommended Lateral Force Requirements and Commentary* [also known as the Blue Book and first published by the Structural Engineers Association of California (SEAOC) in 1959], stated that the intent of the recommended design provisions was to produce a structure that should be able to resist:

- A minor level of earthquake ground motion without damage
- A moderate level of ground motion without structural damage but possibly experience some nonstructural damage
- A major level of ground motion having an intensity equal to the strongest, either experienced or forecast for the building site, without collapse, but possibly with some structural as well as nonstructural damage

Although the SEOAC's seismic design philosophy intended to control building performance for both structural and nonstructural components at different levels of earthquake intensities, both the expected building performance and the ground shaking intensity were described in a qualitative manner. It wasn't until 1995 that SEAOC published Vision 2000 (SEAOC 1995) to outline a performance-based framework to address a broad range of building performance and seismic hazard levels.

In the 1990s, efforts to develop seismic design provisions for rehabilitating existing building structures eventually led to the first performance-based design code: ASCE 41–Seismic Rehabilitation of Existing Building (ASCE 2006). ASCE 41 states the rehabilitation objective in a more quantitative manner. For design of new structures,

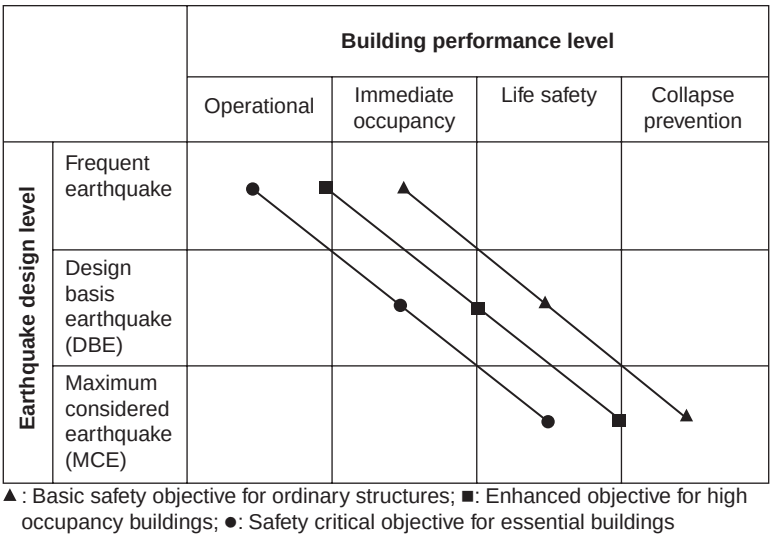

Figure 7.10 ASCE 7 Building seismic performance objectives.

the seismic design objective of ASCE 7 is also stated in a similar manner, expressed in a matrix format in Figure 7.10 (BSSC 2009). The three hazard levels of design ground motions are expressed in a probability format.

Four building performance levels (Operational, Immediate Occupancy, Life Safety, and Collapse Prevention) are used. For example, at the Collapse Prevention level, the seismic force-resisting system is deemed to have lost most of its original stiffness and strength, and little margin against collapse remains. Similarly, at the Life Safety level, significant structural and nonstructural damage are expected, but the damage is not life threatening and a significant margin against collapse still remains. This framework is used to evaluate the seismic design approach adopted in the United States, Canada, and Japan as follows.

7.8.2 USA: ASCE 7

The seismic design provisions in ASCE 7 intend to achieve the Basic Performance Objective for ordinary buildings (Occupancy Category II). As is shown in Section 7.4, only the DBE, which is defined as two thirds of the MCE, is used for design, and the target performance level is Life Safety. Although ASCE 7 explicitly requires design for only one level of ground motions, it is implicitly assumed that structures thus designed will also achieve the other two goals shown in Figure 7.10: collapse prevention at MCE and immediate occupancy at frequent earthquake with a recurrence interval of 72 years.

7.8.3 Canada: NBCC

7.8.3.1 1995 NBCC

National Building Code of Canada (NBCC) also adopts a one-level seismic design procedure. In its 1995 edition, the 475-year DBE elastic design spectrum is expressed as:

$$C_e = \nu SIF \tag{7.30}$$

where ν is the specified horizontal ground velocity, S is a period-dependent seismic response factor, I is a seismic importance factor, and F is a foundation factor. The elastic seismic force is then reduced by two factors to compute the prescribed design base shear ratio:

$$C_s = U\left(\frac{C_e}{R}\right) \tag{7.31}$$

where R is the force modification factor to account for the ductility capacity of the structure, and U (= 0.6) is a calibration factor "representing level of protection based on experience…" (NBC 1995). Although both NBCC and ASCE 7 use the same symbol R for seismic force reduction, their physical meaning is very different. The R values used in NBCC range from 1.0 for nonductile structural systems to 4.0 for the most ductile systems (see Table 7.3 for some typical values), which are significantly smaller than those ($1.0 \le R \le 8.0$) used in ASCE 7 (see Table 7.1).

Equation 7.31 can be rewritten as follows:

$$C_s = U\left(\frac{C_e}{R}\right) = \frac{C_e}{R(1/U)} \tag{7.32}$$

Steel Seismic Force-Resisting System	2005 Edition		1995 Edition	
	R_d	R_o	R	$1/U$
Moment-resisting frames				
• Ductile	5.0	1.5	4.0	1.67
• Moderately ductile	3.5	1.5		
• Limited ductility	2.0	1.3		
Concentrically braced frames				
• Moderately ductile	3.0	1.5	3.0	
• Limited ductility	2.0	1.3		
Eccentrically braced frames	4.0	1.5	3.5	
Ductile steel plate shear walls	5.0	1.6	4.0	

Table 7.3 NBCC Sample Seismic Force Reduction Values

Comparing the previous equation to Eq. (7.18), it is observed that:

$$R_u = R \tag{7.33}$$

$$\Omega_o = \frac{1}{U} \tag{7.34}$$

That is, the R factor in NBCC is the system ductility reduction factor, and a constant system overstrength factor, $1/U$ (= 1.67), is assumed for all the lateral force-resisting systems. Note that the R factor in ASCE 7 includes the contribution from both system ductility reduction and system overstrength; the ductility reduction component of the R factor is not given.

The story drift produced by the prescribed seismic design force is then amplified by R, which corresponds to the C_d factor in ASCE 7. The drift limits are $0.01h$ for post-disaster building and $0.02h$ for all other buildings, where h is the story height.

7.8.3.2 2005 NBCC

Major revisions are made in the 2005 edition of NBCC. The design earthquake used to compute the design seismic forces is similar but not the same as that used in ASCE 7. The procedure to reduce elastic seismic force is maintained but with some adjustments.

NBCC first specifies an elastic base shear ratio based on MCE:

$$C_e = S(T)M_v I_E \tag{7.35}$$

where $S(T)$ is the 5% damped spectral acceleration, expressed as a ratio of gravitational acceleration at period T. M_v, with a value ranging from 0.4 to 2.5, is a factor to account for the higher mode effect, and I_E (1.0, 1.3, or 1.5) is the importance factor. This elastic base shear ratio is then reduced by two factors to compute the prescribed seismic design base shear ratio:

$$C_s = \frac{C_e}{R_d R_o} \tag{7.36}$$

where R_d and R_o are ductility-related and overstrength-related force modification factors. A comparison of the denominator of the above equation with that in Eq. (7.32) shows that R_d is equivalent to R and R_o is equivalent to $(1/U)$ in the 1995 NBCC. The values of R_d range from 1.0 to 5.0; Table 7.3 shows the R_d values for some steel systems. These values are similar to and some are slightly higher than the R values in the 1995 NBCC. Other than using as a constant system overstrength factor (= 1.67), the 2005 NBCC uses R_o, which varies from 1.0 to 1.7. See Mitchell et al. (2003) for the background information on calibrating the R_o values.

The procedure to compute the story drift is also changed. In the 1995 NBCC, only the ductility-related force modification factor, R, is used to amplify the story drift produced by the prescribed seismic design force, and the drift limit is set to $0.02h$ for ordinary buildings. The 2005 NBCC requires the use of the total force modification factor, R_dR_o, to amplify story drift. Although the limit is relaxed to $0.025h$ based on the recommendation of SEAOC Vision 2000 (Devall 2003), the resulting structure is likely to be much stiffer than that designed based on the 1995 NBCC (and ASCE 7) for two reasons. First, the seismic design force is based on MCE, not DBE, yet the values of the total force modification factor are similar to those ($= R/U$) used in the 1995 NBCC (or R in ASCE 7). Therefore, the prescribed seismic design base shear ratio and the corresponding story drift is about 50% higher. Second, this higher story drift is amplified by the total force modification factor, not the ductility-related component of the total force modification factor as was done in the 1995 NBCC. Because the slightly relaxed story drift limit in the 2005 NBCC is not likely to compensate for this much larger design story drift, the 2005 NBCC could, in some instances, result in more conservative designs.

7.8.4 Japan: BSL

Based on the discussions presented so far, both the US and Canadian seismic design provisions attempt to achieve similar seismic performance objectives. For ordinary structures (Occupancy Category II in ASCE 7), the Basic Performance Objective is the target for design. As is shown in Figure 7.10, in concept three levels of design earthquake intensities (i.e., seismic hazards) need to be considered. For ease of design in actual implementation, however, both the US and Canadian codes adopt the same approach by explicitly considering only one seismic hazard level and the associated building performance level, while implicitly assuming that the other two building performance levels at the associated hazard levels will be met automatically. Although both ASCE 7 and NBCC use this "one-level" seismic design procedure, they differ because the ASCE 7 design procedure is anchored at the DBE for Life Safety, whereas the 2005 NBCC is anchored at the MCE for Collapse Prevention.

Unlike the North American seismic codes, the Building Standard Law (BSL) of Japan adopted a "two-level" seismic design procedure since 1981 (IAEE 2004). Although the BSL provides exceptions, allowing the designer to consider only a one-level design when certain height limitation and regularity requirements are met, the central concept in the BSL is to anchor the seismic design on two points along a performance objective line similar to that shown in Figure 7.10, and explicitly consider two seismic hazard levels in design.

As such, the BSL constitutes a two-level design procedure. Designers must consider service limit state requirements for the moderate

earthquake associated with the Level 1 design and ultimate limit state requirements for the severe earthquake associated with the Level 2 design.

7.8.4.1 Level 1 Design

In Japan, moderate earthquake shaking corresponds to a peak ground acceleration of between 0.07 g and 0.10 g (Kato 1986), and with a recurrence interval between 30 and 50 years (Kuramoto 2006). The BSL service limit state requires that a regular building remains in the elastic range when subjected to lateral seismic forces associated with a base shear ratio, C_w:

$$C_w = 0.2ZR_t \tag{7.37}$$

where ZR_t ($\equiv C_e$) represents the linear elastic design response spectrum for *severe* earthquake shaking. The intensity of the moderate earthquake is one-fifth that of the severe earthquake. To control nonstructural damage, the maximum story drift is limited to 0.5% of the story height, which is very similar to that used in the Uniform Building Code before 1997 (Uang and Bertero 1991). To avoid structural damage, the maximum allowable stress for steel design is limited to approximately 90% of the yield stress. One establishes this stress level by increasing the basic allowable stress for gravity-load design, which is about 60% of the yield stress, by 50%. Because the structure is expected to respond in the elastic range, ductility is not considered for the service limit state check.

7.8.4.2 Level 2 Design

A severe earthquake is assumed to have a peak ground acceleration ranging from 0.34 g to 0.4 g (Kato 1986), and the recurrence interval is similar to that of the DBE in ASCE 7. Using the terminology in Figure 7.7, the base shear ratio, C_y, is computed as:

$$C_y = D_s ZR_t \tag{7.38}$$

where D_s is a structural characteristics factor that accounts for the energy dissipation capacity (ductility) of the structure (Kato and Akiyama 1982). For steel building structures, the value of D_s ranges from 0.25 for a ductile system to 0.50 for a nonductile system (see Table 7.4). Note that the BSL requires the designer to check the ultimate strength of the structure, not the first significant yield as is done in the North America, which means the designer has to perform nonlinear analysis in order to ensure that the structure has a sufficient ultimate strength. Based on Eq. (7.16), the BSL effectively provides the following system ductility reduction factor:

$$R_\mu = \frac{1}{D_s} \tag{7.39}$$

Types of Moment-Resisting Portion of Braced Frames*	Types of Braces	
	Moment Frames or Braced Frames with $\beta_u^{\dagger} \le 0.3$	Braced Frames with $\beta_u^{\dagger} > 0.7$
FA	0.25	0.35
FB	0.30	0.35
FC	0.35	0.40
FD	0.40	0.50

*Classification of moment-resisting frames is based on the compactness ratio of beams and columns. See IAEE (2004) for details.

†β_u = ratio of ultimate shear carried by braces to total ultimate shear.

‡For braces with effective slenderness ratio between $50/\sqrt{F_y}$ and $90/\sqrt{F_y}$ only, where yield stress F_y has a unit value of t/cm^2. See IAEE (2004) for other ranges of effective slenderness ratio.

Table 7.4 Typical BSL D_s Values For Steel Structures

Therefore, it is appropriate to compare $1/D_s$ with either the R factor in the 1995 NBCC or the R_d factor in the 2005 NBCC, but not the R factor in ASCE 7. See Uang (1991b) for a comparison of the seismic force reduction factors used in the US and Japanese codes.

In summary, the C_w force level is used for the service limit state design, and the C_y force level is used to check the ultimate limit state design. For buildings that satisfy certain height limitations and regularity requirements, a simplified, yet conservative, one-level design procedure can be used. Also see Uang (1993) for a comparison of one-level and two-level seismic design procedures.

7.8.5 Seismic Design of Tall Buildings

The performance-based methodology also finds its way into the seismic design of tall buildings in high seismic regions in the United States. Building code provisions (e.g., ASCE 7) are intended for a wide range of building types. As a result of this broad intended applicability, code provisions produce tall building design that may not be optimal, both from cost and safety perspectives. One limitation of the current prescriptive building codes is the building height. For buildings in the high seismic design categories, ASCE 7 sets a height limit to many popular lateral force-resisting systems. For example, steel braced frames and reinforced concrete shear walls are limited for buildings up to either 160 ft (49 m) or 100 ft (30 m), depending on the SDC. However, building codes always allow the use of alternative analysis and design methods that can be justified by well-established principles of mechanics and supported by tests. Therefore, several efforts have been made in the United States to develop performance-based design

procedures such that the intended performance objectives in the model codes are met.

The Los Angeles Tall Buildings Structural Design Council (LATBSDC) published in 2005 a document entitled, *An Alternative Procedure for Seismic Analysis and Design of Tall Buildings Located in the Los Angeles Region*. This document led to the development of a similar document *AB-083–Recommended Administrative Bulletin on the Seismic Design and Review of Tall Buildings Using Non-prescriptive Procedures* for the City of San Francisco Department of Building Inspection (SFDBI) in 2007 (SEAONC 2007). In this document, tall buildings are defined as those with an overall height exceeding 160 ft (49 m). Unlike the model building codes, this performance-based design procedure requires two levels of earthquakes to be considered. The conventional code-level, 475-year DBE, is used to define the minimum lateral strength and stiffness requirements for Life Safety. In addition, the 2475-year MCE is evaluated to check for collapse prevention building performance. This latter evaluation requires nonlinear dynamic analysis by using a minimum of seven sets of properly scaled earthquake ground motion records. As part of the acceptance criteria, the average story drift should not be larger than 3% of the story height. For those deformation-controlled members that are designed to yield, the deformation demand cannot exceed the deformation capacity obtained from either test results or applicable documents. For force-controlled members and elements that are not designed to yield and are protected by capacity design principles, the design strength can be based on the expected, not nominal, material strength. However, this document does not require checking nonstructural elements at the MCE level.

The serviceability evaluation for a lower seismic hazard level is generally not required. It is required only when there is a reason to believe that the serviceability performance of the design would be worse than that anticipated for a code-prescriptive design. When needed, the serviceability ground motion shall be that having a recurrence interval of 43 years (i.e., a 50% probability of exceedance in 30 years).

The LATBSDC issued an updated edition on the Alternative Procedure in 2008. Like its 2005 edition, this document intends to meet the Basic Performance Objective. Several significant changes were made over the 2005 edition. First of all, this document explicitly adopts the capacity design approach, followed by performance-based evaluations. Unlike the 2005 edition, the prescriptive code-level Life Safety evaluation is eliminated. Instead, both the serviceability evaluation for a Frequent Earthquake (a 43-year recurrence interval) and Collapse Prevention evaluation for a 2475-year MCE are needed. For serviceability evaluation, the building response is not intended to be limited to be fully elastic. Instead, limited yielding is allowed in deformation-controlled members. But the story drift cannot exceed 0.5% of the story height, which is similar to the drift requirement of the Japanese BSL Level 1 design. For Collapse Prevention evaluation

through the nonlinear dynamic analysis, this document refers to ASCE 41 for the deformation capacities.

The latest guidelines for performance-based seismic design of tall buildings are publisher by the Pacific Earthquake Engineering Research Center. See PEER, 2010 for details.

7.8.6 Next-Generation Performance-Based Seismic Design

All the performance-based design procedures presented above introduced the concept of performance in terms of discretely defined performance levels with names intended to connote the expected level of damage: Collapse Prevention, Life Safety, Immediate Occupancy, and Operational Performance. They also introduced the concept of performance related to damage of both structural and nonstructural components. Performance Objectives were developed by linking one of these performance levels to a specific level of earthquake hazard. These procedures also introduced a set of analytical procedures of varying levels of complexity that could be used to simulate the seismic response of buildings. Also, all these procedures require a MCE response evaluation in order to demonstrate adequate safety against collapse in an implicit manner. This response evaluation does not provide a quantifiable margin against (or a probability of) collapse, but is intended to demonstrate that collapse under the selected ground motions does not occur, that is, the structure maintains stability, and forces and deformations are within acceptable limits.

In order to fulfill the promise of performance-based engineering and help ensure that performance-based seismic design delivers on its full potential for reducing future losses from earthquakes, next-generation performance-based design procedures are being developed under an ATC-58 project funded by FEMA (ATC 2009). This long-range effort includes the following tasks:

- Revise the discrete performance levels defined in first-generation procedures to create new performance measures (e.g., repair costs, casualties, and time of occupancy interruption) that better relate to the decision-making needs of stakeholders, and that communicate these losses in a way that is more meaningful to stakeholders (Krawinkler and Miranda 2004).
- Create procedures for estimating probable repair costs, casualties, and time of occupancy interruption, for both new and existing buildings.
- Expand current nonstructural procedures to explicitly assess the damageability and post-earthquake functionality of nonstructural components and systems, which can constitute a significant percentage of the economic loss associated with damaging earthquakes.
- Develop a framework for performance assessment that properly accounts for, and adequately communicates to

stakeholders, limitations in our ability to accurately predict response, and uncertainty in the level of earthquake hazard.

In a significant way, this also ties with broader efforts to quantify seismic resilience (Bruneau et al. 2003; Bruneau and Reinhorn 2007; MCEER 2008; Cimellaro et al. 2010a, 2010b).

7.9 Historical Perspective of Seismic Codes

Although the design practice is likely to move toward the performance-based seismic design in the next decade, it is proper and instructive, in closing this chapter to provide a historical basis for the seismic force reduction factor, R. The numerical values assigned to those factors by codes for various types of structural systems were not obtained by rigorous analysis and experimentation, but rather by consensus of expert engineers.

The first North American design requirements intended to prevent building collapse during earthquakes originated in California. Interestingly, after a major earthquake struck San Francisco in 1906, reconstruction of the devastated city proceeded with an updated building code that required the consideration of a wind force of 30 pounds per square ft (1.44 kPa) for the design of new buildings (Bronson 1986). No specific earthquake-resistant design clauses were introduced. Given that many building codes of that time did not even have requirements for wind resistance (such as the Los Angeles building code in which wind pressure was not considered in design until 1924), it was hoped that the new "stringent" wind pressure requirement would simultaneously address both wind and earthquake effects.

The 1927 Uniform Building Code (UBC) introduced the first seismic design requirements in North America, partly in response to the Santa Barbara earthquake of 1925. This model code proposed clauses for consideration for possible inclusion in the building codes of various cities, at their discretion, and was not binding. The 1927 UBC proposed that a single horizontal point load, F, equal to 7.5 or 10% (depending on the soil condition) of the sum of the building's total dead and live load, W, be considered to account for the effect of earthquakes.

Hard soil/rock

$$F = CW = 0.075W \tag{7.40a}$$

Soft soil

$$F = CW = 0.10W \tag{7.40b}$$

where C is a seismic coefficient. No justification can be found for these values of C, but they likely reflected the consensus of the engineering

community. Interestingly, Prof. Toshikata Sano in Japan who visited San Francisco after the 1906 earthquake got the idea of using seismic inertia force as the design earthquake action (Towhata 2008). Sano stated that the seismic force is given by the ground acceleration multiplied by the mass of a structure and then recommended the acceleration to be 10 to 30% of that of gravity. This proposal of using a seismic coefficient of 0.1 was adopted in Japanese building design regulations in 1924. Dr. Kyoji Suyehiro of Japan visited California and reported in a series of lectures that buildings designed using a value of C equal to 0.10 in Japan survived the tragic Kanto (Tokyo) earthquake of Richter Magnitude 8.2 in which 140,000 died (Suyehiro 1932).

Enforceable earthquake-resistant design code provisions in North America were implemented following the 1933 Long Beach earthquake of Richter Magnitude 6.3. This earthquake produced damage in Long Beach and surrounding communities in excess of $42 million in 1933 dollars (more than $400 million in 1995 dollars), and the death toll exceeded 120 (Alesch and Petak 1986, Iacopi 1981). It was significant that a large number of the buildings that suffered damage were schools and that the total number of casualties and injuries would have undoubtedly been considerably larger had this earthquake not occurred at 5:54 P.M., when the schools were fortunately empty. Nonetheless, this economic and physical loss provided the necessary political incentive to implement the first mandatory earthquake-resistant design regulations. The California State Legislature passed the Riley Act and the Field Act, the former requiring that all buildings in California be designed to resist a lateral force equal to 2% of their total vertical weight, the latter mandating that all public schools be designed to resist a similar force equal to between 2 and 10% of the dead load plus a fraction of the live load; the magnitude of the design lateral force depended on the building type and the soil condition. At the same time, a Los Angeles building ordinance was issued, calling for 8% of the sum of the dead load plus half of the live load to be used as a design lateral force.

Once researchers brought forth the difference between the dynamic and static response of structures, showing that the seismically induced forces in a flexible (high-rise) building are typically smaller than those in stiff (low-rise) ones, simplified empirical equations to attempt to capture this observed dynamic behavior, and suitable for hand calculations, were developed. The 1943 Los Angeles Building Code was the first to introduce a seismic coefficient and a lateral force distribution that indirectly reflected building flexibility. The lateral forces were calculated as $V = CW$, where V and W were the story shear and total weight of the building above the story under consideration, respectively. The seismic coefficient was calculated as:

$$C = \frac{0.60}{N + 4.5} \tag{7.41}$$

where N is the number of stories above the story under consideration. This formula was slightly modified (SEAOC 1980) when the building height restriction of 13 stories, in effect in Los Angeles in 1943, was removed in 1959.

The 1950s saw the introduction into the lateral force equation of a numerical coefficient, K, intended to reflect the relative seismic performance of various types of structural systems and a more refined consideration of building flexibility through calculation of the fundamental period of vibration, T, of the building in the direction under consideration (Anderson et al. 1952, Green 1981). The generic expression for the base shear became:

$$V = KCW \tag{7.42}$$

where

$$C = \frac{0.05}{T^{1/3}} \tag{7.43a}$$

and

$$T = \frac{0.05H}{\sqrt{D}} \tag{7.43b}$$

where V is the base shear, W is the total dead load, and H and D are, respectively the height of the building and its dimension (in ft) in the direction parallel to the applied forces. The distribution of the base shear along the building height was specified to be inverted-triangular. Types of construction that had been observed to perform better in past earthquakes were assigned low values of K, whereas those that had not performed as well were assigned high values of K. Buildings relying on ductile moment-resisting space frames to resist seismic forces were designed with $K = 0.67$. Buildings with dual structural systems were assigned a value of K equal to 0.8; K for bearing wall systems was set equal to 1.33, and buildings with types of framing systems other than those specified above were assigned a value of K equal to 1.00 (SEAOC 1959). Over time, the equation evolved slightly to include an importance factor, I (equal to 1.0 for normal buildings), a seismic zone factor, Z (equal to 1.0 in the more severe seismic zones), and a soil condition factor varying between 1.0 and 1.5, depending on site conditions. The magnitude of the specified base shear was also increased in 1974, following the San Fernando earthquake of 1971, because many felt that it was too low. This was accomplished by changing the seismic coefficient to the following:

$$C = \frac{1}{15\sqrt{T}} \tag{7.44}$$

Detailed descriptions of the significance of each of the above factors and the way to calculate them, as well as descriptions of the various changes that occurred in seismic codes in the 1960s, 1970s, and some of the 1980s, are available elsewhere (SEAOC 1980, Green 1981, ATC 1995b). However, it is of utmost importance to appreciate that numerical values for K that were introduced into the SEAOC Recommended Lateral Force Requirements in 1959 (and that eventually made their way into other codes worldwide) were based largely on judgment, reflecting the consensus of the SEAOC code committee membership (consisting of expert design professionals and academicians).

A fundamental change in the format of the base shear equation was proposed in 1978 with publication of the ATC-3-06 (ATC 1978) report "Tentative Provisions for the Development of Seismic Regulations for Buildings." That document, prepared by multidisciplinary task groups of experts, proposed new comprehensive seismic provisions that introduced many innovative concepts, among which were the elastic design spectrum and the seismic performance factors, R and C_d. The elastic design spectrum is expressed as follows:

$$C_e(T) = \frac{1.2C_v}{T^{2/3}} \leq 2.5C_a \tag{7.45}$$

where C_v and C_a are seismic coefficients based on the soil profile and the effective peak velocity or the effective peak acceleration, respectively. This elastic seismic force demand is then reduced by the R factor for strength design:

$$C_s(T) = \frac{C_e(T)}{R} = \frac{1.2C_v}{RT^{2/3}} \leq \frac{2.5C_a}{R} \tag{7.46}$$

The authors of the ATC-3-06 elected not to substantially change the required force levels but rather to concentrate on providing ductile detailing (ATC 1995a). This was a paradigm shift that essentially promoted ductile detailing as a top consideration for design.

Numerical values for R were determined largely by calibration to past practice (ATC 1995a). For example, for ductile steel moment-resisting space frames, equating the proposed ATC equation for base shear at the strength level V_{ATC}, to that in effect at the time, V_{SEAOC} (SEAOC 1974):

$$V_{SEAOC}\left(\frac{1.67}{1.33}\right) = \frac{V_{ATC}}{0.9} \tag{7.47}$$

where 1.67 was the typical margin of safety between allowable-stress and ultimate-strength design values, 1.33 accounted for the 33% increase in allowable stresses that was permitted by these codes for load combinations involving earthquakes or wind, and 0.9 was the

capacity reduction factor for flexure in the context of ultimate strength design. Substituting the respective base shear equations in this expression:

$$(ZIKCSW)_{SEAOC} W\left(\frac{1.67}{1.33}\right) = \frac{V_{ATC}}{0.9} \tag{7.48}$$

Assuming a site in California, a fundamental period of 1.0 s, identical soil conditions for which $S_{SEAOC} = 1.5$ and $S_{ATC} = 1.2$, and using $Z = 1.0$, $A = 0.4$, $I = 1.0$, $T = 1.0$:

$$(1.0)(1.0)K\left(\frac{1}{15\sqrt{(1.0)}}\right)(1.5)W\left(\frac{1.67}{1.33}\right) = \frac{1.2(0.4)(1.2)}{0.9R(1.0)^{2/3}}W \tag{7.49}$$

and

$$R = \frac{5.1}{K} \tag{7.50}$$

For a ductile steel moment-resisting frame, K per SEAOC (1959) was 0.67 giving a value of R equal to approximately 8.0 (rounded up from the calculated value of 7.61). Values of R for other types of structural systems (see Table 7.1) were also calculated using Eq. (7.47) and adjusted to reflect the consensus of the ATC-3-06 committee members. The ATC-3-06 equations have also been implemented in the 1988 Uniform Building Code, with some minor modifications, including calibration to accommodate the working stress design (a.k.a. allowable stress design) format of the UBC at the time. The 1988 UBC specifies the DBE elastic design spectrum in the following form:

$$C_e(T) = \frac{1.25ZIS}{T^{2/3}} \le 2.75ZI \tag{7.51}$$

where Z is a seismic zone factor, I is the importance factor, and S is a site soil coefficient. For working stress design, the elastic seismic force demand is reduced by a seismic force reduction factor R_w, not R, for design:

$$C_w(T) = \frac{C_e(T)}{R_w} = \frac{1.25ZIS}{R_w T^{2/3}} \le \frac{2.75ZI}{R_w} \tag{7.52}$$

Through use of a procedure similar to that described above (ATC 1995a), the following relationship was used to obtain R_w factors for use in working stress design:

$$R_w = \frac{7.86}{K} = \frac{7.86R}{5.1} = 1.54R \approx \frac{8}{K} \tag{7.53}$$

Before it was replaced by the International Building Code in the United States, the 1997 UBC specified the design base shear ratio for strength design and replaced R_w by R as the seismic force reduction factor:

$$C_s(T) = \frac{C_v I}{RT} \leq \frac{2.5 C_a I}{R} \tag{7.54}$$

This expression was modeled after ATC-3-06. Instead of using C_d as a deflection amplification factor, UBC used $0.7R$ for the same purpose.

Since then, with the objective of providing a more rigorous and systematic framework on how the values of the seismic performance factor described in this chapter (i.e., R, C_d, and Ω_o) are established for various structural systems, particularly for new systems proposed for adoption in future editions of the seismic design provisions, a detailed procedure has been developed and is outlined in the FEMA P-695 report (FEMA 2009). This methodology provides a thorough framework to assess the appropriateness of such factors, complete with consideration of collapse probabilities and other uncertainties inherent to seismic analysis and design. The proposed methodology is being considered by various code-writing bodies for possible use, as a desirable approach to determine the substantiating data required for adoption of any new structural system into codes and specifications. A complete description of this complex procedure is however beyond the scope of this book.

References

AISC. 2010. *Prequalified Connections for Special and Intermediate Steel Moment Frames for Seismic Applications, ANSI/AISC 358*. Chicago: AISC.

AISC. 2010. *Seismic Provisions for Structural Steel Buildings, ANSI/AISC 341*. Chicago: AISC.

AISC. 2010. *Specification for Structural Steel Buildings, ANSI/AISC 360*, 2005 and 2010. Chicago: AISC.

Alesch, D. J., and Petak, W. J. 1986. *The Politics and Economics of Earthquake Hazard Mitigation*. Boulder: Institute of Behavioral Science, University of Colorado.

Anderson, A. W., Blume, J. A., Degenkolb, H. J., Knapik, E. M., Marchand, H. L., Powers, H. C., Rinne, J. E., Sedgwick, G. A., and Sjoberg, H. O. 1952. "Lateral Forces of Earthquake and Wind." *Transaction of ASCE*, vol. 117.

ASCE. 2006. *Seismic Rehabilitation of Existing Buildings, ASCE/SEI 41*: Reston, VA: ASCE.

ASCE. 2010. *Minimum Design Loads for Buildings and Other Structures, ASCE/SEI 7*, 2005 and 2010. Reston, VA: ASCE.

ATC. 1978. *Tentative Provisions for the Development of Seismic Regulations for Buildings*. Redwood City, CA: Applied Technology Council.

ATC. 1995a. *Structural Response Modification Factors, Report No. ATC-19*. Redwood City, CA: Applied Technology Council.

ATC. 1995b. *A Critical Review of Current Approaches to Earthquake Resistant Design, Report No. ATC-34*. Redwood City, CA: Applied Technology Council.

ATC. 2009. *Guidelines for Seismic Performance Assessment of Buildings, Report No. ATC-58*, (50% Draft). Redwood City, CA: Applied Technology Council.

Bronson, W. 1986. *The Earth Shook, the Sky Burned—A Moving Record of America's Great Earthquake and Fire*. San Francisco: Chronicle Book.

Bruneau, M., Chang, S., Eguchi, R., Lee, G., O'Rourke, T., Reinhorn, A., Shinozuka, M., Tierney, K., Wallace, W., and von Winterfelt, D. 2003. "A Framework to Quantitatively Assess and Enhance the Seismic Resilience of Communities." *EERI Spectra Journal*, vol. 19, no. 4, 733–752.

Bruneau, M., and Reinhorn, A. 2007. "Exploring the Concept of Seismic Resilience for Acute Care Facilities." *Earthquake Spectra*, vol. 23, no.1, 41–62, EERI.

BSSC. 2009. *NEHRP Recommended Seismic Provisions for New Buildings and Other Structures, FEMA P-750*. Washington, D. C. :Federal Emergency Management Agency.

Cimellaro, G., Reinhorn, A., and Bruneau, M. 2010a. "Framework for Analytical Quantification of Disaster Resilience." *Engineering Structures Journal*, vol. 32, no. 11, 3639–3649.

Cimellaro, G., Reinhorn, A., and Bruneau, M. 2010b. "Performance-Based Metamodel for Health Care Facilities." *Journal of Earthquake Engineering and Structural Dynamics*, DOI: 10.1002/eqe.1084.

Chopra, A. K. 2007. *Dynamics of Structures*. Upper Saddle River, NJ: Pearson Prentice Hall.

Devall, R. H. 2003. "Background Information for Some of the Proposed Earthquake Design Provisions for the 2005 Edition of the National Building Code of Canada." *Canadian Journal of Civil Engineering*, vol. 30, no. 2, 279–286.

FEMA. 2009. *Qualification of Building Seismic Performance Factors, FEMA P695*. Washington, D. C.: Federal Emergency Management Agency.

Green, N. B. 1981. *Earthquake Resistant Building Design and Construction*. New York: Van Nostrand Reinhold.

Iacopi, R. 1981. *Earthquake Country—How, Why, and Where Earthquakes Strike in California*. Menlo Park, CA: Sunset Books, Lane Publishing.

IAEE. 2004. *Earthquake Resistant Regulations, a World List–2004* . Tokyo: IAEE.

ICBO. 1997. *Uniform Building Code*. Whittier, CA: International Building Code Council.

ICC. 2009. *International Building Code*. Falls Church, VA: International Code Council.

Kato, B. 1986. "Seismic Design Criteria for Steel Building." *Proceedings of Pacific Structural Steel Conference*, vol. 1, 133–147, Auckland, NZ.

Kato, B., and Akiyama, H. 1982. "Seismic Design of Steel Buildings." *Journal of Structural Engineering, ASCE*, vol. 108, no. ST8, 1709–1721.

Krawinkler, H., and Miranda, E. 2004. "Performance-Based Earthquake Engineering." *Earthquake Engineering: from Engineering Seismology to Performance-Based Engineering*, Chapter 9, editors Bozorgnia and Bertero, V.V., CRC Press, Boca Raton, FL.

Kuramoto, H. 2006. "Seismic Design Codes for Buildings in Japan." *Journal of Disaster Research*, vol. 3, no. 3, 341–356. Fuji Technology Press.

LATBSDC. 2008. *An Alternative Procedure for Seismic Analysis and Design of Tall Buildings Located in the Los Angeles Region.* Los Angeles: Los Angeles Tall Buildings Structural Design Council.

Miranda, E., and Bertero, V. V. 1994. "Evaluation of Strength Reduction Factor for Earthquake-Resistant Design." *Earthquake Spectra*, vol. 10, 357–379.

Mitchell, D., Tremblay, R., Karacabeyli, E., Paultre, P., Saarcioglu, M., and Anderson, D. L. 2003. "Seismic Force Modification Factors for The Proposed 2005 Edition of the National Building Code of Canada." *Canadian Journal of Civil Engineering*, vol. 30, no. 2, 308–327.

MCEER. 2008. "Engineering Resilience Solutions: From Earthquake Engineering to Extreme Events: 1997–2007—A Decade of Earthquake Engineering and Disaster Resilience." *MCEER-08-SP09*. Multidisciplinary Center for Earthquake Engineering Research, University at Buffalo, State University of New York.

NBC. 2005. *National Building Code of Canada (NBCC)*, 1995 and 2005. Ontario: National Research Council.

Newmark, N. M., and Hall, W. J. 1982. *Earthquake Spectra and Design*. Berkeley, CA: EERI.

PEER. 2010. "Guidelines for Performance-Based Seismic Design of Tall Buildings." PEER Report No. 2010/05. Pacific Earthquake Engineering Research Center, University of California, Berkeley.

SEAOC. 1995. *Vision 2000–Performance Based Seismic Engineering of Buildings*. Sacramento, CA: Structural Engineers Association of California.

SEAOC. 1980. *Recommended Lateral Force Requirements and Commentary*. 1959, 1974, and 1980,Structural Engineers Association of California, Sacramento, CA.

SEAONC. 2007. *Recommended Administrative Bulletin on the Seismic Design and Review of Tall Buildings Using Non-prescriptive Procedures*. San Francisco: Structural Engineers Association of Northern California.

Suyehiro, K. 1932. "Engineering Seismology Notes on American Lectures." *Proceedings of ASCE*, vol. 58, no. 4. 9–110.

Towhata, I. 2008. "History of Geotechnical Earthquake Engineering in Japan." *Proceedings of 14th World Conference on Earthquake Engineering*, Oct. 12–17, Beijing, China, IAEE.

Uang, C. M. 1991a. "Establishing R (or R_w) and C_d Factors for Building Seismic Codes." *Journal of Structural Engineering, ASCE*, vol. 117, no. 1, 19–28.

Uang, C. M. 1991b. "Comparison of Seismic Force Reduction Factors Used in U.S.A. and Japan." *Earthquake Engineering and Structural Dynamics*, vol. 20, 389–397.

Uang, C. M. 1993. "An Evaluation of Two-Level Seismic Design Procedure." *Earthquake Spectra, EERI*, vol. 9, no. 1, 121–135.

Uang, C. M., and Bertero, V. V. 1991. "UBC Seismic Serviceability Regulations: Critical Review." *Journal of Structural Engineering, ASCE*, vol. 117, no. 7, 2055–2068.

This page intentionally left blank

CHAPTER 8

Design of Ductile Moment-Resisting Frames

8.1 Introduction

This chapter provides an overview of the behavior and design of ductile steel moment frames. Section 8.2 discusses some basic concepts of overall frame behavior. Sections 8.3 and 8.4 cover basic concepts of column and panel zone behavior and design, which both influence the behavior of steel moment frames. Section 8.5 discusses beam-to-column connections. Typical North American practice for beam-to-column moment connections prior to the 1994 Northridge earthquake is presented, along with observations of connection damage from this earthquake and a review of the reasons for this damage. Some of the moment-connection strategies developed after the Northridge earthquake are presented, together with detailed information on connections prequalified for use in special moment-resisting frames. The corresponding moment frame design procedures specified by AISC 358 (AISC 2010a) are addressed in Section 8.6. Issues related to the consideration of P-Δ effects follow in Section 8.7. Finally, Section 8.8 presents a design example for a special moment-resisting frame designed in compliance with the AISC requirements.

Throughout this chapter, the AISC Seismic Provisions (2010b), a.k.a. AISC 341, are used when necessary to illustrate how principles of ductile design have been implemented in codes. Numerous code documents have introduced and updated specific detailing requirements for earthquake-resistant steel structures since the first comprehensive provisions formulated in code language appeared in 1988 (SEAOC 1988). Although differences remain across international codes and standards (e.g., CSA 2009), the fundamental principles are similar to a broad extent. Emphasis on the AISC requirements here is solely intended to help focus the discussion. Finally, note that although

steel frames damaged by the Northridge earthquake were generally designed per the Uniform Building Code—a forerunner to the International Building Code—the ductility detailing requirements of the 1992 Edition of AISC Seismic Provisions in effect at the time were similar to those of the Uniform Building Code.

8.1.1 Historical Developments

The history of steel moment frames is tied to the emergence of high-rise construction in Chicago and New York City in the late 1880s, the 12-story Home Insurance Building in Chicago being often credited as the first building that used a "skeleton construction" steel frame (Bennett 1995). In those early concepts, steel frames were designed to carry gravity loads, including those from the non–load-bearing unreinforced masonry walls. Although engineers often intuitively relied on the stiff cladding to resist lateral loads, beams were connected to columns in a manner that allowed for the development of some frame action. Requirements for wind and earthquake design only became mandated decades later. For example, in San Francisco's building code, wind forces were first specified following the 1906 San Francisco earthquake, whereas, paradoxically, earthquake design was not required until 1948 (EERI 1994, 1997).

Although seismic design didn't formally exist at the time, empirical evidence from that 1906 San Francisco earthquake convinced many engineers of the unparalleled effectiveness of steel moment frames to resist earthquakes, as photos taken after the earthquake but before the ensuing conflagration showed that many such tall buildings survived, either intact or without part of their facade (Bronson 1959, Freeman 1932). However, steel frame construction evolved and changed substantially over the subsequent decades, with striking differences between the framing connections used at the beginning and end of that century (Hamburger et al. 2009). As a result, these perceptions regarding the expected ductile performance of steel moment frames in earthquakes were significantly challenged by the 1994 Northridge (Los Angeles) earthquake in the United States, and by the 1995 Hyogo-ken Nanbu (Kobe) earthquake in Japan. In both earthquakes, steel moment frames did not perform as well as expected. Brittle failures were observed at beam-to-column connections in modern steel moment frame structures, challenging the assumption of high ductility and demonstrating that knowledge on the behavior of steel moment-resisting frames was incomplete.

To best understand the factors that contribute to either desirable or undesirable seismic performance of moment-resisting frames, and because many engineers are involved in retrofitting older buildings, parts of this chapter are structured as a chronology to differentiate the state of knowledge before and after the Northridge earthquake.

8.1.2 General Behavior and Plastic Mechanism

Moment-resisting frames (also called moment frames) are, in their simplest form, rectilinear assemblages of beams and columns, with the beams rigidly connected to the columns. Resistance to lateral forces is provided primarily by rigid frame action—that is, by the development of bending moments and shear forces in the frame members and joints. By virtue of the rigid beam-to-column connections, a moment frame cannot displace laterally without bending the beams and columns. The bending rigidity and strength of the frame members is therefore the primary source of lateral stiffness and strength for the entire frame. Sway frame action under loads is generally well understood, because it is a fundamental behavior studied as part of the undergraduate structural engineering curriculum (Leet et al. 2011).

Steel moment-resisting frames have been popular in many regions of high seismicity for several reasons. First, as described above, and based on evidence from experimental research (presented in the later sections), moment frames have been viewed as highly ductile systems. Building code formulae for design earthquake forces typically assign the largest force reduction factors (and therefore the lowest lateral design forces) to moment-resisting frames, reflecting the opinion of code writers that moment-resisting frames are among the most ductile of all structural systems. Second, moment frames are popular because of their architectural versatility. There are no bracing elements present to block wall openings, providing maximum flexibility for space utilization. A penalty for this architectural freedom results from the inherent lateral flexibility of moment-resisting frames. Compared with braced frames, moment frames subjected to lateral loads generally require larger member sizes than those required for strength alone to keep the lateral deflections within the code-mandated drift limits. The inherent flexibility of moment frames may also result in greater drift-induced nonstructural damage under earthquake loading than with other stiffer systems.

As described in Chapter 6, the most ductile system behavior is achieved when the desirable sway plastic mechanism can develop, with plastic hinging at the ends of all beams over the frame height. Plastic hinging of columns, which would lead to a plastic mechanism confined to a single story, is undesirable.

8.1.3 Design Philosophy

The design of moment-resisting frames is a direct extension of the plastic analysis and capacity design principles presented in Chapters 3 to 6, with a few major differences. First, to ensure achievement of the desirable yielding hierarchy, the simple plastic properties assumed in these earlier chapters must be modified to account for a number of practical considerations, such as expected yield strength, strain-hardening

effects, panel zones, and others that are in part the subject of this chapter. Second, for reasons described later in this chapter, in some cases, the development of plastic hinges a small distance away from the face of columns is preferable to hinging immediately at the face of the column. All other aspects of the design of moment-resisting frames are predicated by these concepts and other details intended to allow development of the desired plastic mechanism.

8.2 Basic Response of Ductile Moment-Resisting Frames to Lateral Loads

8.2.1 Internal Forces During Seismic Response

A steel moment-resisting frame is composed of three basic components: beams, columns, and beam-column panel zones. These are illustrated in Figure 8.1 for a simple two-story, single-bay moment frame. Beams span the clear distance from face-of-column to face-of-column, L_b, and columns are divided into a clear span portion, h_{ci}, and a panel zone region of height, h_{pzi}. The panel zone is the portion of the column contained within the joint region at the intersection of a beam and a column. This definition is useful when one is considering sources of elastic and inelastic deformations, as well as possible plastic hinge locations.

In traditional structural analysis, moment frames are often modeled as line representations of horizontal and vertical members, with the lines intersecting at dimensionless nodes. Such models do not explicitly consider the panel zone region, and they provide an incomplete picture of moment frame behavior. Design of ductile moment frames requires explicit consideration of the panel zone region (inelastic behavior and design of the panel zone are addressed in Section 8.5).

Figure 8.1 also shows qualitatively the distribution of the bending moment, shear force, and axial force in a moment frame under lateral load. These internal forces are shown for the beam, clear span portion of the column, and the column panel zone and they do not include gravity load effects. The beams exhibit high bending moments, typically under reverse curvature bending, with maximum moments occurring at the member ends. The shear and axial force in the beam are generally much smaller and less significant to the response of the beam as compared with bending moment, although they must be considered in design. Similarly, the clear span portions of the columns are typically subjected to high moments, with relatively low shear forces. Axial forces in columns, both tension and compression, can be significant because of overturning moments on the frame. Finally, the column panel zone is subjected to high moments, high shear forces due to a severe moment gradient, and possibly high axial forces.

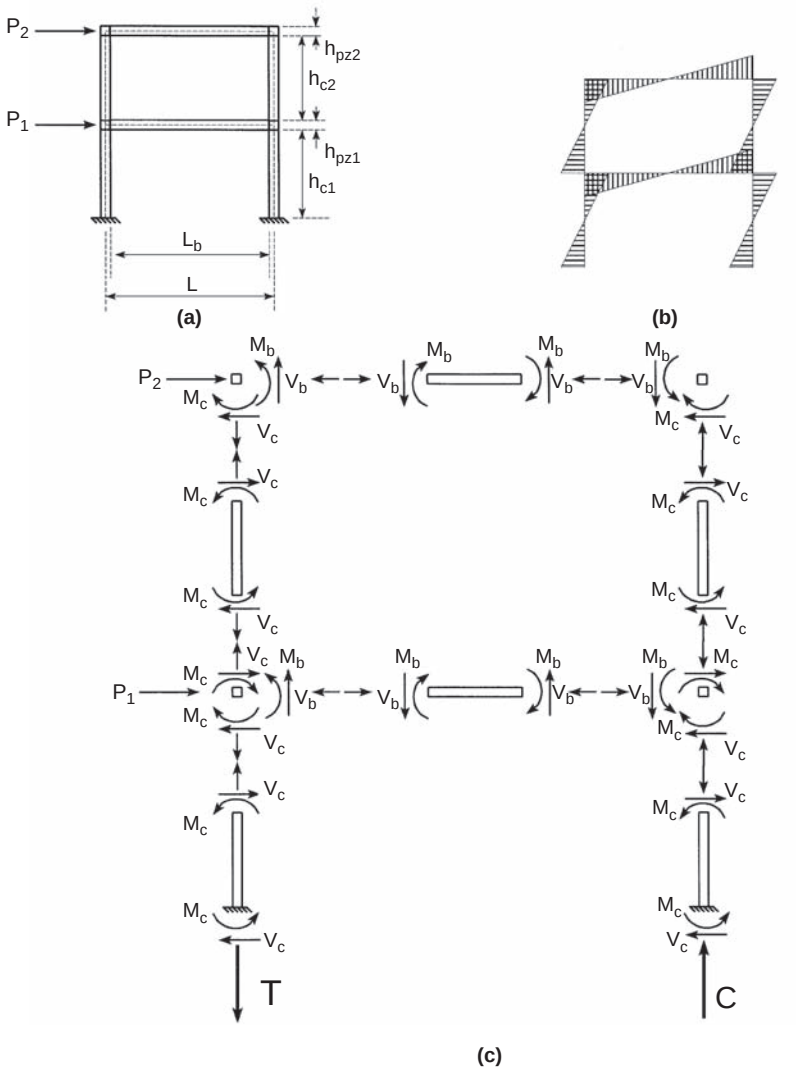

Figure 8.1 Ductile moment-resisting frame: (a) geometry considering finite dimensions of members, (b) typical moment diagram under lateral loading, and (c) corresponding member forces on beams, columns, and panel zones.

The qualitative distribution of internal forces illustrated in Figure 8.1 is fundamentally the same for both elastic and inelastic ranges of behavior. The specific values of the internal forces will change as elements of the frame yield and internal forces are redistributed. The basic patterns illustrated in Figure 8.1, however, remain the same. Inelastic step-by-step response-history analysis is needed to obtain exact values for the internal forces in moment frames, but this

analytical complexity can be avoided if capacity design principles are integrated into the design process along with the conventional elastic analyses.

Plastic analysis of moment frames was described in Chapters 4 through 6. It was shown that, depending on the relative strength of beams and columns framing into a joint, different plastic collapse mechanisms can develop and that, as described in Chapter 6, the development of plastic hinges in the beams is the superior mechanism (see Figure 6.10). In actual frames, however, as opposed to frames studied using simple plastic analysis, strain-hardening makes possible yielding of more than one component at any given joint. In an example sequence of events, the panel zone may yield first, but still exhibit significant postyielding stiffness because of strain-hardening and other effects described in Section 8.4. As a result, greater forces can be applied at the joint, and other framing members, such as a beam, may reach their plastic capacities. Thus, the beam, column, and even panel zone could contribute to the total plastic deformation at the joint, depending on their relative yield strengths and yield thresholds. A structural component considerably weaker than the others framing into the joint will have to provide alone the needed plastic energy dissipation, whereas components of comparable strength would share this burden.

Once identified, those structural components expected to dissipate hysteretic energy during an earthquake must be detailed to allow development of large plastic rotations, without significant loss of strength. Only those components and connection details capable of providing cyclic plastic rotation capacities in excess of the demands should be used to ensure satisfactory seismic performance.

8.2.2 Plastic Rotation Demands

Estimates of the plastic rotation demands for a given moment frame are typically obtained by inelastic response-history analyses. Results from such analyses are sensitive to modeling assumptions and vary when different ground motion records are considered. The amount of the plastic energy dissipated by beams, panel zones, and columns will also be a function of the design philosophy adopted.

For those reasons, general expectations of plastic rotation demand for generic moment frames are based on the synthesis of observations from past analytical studies. Prior to the Northridge earthquake, the largest plastic rotations expected in beams alone (in the absence of panel zone plastic deformations) were expected to be 0.02 radian (Popov and Tsai 1989, Tsai and Popov 1988), although some studies reported values as high as 0.025 radian (Roeder et al. 1989). Smaller plastic rotation demands are obviously expected in flexible frames whose design is governed by compliance to code-specified drift limits.

An approximate way to estimate the plastic rotation demands in a frame is to examine its plastic collapse mechanism at the point of maximum drift. For example, if the beam sway mechanism shown in Figure 6.10 develops in a frame designed in compliance with the code-specified interstory drift limit, the maximum plastic hinge rotations in a beam can be estimated as Δ_e/h, where h is the story height and Δ_e is the inelastic interstory drift. Inelastic interstory drifts are approximately related to those one calculates using design-level forces, Δ_c, by simple relationships such as $\Delta_e = R\,\Delta_c$ (NRCC 2010) or $\Delta_e = C_d\,\Delta_c$ (ASCE 2010), where $R = R_d R_o$ is a seismic force reduction factor per the National Building Code of Canada and C_d is a deflection amplification factor serving the same purpose in U.S. practice (see Chapter 7 for more details). Typically, for code-specified drift limits, the use of these relationships produces plastic rotation demands of approximately 0.02 radian. This procedure is conservative because a large percentage of the total frame drift occurs elastically before plastic hinges form, provided that the method to calculate Δ_e and the seismic hazard characterization are accurate.

After the Northridge earthquake, the required connection plastic rotation capacity was increased to 0.03 radian for new construction and 0.025 radian for postearthquake modification of existing buildings (SAC 1995b). This target rotation was a consensus value developed following the earthquake based on analysis of code-compliant moment frames using ground motion histories recorded during the earthquake (e.g., Bertero et al. 1994). Although this rotation capacity may exceed real earthquake demands on most structural connections, it will likely remain as the target value until substantial research demonstrates that lower values are acceptable.

8.2.3 Lateral Bracing and Local Buckling

Selected structural members must be able to reach and maintain their plastic moment through large plastic rotations that permit hysteretic dissipation of earthquake-induced energy. The engineer must therefore delay local flange and web buckling, and lateral-torsional buckling, to prevent premature failures due to member instability.

For that reason, only seismically compact structural shapes should be used for structural members expected to develop plastic hinges. For example, AISC 341 (AISC 2010b) limits the flange width-to-thickness ratios, $b_f/2t_f$, of W shapes to $0.3\sqrt{E/F_y}$, for F_y in ksi (which roughly corresponds to the $145/\sqrt{F_y}$ limit in CSA 2009, for F_y in MPa). Moreover, lateral bracing to both flanges of these members should be provided at each plastic hinge location and spaced at no more than $0.086 r_y E/\sqrt{F_y}$, with F_y in ksi and where r_y is the member's radius of gyration about its weak axis; ASCE 358 (AISC 2010) may also prescribe alternate limits for specific types of prequalified connections, as will be discussed later. This requirement recognizes that

top and bottom flanges will alternatingly be in compression during an earthquake and accounts for some uncertainty in the location of plastic hinges under various load conditions. Local buckling of flanges and webs and lateral-torsional buckling will unavoidably develop at very large plastic rotations (at least in commonly used structural shapes), but compliance with the above requirements will slow the progressive loss in strength and help ensure good inelastic energy dissipation. This topic is further discussed in Chapter 14.

8.3 Ductile Moment-Frame Column Design

8.3.1 Axial Forces in Columns

Column buckling is not a ductile phenomenon and must be prevented. Columns should therefore be designed to remain stable under the maximum forces they can be subjected to during an earthquake. These forces will generally exceed those predicted by elastic analysis using code-specified earthquake loads, but may be difficult to estimate. As an upper bound, with some allowance for strain-hardening effects, one can obtain maximum axial forces using capacity design principles (as described in Figure 6.8). However, during an earthquake, plastic hinges do not form simultaneously at all stories, but rather develop in only a few stories at a time, often in a succession of waves traveling along the height of the building. As a result, the capacity design approach may be conservative, particularly in multistory buildings.

There is no agreement on what constitutes a proper alternative method to capture the maximum axial force acting on a column during earthquake shaking. Some codes typically resort to an additional load case, with higher specified earthquake loads to be considered only for the design of columns. For example, AISC 341 uses a special "amplified" seismic load combination in which the seismic forces are multiplied by an overstrength factor, Ω_o, only to be used for specific purposes, such as column design (note that some earlier editions now obsolete used a constant $2R/5$ overstrength factor). Application of the SRSS technique in conjunction with capacity design principles, presented in Chapter 9 for ductile concentric braced frames, is another method to estimate more realistic maximum column axial forces. All of these methods have flaws and limitations as discussed in that chapter.

8.3.2 Considerations for Column Splices

Typically, the bending moment diagram for the beams and columns will show a point of inflection somewhere along the length of the member. Frequently, for preliminary design, the points of inflection are assumed to be at midlength of the members. Although this is a convenient assumption, it is important to recognize that the location of the inflection points will vary significantly. This is particularly true as yielding occurs in the frame during an earthquake and bending

moments are redistributed within the frame. Even though the basic pattern of bending moments remains the same, the location of inflection points can shift substantially from the locations indicated by an elastic frame analysis.

Assumptions regarding the location of inflection points can substantially impact the design of column splices. A designer may elect to locate a column splice near an inflection point based on elastic frame analysis (or slightly lower than midheight to provide convenient site-welding conditions) and design the splice for a relatively small bending moment, based on those same elastic frame analysis results. This would be an error because the possibility of significant bending moments at the splice location must be considered, regardless of the results of elastic analysis.

Tests have showed partial penetration welds in thick members to be brittle under tensile loads (Bruneau et al. 1987, Bruneau and Mahin 1991, Popov and Stephen 1977). For example, a standard partial penetration splice detail frequently used in seismic regions, shown in Figure 8.2a, was tested for the largest column sizes that could be accommodated in a 17,800 kN (4000 kips) capacity universal testing machine (Bruneau and Mahin 1991). This specimen, fabricated from A572 Grade 50 steel, was tested in flexure instead of tension to permit consideration of the largest specimen for which cross-section could be kept whole; cutting away part of the section that would have released some of the lock-in residual stresses. The test setup is illustrated in Figure 8.2b. As shown in Figure 8.2c, the moment-curvature relationship remained practically linear up to a value corresponding to approximately 60% of the nominal plastic moment of the smaller column section at the splice, at which the weld fractured in a brittle manner (Figure 8.2d).

For the above reasons, partial penetration welded joints in column splices are viewed apprehensively. Therefore, seismic codes typically require splices subjected to net tension forces to be designed for no less than half of the column axial cross-sectional plastic strength, or 150% of the required splice strength calculated by analysis.

8.3.3 Strong-Column/Weak-Beam Philosophy

Structural frames can dissipate a greater amount of hysteretic energy when plastic hinges develop in the beams rather than in the columns (see Figure 6.10). This beam-sway mechanism enhances overall seismic resistance and prevents development of a soft-story (column-sway) mechanism in a multistory frame. Frames in which measures are taken to promote plastic hinges in the beams rather than in the columns are said to be strong-column/weak-beam (SCWB) frames. The alternative is weak-column/strong-beam (WCSB) frames.

Most codes and design guidelines have moved toward the SCWB philosophy by requiring that, at a joint, the sum of the columns' plastic moment capacities exceed the sum of the beams' plastic

moment capacities, based on simple moment equilibrium at the joint (as in Figure 8.1), in which case:

$$\sum M_{pc} = \sum Z_{cr} F_{yc} = \sum Z_c \left(F_{yc} - \frac{P_{uc}}{A_g} \right) \geq \sum M_{pb} \tag{8.1}$$

and, generally, at least

$$\sum M_{pc} = \sum Z_{cr} F_{yc} = \sum Z_c \left(F_{yc} - \frac{P_{uc}}{A_g} \right) \geq \sum Z_b F_{yb} \tag{8.2}$$

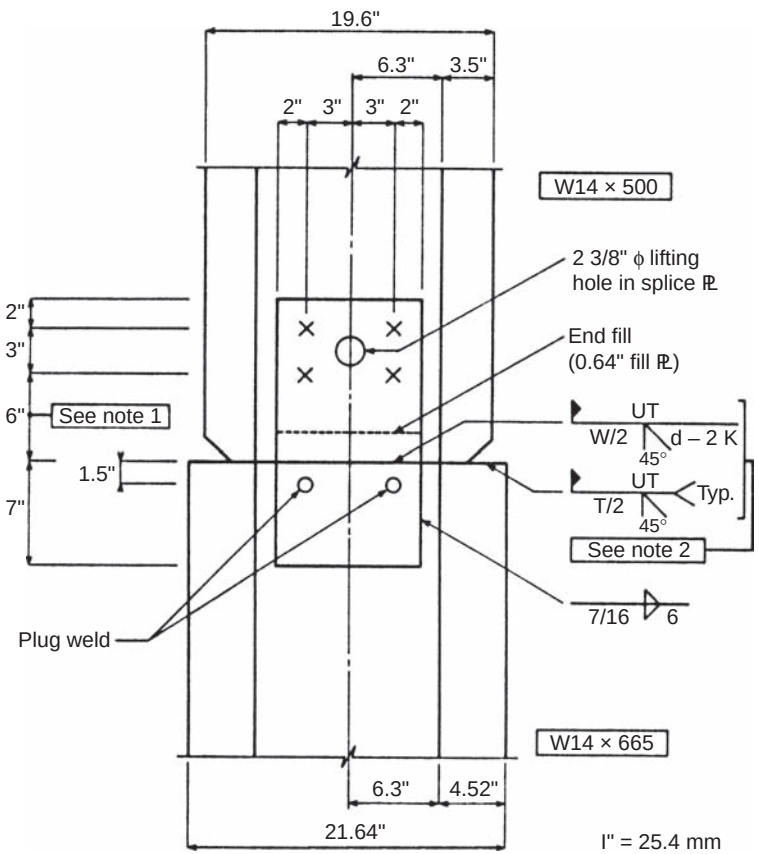

Notes:
1. Provide 6" *as specified* instead of 3" as on standard detail.
2. A certified inspector is to be present during construction and perform ultrasonic testing of the weld.

(a)

Figure 8.2 Test column splice with partial penetration welds in thick members: (a) splice detail; (b) test setup; (c) moment-curvature results; (d) splice after brittle fracture.

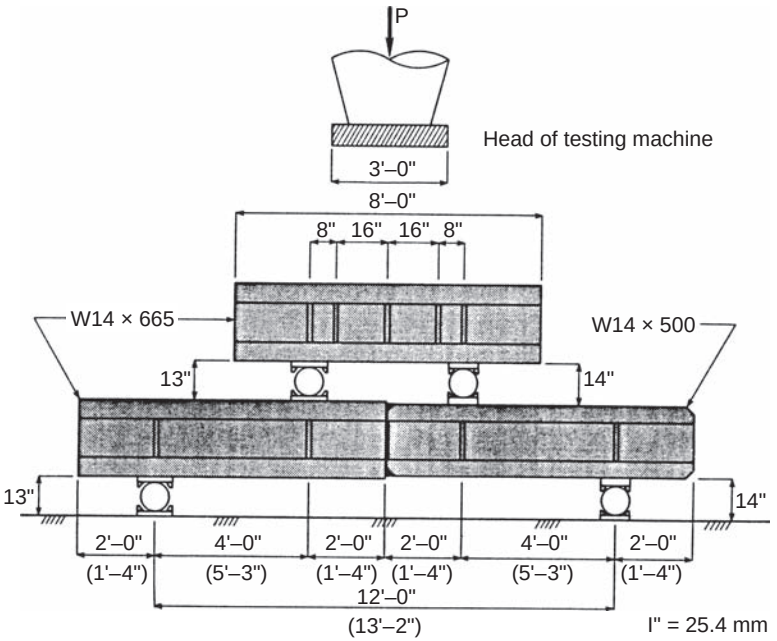

(b)

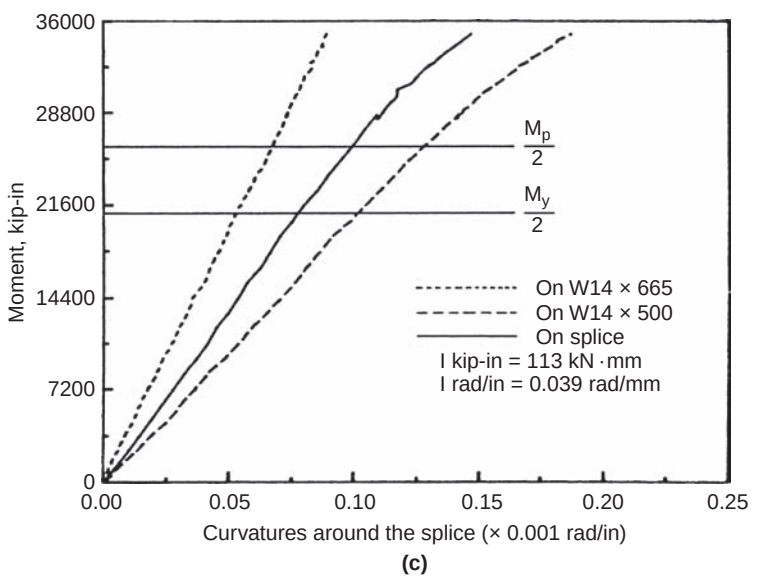

(c)

Figure 8.2 (*Continued*)

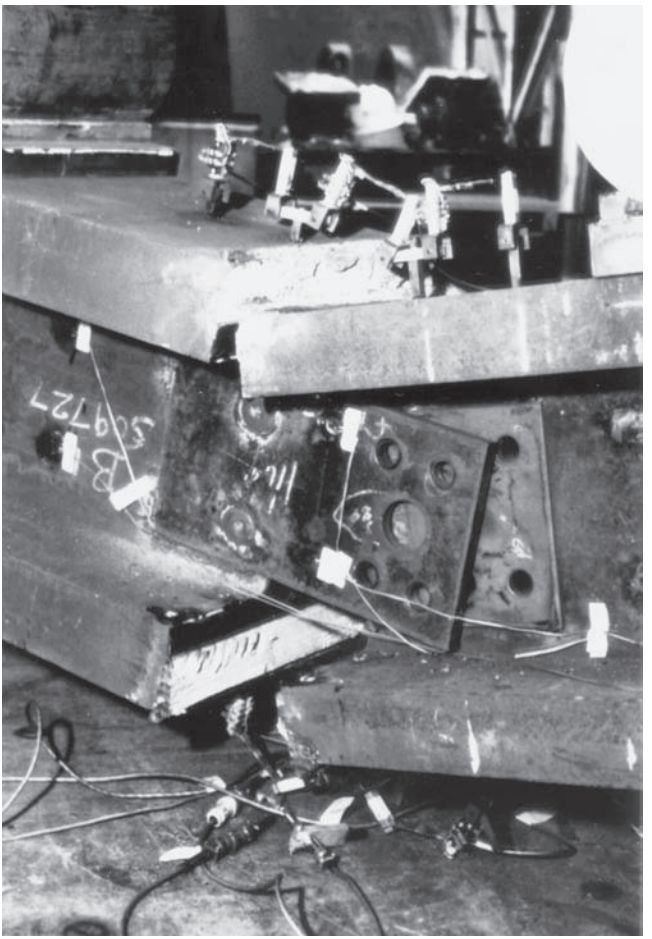

(d)

Figure 8.2 (*Continued*)

where ΣM_{pc} is the sum of the projections to the beam centerline of the *nominal* flexural strengths of the columns above and below the joint, A_g is the gross area of the column, F_{yc} is the column nominal yield strength, P_{uc} is the required axial strength in the column from the load-combination considered, Z_c is the column plastic section modulus, and Z_{cr} is the plastic modulus reduced to account to the presence of axial force (see Chapter 3), and ΣM_{pb} is the sum of the *expected* (i.e., *probable*) flexural strengths of the plastic hinges in the beams, projected from the hinge location to the column centerline. Here, *probable* capacities (as opposed to *nominal* capacities) are obtained by taking into account the impact of strain-hardening, larger-than-specified

beam yield strength, and other factors contributing to reserve strength (many of these concepts will become clear after a reading of the material presented in Section 8.6).

Conceptually, however, the above requirements cannot fully prevent column plastic hinging at beam-to-column joints because the ratio of the column moments acting at the top and bottom faces of a joint varies greatly during an earthquake because of the movement of each column's inflection point. The column demands also increase significantly as a function of ground motion severity (FEMA 2000e, Nakashima and Sawaizumi 2000). It is believed that satisfying the above equation will limit column yielding to a level that is not detrimental, and, most importantly, result in columns strong enough to spread beam plastic hinging over multiple frame levels.

8.3.4 Effect of Axial Forces on Column Ductility

Exceptions to the SCWB philosophy are sometimes permitted in single-story buildings or at the top story of a multistory building, when the risk of soft-story plastic mechanisms is not significant. For example, according to AISC 341, the SCWB requirement can be waived for such columns provided that the maximum axial load acting on them is less than $0.30P_y$, where P_y equals $F_{yc}A_g$, F_{yc} is the column nominal yield strength, and A_g is the gross area of the column. Engineers taking that route must recognize that plastic hinges may form in columns of WCSB frames and recognize the possible deleterious impact of axial forces on the rotation capacity of columns. Other exemptions exist when the capacity design approach is difficult to implement and other precautions can be taken to prevent soft-story mechanisms.

There is a paucity of research results on the effect of axial loads on the ductility of steel columns. Adherence to the above strong-column/weak-beam philosophy may partially explain this situation. Popov et al. (1975) showed that the cyclic behavior of W-shaped columns is a function of the applied load to yield load ratio, P/P_y, and the magnitude of interstory drifts. In those tests, for specimens braced to prevent lateral buckling about their weak axis, sudden failure due to excessive local bucking and strength degradation were observed when P/P_y exceeded 0.5. The aforementioned limit of $0.30P_y$ ($0.40P_y$ in some other codes) is historically tied to this series of tests.

The adequacy of the existing code limits has been challenged by Schneider et al. (1992); test results showed that moment-resisting steel building frames designed according to the WCSB philosophy suffered rapid strength and stiffness deterioration when the columns were subjected to axial loads equal to approximately $0.25\ P/P_y$.

Beyond the above concerns, large axial loads on a ductile column can also lead to column shortening during plastic hinging, which can be problematic in many ways, particularly if developing unevenly in various columns. MacRae et al. (1990) tested columns subjected to

constant axial compression, P, and reverse cyclic horizontal displacements, for P/P_y values of 0.0, 0.3, 0.4, 0.5, 0.6, 0.7, and 0.8. Although column shortening of more than 7% of their length was obtained for the larger ratios, this is a function of cumulative plastic rotations, and shortening due to actual earthquake excitations were less than 1% of column length (MacRae et al. 2009).

Columns subject to plastic deformations should be compact sections and be laterally braced in accordance with the requirements for plastic design. This requires lateral bracing at each plastic hinge location and a maximum brace spacing of $0.086 r_y E/\sqrt{F_y}$ as discussed earlier for beams.

8.4 Panel Zone

The satisfactory seismic response of a ductile moment-resisting frame depends on the adequate performance of its beam-column joints. For multistory building frames, in which beams connected to columns are expected to develop their plastic moment, the designer must prevent undesirable beam-column joint failures. In steel structures, doing so requires measures to avoid column flange distortion, column web yielding and crippling, and panel zone failure. This section mostly focuses on the behavior and design of ductile panel zones, but matters relevant to the first and second failure modes are first addressed.

8.4.1 Flange Distortion and Column Web Yielding/Crippling Prevention

The addition of continuity plates (i.e., stiffeners joining the beam flanges across the column web) can effectively prevent flange distortion and column web yielding/crippling. Examples of continuity plates are shown in Figure 8.3. When beams reach their plastic moment at the column face (Figure 8.4a), the beam flanges apply large localized forces to the columns (Figure 8.4b). The beam flange in tension pulls on the column flange. In the absence of continuity plates, and if otherwise unrestrained, the column flange would bend under that pulling action, with greater deflections in column flanges of low stiffness and small thickness (Figure 8.4c). However, the column flange is not free to deflect because the beam flange framing into it is rigid in its plane (Figure 8.4d). Because deformations of the connected elements must be compatible, stresses concentrate in the beam flange where column flange is stiffest, that is, near the column web (Figures 8.4e and f).

In some tests of connections without continuity plates, localized cracking originated in the beam flange weld at the column centerline and rapidly propagated across the entire flange width and thickness. To prevent this type of failure, most seismic codes require the addition

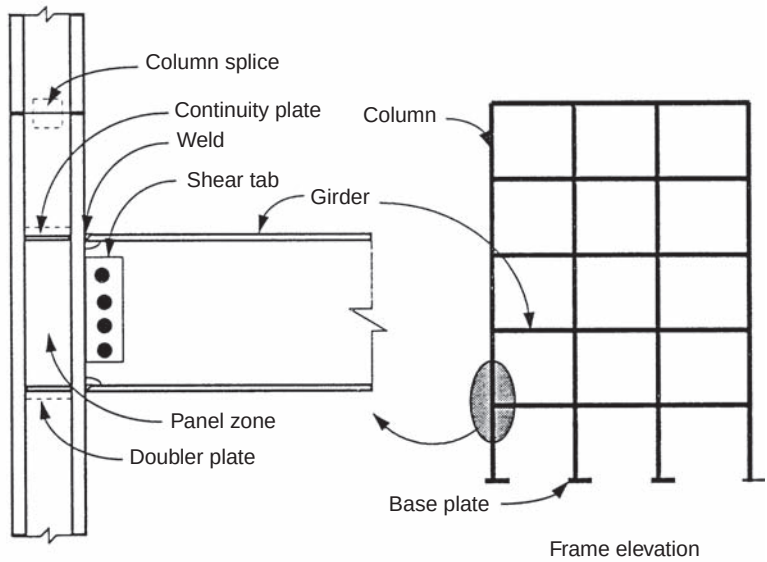

Figure 8.3 Fundamental elements of a ductile moment-resisting frame. (*From* Interim Guidelines: Evaluation, Repair, Modifications, and Design of Steel Moment Frame Structures, *SAC Joint Venture, 1995b, with permission.*)

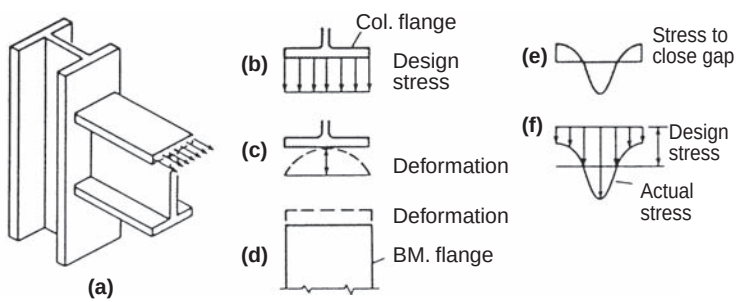

Figure 8.4 Stress distribution in welded beam flange at column face in absence of column continuity plates (stiffeners). (*From* Journal of Constructional Steel Research, *vol. 8, E.G. Popov*, Panel Zone Flexibility in Seismic Moment Joints, 1987, *with permission from Elsevier Science Ltd., Kidlington, U.K.*)

of continuity plates if the maximum expected beam flange force exceeds the factored flange strength of ϕR_n where:

$$R_n = 6.25 t_{cf}^2 F_{yf} \tag{8.3}$$

where t_{cf} is the column flange thickness, F_{yf} is the column flange nominal yield strength, and ϕ is equal to 0.9. This equation is based

on yield line analyses by Graham et al. (1959). Note that AISC (1992) specified that maximum expected beam flange force to be taken as 1.8 $A_f F_y$, where A_f is the flange area of the connected beam and F_y is the nominal strength of the beam. This value assumes a strain-hardened beam moment 30% greater than the nominal plastic moment, and it assumes that the bolted beam web is ineffective in transferring moment. Thus, if only the beam flanges can effectively transfer the maximum beam moment at the connection, and assuming that the flanges-only plastic modulus, $Z_f (\approx A_f d$, where d is the beam depth), is approximately 70% of a beam's plastic modulus, Z, the maximum expected beam flange force becomes:

$$T_{max} = \frac{M_{max}}{d} = \frac{1.3M_p}{d} = \frac{1.3(ZF_y)}{d} = \frac{1.3\left(\frac{Zf}{0.7}\right)F_y}{d} \approx \frac{1.8A_f dF_y}{d} = 1.8A_f F_y \tag{8.4}$$

Other codes (e.g., CSA 2009) arrive at a similar result by specifying a reduced column flange resistance for seismic applications [e.g., 0.6 of (Eq. 8.3)], instead of using the 1.8 magnification factor for the beam flange forces in Eq. (8.4).

Opinions varied substantially over time on the effectiveness of the above equations. Prior to the Northridge earthquake, AISC (1992) suggested that designers use continuity plates even when the above requirement was satisfied because continuity plates had been used in nearly all cyclic tests (prior to 1994) that exhibited satisfactory ductile behavior. Interim design guidelines released following the Northridge earthquake (SAC 1995b) also recommended the use of continuity plates in all ductile moment frame connections, to avoid the stress concentration depicted in Figure 8.4 in the highly stressed welded region. Subsequent review of past test data (FEMA 2000f) showed that good seismic performance was still possible in the absence of continuity plates when the above equations were satisfied, even recognizing that those equations were at best approximations given the complex behaviors at play. Limited experiments by Ricles et al. (2000) led to similar conclusions, demonstrating that although connections having continuity plates exhibited better inelastic seismic performance, comparable ones without such plates still developed appropriate plastic rotations provided that the heavy column flanges met the above requirement, and provided that $t_{cf} \geq b_{cf}/6$, where b_{cf} is the column flange width. Hajjar et al. 2003 summarizes this evolution in thinking and the supporting research evidence.

Accordingly, AISC 341 specifies that continuity plates of thickness at least equal to the thicker of the two beam flanges connecting to a column in two-sided connections (or equal to half of the beam

flange thickness in a one-sided connection) be provided, except when:

$$t_{cf} \geq 0.4\sqrt{1.8 b_{bf} t_{bf} \frac{F_{yb} R_{yb}}{F_{yc} R_{yc}}} \tag{8.5}$$

$$t_{cf} \geq \frac{b_{bf}}{6} \tag{8.6}$$

where R_{yb} and R_{yc} are respectively the ratios of the expected yield stress to the specified minimum yield stress of the beam and column framing at the joint under consideration, or except when superseded by results from qualification testing or alternate requirements for connections prequalifed by the AISC 358 specification (2010a) discussed in later sections. Note that Eq. (8.5) is obtained by equating and rearranging Eqs. (8.3) and (8.4) and substituting expected yield strengths instead of minimum specified strengths.

When the beam flange applies compression to the column flange, column web yielding must be prevented, as would normally be done in nonseismic applications, using the traditional equations for bearing resistance:

$$B_r = (5k + N)\ t_{cw} F_{yw} = (5k + t_{bf})\ t_{cw} F_{yw} \tag{8.7}$$

where k is the distance from the outer face of the column to the web toe of the fillet, N is the bearing length of the applied force, F_{yw} is the yield strength of the column web, and t_{bf} and t_{cw} are the beam flange and column web thicknesses, respectively. Resistance to web crippling must also be checked, using:

$$B_r = 0.8 t_w^2 \left[1 + 3\left(\frac{N}{d}\right)\left(\frac{t_w}{t_f}\right)^{1.5}\right]\sqrt{\frac{E F_{yw} t_f}{t_w}} \tag{8.8}$$

where B_r is the bearing resistance. Again, variations of these equations and additional requirements are prescribed for specific AISC 358 prequalified connections.

Note that seismic design codes generally do not require consideration of strain-hardening in the beam flange in compression because web-crippling is not a brittle failure mode. Also note that doubler plates are frequently used instead of continuity plates when increases in web crippling or web yielding resistance are necessary.

8.4.2 Forces on Panel Zones

The panel zone of a beam-column joint is the rectangular segment of the column web surrounded by the column flanges (left and right vertical boundaries) and the continuity plates (top and bottom horizontal boundaries). Typically, the panel zone is simultaneously subjected to axial forces, shears, and moments from the columns and beams, as shown in Figure 8.5.

Resolving equilibrium on the free-body diagram of Figure 8.5 and taking the forces shown acting on the face of the panel as positive, the horizontal shear acting in the panel zone can be calculated as:

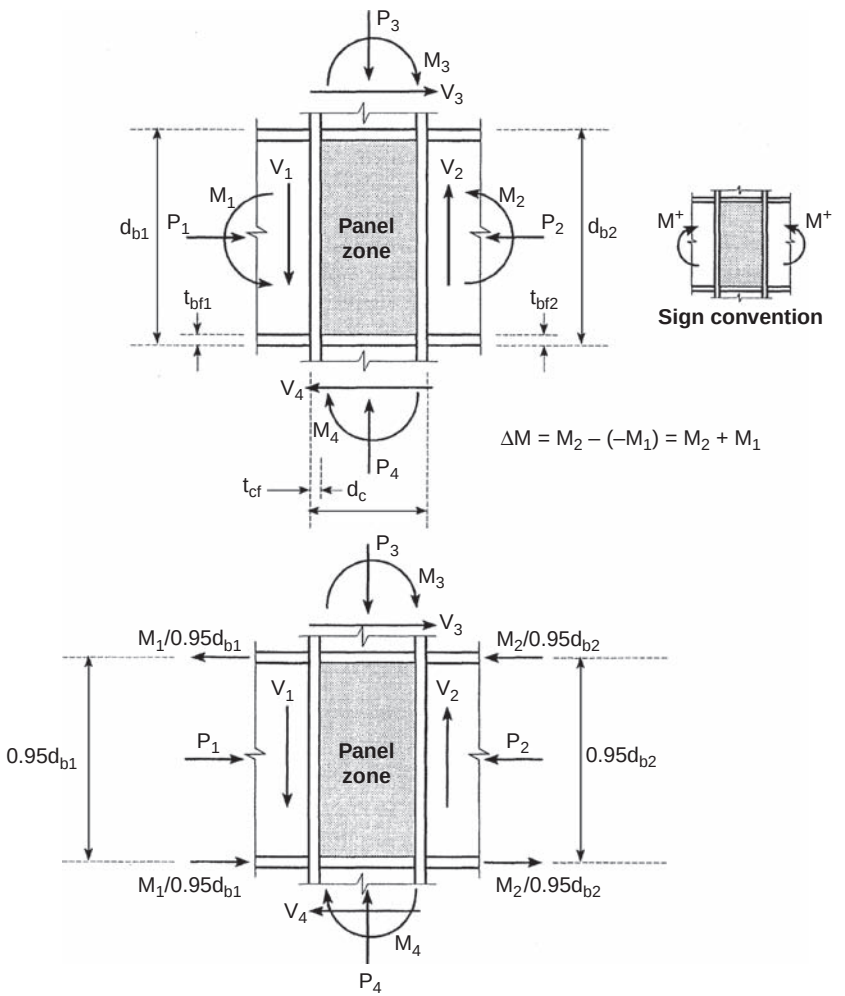

Figure 8.5 Moments, shear forces, and axial forces acting on the panel zone of a ductile moment-resisting frame subjected to lateral loading.

$$V_w = \frac{M_1}{0.95d_{b1}} + \frac{M_2}{0.95d_{b2}} - V_c \tag{8.9}$$

where d_{b1} and d_{b2} are the depths of beams 1 and 2, respectively, and 0.95 d_{b1} and 0.95 d_{b2} are approximations for the lever arm of the beam flange forces resulting from the applied moments, as shown in Figure 8.5. V_c is the subassembly equilibrating shear given by:

$$V_c = \frac{M_1\left(\frac{L_1}{L_{b1}}\right) + M_2\left(\frac{L_2}{L_{b2}}\right)}{h} \tag{8.10}$$

where h is the average of story heights above and below the joint, L_i is the total span length of beam i measured center-to-center of the columns to which it connects, and L_{bi} is the clear span length of beam i equal to the distance from face-to-face of the columns (i.e., deducting half of the column width at each end of the beam) as shown in Figure 8.1. When member forces are available from computer analysis, one can obtain an estimate of V_c by averaging the column shears at the edges of the panel zone:

$$V_c = \frac{V_3 + V_4}{2} \tag{8.11}$$

This approximation is usually conservative because it gives smaller values of V_c and thus higher values of V_w.

The above equations show that the critical loading condition for the panel zone occurs when it is subjected to large unbalanced moments from the beams framing into the columns. Large shear forces will develop in the panel zones of interior columns participating in a sway frame collapse mechanism (of the type shown in Figure 6.10a) when the beams on all sides of such a panel zone reach their plastic moment. In fact, the panel zone shear in that case is substantially greater than the shear in the adjacent columns and beams, and the possibility of panel zone yielding must be considered.

If Eq. (8.8) is substituted into Eq. (8.7), the panel zone shear, V_w, can be shown to depend only on beam moments M_1 and M_2. In other words, the magnitude of the unbalanced moment, $\Delta M = M_1 + M_2$, controls the force demand on the panel zone. Different philosophies regarding the magnitude of ΔM to be considered for design had been developed prior to the Northridge earthquake. Tsai and Popov (1990b) reported three such philosophies: strong panel zones, intermediate-strength panel zones, and minimum-strength panel zones. For strong panel zone design, $\Delta M = M_{p1} + M_{p2} = \Sigma M_p$, following capacity design principles (SEAOC 1980). For intermediate strength panel zone design, $\Delta M = \Sigma M_p - 2M_g$, where M_g is the moment due to gravity loads. Assuming

this moment to be 20% of M_p, the design requirement becomes $\Delta M = \Sigma 0.8M_p$ (Popov 1987, Popov et al. 1989). For minimum-strength panel zone design, in an allowable stress design perspective, $\Delta M = \Sigma(M_g + 1.85M_e) < \Sigma 0.8M_p$, where M_e is the beam moment obtained when the specified earthquake loads are acting alone, and 1.85 is a factor chosen to further reduce the design force on the panel zone and promote a greater energy dissipation by panel zone yielding. Prior to the Northridge earthquake, only a few studies had investigated the consequences of these various design approaches in terms of the relative levels of plastic deformation in beam and panel zones (Popov et al. 1989, Tsai and Popov 1990b, Tsai et al. 1995). These indicated larger panel zone inelastic demands and interstory drifts in frames designed per the minimum-strength panel zone approach. However, arbitrarily reducing the demands to create weaker panel zones is an approach that lacks transparency by confounding actual demands and capacities.

The strong panel zone philosophy was used prior to 1988 in the United States, together with a panel zone shear strength of $0.55F_yA_w$, where A_w is the column web area (SEAOC 1980). The intermediate strength and minimum strength approaches are indirect means to obtain weaker panel zones that will yield sooner and respectively dissipate a greater percentage of the total hysteretic energy. Despite the lack of a sound theoretical basis, the latter two approaches were adopted by many codes and guidelines in the United States (e.g., SEAOC 1988, AISC 1992) after 1988 to be used in conjunction with the panel zone shear strength equation described in Section 8.4.5 below. However, in the post-Northridge context, further to multiple successive changes in code requirements (summarized in Lee et al. 2005b), AISC 341 and 358 requires that the shear in the panel zone be determined from the moments acting at the column face, determined by projection of the expected plastic moment developing in the beam, considering strain-hardening of the plastic hinge and consistently with the free-body diagrams presented in Section 8.6. In that instance, strength of panel zones is independently assessed as a function of intended ultimate behavior.

8.4.3 Behavior of Panel Zones

Studies of panel zone inelastic behavior started in the 1970s and included the work of Krawinkler et al. (1971, 1975, 1978), Fielding and Huang (1971), Fielding and Chen (1973), and Becker (1975). Tests of large-scale specimens clearly revealed the dominance of shear distortions on panel zone behavior. Krawinkler et al. (1971) visually captured this phenomenon using photogrammetric techniques, as shown in Figures 8.6c and d, at large shear strains for the specimens shown in Figures 8.6a and b. These tests also demonstrated that panel zones, when carefully detailed to avoid column web yielding and crippling, as well as column flange distortion, can exhibit

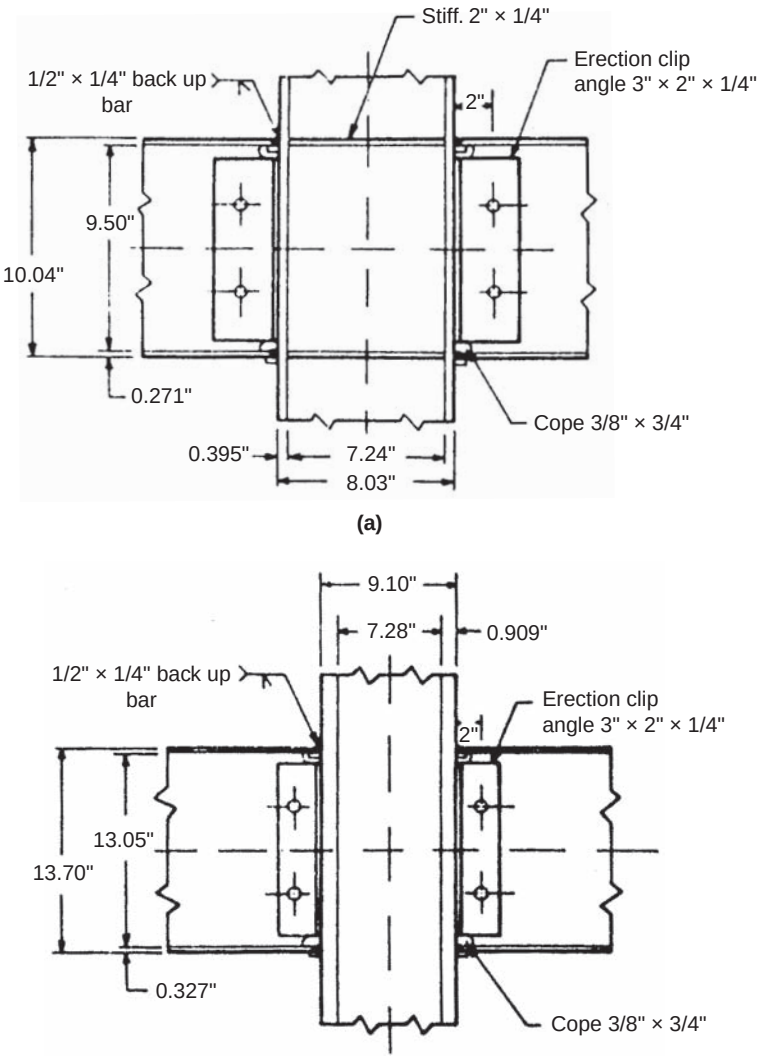

Figure 8.6 Panel zone deformation experimental results: (a) Connection details of specimen A; (b) specimen B. Column in specimen A is W200 × 36 section (W8 × 24 in U.S. units) with flanges milled to simulate W360 × 101 (W14 × 68 in U.S. units), and column in specimen B is W200 × 100 (W8 × 67 U.S. units) to simulate W360 × 339 (W14 × 228 U.S. units); (c) deformation pattern in panel zone of specimen A; (d) deformation pattern in panel zone of specimen B; (e) ΔM versus γ_p diagram for specimen A; (f) ΔM versus γ_p diagram for specimen B; (g) effects of excessive panel zone distortions. (*Parts a to g from* Earthquake Engineering Research Center Report UCB/EERC 71-7, *"Inelastic Behavior of Steel Beam-to-Column Subassemblages" by H. Krawinkler et al., 1971, with permission from the author.*)

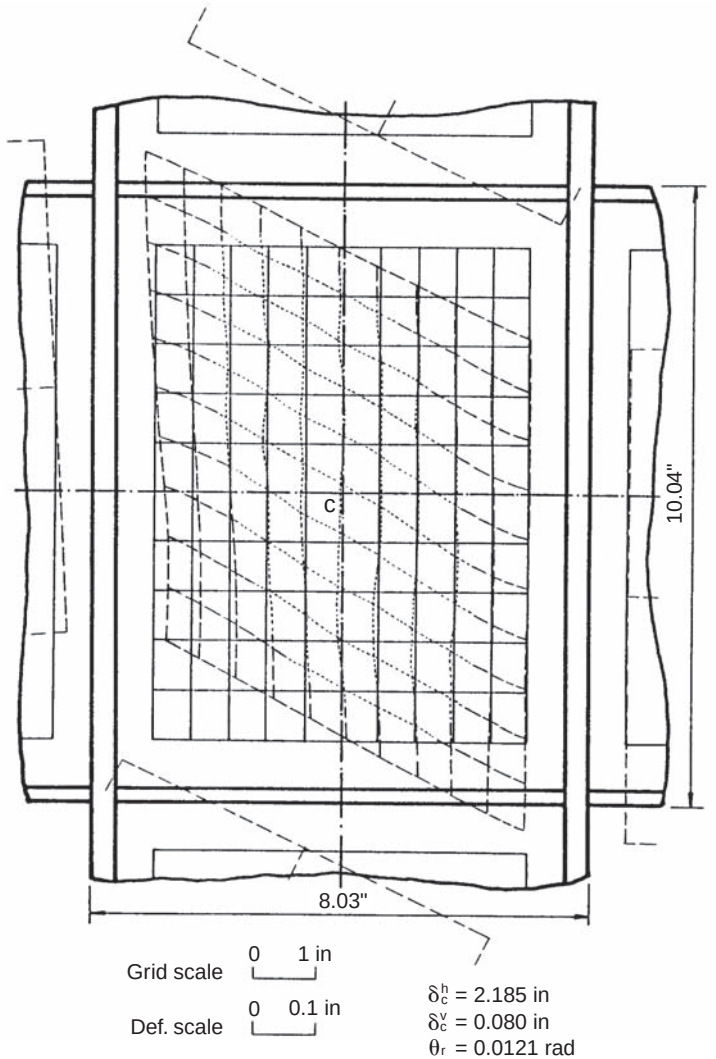

Figure 8.6 (*Continued*)

excellent hysteretic energy dissipation characteristics in shear, up to large inelastic deformations. Typical results from cyclic inelastic testing are presented in Figures 8.6e and f, expressed in terms of the unbalanced beam moment ($\Delta M = M_1 + M_2$) versus average panel zone shear distortions (γ_p, also called shear strains or shear deformations in the literature).

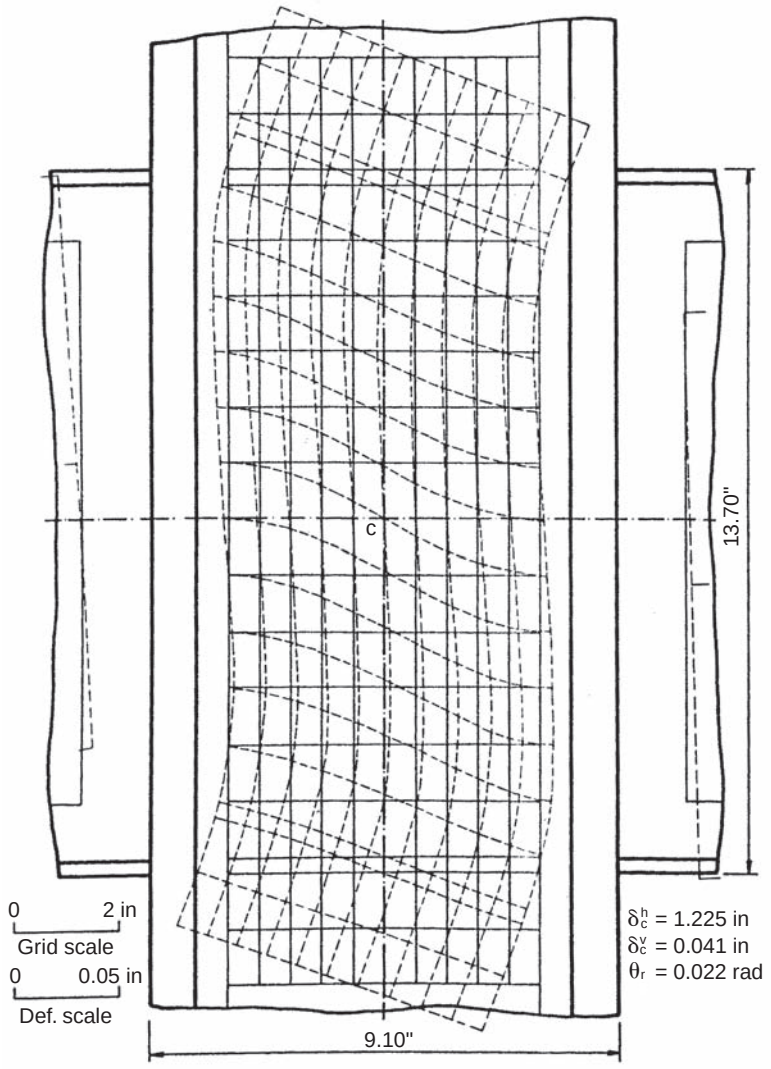

FIGURE 8.6 (*Continued*)

Examination of these hysteretic loops shows that panel zones exhibit considerable reserve strength beyond first yield, with a steep strain-hardening slope. This results from the complex state of stress that develops inside the panel zone as shear stresses are progressively increased. Typically, yielding starts in the middle of the panel, consistently with elastic theory, and progresses approximately in a radial

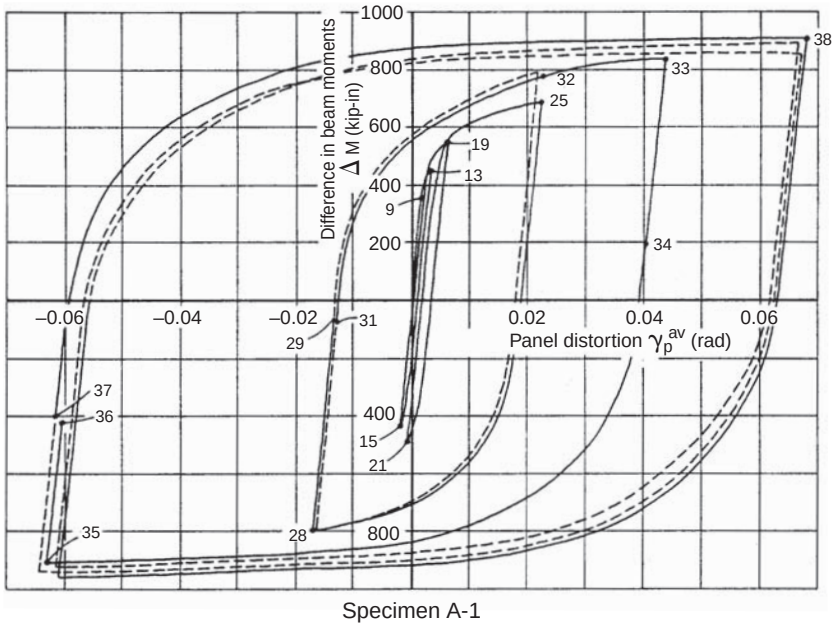

Figure 8.6 (*Continued*)

manner over the entire panel zone as the unbalanced moment further increases. As a result, shear distortion is largest at the center of the panel and smallest at the corners. Once the web is fully yielded, the panel zone stiffness depends in a complex manner on the panel aspect ratio, d_c/d_b per Figure 8.5, and the stiffness of its surrounding elements, such as the column flanges and the webs of the connecting beams. These factors, together with strain-hardening of the web in shear, produce the considerable post-yield stiffness observed during tests (see Figures 8.6e and f).

The column axial load also has an impact on the behavior of the panel zone. In the presence of axial stress, the onset of shear yielding in the panel zone is hastened, in accordance with the Von Mises yield criterion. Nonetheless, experiments have shown that the ultimate shear strength of the panel is not substantially affected by column axial loads; column flanges were observed to provide axial load resistance when the panel yielded in shear. This redistribution is possible when the column flanges remain elastic during panel zone yielding. Ultimately, at large shear strains, the column flanges will in turn develop their full plastic flexural capacity, in a state of combined flexure and axial force. When that occurs, large kinks in column

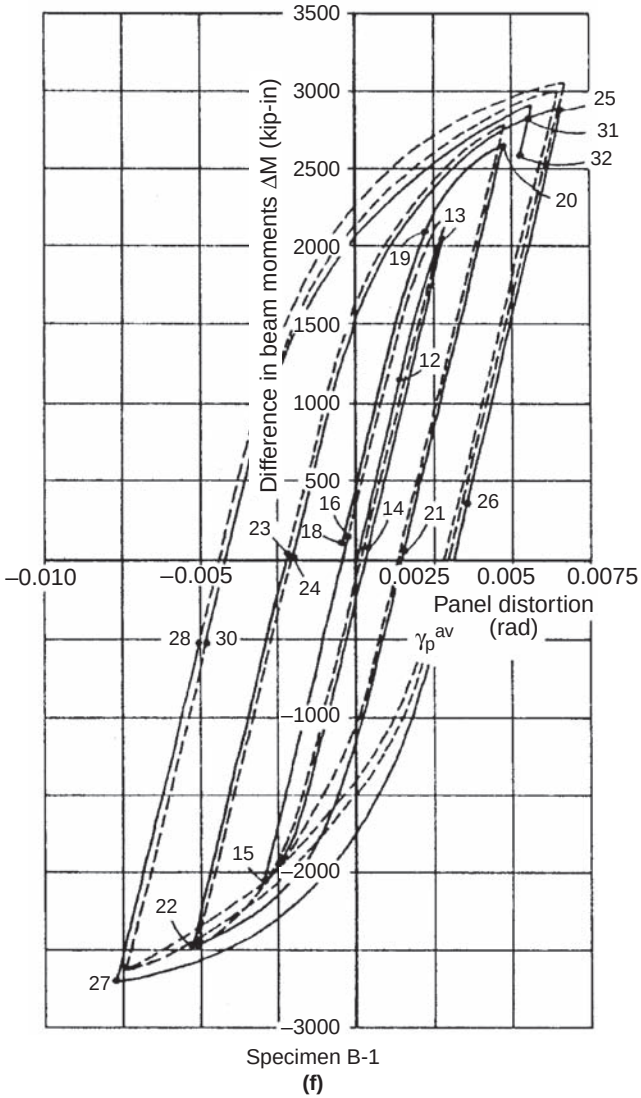

FIGURE 8.6 (*Continued*)

flanges may develop, producing large strains in or near the welds connecting the beam flanges to the column, and possibly joint fracture. For this reason, researchers have recommended that the maximum shear distortion in a panel zone, γ_{max}, be limited to four times the shear yield distortion, γ_y (Krawinkler et al. 1971).

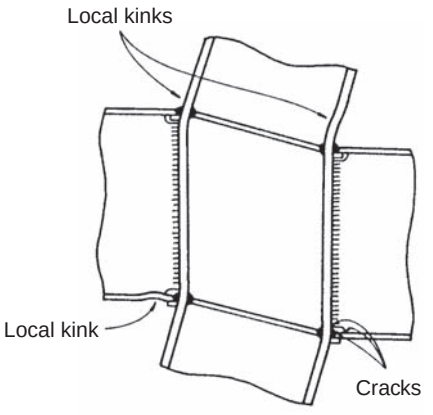

Figure 8.6 (*Continued*)

8.4.4 Modeling of Panel Zone Behavior

Formulation of a simple model that captures the complex behaviors described above remains elusive. Elastic stiffness and yield threshold are relatively simple matters, but modeling postyield stiffness, which was observed to vary considerably from specimen to specimen, is particularly difficult. Krawinkler et al. (1971) proposed a model "… simple enough to permit its inclusion into practical computer programs…" at the "…sacrifice [of] accuracy in modeling actual boundary conditions." The model proposed, presented in Figure 8.7a, consists of an elastic-perfectly plastic column web surrounded by four rigid sides connected by springs at the corners.

These springs mostly capture the effect of the column flanges on panel zone behavior and neglect other behaviors. In the elastic range, the stiffness of the panel zone is approximately:

$$K_e = \frac{V}{\gamma} = \frac{1}{\dfrac{1}{0.95 d_c t_{cw} G} + \dfrac{d_b^2}{24 E I_{cf}}} \tag{8.12}$$

where G is the shear modulus, E is the modulus of elasticity, I_{cf} is the moment of inertia of a single column flange, t_{cw} is the column web thickness, and all other terms have been defined previously. Recognizing that the flange typically contributes approximately only 10% of the total elastic stiffness, one can ignore the second term in the

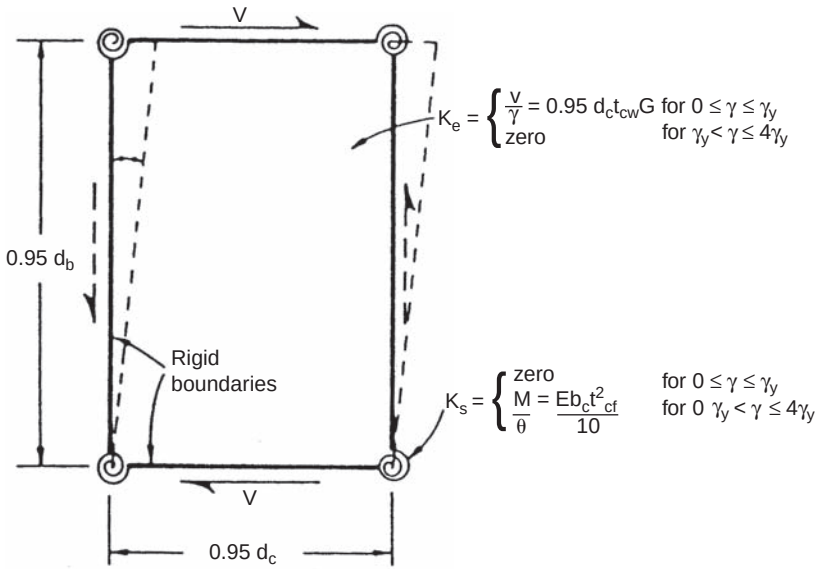

(a)

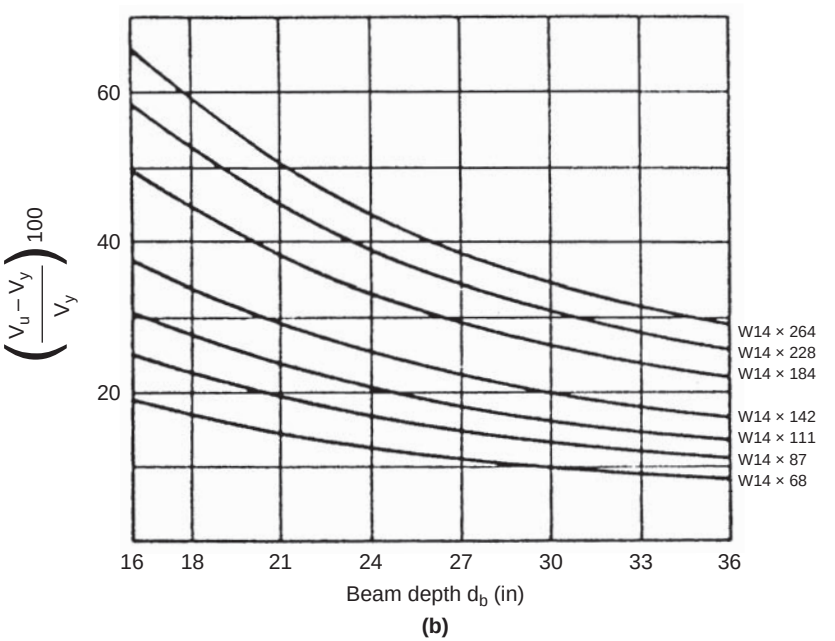

(b)

FIGURE 8.7 Panel zone behavior: (a) mathematical model; (b) Example of ultimate strength per Krawinkler model, V_u, compared with Von Mises yield strength, V_y; (c) experimental versus theoretical panel zone shear (expressed in terms of ΔM) for specimen A; (d) experimental versus theoretical panel zone shear (expressed in terms of ΔM). Specimen B (Krawinkler model is identified as Model 3 on that figure). (*Parts a to d from* Engineering Journal, *3rd Quarter 1978*, *"Shear in Beam-Column Joints in Seismic Design of Steel Frames" by H. Krawinkler, with permission from the American Institute of Steel Construction.*)

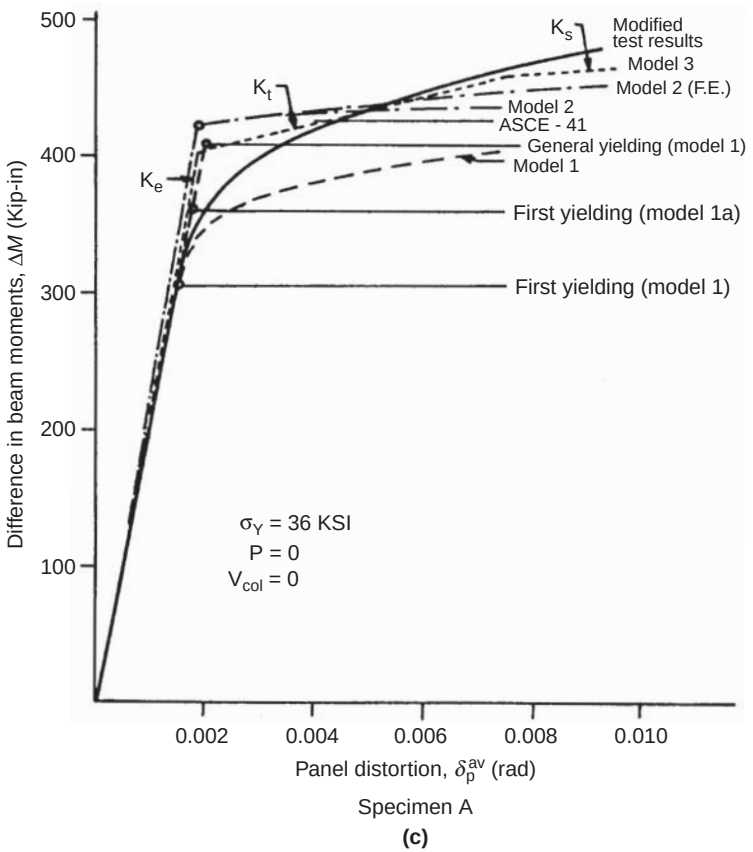

Figure 8.7 (*Continued*)

denominator, which results in the following simpler expression for the elastic stiffness:

$$K_e = \frac{V}{\gamma} = 0.95\, d_c t_{cw} G \tag{8.13}$$

In the postyield range, the panel zone shear stiffness is taken as zero, whereas the spring stiffness is taken as:

$$K_s = \frac{M}{\theta} = \frac{E b_c t_{cf}^2}{10} \tag{8.14}$$

where θ is the concentrated spring rotation, and b_c and t_{cf} are the width and thickness of the column flange, respectively. This definition of K_s cannot be proven through the use of simple models. Krawinkler et al. (1971) report that finite element analyses have been used to

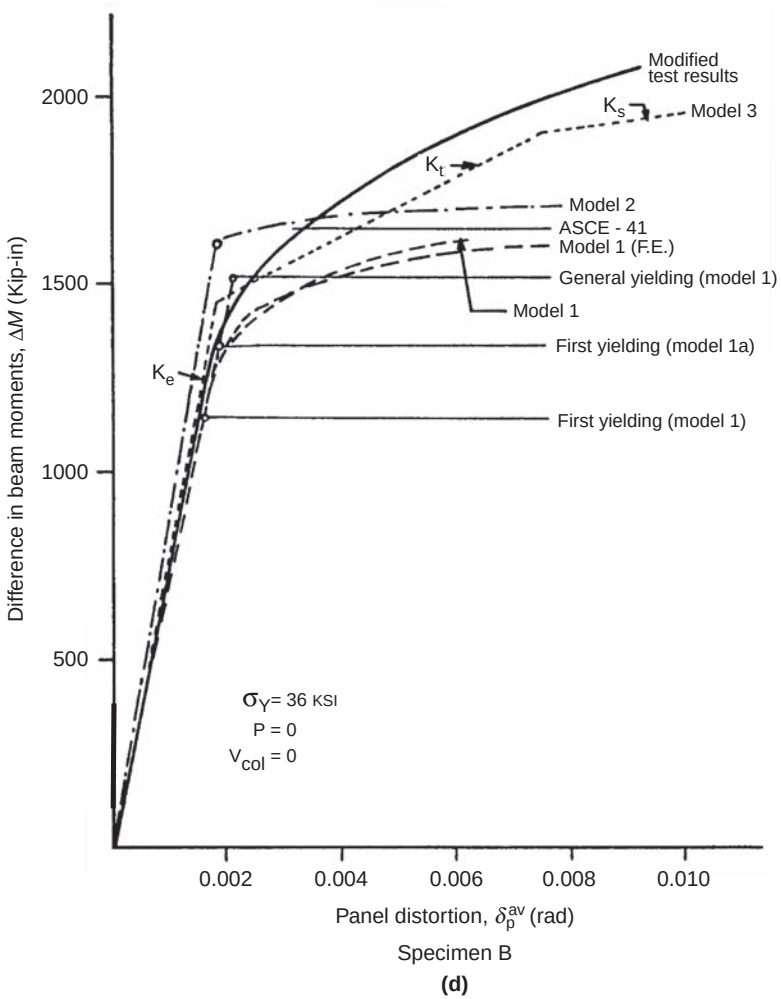

Figure 8.7 (*Continued*)

determine the concentrated column flange rotation at each corner corresponding to this model. The post yielding stiffness of the panel is thus given by:

$$K_t = \frac{V}{\gamma}\left[\frac{4M}{0.95d_b}\right]\frac{1}{\gamma} = \left[\frac{4}{0.95d_b}\right]\frac{M}{\theta} = \frac{1.095b_c t_{cf}^2 G}{d_b} \tag{8.15}$$

using static equilibrium on the panel and knowledge that γ is equal to θ for this model. This equation is reasonable over the range $\gamma_y < \gamma < 4\gamma_y$,

where γ_y is the shear yield distortion. Hence, the panel zone shear strength, reached at an angle of distortion of $4\gamma_y$, is:

$$V_u = K_e\gamma_y + 3K_t\gamma_y = V_y\left(1+3\frac{K_t}{K_e}\right) = 0.55F_y d_c t_{cw}\left(1+\frac{3.45b_c t_{cf}^2}{d_b d_c t_{cw}}\right) \quad (8.16)$$

The ratio of the second term over the first term inside the parenthesis represents the increase in panel zone shear resistance beyond that predicted by the Von Mises criterion. Heavy columns with large flanges will benefit more from the higher resistance provided by this second term, as illustrated in Figure 8.7b. However, tests to date have been conducted on specimens scaled to represent moderate size columns, such as those indicated in Figure 8.6.

Note that the above model fails to check whether the flange flexural plastic capacity is reached before the shear deformation reaches $4\gamma_y$. It also does not consider many other effects that influence panel zone inelastic behavior, such as shear strain-hardening and true boundary conditions (in particular, plastic hinges in column flanges can be closer than $0.95d_b$ for different boundary conditions). However, given that this model was found to capture the few available experimental results reasonably well (as shown in Figures 8.7c and d where this model is called Model 3), it has been adopted in many seismic codes.

8.4.5 Design of Panel Zone

Until the Northridge earthquake, inelastic panel zone action was generally considered to be desirable for energy dissipation. By comparing the behavior of frame subassemblies tested to identical interstory drift levels, Krawinkler et al. (1971) observed that specimens exhibited greater energy dissipation when panel zone shear yielding occurred in combination with beam flexural yielding. When the panel zones tested by Krawinkler did not yield, greater beam flexural plastic rotations were necessary to reach the same interstory drifts, and the beams suffered more of the inelastic local buckling and lateral-torsional buckling that typically develop at large hysteretic flexural deformations, and thus exhibited more strength degradation (a logical consequence consistently observed in other tests, such as by Lee et al. 2005a for example). It was therefore suggested that "controlled" inelastic panel zone deformations would improve the overall seismic behavior of steel frames, particularly because the cyclic shear hysteretic behavior of well-designed panel zones does not exhibit strength degradation. Designers were also advised to consider panel shear deformations when calculating drifts.

Post-Northridge, the prevailing view is that, even though past studies have shown properly proportioned panel zones to be ductile, large panel zone distortions are not desirable because they can have a

detrimental impact on behavior of beam-to-column connections (El-Tawil et al. 1999, El-Tawil 2000, Englekirk, 1999). Statistical variations in beam and column yield strengths also make it difficult to achieve in practice an ideal target "balance" of shared panel zone and beams yielding. For those reasons, the panel zone strength per the above equation can only be used to resist the panel shear demands corresponding to the beam plastic hinges having developed their expected strain-hardened strengths (AISC 341 and 358), when panel zone flexibility is considered in analysis (AISC 360). However, sharing of inelastic deformations between the panel zones and beams is not encouraged when beam flanges are directly welded to column flanges, because of the risk of crack initiation and propagation at that location under large panel shear distortions (Hamburger et al. 2009).

Unless superseded by requirements for specific prequalified connections, the panel zone design equation typically implemented in AISC 360 and CSA S16 respectively is:

$$V_u = 0.60 F_y d_c t_w \left(1 + \frac{3 b_{cf} t_{cf}^2}{d_b d_c t_w}\right) \tag{8.17}$$

and

$$V_u = 0.55 F_y d_c t_w \left(1 + \frac{3 b_{cf} t_{cf}^2}{d_b d_c t_w}\right) \leq 0.66 F_y d_c t_w \tag{8.18}$$

with ϕ factors of 1.0 and 0.9, respectively for seismic applications, where t_w is the thickness of the panel zone including doubler plates if any, and all other terms have been defined previously (Lee et al. 2005b summarizes the ϕ factors used in various design code editions). The upper bound in CSA S16 is to limit the extent of panel zone deformations. When beams of different sizes frame into the column, it is conservative to use the largest of the beam depths for d_b. In nonseismic applications, the AISC 360 decreases the strength given by Eq. (8.15) to as low as 70% of the calculated value when the axial load exceeds 75% of the column plastic axial strength (i.e., 0.75 P_y); some researchers have argued that further reductions are necessary to properly account for the effect of axial forces (Chen and Liew 1992). However, in seismic applications, such high axial loads are rarely found in the columns of ductile moment frames.

When the panel zone of a column has insufficient strength, doubler plates can be added locally to increase the column web thickness; this has proven to be an economical solution in North America. To be considered effective in seismic applications, doubler plates must be detailed in accordance to AISC 341 requirements. In one such detail, for which doubler plates are placed next to the column web, typically

fillet welded along the plate width and welded to the column flanges to develop the design shear strength of the doubler plate, magnetic particle testing is required to ensure that flaws have not been induced in the k-area region (see Chapter 2). An alternative detail permitted by AISC 341 uses a pair of doubler plates symmetrically located away from the column web, one-third to two-thirds of the distance between the beam flange tip and column centerline (Lee et al. 2005b), but has been reported to be more expensive as thicker plates are required due to stability requirements (Hamburger et al. 2009).

In addition to traditional web slenderness limits, seismic design codes typically require that panel zone thickness be at least:

$$t_z \geq \frac{d_z + w_z}{90} \tag{8.19}$$

to prevent premature local buckling under large cyclic inelastic shear deformations. In this empirical equation, d_z is the panel zone depth between the continuity plates, w_z is the panel zone width between the column flanges, and t_z is the panel zone thickness. If doubler plates are used to increase the thickness of the panel zone, their individual thickness must also satisfy the above equation. Note that t_z can be taken as the sum of the panel zone and doubler plate thicknesses only if the doubler plates are connected to the panel zone with plug welds in a manner to preclude independent buckling of these individual elements. Hamburger et al. (2009) indicated that selecting bigger columns that would not need doubler plates can be more economical that installing doubler plates (for column weight increases of up to 100 lb/ft for standard frame geometries).

Finally, note that one should consider panel zone deformations when calculating frame deformations. However, designers have typically neglected panel zone flexibility when conducting analyses with line representations of frames. In such models, finite joint sizes are ignored, structural members are modeled by line elements at their centers of gravity, and the flexible lengths of beams and columns are taken as the center-to-center distances between their intersection points. In more exact models, finite joint sizes are considered, member flexibility is derived from the free lengths between the faces of columns and beams, and the flexibility of panel zones is included. For the types and geometries of frames typically used in buildings, the error obtained through use of the simpler model has been reported to be negligible, particularly in view of all other uncertainties involved in the process (Englekirk 1994, Wakabayashi 1986), and AISC 341 considers that use of that simpler model meets the AISC 360 requirement to account for the effect of panel zone deformations in the analysis. The engineer should nonetheless beware of instances when design conditions and/or frame geometry would make this error significant.

8.5 Beam-to-Column Connections

The seismic response of a ductile moment frame will be satisfactory only if the connections between the framing members have sufficient strength to permit attainment of the desired plastic collapse mechanism, sufficient stiffness to justify the assumption of fully rigid behavior typically assumed for analysis, and adequate detailing to permit development of the large cyclic inelastic deformations expected during an earthquake without any significant loss of connection strength. Beams, panel zones, and to some extent, columns can dissipate seismic energy through plastic cyclic rotations, but connection failure is not acceptable. From that perspective, bolts and welds are considered to be nonductile elements that must be designed with sufficient strength to resist the maximum forces that can develop in the connected elements. Even though bolts and, to some extent, welds are capable of plastic deformations, their small size and limited ductility generally make those deformations ineffective at the structural level.

Moment frames acquired their excellent reputation as seismic framing systems following the San Francisco 1906 earthquake. However, even though the few midrise steel buildings constructed at that time weathered the earthquake well, one must recognize that the heavily riveted moment connections of that era bear little resemblance to current seismic moment connections. Examples of connections used in the first half of the 1900s are shown in Figure 8.8 for comparison with the standard modern connections illustrated later in this chapter. The oft-stated "excellent performance of steel moment frames in past earthquakes" was biased, to some degree, by the track record of buildings with details that became obsolete in the 1960s when high-strength bolts and welding became the preferred fastening methods in seismic regions. It is the behavior of these modern moment connections that is addressed here.

8.5.1 Knowledge and Practice Prior to the 1994 Northridge Earthquake

The welded moment connection details widely used in many North American seismic regions (notably California) during the 25 years preceding the Northridge earthquake are shown at the top of Figure 8.9. Although the simple plastic theory formulated in the first chapters of this book would suggest that full-penetration groove welds are required in both flanges and the web of a beam to create a connection capable of resisting the beam's plastic moment, by the 1960s the building industry was already frequently using an alternative more economic (easier to construct) connection detail with fully welded flanges and a bolted web connection.

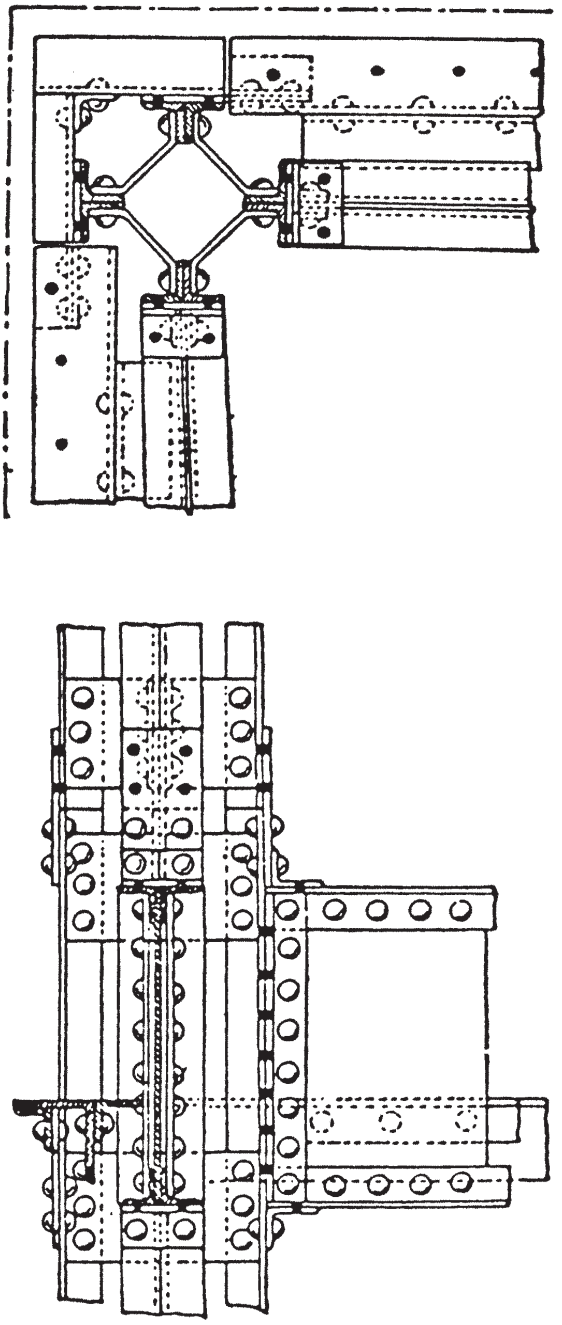

(a)

Figure 8.8 Examples of frame connections: (a) at turn-of-the-century; (b) in the 1930s. (*Part a from* Journal of Constructional Steel Research, *vol. 10, William McGuire, Introduction to Special Issue, 1988, with permission from Elsevier Science Ltd., U.K. Part b from* Steel Tips—Structural Steel Construction in the '90s *by F. R. Preece and A. L. Collin, with permission from the Structural Steel Education Council.*)

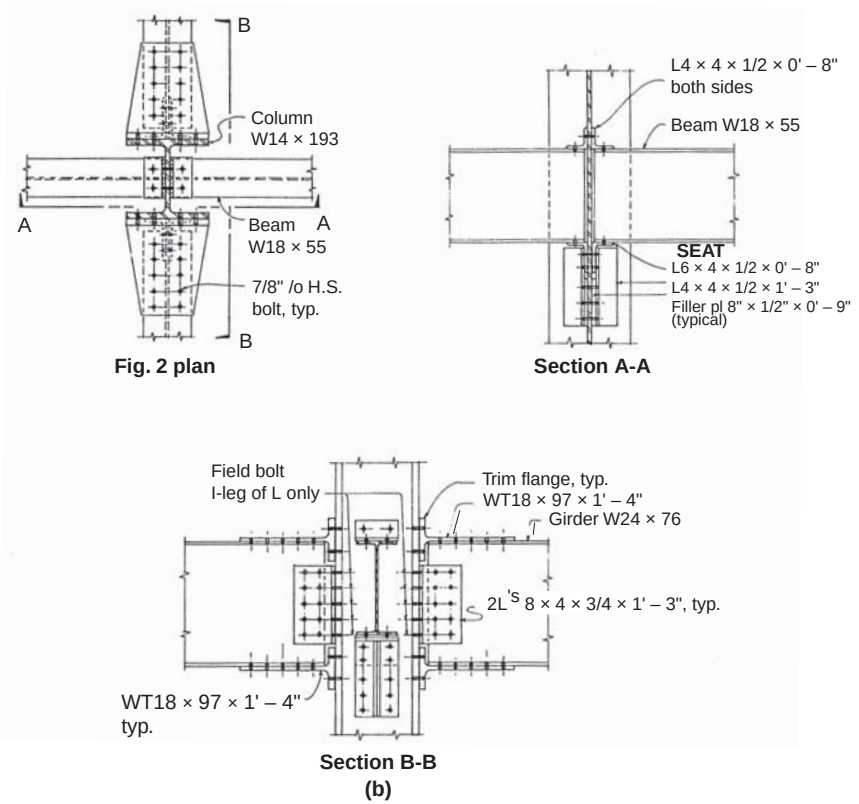

Figure 8.8 (*Continued*)

The first tests to investigate the cyclic plastic behavior of moment connections were conducted in the 1960s (Popov and Pinkney 1969). Various popular details were considered, as shown in Figure 8.9, and specimens with welded flanges and bolted web connections showed superior inelastic behavior compared with the cover-plated moment connection and the fully bolted moment connection alternatives. Typical hysteretic loops are presented in Figure 8.10. The fully bolted detail was considered less desirable because slippage of the bolts during cyclic loading produced a visible pinching of the hysteretic loops and because tensile rupture occurred along a net section between bolt holes.

Further tests in the 1970s (Popov and Stephen 1970) compared the relative performance of the commonly used welded flange-bolted web detail and fully welded connections. Sample results are shown in Figure 8.11. Both details were significantly stronger than predicted by the simple plastic theory (with F_y = 36 ksi), as clearly shown in Figure 8.11, and the fully welded connection exhibited more ductile behavior (Figure 8.11a versus 8.11b). The moment connections with

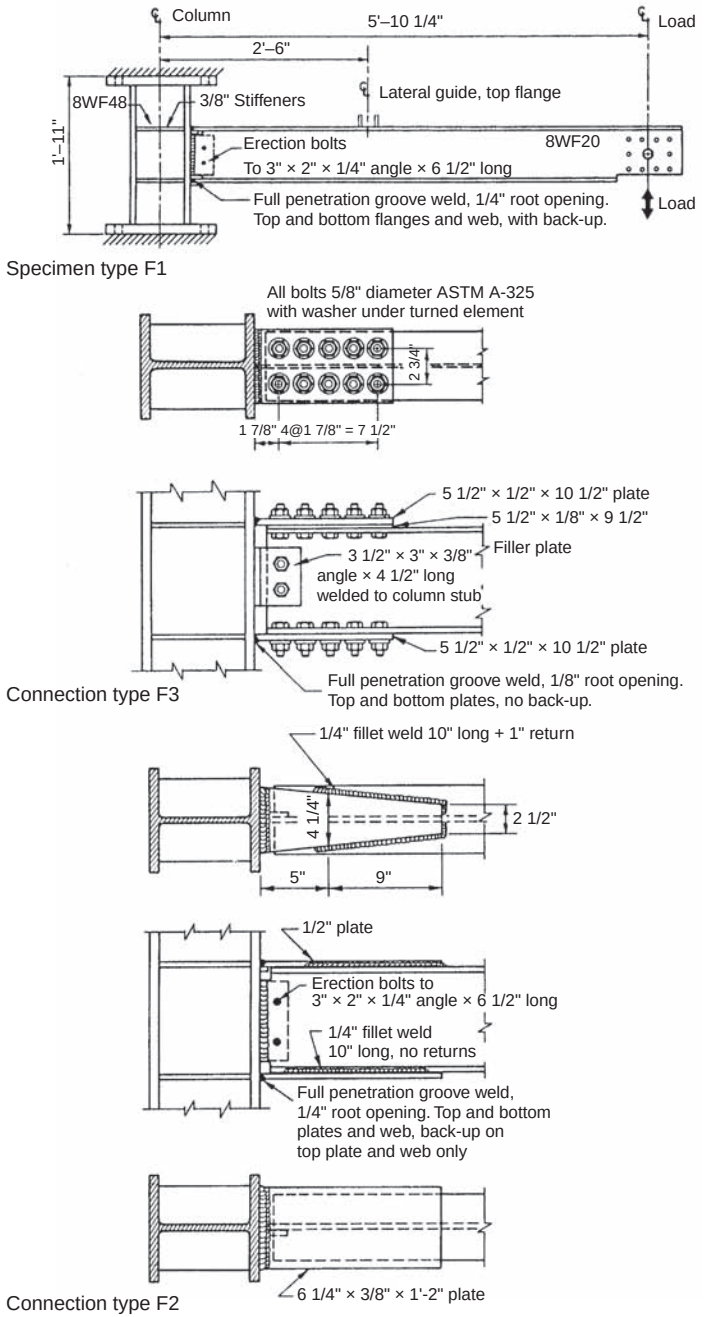

Figure 8.9 Typical connection details considered in early tests of moment connections by Popov and Pinkney. (*From ASCE* Journal of the Structural Division, *vol. 95*, *"Cyclic Yield Reversal in Steel Building Connections" by E. P. Popov and R. B. Pinkney, 1969, with permission from the American Society of Civil Engineers.*)

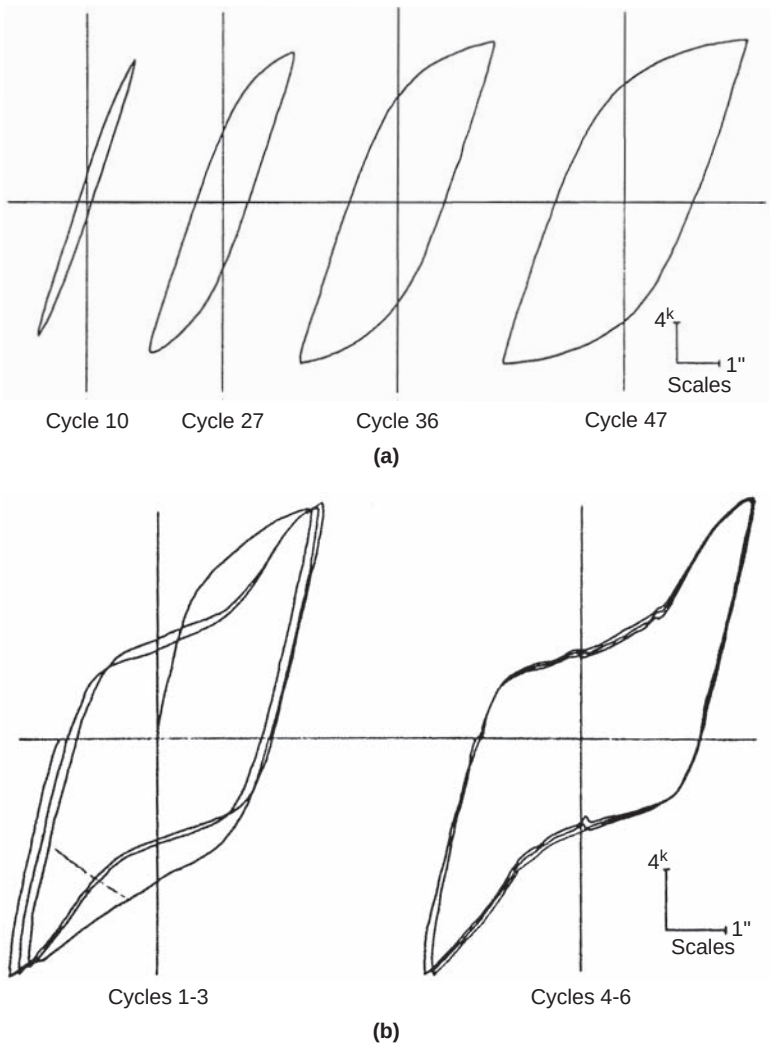

Figure 8.10 Examples of hysteretic behavior obtained in Popov and Pinkney's experiments for (a) specimen type F1, (b) specimen type F3—See Figure 8.9. (*From* ASCE Journal of the Structural Division, *vol. 95*, "*Cyclic Yield Reversal in Steel Building Connections" by E. P. Popov and R. B. Pinkney, 1969, with permission from the American Society of Civil Engineers*.)

bolted webs were also reported to fail abruptly, and their ductility was more erratic (Popov 1987, in a retrospective of past research). Nonetheless, connections with bolted web were judged to be sufficiently ductile and reported to be less costly to fabricate. It is interesting to note that Popov and Stephen (1972) also concluded that "the quality of workmanship and inspection is exceedingly important for the achievement of best results."

Further studies on frame subassemblies (Bertero et al. 1973, Krawinkler et al. 1971, Popov et al. 1975) investigated the effect of panel zone and column plastic hinging and helped make the welded flange-bolted web detail a prequalified moment connection provided that it was detailed according to predetermined rules. This standard

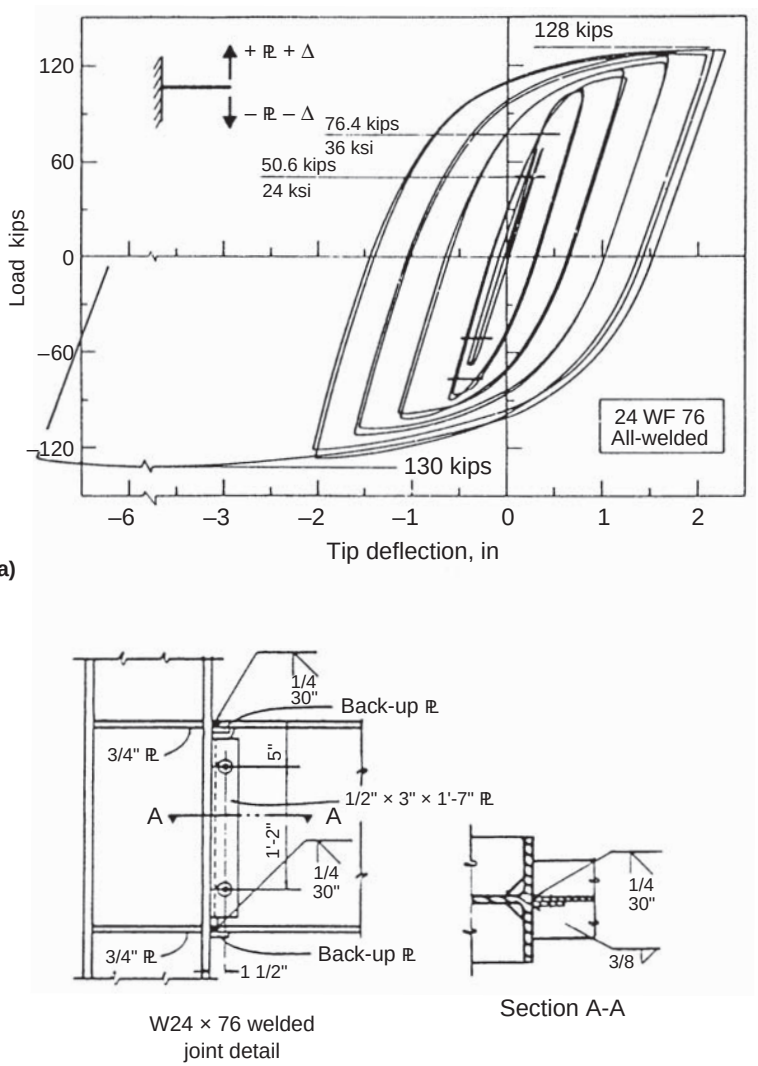

Figure 8.11 Hysteretic behavior of typical connection details having (a) fully welded webs. Results from tests conducted in early 1970s; (b) bolted webs. This connection is otherwise identical to the one shown in (a). Results from tests conducted in early 1970s. (*Parts a and b from* Journal of Constructional Steel Research, *vol. 8, E. G. Popov, "Panel Zone Flexibility in Seismic Moment Joints," 1987, with permission from Elsevier Science Ltd., U.K.*)

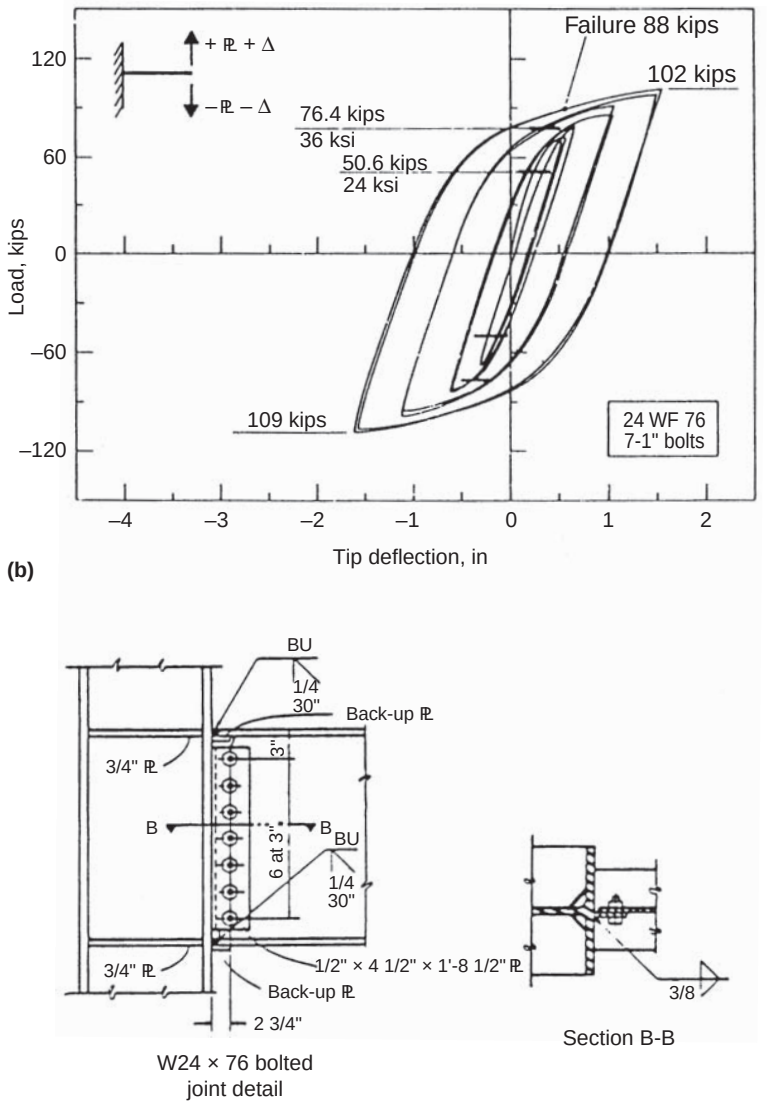

Figure 8.11 (*Continued*)

connection is illustrated in Figure 8.12, although some aspects shown on that detail (such as the supplemental fillet welds along part of the web tab) were actually implemented only in the late 1980s (ICBO 1988). This figure also summarizes some of the doubler plate details described in Section 8.4.5. Note that self-shielded flux-cored arc welding was commonly used, with E70T-4 or E70T-7 electrodes as the filler metal, as there was no specified notch toughness requirement for the filler metal.

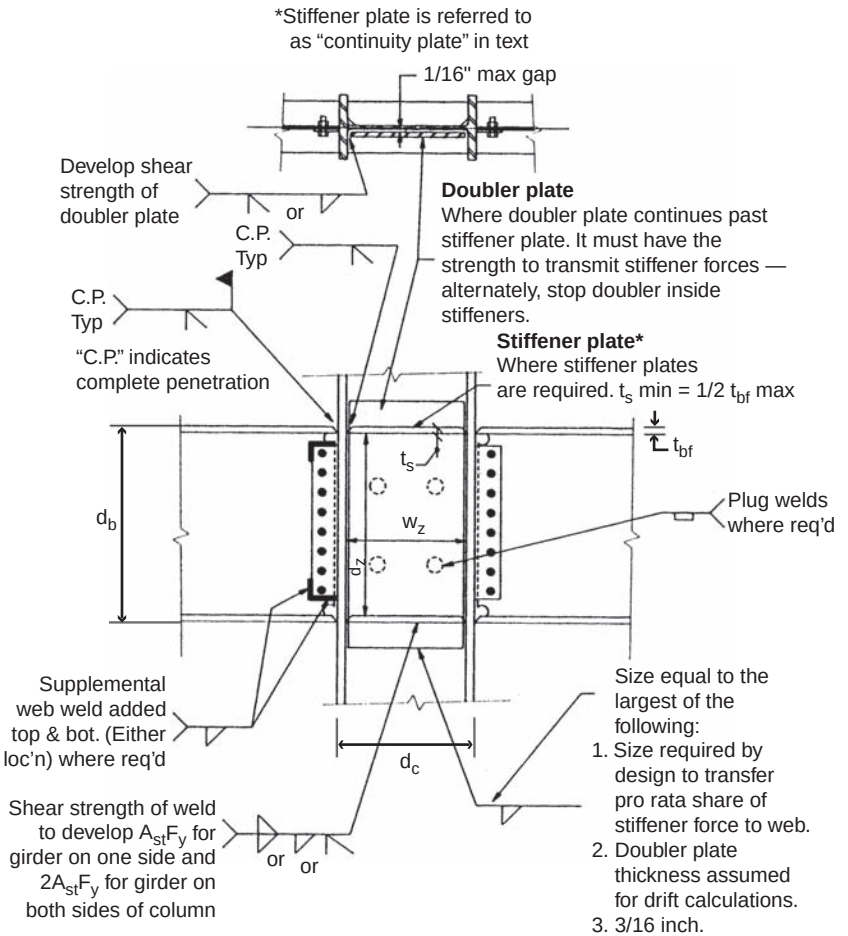

Figure 8.12 Prequalified moment-resisting frame detail in use prior to Northridge earthquake.

For a number of years, nearly all beam-to-column connections in structural systems designated as ductile moment-resisting frames were detailed to be able to transfer the nominal plastic moment of the beams to the columns (Roeder and Foutch 1995). As a result, relatively modest column and beam sizes were sufficient in those moment frames to provide the necessary seismic resistance. However, over the years, as a result of the cost premium commanded by full moment connections compared with shear connections, many engineers concluded that it was economically advantageous to limit the number of bays of framing designed as ductile moment-resisting frames. In the extreme, prior to the Northridge earthquake, some engineers routinely designed buildings having only four single-bay ductile moment frames (two in each principal direction, with each in a different plane

to provide torsional resistance). This trend developed at the expense of a dramatic loss in structural redundancy, which can be argued to be a nonnegligible reduction in overall structural safety, particularly in the event of construction defects. Moreover, considerably deeper beams, columns with thicker flanges, and bigger foundations were needed in these single-bay ductile moment frames than in the multi-bay ones previously used to resist the same seismically induced forces.

In that regard, some pre-Northridge tests on beam-to-column subassemblies provided an opportunity to investigate potential size effects. In particular, tests by Tsai and Popov (1988, 1989) indicated that some prequalified moment connections in ductile moment frames with W460 and W530 beams, equivalent to W18 and W21 in U.S. units and thus similar in depth to those tested by Popov and Stephen (1970, 1972), were not as ductile as expected when the web accounted for a substantial portion of the beam's plastic moment capacity. As shown in Figure 8.13, specimens with the welded flange-bolted web connections (specimens 3 and 5) failed abruptly before developing adequate plastic rotations. These specimens were constructed by a commercial fabricator, and the welds had been inspected ultrasonically and found to be satisfactory. The use of bolts with twist-off ends for tension control in the beam web (specimens 17 and 18) or the use of supplemental web welds (specimens 13 and 14) improved hysteretic performance and delayed abrupt failure. It is noteworthy that two specimens with bolted webs failed prior to reaching M_p (even though they were supplied from a commercial fabricator), and two other specimens with fully welded flanges and webs exhibited significant ductility (specimens 9 and 11), as shown in Figure 8.13.

Further to these findings, the prequalified welded flange-bolted web connection detail was modified in the late 1980s for beams having a ratio Z_f/Z less than 0.7, where Z_f is the plastic modulus of the beam flanges alone, and Z is the plastic modulus of the entire beam section. For those beams, supplemental welds on the bolted web shear tabs were required (i.e., in addition to the usual complete penetration single-bevel groove welds on the beam flanges and the bolted shear tab for the web), as shown in Figure 8.12. The supplemental welds were also required to have a minimum strength of 20% of the nominal flexural strength of the beam web.

Given that those new requirements were supported by only limited test data, Engelhardt and Husain (1993) conducted additional tests to investigate the effect of Z_f/Z on rotation capacity using slightly deeper beams than those tested by Tsai and Popov (W460 to W610 shapes, equivalent to W18 to W24 in U.S. units). Interestingly, some of the specimens tested by Engelhardt and Husain showed a disturbing lack of ductility, even though all specimens had been constructed by competent steel fabricators using certified welders, and all welds had been ultrasonically tested by certified inspectors. Some specimens exhibited almost no ductile hysteretic behavior (e.g., Figures 8.14a and d), whereas others behaved in a ductile manner

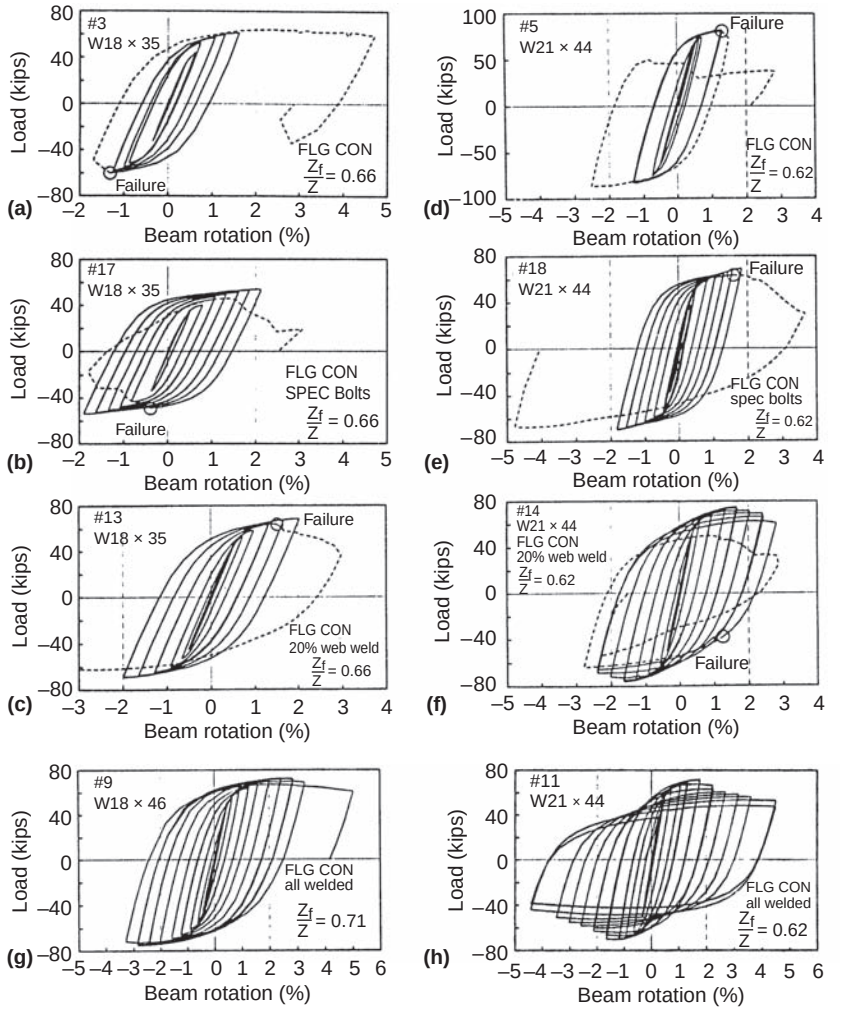

Figure 8.13 Hysteretic loops for moment-resisting frame connections with low Z_f/Z values and different beam web connection methods: (a) W460 × 52 (W18 × 35) beam with bolted web, (b) W460 × 52 beam with tension-control bolts (special bolt whose ends twist off upon reaching specified bolt tension), (c) W460 × 52 beam with bolted web and 20% supplementary weld, (d) W530 × 66 (W21 × 44) beam with bolted web, (e) W530 × 66 beam with tension-control bolts, (f) W530 × 66 beam with bolted web and 20% supplementary weld, (g) W460 × 68 (W18 × 46) beam with fully welded web, and (h) W530 × 66 beam with fully welded web. (*From* Engineering Journal, *2nd Quarter 1989*, *"Performance of Large Seismic Steel Moment Connections under Cyclic Loads" by E. P. Popov and K. C. Tsai, with permission from the American Institute of Steel Construction.*)

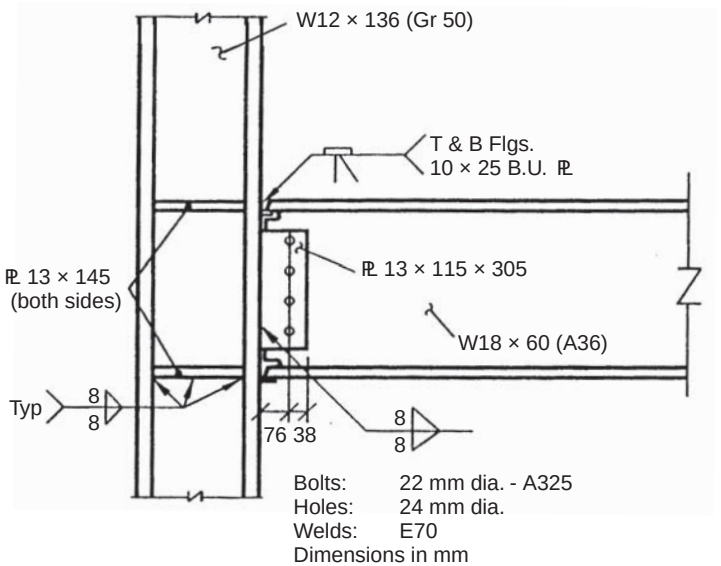

(a)

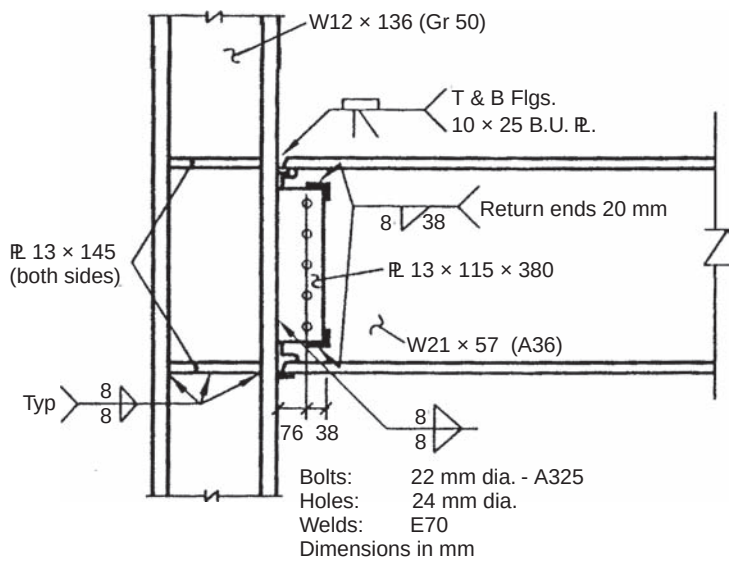

(b)

Figure 8.14 Engelhardt and Husain's tests: (a) specimen 4 details; (b) specimen 7 details. (c) typical weld and cope details; (d) resulting moment versus plastic rotation hysteretic curves for Specimen 4; (e) resulting moment versus plastic rotation hysteric curves for specimen 7. (*Parts a to e courtesy of M. D. Engelhardt, Dept. of Civil Engineering, University of Texas, Austin.*)

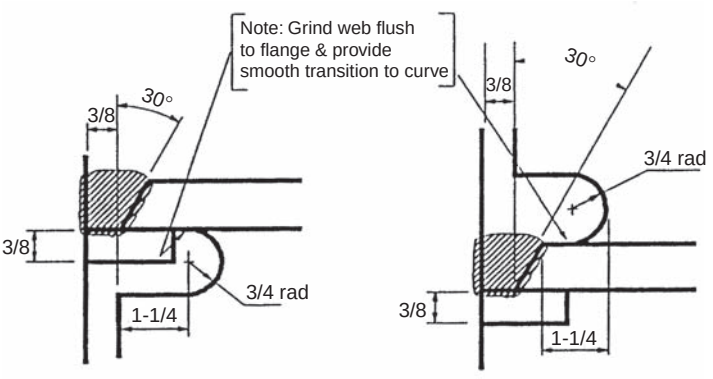

(c)

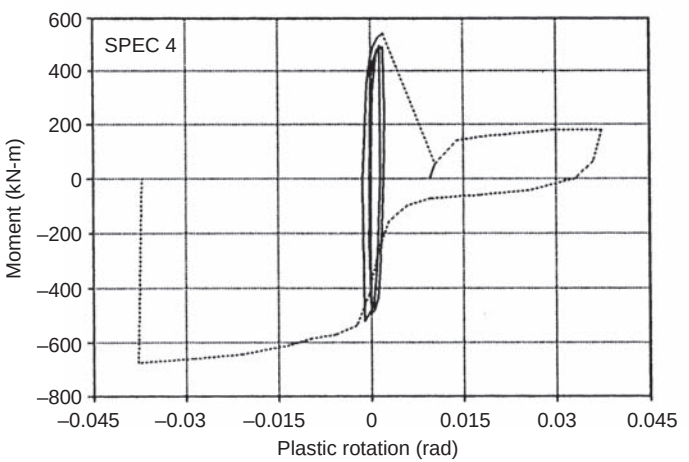

(d)

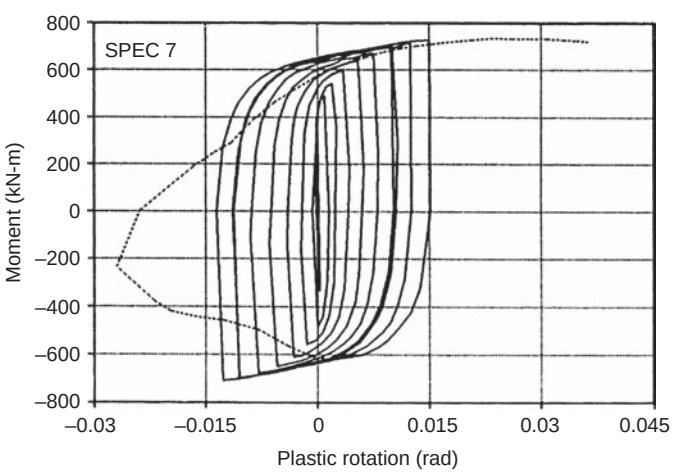

(e)

Figure 8.14 (*Continued*)

until a sudden rupture developed in the connection (e.g., Figures 8.14b and e). The amount of hysteretic behavior developed prior to failure bore no relationship to Z_f/Z. Three specimens suffered sudden fracture at the weld-to-column interface at the beam bottom flange (such as the specimen shown in Figure 8.14a); the remaining specimens suffered gradual fracture at the same location (three specimens), at the top flange (one specimen), or through the bottom beam flange outside the weld (one specimen).

Engelhardt and Husain also compared their results with past experimental data. Assuming that connections must have a beam plastic rotation capacity of 0.015 radian to survive severe earthquakes, they found that none of their seven specimens could provide this rotation capacity (Figure 8.15), nor could most connections in tests conducted by other researchers. As a result of these observations, Engelhardt and Husain expressed concerns about the welded flange-bolted web detail commonly used in ductile moment frames in severe seismic regions.

And then the Northridge earthquake happened.

8.5.2 Damage During the Northridge Earthquake

On January 17, 1994, an earthquake of moment magnitude 6.7 struck the Los Angeles area. The epicenter of the earthquake was at Northridge in the San Fernando valley, 32-km northwest of downtown Los Angeles. This earthquake caused over $20 billion in damage, becoming the most costly disaster ever to strike the United States at the time (EERI 1995). Structural and nonstructural damage to buildings and infrastructure was widespread and considerable, but there were no reports of significant damage to steel building structures immediately following the earthquake. This should not come as a surprise. Inspectors, as well as reconnaissance teams dispatched by various engineering societies and research centers following a major earthquake can report only readily visible damage not obstructed by nonstructural elements. Careful inspection of a building's steel frame requires the removal of architectural finishes (cladding, ceiling panels, etc.) and of the fireproofing material covering the steel members—an expensive and time-consuming process. Given that no steel building collapsed or exhibited noticeable signs of structural distress (EERI 1996; Tremblay et al. 1995), the discovery of critical but nonfatal damage was precluded without authority to expose part of the structure.

However, in the months following the earthquake, engineers discovered important damage to steel structures, including a large number of beam-to-column connection fractures. Initially, damage was often found accidentally, while engineers were trying to resolve nonstructural problems reported by owners following the earthquake. In one case, for example, beam-to-column connection fractures would

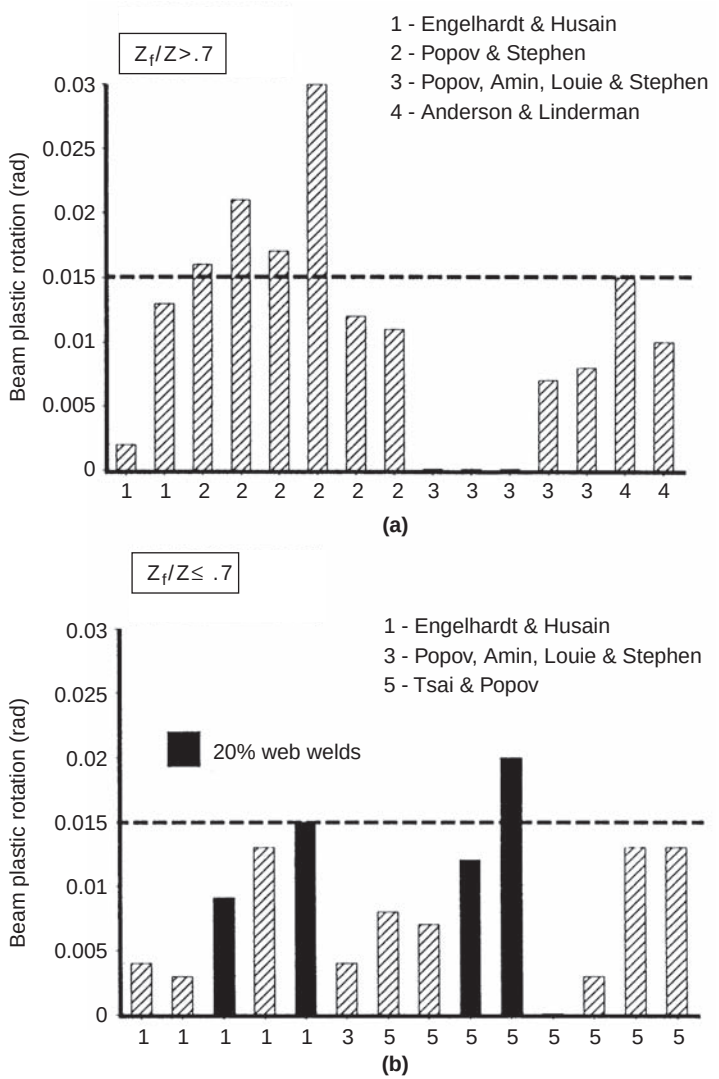

Figure 8.15 Engelhardt and Husain's comparison of beam plastic rotations obtained in past test for (a) specimens with $Z_f/Z > 0.70$ and (b) specimens with $Z_f/Z \leq 0.70$. (*Courtesy of M. D. Engelhardt, Dept. of Civil Engineering, University of Texas, Austin.*)

have remained hidden, if not for complaints by occupants about persisting elevator problems.

The structural engineer noticed that the building was leaning in one direction and requested that some connections be exposed. Informal discussion of such problems within the profession led other structural

engineers to recognize the potential significance of the problem and to require random inspection of joints in various steel structures. This led to the discovery of more failures. Connection fractures were found in buildings of various vintages and heights (1 to 27 stories), including new buildings under construction at the time of the earthquake (Engelhardt and Sabol 1995, FEMA 2000g, SAC 1995a, Youssef et al. 1995). For example, in a steel building still under construction at the time of the Northridge earthquake, one that had apparently survived the earthquake intact, random inspection revealed severe fractures in nearly all beam-to-column connections in one moment-resisting frame. Typically, in the damaged connections of that building, the column flange fractured at the level of the full-penetration weld of the beam's bottom flange to the column, and the crack propagated horizontally a short distance into the column web and then vertically toward the other flange of the same beam (Figure 8.16).

Within two months, more than a dozen buildings with brittle failures of beam-to-column moment connections attributable to the Northridge earthquake had been reported. This became a rather delicate issue given that most buildings in which fractures were discovered were still occupied after the earthquake. A first special AISC task committee meeting allowed researchers and practicing engineers to meet and exchange information (AISC 1994). Tentative provisions for the repair of observed damage were formulated, and although many potential causes for the problem could be identified, failures could not be conclusively explained.

Three months following the earthquake, approximately 50 steel buildings were known to have suffered moment frame damage, based on records from the Los Angeles Department of Building and Safety. By the end of 1994, approximately 100 had been identified, but the actual number of buildings with damaged moment frames was suspected to be higher, given that some owners disallowed inspection of their buildings (SAC 1995a, SAC 1995b, FEMA 2000g). For perspective, approximately 500 buildings with steel moment frames were located where severe ground shaking occurred during that earthquake. Lessons from the Northridge earthquake also prompted engineers to suspect that damage to steel moment frames might have occurred in previous earthquakes, and remained hidden. In the San Francisco Bay Area, hit by the Loma Prieta earthquake in October 1989 (EERI 1990), this suspicion has been confirmed as buildings with damaged connections were discovered as inspection opportunities arose (Rosenbaum 1996). Similar damage was also reported in a limited number of buildings previously affected by the 1992 Landers and 1992 Big Bear earthquakes (FEMA 2000a).

Various types of damage were discovered during the surveys conducted following the Northridge earthquake. Cracks that developed at or near beam bottom flanges were most frequently reported.

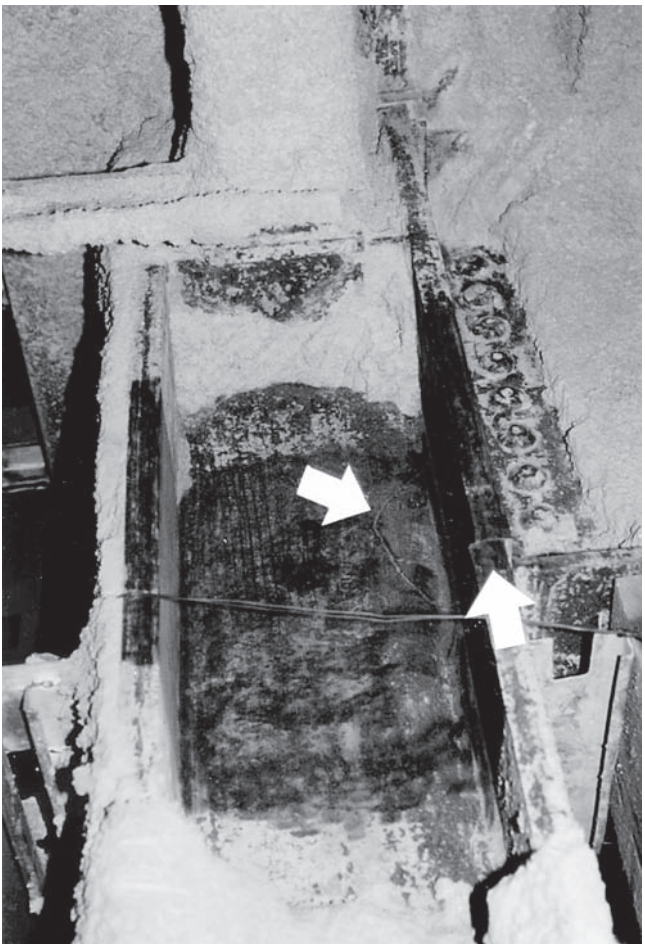

(a)

Figure 8.16 Examples of Northridge fractures propagating through column flanges: (a) column without stiffener, with fracture propagating into column web and vertically toward top flange; (b) close-up view of fracture shown in (a); (c) column with partial stiffener, with fracture through column flange; (d) close-up view of fracture shown in (c).

Figure 8.17 summarizes the various types of fractures observed in that case (types 1 to 8). Most frequently, cracking initiated near the steel backup bar in the root pass of the weld. Those cracks either remained within the weld material, propagating through part or all of the flange weld (type 1 and 2 respectively), or spread into the adjacent base metal (types 3 to 6). Cracks in the adjacent steel propagated into the column flange either vertically (types 3 or 4, depending on

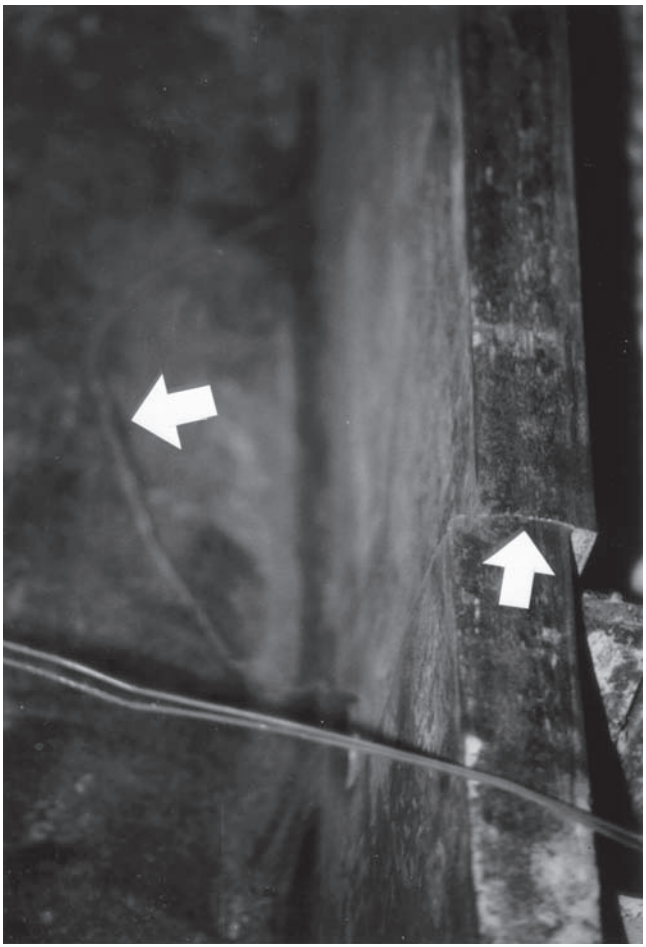

(b)

Figure 8.16 (*Continued*)

whether a piece of the column was completely pulled out in the process) or horizontally by fracturing the entire column flange (type 5) and sometimes a significant portion of the column web (type 6). In some cases, cracks that extended into the column web ruptured the entire column section horizontally or were found to bifurcate and propagate vertically toward the other flange of the beam in which it initiated. In a few instances, cracking initiated at the weld toe and propagated through the flange heat-affected zone (type 7), and at least one case of lamellar tearing of a column flange has been reported (type 8) (Bertero et al. 1994). Examples of such damage are shown in Figures 8.18, 8.19, and 8.20.

(c)

Figure 8.16 (*Continued*)

These cracks and fractures were frequently reported in the absence of similar damage to the top flange. In a few buildings, there were instances of weld damage at the beam top flanges without damage to the corresponding bottom flange welds, but generally, both flanges were found to have suffered damage when cracks were found in the top flange welds. Only a few instances of base metal fractures adjacent to beam top flanges were reported, but other such failures may have been left undetected in many cases because floor slabs frequently obstruct inspection at that location (Youssef et al. 1995).

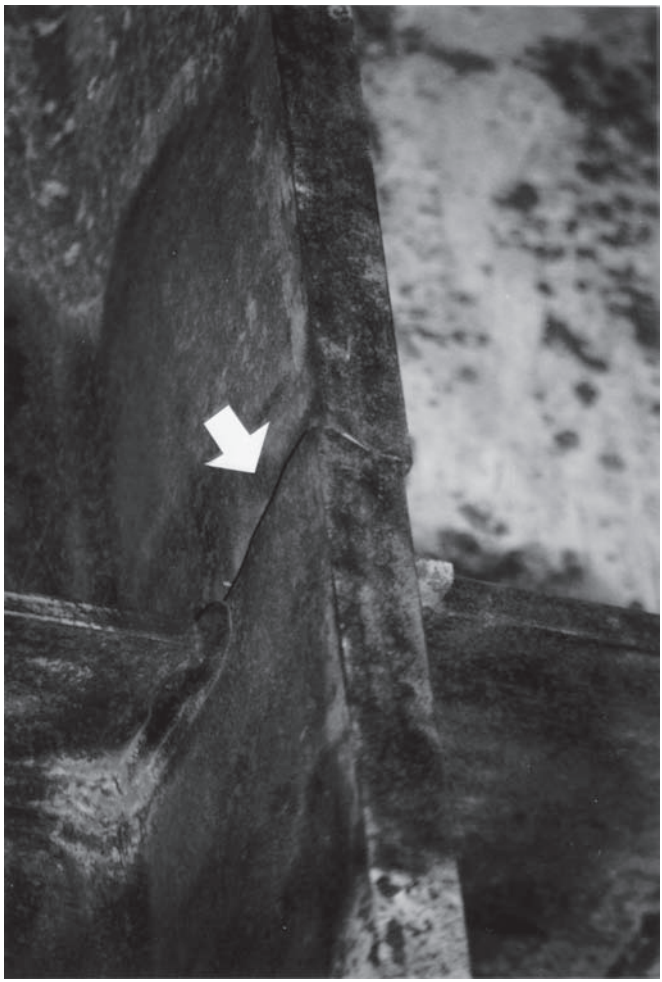

(d)

Figure 8.16 (*Continued*)

The damage reported above was sometimes accompanied by severe damage to the beam's shear tabs, with vertical net section fractures between the bolt holes over part of the height of the web connector (this occurred after the beam flange fractured completely). Note that gravity load resistance could be seriously jeopardized when complete rupture of such shear tabs follows flange fracture. Finally, in a few instances, panel zone yielding was also observed (Youssef et al. 1995).

Given that the above damage was reported in buildings having widely different characteristics, attempts were made to correlate

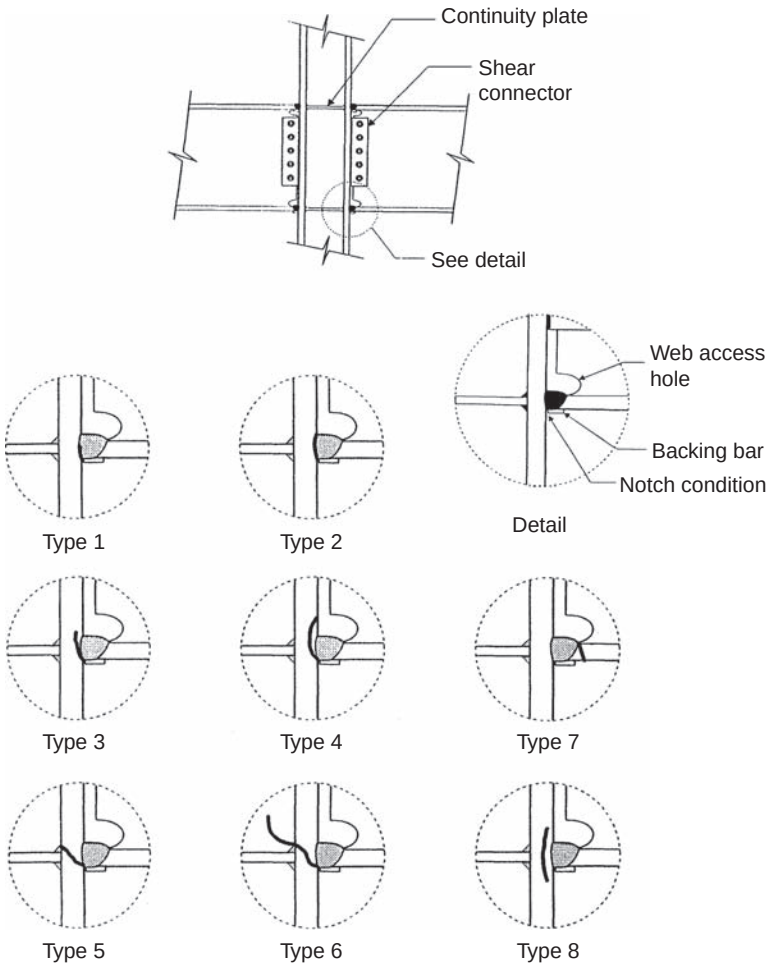

Figure 8.17 Typical welded flange and bolted web beam-to-column connection in moment-resisting frames, with close-up view of notch condition at backing bar, and eight types of reported Northridge fractures. (*Courtesy of R. Tremblay, Dept. of Civil Engineering, Ecole Polytechnique, Montreal, Canada.*)

damage statistics to beam depth, beam span, steel grade, design details, shear connection type, weld process, composite-beam behavior, material, and construction quality. These studies have proven inconclusive (Youssef et al. 1995).

Although no steel buildings collapsed during the Northridge earthquake, the discovery of these unexpected failures forced the structural engineering community to reexamine its design, detailing, and construction practice for steel moment frames. A sense of urgency was fueled by the recognition that the Northridge earthquake was

(a)

(b)

Figure 8.18 Four examples of bottom flange welds fractures. In case (a), for a fracture located near the face of a box column, a business card is dropped in to illustrate that the fracture passes completely through the weld. (*Parts a to c are courtesy of M. D. Engelhardt, Dept. of Civil Engineering, University of Texas, Austin. Part d is courtesy of David P. O'Sullivan, EQE International, San Francisco.*)

(c)

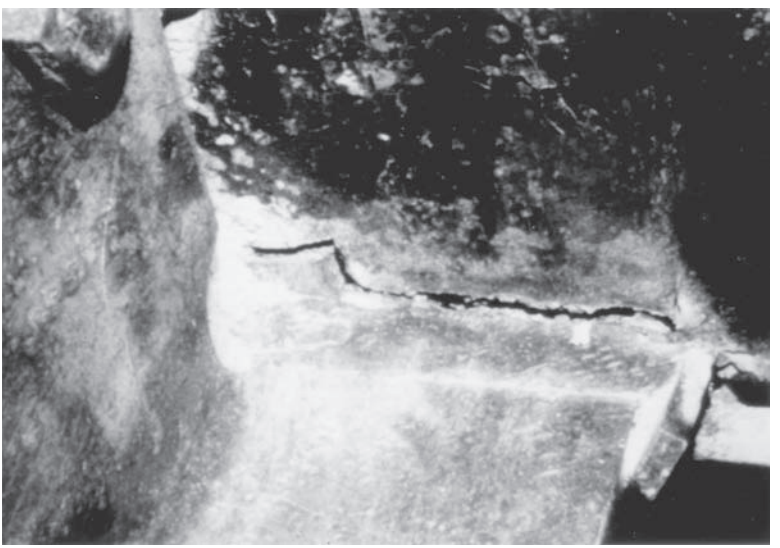

(d)

Figure 8.18 (*Continued*)

certainly not the largest earthquake expected to occur in North America and that steel frames could be subjected to larger inelastic deformation demands in future earthquakes. To develop short-term and long-term solutions, extensive research activities were initiated by federal agencies and private industries. More notable was a

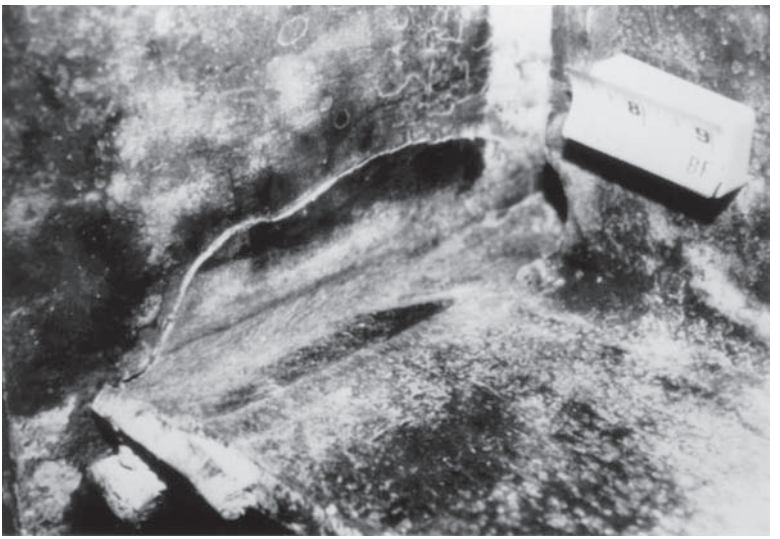

(a)

(b)

Figure 8.19 Two examples of divot fracture at beam bottom flange. (*Courtesy of David P. O'Sullivan, EQE International, San Francisco.*)

coordinated research effort initiated through a joint venture of the Structural Engineers Association of California (SEAOC), the Applied Technology Council (ATC), and the California Universities for Research in Earthquake Engineering (CUREe). The SAC Joint Venture combined the efforts of practicing engineers, code writers, industry

(a)

(b)

Figure 8.20 Examples of fractured columns, with fractures propagating from near the beam bottom flange weld (on the right side in both cases) to the column flange and into the column web. (*Part a courtesy of M. D. Engelhardt, Dept. of Civil Engineering, University of Texas, Austin. Part b courtesy of David P. O'Sullivan, EQE International, San Francisco.*)

representatives, and researchers who share either a professional or a financial interest in the resolution of the problems in beam-to-column connections that arose as a result of the Northridge earthquake. This venture published important documents reporting findings (e.g., SAC 1995a, 1995b, 1997, 1999), and design recommendations (FEMA 2000a, 2000b, 2000c, 2000d) later integrated in various consensus codes, specifications, and standards.

8.5.3 Causes for Failures

Numerous factors have been identified as potentially contributing to the poor seismic performance of the pre-Northridge steel moment connections, and failures may have been caused by different combinations of those factors. After much research, debate, and deliberation, the professional engineering community did not single out a unique or dominant reason for the observed failures, but rather concluded that all of those factors had a relative detrimental influence. Thus, design solutions and changes to practice enacted since then have aimed to redress deficiencies related to every plausible cause of connection damage. A review of some of these conjectured causes is therefore worthwhile and is presented below. The most important concerns are addressed here, and related issues have been grouped under arbitrarily defined broad categories. A more complete summary of all major and minor concerns expressed following the Northridge earthquake is available elsewhere (SAC 1995a).

8.5.3.1 Workmanship and Inspection Quality

A percentage of the damage observed following past earthquakes worldwide has been a consequence of substandard workmanship and improper inspection, particularly in countries with poor code enforcement and contractors who hide construction (detailing) mistakes. Hence, as Northridge failures started to appear, many asserted that deficient workmanship and inspection were to blame. Ignorance of standard welding requirements was found to be disconcertingly widespread among structural engineers (SAC 1995a), and some have reported evidence of poor quality welds with defects that escaped detection prior to the earthquake. Nonetheless, although lack of adherence to standard welding procedure generally made matters worse, improved workmanship and inspection quality alone would not have been sufficient to prevent the Northridge failures (specimens constructed under controlled conditions still exhibited erratic behavior in post-Northridge laboratory tests, as described later).

8.5.3.2 Weld Design

In the pre-Northridge connection described earlier, the beam web creates an obstacle when one is executing the bottom flange groove weld; deposition of weld metal is interrupted at the beam web at every pass. As a result, there is a high probability of defects in the

bottom flange weld at that location. Those defects are particularly difficult to detect through ultrasonic inspection because they are frequently hidden in the portion of the testing signal that is interpreted as interference because of the presence of the beam web.

8.5.3.3 Fracture Mechanics

The backup bars used for downhand welding of beam flanges were typically left in place prior to 1994 after completion of the weld. From a strength perspective, these small bars were perceived as additional material that could be left in place without detrimental effects. However, from a fracture mechanics perspective, the small unwelded gap between the edge of the backup bar and the column flange can be considered a notch or crack that acts as a stress raiser, from where new cracks can originate and propagate into the weld or adjacent base metal (see Figure 8.21). This problem is further compounded if the weld metal has low notch-toughness.

Similarly, a large number of defects can exist in the weld runoff tabs installed to allow extension of the weld passes beyond the flange width (as required by the American Welding Society). Runoff tabs collect the defects commonly introduced by the starting and ending of each weld pass in a zone removed from the flange. If left in place, the weld runoff tabs provide an opportunity for these defects, even though located outside the flange, to propagate into the weld proper. This propensity to crack propagation was further accentuated by the very low Charpy-V notch toughness of the E70T-4 electrodes (Figure 8.22) that were commonly used as filler metals in pre-Northridge welds (Kaufman et al. 1996).

8.5.3.4 Base Metal Elevated Yield Stress

Many engineers had resorted to using A36 steel for beams and A572-Grade 50 for columns to facilitate compliance with the philosophy of strong-column/weak-beam design. The use of Grade 50 steel for columns also increased the panel zone strength, minimizing the need for doubler plates. However, a significant increase in the actual yield and ultimate strengths of the standard A36 steel produced in the United States has been observed over the years, in spite of the absence of changes to the steel grade specification itself. This increase is primarily due to changes in the steel-making process in the 1980s, when integrated mills were replaced by mini-mills that use highly efficient electric arc furnaces to produce steel shapes from scrap steels. SSPC (1994) and SAC (1995b) reports average yield and ultimate strengths of 338 MPa (49 ksi) and 475 MPa (69 ksi) for A36 steel, and maximum yield strengths as high as 496 MPa (72 ksi), as shown in Table 8.1. Some steel producers have also introduced dual-certified steel, which is steel simultaneously in compliance with all the minimum chemical and strength requirements of both A36 and A572-Grade 50 steels.

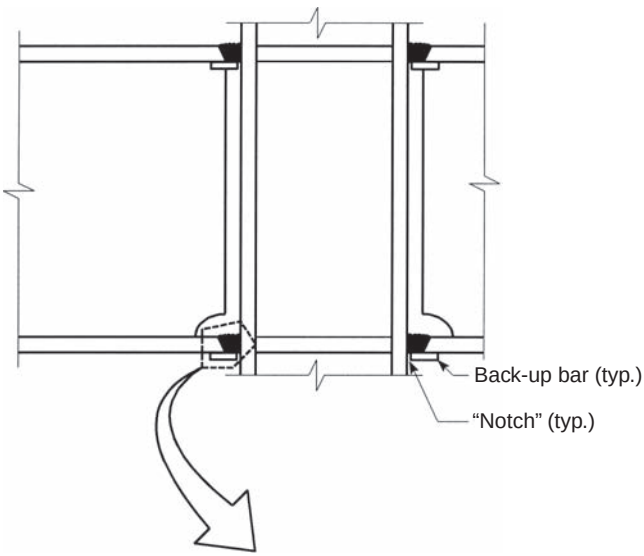

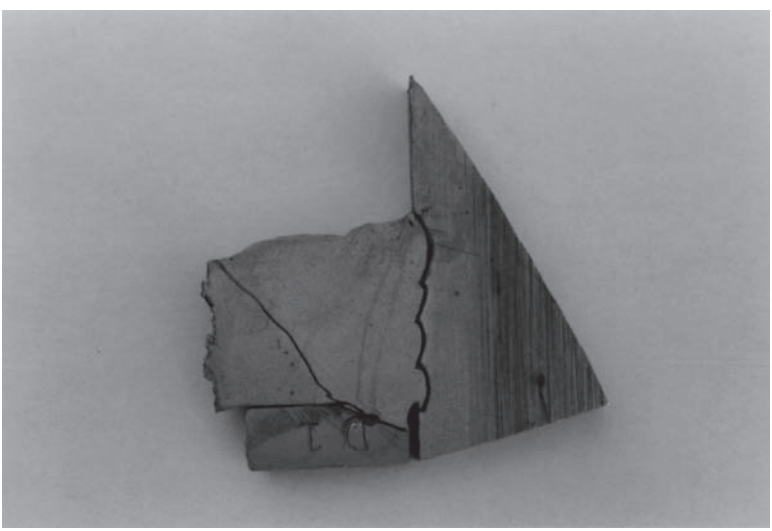

Figure 8.21 Example of fractured beam bottom flange in which a crack originated at the unwelded gap between the edge of the backup bar and the column flange. (*Courtesy of J. E. Patridge, Smith-Emery Co., Los Angeles.*)

Therefore, engineers who assume A36 steel properties for the design of beams may seriously underestimate the beam flange forces acting on the groove welds, and unintentionally select welds weaker than the base metal, if the contractors supply steel with yield strength in excess of 350 MPa (50 ksi). Furthermore, the intended strong-column/

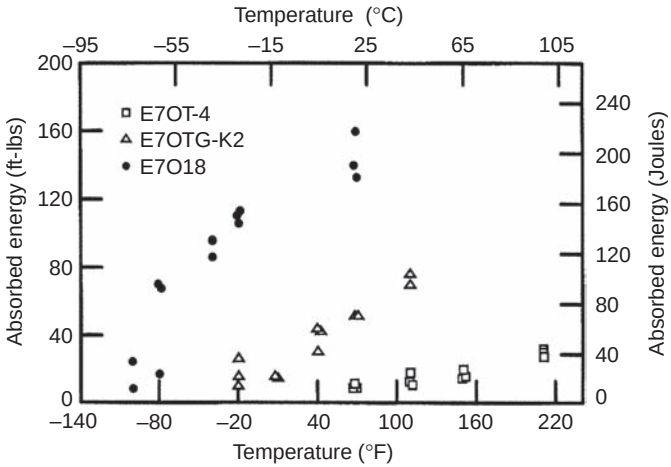

Figure 8.22 Charpy-V notch test results on three different types of weld filler metal. (*From* Modern Steel Construction, *vol. 36, no. 1, "Achieving Ductile Behavior of Moment Connections" by E. J. Kaufmann et al., 1996, with permission from the American Institute of Steel Construction.*)

weak-beam design may in practice be a weak-column/strong-beam system if the yield strength of the beam substantially exceeds the nominal value.

To ensure that representative yield and tensile strength values are used in design when this knowledge is critical, correction factors were developed to relate actual expected strength to minimum specified strengths, using the data from Table 8.1 and other complementary studies (Bartlett et al. 2003, Liu 2003). The corresponding expected yield strength, F_y^{exp}, and expected tensile strength, F_u^{exp}, (called "actual" strengths in some references) are defined as $F_y^{exp} = R_y F_y$ and $F_u^{exp} = R_t F_u$, where R_y is the ratio of the expected yield stress to the specified minimum yield stress, and R_t is the ratio of the expected tensile strength to the specified minimum tensile strength.

Table 8.2 shows sample results specified by AISC 341 for various structural shapes and steel grades, including the A992 and A913 grades having specified upper limits on yield strength (see Section 2.2.5). Values for other structural shapes and steel are provided in AISC 341.

8.5.3.5 Welds Stress Condition

The ultimate stress applied to the weld of the beam flange can be estimated if one assumes that the bolted web cannot transfer bending moments. Indeed, researchers have observed that web bolts

Statistics	A36 Steel	Dual Grade	A572 Grade 50
Yield Stress (ksi)*			
Specified	36.0	50	50
Mean	49.2	55.2	57.6
Minimum	36.0	50	50
Maximum	72.4	71.1	79.5
Standard deviation	4.9	3.7	5.1
Mean plus one standard deviation	54.1	58.9	62.7
Tensile Stress (ksi)*			
Specified	58–80†	65 (min)	65 (min)
Mean	68.5	73.2	75.6
Minimum	58.0	65.0	65.0
Maximum	88.5	80.0	104.0
Standard deviation	4.6	3.3	6.2
Mean plus one standard deviation	73.1	76.5	81.8
Yield/Tensile Ratio			
Specified	0.62 (max)	0.77 (max)	0.77 (max)
Mean	0.72	0.75	0.76
Minimum	0.51	0.65	0.62
Maximum	0.93	0.92	0.95
Standard deviation	0.06	0.04	0.05
Mean plus one standard deviation	0.78	0.79	0.81

*1 ksi = 6.895 MPa.
†No maximum for shapes heavier than 426 lb/ft.
(*SSPC 1994*)

Table 8.1 Statistical Yield and Tensile Properties for Structural Shapes Based on Data Reported by the Structural Shape Producers Council (SSPC)

typically slip during testing, leaving the stiffer welded flanges alone to resist the total applied moment at the connection (Popov et al. 1985, Tsai and Popov 1988). As a result of the incompatible stiffnesses of the bolted web and the welded flanges, the connection resistance is reached when the flanges reach their ultimate tensile stress, F_u (Figure 8.23).

Structural Shape and Steel Grades	R_y	R_t
Hot-rolled structural shapes and bars:		
• ASTM A36/A36M,	1.5	1.2
• ASTM A1043/1043M Gr. 36 (250)	1.3	1.1
• ASTM A572/572M Gr. 50 (345) or 55 (380), ASTM A913/A913M Gr. 50 (345), 60 (415), or 65 (450), ASTM A588/A588M, ASTM A992/A992M,	1.1	1.1
• ASTM A1043/A1043M Gr. 50 (345)	1.2	1.1
Hollow structural sections (HSS):		
• ASTM A500 (Gr. B or C), ASTM A501	1.4	1.3
Pipe:		
• ASTM A53/A53M	1.6	1.2
Plates, Strips and Sheets:		
• ASTM A36/A36M	1.3	1.2
• ASTM A1043/1043M Gr. 36 (250)	1.3	1.1
• A1011 HSLAS Gr. 55 (380)	1.1	1.1
• ASTM A572/A572M Gr. 42 (290)	1.3	1.0
• ASTM A572/A572M Gr. 50 (345), Gr. 55 (380), ASTM A588/A588M	1.1	1.2
• ASTM 1043/1043M Gr. 50 (345)	1.2	1.1

Table 8.2 R_y and R_t Values for Steel

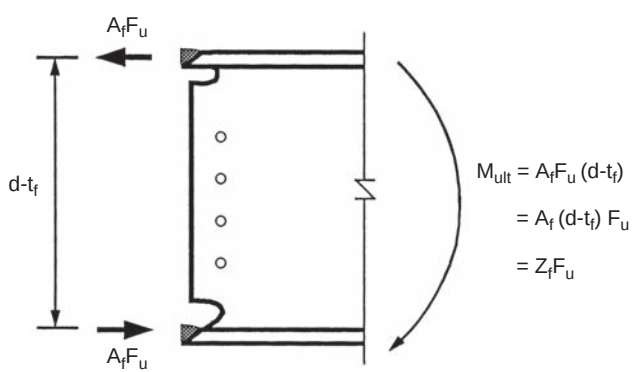

Figure 8.23 Free-body diagram for simplified model of connection strength. (*Courtesy of M. D. Engelhardt, Dept. of Civil Engineering, University of Texas, Austin.*)

As a result of strain-hardening, beams will reach bending moments of 1.2 to 1.3 times the expected plastic moment, M_p^{exp}, at the required plastic rotations, and flange fracture will develop unless:

$$A_f F_u (d - t_f) = Z_f F_u \geq 1.2 M_p^{exp} = 1.2 Z F_y^{exp} \tag{8.20}$$

where A_f and t_f are, respectively, the area and thickness of a beam flange, d is the beam depth, and F_y^{exp} is the expected yield stress of the beam. Assuming the plastic section modulus of the flanges alone, Z_f is approximately 70% of the beam plastic modulus, Z, the ratio of F_y^{exp} over F_u needed to develop significant plastic rotations is given by:

$$\frac{F_y^{exp}}{F_u} \leq \frac{0.83 Z_f}{Z} \approx 0.60 \tag{8.21}$$

Given that the mean ratio of F_y^{exp} over F_u for currently available steels has been reported to vary between 0.72 and 0.76 (SAC 1995a, SAC 1995b), as shown in Table 8.1, it may not be possible to reliably develop the required plastic deformations in beams, even with perfect groove-welded connections.

8.5.3.6 Stress Concentrations

The absence of continuity plates opposite the beam flanges in a column produces stress concentrations in the flange near the column web (see Figure 8.4). Some engineers also alleged that this stress concentration could not be eliminated by the addition of thick continuity plates (Allen et al. 1995). Note that the use of overly thick continuity plates will generally require large welds that will introduce greater residual stresses in the connection: another condition conducive to crack initiation.

8.5.3.7 Effect of Triaxial Stress Conditions

Triaxial stress conditions can have an adverse effect on the ductility of steel. This is illustrated in Figure 8.24 in a comparison of the Mohr circles for steel elements with free or constrained lateral deformations when they are subjected to uniaxial yield stress (Blodgett 1995).

As described in Chapter 2, yielding requires the development of slip planes. For a steel element unrestrained laterally and subjected to uniaxial stress, ductile behavior develops when the shear stress equivalent to the uniaxial yield stress is exceeded. For a steel with $\sigma_y = \sigma_3 = 350$ MPa (50.8 ksi), the corresponding yield shear stress is 175 MPa (25.4 ksi) from Mohr's circle (Figure 8.24). The corresponding axial strains, obtained from the classical equations of elasticity (Popov 1968), using a value of Poisson's ratio, μ, of 0.3 are $\varepsilon_3 = \sigma_3/E = 0.00175$, and $\varepsilon_2 = \varepsilon_1 = -\mu\sigma_3/E = -0.00053$. However, if the same axial strain

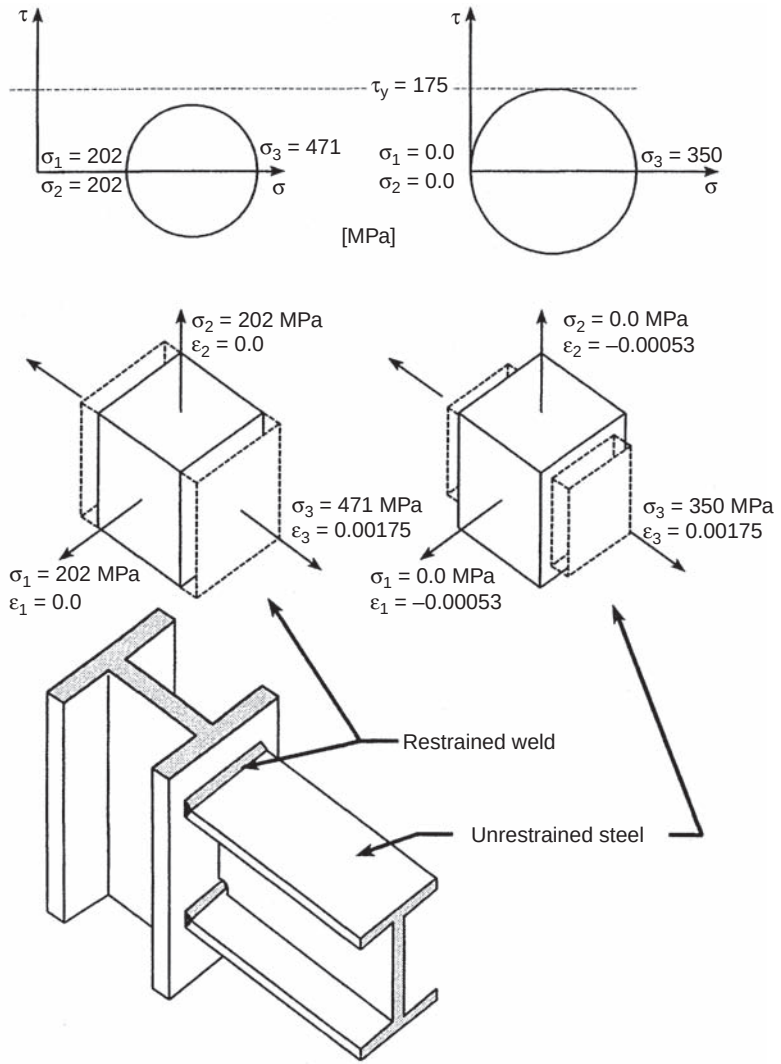

Figure 8.24 Comparison of triaxial stresses in unrestrained and restrained steel elements. (*Adapted from Blodgett 1995.*)

$\varepsilon_3 = 0.00175$ is applied when lateral deformations of the steel element are fully restrained (i.e., $\varepsilon_2 = \varepsilon_1 = 0$), the resulting stresses are:

$$\sigma_3 = \frac{E[1-\mu]\varepsilon_3 + \mu\varepsilon_2 + \mu\varepsilon_1}{(1+\mu)(1-2\mu)}$$

$$= \frac{200000[(1.0-0.3)(0.00175)]}{(1.3)(0.4)} \qquad (8.22a)$$

$$= 471 \text{ MPa } (68.3 \text{ ksi})$$

$$\sigma_2 = \frac{E[\mu\varepsilon_3 + (1-\mu)\varepsilon_2 + \mu\varepsilon_1]}{(1+\mu)(1-2\mu)}$$
$$= \frac{(200000)[0.3\ (0.00175)]}{(1.3)(0.4)} \qquad (8.22b)$$
$$= 202\ \text{MPa}\ (29.3\ \text{ksi})$$

$$\sigma_1 = \frac{E[\mu\varepsilon_3 + \mu\varepsilon_2 + (1-\mu)\varepsilon_1]}{(1+\mu)(1-2\mu)}$$
$$= \frac{(200000)[0.3\ (0.00175)]}{(1.3)(0.4)} \qquad (8.22c)$$
$$= 202\ \text{MPa}\ (29.3\ \text{ksi})$$

As can be seen from the corresponding Mohr circle, even though the axial stress has exceeded the uniaxial yield stress of 350 MPa (50.8 ksi), the maximum shear stress is only 135 MPa (19.6 ksi). The shear stress needed to initiate slip planes would be reached only at an axial stress of 610 MPa (88.5 ksi), a value most likely in excess of the ultimate yield stress of the material (based on data in Table 8.1). Hence, ductile behavior will not develop, and brittle failure will occur instead. This simplified model also suggests that compression in the column ($\varepsilon_2 < 0$) would enhance the potential for ductile behavior at the weld, whereas tension ($\varepsilon_2 > 0$) would reduce it. Practically, the above condition of full restraint against lateral deformations is an extreme constraint not encountered in most welds of small to moderate sizes, but may be approached when large welds are executed on very thick steel members. Elasto-plastic studies of the behavior of constrained welds would help clarify the relationship between degrees of restraint and ductility.

8.5.3.8 Loading Rate

Given that all large-scale specimens in past experimental studies prior to the Northridge earthquake had been subjected to quasi-static loading, it was suggested that rate of loading may have had a detrimental effect on the behavior of beam-to-column moment connections. Dynamic testing of pre-Northridge full-size beam-to-column connections with W760 × 147 beams (W30 × 99 in U.S. units) revealed that beam flanges experienced strain rates on the order of 10^{-1} mm/mm/s for moment frames located in buildings having a fundamental period of vibration of approximately 1 s (Uang and Bondad 1996). At such a strain rate, yield stress can be increased by 10% (see Figure 2.8), thereby increasing the force demand on the groove-welded joint. It is also known that strain rate will decrease the notch toughness of the material. The combined effects resulted in a poorer cyclic behavior under dynamic loading conditions.

8.5.3.9 Presence of Composite Floor Slab

The development of composite action due to the presence of a concrete floor slab may have been responsible for the dominant number of beam bottom flange fractures (compared with top flange fractures). The different neutral axis positions in positive (composite) flexure versus negative (noncomposite) flexure translate into greater axial deformation demands on the beam bottom flange than on the top flange. However, other factors also likely contributed to the greater damage to the beam bottom flanges. For example, the top flange groove weld is easier to accomplish and inspect than the bottom flange weld. Furthermore, the strain demands at the level of the backup bar to the top flange weld are smaller than those on the backup bar to the bottom flange weld, which is farther from the center of the steel section.

Note that in California, engineers have commonly ignored composite action in design of moment-resisting frames, even though 19-mm (¾-inch) diameter shear studs spaced 300 mm (12 in) on center are popular to transfer seismic forces from the slab to the steel frame. Welded wire fabric is commonly used there as reinforcement in the concrete slab.

8.5.4 Reexamination of Pre-Northridge Practice

8.5.4.1 Reexamination of Past Literature

The extensive damage to steel moment frames in the Northridge earthquake prompted a reexamination of past experimental data. This review essentially revealed that the Northridge failures should have been expected (Bertero et al. 1994, Roeder and Foutch 1995, Stojadinovic et al. 2000). Although past experimental studies on standard moment connections generally reported satisfactory performance, sometimes with impressive ductile behavior, most studies reported instances of failures after only a limited amount of inelastic energy dissipation. For example, beyond the numerous sudden failures already reported in Section 8.5.1, Popov and Bertero (1973) reported a number of abrupt specimen failures, sometimes with fractures through welds or flanges, and Popov et al. (1985) noted that most of their specimens failed abruptly after exhibiting more or less satisfactory levels of plastic deformations. That latter test series was conducted to verify the adequacy of the design criteria for beam-to-column joints, using larger specimens than tested to that time and A36 beams framing into A572-Grade 50 columns. The beams' flanges were fully welded, webs were bolted only, and researchers reported hearing the slippage of the web bolts at each load reversal during testing. They also noted that specimens with continuity plates and doubler plates performed better than those without.

The abrupt failures reported in past North American beam-to-column tests were limited to fractures of the welded connections; cracks

propagating into columns had not been observed prior to the Northridge earthquake. However, Bertero et al. (1994) reported that Japanese researchers had experienced such column fractures decades earlier (Kato 1973, Kato and Morita 1969). In those tests performed on large columns, cracks were observed to propagate from the beam welds through the entire column cross-section when the column was subjected to low axial forces; crack propagation stopped after rupture of the column flange when columns were subjected to high axial compression forces.

Thus, beam, column, and weld fractures similar to those documented following the Northridge earthquake had been observed in past studies. Unfortunately, although some of the specimens that exhibited inadequate ductility were brought forth (e.g., Engelhardt and Husain 1993), other instances of erratic behavior received cursory treatment and were attributed to faulty workmanship, even when the test specimens were provided by commercial fabricators.

8.5.4.2 Post-Northridge Tests of Pre-Northridge Details

Shortly after the Northridge earthquake, many tests of typical pre-Northridge connections were conducted in an attempt to replicate the observed failures under controlled conditions. A first series of tests involved heavy beam and column specimens (W360 × 677 A572-Grade 50 columns and W920 × 233 A36 beams, corresponding to W14 × 455 and W36 × 150, respectively, in U.S. units) representative of those that fractured during the earthquake (Engelhardt and Sabol 1994). Special care was taken to ensure superior welding quality and inspection. Backup bars and weld runoff tabs were also removed, and the weld root pass was gouged out and filled with new weld material to locally reinforce the weld. Two specimens had bolted webs (with supplemental welds on the web connector plate), and two specimens had webs fully welded to the column flanges; continuity plates were not used. The four specimens were tested by a standard quasi-static method, which is at strain rates much less than those that typically occur during earthquakes. All specimens failed at a low level of inelastic deformation (attaining plastic rotations of 0.0025 rad to 0.009 rad, depending on the specimen), with brittle fractures observed in both top and bottom flanges. Specimens with fully welded webs did not perform any better than those with bolted webs. These results showed the need for joint reinforcement and/or an alternative welding procedure to be validated through an extensive experimental program.

Tests on eight full-scale specimens of other pre-Northridge connections (W360 × 262 A572 Grade 50 columns with W760 × 147 A36 beams, corresponding to W14 × 176 and W30 × 99, respectively, in U.S. units) showed similar results (Whittaker et al. 1995, Uang and Bondad 1996). All eight specimens had the supplemental welds required on the web connector plate. First, three nominally identical specimens (Whittaker et al. 1995) were constructed under close supervision and rigorous inspection and thus were likely of greater than

average quality. Tested at low strain rates, these pre-Northridge specimens suffered top flange weld fracture at beam plastic rotations of approximately 0.4%, 0.4%, and 1.0%, respectively (Whittaker et al. 1995). Panel zone yielding, observed in all three specimens, increased the total plastic deformation of the specimens by 0.7%, 0.7%, and 1.1%, respectively. Repairs that consisted of rewelding the failed flanges with toughness-rated filler metal failed in a similar manner at beam plastic rotations of 0.3%. Five different specimens tested by Uang and Bondad (1996) failed in a similar manner. Three specimens, tested quasi-statically, achieved maximum beam plastic rotations ranging between 0.2% and 1.6%, and total plastic rotations varied from 0.8% to 2.3% when panel zone plastic deformations were included. Two additional specimens tested at strain rates of 0.1 cm/cm/s failed without exhibiting any beam plastic rotation; maximum panel zone plastic rotations of 0.15% and 1.0% were measured respectively in the two tests. The fractures propagated into the column flanges and bolted beam web plates in the dynamically tested specimens, suggesting that loading rate may have contributed to that failure pattern observed in many Northridge-type failures. The propagation of damage in the dynamic tests has been documented on video (Uang 1995).

As soon as the first preliminary test results became available, the prequalified standard moment connection was deleted from most building codes and regulations for applications in moderate to high seismic regions, and it was replaced by general clauses requiring that welded or bolted moment connections be able to sustain inelastic rotations and develop the required strength, as demonstrated by approved cyclic tests or calculations supported by test data. Interpretation of these clauses, particularly regarding what constitutes acceptable levels of inelastic rotations and test procedures, had been left to the regulatory authorities and professional organizations (e.g., SEAOC 1995) while awaiting consensus agreement. As a result, for a few years, building officials in many jurisdictions required mandatory testing of any new connection detail not previously proven by cyclic inelastic tests, or any connection with beams and columns larger than tested previously. This expensive proposition pushed many engineers toward other lateral-load resisting systems. The findings from an extensive coordinated research program conducted to establish acceptable moment-resisting connections is described in the next section.

8.5.5 Post-Northridge Beam-to-Column Connections Design Strategies for New Buildings—Initial Concepts

Numerous proposed solutions to the moment frame connection problem were attempted in the years following the Northridge earthquake, as part of a coordinated research effort funded by the Federal Emergency Management Agency and the California Office of Emergency Services, as well as from other initiatives. A broad range

of innovative ideas were proposed, often boldly departing from existing practice, sometimes with an entrepreneurship spirit. This section focuses on some successful and nonsuccessful initial concepts, to provide a useful perspective of the context that led to the solutions and constraints adopted in design provisions that are presented later.

Generally, two key concepts were originally pursued to circumvent the problems associated with the pre-Northridge moment frame connection, namely:

- Strengthening the connection, or
- Weakening the beam(s) that frame into the connection

In both cases, the objective is to move the plastic hinge away from the face of the column, to avoid the aforementioned problems related to the potential fragility of groove welds subjected to triaxial stress conditions. Figure 8.25 schematically illustrates the corresponding beam moment diagrams to achieve this. For the strengthening case (reinforced beam ends), developing the plastic moment of the beam, M_p, at a distance e from the face of a column induces greater moments at the column face. On the contrary, weakening solutions locally reduce the beam plastic moment at that same distance e, and ensure plastic hinging at that location by selecting a strength, m_p such that the maximum moment reached at the column face is less than M_p, which can be advantageous given that this moment dictates column and panel zone design.

Solutions that circumvented the need to develop the plastic moment of the beam were also proposed (such as friction-based energy dissipation concepts, or pre-tensioned connections, to name a few), but such

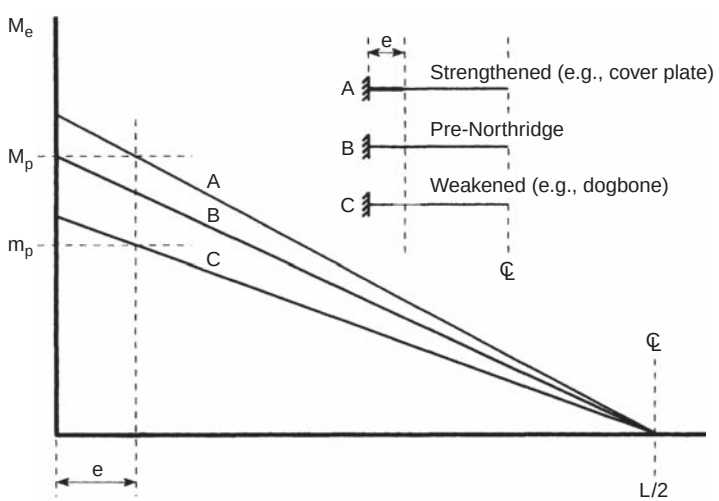

Figure 8.25 Consideration of moment gradient to promote development of plastic hinges at distance *e* from face of column.

outright departures from design approaches relying on hysteretic behavior are presented in Chapter 13, the focus here being on connections that can develop the plastic hinging of the connected beam.

On the strength of results from nonlinear inelastic analyses of example buildings conducted using contemporary knowledge on seismic demands (FEMA 2000e), it was shown that drifts of 4% could develop in special moment-resisting steel frames. Therefore, to ensure the satisfactory performance of such ductile moment-resisting connections, proposed connections were required to experimentally achieve plastic rotations of 0.03 radian without exhibiting strength degradation of more than 20% of their plastic moment (SAC 1995b, FEMA 2000a) when subjected to a specified protocol of cyclic inelastic deformations (e.g., similar to the one in Appendix S of the 2005 edition of AISC 341, or Appendix K of the 2010 edition). A minimum of three satisfactory tests was required to ensure reliable results.

Incidentally, all proposed post-Northridge connections were recommended to be implemented in conjunction with the use of high toughness weld filler metal, better welding practice, and high-quality inspection. Furthermore, even though removal of the backup bars and weld runoff tabs did not enhance performance noticeably in the tests of pre-Northridge connections, the arguments presented earlier regarding the notch effect created by the backup bar are compelling, and their removal is recommended. In some of the post-Northridge test though, a fillet weld applied between the backup bar and column flange was alternatively used to seal the cracklike gap described in Section 8.5.3.

8.5.5.1 Initially Investigated Strengthening Strategies: Cover Plates and Flange Ribs

Many ideas were initially proposed to make the connection stronger than the beam framing into the connection, some of which being illustrated in Figure 8.26. The use of beam strengthening schemes to reinforce beam-to-column connections has the advantage of relocating the plastic hinge(s) away from the column face(s), but the disadvantages of: (1) increasing the beam moment(s) at the face(s) of the column, thereby increasing the column size to maintain the strong-column/weak-beam system; (2) increasing the unbalanced moment on the panel zone; and (3) increasing the plastic hinge rotation demand (see Section 8.6)—all issues that must be considered by the designer.

Among the strengthening strategies, the use of cover plates or flange ribs appeared to be an obvious and promising solution to strengthen the beam at the column face (e.g., Engelhardt and Sabol 1996; Noel and Uang 1996; Kim et al. 2000; Whittaker et al. 1995, 2002). In nearly all cases (Noel and Uang, 1996 and Kim et al., 2000 providing typical exceptions), to make downhand welding possible for both flanges, the top cover plate was tapered and narrower than the beam top flange, whereas the bottom plate was rectangular and

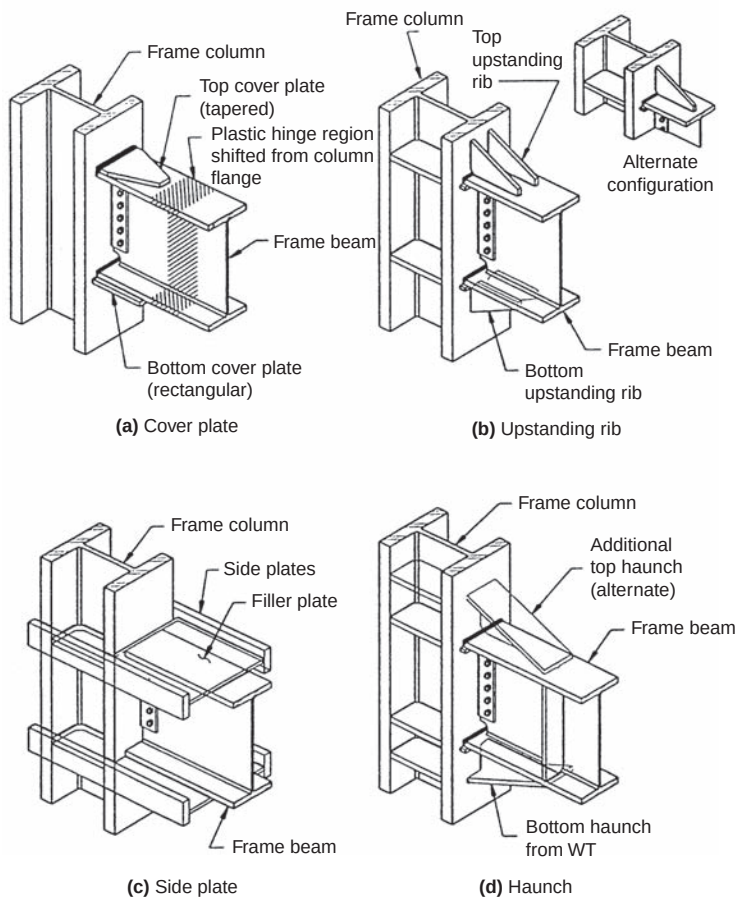

Figure 8.26 Examples of initially proposed moment connections per strengthening strategies. (*Courtesy of M.D. Engelhardt, Dept. of Civil Engineering, University of Texas, Austin.*)

wider than the bottom flange (Figure 8.26a). Plate tapering was also believed to result in a smoother stress transfer between each flange and its cover plate. However, this originally envisioned simple cover plate details ended-up not being prequalified for new construction, for the reasons described below.

Results from a series of cover plate tests by Engelhardt and Sabol (1996) are instructive. Details of 12 specimens considered are summarized in Table 8.3, along with brief description of their performance. Details with bolted web or welded web connections were evaluated, as shown in Figures 8.27a and b, respectively. Note that for new construction with that proposed cover plate detail, the

Specimen	Beam Size§	Beam Flange Strength		Beam Web Strength		Column Size§ W14×	Top Cover Plate (tapered) (thickness × width × length) (mm)	Bottom Cover Plate (rectangular) (thickness × width × length) (mm)	Web Connection	Electrode*	Maximum Plastic Rotation (rad)	Description of Failure
		Fy (MPa)	*Fu* (MPa)	*Fy* (MPa)	*Fu* (MPa)							
AISC-3A	W36 × I50	294	425	320	435	455	19 × 300 × 430	16 × 355 × 405	bolted	E70T-4	1.5%	Brittle fracture at top flange and cover plate groove weld
AISC-3B	W36 × I50	294	425	320	435	455	19 × 300 × 430	16 × 355 × 405	bolted	E70T-4	2.5%	Gradual strength deterioration due to local budding, followed by gradual tearing of bottom flange at end of cover plate
AISC-5A	W36 × I50	318	460	375	494	426	25 × 300 × 610	25 × 300 × 585†	bolted	E70TG-K2‡	2.5%	Same as AISC-3B
AISC-5B	W36 × 150	370	492	380	520	426	25 × 300 × 610	25 × 300 × 585†	bolted	E70TG-K2‡	0.5%	Brittle fracture at beam bottom flange connection. Fracture contained within column flange base metal
AISC-7A	W36 × I50	318	460	375	494	426	19 × 300 × 430	16 × 355 × 405	bolted	E70T-7	3.5%+	Gradual strength deterioration due to local buckling, and gradual tearing of fillet welds of cover plates to beam flanges

AISC-7B	W36 × l50	318	460	375	494	426	19 × 300 × 430	16 × 355 × 405	bolted	E70T-7	5.0%+	Same as AISC-7A
AISC-8A	W36 × l50	311	444	343	465	426	19 × 300 × 430	16 × 355 × 405	bolted	E70T-7	3.5%+	Same as AISC-7A
AISC-8B	W36 × l50	311	444	343	465	426	19 × 300 × 430	16 × 355 × 405	bolted	E70T-7	3.5%+	Same as AISC-7A
SAC-4	W36 × l50	292	421	329	437	257	25 × 300 × 405	25 × 355 × 405	bolted	E70T-8	3.7%+	Same as AISC-7A + significant panel zone yielding
NSF-5	W36 × l50	296	417	310	415	426	12 × 300 × 355	12 × 380 × 355	welded	E70T-8	3.3%+	Same as AISC-7A
NSF-6	W30 × l48	321	445	334	450	257	16 × 266 × 355	16 × 300 × 355	welded	E70T-8	3.8%+	Gradual tearing of fillet welds of cover plates to beam flanges; panel zone dominated inelastic response
NSF-7	W36 × l50	340	456	360	467	455	12 × 300 × 355	12 × 380 × 355	welded	E70T-8	3.8%+	Same as AISC-7A

*All bolted webs with fully tensioned high strength bolts and supplemental welds on web shear tab to develop 20% of nominal plastic moment of beam web; all welded webs by directly welding to column using complete joint penetration groove weld.
†Tapered bottom cover plate
‡Except E70T-7 used for bottom cover plate to column flange weld
§In S.I. units, W36 × 150 is W920 × 223, W30 × 148 is W760 × 221, W14 × 455 is W360 × 677, W14 × 426 is W360 × 634, W14 × 257 is 360 × 382.
(*From Engelhardt and Sabol 1996*)

TABLE 8.3 Summary of Results for Cover-Plated Connection Test Series

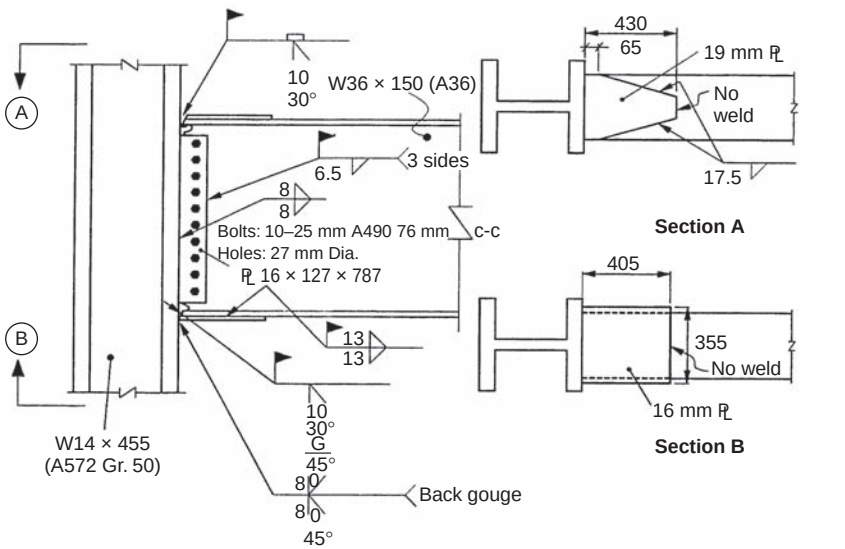

(a)

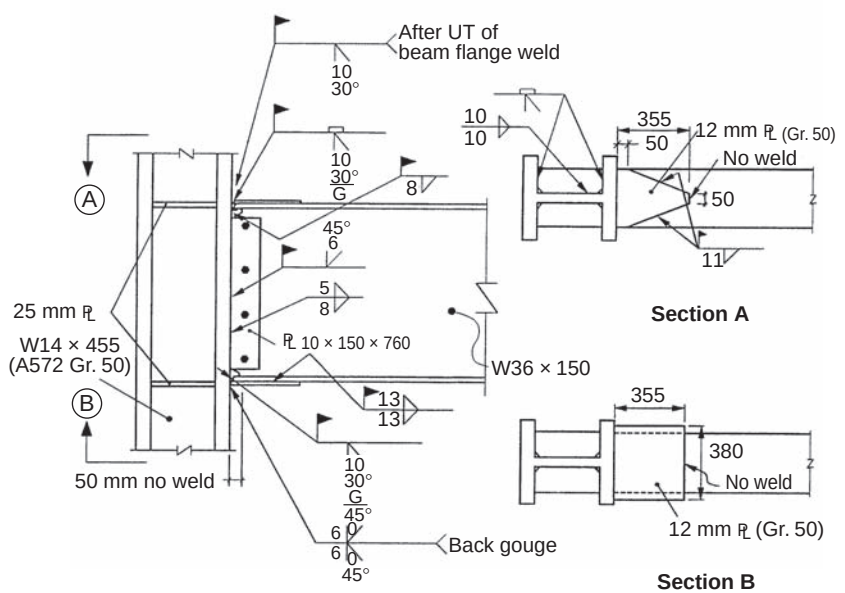

(b)

Figure 8.27 Moment connections with cover plates: (a) bolted web (specimen AISC-3A), (b) fully welded web (specimen NSF-7). (*Courtesy of M. D. Engelhardt, Dept. of Civil Engineering, University of Texas, Austin.*)

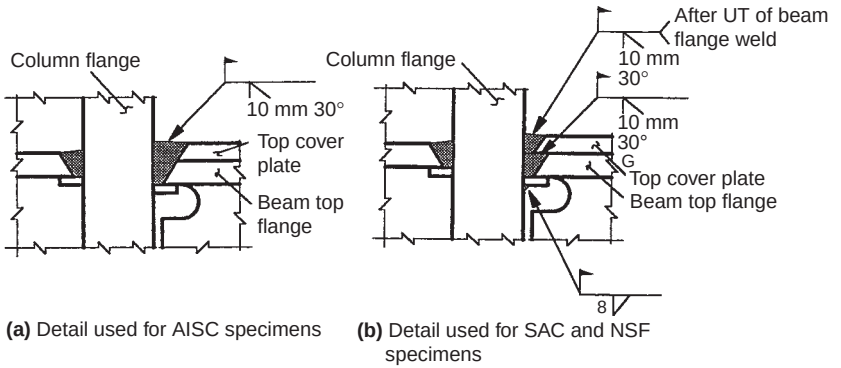

Figure 8.28 Typical groove weld details at top flange used for moment connection strengthened by cover plates. (*Courtesy of M. D. Engelhardt, Dept. of Civil Engineering, University of Texas, Austin.*)

bottom cover plate would have been shop-welded to the column flange and used in the field as an erection seat for the beam. This particular construction sequence also would have made it possible to perform ultrasonic testing at various stages of connection assembly and to fully weld the beam web, using the web tab as a backup plate. A welded web can transfer its share of the beam plastic moment, which makes possible the use of smaller cover plates. Smaller plates also minimize residual stresses due to weld shrinkage, and the likelihood of high triaxial tensile stresses at the column face. Separate welds for the flange and cover plate (Figure 8.28) also reduce this likelihood of developing detrimental triaxial stresses in the connection and enable individual ultrasonic inspection of the two welds.

As shown in Table 8.3, two-thirds of the cover-plated specimens developed total plastic rotations of 0.03 rad without brittle fracture. Note that in those specimens, the columns were designed with a strong panel zone that remained elastic throughout testing, with the exception of specimens SEC-4 and NSF-6 designed with lighter columns and for which panel zone yielding dominated the inelastic response. Results for a specimen with a fully welded web connector plate are shown in Figure 8.29. Yet, cover plates by themselves are not a panacea. As seen in Table 8.3, two of the specimens with bolted webs tested by Engelhardt and Sabol (AISC-3A and AISC-5B) failed in a brittle manner at plastic rotations of less than 0.02 rad, even though the groove welds had passed ultrasonic inspection. Each specimen that failed had a counterpart that exhibited satisfactory behavior.

Note that for the AISC-#B specimens, a Welding Procedure Specification was written and enforced, whereas for the AISC-#A specimens, the welder was permitted to weld on the basis of his experience.

Two different welders executed the AISC-3A and -3B specimens; both were uncomfortable with the setting recommendations from the

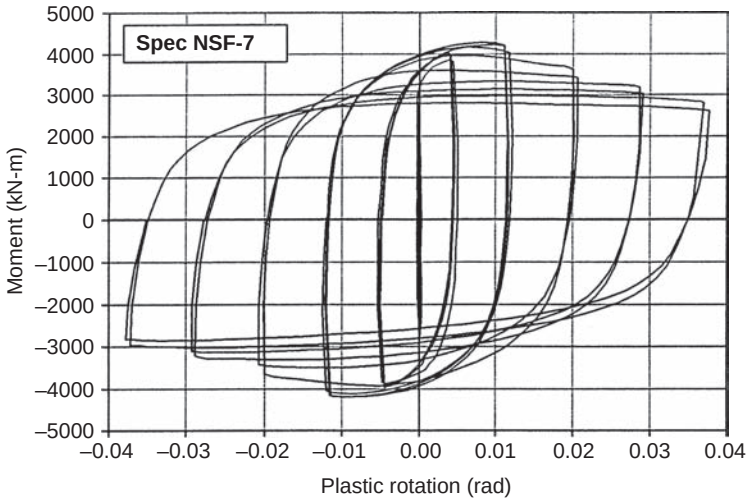

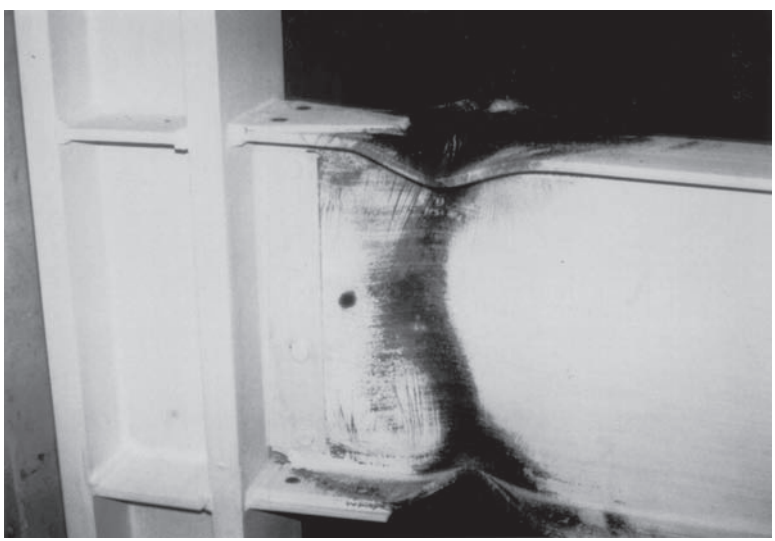

Figure 8.29 Moment connection with cover plates and fully welded web (specimen NSF-7): (a) hysteretic behavior. (b) specimen state at completion of test. (*Parts a and b courtesy of M. D. Engelhardt, Dept. of Civil Engineering, University of Texas, Austin.*)

electrode manufacturers. The Welding Procedure Specification was enforced for specimen AISC-3B, but the welder of specimen AISC-3A increased the voltage and current of the welding machine to enhance workability. Metallurgical study of the groove welds revealed the greater heat input to AISC-3A (that suffered brittle fracture) resulting in a fivefold lower weld toughness than in AISC-3B. As for the other

specimen with poor performance, AISC-5B, fracture was attributed to the larger-than-anticipated beam yield strength and the fact that long cover plates were used. These long plates developed the beam plastic moment farther from the column, resulting in larger bending moments at the column face.

Reviewing all the evidence, concerns remained regarding the use of cover plates. First, the panel zones in the very large columns tested by Engelhardt and Sabol (1996) did not yield—poor performance was reported in other tests that developed large panel zone deformations (Obeid 1996, Whittaker and Gilani 1996). Second, it was cautioned that overlaid welds should be accomplished only through use of identical electrodes; loss of weld toughness due to the mixing of weld metals has been reported (Wolfe et al. 1996). Note that section J2.7 of AISC (2010c) also warns that low notch-toughness welds may result from the mixing of two incompatible weld metals of high notch-toughness. Third, Hamburger (1996) reported that an estimated failure rate of 20% has been experienced when laboratory qualification testing of these connections was performed for specific design projects, which suggests that the cover plate detail may not be sufficiently reliable; Kim et al. (2000) also listed past instances of brittle failures. Fourth, the SAC Interim Guidelines (1995b) indicated that, conceptually, this connection could be exposed to some of the same flaws that plagued the pre-Northridge connections, namely, dependence on weld quality and through-thickness behavior of the column flange, potentially exacerbated by the thicker groove welds made necessary by the addition of cover plates. Finally, SAC (1997) reported that when the bottom cover plate is shop-welded to the column flange to be used as an erection seat for the beam, premature fracture can develop across the column flange as the seam between the bottom flange and cover plate acts as a notch that can trigger crack propagation.

Fewer tests on the use of upstanding beam flange ribs (Figure 8.26b) have been conducted since the Northridge earthquake, although this detail was investigated prior to 1994 (Tsai and Popov 1988). Overall, this type of rib detail appeared effective, but it was judged that additional testing was needed to determine how various design and detailing parameters influence its inelastic performance.

8.5.5.2 Initially Investigated Strengthening Strategies: Haunches

Haunches provide another intuitive way to make a connection stronger that its beam. Different haunch details have been tested, and many have exhibited satisfactory performance. Given the availability of less expensive alternatives, haunches have typically not been prequalified for new constructions (FEMA 2000a); however, they have been pre-qualified for the upgrading of existing structures, as fewer solutions can be easily implemented in that case (FEMA 2000b). A sample of typical experimental results is provided here to illustrate their behavior.

Uang and Bondad (1996) tested pre-Northridge specimens repaired with bottom flange triangular T-shaped haunches only, as shown in Figure 8.30. Continuity plates were added to the column at the level of the haunch flange. Two specimens were tested in a quasi-static manner, and two were tested dynamically with a maximum strain rate of 0.1 mm/mm/s. The repaired specimens performed much better than the pre-Northridge specimens, with beam plastic hinges developing

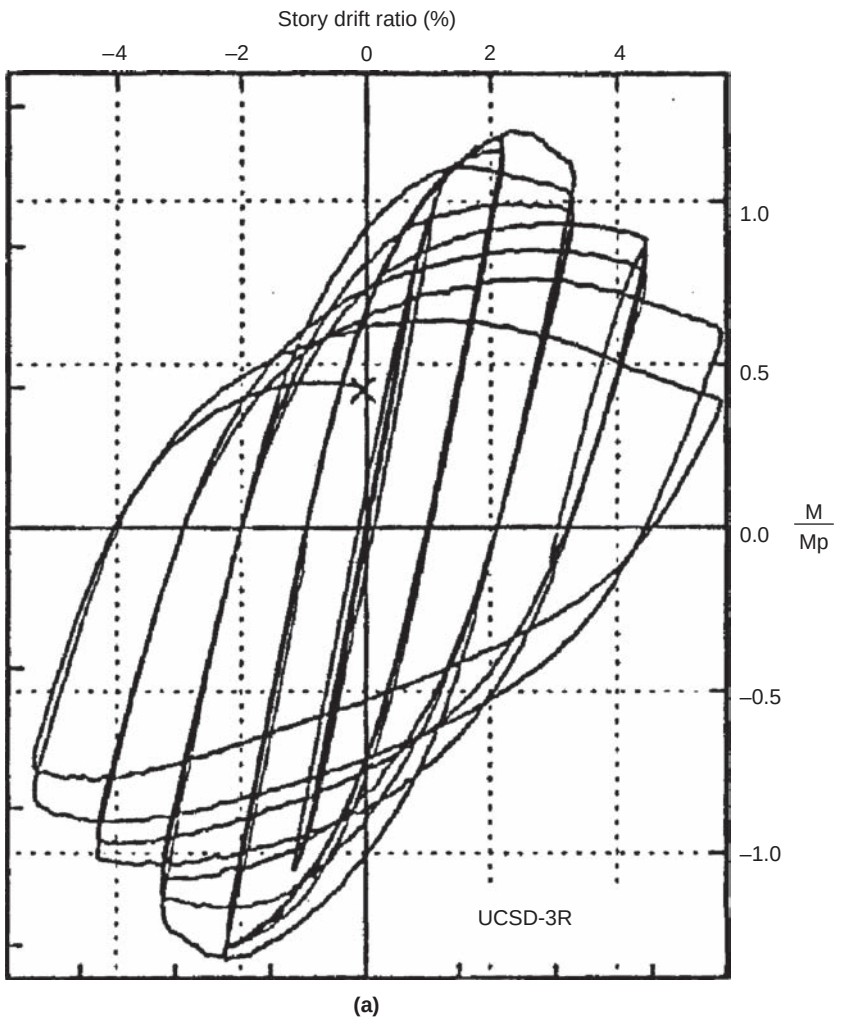

Figure 8.30 Moment connection of W760 × 147 beam (W30 × 99 in U.S. units) of A36 steel to W360 × 262 column (W14 × 176 in U.S. units) of A572 Grade 50 steel, with bottom flange haunch: (a) hysteretic behavior in terms of load versus cantilever beam tip deflection at 3.6 m from centerline of the column; (b) specimen state at first cycle of –7.0 in tip deflection.

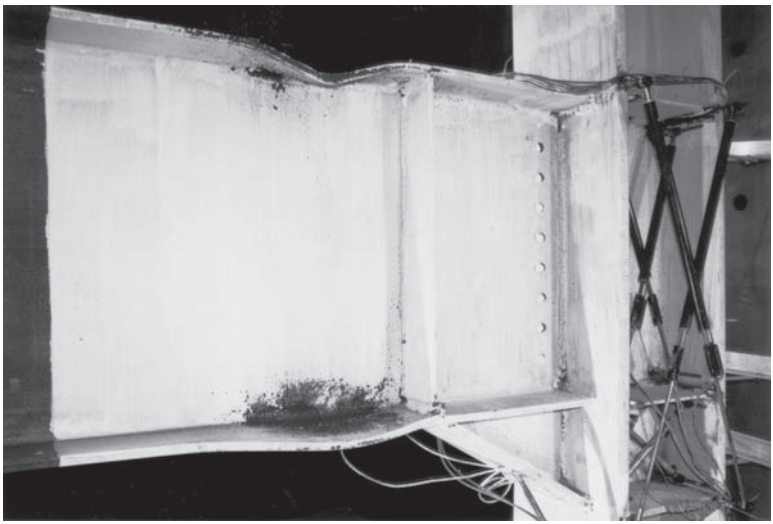

(b)

FIGURE 8.30 (*Continued*)

outside the haunch. Plastic deformation of the panel zones was also reduced, and nearly all of the inelastic action was concentrated in the beams. Note that the presence of a haunch increases the depth of the panel zone, thus reducing the extent of panel zone yielding.

Total beam plastic rotations in excess of 3% were obtained in the quasi-static tests. Failure was defined by excessive strength degradation due to local buckling of the beam flanges (Figure 8.30), although the specimens could sustain larger plastic rotations and dissipate further hysteretic energy while undergoing further strength degradation. In one of the dynamically tested specimens, in addition to repairing the fractured bottom flange with a haunch, the beam top flange with pre-Northridge type of groove-welded joint was strengthened by the addition of a pair of rib plates on the underside of the flange. This detail, developed for strengthening existing connections, avoids the need to remove the concrete slab around the column, but would still require removal of the building's facade (i.e., cladding panel or other architectural finishes) to provide access to one half of the beam flange for perimeter frames. Although the welded top flange joint fractured during retesting, the two vertical ribs served their intended purpose by maintaining the integrity of the connection.

Whittaker et al. (1995) reported adequate performance for pre-Northridge specimens repaired and strengthened by the addition of triangular T-shaped haunches to both top and bottom flanges. Panel zone yielding was substantially eliminated in the strengthened specimen and significant beam plastic rotations were obtained (Figure 8.31). However, with failure defined as the point at which the

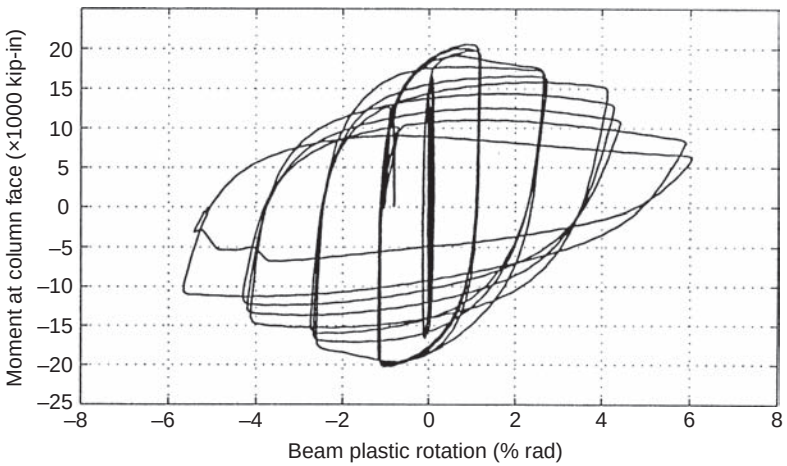

(a)

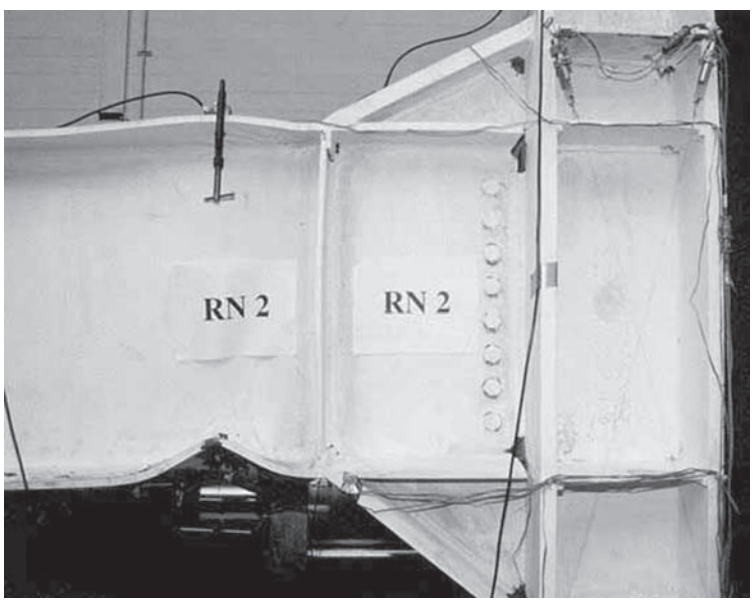

(b)

Figure 8.31 Hysteretic behavior of moment connection with top and bottom flange haunches, in terms of moment versus beam plastic rotation, and specimen state upon completion of test. (*Courtesy of the SAC Joint Venture, a Partnership of the Structural Engineers Association of California, Applied Technology Council, and Consortium of Universities for Research in Earthquake Engineering.*)

resistance degraded to 80% of the maximum value, beam plastic rotations of 2.7% was reached prior to failure.

Hybrid connections with cover plate reinforcement of the top flange and haunch reinforcement of the bottom flange have also been considered. Excellent performance was obtained for a particular configuration and detailing (Figure 8.32). For this particular design, the

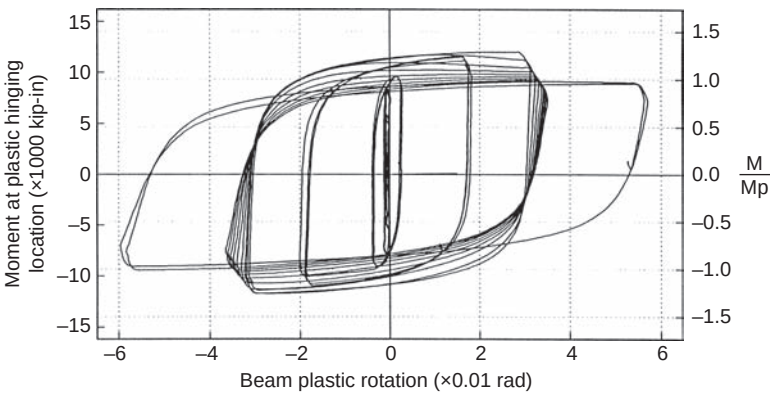

(a)

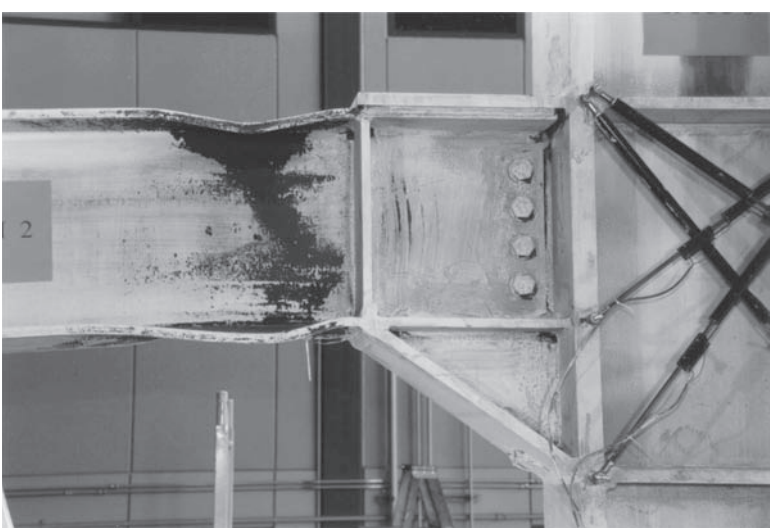

(b)

Figure 8.32 Hysteretic behavior of moment connection with top flange cover plate and bottom flange haunch, in terms of moment at hinge location versus beam plastic rotation at hinge location and specimen state at ninth cycle of +3.5 inches tip deflection. (*Courtesy of M. S. Jokerst, Forell/Elsesser Engineers Inc., San Francisco.*)

cover plate was shop-welded to the beam with a fillet weld, and only the cover plate (not the beam top flange) was groove welded to the column; the backup bar was left in position with a closure fillet weld (Noel and Uang 1996).

In summary, the available experimental data suggest that using triangular T-shaped haunches is an effective means by which to strengthen a connection. Their high redundancy also contributes to preserve good plastic behavior if one of the full penetration groove welds fails. However, haunches are expensive to construct, and the top haunch, when present, can be an obstruction above the floor level.

Straight haunches have been proposed as a more economical alternative solution (Uang and Bondad 1996). The direct strut action that develops in sloped haunch flanges is not possible in this alternative, and the beam flange force must be transferred to the haunch flange via shear in the haunch web. In the specimen tested, stress concentration at the free end of the haunch fractured the weld between the beam flange and haunch web at that free end (Figure 8.33). Additional stiffeners at the free end of the haunch to tie the beam and haunch together, or the use of a sloped free end to reduce the stress concentration, might be effective in preventing the observed fracture, but the adequacy of such enhancements must be validated by testing.

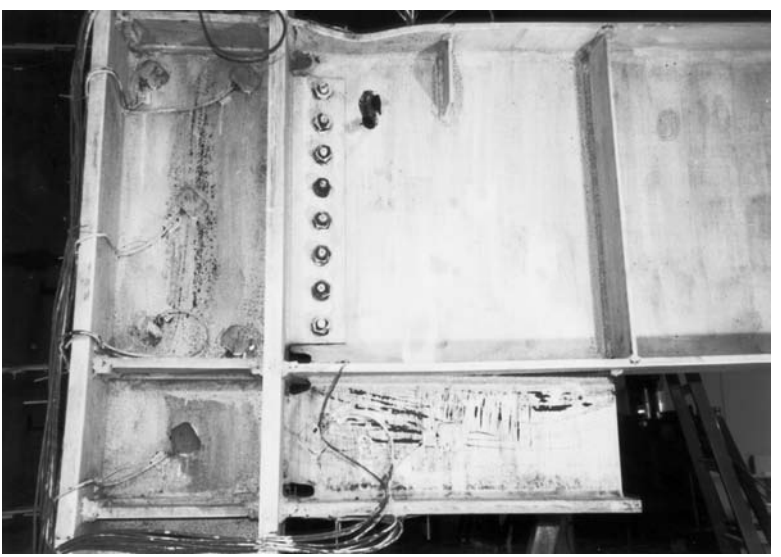

Figure 8.33 Fracture between straight haunches and beam bottom flange at the free end of the haunch and beam top flange local buckling.

8.5.5.3 Initially Investigated Weakening Strategies

Plastic hinges can be moved away from the face of a column if one reduces the area of the beams' flanges at a selected location. By strategically weakening the beam by a predetermined amount over a small length, at some distance from the welded connection, and by taking into account the shape of the moment diagram to ensure that yielding will occur only at this location of reduced plastic moment capacity, one can effectively protect the more vulnerable beam-to-column connection. One can do this in a number of ways, such as by drilling holes in the flanges or by trimming the flanges. The latter solution has found broad acceptance in a relatively short time.

The idea of shaving beam flanges to improve the seismic performance of steel connections was first proposed and tested by Plumier (1990). Chen and Yeh (1994) confirmed the effectiveness of this approach to enhance the ductility of beam-to-column connections. Although this concept was patented in the United States in 1992, the owner of the patent waived any commercial royalty rights for its public use after the Northridge earthquake.

Two flange shapes have received considerable attention following the Northridge earthquake (Figure 8.34). The first type

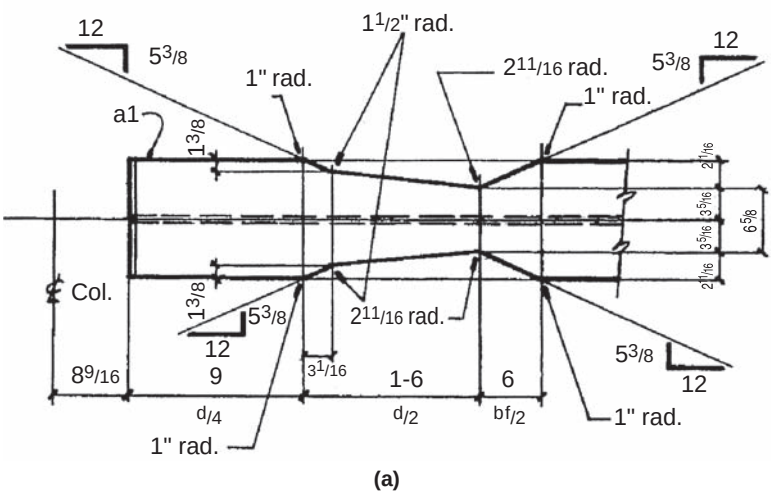

Figure 8.34 Reduced beam section designs: (a) Tapered flange profile. (b) elevation and plan view of radius-cut flange profile; (c) information on radius-cut typical flange profile. (*Part a from* Modern Steel Construction, *vol. 36, no. 4, "The Dogbone: A New Idea to Chew On" by N. R. Iwankiw and C. J. Carter, 1996, with permission from the American Institute of Steel Construction. Parts b and c Courtesy of M. D. Engelhardt, Dept. of Civil Engineering, University of Texas, Austin.*)

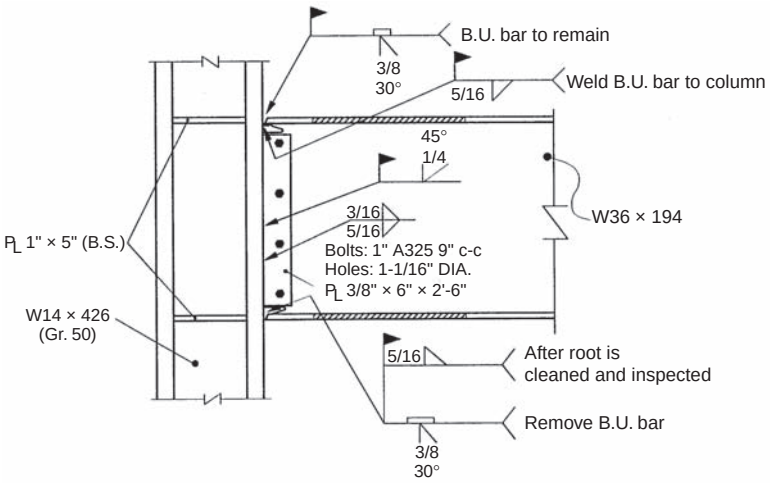

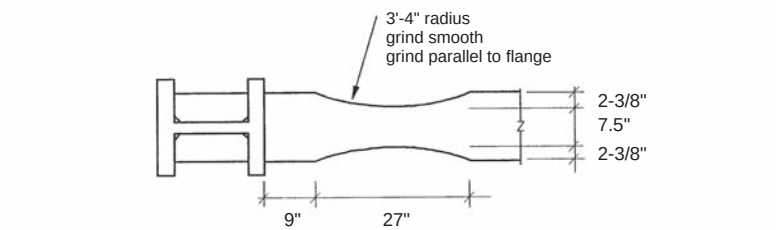

(b)

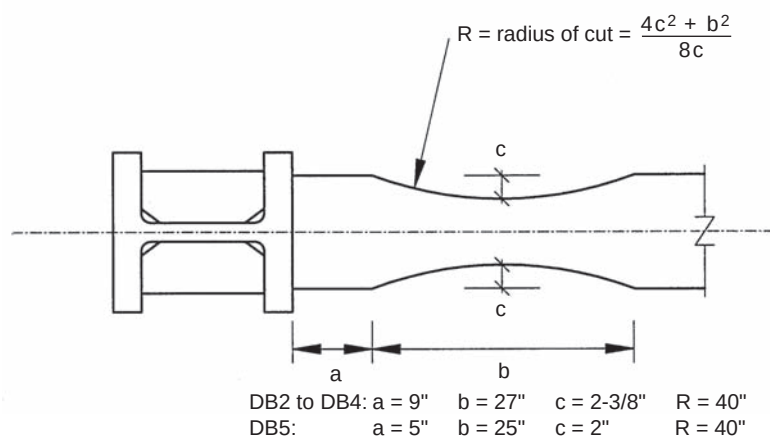

(c)

FIGURE 8.34 (*Continued*)

(Chen et al. 1996, Iwankiw and Carter 1996) has flanges tapered according to a linear profile intended to approximately follow the varying moment diagram (Figure 8.34a). The second profile (Engelhardt et al. 1996 and many others subsequently) is shaved along a circular profile as described in Figures 8.34b and c. Both reduced beam section (RBS) profiles (a.k.a. "dogbone" profiles) have achieved plastic rotations in excess of 3%, as shown in Figure 8.35. A variant of the linear taper, with additional rib plates welded to the beam flanges to further reduce stresses in the flange groove welds, has also been successfully tested (Uang and Noel 1995).

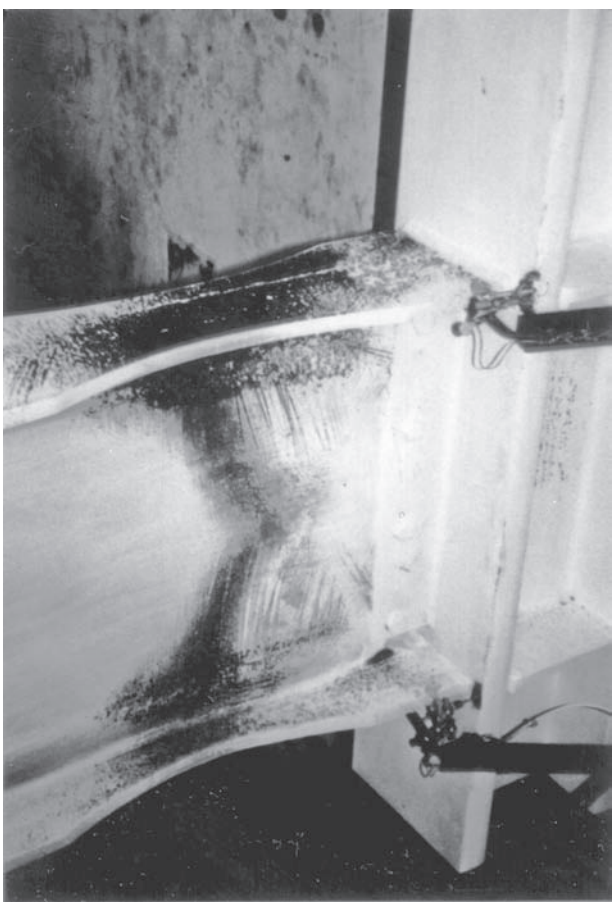

(a)

Figure 8.35 Radius-cut flange profile moment connection: (a) specimen state at completion of test, (b) specimen state at completion of test: side view and top view, (c) hysteretic behavior in terms of moment at column face versus beam plastic rotation. (*Parts a to c courtesy of M. D. Engelhardt, Dept. of Civil Engineering, University of Texas, Austin.*)

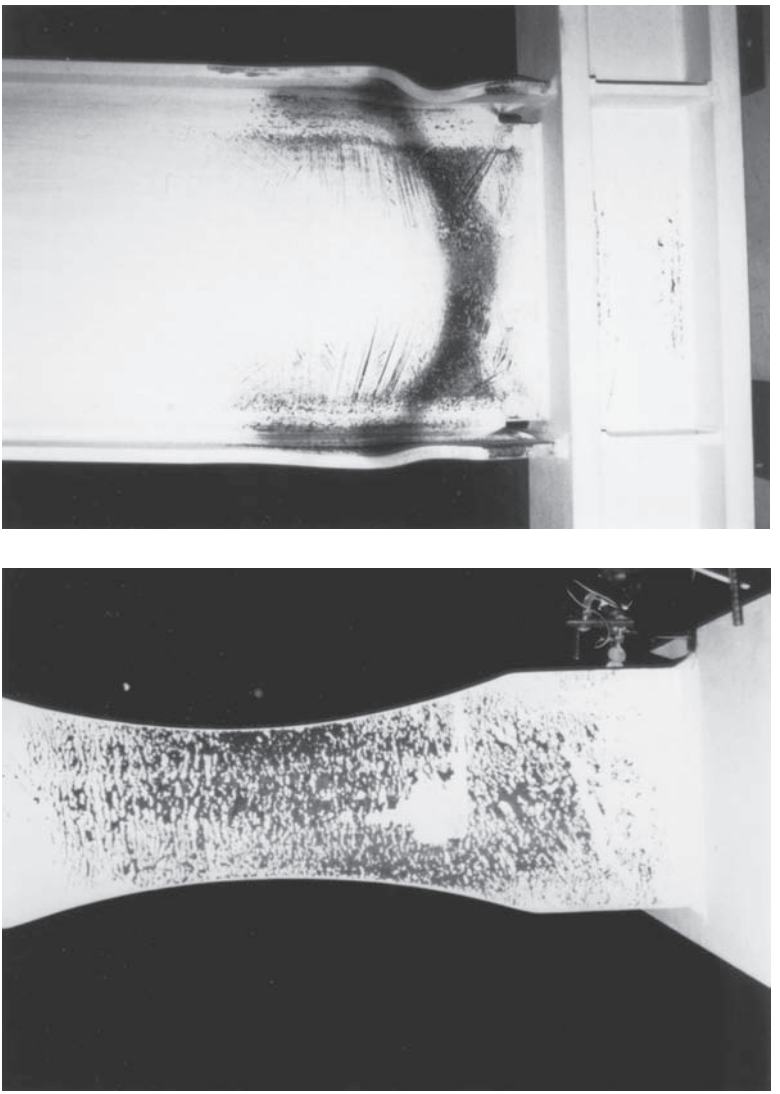

(b)

Figure 8.35 (*Continued*)

In all cases, trimming of the flanges delays local buckling, but increases the likelihood of web buckling and lateral-torsional buckling due to the reduction in flange stiffness. The RBS connection usually experiences web local buckling first, followed by flange local buckling and lateral-torsional buckling, resulting in significant strength degradation. The addition of lateral bracing at the reduced

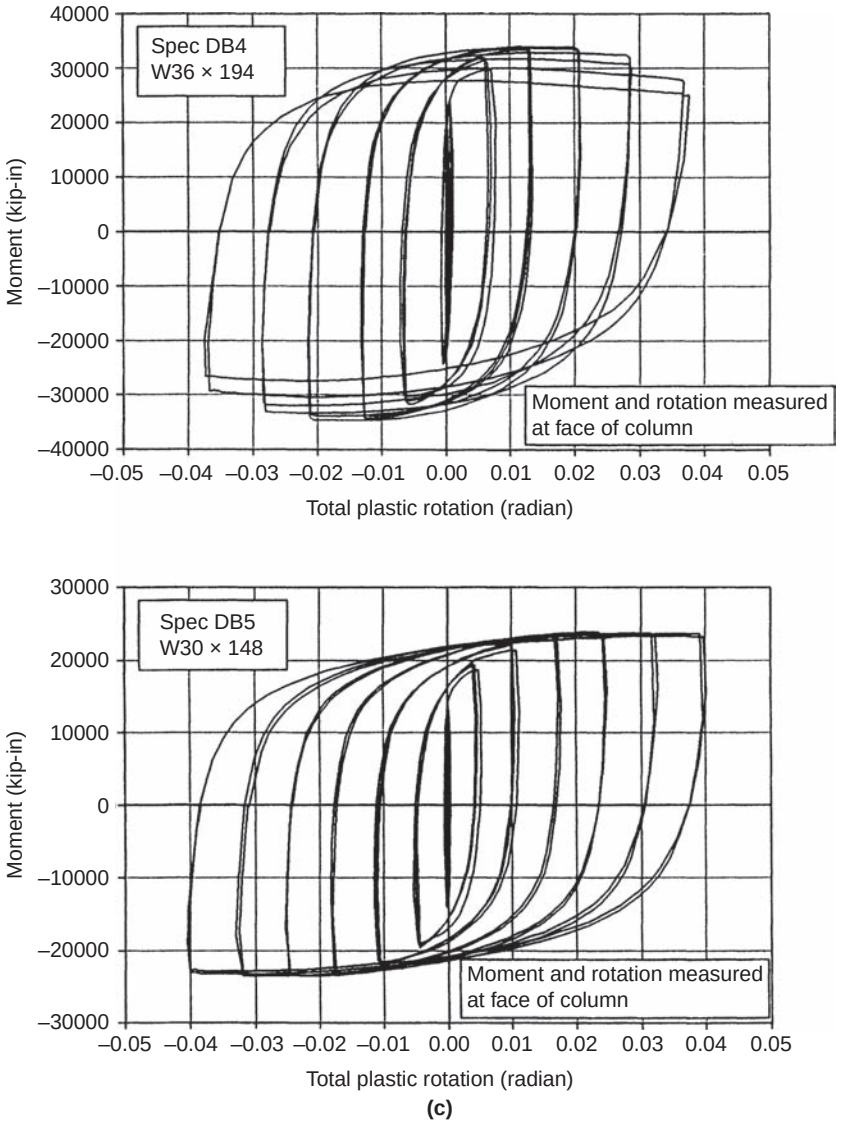

Figure 8.35 (*Continued*)

beam section delays this strength degradation. High plastic rotation capacities have been achieved when lateral bracing was provided at the end of the dogbone farthest away from the column. Tests indicate a required lateral bracing strength of approximately 4% of the actual force developed by the beam flange (Uang and Noel 1996); AISC 341 specifies that 6% of the expected beam flange capacity at the hinge

location be used instead. The RBS concept was eventually prequalified, as described in a later section.

8.5.6 Post-Northridge Beam-to-Column Prequalified Connections

8.5.6.1 New Construction

The selected results presented above provide only a sample of the numerous beam-to-column connection tests conducted in the years following the Northridge earthquake. The online database of tests performed as part of the FEMA/SAC project alone contains results for 513 specimens (available at www.sacsteel.org/connections). Review of this extensive information led to a selected number of pre-qualified connections presented as part of the FEMA 350 "Recommended Design Criteria for Moment Resisting Steel Frames" (FEMA 2000a), to be used together with the design principles described later. This same information was later considered by an AISC Review Panel in developing the AISC 358 "Prequalified Connections for Special and Intermediate Moment Resisting Frames for Seismic Applications," a document referenced by standard specifications and thus more readily accepted by building officials. The FEMA-350 prequalified connections have not all been simultaneous approved into the AISC 358 document; the latter document being an American National Standards Institute (ANSI)-approved consensus-based standard, the critical reassessment of all experimental evidence for some specific types of connections was either incomplete at key publication times, or failed to convince the AISC Review Panel.

Focusing here on connections for SMRF applications, Table 8.4 lists the various prequalified connections recognized by each documents (at various times). Those prequalified by AISC 358-10 are schematically illustrated in Figure 8.36. FEMA 350 prequalifies four welded and three bolted connections, namely, the Welded Unreinforced Flanges-Welded Web (WUF-W), the Free Flange (FF), the Welded Flange Plate (WFP), the Reduced Beam Section (RBS), the Bolted Unstiffened End Plate (BUEP), the Bolted, Stiffened End Plate (BSEP), and the Bolted Flange Plates (BFP)—note that a Double Split Tee (DST) connection is also prequalified as a partially restrained connection. Of those, AISC 358-10 only prequalifies the WUF-W, RBS, BUEP, BSEP, and BFP connections, and adds the proprietary cast-steel Kaiser Bolted Bracket (BB) connection for which licensing fees have been waived (Hamburger et al. 2009).

The characteristics of the RBS detail have been thoroughly described in a previous section; the prequalified connection is a radius cut of prescribed geometry, allowing up to a 50% reduction of the flange width. The WUF-W connection essentially relies on complete joint penetration welded web and flanges using a shear tab of specified

	WUFW*	FF*	WFP*	RBS*	BUEP*	BSEP*	BFP*	BB*
Prequalified By:								
FEMA 350	X	X	X	X	X	X	X	
AISC 358 2005†				X	X	X		
AISC 358 2010	X			X	X	X	X	X
Critical Beam Parameters								
Max. Depth	W36	W30	W36	W36	W24 (55")	W36 (Table)	W30 (W36)	– (W33)
Max. Beam Weight (lb/ft)‡	– (150)	– –	– –	– (300)	– (None)	– (None)	– (150)	– (130)
Min. Span to Depth Ratio	7	7	7	7	7	7	8 (9)	– (9)
Max. $b/2t_f$ ‖	–	$52/\sqrt{F_y}$	–	$52/\sqrt{F_y}$ §	–	–	–	–
Max. Flange Thickness	1"	0.75"	1"	1.75"	0.75"	1" (Table)	0.75" (1")	– (1")

Note: Permissible material per FEMA 350: Beam can be A572 Grade 50, A992, A913 Grade 50/S75; columns can be A572 Grade 50, A913 Grade 50 and 65, A992. Note that A913 Grade 50/S75 has a specified maximum yield point to tensile strength ratio. AISC 358 permitted material are same as in AISC 341, except BB which is an ASTM A958 Grade SC8620 class 80/50 cast steel.

FEMA 350 only prequalifies W12 and W14 columns, except for BUEP case for which W8 and W10 are also permitted. AISC 358-10 permits a broad range of rolled and built-up columns (I-shaped, cruciform, box-shaped, and boxed wide-flange).

*WUF-W = Welded Unreinforced Flanges-Welded Web; FF = Free Flange; WFP = Welded Flange Plate; RBS = Reduced Beam Section; BUEP = Bolted, Unstiffened End Plate; BSEP = Bolted, Stiffened End Plate; BFP = Bolted Flange Plates; BB = Kaiser Bolted Bracket

†Prior to Supplement 1, published in 2009

‡Required only by AISC 358

§Measured at the ends of the center 2/3 of the reduced section of the beam

‖AISC 358 requires web and flange width-to-thickness ratios to conform to AISC 341 limits. Values in Table are listed when specified by FEMA 350.

TABLE 8.4 Partial List of Limits of Applicability of Prequalified SMRF Connections (Values in Parenthesis Are AISC 358-10 Values when Different from FEMA 350)

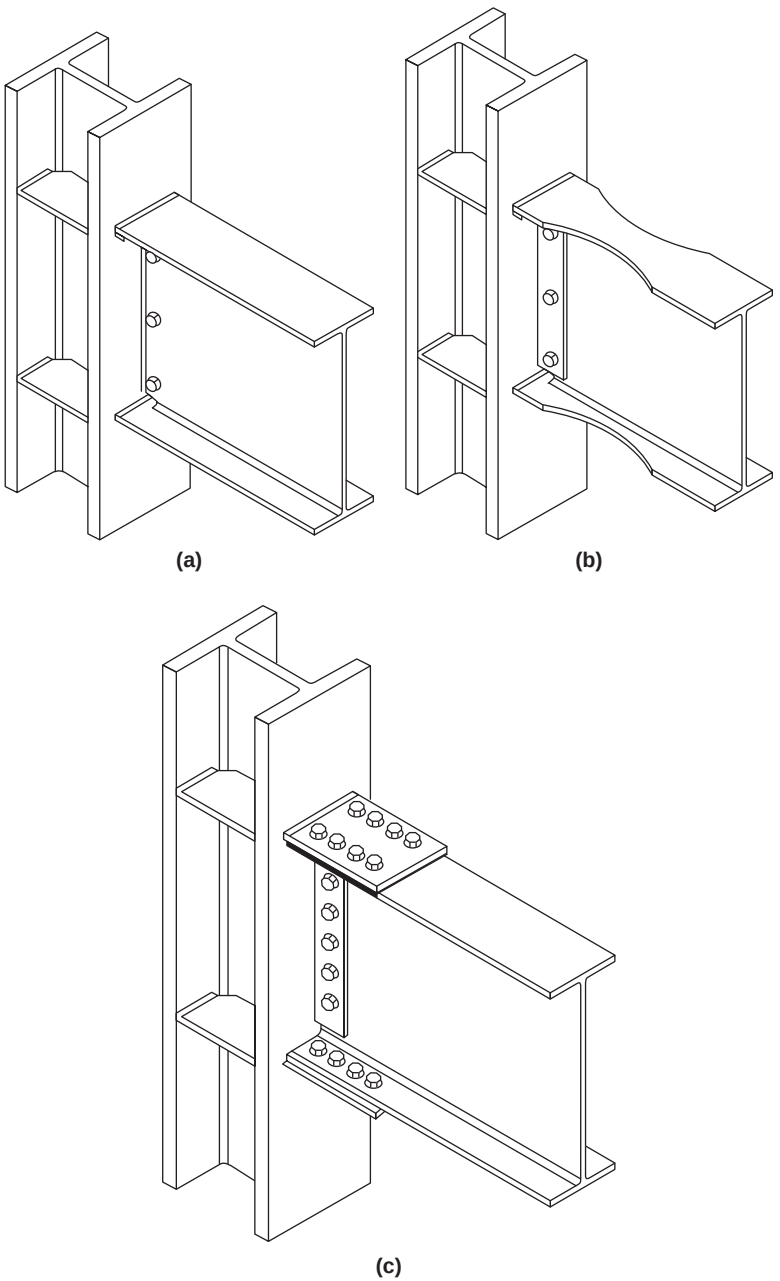

Figure 8.36 Sketch of AISC 358 2010 prequalified SMRF connections: (a) WUF-W; (b) RBS; (c) BFP; (d) BUEP and BSEP, and; (e) BB. Acronyms are defined in a footnote of Table 8.4. (*Courtesy of Ron Hamburger, Simpson Gumpertz & Heger, San Francisco, CA.*)

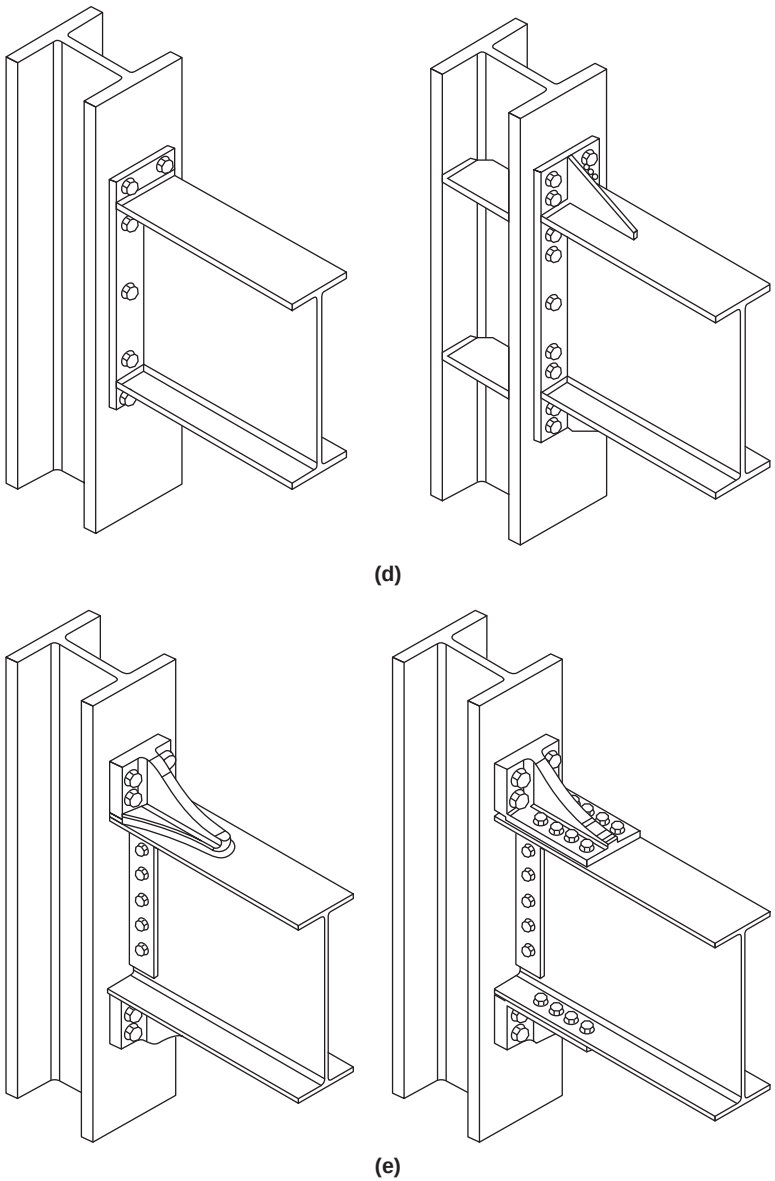

Figure 8.36 (*Continued*)

minimum geometry, prescribed detailing and welding procedures, and rigorous quality controls. The FF (Figure 8.37) detail was developed building on the observation from finite element analyses that, contrary to classic beam theory, the beam flanges in pre-Northridge moment connections contributed substantially in transferring the

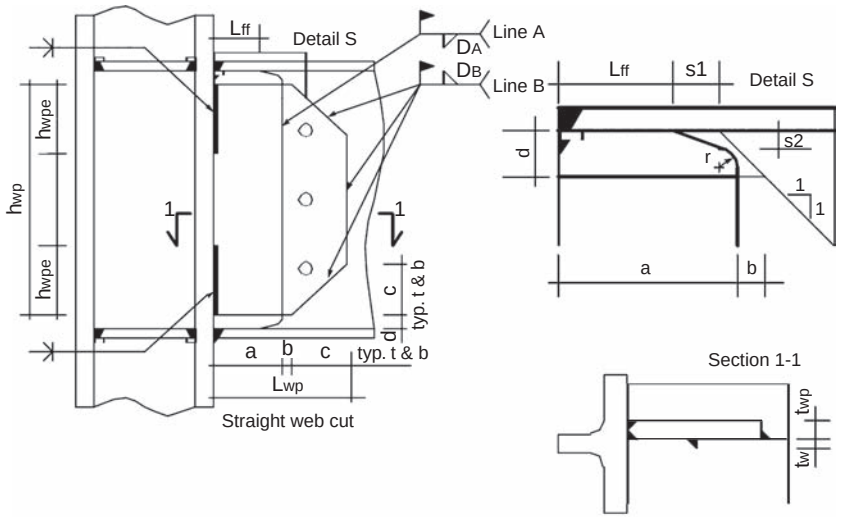

Figure 8.37 Free flange connection concept. (*Courtesy of B. Stojadinovic, Dept. of Civil and Environmental Engineering, University of California, Berkeley.*)

shear to the columns, resulting in "flange overload" (Goel et al. 1997). The particular geometry of FF connections is designed to prevent that shift of the shear from the web to the flanges, by substantially cutting back the beam web and using a large welded shear tab to transfer the beam's shear to the column (Choi et al. 2003). The WFP connection uses welded shear tabs and flange cover plates, without welding the ends of the beam flanges to the column.

The prequalified bolted connections require that substantially more limit states be checked, and are sometimes only workable for smaller beams. The BFP connection is analogous to the WFP one, but with cover plates and shear tabs bolted to the beam. The BUEP and BSEP connections are sized to remain elastic and allow development of beam plastic hinging. As such, bolts or end-plate yielding are undesirable failure modes. Bolted end-plate moment connections are popular where shop-welding and field-bolting is the preferred assembly method. Connections with added plate stiffeners, or with a thicker end plate and stronger bolts, detailed per the BUEP or BSEP requirements, have exhibited superior energy dissipation capacity compared with the limited cyclic plastic deformation capacity of others sized in compliance with the conventional design procedure in place prior to the Northridge earthquake (Ghobarah et al. 1990; Ghobarah et al. 1992; Osman et al. 1990; Tsai and Popov 1988, 1990a).

The BB connection consists of high-strength cast steel brackets, either welded or bolted to the beam flanges and bolted to the column, and available in a fixed number of sizes. These castings are subjected to prescribed quality control measures.

Table 8.4 summarizes some of the limits that restrict the applicability of each connection type. Beyond those listed in that table, AISC 358 specifies additional limits that restrict various column parameters, various geometry aspects for welded and bolted configurations, and various other connection-specific details. Guidance is also provided with respect to the lateral bracing requirements, protected zone region, and respective location of plastic hinging, that are to be considered for the design of each connection (as will be discussed later). A testing program conducted in compliance with the requirements outlined in the Appendix of AISC 341 is required to qualify connections that exceed any of the limits listed in that table, or for different types of connections altogether, which in either case can be an expensive endeavor.

In that perspective note that some proprietary connection systems have also been developed (Nelson 1995), and although these are not prequalified by either FEMA 350 or AISC 358, some jurisdictions and authorities have accepted their implementation in various projects on the basis of experimental evidence. The database of past tests conducted to investigate and demonstrate satisfactory seismic performance varies from one type of patented connection to the other, and peer review is sometimes required before project-specific implementation. Examples of proprietary systems used in a number of past projects include the Side Plate (SP) connection and the Slotted Web (SW) connection; information on their performance and implementations can be obtained from the respective licensors of these technologies.

There is no definite answer either as to which of the above connections is the most cost effective. Cost comparisons need to account for cost of connections, royalty fees for proprietary systems, and influence of the connection detail on the weight of the steel frame and the cost of the foundations.

The FEMA 350 and AISC-358 procedures to design beam-to-column connections of the type described above are sensibly similar; however, only the AISC procedures are considered from this point onward—and presented in Section 8.6. Nonetheless, the FEMA 350 report is a comprehensive resource that documents much of the fine points that are part of this methodology and refers to the relevant literature. As such, it is a valuable recommended reading.

8.5.6.2 Retrofits and Repair of Existing Construction

FEMA 350 and AISC-358 are focused on new construction. Different types of connections and levels of expected seismic performance may be adopted with respect to repair and rehabilitation works. Often, repairs are emergency measures that bring a damaged structure back to its pre-earthquake condition. If the exact same earthquake that initially damaged a structure would strike again after completion of repairs to the structure, one could reasonably expect the same damage to recur (assuming, obviously, that repairs were not accompanied by some measures of strengthening). Rehabilitations (also called

retrofits or modifications in some documents) are measures intended to enhance the seismic performance of an existing structure.

Seismic rehabilitation is a complex subject whose breadth exceeds the scope of this book. In principle, the connection strategies developed for new construction should be equally effective in existing buildings. Unfortunately, many of those solutions cannot be economically implemented in existing buildings without major modifications. For example, new structural elements added to a connection, such as haunches, will have to work in parallel with the existing flange groove welds recognized as likely to perform poorly in future earthquakes, and additional measures may also be necessary to correct these weld deficiencies. Likewise, moment-resisting frames in existing buildings are frequently located at the edge of buildings (i.e., the optimal location to provide seismic torsional resistance in plan); as a result, access to the outside face of the connection is not possible without removal of the exterior cladding, by itself a practical impediment to the implementation of some seismic rehabilitation strategies. Although many of the concepts and details presented here for new construction can be applied to seismic rehabilitation, the FEMA 351 and FEMA 352 reports (FEMA 2000b, 2000c) provide specific information respectively targeted to address retrofits and repairs.

8.5.7 International Relevance

Moment frame connections identical to those that fractured during the Northridge earthquake have also been commonly used in other countries (e.g., Tremblay et al. 1995). Furthermore, irrespective of the types of moment connections used, the Northridge experience reinforces the need for substantial full-scale experimental verification of connection details, for quality workmanship and inspection, and for periodic experimental re-evaluation of accepted practices to assess the significance of accumulated changes in materials properties, welding procedures, and other issues as the steel industry further evolves. A brief review of the Japanese experience is instructive in this regard.

8.5.7.1 Kobe Earthquake Experience

Steel design practice in Japan has favored the use of "column trees" in the construction of moment-resisting frames. This concept typically involves the welding of stub-beams to a column prior to its shipment to the building site where the remaining beam segments are field-bolted to the stub-beams (Figure 8.38). In principle, all welds of columns, beams, and continuity plates (known as diaphragms in Japan) are accomplished in the shop, with automated welding processes and under tight quality control (Nakashima et al. 2004). For that reason, such connections were thought to be superior to the prequalified moment connection used in the United States prior to the Northridge earthquake. Unfortunately, the Kobe earthquake, striking exactly one year after the Northridge earthquake, revealed this belief to be partly unfounded (Tremblay et al. 1996).

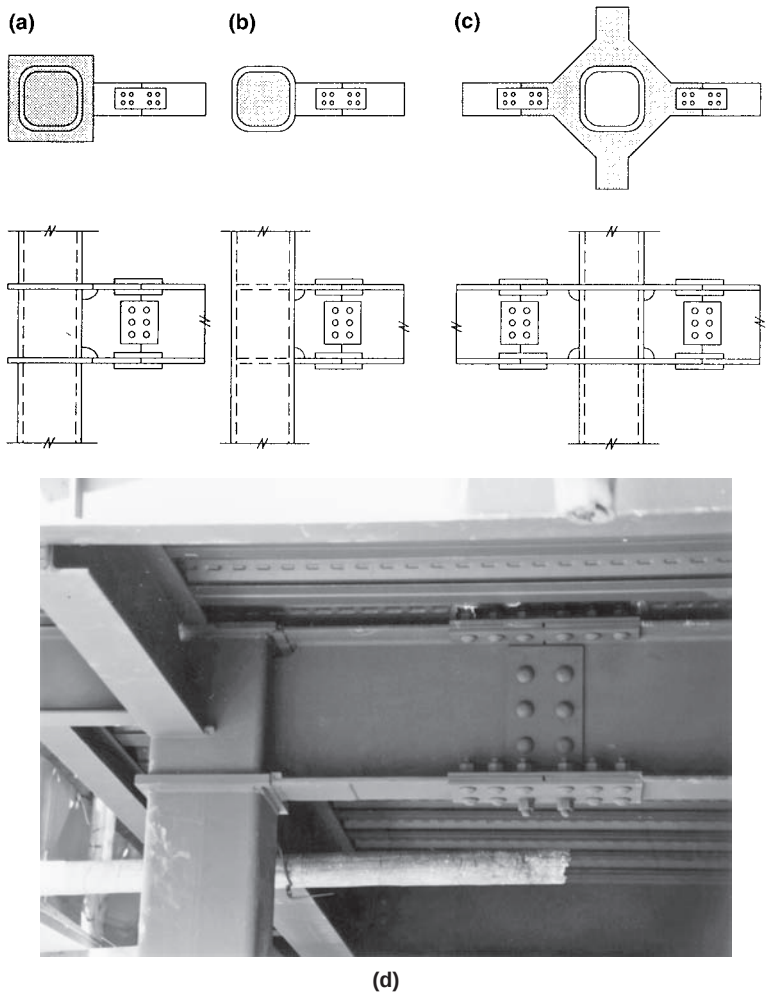

Figure 8.38 HSS columns in Japanese column-tree moment-resisting frames, with: (a) through-diaphragm; (b) interior diaphragm; (c) exterior diaphragm; (d) typical column-tree construction with through-diaphragm.

An investigation by the Steel Committee of the Architectural Institute of Japan covering 988 modern steel buildings following the 1995 Hyogo-ken Nanbu (Kobe) earthquake reported 332 cases of severely damaged buildings, 90 collapses, and 113 buildings for which damage to beam-to-column connections was observed (AIJ 1995, Nakashima 2001, Nakashima et al. 1998, Nakashima et al. 2000). Numerous cases of brittle fractures occurred, and 47 of the buildings that collapsed were moment frames constructed with the column tree system. The tallest steel frame buildings that collapsed had five stories. It is significant in this regard that in typical Japanese buildings, all

frames throughout a building have rigid moment-resisting beam-to-column connections, contrary to North American practice, in which moment-resisting connections are limited to a few frames in each principal directions of a building.

The beam-to-column failures observed during the Kobe earthquake differed somewhat from the Northridge failures in that cracking and fractures were frequently (but not always) accompanied by plastic hinging in the beams. This evidence of plastification was observed mostly in the more modern moment frames having square-tube columns and full penetration welds of the stub-beams to the diaphragms. In the majority of these cases, no sign of plastification was observed in the columns. Most of the fractures occurred in the lower flange of the beams, and the beams exhibited clear signs of plastic hinging accompanied by local buckling of the flanges (Figure 8.39), although, in some cases, the level of plastification was modest. Typically, fracture initiated either from the corner of a weld access hole, near a run-off tab or a weld toe, or in the heat-affected zones in the beam flange or diaphragm. In many cases, the fracture progressed into the beam's web (e.g., Figure 8.39b), and, in some cases, propagated into the column flanges (e.g., Figure 8.39d).

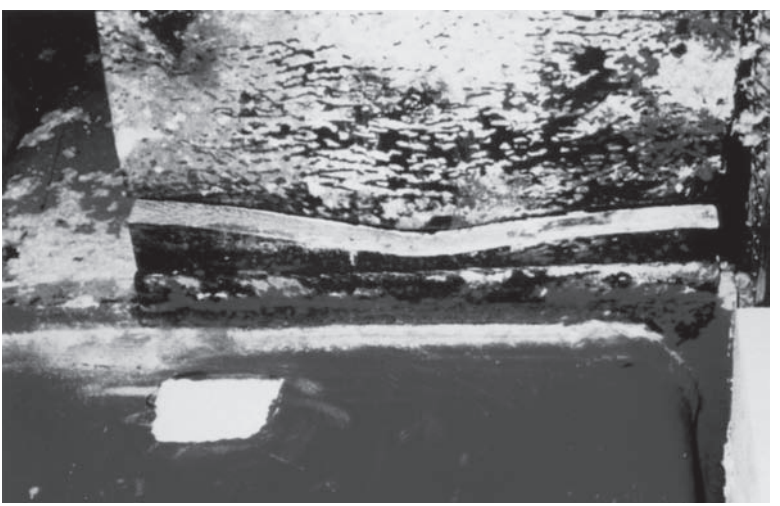

(a)

Figure 8.39 Damage to Japanese column-tree moment connections in modern moment-resisting frames with square-tube columns and full penetration welds at the beams, due to the Hyogo-ken Nanbu (Kobe, Japan) earthquake: (a) fracture at the lower beam flange; (b) propagation of fracture in the beam web; (c) fracture initiated in the heat-affected zone of the diaphragm, (d) propagation of fracture in the column. (*Parts a to d from* Performance of Steel Buildings during the 1995 Hyogo-ken Nanbu Earthquake *by Architectural Institute of Japan, courtesy of the Committee on Steel Structures of the Kinki Branch of the Architectural Institute of Japan.*)

(b)

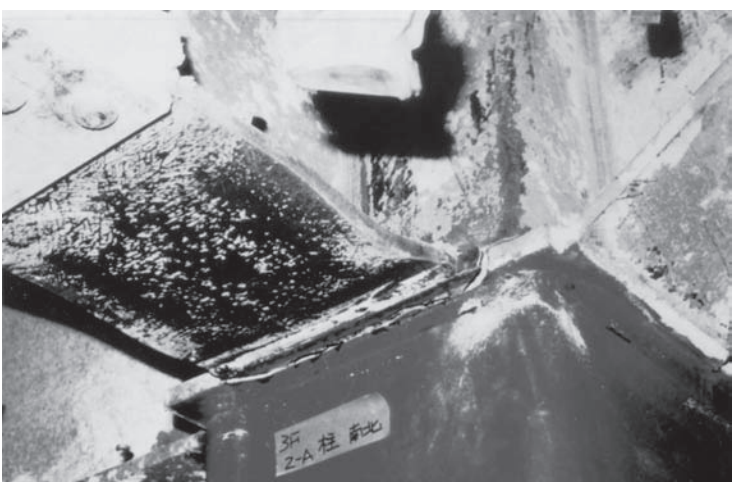

(c)

Figure 8.39 (*Continued*)

(d)

Figure 8.39 (*Continued*)

Many beam-to-column connections cracked and fractured without any signs of plastification when fillet welds were used in lieu of full penetration groove welds. These fillet welds were often too small to develop the capacity of the connected members (Figure 8.40a). Many other types of moment connections also suffered serious damage (Figure 8.40b). Notably, when tube columns were used, cracking and fracture frequently occurred in the columns above or below the top or bottom diaphragm (Figure 8.41a), sometimes leading to complete overturning and collapse of the structure (Figure 8.41b). Damage to the beam-to-column connections of at least 59 moment frames having square-tube columns was reported by the AIJ, with about 70% of those rated as either collapsed or severely damaged. Although most of those surveyed buildings that collapsed had fillet-welded moment connections, at least three buildings having full-penetration welded moment connections collapsed (AIJ 1995).

8.5.7.2 Post-Kobe Beam-to-Column Connections

Notable differences existed between North-American pre-Northridge and Japanese pre-Kobe practices (Nakashima et al. 2000), and logically still remains after these two earthquakes (Nakashima 2001, Nakashima et al. 2000). Moment frames designed and constructed in compliance with the best Japanese practices at the time of the Kobe earthquake arguably performed relatively well in spite of the reported failures. Consequently, the post-Kobe modifications to beam-to-column connection details were more evolutionary than revolutionary. Although

(a)

(b)

Figure 8.40 Examples of beam-to-column welded connections damaged by the Hyogo-ken Nanbu (Kobe, Japan) earthquake: (a) fracture along fillet welds of moment connection at the first story of a multistory residential building; (b) large residual interstory drift in a moment frame with damaged connections; (c) close-up view of fractured welds along box-column plate for frame shown in Figure 8.40b.

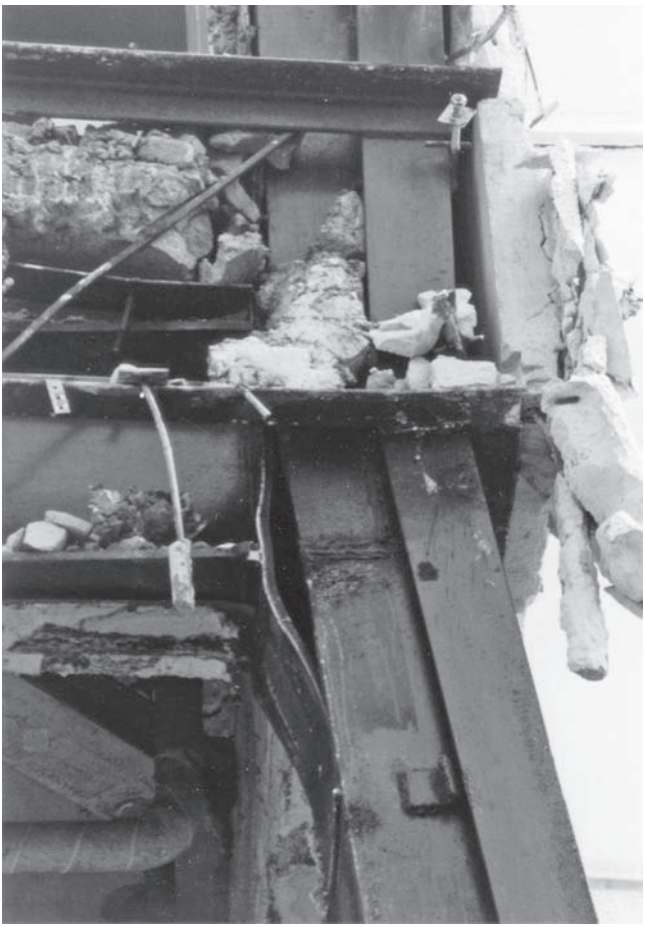

(c)

Figure 8.40 (*Continued*)

no single factor alone could explain the observed failures, a number of issues of paramount importance with respect to the Northridge failures had already been addressed in Japan prior to the Kobe earthquake. For one, existing Japanese steels having good notch toughness were already being used—for example, tests on the base metal of a fractured beam gave Charpy-V values of 50 J at 0°C (Nakashima et al. 1998). Likewise, steels having both upper and lower yield and tensile strengths, and an upper bound of 0.8 for the ratio of the yield to the tensile strength, were being introduced at the time of the earthquake, and became rapidly accepted (although not mandatory).

Given that 20.5% of the damaged moment connections fractured in the base metal, with cracks initiating from the toe of the weld access

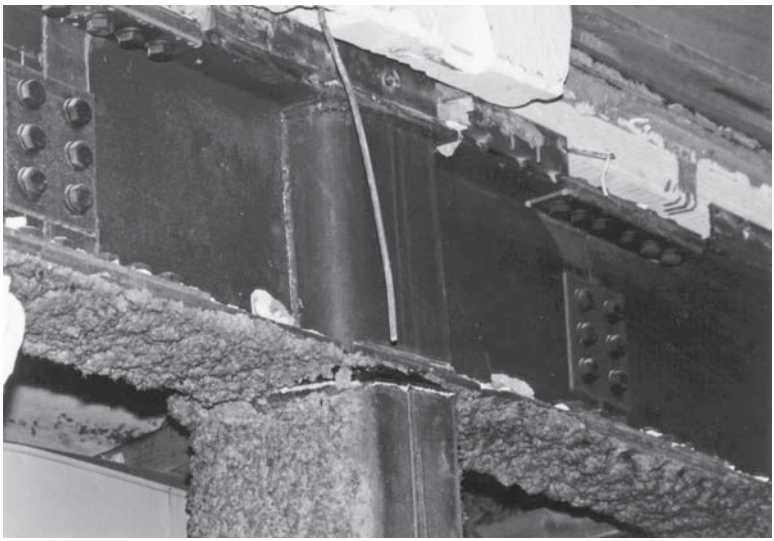

(a)

(b)

Figure 8.41 Examples of beam-to-column damage due to the Hyogo-ken Nanbu (Kobe, Japan) earthquake: (a) fracture in column-to-diaphragm welded connections; (b) overturning of a building as a consequence of such fractures.

hole, many post-Kobe studies focused on modifying connection details to minimize the stress and strain concentrations at that access hole location. Interestingly, although 24.4% of the damaged moment connections fractured in the weld metal, 10.3% had cracks at craters, and 37.2% had fractures initiating from run-off tabs, these were

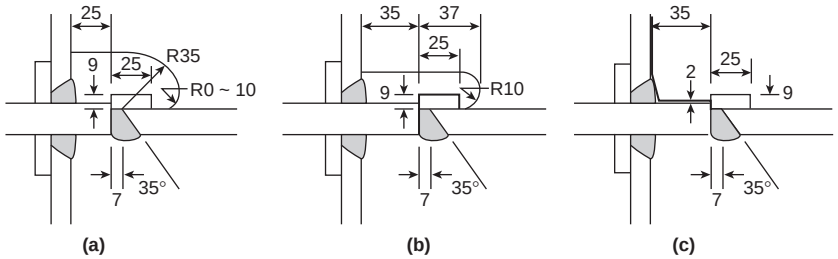

Figure 8.42 Weld access hole: (a) pre-Kobe standard detail; (b) post-Kobe modified detail with smaller hole; (c) post-Kobe no-hole detail. (*Courtesy of M. Nakashima, Disaster Prevention Research Institute, Kyoto University, Japan.*)

speculated to have been caused by welding voltages and deposition rates exceeding specified values, together with excessive weld "weaving" (i.e., welding along a zigzag path rather than directly along the weld axis), given that the use of gas-shielded arc welding (which typically contribute to greater weld toughness) was already a common practice (Nakashima 2001).

The revised JASS-6 steel fabrication specifications published following the Kobe earthquake (AIJ 1996) proposed revised shapes and sizes for weld access holes, but did not require removal of the backing bars and run-off tabs. Along that same line of thinking, subsequent research demonstrated that details without any access hole could ensure highly ductile seismic performance (Suita et al. 1999). Figure 8.42 shows the Japanese access hole details specified before and after the Kobe earthquake, together with the proposed no-hole detail. A test specimen with the no-hole detail is shown in Figure 8.43 together with a reference specimen having a RBS connection representative of North American best practice at the time. The moment-rotation hysteretic curves obtained for both of these connections are shown in Figure 8.44, together with that for a pre-Kobe detail. The no-hole and RBS connections exhibited stable hysteretic behavior up to plastic rotations of 0.03 to 0.04 radians. The pre-Kobe connection, although relatively ductile, did not perform as well.

8.5.8 Semi-Rigid (Partially Restrained) Bolted Connections

Although fully rigid moment connections are preferred in contemporary seismic design, all connections have an inherent flexural resistance; this strength may be marginal in the case of connections considered as "flexible" (or "pin" connections), or more substantial in the case of semi-rigid or partially restrained connections. In many instances, particularly in older frames, these connections were present at the ends of every beam throughout the entire building—

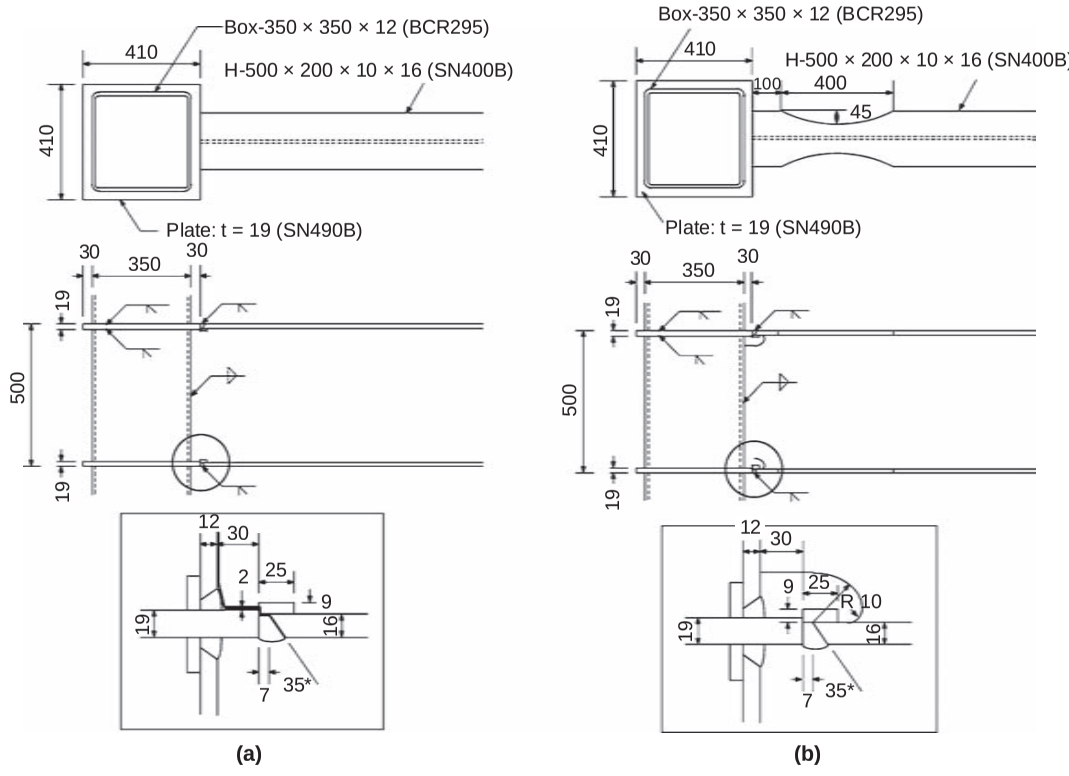

FIGURE 8.43 Moment connection specimens considered for Japanese practice: (a) no-hole detail; (b) RBS detail. (*Courtesy of M. Nakashima, Disaster Prevention Research Institute, Kyoto University, Japan.*)

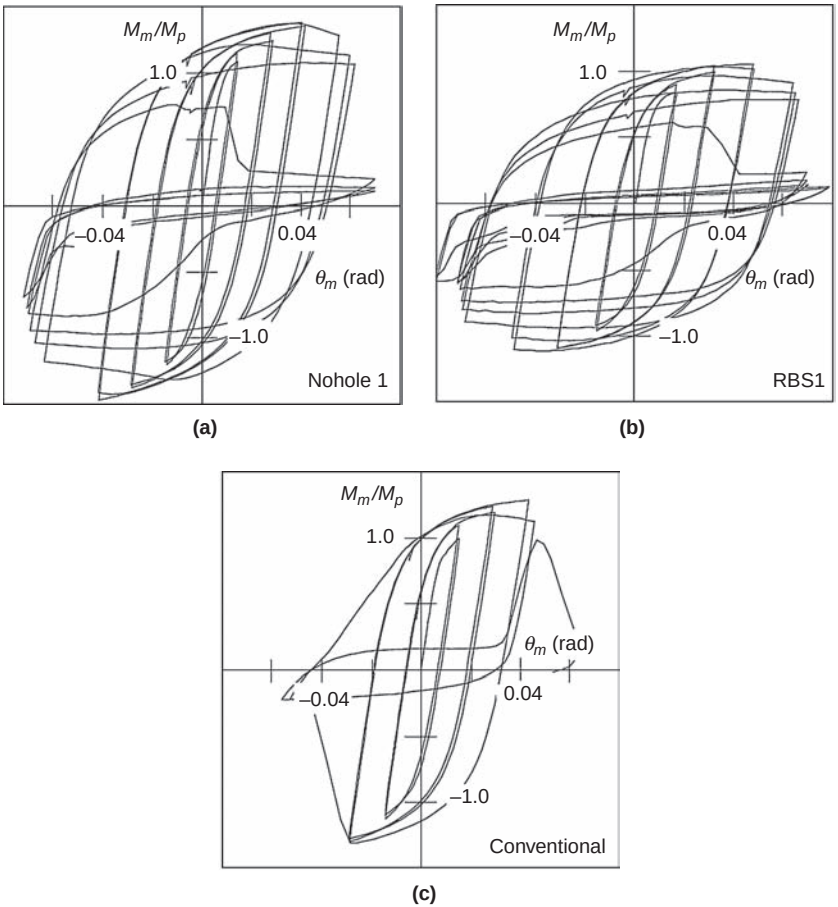

Figure 8.44 Hysteretic behavior of moment connections: (a) no-hole connection detail; (b) RBS connection detail; (c) pre-Kobe connection detail. (*Courtesy of M. Nakashima, Disaster Prevention Research Institute, Kyoto University, Japan.*)

a redundancy that compensated somewhat for the fact that each individual connection developed less than the beam's flexural capacity.

Much of the past research on seismic beam-to-column connections has focused on fully rigid welded connections. Semi-rigid connections may be viable alternatives in some cases, but they have not received as much attention as fully rigid ones from engineers practicing in regions of high seismic risk. Although the behavior of semi-rigid connections subjected to a limited level of reverse loading (to assess their rigidity under wind loads) was first investigated approximately a century ago (e.g., Moore and Wilson 1917), full-scale cyclic tests intended to be representative of seismic demands started in the mid-1980s (e.g., Astaneh et al. 1989, Elnashai and Elghazouli 1994,

Leon et al. 1994, Liu and Astaneh 2000, Radziminski and Azizinamini 1986, Roeder et al. 1996, Sarraf and Bruneau 1996). Notably, FEMA 350 included design requirements for a Double Split Tee detail prequalified as a full-strength but partial stiffness connection (FEMA 2000a), and FEMA 355d (2000d) discusses the cyclic behavior of a number of semi-rigid partial-strength connection details.

Bolted partial-strength semi-rigid connections are easier to implement than fully rigid connections for deep beams framing into heavy columns, given that the strength, stiffness, and ductility of such typical semi-rigid connections are governed by that of the connecting elements (e.g., angles, plates). Semi-rigid connections are often capable of developing plastic rotations of 0.03 radian, as shown in Figure 8.45 for an existing riveted connection retrofitted to develop a

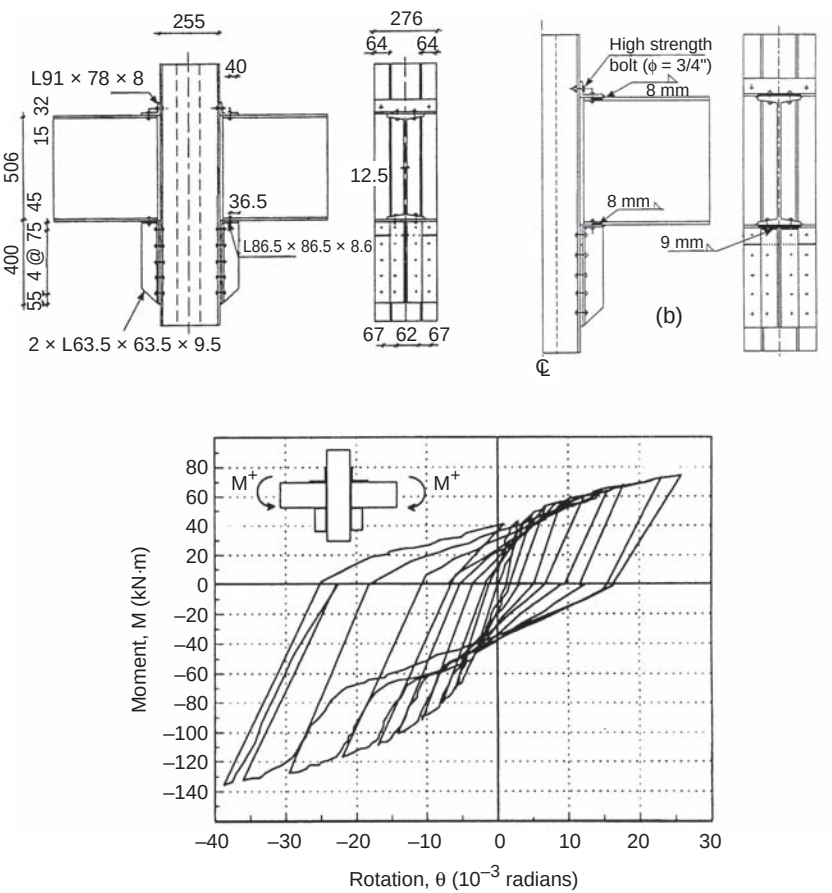

Figure 8.45 Hysteretic behavior of riveted stiffened seat-angle semi-rigid connection retrofitted using selective welding strategy, in terms of moment versus beam plastic rotation. (*From Sarraf and Bruneau 1994.*)

ductile semi-rigid behavior. Semi-rigid connections can also be easily repaired if necessary following an earthquake. However, the lower stiffness of semi-rigid connections with respect to fully rigid connections will require stiffer (and heavier) beams and columns to comply with code-specified drift limits and thus larger beam-to-column connections. In computer models, beams are typically connected to columns using spring, or modeled with equivalent flexural rigidities, and the additional flexibility of these frames often require rigorous consideration of P-Δ effects.

Seismic behavior of semi-rigid connections, an enormous topic by itself, is beyond the scope of this book. Some of that information is presented in Chen et al. (2010).

8.6 Design of a Ductile Moment Frame

8.6.1 General Connection Design Issues

AISC 358, with appropriate references to AISC 341, systematically outlines the issues that must be addressed for each type of prequalified connection. Specifically, the specific steps of that process include:

- A description of the prequalified connections and their intended energy dissipation mechanism (which would be, for example, yielding and hinge formation primarily within the reduced section of the beam in an RBS connection).
- A list of the beam and column limits that must be respected for the connection to be prequalified for various types of structural shapes; some of these limits for beams are summarized in Table 8.4. Note that although various types of column cross-sections are permitted, only W-shape beams are allowed (or equivalent built-up beams having their web joined to their flanges by full-penetration welds).
- Seismic compactness requirements (i.e., limits on width-to-thickness ratios) and lateral bracing requirements.
- A description of the location and size of the "protected zone," these being the parts of the structural members or connections over which alterations, perforations, and attachments are prohibited so as to not impair their ability to undergo large inelastic deformations.
- A description of the requirements that must be satisfied to ensure strong-column/weak-beam design, and thus prevent column hinging.
- Specified requirements for column panel zone and continuity plates design.

- Prescribed bolting and welding detailing requirements for the connection to be prequalified. For example, for a beam bottom flange having complete penetration welds to a column, the steel backing plate used at that location must be removed, the exposed root pass must be backgouged to sound weld metal and backwelded with a reinforcing fillet—the fillet leg adjacent to the column flange being at least 5/16 in (8 mm), and the fillet leg adjacent to the beam flange being long enough to ensure that the fillet toe is located on the beam flange base metal.
- Specific fabrication details applicable to individual connections (e.g., the thermal cutting process, maximum permissible surface roughness of the cut, geometry details, tolerances, procedure to repair gouges and notches, and inspection procedure, are specified for the RBS connection).
- A design procedure, outlining in sequence all the limit states that must be checked to obtain a satisfactory prequalified connection (see Section 8.6.2).
- A specified design value for the distance of the plastic hinge located away from the column face.
- Prescribed bolted and welded details required for the connection to be prequalified (as shown in Section 8.8 example).

This chapter has already provided insights into some of the above important aspects governing the behavior of moment frames (e.g., design of panel zones and their modeling in structural analysis described in Section 8.4.5; need to use seismically compact sections and to provide bracing against lateral torsional buckling described in Section 8.2.3). A few additional important considerations follow.

8.6.2 Welding and Quality Control Issues

As mentioned in Section 8.5.3, factors contributing to the connection failures during the Northridge earthquake included the low fracture toughness of the welding metal used (typically E70T-4 electrodes), weld defects (such as those frequently found at the midwidth of bottom flange, on runoff tabs, etc.), and detrimental weld details. For example, dynamic loading tests indicated that the use of weld metals with high notch toughness properties, such as those accomplished with E7018 filler metal, improved performance when used in conjunction with good detailing practice, including among many things removal of backup bars and weld runoff tabs (e.g., Kaufmann et al. 1996, Xue et al. 1996).

The FEMA-353 recommended welding requirements and quality assurance guidelines for seismic applications, developed following the Northridge earthquake (FEMA 2000d), have for the most part been adopted into consensus codes. Minor conflicting requirements

between AISC 341 (2005) published before AWS D1.9 2005 (Stockmann and Schlafly 2008) have been resolved in subsequent editions of these specifications. Both AISC 341 and AISC 358 reference the AWS D1.9 (AWS 2009) for numerous issues related to "demand-critical welds," which are those welds in seismic applications connecting yielding elements and whose failure would produce significant strength and stiffness degradation of the energy dissipating elements. For example, demand-critical welds are specified for beam-to-column complete joint penetration welds or other yielding applications when cross-thickness loading or triaxial stress states exist.

Given the recognized benefits of using filler metal with relatively high notch toughness and better weld quality, demand critical welds are required to have a minimum Charpy-V notch toughness of 20 ft-lbs (27 J) at 0°F (−18°C). More stringent requirements are required if the steel frame is exposed to service temperatures lower than 50°F. AWS D1.8 also limits hydrogen content for all welding electrodes and electrode-flux combinations to prevent hydrogen-induced cracking, and specifies requirements for workmanship, inspection, welder qualification, welding procedure and material, and other issues to ensure quality welds (AWS 2009, Hamburger et al. 2007, Miller 2006).

For each prequalified connection, AISC 358 also refer to the appropriate documents for weld access hole configuration, surface smoothness, and inspection, to prevent notches and surface defects that can lead to cracking in this region of complex stress flow. A similar approach is taken to specify when backing bars need be removed, and when additional weld fillet and special detailing is required.

For example, for WUF-W connections, AISC 358 specifies that the weld access hole geometry shall conform to the requirements of AWS D1.8. Although AWS D1.8 indicates that the standard access hole geometry specified in its main structural welding code (AWS D1.1) is acceptable in most conditions, it also includes an "alternate geometry" access hole detail identical to the one recommended by FEMA 350 on the basis of finite element analyses and experiments that demonstrated improved performance for some connection types (Figure 8.46).

8.6.3 Generic Design Procedure

Selection of a specific type of prequalified connection is typically driven by cost comparisons, past experiences, engineering/fabricator preferences, or other reasons. For each prequalified connection, AISC 358 provides a different step-by-step design procedure—the complexity of the design requirements integral to each procedure being proportional to the number of its limit states, given the need to prevent all undesirable failure modes. However, some basic fundamental principles are applicable to most of the prequalified connections, as described below.

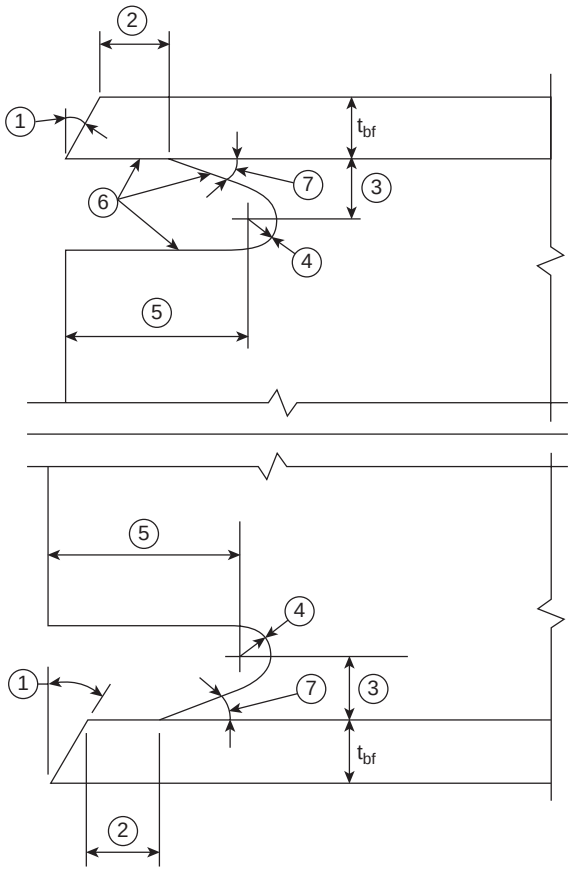

Notes:
1. Bevel as required for the WPS.
2. t_{bf} or 1/2 in [12 mm], whichever is larger (plus 1/2 t_{bf}, or minus 1/4 t_{bf}).
3. The minimum dimension shall be 3/4 t_{bf}, or 3/4 in [20 mm], whichever is greater. The maximum dimension shall be t_{bf} (+1/4 in [6 mm]).
4. 3/8 in [10 mm] minimum radius (–0, +unlimited).
5. 3 t_{bf} (±1/2 in [12 mm]).
6. See 6.10.2.1 for surface roughness requirements.
7. Tolerances shall not accumulate to the extent that the angle of the access hole cut to the flange surface exceeds 25°.

Figure 8.46 AWS D.18 Alternate Geometry for Beam-Flange Weld Access Hole Detail—surface roughness requirements of 500 µin (13 µmm) per clause 6.10.2.1. (AWS D1.8/D1.8M:2009, Figure 6.2; *Reproduced with permission of the American Welding Society* [*AWS*]*, Miami, Florida.*)

8.6.3.1 Free-Body Diagram for Plastic Hinge Away from Column Face

Generically, the design procedures rely on capacity design concepts and strategies to relocate plastic hinges away from the column faces. This forces the development of a plastic mechanism like the one in

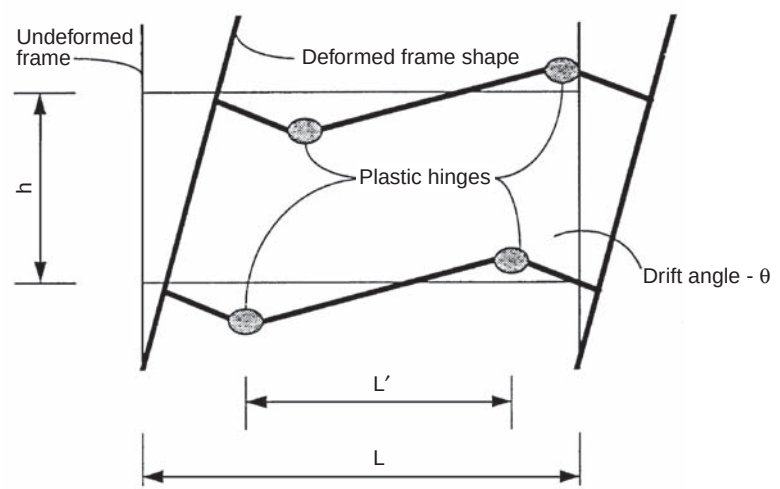

Figure 8.47 Desired plastic collapse mechanism in post-Northridge ductile moment-resisting frames. (*From* Interim Guidelines: Evaluation, Repair, Modifications, and Design of Steel Moment Frames, *SAC Joint Venture, 1995, with permission.*)

Figure 8.47 (shown for a single bay frame for expediency, recognizing that moment-frames of multiple bays are encouraged to promote redundancy).

Figure 8.48 shows the corresponding free-body diagrams that are used as part of the AISC 358 design procedure (showing haunches as beam reinforcement for schematic simplicity and convenience, recognizing that haunch connections are not prequalified per AISC 358). The distance to plastic hinge from the face of the column, S_h, specified by AISC 358 for each connection type based on experimental evidence, is used to determine the moments and shears at the plastic hinge locations, column faces, and center of columns, from which all other needed parameters can be calculated.

For example, for end-plate connections, S_h is specified as the lesser of $d/2$ or $3b_{bf}$ for the BUEP unstiffened connection, and as $L_{st} + t_p$ for the BSEP stiffened connection, where d and b_{bf} are the beam's depth and flange width respectively, L_{st} is the length of the end-plate stiffener, and t_p is the thickness of end plate. For the BFP connection, it is equal to $S_1 + s\ (0.5n - 1)$, where S_1 is the distance from face of column to nearest row of bolts, s is the spacing of bolt rows, and n is the number of bolts rounded to the next higher even number increment. For BB connections, the plastic hinge is located at a distance equal to the length of the bracket.

For an RBS connection, $S_h = a + b/2$, where a is the horizontal distance from the column face to the start of the RBS cut, and b is the

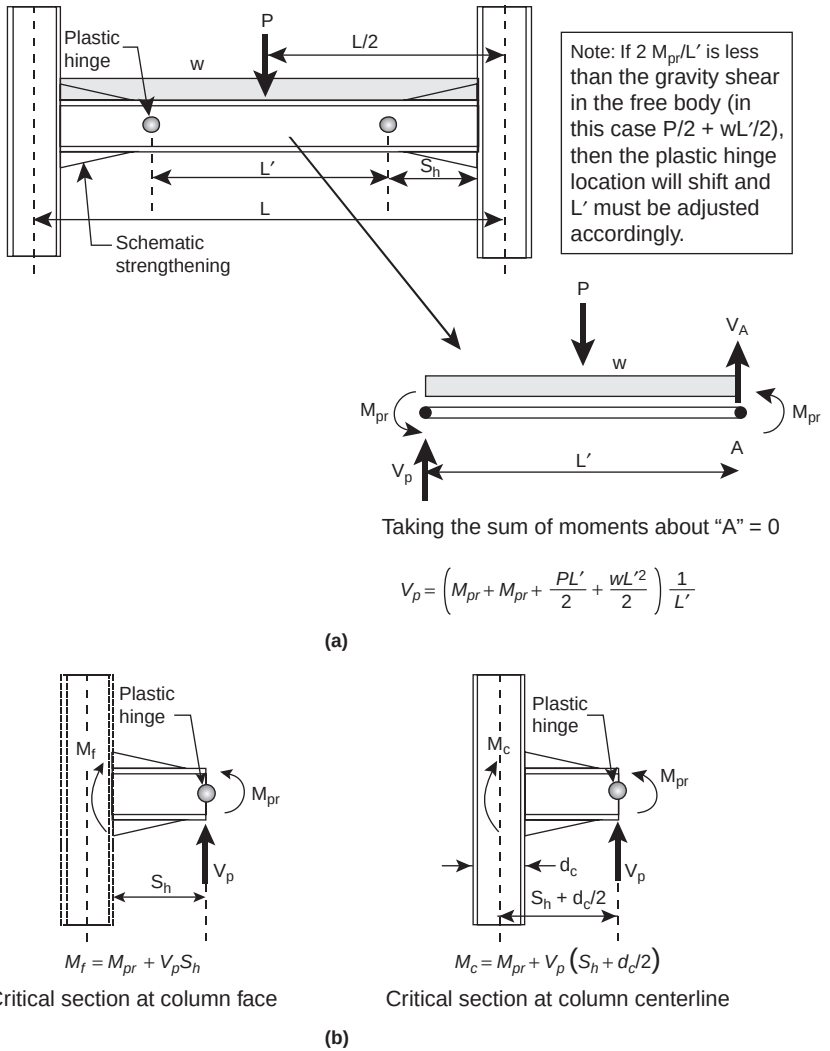

Figure 8.48 Design of post-Northridge ductile moment-resisting frames: (a) free-body-diagram to calculate shear at plastic hinges; (b) free-body diagrams to calculate moments at column face and column centerline. (*Adapted from* Interim Guidelines: Evaluation, Repair, Modifications, and Design of Steel Moment Frames, *SAC Joint Venture, 1995, with permission.*)

length of the RBS cut, as shown in Figure 8.33c. The AISC 358 design procedure also restricts the geometry of RBS connections to

$$0.5b_{bf} \le a \le 0.75b_{bf} \tag{8.23a}$$

$$0.65d \le b \le 0.85d \tag{8.23b}$$

$$0.1b_{bf} \le c \le 0.25b_{bf} \tag{8.23c}$$

where c is the depth of the cut at the center of the reduced beam section (Figure 8.33c), and all other terms have been defined earlier. Note that the RBS section itself, like all other beams and columns throughout the frame, must have adequate strength to resist the moments, shears, and axial forces computed for all the applicable code-specified forces and load combinations. Design story drift limits must also be met, either by specifically accounting for the actual reduction in stiffness at the RBS or, more expeditiously, by increasing by 10% the drifts calculated using beam gross cross-sections for the RBS case having 50% reduction in flange width (this drift magnification factor can be interpolated for lesser flange width reductions).

Note that, in a significant departure from FEMA 350, AISC 358 specifies $S_h = 0$ for WUF-W connections, even though yielding of beams having such connections has been observed to spread from the face of columns up to a distance of one beam depth beyond that point. This was done to simplify the design calculations, with other deviations from the standard design procedure introduced later on to compensate for this simplification.

Caution is also warranted in comparing FEMA 350 and AISC 358, because S_h is inconsistency defined in those documents, being measured from the column centerline in FEMA 350 rather than from the column face as done here and in AISC 358.

8.6.3.2 Probable Maximum Moment at Plastic Hinge Location

The probable maximum moment, M_{pr}, at the plastic hinge location specified for the prequalified connection, is given by:

$$M_{pr} = C_{pr} R_y F_y Z_e \tag{8.24}$$

where R_y is the ratio of the expected yield stress to the specified minimum yield stress F_y, Z_e is the effective plastic section modulus at that plastic hinge location, and C_{pr} is a magnification factor to account for the peak connection strength expected due to the effects of strain-hardening, local restraints, additional reinforcement, and other conditions.

For plastic hinges in beams, Z_e is the plastic section modulus about the x-axis of the full beam cross-section, Z_x, except in RBS connections where it is computed at the center of the reduced beam section and therefore equal to:

$$Z_e = Z_x - 2ct_{bf}(d - t_{bf}) \tag{8.25}$$

where t_{bf} is the thickness of the beam flange and all other terms have been defined previously.

In general, C_{pr} is given as:

$$C_{pr} = \frac{(F_y + F_u)}{2F_y} \leq 1.2 \tag{8.26}$$

except for WUF-W connections, for which C_{pr} shall be taken as equal to 1.4 because the specified plastic hinge distance is zero. In Eq. (8.26), F_u is the specified minimum tensile strength of the yielding steel.

8.6.3.3 Shear Forces at Plastic Hinge Location

Shear forces acting at the plastic hinge locations are obtained by equilibrium equations from a free-body diagram of the beam segment between plastic hinge locations, as shown in Figure 8.48. The largest of the shear forces at these two beams ends, considering the effects of gravity, is called V_p here (for different prequalified connections, AISC 358 uses the terms V_u, V_h, and V_{RBS}, practically for the same purpose), and given by:

$$V_p = \frac{2M_{pr}}{L'} + V_{Gravity} \tag{8.27}$$

For the example shown in Figure 8.48, with a uniformly distributed load and an additional point load at the beam's midspan:

$$V_{Gravity} = \frac{\omega L'}{2} + \frac{P}{2} \tag{8.28}$$

The shears for beams having other gravity loading patterns would be similarly obtained. Note that factored gravity loads per the applicable building code load combinations must be considered.

8.6.3.4 Forces at Column Face and Column Center Line

As shown by the other free-body diagrams in Figure 8.48, the moment acting at the face of the column, M_f, is given by:

$$M_f = M_{pr} + V_p S_h \tag{8.29}$$

while the moment at the column centerline is:

$$M_c = M_{pr} + V_p (S_h + 0.5\, dc) \tag{8.30}$$

where d_c is the column depth.

Note that, for simplicity, the above equations neglect the gravity load over the distance S_h. For consistency, AISC 358 also considers the shear acting at the column face to be V_p. Obviously, consideration of the gravity load over that small segment is permitted, as it would be more rigorous and statically correct.

The moment at the column centerline is required to verify if the strong-column/weak-beam design requirement is met. The shear and moments at the face of the column are needed to size various aspects of the prequalified connections at that location.

For RBS connections, it must also be ensured that the moment at the column face does not exceed the plastic strength of the beam (based on expected yield stress) when the minimum section of the RBS is fully yielded and strain hardened, therefore:

$$M_f \le M_{pe} = R_y Z_x F_y \tag{8.31}$$

Adjusting the geometry of the RBS may be needed to meet this requirement.

8.6.3.5 Other Detailing Requirements

The details of each of the prequalified connection are then designed to resist the above appropriate moments and shears. AISC 358 spells out the various limit states to consider for each prequalified beam-to-column connections (such as tension and shear strength of bolts and filet welds, block shear strength, and effect of prying action, to name a few), providing design equations as appropriate. For bolted connections, it is also required that the tensile strength at the net section of flanges be greater than the yield strength at their gross section (i.e., $R_t A_n F_u > R_y A_g F_y$, where R_t is the ratio of the expected tensile strength to the specified minimum tensile strength for the flange under consideration, and all other parameters have been defined previously). Specific required welding procedures are also outlined as appropriate.

The AISC 341 requirements for strong-column/weak-beam design, continuity plates, and panel zone design are referenced as part of the design procedure. On that latter point, it is worthwhile to caution that even though the combined action of panel zone yielding and beam hinging can be helpful in reducing plastic rotation demands in beams, substantial panel zone yielding will develop (up to $4\gamma_y$ in principle) if Eq. (8.15) is used. For many reasons, it may be preferable to concentrate plastic hinging in the beams. Experimental observations indicate that uncertainties in true material strengths make the intended sharing of plastic rotation between the beam and panel zone impossible to control. For example, panel zones in columns with weaker than average yield values would have to provide all of the required hysteretic energy dissipation if coupled with beams having stronger than average strengths, and vice versa. Also, although panel zones can be reliable energy dissipators, the kinking of column flanges at large panel shear strain deformations generates complex triaxial stress conditions and possible fracture at the beam flange welds.

8.7 *P*-Δ Stability of Moment Resisting Frames

Consideration of *P*-Δ effects in moment frames has long been recognized as important to prevent collapses due to instability during earthquakes. Also, more recently, the topic has been the subject of a renewed research interests to more reliably define the conditions of

incipient collapse during earthquakes and methods to model behavior through all stages of collapse, in parallel with intensified research efforts on progressive collapse. However, a broad consensus is still lacking on many aspects related to these issues.

For the current purpose, a brief overview of some fundamental concepts is presented, followed by a description of the ASCE design requirements. Other design codes and standards internationally have similar, but not identical, provisions. A survey of existing research on structural stability during earthquakes excitations is available in Ziemian (2010).

8.7.1 Fundamental Concept and Parameters

The concept of P-Δ effects under static loading is illustrated in Figure 8.49a using a single degree of freedom (SDOF) structure subjected to gravity and lateral loads: a single column represents the lateral load resisting system, P is the force due to gravity acting on the mass lumped at the top of the structure, L is the column height, V is the lateral force on the mass, and Δ is the horizontal displacement of the mass. As the structure sways by Δ under the effect of the lateral force, the product of P by Δ produces an additional moment at the base of the column, which can be obtained by considering static equilibrium in the deformed configuration. For any given structure, this effect results in an increased demand on the lateral load resisting elements, without any increase in the horizontal forces and base shear.

For the bilinear elastic-perfectly plastic model shown in Fig. 8.49b, the ultimate lateral force, ignoring the P-Δ effect, which can be applied to each identical column of that frame, is reached when the plastic moment of the column, M_p, develops at the top and bottom of the column, and is given by:

$$V_{yo} = \frac{2 \cdot M_p}{L} \tag{8.32}$$

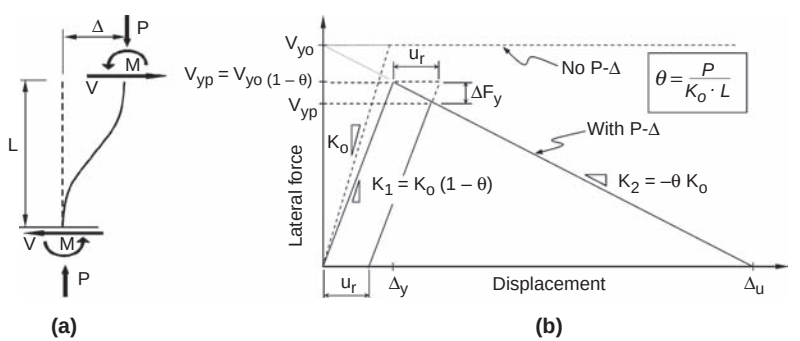

Figure 8.49 SDOF structure subjected to P-Δ effects: (a) free-body diagram; (b) bilinear lateral force versus displacement model. (*Vian and Bruneau 2001, Courtesy of MCEER, University at Buffalo.*)

The corresponding yield displacement is:

$$\Delta_y = \frac{V_{yo}}{K_o} \tag{8.33}$$

Now, as shown in Fig. 8.49b, considering *P*-Δ effects on the single column, moment equilibrium gives:

$$2 \cdot M = VL + P\Delta \tag{8.34}$$

where V is the lateral force at the top of the column.

Rearranging Eq. (8.34), the lateral force, V, can be expressed as:

$$V = \frac{(2 \cdot M - P\Delta)}{L} = \frac{2 \cdot M}{L} - \frac{P\Delta}{L} = V_o - \frac{P\Delta}{L} \tag{8.35}$$

where V_o is the lateral force that would be obtained ignoring the *P*-Δ effect.

Shown in Figure 8.49b, as a consequence of *P*-Δ effects seen in Eq. (8.35), V decreases relative to V_o, as the displacement, Δ, increases. This equation can also be expressed as:

$$V = V_o - \frac{P\Delta}{L} = V_o - \theta \cdot K_o \Delta \tag{8.36}$$

where Δ is the *P*-Δ stability coefficient given by:

$$\theta = \frac{P}{K_o L} = \frac{P\Delta}{V_o L} = \frac{P\Delta_y}{V_{yo} L} \tag{8.37}$$

From Eq. (8.36), the elastic stiffness considering *P*-Δ, K_1, is therefore:

$$K_1 = K_o(1 - \theta) \tag{8.38}$$

Similarly, the lateral force at which the column, including *P*-Δ effects, yields, V_{yp}, is:

$$V_{yp} = V_{yo}(1 - \theta) \tag{8.39}$$

When elastic-perfectly plastic material properties are assumed for the idealized frame, lateral force V_o in Eq. (8.36) remains constant in the post-elastic region of the force-displacement graph as the plastic

moment, M_p, is developed. However, when P-Δ effects are considered, the corresponding lateral force versus displacement curve exhibits a negative slope past the yield point, with a stiffness of:

$$K_2 = -\theta \cdot K_o \tag{8.40}$$

as shown in Figure 8.49b.

Therefore, the monotonic bilinear force-displacement response of this SDOF structure, including P-Δ effects, can be summarized as follows:

$$V = \begin{cases} K_1 \cdot \Delta & if \quad \Delta \le \Delta_y \\ V_{yo} + K_2 \cdot \Delta & if \quad \Delta > \Delta_y \end{cases} \tag{8.41}$$

The ultimate displacement of the structure designated as Δ_u, as shown on Fig. 8.49b, is the point at which the post-elastic lateral strength curve or negative-slope, intersects the displacement axis. This theoretically implies that for any additional lateral displacement, lateral instability develops (i.e., lateral strength becomes negative for any additional positive displacement).

Some additional parameters are useful to further characterize inelastic behavior of columns up to collapse. The ratio of postelastic to elastic stiffness, K_2 and K_1, respectively, known as the stiffness ratio, r, is given by:

$$r = \frac{K_2}{K_1} = \frac{\alpha - \theta}{1 - \theta} \tag{8.42}$$

where $\alpha \cdot K_o$ is the stiffness (in absence of stability effects) of the strain-hardening segment of a bilinear elastic-plastic material model. Here, the value of $\alpha = 0.0$ is considered.

The displacement ductility—displacement as a ratio of yield displacement—at ultimate displacement, Δ_u, known as the static stability limit, μ_s, is derived from the geometry and relations given in Figure 8.49b, in terms of θ and r:

$$\mu_s = \frac{\Delta_u}{\Delta_y} = \frac{1}{\theta} = 1 - \frac{1}{r} \tag{8.43}$$

8.7.2 Impact on Hysteretic Behavior

Figure 8.49b also shows that, for the assumed bilinear force-displacement model, after a first yield excursion and unloading to

a residual displacement, u_r, the structure has a new reduced yield strength, V_{yp}', upon reloading, given by:

$$V_{yp}' = V_{yp} - \Delta F_y = K_1 \cdot (\Delta_y - \theta \cdot u_r) \tag{8.44}$$

where ΔF_y is the structure's yield base shear reduction, and all other terms have been previously defined. As a consequence of the structure's lower yield strength in the direction it has previously yielded, continued yielding in that direction is relatively easier, and the hysteretic behavior obtained from seismic excitations exhibits a bias in one displacement direction compared with the balanced hysteretic loops typically obtained otherwise. The severity of this bias is a function of the stability factor.

Figure 8.50 illustrates this phenomenon for shake table tests of a small-scale single story frame having a θ value of 0.138 and subjected

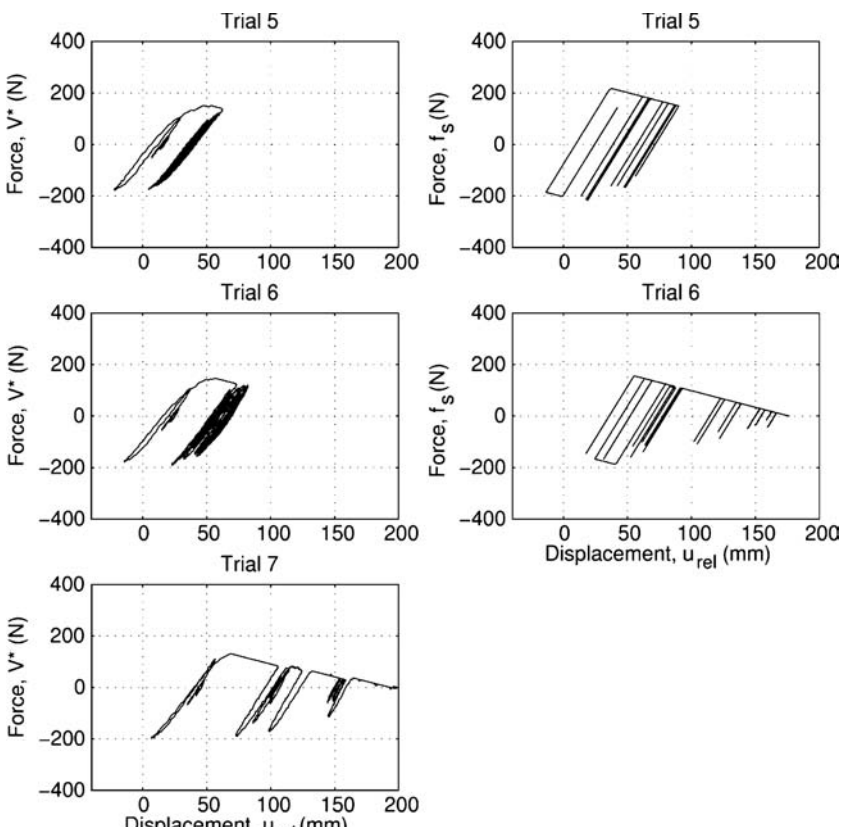

Figure 8.50 Hysteretic force-displacement measured for Specimen 11 upon successive earthquake excitations (left), and results from bi-linear analytical model (right). (*Vian and Bruneau 2001, Courtesy of MCEER, University at Buffalo.*)

to a series of progressively more severe earthquakes until the structure collapsed, together with the results from nonlinear dynamic analyses using a bilinear elastic-perfectly plastic model, a damping ratio of 1.8%, and adjusting the model to account for the reduced yield strength at the experimentally obtained residual displacements. Both the experimental and analytical hysteretic curves exhibit dynamically unstable behavior following a clear negative postyield stiffness, as a consequence of the systems' tendency to drift in a given direction once yielding has started. This results in large cumulative residual displacements and lower cyclic energy absorption capability prior to failure. These detrimental effects become progressively more significant for larger values of the stability coefficient (results for all 15 specimens tested are presented in Vian and Bruneau 2001, 2003).

Analytical results from the above simple analyses are for illustration purposes. More accurate and refined analytical models have been developed to capture behavior up to and through collapse (e.g., Lavan et al. 2009; Sivaselvan and Reinhorn 2002, 2006). Villaverde (2007) also summarizes findings from other shake table experimental results and methods to assess the seismic collapse capacity of building structures.

In addition to the above issues related to idealized frames having bilinear behavior, degradation of structural strength at large inelastic deformations (i.e., beyond the drifts up to which plastic strength can be sustained) can actually produce substantially more steep negative postyield stiffness, and thus more rapidly lead to instability and collapse (Ibarra et al. 2005, Lignos et al. 2008, Rodgers and Mahin 2006, Suita et al. 2008). Attempts to formulate equations quantifying how various response parameters are affected by structural instability during earthquake are further compounded by the fact that such response also varies as a function of many ground motion characteristics (e.g., Bernal et al. 2006, Williamson 2003). This complex variability is often probabilistically considered by subjecting sets of representative structures to incremental dynamic analyses (IDA), which requires using time history analyses for suites of ground motions, progressively increasing the severity of each ground motion until collapse is reached, and using appropriate hysteretic models that appropriately capture strength and stiffness degradation (e.g., FEMA 2009, Krawinkler 2006, Sivaselvan and Reinhorn 2000). Many of the above studies have also reported that collapse of an individual story in a multistory frame is significantly more likely than global instability of the entire building, in part due to the effect of higher vibration modes. Some have recommended special design requirements for continuous columns to better distribute drift demands over the entire frame height and prevent such localized story failures (e.g., Krawinkler 2006, MacRae 1994, MacRae et al. 2004).

8.7.3 Design Requirements

The design objective is to limit the magnitude of lateral drifts to prevent global instability of the entire structure, or of individual stories.

Various strategies have been proposed to that effect. Designing to achieve a post-yield stiffness such that $\alpha \geq \theta$ would eliminate the negative post-yielding stiffness and thus prevent such instability. A similar concept is also possible for more complex hysteretic behaviors (Kawashima et al. 1996, MacRae and Kawashima 1993, MacRae 1994, MacRae et al. 1993). This could be achieved using a structural fuse philosophy (Chapter 13) or a secondary system designed to provide the needed lateral stiffness beyond yielding of the primary lateral load-resisting system. Alternatively, expressions have been proposed to increase the design lateral strength to compensate for the increased displacements induced by P-Δ effects (Bernal 1987, Davidson and Fenwick 2004, Mazzolani and Piluso 1996, Miranda and Akkar 2003, Rutenberg and DeStefano 2000).

For simplicity, given that θ is generally less than 0.060 for actual structures (MacRae et al. 1993), many building codes and standards specify that P-Δ effects can be neglected in seismic design when the stability coefficient is less than a specific value, and prescribe a maximum permitted value for that coefficient. However, various codes differently define the stability coefficient (Ziemian 2010). In accordance to ASCE 7-10, simplifying some terms, the stability coefficient is defined and limited by:

$$\theta = \frac{P_x \Delta}{V_x h_{sx}} \leq \frac{0.5}{\beta C_d} \leq 0.25 \tag{8.45}$$

where P_x is the total vertical design load at and above level x, Δ is the design story drift at that level determined from elastic analysis and occurring simultaneously with V_x which is the seismic shear force acting between levels x and $x - 1$, h_{sx} is the story height below level x, C_d is a deflection amplification described in Chapter 7, and β is the ratio of story shear demand over capacity (accounting for possible overstrength of the lateral-load-resisting system between Levels x and $x - 1$). ASCE states that P-Δ effects can be ignored when $\theta \leq 0.10$, and considered by rational analysis otherwise. Alternatively to such a rational analysis, ASCE permits to multiply displacements and member forces by $1.0/(1 - \theta)$ to simulate the results of such an analysis.

Additional recommendations for design to prevent global instability are available elsewhere (FEMA 2009, Krawinkler 2006, Villaverde 2007, Zareian and Krawinkler 2007).

8.8 Design Example

The following section illustrates the design of a Special Moment Frame. The design applies the requirements of ASCE 7 (2010), AISC 341 (2010b), and AISC 358 (2010a). The example is not intended to be a

S_S	1.0 g
S_1	0.60 g
Site class	D
S_{DS}	0.733 g
S_{D1}	0.60 g
R	8
I	1.0
C_D	5.5
Ω_o	3

Table 8.5 Seismic Design Data

complete illustration of the application of all design requirements. Rather, it is intended to illustrate key proportioning and detailing techniques that are intended to ensure ductile response of the structure.

8.8.1 Building Description and Loading

The example building is a five-story structure located in an area of moderate to high seismicity. Tables 8.5 and 8.6 below give the seismic design data and building information. Figure 8.51 shows the plan and Figure 8.52 shows the typical frame elevation.

8.8.2 Global Requirements

In areas of high seismicity, the required base-shear strength prescribed by the building code does not typically govern the selection of members in SMF systems and it is typically advantageous to select members based on drift control and then check the member strengths later. (In areas of low seismicity the opposite may be true: strength requirements may govern the design.) The drift limit is dependent on system type and occupancy. For this building the drift limit is 0.020 times the story height. Conversely, in areas of low or moderate seismicity drift governs the design much less often and it may be advantageous to design for strength and check drift. Strength-controlled designs are somewhat easier to perform and optimize than are drift controlled ones, which typically require some iteration. However both cases

Typical floor weight	100 psf	2310 kips
Typical cladding weight	20 psf	160 kips
Roof weight	100 psf	2310 kips

Table 8.6 Building Information

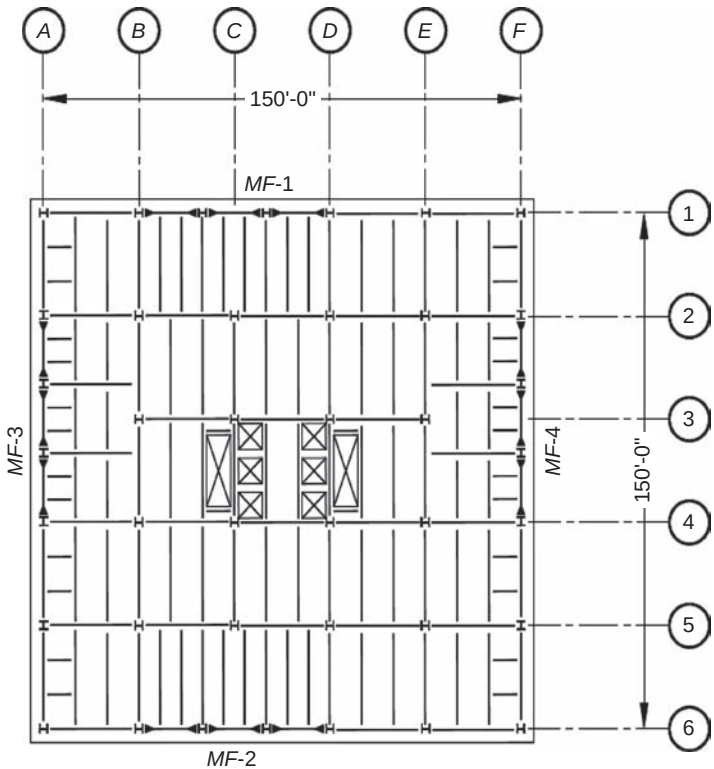

Figure 8.51 Typical floor plan.

involve preliminary design, analysis, and final confirmation of adequate strength and drift control.

This example is set in a zone with high seismicity and thus the former strategy (design for drift; check strength) is adopted.

8.8.3 Basis of Design

The design of SMF is based on the expectation of a global yield mechanism in which plastic hinges form at the ends of some (or all) beams and at the column bases. Although it is acknowledged that some column hinging at other locations may occur in actual building response, the design procedures are derived from the beam-hinging assumption.

The analysis procedure utilized is a linear Modal Response Spectrum (MRS) analysis. This is typically advantageous due to the reduction in design forces. ASCE 7 permits for this method and the reduction in overturning moment that typically results from this approach compared with the vertical force distribution used in the equivalent lateral force procedure of ASCE 7. Based on the seismic-design data

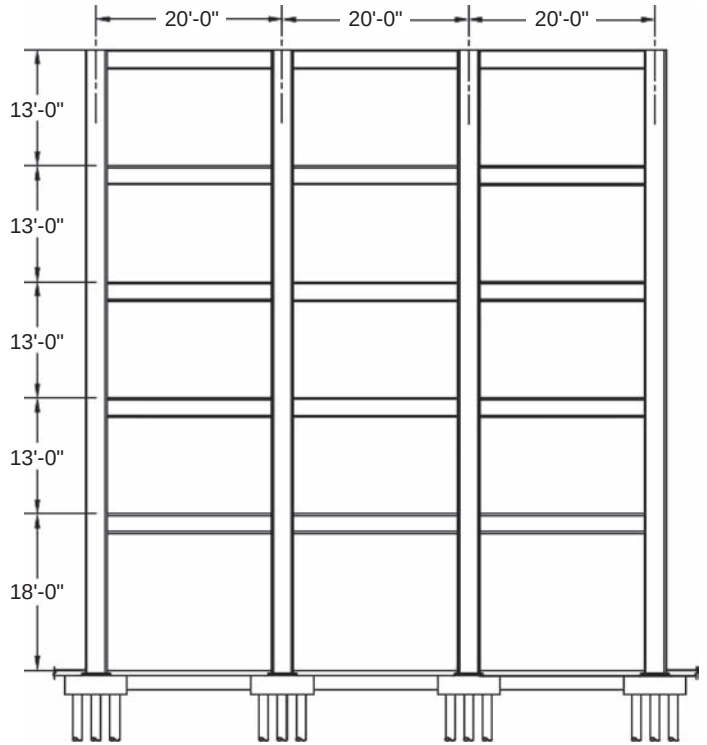

Figure 8.52 Typical frame elevation.

a generic seismic response spectrum is constructed in accordance with ASCE 7.

As required by AISC 341, the design utilizes a connection that can provide a rotation angle of 0.04 radians through a combination of elastic and inelastic deformation. The connection is a Welded Unreinforced Flange-Welded Web (WUF-W) prequalified per AISC 358. AISC 358 prequalifies several connections, many of which have limit states or calculations specific to that connection. However, the general design methodology is similar.

8.8.4 Iterative Analysis and Proportioning

The forces used to evaluate the design drift are dependent on the building period. Thus some iteration is required to select members that satisfy the drift requirements efficiently (i.e., to avoid inefficient overdesign). Initially the building period is assumed to equal the ASCE 7 upper limit for static analyses, $C_u T_a$. Member selection must also satisfy proportioning requirements intended to favor beam hinging over column hinging (the "strong-column/weak-beam" rule addressed in the connection-design section). Thus designers often

apply proportioning rules in preliminary design to prevent failing this rule at a later stage in design. (This is checked in Section 8.6.2 below.) In order for the beam to be able to undergo flexural yielding, "highly ductile" members are selected based on Table D1.1; these members are sufficiently compact that local flange buckling does not limit the ability of the section to undergo large inelastic rotations while maintaining its strength.

In order to ensure adequate drift control, panel zone flexibility must be captured in the model. This is rarely done explicitly by use of a separate panel-zone element permitting relative rotation between beam and column. More often, this is done by centerline modeling (i.e., not employing rigid-end offsets in the model). This reasonably captures panel-zone flexibility for typical spans (Charney and Horvilleur 1995).

Some connection types have an effect on the stiffness of SMF frames. For example, the reduced-beam section connection, by virtue of removing material from the beam, causes additional flexibility that must be modeled, often resulting in larger required members. Other connections add material and thus reduce flexibility, sometimes to a degree that can permit lighter members to be used.

To commence the preliminary design the following steps are taken using the equivalent lateral force procedure:

- Determination of base shear
- Vertical distribution of forces
- Horizontal distribution of forces to frames
- Use of approximate equations relating story shear, beam and column moments of inertia, and deflection to determine preliminary member sizes

A commonly used equation for estimating drift is given below (Wong et al. 1981):

$$\Delta_i = \frac{V_i h_1^2}{12}\left[\sum \frac{h_i}{EI_{ci}} + \sum \frac{L}{EI_{bi}}\right] \tag{8.46}$$

where V_i is the frame shear at level I, h_i is the height of level i (average of adjacent stories), E is modulus of elasticity, I_{ci} is the moment of inertia of each column in the frame at level I, I_{bi} is the moment of inertia of each beam in the frame at level I, and L is the span of each beam in the frame.

In the equation above the design frame shear V_i (reduced by the Response Modification Coefficient R) is used, and thus drifts must be amplified by the factor C_d. The drift can be set equal to the drift limit at each floor level and members can be selected corresponding to that

drift value. The drift limit is a function of the story height and the allowable drift angle, θ_{max}, which is typically 0.02:

$$\Delta_{max} = \theta_{max} h \tag{8.47}$$

For preliminary design the static base shear is used; member sizes can be refined subsequently considering the results of a modal response spectrum analysis. Accidental torsion may be considered in the determination of the frame shear using approximate methods. In this design it was not considered at this stage due to its likely limited effect compared with other approximations.

To simplify the preliminary member selection further, the column moment of inertia can be assumed to be twice the beam moment of inertia. Furthermore, the moment of inertia of the columns at the end of the frame (which connect to one moment frame beam at each floor) can be assumed to be one half that of the interior columns (which connect to two moment frame beams at each floor). This proportioning will make it likely that the strong-column/weak-beam requirements will be met, which can only be checked later in the design.

With the simplifications outlined above the minimum moment of inertia of the beams can be solved for:

$$I_{bi} = \frac{V_i h_i}{12 EN} \frac{C_d}{\theta_{max}} \left[\frac{h_i}{2} + L \right] \tag{8.48}$$

where N = number of bays.

Preliminary beam sizes are presented in Table 8.7.

In the selection of beams the section compactness and the span-to-depth ratio must be considered. With the short 20-ft span used, limiting the depth to no more than 30 inches in the beam selection allows for the use of deep W27 columns, which are more efficient than W14 columns, while maintaining a clear span-to-depth ratio of 7 (the minimum permitted for SMF). The resulting span-to-depth ratio for a W30 beam (from face of column to face of column, based on nominal sizes) is 7, exactly the limit in AISC 358.

Level	Beam Size
Roof	W18 × 50
Fifth Floor	W27 × 94
Fourth Floor	W30 × 108
Third Floor	W30 × 116
Second Floor	W30 × 148

Table 8.7 Preliminary Beam Sizes

	Interior Column	Exterior Column
Upper Column	W27 × 217	W27 × 129
Lower Column	W27 × 307	W27 × 178

Table 8.8 Preliminary Column Sizes

Preliminary column sizes can be determined based on the beam sizes selected. Columns are typically spliced every two or four stories, and so the column size is determined from the strongest connecting beams. The column plastic section modulus Z should be checked in preliminary design so that it will meet the strong-column/weak-beam requirements of AISC 341 E3.4a; for preliminary design a minimum column to beam plastic section modulus ratio of at least 1.75 at interior (low axial load from overturning) moment frame columns and 2.5 at exterior (high axial load from overturning) moment frame columns is recommended to minimize the chance of failing the criterion in the later stages of design. Keep in mind these preliminary plastic section modulus ratios will ultimately be reduced by both connection overstrength in the beam and axial loads in the columns.

In this example columns are only spliced once: 4 ft above the third floor. Preliminary column sizes are shown in Table 8.8. Sizes are determined based on the moment of inertia assumptions, with the plastic section modulus checked as described above.

Using these preliminary sizes a three-dimensional computer model is constructed and a modal response spectrum analysis is performed. The interstory drift is found to be 2.15 in at the critical third story, resulting in an interstory drift ratio of 1.38%. Member sizes are revised so that the calculated drift is just below the allowable.

Because the proportioning assumptions used in the preliminary design are biased toward column strength, to allow for increased building drift the column size may be reduced. Similarly, to stiffen the building the beam sizes may be increased. Also, one might optimize the design by simultaneously increasing beam strength and decreasing column strength. However, in so doing one runs the risk of violating the strong-column/weak-beam proportioning.

Final member sizes based on drift control and stability requirements are presented in Table 8.9.

8.8.5 Member Checks

The column is checked for the combined effects of bending and axial forces. The effective length factor is determined using alignment

Level	Beam		Interior Column	Exterior Column
Roof	W18 × 50	Upper Column	W27 × 114	W27 × 94
Fifth Floor	W24 × 55			
Fourth Floor	W24 × 76			
Third Floor	W24 × 94	Lower Column	W27 × 161	W27 × 146
Second Floor	W24 × 94			

TABLE 8.9 Final Member Sizes

charts and including the destabilizing effects of leaning columns. Forces are determined using the basic load combinations:

$$R_u = 1.2D + 0.5L + E \tag{8.49}$$

$$R_u = 0.9D - E \tag{8.50}$$

Substituting the vertical component of seismic acceleration:

$$R_u = (1.2 + 0.2S_{DS})D + 0.5L + E \tag{8.51}$$

$$R_u = (0.9 - 0.2S_{DS})D - E \tag{8.52}$$

For the first-story interior-column the design forces are:

$$P_u = 284 \text{ kips}$$

$$M_u = 15{,}810 \text{ kip-in}$$

A separate check is performed on the columns for the axial forces determined using the amplified seismic load. For this check it is permitted to neglect moments. Implicit in this check is the expectation that some flexural yielding can be tolerated in the column.

$$R_u = 1.2D + 0.5L + \Omega_o E \tag{8.53}$$

$$R_u = 0.9D - \Omega_o E \tag{8.54}$$

Again, substituting the vertical component of seismic acceleration:

$$R_u = (1.2 + 0.2S_{DS})D + 0.5L + \Omega_o E \tag{8.55}$$

$$R_u = (0.9 - 0.2S_{DS})D - \Omega_o E \tag{8.56}$$

$$P_u = 291 \text{ kips}$$

The beam is likewise checked using the forces from the basic load combinations. Beam axial and flexural forces are considered in

combination. Typically axial forces are small and can be neglected. For the second floor beam the maximum moment is:

$$R_u = (1.2 + 0.2S_{DS})D + 0.5L + E \tag{8.57}$$

$$M_u = 8770 \text{ kip-in}$$

Both column and beam members have been selected from seismically compact shapes. For the column web, the exact compactness limit is a function of the axial force.

8.8.6 WUF-W Connection Design

The connection considered is at an interior column at the second floor. The column is a W27 × 161 and the connecting beams are W24 × 94.

This connection is not actually designed in the strictest sense. The use of a prequalified connection dictates conformance to the details of the connection as defined in AISC 358. The designer checks that this detail is adequate given the members used, the bay proportions, gravity load, and other relevant particulars of the condition under consideration. Figure 8.53 shows the connection design.

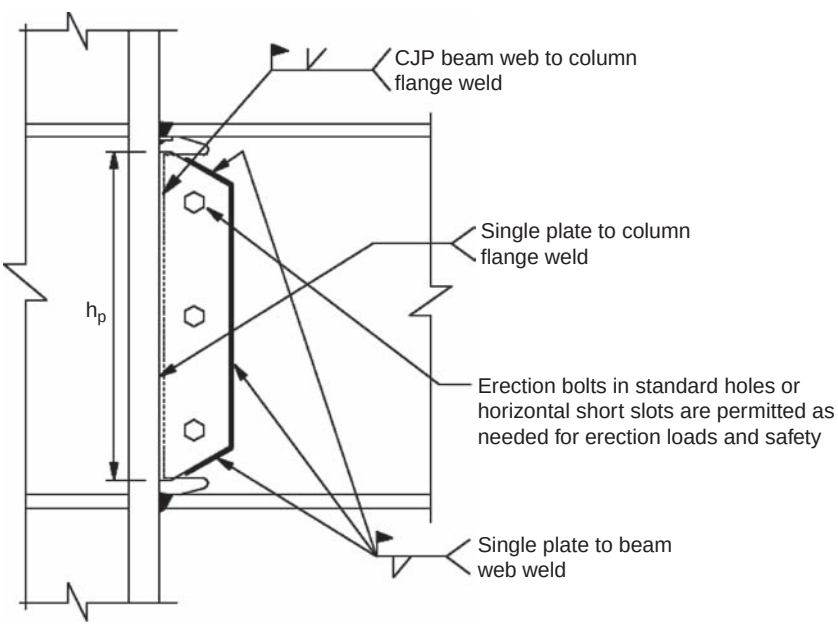

Figure 8.53 WUF-W beam-to-column connection (from AISC 358). (*Copyright © American Institute of Steel Construction. Reprinted with permission. All rights reserved.*)

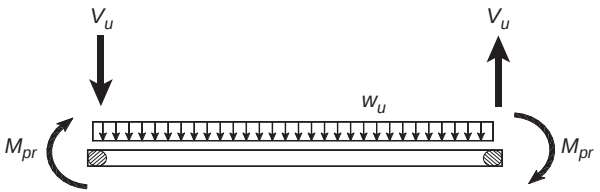

Figure 8.54 Free-body diagram of beam.

The determination of the forces used to check the connection begins with a free-body diagram of the beam (Figure 8.54). For consistency of reference, the frame will be considered to be deforming to the right such that the seismic moments imposed on each end of the beam are clockwise (and the seismic moments imposed on the column by each beam are counter-clockwise).

Following the AISC 358 method for a WUF-W connection the plastic hinge location is assumed to be at the column face. Plastic hinge moments are assumed to be the "probable moment" (M_{pr}), which includes both the expected material overstrength factor, R_y, and a factor for strain-hardening and other sources of connection overstrength, C_{pr}. For the WUF-W connection, $C_{pr} = 1.4$ per AISC 358.

$$\begin{aligned} M_{pr} &= C_{pr} R_y F_y Z \\ &= (1.4)(1.1)(50)(254) \\ &= 19{,}600 \text{ kip-in} \end{aligned} \tag{8.58}$$

The seismic shear is thus:

$$V_E = \frac{2M_{pr}}{L_h} \tag{8.59}$$

where L_h is the distance between plastic hinges. For this connection, L_h is taken to be the distance between column faces. L_h is $L - 2(\frac{1}{2}\, d_c) = 240 - 2(\frac{1}{2}\, 27.6) = 212.4$ in, V_E is 2(19,600)/(212.4) = 184 kips.

The gravity shear is determined from the appropriate load combination:

$$V_g = \frac{w_u L_h}{2} \tag{8.60}$$

$$w_u = 1.2D + 0.5L \tag{8.61}$$

Thus the shear at left side of the beam (where the seismic shear is aligned with gravity) is:

$$V_u = V_E + V_g = 196 \text{ kips} \tag{8.62}$$

and the shear at the right side of the beam is:

$$V_u = V_E - V_g = 172 \text{ kips} \tag{8.63}$$

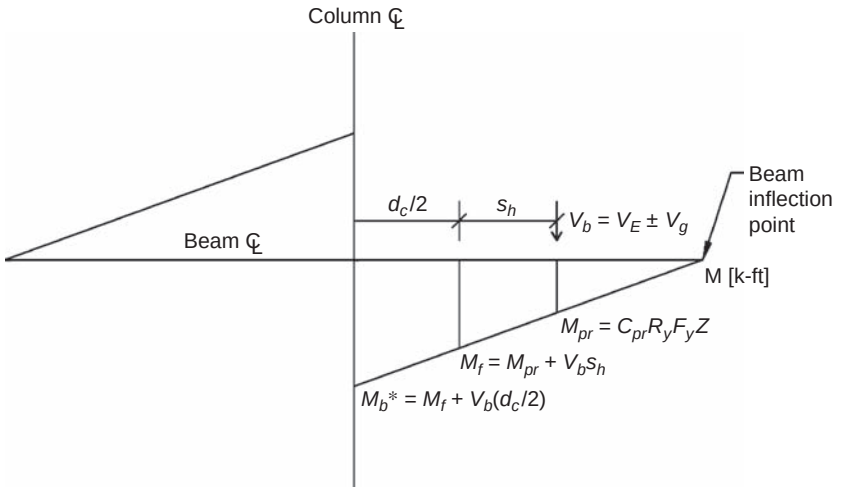

Figure 8.55 Projection of probable beam moment capacity to column centerline.

These shears are used to calculate the beam moments at the column face (for determining panel-zone shear) and at the column centerline (for checking the strong-column/weak-beam requirement). Figure 8.55 shows the projection of the probable moment to the column face and to the column centerline.

For reference, the beams are given the following designations (see Figure 8.56 below): Beam 1 is to the left of the column and Beam 2 is to the right.

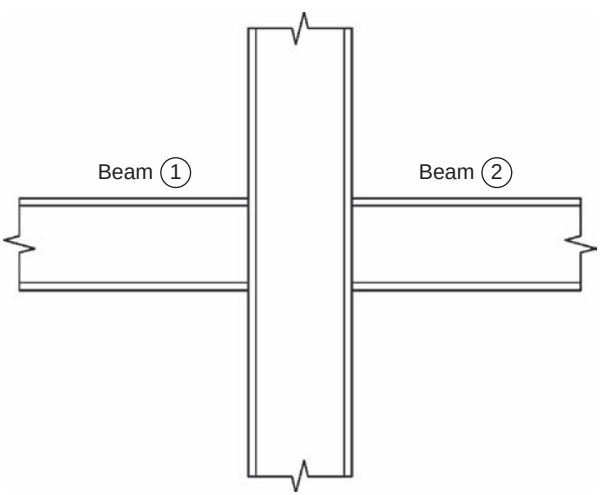

Figure 8.56 Beam identification convention.

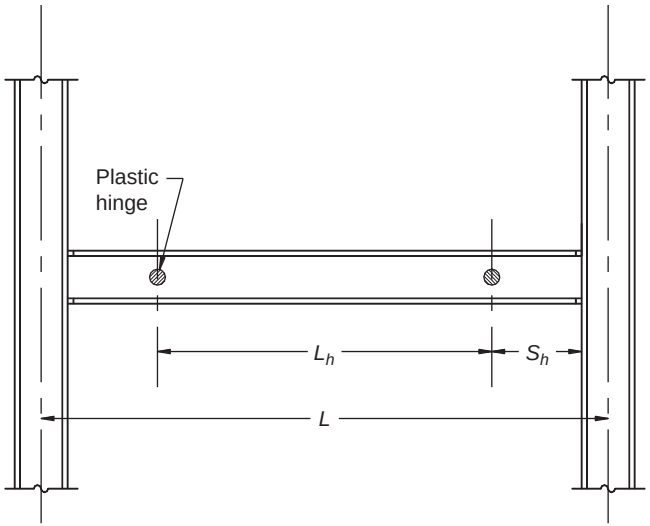

Figure 8.57 Location of plastic hinge.

At the left face of the column (at Beam 1) the moment is:

$$M_{f1} = M_{pr} + V_u s_h \qquad (8.64)$$
$$M_{f1} = 19{,}600 \text{ kip-in}$$

where s_h is the distance from the face of the column to the center of the plastic hinge as shown in Figure 8.57. For this connection, s_h is taken to be 0.

At the right face of the column (at Beam 2) the moment is:

$$M_{f2} = M_{pr} + V_u s_h \qquad (8.65)$$
$$M_{f2} = 19{,}600 \text{ kip-in}$$

At the centerline of the column the moment due to Beam 1 framing in from the left is:

$$M_{b1}{}^* = M_{pr} + V_u(s_h + \tfrac{1}{2} d_c) \qquad (8.66)$$
$$M_{b1}{}^* = 22{,}300 \text{ kip-in}$$

At the centerline of the column the moment due to Beam 2 framing in from the right is:

$$M_{b2}{}^* = M_{pr} + V_u(s_h + \tfrac{1}{2} d_c) \qquad (8.67)$$
$$M_{b2}{}^* = 21{,}900 \text{ kip-in}$$

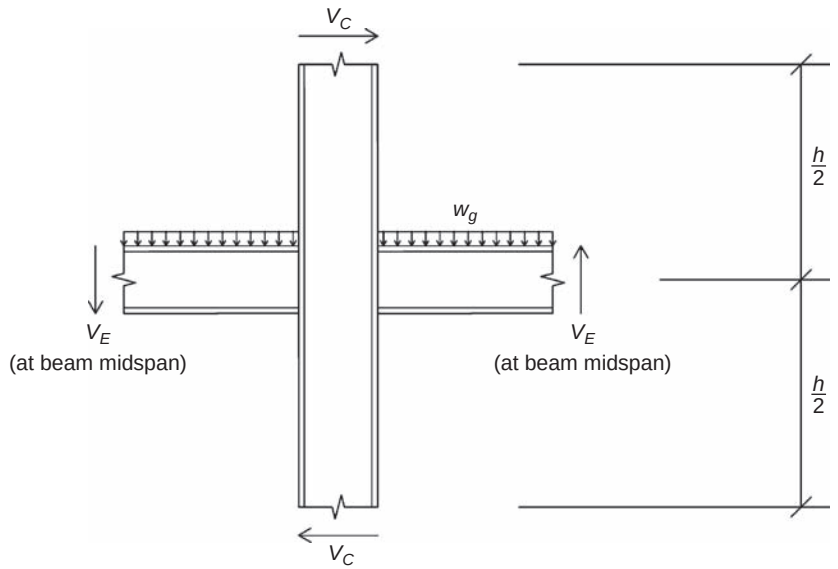

Figure 8.58 Free-body diagram of beam and column assembly.

The column shear corresponding to the probable beam strength can be estimated by assuming an inflection point at the column midheight above the connection and again at the column midheight below. Similarly, the beam inflection points are assumed to occur at midspan. Figure 8.58 shows the free-body diagram of a beam and column assembly from inflection point to inflection point.

To simplify the determination it is conservatively assumed that the column shear is the same above and below the connection. Thus:

$$V_c = \frac{\sum M_b^*}{\sum H/2} \tag{8.68}$$

$$V_c = \frac{(22{,}300 + 21{,}900)}{[(156 + 216)/2]}$$

$$V_c = 238 \text{ kips}$$

Now that these forces have been determined, the beam shear, strong-column/weak-beam, panel-zone, and continuity-plate requirements can be checked.

8.8.6.1 Beam Shear

The shear at the column face is compared with the beam shear strength:

$$\phi V_n = \phi\ 0.6 R_y F_y A_w \tag{8.69}$$

$$\phi V_n = 413 \text{ kips}$$

$$\phi V_n \geq V_u$$

8.8.6.2 Strong-Column/Weak-Beam

A virtual beam moment is calculated by projecting the moment at the column face to the column centerline. It is compared with a virtual column capacity which is determined by projecting the true capacity from the top flange level to the beam centerline.

A typical interior connection involves two beams (one to the left and one to the right of the columns), whereas an exterior one involves just one. At intermediate floors the continuous column is considered to be two columns (i.e., to represent a capacity based on its strength both above and below the connection).

The beam moment at the centerline of the column from the right end of the left beam (where the shear is lower) is: $M_{b1}^{*} = 21{,}900$ kip-in. The beam moment at the centerline of the column from the left end of the right beam (where the shear is greater) is: $M_{b2}^{*} = 22{,}300$ kip-in. The total moment at the column centerline is: $M_{b1}^{*} + M_{b2}^{*} = 44{,}200$ kip-in.

The column capacity is calculated considering both a reduction due to axial force and an increase in projecting the column moment corresponding to that capacity from the beam flange elevation to the beam centerline. The column shear corresponding to the probable beam strength is used to project the column flexural capacity from the point of maximum moment (at the beam flange level) to the beam centerline for purposes of comparison to the projected beam moment. Figure 8.59 shows this projection.

$$\sum M_c^{*} = 2\left[\left(F_y - \frac{P_u}{A}\right)Z + V_c \frac{1}{2} d_b\right]$$

$$\sum M_c^{*} = 2\left[\left(\frac{50 - 291}{47.6}\right)515 + (237.6)\frac{1}{2}(24.3)\right] \tag{8.70}$$

8.8.6.3 Panel-Zone Shear

The panel-zone shear demand is computed from the moments at the column face and reduced by the estimated column shear. The moment at the column face from one of the two connecting beams (Beam 2) has already been converted into a flange force (R_{u2}) for purposes of checking the need for continuity plates. The flange force (R_{u1}) at the opposite column face is similarly calculated from the moment from the other beam (Beam 1), and the resulting column panel-zone shear is computed.

Because the distance s_h is taken to be zero for this connection and identical beam sizes are used on each side, the moments at the opposite column faces are equal. Where s_h is greater than zero the gravity shear affects the projection of the moment to the column

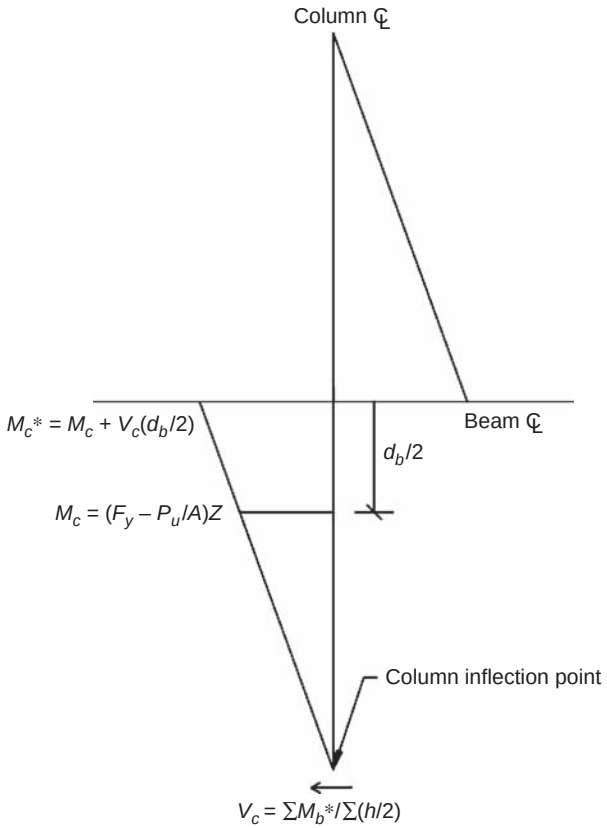

Figure 8.59 Projection of estimated column moment capacity to beam centerline.

face, increasing the moment on one side of the column and decreasing it on the other.

$$V_u = R_{u1} + R_{u2} - V_c \tag{8.71}$$

$$R_u = \frac{M_f}{(d_b - t_{bf})} \tag{8.72}$$

$$V_u = \frac{M_{f1}}{(d_b - t_{bf})} + \frac{M_{f2}}{(d_b - t_{bf})} - V_c$$

$$= 2\left[\frac{19{,}600}{(24.3 - 0.875)}\right] - 238$$

$$= 835 \text{ kips} + 835 \text{ kips} - 238 \text{ kips}$$

$$= 1430 \text{ kips}$$

The panel-zone shear capacity is:

$$\phi R_n = \phi\left(0.6F_y A_w + \frac{1.8b_{cf}t_{cf}^2F_y}{d_b}\right)$$

$$= 1.0\left[0.6(50)(27.6)(0.660) + \frac{1.8(14.0)(1.08)\,2(50)}{(24.3)}\right] \qquad (8.73)$$

$$= 607 \text{ kips}$$

$$\phi R_n \le R_u$$

Doubler plates are required. The deficit in web strength will be corrected by the addition of a doubler.

$$\phi R_n = \phi 0.6F_y t_{dp} d \qquad (8.74)$$

$$\phi R_n \ge R_u$$

$$t_{dp} \ge \frac{R_u}{(\phi 0.6\,F_y\,d)}$$

$$\ge \frac{1430 - 607}{(1.0)\;0.6\;(50)(27.6)}$$

$$t_{dp} \ge 1.00 \text{ in}$$

The minimum doubler thickness (without bracing) is:

$$t_{dp} \ge \frac{d_z + w_z}{90} \qquad (8.75)$$

$$\ge \frac{d_{b-2}t_{bf} + d_{c-2}t_{cf}}{90}$$

$$\ge \frac{24.3 - 2(0875) - 27.6 - 2(1.08)}{90} = 0.53 \text{ in}$$

Both the web and the doubler satisfy the limit. If either did not a plug weld (or series of plug welds) could be added connecting the doubler to the web and thus reducing the unbraced lengths d_z and w_z.

The doubler extends above and below the connection by 6 in. The welds at the top and bottom of the doubler are the AISC minimum welds (Figures 8.60 and 8.61). These help prevent shear buckling of the doubler. However, the main force transfer into the doubler is through the grove weld to the column flange. Note that AISC 341

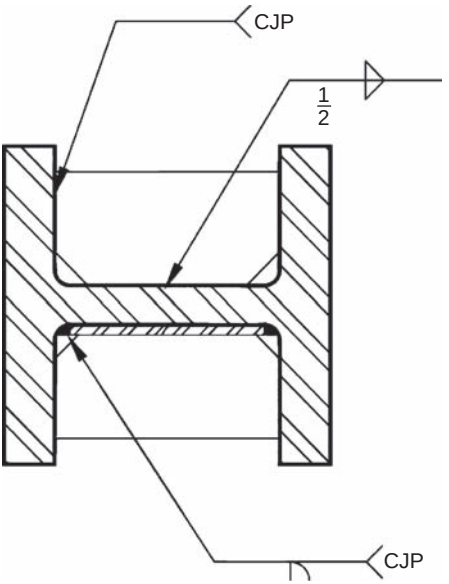

Figure 8.60 Doubler plate.

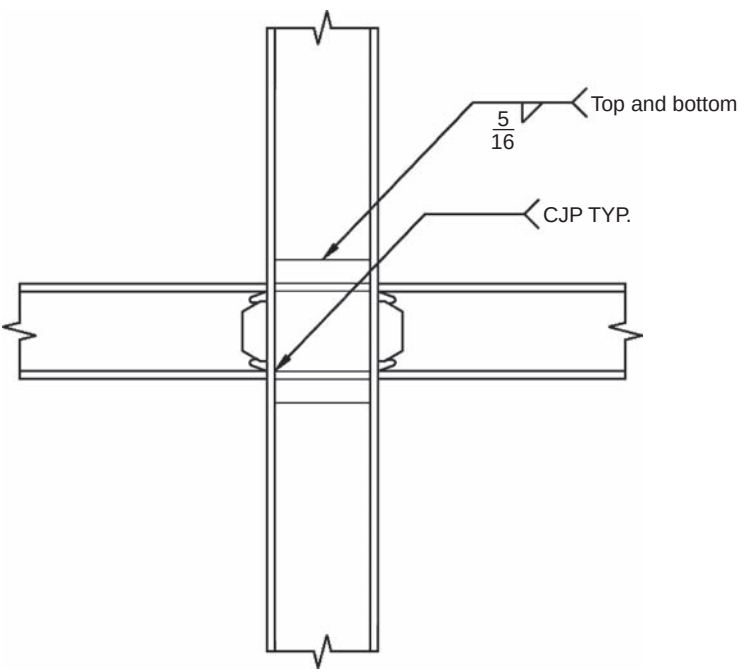

Figure 8.61 Doubler plate together with continuity plates.

indicates that these welds be designed for certain forces; in actuality the force patterns are much more complicated than the code indicates; the approach used here is supported by research (Lee et al. 2005b), although it may be at odds with AISC 341.

8.8.6.4 Continuity Plates

The need for continuity plates is checked considering the moment at the column face to be delivered as a force couple to the column flange:

$$R_u = \frac{M_f}{d_b - t_{bf}} \tag{8.76}$$

$$= \frac{19.558 \text{ kip-in}}{24.3 \text{ in} - 0.875 \text{ in}}$$

$$= 835 \text{ kips}$$

This demand need not exceed the maximum force that the flange can deliver. Based on the continuity plate criterion Eq. (8.77) this maximum is:

$$R_u \le 1.8\, b_{bf}\, t_{bf}\, F_{yb}\, R_{yb} \tag{8.77}$$

$$= 786 \text{ kips}$$

This demand is compared to the column web local yielding and crippling limit states. Two additional checks are performed on the column flange. Should any of these limit states be exceeded, continuity plates are required. The designer may consider a larger column section, smaller beam section, use of a doubler (or thicker doubler), or other adjustments to the design as well.

8.8.6.4.1 Column Web Local Yielding For this check the reinforced web thickness including the doubler is considered. Thus the effective web thickness is:

$$t_w = t_{wc} + t_d = 0.660 + 1.00 = 1.66 \text{ in}$$

$$\phi R_n \le \phi(5k + N) F_y t_w \tag{8.78}$$

$$\phi R_n \le \phi(5k + t_{wf}) F_y t_w$$

$$\phi R_n \le (100)[5(1.87) + (0.875)](50)(1.66) = 848 \text{ kips}$$

$$\phi R_n \le R_u$$

8.8.6.4.2 Column Web Crippling

$$\phi R_n = \phi 0.80 t_w^2 \left[1 + 3\left(\frac{N}{d}\right)\left(\frac{t_w}{t_f}\right)^{1.5}\right]\sqrt{\frac{EF_{yw}t_f}{t_w}} \tag{8.79}$$

$$\phi R_n = (0.75)0.80(1.66)^2 \left[1 + 3\left(\frac{0.875}{27.6}\right)\left(\frac{1.660}{1.08}\right)^{1.5}\right]\sqrt{\frac{29{,}000(50)1.08}{1.660}}$$

$$= 1900 \text{ kips}$$

$$\phi R_n \leq R_u$$

8.8.6.4.3 Column Flange Bending (Strength) This check is mandated by AISC 358. It supersedes the flange-bending check in AISC 360:

$$t_{cf} \geq 0.4\sqrt{1.8 b_{bf} t_{bf}\left(\frac{F_{yb}R_{yb}}{F_{yc}R_{yc}}\right)} \tag{8.80}$$

which can be rearranged into the format of familiar equations for flange local bending:

$$6.25\, tcf^2 F_{yc}R_{yc} \geq 1.8 b_{bf} t_{bf} F_{yb} R_{yb} \tag{8.81}$$

$$401 \text{ kips} \leq 786 \text{ kips}$$

This is no good (reinforcement required).

8.8.6.4.4 Column Flange Bending (Stiffness)

$$t_{cf} \geq \frac{b_{bf}}{6} \tag{8.82}$$

$$1.08 \text{ in} \geq 9.07 \text{ in}/6$$

$$1.08 \text{ in} \leq 1.51 \text{ in}$$

This is no good (reinforcement required).

Two of these checks indicate insufficient capacity in the column. (specifically the column flange, as the web has already been reinforced with a doubler plate), and thus continuity plates are required. The continuity plate must be designed to resist the difference between the demand and the capacity:

$$R_{uCP} = R_u - \phi R_n \tag{8.83}$$

$$= 786 \text{ kips} - 401 \text{ kips} = 385 \text{ kips}$$

In addition, its minimum thickness is governed by AISC 358, which states that the thickness must match the beam flange thickness (0.875 in for a W24 × 94) for two-sided connections.

Assuming the full beam flange width is effective, the required plate thickness is determined:

$$t_{CP} = \frac{R_u}{\phi F_y b_f} = \frac{385}{0.9(50)(9.07)} = 0.94 \text{ in} \tag{8.84}$$

One-inch continuity plates will be used.

8.8.7 Detailing

Detailing of the connection follows the requirements of AISC 358, as illustrated in Figure 8.62.

In addition, all welds of this connection are designated as "demand critical," indicating that they require high notch toughness. Also, the weld access hole requires a special geometry defined in AWS D1.8.

Finally, the region of the connection where inelastic strain is expected must be kept free of notches and defects caused by welded or shot-in attachments. The region to be kept clear, the "protected zone," extends from the column face one full beam depth in, as shown in Figure 8.63.

8.8.8 Bracing

In order for the beam to be able to undergo flexural yielding, lateral torsional buckling must be prevented, not only initially but through large inelastic rotations. This is done through lateral bracing at the beam-to-column connection, near the plastic hinge, and along the beam length.

The required bracing forces and stiffnesses are as shown below.

8.8.8.1 Bracing at the Beam-to-Column Connection

The column is braced at the top and bottom flange level. The required bracing force is:

$$P_{br} = 0.02 F_y b_f t_{bf} \tag{8.85}$$
$$P_{br} = 0.02(50)(9.07)(0.875) = 7.9 \text{ kips}$$

8.8.8.2 Bracing Near the Plastic Hinge

A brace is ostensibly required near the plastic hinge by AISC 358. However, in most building conditions this requirement is waived by

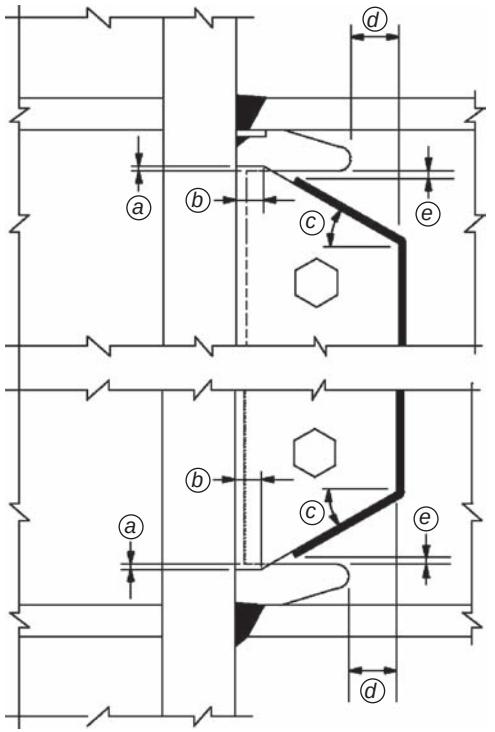

Notes:
a. 1/4 in (3 mm) minimum, 1/2 in (6 mm) maximum.
b. 1 in (25 mm) minimum.
c. 30° (±10°).
d. 2 in (50 mm) minimum.
e. 1/2-in (6 mm) minimum distance, 1-in (25 mm) maximum distance, from end of fillet weld to edge of weld access hole.

Figure 8.62 WUF-W beam-to-column connection (from AISC 358). (*Copyright © American Institute of Steel Construction. Reprinted with permission. All rights reserved.*)

an exception that allows the torsional stabilizing effect of the composite slab to substitute for this discrete brace.

$$P_u = \frac{0.06R_y Z F_y}{h_o} \tag{8.86}$$

$$\beta_{br} = \frac{1}{\phi}\left(\frac{10M_r C_d}{L_b h_o}\right) \tag{8.87}$$

where $h_o = d - t_f$ and $h_o = 24.3$ in $- 0.875$ in $= 23.4$ in

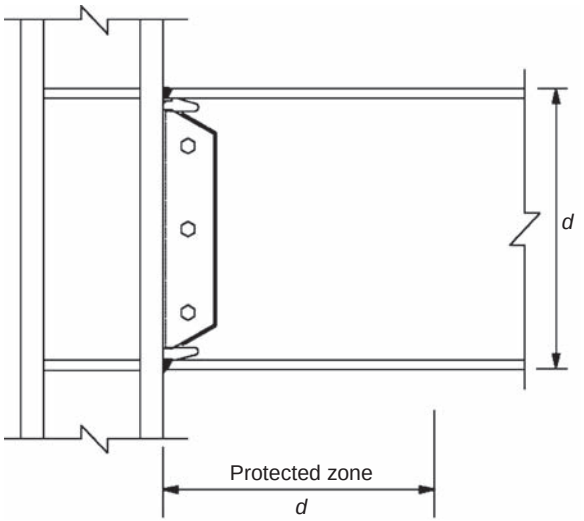

Figure 8.63 Protected zone (from AISC 358). (*Copyright © American Institute of Steel Construction. Reprinted with permission. All rights reserved.*)

Note that L_b should be taken to be L_q, the maximum unbraced length corresponding to the flexural demand, M_r, which is taken to be the expected flexural strength in this application. Thus the length L_q may be assumed to be equal to the limiting length L_p.

$$M_r = M_u = R_y Z F_y \tag{8.88}$$

$$M_r = 1.1(254)(50) = 14{,}000 \text{ kip-in}$$

$$C_d = 1.0$$

$$\phi = 0.75$$

$$P_{br} = \frac{0.06(1.1)(254)(50)}{(23.4)} = 35.8 \text{ kips}$$

$$P_{br} = \frac{10(14{,}000)(1.0)}{0.75(84)(23.4)} = 94.6 \text{ kips/in}$$

8.8.8.3 Bracing Along the Beam

$$P_{br} = \frac{0.02 M_r C_d}{h_o} \tag{8.89}$$

$$\beta_{br} = \frac{1}{\phi}\left(\frac{10 M_r C_d}{L_b h_o}\right) \tag{8.90}$$

$$L_b \le \frac{0.086 r_y E}{F_y} \tag{8.91}$$

$$P_{br} = \frac{0.02(14{,}000)(1.0)}{(23.4)} = 11.9 \text{ kips}$$

$$\beta_{br} = 66.3 \text{ kips/in from above}$$

$$L_b \le \frac{0.086(1.98)(29{,}000)}{(50)} = 98.8 \text{ in}$$

The beams will be braced at third points along the span.

8.8.9 Completion of Design

Several items remain to complete the design. These include:

- Column splices
- Base plates
- Foundations
- Diaphragms, chords, and collectors

Although each one of these items is necessary and important, the execution is similar to that of many other components of a building design.

8.9 Self-Study Problems

Problem 8.1 For the SMF shown, design the beam-to-column connections for the first story beam using only the following types of connections prequalified per AISC 358.

(a) WUFW connections
(b) Welded flange plate (WFP) connections
(c) Reduced beam section (RBS) connections
(d) Bolted stiffened end plate (BSEP) connections
(e) Bolted flange plate (BFP) connections
(f) Bolted bracket (BB) connections
(g) Free flange (FF) connections (using FEMA 350 connections details in this case)

Assume that, at the story under consideration, the beam is W30 × 173, and the columns are W14 × 311. All loads are shown below. Assume ASTM A992 Gr. 50 steel for beams and columns.

Check that the design satisfies the strong-column/weak-beam requirements, as well as all other applicable detailing requirements.

If one or many limits of applicability are found to be violated for a specific connection type, just highlight the violations and continue calculations as if the connection was permitted.

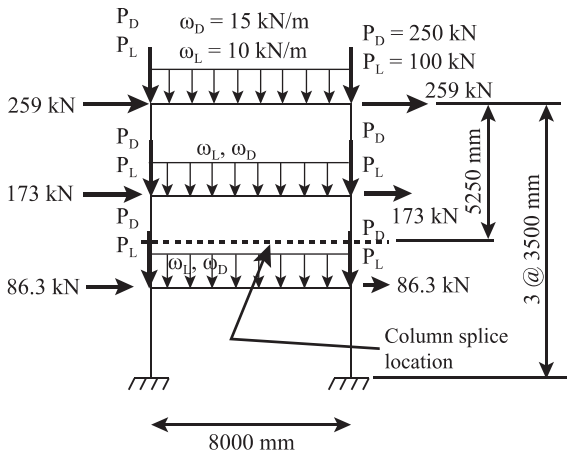

Problem 8.2 A single-story frame like the one shown consists of two exterior vertical members that serve as columns to resist the gravity loads, and a vertical member with RBS at its ends inserted at midbay of the frames to resist the lateral loads.

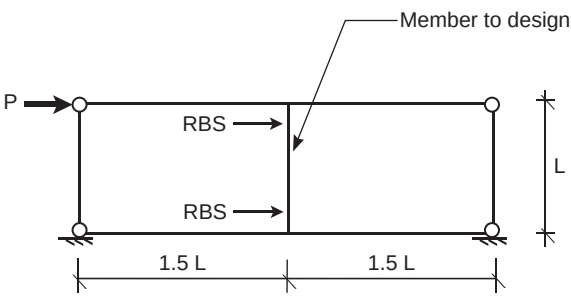

Here, for $L = 10'$ and $P = 100$ kips:

(1) Design the lightest W12 shape that can be used as the mid-bay vertical member, having a 50% reduction in flange width at the RBS locations, to resist the applied loads and to meet the AISC 358 specified limitations for the pre-qualified connection details. Clearly show the geometry/dimensions of the selected RBS.
   (a) Design the vertical member assuming that the shear force in that member does not affect its flexural plastic strength.
   (b) For the resulting vertical member designed in (a), calculate the flexural plastic strength of the member taking into account the presence of shear in that member. Indicate by how much (in %) the calculated strength of the structure is reduced as a result of this more refined calculation.
   (c) Compare the results in (a) and (b) and comment on why the difference is significant or insignificant. If significant, explain what could be done to compensate for this.

(2) Draw the moment and axial force diagrams for the top horizontal beam of that system, indicating the magnitude of the moments and forces that would have to be considered for the design of that beam.

Additional notes:

- The beams have simple connections at their ends.
- Organize design iterations in a tabular format.

There is no gravity load applied to this frame.

Optional design aspects that could be considered in this problem include: (a) design the shear connection of the vertical member to the beams; (b) design the beams, including checking the panel zone strength; and (c) check if continuity plates in the beams are needed.

Problem 8.3 Design a prequalified RBS connection for the beam of the SMRF structure shown. More specifically:

(1) Select an appropriate geometry for the RBS and location of the RBS along the beam length.
(2) Check whether the selected beams and columns meet the specified limitations and details of the prequalified connection.
(3) Check whether moment at face of column is acceptable.
(4) Check whether column panel zone strength is acceptable.

There is no gravity load applied to this frame.

Optional design aspects that could be considered in this problem include: (a) design the shear connection of the beam to the columns; (b) check if continuity plates are needed in the columns.

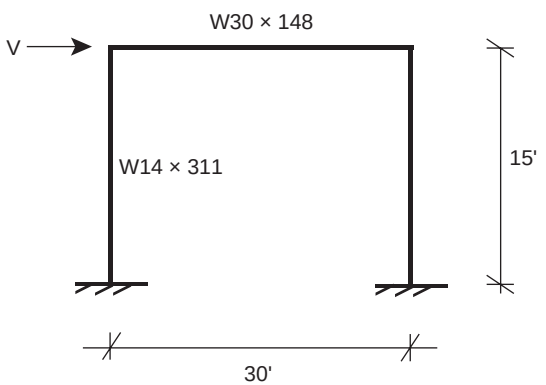

Problem 8.4 The structure shown in the figure below has RBS connections in each of its two beams. For simplicity in this problem:

- The depth of columns and beams are neglected for this problem (i.e., consider stick-members, as shown in the figure).
- The RBS are located at a distance of $L/10$ from the columns, and this eccentricity must be taken into account in calculations and in showing the resulting plastic collapse mechanism.

- M_p of the columns is assumed to be sufficiently large to ensure that plastic hinging only takes place in the two beams.
- All beams are W27 × 161.

Here:

(a) Assuming that the beam flanges have been cut to 50% of their original width, calculate the resulting M_p value at the RBS (in k-ft).
(b) Using the upper bound method, find the maximum load, V, that can be applied (in terms of L, h, M_p), and show the resulting plastic collapse mechanism.

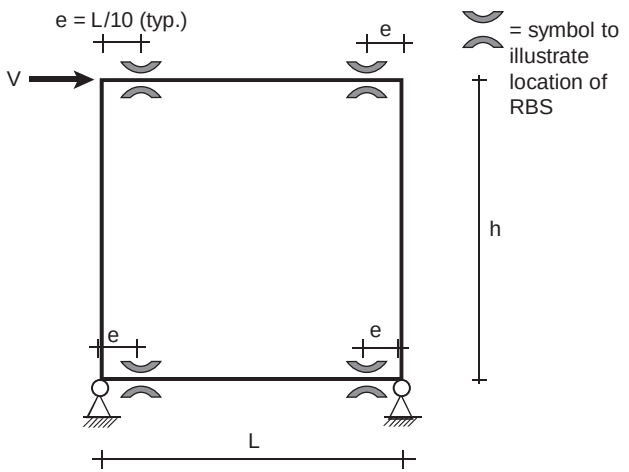

Problem 8.5 A twenty-story building was designed with special moment-resisting frames having RBS beam-to-column connections. The W33 × 354 beams have RBS connections with radius cuts per a geometry in compliance with AISC 358, and fully welded to the web of a W14 × 808 column. Both the columns and beams are of High Performance Steel (HPS) Grade 70.

(a) Identify all issues that make this design noncompliant to the AISC 358 requirements and details for prequalified RBS connections.
(b) Describe in two or three short sentences what would be required to use this proposed RBS connection design on a that specific building project. Cite the appropriate AISC 341 and 358 requirements.

Problem 8.6 What is the physical phenomenon intended to be captured by the C_{pr} factor in AISC 358?

Problem 8.7 Which of the prequalified types of welded connections can be used to connect a W36 × 256 to a W14 column?

Problem 8.8 (Project-Type Problem) Using examples, compare the designs that would result using traditional elastic versus plastic designs.

(a) For low-rise (2 to 5 stories) moment-resisting frames
(b) For mid-rise (8 to 12 stories) moment-resisting frames

Problem 8.9 (Project-Type Problem) Write a computer program to do the lower-bound systematic method of plastic analysis using the simplex algorithm.

References

AIJ. 1995. *Performance of Steel Buildings during the 1995 Hyogoken-Nanbu Earthquake.* (In Japanese with English summary). Tokyo: Architectural Institute of Japan.

AIJ. 1996. *Technical Recommendations for Steel Construction for Buildings* (Part 1 Guide to Steel-Rib Fabrication), 4th ed. Tokyo: Architectural Institute of Japan (in Japanese).

AISC. 1992. *Seismic Provisions for Structural Steel Buildings.* Chicago: American Institute of Steel Construction.

AISC. 1994. Proceedings of the AISC Special Task Committee on the Northridge Earthquake Meeting, American Institute of Steel Construction, Chicago, Illinois.

AISC. 2005. *Seismic Provisions for Structural Steel Buildings—ANSI/AISC 341-05.* Chicago: American Institute of Steel Construction.

AISC. 2010a. *Prequalified Connections for Special and Intermediate Steel Moment Frames for Seismic Applications—ANSI/AISC 358-10.* Chicago: American Institute of Steel Construction.

AISC. 2010b. *Seismic Provisions for Structural Steel Buildings—AISC 341-10.* Chicago: American Institute of Steel Construction.

AISC. 2010c. *Specification for Structural Steel Buildings—ANSI/AISC 360-10.* Chicago: American Institute of Steel Construction.

Allen, J., Partridge, J. E., Radau, S., and Richard, R. M. 1995. "Ductile Connection Designs for Welded Steel Moment Frames," *Proc. 64th Annual Convention, Structural Engineers Association of California*, p. 253–269.

ASCE. 2010. *Minimum Design Loads for Buildings and Other Structures, Standard ASCE/SEI 7-10*. Reston, VA: American Society of Civil Engineers.

Astaneh, A., Nader, M. N., and Malik, L. 1989. "Cyclic Behavior of Double Angle Connections." *Journal of Structural Engineering, ASCE,* vol. 115, no. 5, 1101–1118.

ATC. 1992. *Guidelines for Cyclic Testing of Components of Steel Structures, ATC-24.* Redwood City, CA: Applied Technology Council.

AWS. 2009. *AWS D1.8-09 Structural Welding Code—Seismic Supplement*. Miami, FL: American Welding Society.

Bartlett, F. M., Dexter, J. D., Graeser, M. D., Jelinek, J. J., Schmidt, B. J., and Galambos, T. V. 2003. "Updating Standard Shape Material Properties Database for Design and Reliability." *Engineering Journal, AISC*, vol. 40, no. 1, 2–14.

Becker, R. 1975. "Panel Zone Effect on the Strength and Stiffness of Steel Rigid Frames." *Engineering Journal, AISC*, vol. 12, no. 1, 19–29.

Bennett, D. 1995. *Skyscrapers*. New York: Simon and Schuster.

Bernal, D. 1987 "Amplification Factors for Inelastic Dynamic P-Delta Effects in Earthquake Analysis." *Earthquake Engineering and Structural Dynamics*, vol. 15, no. 5, 635–651.

Bernal, D., Nasseri, A., and Bulut, Y. 2006. Instability Inducing Potential of Near Fault Ground Motions SMIP06 Seminar on Utilization of Strong-Motion Data, p. 41–62.

Bertero, V. V., Anderson, J. C., and Krawinkler, H. 1994. "Performance of Steel Building Structures during the Northridge Earthquake," *Report No. UCB/EERC-94/09*. Berkeley: Earthquake Engineering Research Center, University of California.

Bertero, V. V., Krawinkler, H., and Popov, E. P. 1973. "Further Studies on Seismic Behavior of Steel Beam-to-Column Subassemblages," *Report No. UCB/EERC-73/27*. Berkeley: Earthquake Engineering Research Center, University of California.

Blodgett, O. 1995. "Evaluation of Beam to Column Connections." *SAC Steel Moment Frame Connections, Advisory No. 3, SAC-95-01*. Sacramento: SAC Joint Venture.

Bronson, W. 1959. *The Earth Shook, the Sky Burned—A Moving Record of American's Great Earthquake and Fire: San Francisco April 18, 1906*. San Francisco: Chronicle Books, p. 192.

Bruneau, M., and Mahin, S. A. 1991. "Full Scale Tests of Butt Welded Splices in Heavy Rolled Steel Sections Subjected to Primary Tensile Stresses." *Engineering Journal, AISC*, vol. 28, no. 1, 1–17.

Bruneau, M., Mahin, S. A., and Popov, E. P. 1987. "Ultimate Behavior of Butt Welded Splices in Heavy Rolled Steel Sections." *Report UBC/EERC-87/10*. Berkeley: Earthquake Engineering Research Center, University of California.

Charney, F. A., and Horvilleur, J. F. 1995. "A Technique for Evaluating the Effect of Beam-Column Joint Deformation on the Lateral Flexibility of Steel Frame Building Structures." *The Structural Design of Tall Buildings*, vol. 4, no. 1, 3–13.

Chen, S. J., and Yeh, C. H. 1994. "Enhancement of Ductility of Steel Beam-to-Column Connections for Seismic Resistance," *SSRC Technical Session*. Bethlehem, PA: Lehigh University.

Chen, S. J., Yeh, C. H., and Chu, J. M. 1996. "Ductile Steel Beam-to-Column Connections for Seismic Resistance." *Structural Journal, ASCE,* vol. 122, no. 11, 1292–1299.

Chen, W. F., and Liew, J. Y. R. 1992. "Seismic Resistant Design of Steel Moment-Resisting Frames Considering Panel-Zone Deformations." *Stability and Ductility of Steel Structures under Cyclic Loading*, Fukumoto, Y., and Lee, G., editors. p. 323–334.

Chen, W. F., Kishi, N., and Komuro, M. 2010. *Semi-Rigid Connections Handbook*. Fort Lauderdale, FL: J Ross Pub.

Choi, J., Stojadinovic, B., and Goel, S. C. 2003. "Design of Free Flange Moment Connection." *Engineering Journal*, *AISC*, vol. 40, no. 1, 25–41.

CSA. 2009. *Design of Steel Structures*., Mississauga, Ont, Canada: Canadian Standard Association.

Davidson, B. J., and Fenwick, R. C. 2004. "Design for P-Delta Effects as Proposed for the Australian and New Zealand Loadings Standards." SSRC/NASCC 2004 Joint Annual Stability Conference, Long Beach, California, March 2004.

EERI. 1990. "Loma Prieta Earthquake Reconnaissance Report." *Earthquake Spectra,* supplement C to vol. 6, Oakland, CA.

EERI. 1995. "Northridge Earthquake Reconnaissance Report. Vol. 1." *Earthquake Spectra,* supplement C to vol. 11, Oakland, CA.

EERI. 1996. "Northridge Earthquake Reconnaissance Report. Vol. 2." *Earthquake Spectra,* supplement C to vol. 11, Oakland, CA.

EERI. 1994. "Connections: Henry J. Degenkolb." *EERI Oral History Series*. Oakland, CA: Earthquake Engineering Research Institute, p. 226.

EERI. 1997. "Connections: George W. Housner." *EERI Oral History Series*. Oakland, CA: Earthquake Engineering Research Institute, p. 275.

Elnashai, A. S., and Elghazouli, A. Y. 1994. "Seismic Behavior of Semi-Rigid Steel Frames." *Journal of Constructional Steel Research,* vol. 29, no. 1–3, 149–174.

El-Tawil, S., Mikesell, T. D., Vidarsson, E., and Kunnath, S. K. 1999. "Inelastic Behavior and Design of Steel Panel Zones." *Journal of Structural Engineering, ASCE*, vol. 125, no. 2, 183–193.

El-Tawil, S. 2000. "Panel Zone Yielding in Steel Moment Connections." *Engineering Journal, AISC*, vol. 37, no. 3, 120–135.

Engelhardt, M. D., and Husain, A. S. 1993. Cyclic Loading Performance of Welded Flange-Bolted Web Connections. *Journal of Structural Engineering. ASCE*, vol. 119, no. 12, 3537–3550.

Engelhardt, M. D., and Sabol, T. A. 1994. "Testing of Welded Steel Moment Connections in Response to the Northridge Earthquake." *Progress Report to the AISC Advisory Committee on Special Moment-Resisting Frame Research*.

Engelhardt, M. D., and Sabol, T. A. 1995. "Lessons Learned from the Northridge Earthquake: Steel Moment Frame Performance." *Proceedings, New Directions in Seismic Design*. Tokyo. October. 1–12.

Engelhardt, M. D., and Sabol, T. A. 1996. "Reinforcing of Steel Moment Connections with Cover Plates: Benefits and Limitations." *Proceedings, U.S.-Japan Seminar on*

Innovations in Stability Concepts and Methods for Seismic Design in Structural Steel, Honolulu, Hawaii.
Engelhardt, M. D., Winneberger, T., Zekany, A. J., and Potyraj, T. J. 1996. "The Dogbone Connection: Part II." *Modern Steel Construction*, vol. 36, no. 8, 46–55.
Englekirk, R. 1994. *Steel Structures—Controlling Behavior through Design*. New York: John Wiley & Sons.
Englekirk, R. E. 1999. "Extant Panel Zone Design Procedures for Steel Frames are Questioned." *Earthquake Spectra, EERI*, vol. 15, no. 2, 361–370, Oakland, CA.
FEMA. 2000a. "Recommended Seismic Design Criteria for New Steel Moment-Frame Buildings," *Report FEMA-350*. Washington, D. C.: Federal Emergency Management Agency.
FEMA. 2000b. "Recommended Seismic Evaluation and Upgrade Criteria for Existing Welded Steel Moment-Frame Buildings." *Report FEMA-351*. Washington, D. C.: Federal Emergency Management Agency.
FEMA. 2000c. "Recommended Postearthquake Evaluation and Repair Criteria for Welded Steel Moment-Frame Buildings." *Report FEMA-352*. Washington, D. C.: Federal Emergency Management Agency.
FEMA. 2000d. "Recommended Specifications and Quality Assurance Guidelines for Steel Moment-Frame Construction for Seismic Applications." *Report FEMA-353*. Washington, D. C.: Federal Emergency Management Agency.
FEMA. 2000e. "State of the Art Report on Systems Performance of Steel Moment Frames Subject to Earthquake Ground Shaking." *Report No. FEMA-355C*. Washington, D. C.: Federal Emergency Management Agency.
FEMA. 2000f. "State-of-the-Art Report on Connection Performance." *Report No. FEMA-355D*. Washington, D. C.: Federal Emergency Management Agency.
FEMA. 2000g. "State of the Art Report on Past Performance of Steel Moment-Frame Buildings in Earthquakes." *Report No. FEMA-355E*. Washington, D. C.: Federal Emergency Management Agency.
FEMA. 2009. "Quantification of Building Seismic Performance Factors." *FEMA Report P-695*, Washington, D. C.: Federal Emergency Management Agency.
Fielding, D. J., and Chen, W. F. 1973. "Steel Frame Analysis and Connection Shear Deformation." *Journal of the Structural Division, ASCE*, vol. 99, ST1, 1–18.
Fielding, D. J., and Huang, J. S. 1971. "Shear in Steel Beam-to-Column Connections." *Welding Journal*. July.
Freeman, J. R. 1932. *Earthquake Damage and Insurance*. New York: McGraw-Hill, p. 904.
Ghobarah, A., Osman, A., and Korol, R. M. 1990. "Behaviour of Extended End-Plate Connections under Cyclic Loading." Engineering Structures, vol. 12, 15–26, ElsevierScience Publishers, London, England.
Ghobarah, A., Korol, R. M., and Osman, A. 1992. "Cyclic Behavior of Extended End-Plate Joints." ASCE *Structural Journal*, vol. 118, no. 5, 1333–1353.
Graham, J. D., Sherbourne, A. N., and Khabbaz, R. N. 1959. *Welded Interior Beam-to-Column Connections.* Chicago: American Institute of Steel Construction.
Goel, S. C., and Stojadinovic, B., and Lee, K. H. 1997. "Truss Analogy for Steel Moment Connections," *Engineering Journal, AISC*, vol. 33, no. 2, 2nd Quarter, 43–53.
Hajjar, J. F., Dexter, R. J., Ojard, S. D., Ye, Y., and Cotton, S. C. 2003. *Continuity Plate Detailing for Steel Moment-Resisting Connections*, vol., no. 4, 189–211.
Hamburger, R. O. 1996. "More on Welded Moment Connections." *NEWS*. April. San Francisco: Structural Engineers Association of California (also available at http://www.seaoc.org/seaoc/seaonc/nl496/ncnl496.htm).
Hamburger, R. O., Malley, J. O., and Miller, D. K. 2007. "New AWS D1.8 Seismic Welding Supplement Outlined." *Welding Journal*, p. 28–31, February 2007.
Hamburger, R. O., Krawinkler, H., Malley, J. O., and Adan, S. M. 2009. "Seismic Design of Steel Special Moment Frames: A Guide for Practicing Engineers." *NEHRP Technical Brief No. 2, Report NIST GCR 09-917-3*. Gaithersburg, MD: National Institute of Standards and Technology.
Ibarra, L. F., Medina, R. A., and Krawinkler, H. 2005. "Hysteretic models that incorporate strength and stiffness degradation." *Earthquake Engineering and Structural Dynamics*, 34, 1489–1511.

ICBO. 1988, 1997. *Uniform Building Code*. Whittier, CA: International Conference of Building Officials.

Iwankiw, R. N., and Carter, C. J. 1996. "The Dogbone: A New Idea to Chew On." *Modern Steel Construction*, vol. 36, no. 4, 18–23.

Kato, B. 1973. "Brittle Fracture of Heavy Steel Members," *Proceedings of the National Conference on Tall Buildings. Architectural Institute of Japan*, August, Tokyo, 99–100.

Kato, B., and Morita, K. 1969. "Brittle Fracture of Heavy Steel Structural Members" (in Japanese). *Transactions of the Architectural Institute of Japan*, no. 156, February, Tokyo.

Kaufmann, E. J., Xue, M., Lu, L. W., and Fisher, J. W. 1996. "Achieving Ductile Behavior of Moment Connections." *Modern Steel Construction*, vol. 36, no. 1, 30–39.

Kawashima, K., MacRae, G. A., Hoshikuma, J., and Nagaya, K. 1996. "Residual Displacement Response Spectrum And Its Application To Reinforced Concrete Bridge Piers." *Wind and Seismic Effects: Proceedings of the 28th Joint Meeting of the US-Japan*, August 1996.

Kim, T., Whittaker, A. S., Gilani, A. S. J., Bertero, V. V., and Takhirov, S. M. 2000. "Cover-plate and flange-plate reinforced steel moment-resisting connections." Report PEER 2000/07, Pacific Earthquake Engineering Research Center, University of California at Berkeley, Berkeley, California.

Krawinkler, H. 1978. "Shear in Beam-Column Joints in Seismic Design of Steel Frames." *Engineering Journal, AISC*, vol. 5, no. 3, 82–91.

Krawinkler, H., Bertero, V. V., and Popov, E. P. 1971. "Inelastic Behavior of Steel Beam-to-Column Subassemblages." *Report No. UCB/EERC-71/7*. Berkeley: Earthquake Engineering Research Center, University of California.

Krawinkler, H., Bertero, V. V., and Popov, E. P. 1975. "Shear Behavior of Steel Frame Joints." *Journal of the Structural Division, ASCE*, vol. 101, ST11, 2317–2336.

Krawinkler, H. 2006. "Importance of Good Nonlinear Analysis." *Struct. Design Tall Spec. Build*, vol. 15, 515–531.

Lavan O., Sivaselvan, M. V., Reinhorn A. M., and Dargush, G. F. 2009. "Progressive Collapse Analysis Through Strength Degradation and Fracture in the Mixed Lagrangian Framework." *International Journal of Earthquake Engineering and Structural Dynamics*, 38, no. 13, 1483–1504.

Lee, C. H., Jeon, S. W., Kim, J. H., and Uang, C. M. 2005a. "Effects of Panel Zone Strength and Beam Web Connection Method on Seismic Performance of Reduced Beam Section Steel Moment Connections." *Journal of Structural Engineering, ASCE,* vol. 131, no. 12, 1854–1865.

Lee, D., Cotton, S. C., Hajjar, J. F., Dexter, R. J., and Ye, Y. 2005b. "Cyclic Behavior of Steel Moment-Resisting Connections Reinforced by Alternative Column Stiffener Details: II. Panel Zone Behavior and Doubler Plate Detailing." *Engineering Journal, AISC*, vol. 42, no. 4, 215–238.

Leet, K., Uang, C. M., and Gilbert, A. 2011. "*Fundamentals of Structural Analysis*," 4th ed. New York: McGraw-Hill.

Leon R, Forcier, G. P., Roeder, C. W., and Reece, F. R. 1994. "Cyclic Performance of Riveted Connections." *ASCE Struct Congr XII*, Atlanta, p. 1490–1495.

Lignos, D. G., Krawinkler, H., and Whittaker, A. S. 2008. "Shaking Table Collapse Tests of Two Scale Models of a 4-Story Moment Resisting Frame." *Paper No. 12-01-0186, Proceedings of the 14th World Conference on Earthquake Engineering*, Beijing.

Liu, J., and Astaneh, A. 2000. "Cyclic Testing of Simple Connections Including Effects of Slab." *Journal of Structural Engineering*. vol. 126, no. 1, 32–39.

Liu, J. 2003. "Examination of Expected Yield and Tensile Strength Ratios," *Draft Addendum Report*. Chicago: American Institute of Steel Construction.

MacRae, G. A., Carr, A. J., and Walpole, W. R. 1990. "The Seismic Response of Steel Frames." *Research Report 90-6*. Christchurch, NZ: Department of Civil Engineering, University of Canterbury.

MacRae, G. A., and Kawashima, K. 1993. "The Seismic Response of Bilinear Oscillators Using Japanese Earthquake Records." *Journal of Research*, vol. 30, Public Works Research Institute, Tsukuba, Japan.

MacRae GA. 1994. "P–Δ effects on single-degree-of-freedom structures in earthquakes." *Earthquake Spectra*; vol. 10, no. 3, 539–568.
MacRae, G. A., Priestley, M. J. N., and Tao, J. 1993. "*P*-Δ Effects in Seismic Design." *Report No. SSRP-93/05*. San Diego: Department of Applied Mechanics and Engineering Sciences, University of California.
MacRae, G. A., Urmson, C. R., Walpole, W. R., Moss, P., Hyde, K., and Clifton, G. C. 2009. "Axial Shortening of Steel Columns in Buildings Subjected to Earthquakes." *Bulletin of the NZ Society of Earthquake Engineering*, vol. 42, no. 4, 275–287.
MacRae, G. A., Kimura, Y., and Roeder, C. 2004. "Effect of Column Stiffness on Braced Frame Seismic Behavior." *Journal of Structural Engineering*, *ASCE*, vol. 127, no. 5, 490–497.
NRCC. 2010. *National Building Code of Canada*. Ottawa, Ont., Canada: National Research Council of Canada.
Mazzolani, F. M., and Piluso, V. 1996. *Theory and Design of Seismic Resistant Frames*. London: E&FN Spon.
Miller, D. K. 2006. *Design Guide 21: Welded Connections—A Primer for Engineers.* Chicago: American Institute of Steel Construction.
Miranda, E., and Akkar, S. D. 2003. "Dynamic Instability of Simple Structural Systems." *Journal of Structural Engineering*, *ASCE*, vol. 129, no. 1, 1722–1726.
Nakashima, M., Inoue, K., and Tada, M. 1998. "Classification of Damage to Steel Buildings Observed in the 1995 Hyogoken-Nanbu Earthquake." *Engineering Structures*, vol. 20, no. 4–6, 271–281.
Nakashima, M., and Sawaizumi, S. 2000. "Column-to-Beam Strength Ratio Required for Ensuring Beam-Collapse Mechanisms in Earthquake Response of Steel Moment Frames," *Proceedings, 12WCEE, paper #1109/6/A*, Auckland, New Zealand.
Nakashima, M., Roeder, C. W., and Maruoka, Y. 2000. "Steel Moment Frames for Earthquakes in the United States and Japan." *Journal of Structural Engineering, ASCE*, vol. 126, no. 8, 861–868.
Nakashima, M., Kato, M., and Okazaki, T. 2004. "Collaboration between Practice and Research for Development of Steel Construction in Japan." *Journal of Steel Structures, Korean Society of Steel Construction*, vol. 4, no. 4, 249–262.
Nakashima, M. 2001. "APPENDIX C. Overview of Damage to Steel Building Structures Observed in the 1995 Kobe Earthquake." *Past Performance of Steel Moment-Frame Buildings in Earthquakes, Federal Emergency Management Agency, Report FEMA-355E*, June 2001, C-1-C24.
Nelson, R. F. 1995. "Proprietary Solution." *Modern Steel Construction*, vol. 36, no. 1, 40–44.
Noel, S., and Uang, C. M. 1996. "Cyclic Testing of Steel Moment Connections for the San Francisco Civic Center Complex." *Test report to HSH Design/Build Structural Systems Research Project. Division of Structural Engineering Report No. TR-96/07,* San Diego: University of California.
Obeid, K. 1996. "Steel Moment Frame Connections: Shear in the Panel Zone." *NEWS*. April. San Francisco: Structural Engineers Association of California.
Osman, A., Korol, R. M., and Ghobarah, A. 1990. "Seismic Performance of Extended End-Plate Connections." *Proceedings of the 4th National U.S. Conference on Earthquake Engineering*. Oakland, CA: Earthquake Engineering Research Institute.
Plumier, A. 1990. "New Idea for Safe Structures in Seismic Zones." *IABSE Symposium*, Brussels, Belgium: University of Liege.
Popov, E. P. 1968. *Introduction to Mechanics of Solids*, Englewood Cliffs, NJ: Prentice Hall.
Popov, E. P. 1987. "Panel Zone Flexibility in Seismic Moment Joints." *Journal of Constructional Steel Research*, vol. 8, no. 1, 91–118.
Popov, E. P., Amin, N. R., Louie, J. J., and Stephen, R. M. 1985. "Cyclic Behavior of Large Beam-Column Assemblies." *Earthquake Spectra*, *Earthquake Engineering Research Institute,* vol. 1, no. 2, 203–238.
Popov, E. P., and Bertero, V. V. 1973. "Cyclic Loading of Steel Beams and Connections." *Journal of the Structural Division, ASCE*, vol. 99, ST6, 1189–1204.

Popov, E. P., Bertero, V. V., and Chandramouli, S. 1975. "Hysteretic Behavior of Steel Columns," *Report UCB/EERC-75-11*. Berkeley: Earthquake Engineering Research Center, University of California.

Popov, E. P., and Pinkney, R. B. 1969. "Cyclic Yield Reversals in Steel Building Connections." *Journal of the Structural Division, ASCE*, vol. 95, no. ST3, 327–353.

Popov, E. P., and Stephen, R. M. 1972. "Cyclic Loading of Full-Size Steel Connections," *Bulletin No. 21*. New York: American Iron and Steel Institute.

Popov, E. P., and Stephen, R. M. 1970. "Cyclic Loading of Full-Size Steel Connections," *Report UCB/EERC-70-3*. Berkeley: Earthquake Engineering Research Center, University of California.

Popov, E. P., and Stephen, R. M. 1977. "Tensile Capacity of Partial Penetration Welds." *ASCE Journal of the Structural Division*, vol. 103, no. ST9.

Popov, E. P., and Tsai, K. C. 1989. "Performance of Large Seismic Steel Moment Connections under Cyclic Loads." *Engineering Journal, AISC*, vol. 26, no. 2, 51–60.

Popov, E. P. Tsai, K. C., and Engelhardt, M. D. 1989. "On Seismic Steel Joints and Connections." *Engineering Structures*, vol. 11, no. 4, 193–209.

Radziminski, J. B., and Azizinamini, A. 1986. "Low Cyclic Fatigue of Semi-Rigid Steel Beam-to-Column Connections." *Proceedings of the 3rd U.S. National Conference on Earthquake Engineering*, vol. 2, 1285–1296. Oakland, CA: Earthquake Engineering Research Institute.

Ricles, J. M., Mao, L., Kaufmann, E. J., Lu, L., and Fisher, J. W. 2000. "Development and Evaluation of Improved Details for Ductile Welded Unreinforced Flange Connections." *Report No. SAC/BD-00/24*. Sacramento, CA: SAC Joint Venture.

Roeder, C. W. Carpenter, J. E., and Taniguchi, H. 1989. "Predicted Ductility Demands for Steel Moment-Resisting Frames." *Earthquake Spectra*, vol. 5, no. 2, 409–427.

Roeder, C. W., and Foutch, D. A. 1995. "Experimental Results for Seismic Resistant Steel Moment Frame Connections." *Journal of Structural Engineering, ASCE,* vol. 122, no. 6, 581–588.

Roeder, C. W., Knechtel, B, Thomas, E., Vaneaton, A, Leon, R. T., and Preece, F. R. 1996. "Seismic Behavior of Older Steel Structures." *Journal of Structural Engineering, ASCE,* vol. 122, no. 4, 365–373.

Rodgers, J. E., and Mahin, S. A. 2006. "Effects of Connection Fractures on Global Behavior of Steel Moment Frames Subjected to Earthquakes." *Journal of Structural Engineering, ASCE,* vol. 132, no. 1, 78–88.

Rosenbaum, D. B. 1996. "Welds in Bay Area Hit by Quake, Too." *Engineering News Record*, vol. 237, no. 11, 10.

Rutenberg, A., and DeStefano, M. 2000. "Approximate Stability Bounds on the Seismic Force Reduction Factor," *Paper no. 1635, Proceedings of the 12th World Conference on Earthquake Engineering*, Auckland, New Zealand.

SAC. 1995a. "Steel Moment Frame Connections—Advisory No. 3." *SAC-95-01*. Sacramento, CA: SAC Joint Venture.

SAC. 1995b. "Interim Guidelines: Evaluation, Repair, Modification and Design of Welded Steel Moment Frame Structures." *Program to Reduce the Earthquake Hazards of Steel Moment Frame Structures. Federal Emergency Management Agency, Report FEMA 267/SAC-95-02*. Sacramento, CA: SAC Joint Venture.

SAC. 1997. "Interim Guidelines Advisory No. 1: Supplement to FEMA 267." *Program to Reduce the Earthquake Hazards of Steel Moment Frame Structures. Federal Emergency Management Agency, Report FEMA 267A/SAC-96-03*. Sacramento, CA: SAC Joint Venture.

SAC. 1999. "Interim Guidelines Advisory No. 2: Supplement to FEMA 267." *Program to Reduce the Earthquake Hazards of Steel Moment Frame Structures. Federal Emergency Management Agency, Report FEMA 267B/SAC-99-01*. Sacramento, CA: SAC Joint Venture.

Sarraf, M., Bruneau, M. 1994. "Experimental Study on Cyclic Behavior of Riveted Stiffened-Seat Angle Connections." *Ottawa Carleton Earthquake Engineering Research Centre report OCEERC 94-01*, Ottawa, December 1994, p. 172.

Sarraf, M., and Bruneau, M. 1996. "Cyclic Testing of Existing and Retrofitted Riveted Stiffened-Seat Angle Connections." *ASCE Structural Journal*, vol. 122, no. 7, 762–775.

Schneider, S. P., Roeder, C. W., and Carpenter, J. E. 1992. "Seismic Behavior of Moment-Resisting Steel Frames: Experimental Study." *ASCE Structural Journal*, vol. 119, no. 6, 1885–1902.

SEAOC. 1995. *Interim Recommendations for Design of Steel Moment-Resisting Connection*. Sacramento, CA: Structural Engineers Association of California.

SEAOC. 1980, 1988, 1990. *Recommended Lateral Force Requirements and Commentary*. Sacramento, CA: Seismology Committee, Structural Engineers Association of California.

Sivaselvan, M. V., and Reinhorn, A. M. 2000. "Hysteretic models for deteriorating structures." *J. Eng. Mech., ASCE*, vol. 126, 633–640.

Sivaselvan, M. V., and Reinhorn, A. M. 2002. "Collapse Analysis: Large Inelastic Deformations Analysis of Planar Frames." *Journal of Structural Engineering, ASCE*, vol. 128, no. 12, 1575–1583.

Sivaselvan, M. V., and Reinhorn, A. M. 2006. "Lagrangian Approach to Structural Collapse Simulation." *J. Eng. Mech., ASCE*, vol. 132, 795–805.

SSPC. 1994. *Statistical Analysis of Tensile Data for Wide Flange Structural Shapes*. Structural Shape Producers Council, Washington, D.C.

Stockmann, M., and Schlafly, T. J. 2008. "Digging Through the Rubble, Part 1 and 2." *Modern Steel Construction*, October and November.

Stojadinovic, B., Goel, S. C., Lee, K. H., Margarian, A. G., and Choi, J. 2000. "Parametric Tests on Unreinforced Steel Moment Connections." *Journal of Structural Engineering, ASCE*, vol. 126, no. 1, 40–49.

Suita, K., Tamura, T., Morita, S., Nakashima, M., and Engelhardt, M. D. 1999. "Plastic Rotation Capacity of Steel Beam-to-Column Connection Using a Reduced Beam Section and No Weld Access Hole Design—Full-Scale Tests for Improved Steel Beam-to-Column Subassemblies Part 1." *Journal of Structural and Construction Engineering, AIJ*, vol. 526, 177–184.

Suita, K., Yamada, S., Tada, M., Kasai, K., Matsuoka, Y., and Sato, E. 2008. "Results of Recent E-Defense Tests on Full-Scale Steel Buildings: Part I—Collapse Experiments on 4-Story Moment Frames," *Paper no. 266, Proceedings, ASCE Structures Congress*, Vancouver, Canada.

Tremblay, R., Bruneau, M., Nakashima, M., Prion, H. G. L., Filiatrault, A., and DeVall, R. 1996. "Seismic Design of Steel Buildings: Lessons from the 1995 Hyogoken Nanbu Earthquake." *Canadian Journal of Civil Engineering*, vol. 23, no. 3, 757–770.

Tremblay, R. Timler, P., Bruneau, M., and Filiatrault, A. 1995. "Performance of Steel Structures during the January 17, 1994, Northridge Earthquake." *Canadian Journal of Civil Engineering*, vol. 22, no. 2, 338–360.

Tsai, K. C., and Popov, E. P. 1990a. "Cyclic Behavior of End-Plate Moment Connections." *ASCE Structural Journal*, vol. 116, no. 11, 2917–2930.

Tsai, K. C., and Popov, E. P. 1990b. "Seismic Panel Zone Design Effect on Elastic Story Drift in Steel Frames." *ASCE Structural Journal*, vol. 116, no. 12, 3285–3301.

Tsai, K. C., and Popov, E. P. 1988. "Steel Beam-Column Joints in Seismic Moment-Resisting Frames," *Report UCB/EERC-88/19*. Berkeley: Earthquake Engineering Research Center, University of California.

Tsai, K. C., Wu, S., and Popov, E. P. 1995. "Experimental Performance of Seismic Steel Beam-Column Moment Joints." *ASCE Structural Journal*, vol. 121, no. 6, 925–931

Uang, C. M. 1995. *Dynamic Testing of Large-Size Steel Moment Connections*. VHS-video of tests. San Diego: University of California.

Uang, C. M., and Bondad, D. M. 1996. "Dynamic Testing of Full-Scale Steel Moment Connections." *Proceedings of 11th World Conference on Earthquake Engineering, Acapulco, Paper 407*. CD-ROM. New York: Pergamon Press.

Uang, C. M., and Noel, S. 1995. "Cyclic Testing of Rib-Reinforced Steel Moment Connection with Reduced Beam Flanges." *Test report to Ove Arup & Partners. Structural systems research project. Division of Structural Engineering Report No. TR-95/04*. San Diego: University of California.

Uang, C. M., and Noel, S. 1996. "Cyclic Testing of Strong- and Weak-Axis Steel Moment Connection with Reduced Beam Flanges." *Final Report to the City of*

Hope. Division of Structural Engineering Report No. TR-96/01. San Diego: University of California.

Vian, D., and Bruneau, M. 2001. "Experimental Investigation Of P-Delta Effects To Collapse During Earthquakes," *Technical Report MCEER 01-0001*. Buffalo, NY: Multidisciplinary Center For Earthquake Engineering Research, University at Buffalo (available at http://civil.eng.buffalo.edu/users_ntwk/experimental/case_studies/vian/).

Vian, D., and Bruneau., M. 2003. "Tests to Structural Collapse of Single Degree of Freedom Frames Subjected to Earthquake Excitation." *Journal of Structural Engineering, ASCE*, vol. 129, no. 12, 1676–1685.

Villaverde, R. 2007. "Methods to Assess the Seismic Collapse Capacity of Buildings Structures: State of the Art." *Journal of Structural Engineering, ASCE*, vol. 133, no. 1, 57–66.

Wolfe, J., Nienberg, M., Manmohan, D., Halle, J., and Quintana, M. 1996. "Welding Alert, Cover Plated Moment Frame Connections." *NEWS*, April. San Francisco: Structural Engineers Association of California.

Wakabayashi, M. 1986. *Design of Earthquake-Resistant Buildings*. New York: McGraw-Hill.

Whittaker, A., Bertero., V., and Gilani, A. 1995. "Testing of Full-Scale Steel Beam-Column Assemblies." *SAC Phase I Report*. Sacramento, CA: SAC Joint Venture.

Whittaker, A., and Gilani, A. 1996. "Cyclic Testing of Steel Beam-Column Connections." *Report No. EERC-STI/96-04*. Berkeley: Earthquake Engineering Research Center, University of California.

Whittaker, A., Gilani, A., Takhirov, S. and Ostertag, C. 2002. "Forensic studies of a large cover-plate steel moment-resisting connection." The Structural Design of Tall Buildings, no. 11, 265–283.

Wong, C. H., El Nimeiri, M. M., and Tang, J. W. 1981. "Preliminary Analysis and Member Sizing of Tall Tubular Steel Buildings." *AISC Engineering Journal*, 2nd quarter.

Xue, M., Kaufmann, E. J., Lu, L. W., and Fisher, J. W. 1996. "Achieving Ductile Behavior of Moment Connections—Part II." *Modern Steel Construction*, vol. 36, no. 6, 38–42.

Youssef, N. F. G., Bonowitz, D., and Gross, J. L. 1995. "A Survey of Steel Moment-Resisting Frame Buildings Affected by the 1994 Northridge Earthquake." *Report NISTIR 5625*. Gaithersburg, MD: National Institute of Standards and Technology, Technology Administration, United States Department of Commerce.

Zareian, F., and Krawinkler, H. 2007. Assessment of probability of collapse and design for collapse safety. Earthquake Engineering and Structural Dynamics, no. 36, 1901–1914.

Ziemian, R. D. 2010. "Guide to Stability Design Criteria for Metal Structures, 6th Edition." Wiley, p. 1120.

This page intentionally left blank

CHAPTER 9

Design of Ductile Concentrically Braced Frames

9.1 Introduction

9.1.1 Historical Developments

A braced frame is essentially a planar vertically cantilevered truss. Notwithstanding cast iron trussed arches, such as those built by Tilford as early as 1796, straight metal trusses were first used in Earl Trumbull's 1840 bridge spanning the Erie canal, and frequently thereafter using Squire Whimple's more economical bowstring truss concept that relied on brittle cast iron for compression members and more forgiving wrought iron for tension members (DeLony 1992, Griggs 2009). Not surprisingly, in early steel buildings without heavy masonry cladding that could provide lateral stability, trusses were also introduced—for example, discrete bracing rods are visible in sketches of the cast iron Crystal Palace built in London in 1851 (lost to fire in 1936). Likewise, the architects of the 1853 New York Crystal Palace (lost to fire in 1858) described its roof as "braced against the action of the wind by a system of horizontal wrought-iron trusses similar to the vertical supports of the gallery floors" (Carstensen and Gildemeister 1918).

With the arrival of processes to economically make steel of reliable quality, steel bridges followed, the 6442-foot (1964-meter) James Eades trussed-arch bridge built in 1874 in St. Louis being the first major bridge to use steel, and the 2.5 km (1.5 m) 1890 Forth Bridge in Scotland being the first all-steel bridge [with a world record span of 521.3 m (1710 ft) until 1917] (Bennett 1999). Note that the 1889 Eiffel tower, which is conceptually a tall tapered three-dimensional braced frame, was made of puddled iron (a refined form of wrought iron). Because of their high strength and stiffness to resist lateral loads, steel braced frames rapidly became popular to resist wind forces

when implemented in buildings and industrial structures in the nineteenth century, and particularly so as architects pushed high-rise construction to greater heights in the early twentieth century. Ketchum (1918) described how diagonal bracing, knee-bracing, portal bracing, and brackets could be used to resist wind loads, providing plans and elevations for actual buildings, and described diagonal bracing as being the most effective and desirable for this purpose (noting that architects at the time required braces to be hidden in walls). Many of these diagonal braces were slender rods, only able to resist tension forces (a.k.a. tension-only braces), and braces, like the rest of the steel frame, were often encased in concrete or masonry for fireproofing. Interestingly, formal regulations for wind design requirements only appeared in the earliest part of the twentieth century—specified earthquake design requirements following only much later—as mentioned in Chapter 8.

Design requirements for braced frames evolved continuously over time, and the engineer is cautioned that noncompliance with all of the latest specified design requirements may not necessarily lead to inadequate performance. For example, nowadays, members subjected to axial compression in nonseismic applications are required to be compact, which means that the width-to-thickness ratio of the parts that constitute the cross-section must be sufficiently large to ensure that the stress at which local buckling would develop is greater than F_y. In early steel design practice (in an allowable stress perspective), some design codes only required that this local buckling critical stress be greater than the stress at which global member buckling occurred, which for slender members in compression, can result in substantially more liberal width-to-thickness ratios and satisfactory behavior nonetheless (in a non-seismic context). Information on archaic steel design practices can be found in older steel design textbook (e.g., Ketchum 1918) and various other documents (e.g., Brockenbrough 2002, Friedman 1995).

Although architects in many applications predominantly preferred the open spaces afforded by moment-resisting frames, with the emergence of seismic regulations in the 1960s and 1970s, braced frames slowly gained popularity in regions of high seismicity because they required less steel than moment-resisting frames to resist the prescribed seismic forces, and more easily could meet the specified frame drift limits.

The initial studies on the seismic performance of braced frames were conducted in the 1970s for the oil industry to characterize the inelastic cyclic behavior of axially loaded tubular steel members used in offshore drilling platforms. Although braces having circular and rectangular hollow sections are also used as braces in buildings, the scope of subsequent research expanded to include other cross-sections typically encountered in buildings, such as I-shaped sections, double angles stitched together to form T-shaped sections, solid T-shaped sections, single angles, channels, and tension-only rods and angles. Behavior of the welded or bolted gusset plates providing brace connections to the framing system were also found to play an

important role on system behavior. Much of that early research instructed many of the specified code provision, details, and limitations in effect since.

Seismic provisions for the analysis, design, and detailing of concentrically braced frames (CBFs) were gradually introduced into seismic regulations and guidelines. In the United States, this started in California in the late 1970s (SEAOC 1978) and on a nationwide basis in the early 1990s (AISC 1992). These were progressively updated in subsequent editions of various regulations and guidelines, such as the Structural Engineers Association of California (SEAOC) Recommended Lateral Force Requirements (SEAOC 1996), the Uniform Building Code (ICBO 1994), the NEHRP Recommended Provisions for the Development of Seismic Regulations for New Buildings (BSSC 1995), and the AISC LRFD Specification (AISC 1993). The consolidation of building codes that occurred in the United States in 2000 made it possible to concentrate the seismic design requirements for steel structures in the AISC Seismic Provisions (ANSI Standard AISC 341) (AISC 1997, 2002, 2005, 2010a), then referenced by the International Buildings Code or other state or city buildings codes as appropriate.

Note that in the aftermath of the Northridge earthquake, in light of the fractures discovered in moment-resisting frames, new steel buildings in California became more frequently designed with braced frames. Owners and architects who earlier wished to avoid at all cost the obstructions created by braces, suddenly were able to charge a premium for the offices having windows crossed by braces, which the public came to associate with seismic safety. Ironically, although a large number of tests were conducted to investigate and better understand how to design reliable ductile moment-resisting frames after the 1994 Northridge earthquake, relatively fewer tests investigated the cyclic behavior of concentrically braced frames (CBFs); research relying on past experimental results for individual braces typically reports less than a hundred data points (e.g., Lee and Bruneau 2002; Tremblay 2002, 2008; Uriz and Mahin 2008). This is surprising given the reliance on compression brace energy dissipation by existing codes and guidelines for many years, and the complex mechanisms leading to substantial strength degradation upon cyclic plastic hinging at midspan of braces, as explained throughout this chapter. As such, contemporary research has been most instructive and findings have been implemented in the latest editions of AISC 341 (AISC 1997, 2002, 2005, 2010a) and CSA S16 (CSA 1994, 2001, 2009).

Note that, in this chapter, given that providing an understanding of the evolution of seismic design requirements is within the scope of this book, a number of obsolete design provisions are reviewed and contrasted with current requirements. This is useful in the perspective of seismic retrofit.

Also, because differentiation is necessary for clarity, C_u and T_u are used in this chapter for the axial compression and tension strength of

braces, respectively, instead of P_u, which is used interchangeably in AISC 341 and 360 (AISC 2010a and 2010b, respectively) for both values. Likewise, C_r and T_r are used instead of ϕP_u. Acronyms are also used to refer to concentrically braced frames (CBFs), special concentrically braces frames (SCBFs), and ordinary concentrically braces frames (OCBFs), the latter two being defined in Section 9.1.3.

9.1.2 General Behavior and Plastic Mechanism

As described in Chapter 7, seismic design considers forces substantially smaller than those that would have to be considered to achieve full elastic response during an earthquake. This is possible provided that designated elements of the structural system are designed to yield at these lower forces, and detailed to have a ductile response. These ductile elements then limit the forces applied to the rest of the system, per capacity design principles.

During earthquakes, CBFs are expected to yield and dissipate energy through postbuckling hysteretic behavior of their bracing members. For drift in one specific direction, this is achieved by buckling of the braces in compression, followed by yielding of the braces in tension, as schematically illustrated in Figure 9.1. Under cyclic loading, for loads acting in the reversed direction, the previously buckled brace will yield in tension, whereas the brace previously yielded in tension will buckle. Typical postearthquake evidence of brace inelastic buckling is shown in Figure 9.2. Therefore, to survive an earthquake, the braces must be able to sustain large inelastic displacement reversals without significant loss of strength and stiffness.

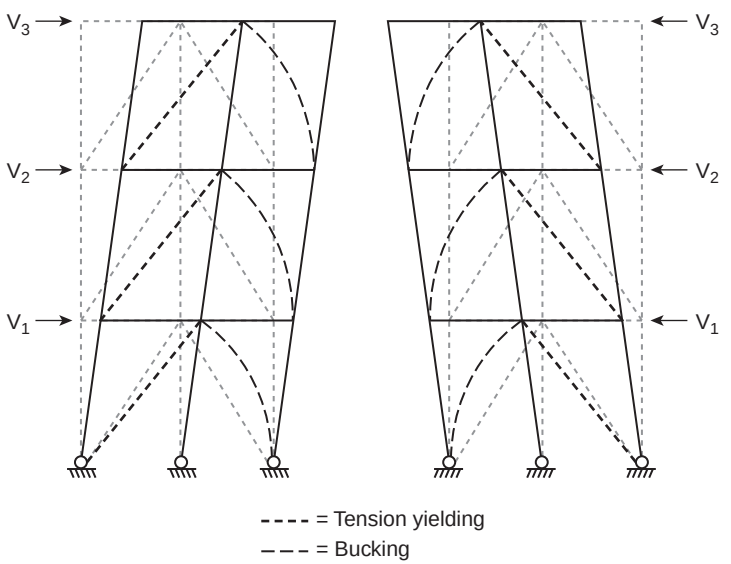

Figure 9.1 Schematic of CBF inelastic behavior.

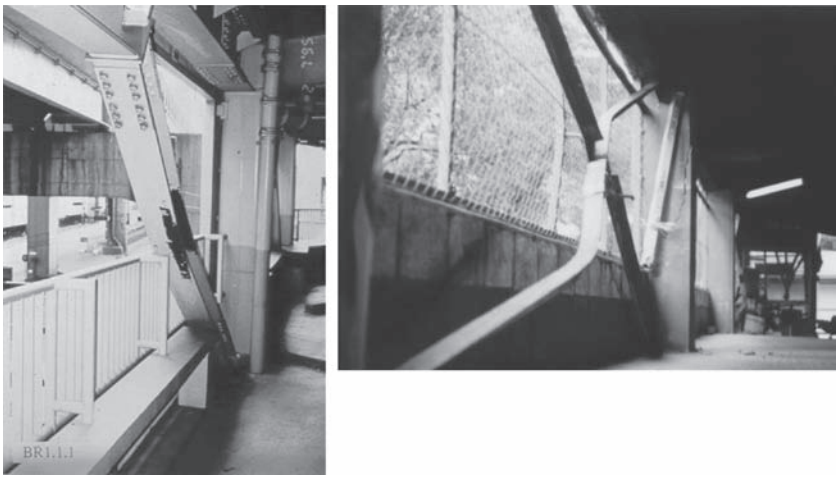

(a) (b)

Figure 9.2 Postearthquake residual inelastic brace buckling: (a) brace with low member slenderness; (b) brace with high member slenderness. (*Part a, courtesy of M. Nakashima, Disaster Prevention Research Institute, Kyoto University, Japan.*)

To achieve this behavior, special ductile detailing is required. Many braced frame structures designed without such ductile detailing consideration have suffered extensive damage in past earthquakes, including failure of bracing members and their connections (e.g., AIJ 1995; Tremblay et al. 1995, 1996)—examples of such failures are presented as appropriate throughout this chapter.

Given that braces are the designated energy dissipating element in CBFs, a review of their cyclic inelastic behavior is presented in Section 9.2. An understanding of the characteristics of that cyclic behavior is key to integrate capacity design principles in the design of CBFs to achieve the intended ductile performance. Hysteretic behavior and design of CBFs are both addressed in Section 9.3.

9.1.3 Design Philosophy

To provide adequate earthquake resistance, CBFs must be designed to have appropriate strength and ductile response. To achieve this, diagonal braces must be specially designed to sustain plastic deformations and dissipate hysteretic energy in a stable manner through successive cycles of buckling in compression and yielding in tension. The design strategy is to ensure that plastic deformations only occur in the braces, leaving the columns and beams undamaged, thus allowing the structure to survive strong earthquakes without losing its gravity-load resistance.

Early thinking on the design and detailing of such braces, as implemented in seismic regulations and guidelines at the time, was that bracing members with low member slenderness, KL/r (Section 9.2.2),

and width-to-thickness ratio, *b/t* (Section 9.2.3), have superior seismic performance, on the premise that compressed braces with low *KL/r* can provide more significant energy dissipation. As described in more details in Section 9.2, upon buckling, flexure develops in the compression member and a plastic hinge eventually develops at the middle length of the brace, that is, at the point of maximum moment. It is through the development of this plastic hinging that a member in compression can dissipate energy during earthquakes. Low *b/t* limits are prescribed to prevent brittle failure due to local buckling during this plastic hinging, because the reversed cyclic loading induced by earthquakes leads to repeated buckling and straightening of the material at the local buckling location, which, combined with high strains at the tip of the local buckle, precipitate low-cycle fatigue.

The more recent thinking on these matters recognizes the importance of delaying low-cycle fatigue at the plastic hinge location, and allows the use of more slender braces that correspondingly have lower ductility demands in compression, relying proportionally more on tension yielding of the braces to dissipate seismic energy. The drawback of this approach is a greater difference between the strength of the braces in compression and tension, and thus greater demands that this imbalance can impose on the elements of the CBFs that must be protected (i.e., remain elastic) through application of capacity design principles.

Various editions of the design specifications have reflected this change in philosophy, along with other tweaks intended to make the design intent transparent. However, the most ductile CBFs have consistently been assigned structural response modification factor, *R*, on the order of 75% of the maximum value assigned to special moment-resisting frames (see Chapter 7). This penalty is attributed mainly as a consequence of the less ideal energy dissipation provided by the compression brace, the observed pinching of the hysteretic curves of the braced frame due to the strength degradation of the compression brace, and the absence of effective strength hardening as typically occurs in moment frames.

Note that two types of CBF systems are permitted by AISC 341, namely, *Special Concentrically Braced Frames (SCBFs)* and the *Ordinary Concentrically Braced Frames (OCBFs)*. Emphasis here is on SCBFs, which are designed for stable inelastic performance and energy dissipation capability, and correspondingly for the largest force reduction factor, *R*. Some of the ductile detailing requirements are relaxed for the OCBF in the perspective that these would be subjected to less inelastic demand, being designed to a smaller reduction factor. However, if demands from an earthquake were to exceed the design level, structures with SCBFs could be advantaged over OCBFs, in spite of the higher design force level considered in the latter case.

Typical CBF configurations are presented in Figure 9.3. These were originally developed to resist wind loads in the linearly elastic range, but are not necessarily adequate for seismic design. Some

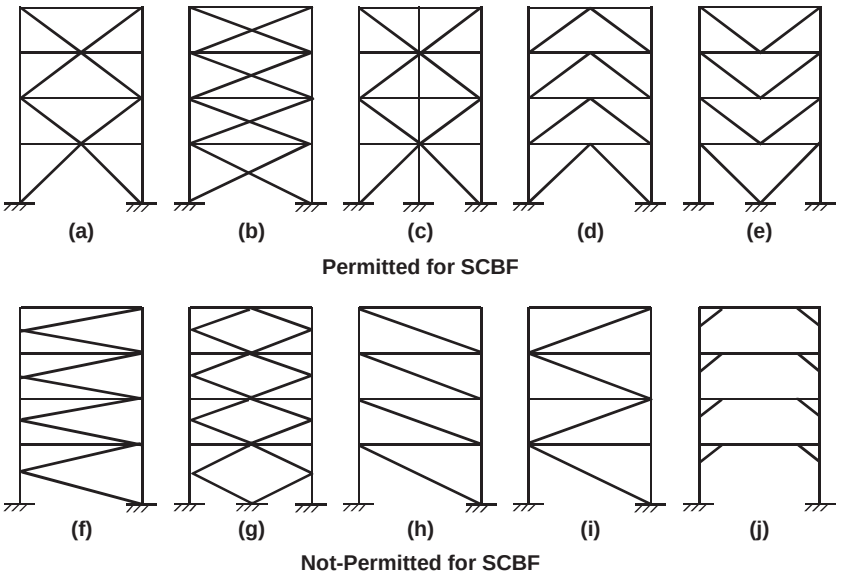

Figure 9.3 CBF configurations permitted and prohibited in seismic regions: (a to c) X-braced frames; (d to e) inverted V-braced and V-braced frames, also known as inverted chevron-braced and chevron-braced frames, respectively; (f to g) K-braced and double K-braced frames; (h to i) single diagonal braced frames; (j) knee-braced frame.

configurations are prohibited in seismic regions because they exhibit poor cyclic inelastic response or induce undesirable demands in other structural elements. For example, the K-braced frame configuration shown in Figure 9.3f is problematic. If one of the diagonal braces were to buckle, increasing force in the tension brace would be transferred as shear in the adjacent column. The resultant horizontal force from these two unequal brace forces, applied at midheight of the column, could produce a plastic hinge in the column at the brace-to-column intersection point and result in undesirable column failure. Note that the single brace configurations of Figures 9.3h and 9.3i, although prohibited, would be permitted if used together with their respective mirror image along the same line of bracing (Figure 9.3c can be seen as one such example for single-braced frames of the type shown in Figure 9.3i).

The severely pinched hysteresis curves exhibited by *tension-only* braced frames have been presented in Chapter 6. Such frames have been commonly used to resist wind forces in nonseismic regions, typically with X-braced configuration (Figure 9.3b) having angles, rods, or flat bar braces of high slenderness (often $KL/r > 300$). The cyclic inelastic behavior of a tension-only braced frame is characterized by yielding and elongation of the tension braces, and buckling of the compression braces at near-zero levels of axial load due to their

high slenderness. Upon repeated cyclic loading, each brace accumulates residual axial displacements, and the X-braced frame loses its lateral stiffness in the vicinity of zero frame displacement, defeating to some degree the intent of adding the braces to the frame. AISC 341-10 does not permit the use of tension-only braces in SCBFs, but allows it for OCBFs. CSA S16-09 allows their use for low-rise buildings up to a height of 20 m (with a progressively reducing R factor between 16 m and 20 m in height), provided all columns in the building are continuous and of constant cross-section over the entire building height. Tremblay and Filiatrault (1996) demonstrated that, contrary to earlier expectations, impact forces on the braces and their connections due to the sudden straightening of previously taut slender tension-only braces are limited by the yield strength of the braces; they observed an increase in yield strength of up to 15% due to strain rate effects (Chapter 2), as commonly observed in other CBF studies with conventional braces. Strain-rate effects are generally not considered by seismic design codes and specifications at this time.

9.2 Hysteretic Behavior of Single Braces

9.2.1 Brace Physical Inelastic Cyclic Behavior

An understanding of the physical inelastic behavior of an individual brace member subjected to reversed cycles of axial loading is necessary to design ductile braced frames using the concepts presented in this chapter.

The behavior of axially loaded members is commonly expressed in terms of the axial load, P, axial deformation, δ, and transverse displacement at midlength, Δ. According to convention, tension forces and deformations are taken as positive, and compression forces and deformations as negative. A simplified hysteretic curve for a generic brace member is presented in Figure 9.4.

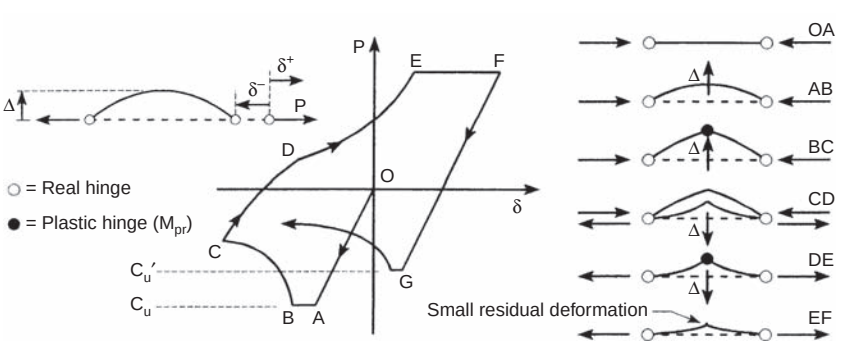

Figure 9.4 Sample hysteresis of a brace under cyclic axial loading.

Starting from the unloaded condition (point O in Figure 9.4), the brace is compressed in the linearly elastic range. Buckling occurs at point A, when $P = C_u$. Slender braces that buckle elastically at point A can sustain their applied axial load as the brace deflects laterally, with a corresponding axial shortening (shown as the plateau AB in Figure 9.4). At that point, if brace behavior remained elastic, unloading would occur along the line BAO if the axial compressive load was removed.

During buckling, due to its transverse deflections, the brace is subjected to flexural moments. Considering equilibrium in the deformed configuration, using a free-body diagram of a segment of the brace from its end to a distance x from it, the flexural moment at any point x is calculated as the product of the axial force and the lateral displacement at that point. As such, the shape of the moment diagram is proportional to the deflected shape, with the maximum moment occurring at the point of maximum transverse displacement (i.e., at midspan for the pin-pin brace shown in Figure 9.4). Assuming bilinear elasto-plastic flexural behavior, as transverse displacement of the brace further increases under the constant axial force, the plastic moment of the brace is eventually reached and a plastic hinge forms (point B in Figure 9.4). The value of the transverse displacement, Δ, when this happens can be obtained accounting for flexure-axial load interaction in the brace (Chapter 3)—recognizing, however, that for actual material behavior and residual stresses, the development of plastic hinging would be gradual.

Further increases in axial displacements produce corresponding increases in Δ and in plastic hinge rotations (segment BC), resulting in a deflected shape having a plastic kink, as schematically shown in Figure 9.4. The axial resistance of the brace drops along segment BC: because the moment at midlength ($M = P\Delta$) cannot increase beyond the plastic moment, an increase in Δ must be accompanied by a decrease in P. However, the path from point B to point C is nonlinear due to flexure-axial load interaction at the plastic hinge, recognizing that a decrease in axial load produces an increase in moment capacity.

Upon unloading (from point C in Figure 9.4) to $P = 0$, the brace retains a residual axial deflection, δ, and a residual transverse deflection, Δ, including a kink in the brace due to residual plastic rotations.

When the brace is loaded in tension from $P = 0$ to point D, the behavior is elastic. At point D, the product of the axial load and the transverse displacement equals the plastic moment of the brace (similar to the equilibrium described at point B earlier), and a plastic hinge forms at midlength of the brace. However, along segment DE, the plastic hinge rotations act in the reverse direction of that along segment BC and effectively reduce the magnitude of the transverse deflection, Δ. As a result, axial forces larger than that at point D can be applied.

It is not possible to completely remove the transverse displacement and return the brace to a perfectly straight condition. The

theoretical axial force required to produce additional plastic hinge rotations tends to infinity as the transverse displacement approaches zero, but the axial force in the brace cannot exceed its tensile yielding resistance (= AF_y), and residual transverse deflections cannot be avoided. Tension yielding is shown as segment EF in Figure 9.4.

Upon reloading in compression, the brace therefore behaves as a member having an initial deformation, and its buckling capacity upon reloading (C_u' at point G) is typically lower than its buckling capacity upon first loading (C_u at point A). The ratio C_u'/C_u depends primarily on the slenderness ratio (KL/r), and expressions used in the past to capture this relationship are presented in Section 9.2.3. The length of the elastic buckling plateau (segment AB) also reduces upon each subsequent inelastic cycle as a result of the residual initial deflection. Beyond these two differences, the shape of the hysteresis curves (OABCDEF) in subsequent inelastic cycles remains basically unchanged. Analytical models to capture all phases of this hysteretic behavior are briefly discussed in a later section.

Quantitative assessments of the hysteretic behavior and energy dissipation capacity of braces have typically been obtained from tests of members subjected to repeated cyclic inelastic axial displacements. Results have included either complete hysteresis curves for a given experiment's loading history or simply the envelope of all hysteresis curves (Black et al. 1980). Both approaches are used in the following sections. Slenderness ratio has a dominant impact on the shape of the hysteresis curves. For a slender brace (large KL/r), segment OA will be rather small, whereas the plateau segment AB could be rather long, resulting in relatively small hysteretic energy dissipation capacity in compression. For stocky braces (small KL/r), the reverse is true, and segment AB may not exist. The effect of slenderness is further investigated in the next section.

9.2.2 Brace Slenderness

The cyclic behavior of a brace largely depends on its slenderness, KL/r, where K is an effective length factor, L is the brace clear span, and r is the radius of gyration of the member about the buckling axis under consideration. The radius of gyration, r_i, about axis i, is equal to $\sqrt{I_i/A}$, where I_i is the second moment of area of the component about axis i, and A is the cross-sectional area of the member. Note that some design standards or research documents alternatively refer to the non-dimensional slenderness ratio, λ, defined as $(KL/r)(\sqrt{F_y/\pi^2 E})$.

Data for A, I_i, and r_i for standard structural shapes is typically tabulated in design manuals and handbooks (AISC 2011 and CISC 2010). The largest slenderness ratio obtained, considering the possible buckling axes for a given member, governs behavior and is used for design.

Representative hysteresis curves for braces having slenderness ratios of 120, 80, and 40 are shown in Figure 9.5 in terms of axial force, P, and axial deformations, δ, along with their corresponding brace lateral displacements, Δ. In all cases, large residual lateral deformations remains upon unloading (i.e., when $P = 0$) as a consequence of inelastic buckling. Increasing magnitude of the lateral deformations is a consequence of brace "growth" due to incremental plastic elongations in subsequent cycles of tension yielding, and the relative lesser plastic axial shortening of the brace before its buckling in compression; the progressively longer brace must therefore displace laterally more to fit in its same original clear span. Note that, as this residual lateral displacement increases in subsequent cycles, the buckling capacity of the brace reduces, equivalently to that of a brace having an initial curvature or camber. The Bauschinger effect (Chapter 2) also contributes to this reduction in compressive strength in subsequent cycles.

It is also observed in Figure 9.5 that increases in slenderness correspond to reductions in hysteretic energy dissipated by the brace in compression (i.e., area under the hysteresis curves), together with reductions of the compression strength (as a percentage of the corresponding tensile strength). Similar observations are possible from Figure 9.6a, using envelopes of the hysteresis curves for different braces having slenderness ratios of 40, 80, and 120, in terms of normalized axial load versus normalized axial displacement. An example of how such an envelope is obtained is shown in Figure 9.6b.

The hysteresis curves for more compact members would approach that of the material itself, whereas those for more slender ones would approach the tension-only behavior described in Chapter 6.

Figure 9.5 also illustrates the variation of axial stiffness at various displacements, and the consequent corresponding loss of tangent stiffness of a braced frame as it is unloaded (to zero axial load) or returns to its original plumb position. For example, data in Figure 9.5a shows the axial tangent stiffness of the brace at zero axial load to be approximately 1700 kips/in (29.4 kN/mm) in the first loading cycle and approximately 20 kips/in (0.35 kN/mm) in the loading cycle to $\delta = 35$ mm (1.38 in). If two such braces formed an inverted-V CBF configuration, the lateral stiffness of the braced frame near the point of zero lateral displacement would be less than 5% of the elastic stiffness of the frame. Large drifts are required to re-engage the brace in tension to its full stiffness.

The normalized lateral deflected shape of two braces having different end-conditions and slenderness ratios are shown in Figure 9.7. For the pin–pin brace shown in Figure 9.7a, the somewhat parabolic elastic deflected shape becomes progressively more linear in segments between the midspan plastic hinge and actual hinges as inelastic behavior further develops (the non-normalized magnitude of the

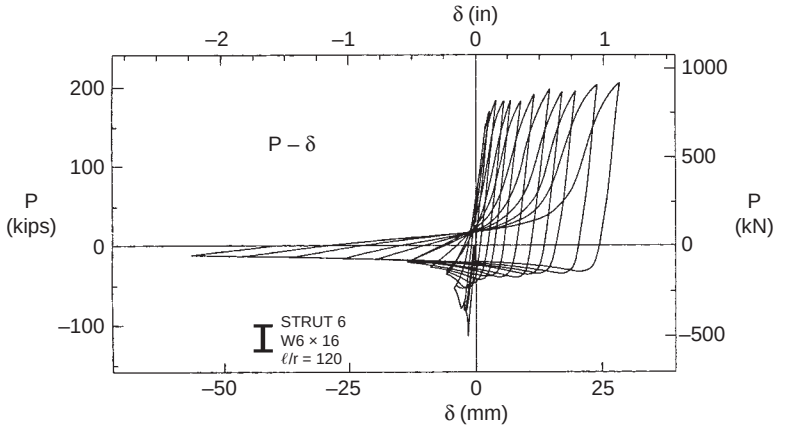

(a) Axial load versus axial displacement

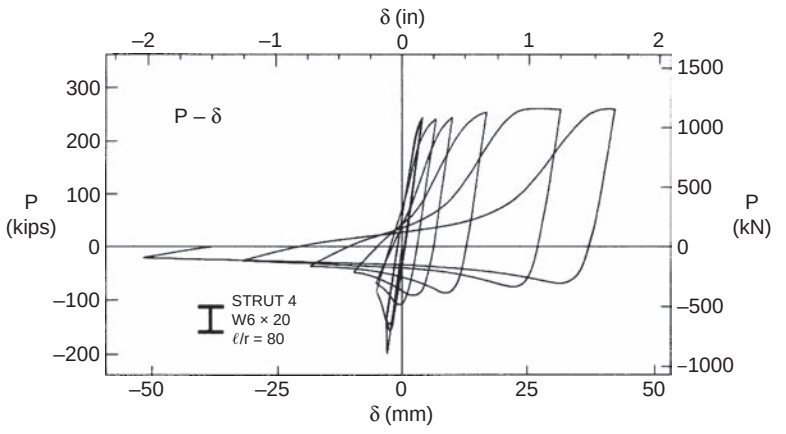

(b)

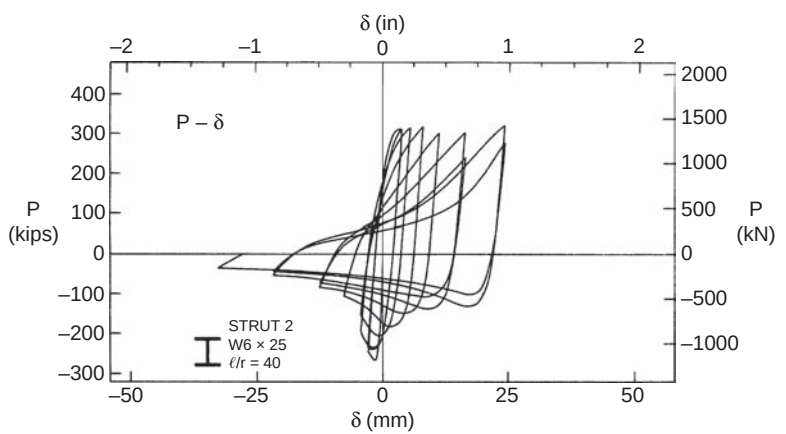

(c)

Figure 9.5 Cyclic behavior of braces having slenderness ratios of 120, 80, and 40: (a, b, c) axial force versus axial displacement hysteresis curves; (d, e, f) axial force versus brace lateral displacement. (*Black et al. 1980, with permission from EERC, University of California, Berkeley.*)

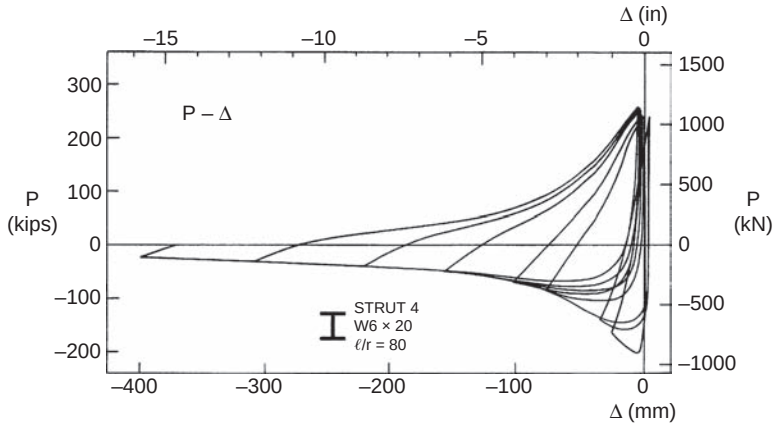

(d)

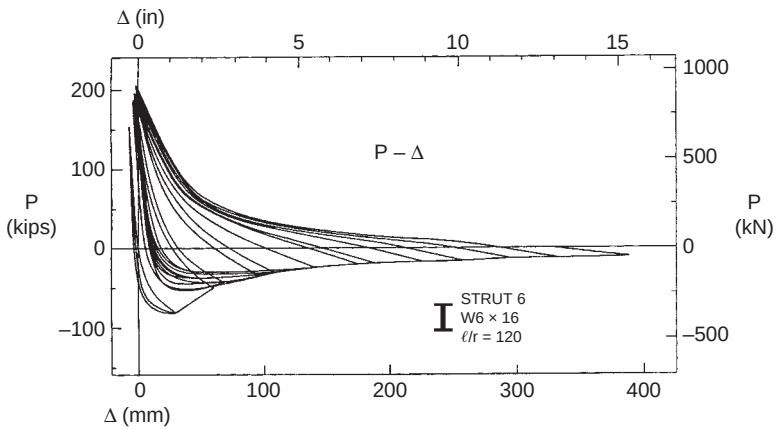

(e)

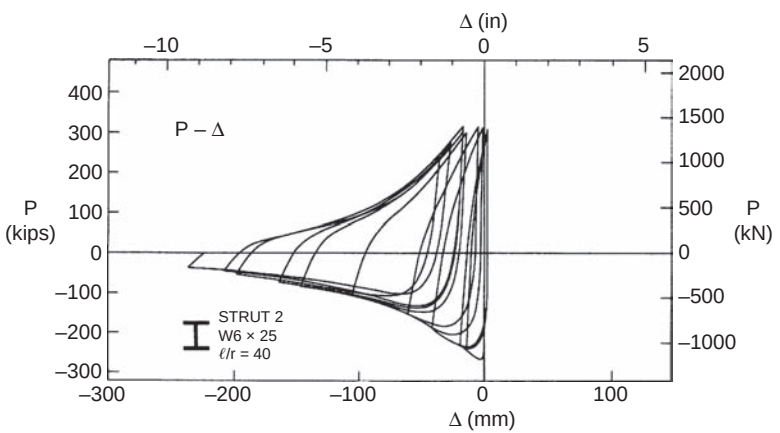

(f)

Figure 9.5 (*Continued*)

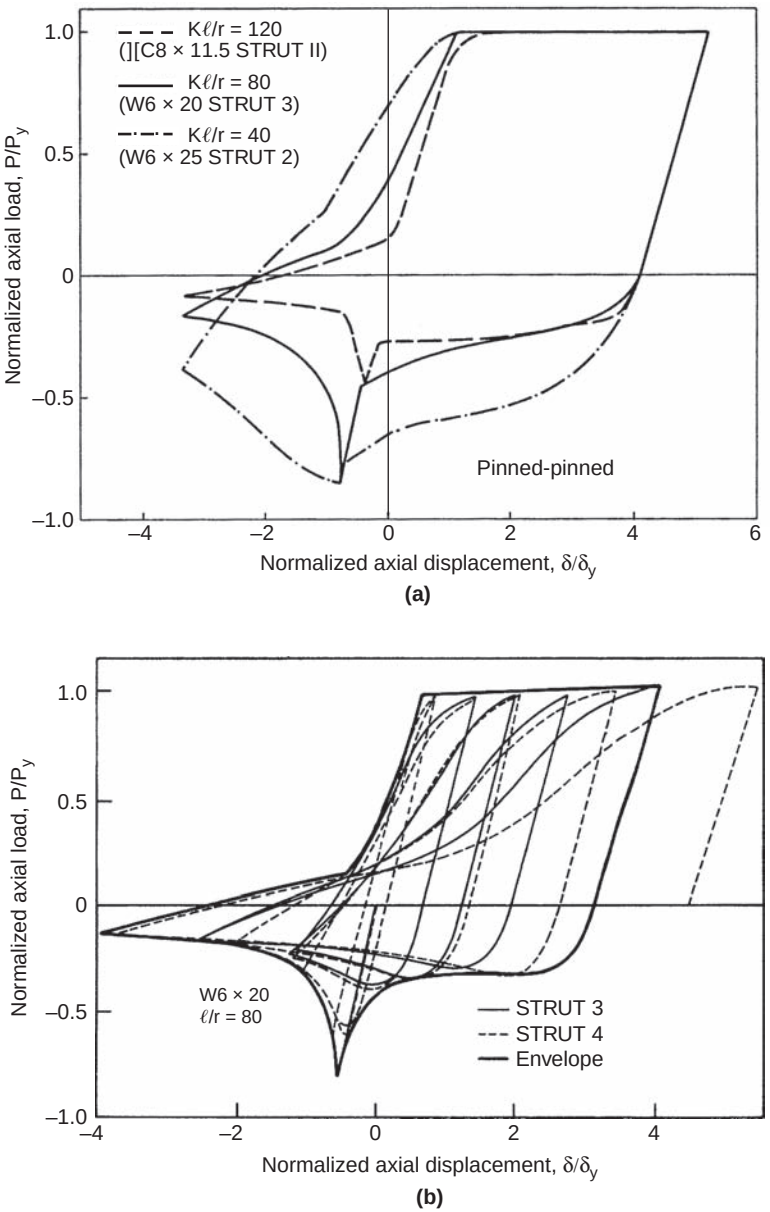

Figure 9.6 Normalized envelopes for braces: (a) comparison of normalized axial force versus normalized axial displacement; (b) graphical definition of envelope. (*Black et al. 1980, with permission from EERC, University of California, Berkeley.*)

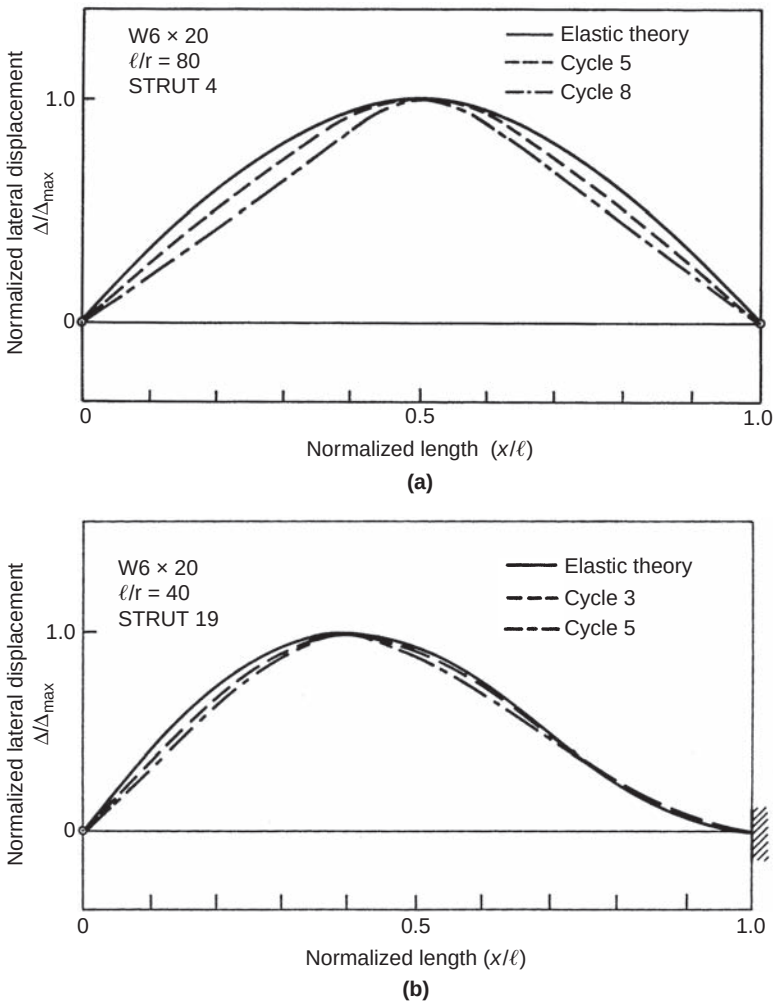

Figure 9.7 Elastic and inelastic buckled shapes for I-shaped beams: (b) pinned-fixed end conditions. (*Black et al. 1980, with permission from EERC, University of California, Berkeley.*)

lateral displacements would correspondingly increase as this happens). Likewise, for the brace pinned at one end and fixed at the other shown in Figure 9.7b, straight segments connect the plastic and actual hinges at large inelastic excursions. Nonetheless, the deflected shapes are quite similar, and use of the effective length, KL, based on elastic analysis, is appropriate to calculate the strength and characterize behavior of braces undergoing cyclic inelastic buckling. This conclusion is further supported by comparison of the envelopes of hysteresis curves of braces having various end-conditions, shown in Figure 9.8.

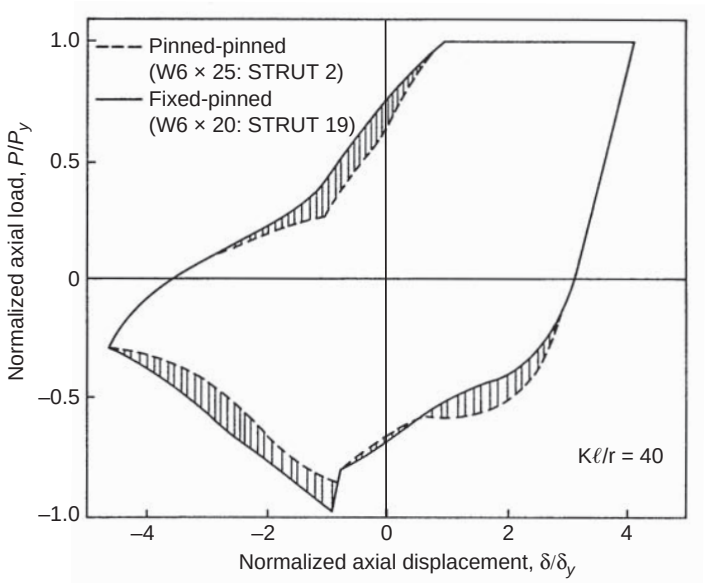

(a) I-shaped brace response

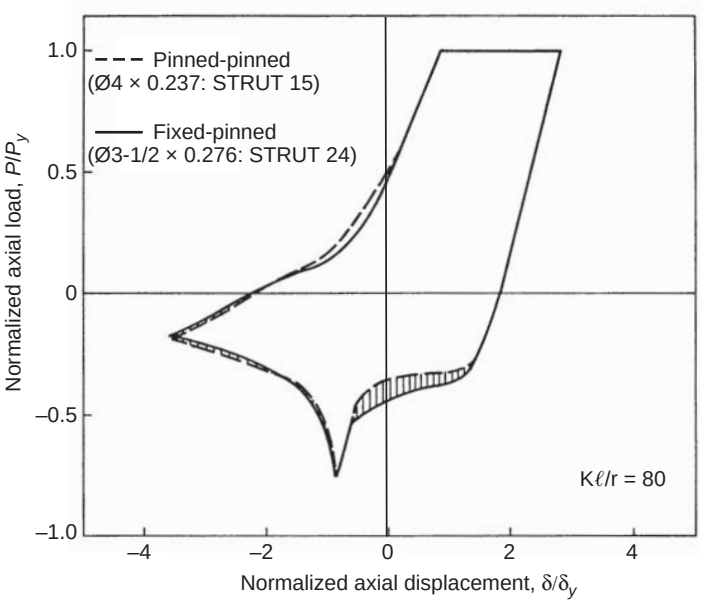

(b) Circular tube brace response

Figure 9.8 Hysteretic curves for braces with different end conditions. (*Black et al. 1980, with permission from EERC, University of California, Berkeley.*)

Marginal differences in hysteretic energy dissipation can be seen between braces having pinned–pinned and fixed-pinned end conditions, for either I-shaped (Figure 9.8a), circular tube braces (Figure 9.8b), or double-angle braces (Black et al. 1980, Popov and Black 1981).

Incidentally, cross-sectional shape also has a marginal impact on the envelope of hysteretic response for braces having the same slenderness ratio, as shown in Figure 9.9 (Black et al. 1980), although different shapes can have substantially different behavior in terms of local buckling and low-cycle fatigue life, as described later.

On the strength of the above observations, early seismic design requirements for ductile CBFs were formulated promoting the use of stockier braces that could contribute to the total hysteretic energy dissipation. Representatively, the 1992 edition of the AISC seismic provisions only permitted the use of braces having slenderness ratio less or equal to $720/\sqrt{F_y}$ (= $1900/\sqrt{F_y}$ in S.I. units), which corresponded to KL/r values of 102 and 120 for F_y of 50 ksi and 36 ksi, respectively. The 1995 edition increased this limit to $1000/\sqrt{F_y}$, corresponding to 141 and 167 for the same two steel grades respectively. The 2010 edition allows the use of KL/r values of up to 200 when capacity design principles are considered in the design of the columns. The rationale for these changes is presented later.

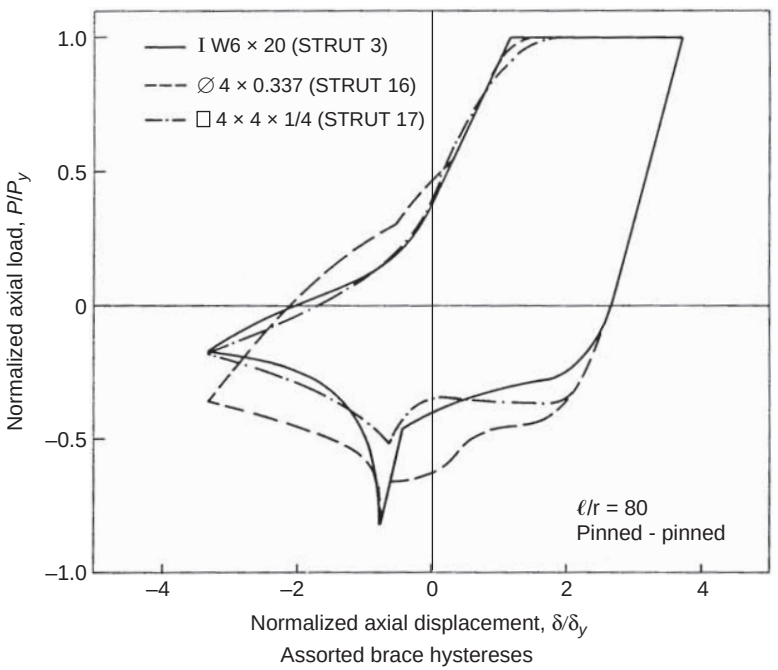

Figure 9.9 Hysteretic curves for braces with different cross-sectional shapes. (*Black et al. 1980, with permission from EERC, University of California, Berkeley.*)

Note that because minimum weight considerations often drive the design of braces, actual ductile CBFs typically have braces with slendernesses close to the specified upper limit.

9.2.3 Compression Strength Degradation of Brace Under Repeated Loading

Knowledge of the actual force resisted by a brace throughout its cyclic response is important, as variations in this value affect how forces flow throughout the structural system, and consequently how connections and other structural members must be designed to resist these demands (as is further described in later sections).

Figures 9.5 and 9.6 above also show the progressive reduction in buckling strength in subsequent inelastic loading cycles (i.e., point G in Figure 9.2). Early seismic design requirements specified that a reduced compressive strength, C_r', be considered in design instead of the value otherwise used in nonseismic applications, C_r. The ratio C_r'/C_r was understood to depend primarily on the slenderness ratio, KL/r; sample expressions that were used then to capture this relationship include:

SEAOC 1990

$$C_r' = \frac{C_r}{1 + 0.50\left(\frac{KL}{r\pi}\sqrt{\frac{0.5F_y}{E}}\right)} \tag{9.1a}$$

CSA 1994

$$C_r' = \frac{C_r}{1 + 0.35\left(\frac{KL}{r\pi}\sqrt{\frac{F_y}{E}}\right)} \tag{9.1b}$$

Using these equations, for a slenderness ratio equal to 0, $C_r' = C_r$, whereas for a Grade A36 steel brace with a slenderness ratio of 130, $C_r' = 0.67C_r$. For simplicity, the design strength of a brace per the AISC LRFD Specification (AISC 1992) was calculated as $0.8\phi_c P_n$ where ϕ_c was the resistance factor for compression components, and P_n the nominal axial strength of the brace (i.e., $C_r = \phi_c P_n$). Interestingly, $C_r' = 0.8C_r$ would be obtained from Equation 9.1a with a slenderness ratio of approximately 65, which was equivalent to the average C_r' obtained over the range of permissible KL/r values at the time. Designing braces assuming their strength to be C_r' was equivalent to neglecting the first cycle strength C_r and assuming that brace compression strength did not further degrade after the second cycle (which is incorrect). Note that both C_r' or C_r were to be considered in capacity design calculations, depending on which case would deliver the

maximum load to other components or systems (as shown in later sections). Later editions of the AISC Seismic Provisions dropped the 0.8 factor, recognizing that other factors had a greater impact on achieving satisfactory CBF cyclic response.

One such factor is degradation of brace strength after repeated cycles of inelastic deformations. For capacity design purposes, the capacity of the brace in compression when the entire frame reaches its maximum sway deformation, which is defined as C_r'' here, can be substantially lower than C_r' and thus more relevant to consider in design. Indeed, as plastic hinging develops in the middle of the brace, C_r'' drops as deformation increases. This means that at maximum sway, when the tension brace has yielded, only a small fraction of the original compression buckling strength of the other brace is effective.

Lee and Bruneau (2002, 2005) quantified the strength degradation of braces upon repeated cycling by extracting compression excursion from the complete hysteretic force-displacement curve obtained from 66 tests by various researchers, and overlaying them to start from the same zero displacement, as shown in Figure 9.10 (ϕ taken as 1.0 for this purpose) in terms of δ/δ_B, where δ_B is the axial displacement at first buckling. For a typical curve, schematically idealized in that figure, the magnitude of axial deformations typically increased in subsequent cycles as a consequence of the testing protocols adopted (note that only cycles that produced displacements exceeding the

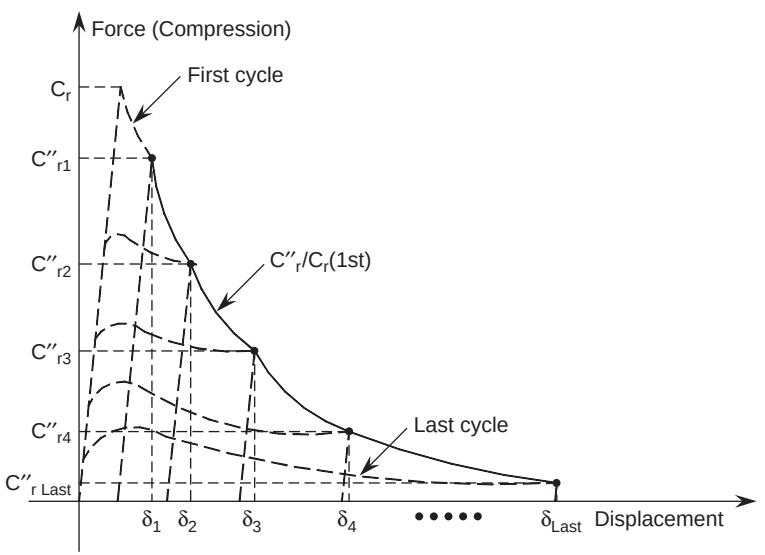

Figure 9.10 Definition of normalized buckling capacity, $C_r''/C_r(1st)$. (*Lee and Bruneau 2002, courtesy of MCEER, University at Buffalo.*)

previously obtained values were considered). In the "*nth*" cycle, beyond first buckling (defined experimentally as C_r), compressive strength of the brace at the point of maximum displacement for that compressive excursion, δ_n, was labeled C_{rn}'', the numeral subscript indicating the cycle number. These value of C_r'' were then divided by C_r for normalization. This normalized strength is labeled $C_r''/C_r(1st)$, the qualifier "1st" implying "the strength obtained the first time this displacement is reached." Figure 9.11 shows a typical curve obtained following this procedure. That curve can be considered a normalized force-displacement envelope of the brace in compression.

Furthermore, the brace compressive strength recorded during the last cycle of testing was also of interest. It was calculated at each of the previously considered displacement points, δ_n, as shown in Figure 9.12, giving results as typically shown in Figure 9.13. This normalized strength was labeled $C_r''/C_r(last)$, the qualifier "last" implying "the strength obtained during the last cycle of testing."

Using the same displacement points to calculate both $C_r''/C_r(1st)$ and $C_r''/C_r(last)$ makes it possible to calculate the ratio of these values. A large ratio indicates a considerable drop in strength at a specific displacement, δ/δ_B, whereas a lower ratio expresses rather stable strength degradation from the first to last cycle. A typical result is shown in Figure 9.14. Lee and Bruneau (2002) present results for all braces considered, together with similar data on the normalized hysteretic energy dissipation of compression braces.

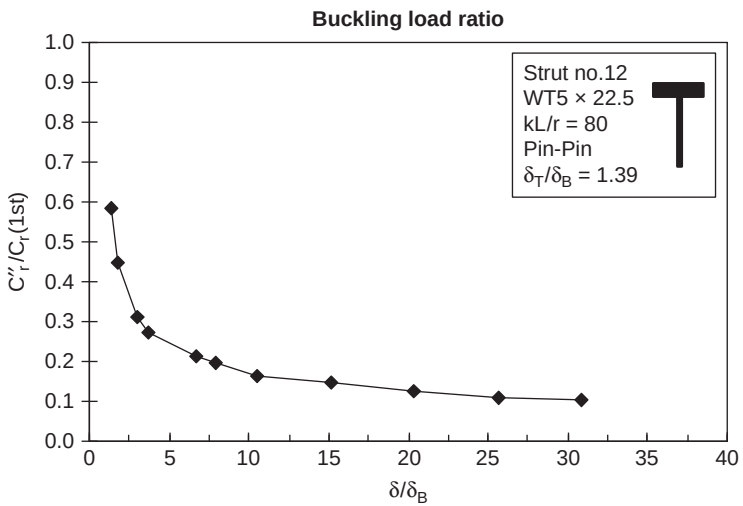

Figure 9.11 Example of normalized maximum compression strength reached upon repeated cyclic inelastic displacements, $C_r''/C_r(1st)$. (*Lee and Bruneau 2002, courtesy of MCEER, University at Buffalo.*)

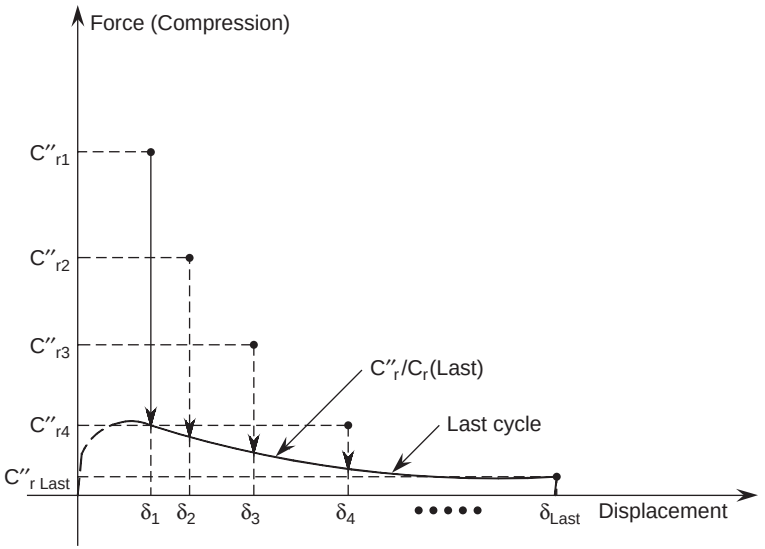

FIGURE 9.12 Definition of normalized buckling capacity, $C_r''/C_r(last)$. (*Lee and Bruneau 2002, courtesy of MCEER, University at Buffalo.*)

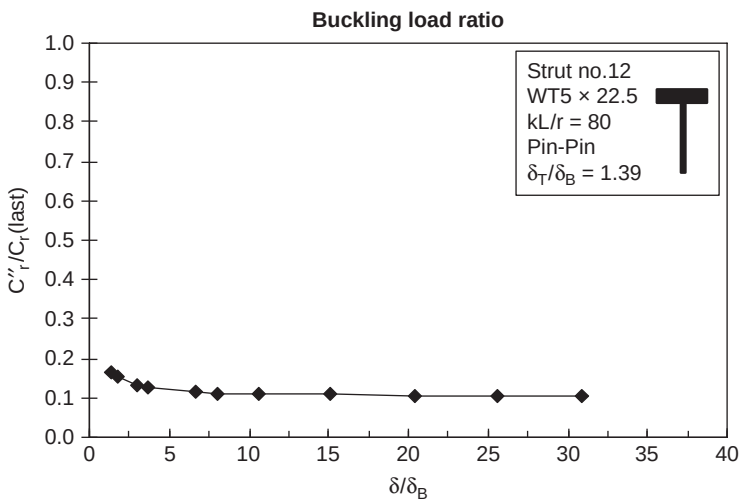

FIGURE 9.13 Example of normalized maximum compression strength reached upon repeated cycling data, $C_r''/C_r(last)$. (*Lee and Bruneau 2002, courtesy of MCEER, University at Buffalo.*)

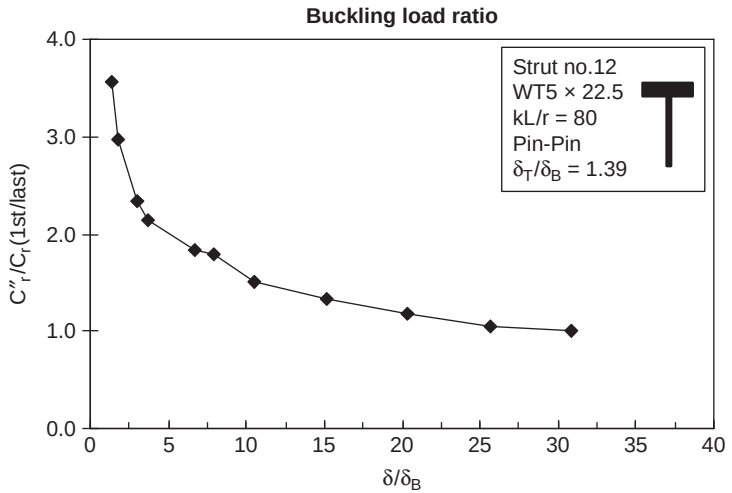

Figure 9.14 Example of normalized maximum compression strength reached upon repeated cyclic inelastic displacements, $C_r''/C_r(1st/last)$. (*Lee and Bruneau 2002, courtesy of MCEER, University at Buffalo.*)

Results obtained indicated that reduction in the normalized C_r''/C_r (1*st*) envelope is particularly severe for the W-shaped braces having KL/r above 80, dropping to approximately 0.2 when the normalized displacements exceed 5. Behavior is not significantly worse for KL/r in the 120 to 160 range. Tubes perform relatively better, over all slenderness range, with double-angle braces in-between these two cases. Results for $C_r''/C_r(last)$ and $C_r''/C_r(1st/last)$ showed that the compression capacity at low δ/δ_B values drops rapidly upon repeated cycling, and that $C_r''/C_r(1st)$ is effectively equal to $C_r''/C_r(last)$ at normalized displacements above 3 in most instances.

These results indicated that when a braced bent having braces with *KL/r* greater than 80 reaches its expected displacement ductility of 3 to 4, the compression strength of a brace has already dropped to approximately 20% of its original buckling strength (40% for square HSS). Similar results were obtained for normalized energy dissipation capacity in compression. Given that most braces in actual design have slenderness above 80, this confirmed that limits on *KL/r* specified by the various seismic design specifications are not correlated to brace effectiveness in compression—they can, however, relate to other factors, as shown in the next sections.

A similar study conducted in parallel by Tremblay (2002), considering 76 tests from 9 experimental programs, compared various approaches to quantify postbuckling brace compression strength (expressed as C_u' in that case, but equivalent to C_r'' with $\phi = 1$ considered above). Recognizing that the postbuckling strength depends on

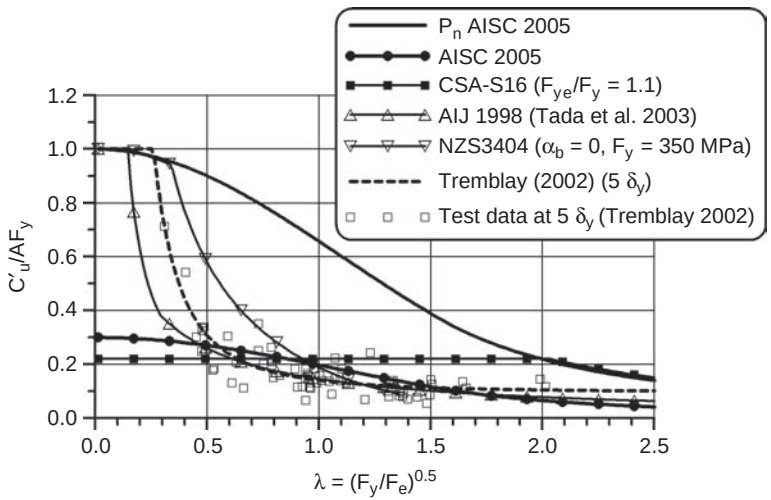

Figure 9.15 Postbuckling compression strength. (*Courtesy of Robert Tremblay, Département des génies civil, géologique et des mines, EcolePolytechnique, Montréal.*)

the magnitude of inelastic deformations, Figure 9.15 presents resulting strength degradations as a function of the normalized slenderness ratio for the case of braces axially deformed up to five times their tension yield displacement. Note that the actual effective braced length for each of the experiments considered was used in this study. The equations for minimum postbuckling strength provided by various design codes and standards are plotted in this figure for comparison against the test data and average compression strength obtained from regression analysis of the data. Results in Figure 9.15 show that the value of $0.3\phi_c Pn$ introduced for V and inverted V braces in the 1995 AISC Seismic Provisions (based on the work of Hassan and Goel, 1991) matches well the data over λ ranging from 0.5 to 1.5 (i.e., KL/r of 38 to 113 for $F_y = 50$ ksi), but becomes quite conservative for stockier braces. Results also show that using a constant value independent of slenderness provides a poor match (such as for the case of the value $0.2A_g R_y F_y$ introduced in CSA S16.1-01, and retained in CSA S16-09).

Note that both C_r'' or C_r are to be considered in capacity design calculations, depending on which case would deliver the maximum load to other components or systems (as shown in later sections), although this has not always been stated explicitly in design codes or standards.

9.2.4 Brace Compression Overstrength at First Buckling

Tremblay (2002) also quantified the brace initial compression strength compared with AISC and CSA design equations (Figure 9.16—the Class 1 designation refers to compact sections per CSA S16). This

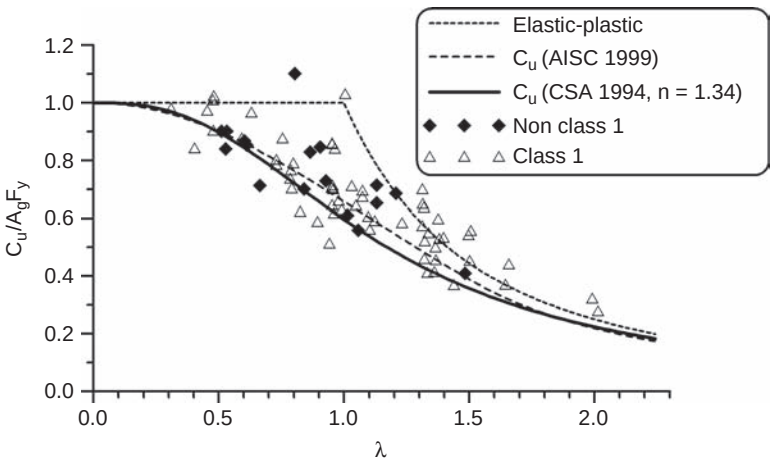

Figure 9.16 Experimentally obtained compression strengths at first buckling. (*Courtesy of Robert Tremblay, Département des génies civil, géologique et des mines, EcolePolytechnique, Montréal.*)

value is important to estimate the maximum forces applied by braces in compression to their connections and other structural elements.

Expected compression strength was found to be typically greater than the calculated nominal strength, particularly for more slender braces, likely as a consequence of conservative assumptions built in the design equations with respect to initial imperfections and residual stress conditions. Tremblay found the average overstrength over all slenderness ranges to be 1.09 and 1.16 compared with the AISC 341 and CSA S16 design equations, respectively, with coefficients of variation of 0.16 and 0.17.

Subsequently, the AISC 341-05 required that connections be designed for $1.1R_yP_n$, with P_n being the nominal compression strength per AISC 360, whereas AISC 341-10 further defined P_n for this particular application to be 1.1 times the lesser of $R_yF_yA_g$ and $1.14\,F_{cre}A_g$, where F_{cre} is F_{cr}, determined per AISC 360 Chapter E, substituting the expected yield stress R_yF_y in lieu of F_y in these equation. Note that 1.14 is equal to 1/0.877. Recall that the compressive flexural-buckling strength of compact members per AISC 360 is given by:

$$F_{cr} = \left[0.658^{\frac{F_y}{F_e}}\right]F_y \quad \text{when} \quad \frac{KL}{r} \le 4.71\sqrt{\frac{E}{F_y}} \ (\text{equivalent to } F_e \ge 0.44F_y) \tag{9.2a}$$

and

$$F_{cr} = 0.877F_e \quad \text{when} \quad \frac{KL}{r} \ge 4.71\sqrt{\frac{E}{F_y}} \tag{9.2b}$$

where

$$F_e = \frac{\pi^2 E}{\left(\frac{KL}{r}\right)^2} \tag{9.2c}$$

The equivalent CSA S16 clause uses $1.2R_yC_u$.

Note that these overstrength values were determined considering the actual KL/r values corresponding to the experiments reviewed. Designer are cautioned that, for the same reasons, although considering higher values of KL/r may be conservative for brace design, it would be inappropriate for assessing the demands imposed by the brace on its connections and other frame elements.

9.2.5 Evolution of Codified Strength and Slenderness Limits

Table 9.1 summarizes how the AISC Seismic Provisions, from their 1992 edition through 2010, have accounted for some of the parameters described above. This timeline perspective of codified requirements can be useful when reviewing the seismic design of existing buildings, or when studying design aids and tutorials developed referencing earlier editions of the provisions, as the frequent changes that occurred over those two decades can be perplexing.

9.2.6 Local Buckling

Local buckling is another factor that has a major impact on the behavior of braces. First, local buckling leads to rapid degradation of compressive and flexural strength of the brace. Second, and more importantly, the large local strains that develop at the buckled plate surfaces are susceptible to low-cycle fatigue upon repeated cycles of inelastic deformations, and thus cracking leading to fracture. Because braces in a concentrically braced frame provide a structure's lateral stiffness and strength and are the elements that dissipate the seismic energy, their fracture risks leading to frame collapse.

In stocky braces, it is desirable to delay local buckling as much as possible during compression yielding (beyond preventing its development before axial yielding). Instances of axial local buckling, rapidly followed by fracture of the brace, are shown in Figure 9.17 for built-up braces (Lee and Bruneau 2004). Note that, in some stocky braces, local buckling produces lateral displacements that can trigger global brace buckling. Instances of stocky braces are less common in practice, because design for minimum weight typically leads to smaller braces of slenderness close to the permitted upper limits.

In braces that buckle inelastically, compression energy dissipation develops through plastic flexural hinging at midspan of the brace. The large plastic curvatures that typically develop at that location can potentially lead to local buckling. Upon repeated cyclic loading, the local buckling and straightening of the material at that location induces cracks that may propagate and lead to fracture.

Categories	1992 Edition	1997 Edition		2002 Provisions[b]		2005 Provisions		2010 Provisions	
		OCBF	SCBF	OCBF[c]	SCBF	OCBF	SCBF	OCBF	SCBF
R	5	5	6	5	6	3.25	6	3.25	6
C_r	$0.8\phi_c P_n$	$0.8\phi_c P_n$	$\phi_c P_n$	—	$\phi_c P_n$	$0.8\phi_c P_n$	$\phi_c P_n$	$\phi_c P_n$	$\phi_c P_n$
$(KL/r)_{max.}$	$\frac{720}{\sqrt{F_y}}$	$\frac{720}{\sqrt{F_y}}$	$\frac{1000}{\sqrt{F_y}}$	—	$\frac{1000}{\sqrt{F_y}}$	$\frac{720}{\sqrt{F_y}}$	$\frac{680}{\sqrt{F_y}}$ or 200[e]	$\frac{680}{\sqrt{F_y}}$[f]	200
Tension on Connection	$A_g F_y$	$R_y A_g F_y$	$R_y A_g F_y$	—	$R_y A_g F_y$	$R_y A_g F_y$	$R_y A_g F_y$	Note[g]	$R_y A_g F_y$
Moment on Connection[d]	M_n	$1.1 R_y M_p$	$1.1 R_y M_p$	—	$1.1 R_y M_p$	—	$1.1 R_y M_p$	Note[g]	$1.1 R_y M_p$
Compression on Connection	—	GS[h]	GS[h]	—	GS[h]	—	$1.1 R_y P_n$	Note[g]	1.1 times (lesser of $R_y F_y A_g$ and $1.14 F_{cre} A_g$[i])
Expected Postbuckling Compression Strength	—	—	$0.3\phi_c P_n^f$	—	$0.3\phi_c P_n^f$	—	$0.3 P_n^f$	Note[g]	0.3 times (lesser of $R_y F_y A_g$ and $1.14 F_{cre} A_g$)[j]

[a]($\phi_c = 0.85$ for 2002 editions and earlier; $\phi_c = 0.9$ since 2005 edition)
[b]Provisions for OCBF were eliminated, except for what was previously required for low-rise buildings
[c]Low-rise and roof structures only, designed for the Amplified Seismic Loads, $\Omega_o E$, with $\Omega_o = 2$.
[d]Except when brace connection can accommodate inelastic rotation associated with brace postbuckling deformations (e.g., gusset hinging).
[e]KL/r up to 200 permitted when columns designed considering maximum load transferred to the column (considering R_y times the nominal strength of the connecting brace elements).
[f]Only required for *V* or Inverted *V* configurations
[g]Designed for Amplified Seismic Loads, unless designed as per SCBF requirements
[h]Generic statement: "The design of gusset plates shall include consideration of buckling"
[i]F_{cre} is F_{cr}, determined per AISC 360 Chapter E using expected yield stress $R_y F_y$ in lieu of F_y. Note that 1.14 is equal to 1/0.877.
[j]Commentary states that two separate analyses are required: one with all braces at their maximum forces, and one with tension braces at their maximum strength and compression braces at their low postbuckling strength

TABLE 9.1 Changes in AISC CBF Provisions from 1992 to 2010[a]

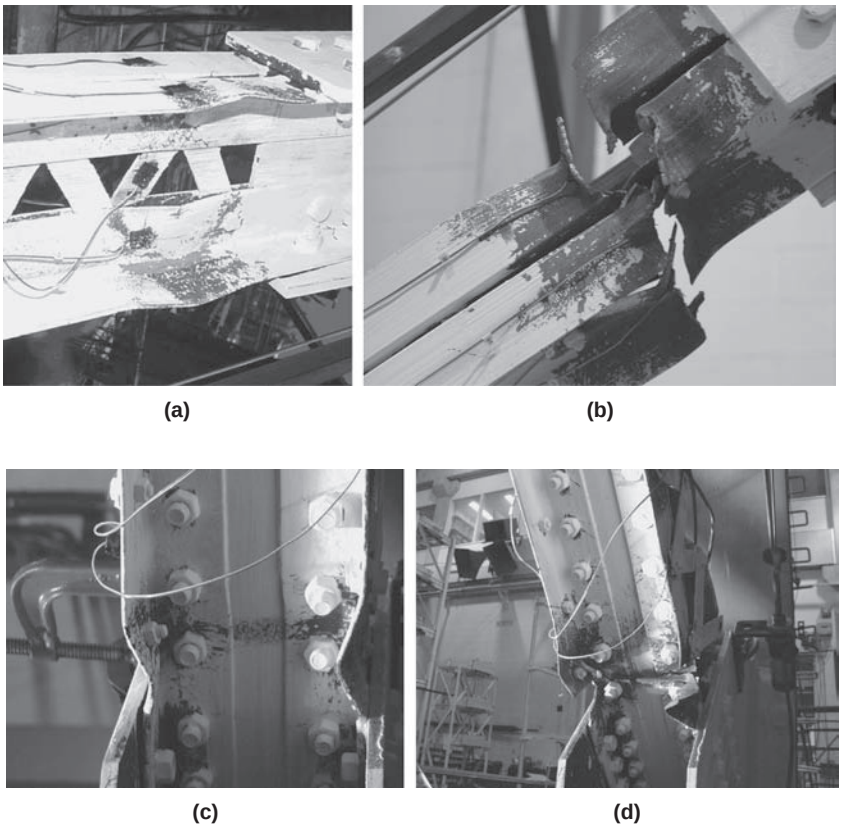

FIGURE 9.17 Axial local buckling in stocky built-up brace: (a) initiation of local buckling; (b) fracture subsequent to cycles of inelastic displacements, for brace with latticed web; (c) and (d) same for beam with solid web. (*Lee and Bruneau 2004, Courtesy of MCEER, University at Buffalo.*)

Braces of rectangular hollow structural shapes (a.k.a. tubes) are particular prone to local buckling and subsequent fractures during cyclic inelastic deformations (e.g., Bonneville and Bartoletti 1996, Gugerli and Goel 1982, Liu and Goel 1987, Shaback and Brown 2003, Tremblay 2002, Tremblay et al. 2003, Uang and Bertero 1986), with cracking often initiating at their rounded corners where high strains have been introduced during their fabrication (by bending of a flat plate into the final tubular shape). This is unfortunate because the high radius of gyration of rectangular tubes for a given cross-sectional area makes them otherwise highly desirable and commonly used as seismic braces. In some instances, fracture has been observed to develop rapidly following the onset of local buckling. This phenomenon, from local buckling to fracture, is illustrated in Figure 9.18 for a tubular brace. Example of such brace buckling and fractures observed following earthquakes are shown in Figure 9.19.

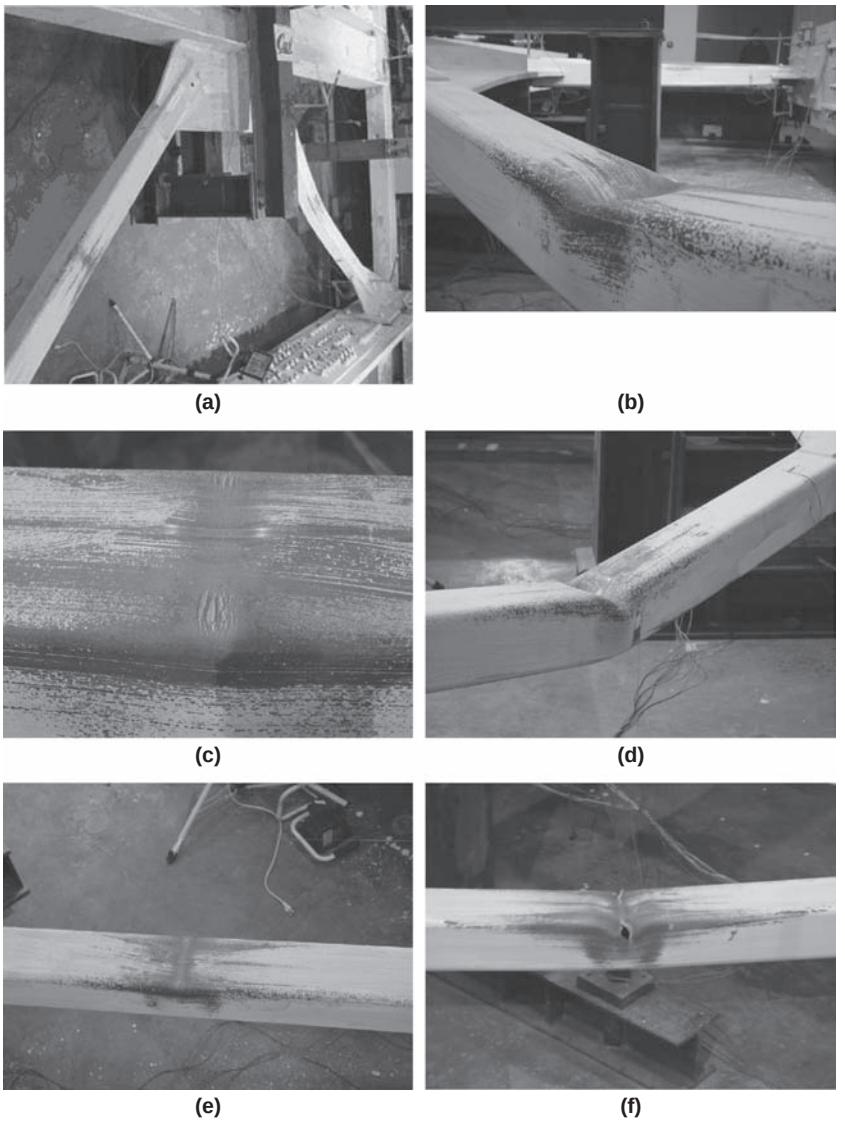

Figure 9.18 Stages in fracture of cyclically loaded braces: (a) buckled and restraightened brace at 0.67% drift; (b) local buckle developed during out-of-plane buckling; (c) initial tears at corner of straightened brace at 0.67% drift; (d) out-of-plane buckling of brace; (e) corresponding point of fracture initiation in strengthened brace at 1.34% drift; (f) fractured corners; (g) fractured face; (h) complete fracture. (*Uriz and Mahin 2008, with permission from PEER, University of California, Berkeley.*)

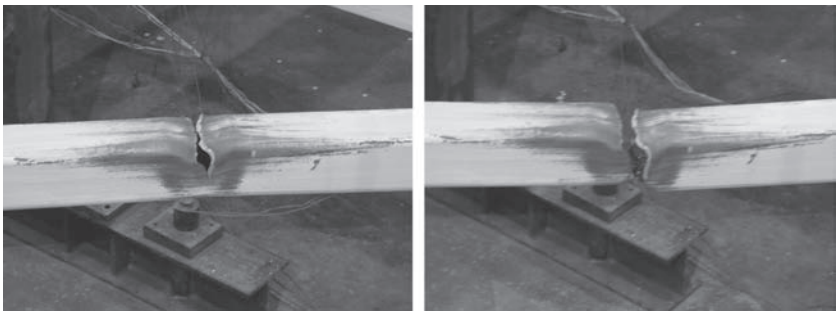

(g) (h)

Figure 9.18 (*Continued*)

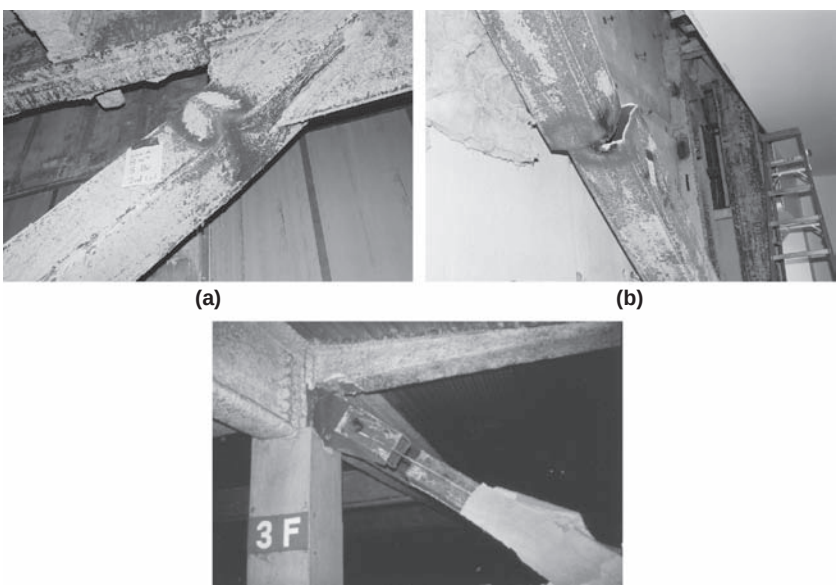

(a) (b)

(c)

Figure 9.19 Rectangular HSS braces: (a and b) buckled and fractured—Northridge earthquake. (*Courtesy of Degenkolb Engineers*); (c) fractured—Kobe earthquake. (*Courtesy of Dennis Mitchell, Department of Civil Engineering and Applied Mechanics, McGill University.*)

Preventing local buckling is paramount to precluding premature material fracture. For all structural shapes, the strategy adopted by codes and standards for delaying the onset of local buckling has been to limit the width-to-thickness ratio of braces. Given that braces develop flexural plastic hinges during their buckling, limits on width-to-thickness ratios must be at least as stringent as those for highly

ductile flexural members, and more stringent in some cases given the large axial loads simultaneously resisted by braces.

Given that the limits specified for seismic design were more stringent than those defining compact members (i.e., smaller than λ_p in AISC 360), members meeting these requirements were called "seismically compact" in some past codes and specifications (e.g., AISC 341-05). This terminology has been superseded in AISC 341-10 by the designations of "moderately ductile" for members anticipated to undergo plastic rotation of up to 0.02 rad, and "highly ductile" for members anticipated to undergo plastic rotation of 0.04 rad or more.

The width-to-thickness ratio for the flanges of rolled or built-up I-shaped sections, channels, and tees, as well as legs of angles (single angles, double angle members with separators, or outstanding legs of pairs of angles in continuous contact) and stem of tees, is limited to $0.30\sqrt{E/F_y}$ for highly ductile members (which includes braces of SCBF), and $0.38\sqrt{E/F_y}$ for moderately ductile members (which includes braces of OCBF). Except for round and rectangular HSS, stems of WTs and webs in flexural compression, the width-to-thickness ratio limits for moderately ductile members correspond to λp values in AISC 360.

The rapid strength deterioration and fracture under inelastic cyclic loading of braces having hollow structural shapes has long been recognized. Based on results from their respective research, Tang and Goel (1987) and Uang and Bertero (1986) recommended that the limit on the width-to-thickness ratio (b/t) for rectangular tubes be reduced from the value then specified. Tang and Goel recommended a b/t limit of $95/\sqrt{F_y}$ ($= 250/\sqrt{F_y}$ in S.I. units) for rectangular tube sections. Uang and Bertero (1986) recommended a limit of $125/\sqrt{F_y}$ ($= 330/\sqrt{F_y}$ in S.I. units) with a slenderness ratio, KL/r, limit of 68, (their study considered braces having $48 \le KL/r \le 61$ and $12.7 \le b/t \le 20.5$, these latter values being less than the AISC b/t limit of 26 at the time). From 1992 to 2005, the AISC Seismic Provisions limit for seismically compact rectangular HSS braces was $110\sqrt{F_y}$, equivalent to $0.64\sqrt{E/F_y}$. In AISC 341-10, this limit was retained for moderately ductile braces, but reduced to $0.55\sqrt{E/F_y}$, equivalent to $94\sqrt{F_y}$, for highly ductile braces, on the basis of additional research results (Fell et al, 2006, Uriz and Mahin 2008). AISC 341-10 similarly reduced by 15% the previous seismically compact limit of $0.044E/F_y$ for the diameter-to-thickness ratio limit of round HSS in SCBF, to $0.038E/F_y$ for highly ductile braces; moderately ductile braces (in OCBF) remained at the previous limit. However, as local buckling and low-cycle fatigue life of braces also correlate to member slenderness, future research is anticipated to further affect these limits.

As an alternate approach to delay the onset of local buckling in tubular braces, Liu and Goel (1987) and Lee and Goel (1987) proposed filling them with expansive concrete. They investigated

the hysteretic response of similar braces, comparing hollow steel braces b/t ratios approximately equal to 30 and 14, with a brace having the lower b/t ratio and filled with concrete. Liu and Goel reported similar overall buckling modes for the three specimens prior to plastic hinge formation and local buckling, but that following plastic hinge formation, the braces with the smaller b/t ratio and concrete fill performed substantially better because local buckling in the plastic hinge zones was delayed and the strength of the brace remained relatively constant with repeated cycling. For the two hollow tubular sections tested, the compression flange in the brace at the plastic hinge buckled inward and the brace webs bulged outward (Figure 9.20a). For the concrete-filled braces, because of concrete restraining any significant inward buckling, the flange of the tube buckled outward; the zone of local buckling lengthened to approximately the width of the tube and its severity was reduced (Figure 9.20b), reducing the magnitude of strains in the plastic hinge zone due to local buckling, delaying the onset of fracture, and lessening degradation of the brace compression strength. Other researchers reported similar benefits with concrete filled tubes (e.g., Broderick et al. 2005, Zhao et al. 2002).

9.2.7 Low-Cycle Fatigue Models

While the emphasis of early editions of seismic provisions was on limiting member slenderness, KL/r, to relatively low values, research results raised concerns that ductile braces designed in full compliance with these requirements would not necessarily have a low-cycle fatigue life sufficient to survive the large cyclic deformations imposed by severe earthquakes (Archambault et al. 1995, Fell et al. 2009, Tang and Goel 1987), as cracking and early fracture develop due to severe local buckling in the regions of plastic hinges. Global member slenderness limits for braces were relaxed in more recent editions of seismic design code and standards as a way to reduce plastic hinge rotation demands in the braces, and thus to delay or prevent low-cycle fatigue fractures. As KL/r increases, inelastic demand during brace buckling decreases, leading to lower strains at the plastic hinge location, suggesting that increased member slenderness is beneficial, and that KL/r is the most important parameter controlling global behavior and response (e.g., Fell et al. 2009, Jain et al. 1978, Lee and Bruneau 2005, Tang and Goel 1989, Tremblay 2002, Tremblay et al. 2003). Arguably, slender braces only developing elastic buckling (i.e., without plastic hinging) could have a more desirable behavior, at the cost of low compression strength and no energy dissipation in compression. In the absence of plastic hinging in the middle of the brace, provided no local buckling otherwise developed in the brace, there is no need to be concerned about low-cycle fatigue life of the brace. Future research will enlighten design decisions in this regard.

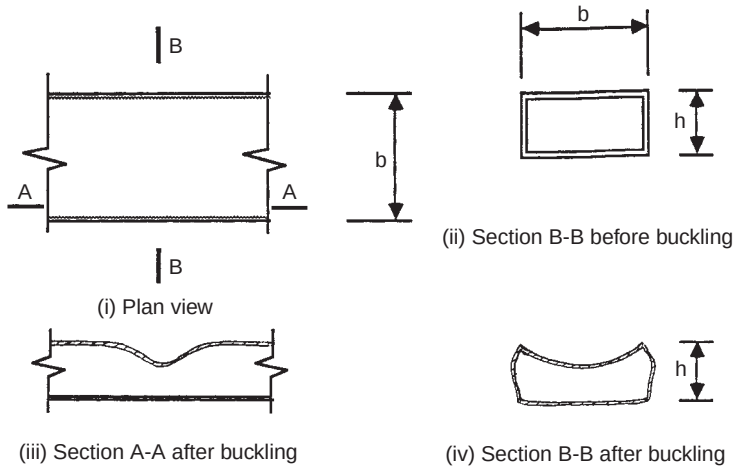

(a) Hollow tubular braces

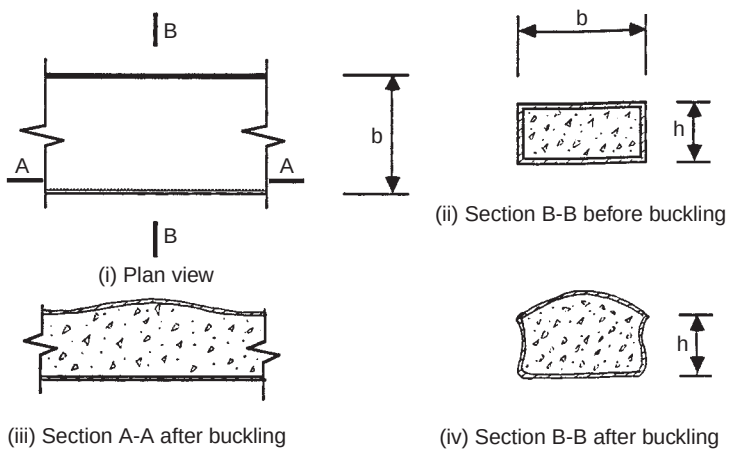

(b) Concrete-filled tubular braces

Figure 9.20 Buckled sections in tubular steel braces at plastic hinge locations. (*Courtesy of S. Goel, Department of Civil and Environmental Engineering, University of Michigan.*)

Tools to assess the low-cycle fatigue life of braces will be required for this purpose. This section briefly reviews some of the fracture criteria that have been developed for tubular bracing members. Note that, typically, wherever Δ has been used in fracture models, it actually corresponds to the axial elongation of the brace, that is, δ per the notation used in all other sections.

9.2.7.1 Member Hysteresis Models (Phenomenological Models)

One category of low-cycle fatigue models consists of criteria related to the hysteretic behavior of brace members. Tang and Goel (1987) first proposed the following empirical equation to quantify the fracture life of rectangular tubular bracing members:

$$N_f = 262\frac{(B/D)(60)}{[(B-2t)/t]^2} \quad \text{for} \quad \frac{KL}{r} \le 60 \tag{9.3a}$$

$$N_f = 262\frac{(B/D)(KL/r)}{[(B-2t)/t]^2} \quad \text{for} \quad \frac{KL}{r} > 60 \tag{9.3b}$$

where N_f is the fracture life expressed in terms of a number of equivalent cycles, B and D are respectively the gross width and depth of the section defined such that $B > D$, and t is the thickness of the section. To determine if fatigue life is exceeded, the calculated time history of brace deformations must be converted into equivalent cycles per a procedure outlined in Tang and Goel (1987), equivalent to a rainflow counting method (Chapter 2) in which only the half cycles from a compression peak to the point of maximum tension (or minimum compression) in a cycle are counted to contribute to fatigue life.

Lee and Goel (1987) reformulated this model by considering the effect of F_y and eliminating the dependency on KL/r. In this criterion, the nondimensional parameter Δ_f is used instead of N_f to quantify the fracture life of a tubular bracing member. This method proceeds per the following steps:

(a) The hysteresis curves (P vs. Δ) are converted to normalized hysteresis curves (P/P_y vs. Δ/Δ_y).

(b) The deformation amplitude (tension excursion in a cycle) is divided into two parts, Δ_1 and Δ_2, defined at the axial load $P_y/3$ point, as illustrated in Figure 9.21. Δ_1 is the tension deformation from the load reversal point to $P_y/3$, whereas Δ_2 is from $P_y/3$ point up to the unloading point.

(c) $\Delta_{f,exp}$ is obtained by adding 0.1 times Δ_1 to Δ_2 in each cycle and summing up for all cycles up to the failure [i.e., $\Delta_f = \Sigma(0.1\Delta_1 + \Delta_2)$]. This reflects a belief that straightening and stretching of the brace has a greater impact on fracture life than compressive deformation excursions.

(d) The theoretical fracture life, Δ_f is expressed as follows:

$$\Delta_f = C_s \frac{(46/F_y)^{1.2}}{[(B-2t)/t]^{1.6}}\left(\frac{4B/D+1}{5}\right) \tag{9.4}$$

where C_s is an empirically obtained constant calibrated from test results, and F_y is the yield strength of the brace (ksi). The numerical

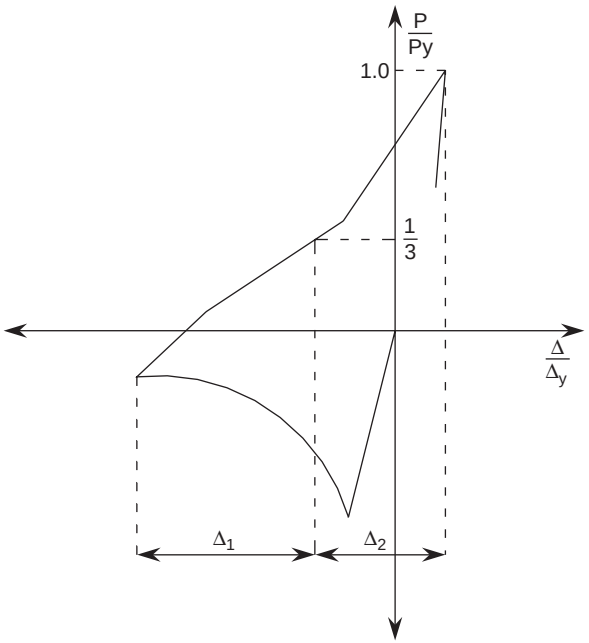

Figure 9.21 Definition of Δ_1 and Δ_2. (*Lee and Goel model.*) (*Lee and Bruneau 2002, courtesy of MCEER, University of Buffalo.*)

constant C_s, originally given as 1335 by Lee and Goel (1987), was recalibrated using the test results of Gugerli and Goel (1982) and Lee and Goel (1987), and found to be 1560 by Hassan and Goel (1991). Fracture is assumed to occur when $\Delta_{f,exp} = \Delta_f$.

Based on a review of additional and previous test results, Archambault et al. (1995) found the Lee and Goel model to underestimate the fracture life of tubular bracing members having large slenderness ratios, and modified it by reintroducing the effect of slenderness ratio, KL/r, and recalibrating against the available data. They introduced the term, Δ_f^* (to differentiate it from Δ_f used by Lee and Goel), and expressed fatigue life as:

$$\Delta_f^* = C_s \frac{(317/F_y)^{1.2}}{[(B-2t)/t]^{0.5}} \left(\frac{4B/D+1}{5}\right)^{0.8} \times (70)^2 \qquad \text{for} \qquad \frac{KL}{r} < 70 \tag{9.5a}$$

$$\Delta_f^* = C_s \frac{(317/F_y)^{1.2}}{[(B-2t)/t]^{0.5}} \left(\frac{4B/D+1}{5}\right)^{0.8} \times (KL/r)^2 \qquad \text{for} \qquad \frac{KL}{r} \geq 70 \tag{9.5b}$$

where the C_s = 0.0257 based on calibration to experimental results and F_y is in MPa. Figure 9.22 compares the trends in predicted

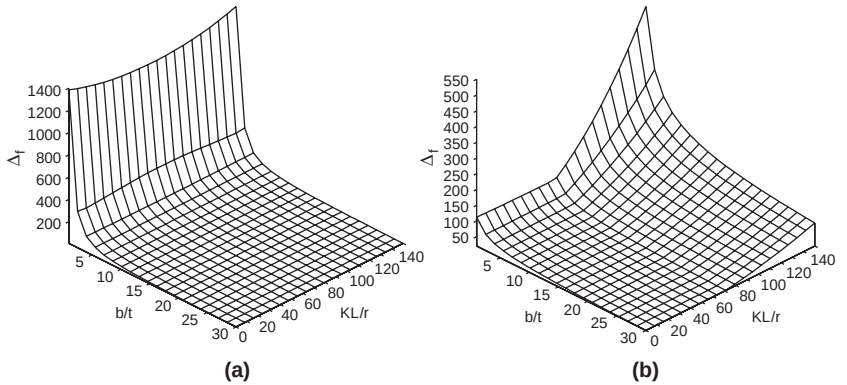

FIGURE 9.22 Trends in predicted fracture life, as a function of b/t and KL/r, per: (a) Tang and Goel model; (b) Archambault et al. (1995) model. (*Lee and Bruneau 2002, courtesy of MCEER, University at Buffalo.*)

fracture life, for the Lee and Goel versus the Archambault et al. (1995) models (Lee and Bruneau 2002).

Additional test results and recalibration by Shaback and Brown (2003) led to the following revisions to the model:

$$\Delta_f^* = 0.065 \frac{(350/F_y)^{-3.5}}{[(B-2t)/t]^{1.2}} \left(\frac{4B/D - 0.5}{5} \right)^{0.55} \times (70)^2 \quad \text{for} \quad \frac{KL}{r} < 70 \tag{9.6a}$$

$$\Delta_f^* = 0.065 \frac{(350/F_y)^{-3.5}}{[(B-2t)/t]^{1.2}} \left(\frac{4B/D - 0.5}{5} \right)^{0.55} \times \left(\frac{KL}{r} \right)^2 \quad \text{for} \quad \frac{KL}{r} \geq 70 \tag{9.6b}$$

Phenomenological models for assessing the low-cycle fatigue life of braces having other types of cross-sectional shapes have not been as intensely pursued, even though such fractures have been observed following local buckling at the plastic hinge locations, such as in circular hollow sections (e.g., Elchalakani et al. 2003, Tremblay et al. 2008) and W shapes (http://exp.ncree.org/cbf/index.html, Roeder et al. 2010). Lee and Bruneau (2002) adapted the above equations for built-up latticed braces made of angles, on the basis of limited experimental results, and Goel and Lee (1992) proposed a fracture criterion for concrete-filled tubular bracing members.

9.2.7.2 Continuum Mechanics Models (Physical Models)

A second approach taken to model the low-cycle fatigue of cyclically loaded brace members has been to implement fatigue models in finite element programs, either tracking plastic strain histories at all locations of interest (e.g., Yoo et al. 2008) or explicitly modeling plastic

damage and fracture (e.g., Huang and Mahin 2010, Kanvinde and Deierlein 2007), and calibrating model parameters based on past experimental data for braces.

For example, Huang and Mahin (2010) developed a continuum mechanics damage plasticity model to account for low-cycle fatigue, combined with an existing erosion algorithm to simulate cracking. Recognizing that additional research is required to determine how to best calibrate the damage parameters of such models, analyses provided good correlation with experimental results in chosen illustrative examples. Sample simulation results are shown in Figure 9.23.

As an intermediate step between phenomenological models and full-blown continuum mechanics, Uriz and Mahin (2008) developed an approach for modeling low-cycle fatigue using fiber-hinge models (Uriz et al 2007), a Menegotto-Pinto material model, a modified

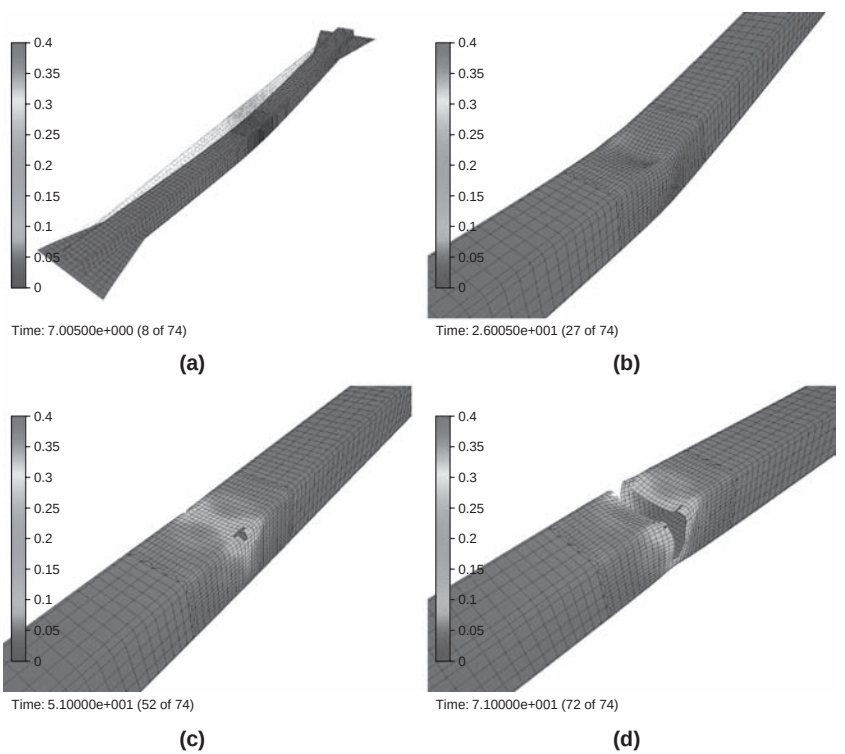

Figure 9.23 Finite element modeling of low-cycle fatigue of brace: (a) global buckling; (b) local buckling; (c) crack initiation; (d) fracture. (*Huang and Mahin 2010, with permission from PEER, University of California, Berkeley.*)

rainflow cycle counting procedure with the Coffin-Manson model (Chapter 2), and calibration using data for rectangular tubular braces. Although the accuracy obtained with this approach was comparable with that obtained with the phenomenological models, calibration allows further investigation of other cross-sectional types, boundary conditions, lengths, b/t ratios, and material properties; using such an approach, Uriz and Mahin verified that braces using wide-flange shapes typically have a significantly better low-cycle fatigue life than other cross-sections. However, fiber model elements are limited in that they cannot model cross-sectional changes due to local buckling, nor strain and stress concentrations due to crack opening.

9.2.8 Models of Single Brace Behavior

Computationally efficient element models of single brace for use in nonlinear inelastic analysis programs have been developed since the mid 1970s to capture the hysteretic axial force versus axial displacement behavior of braces. Use of these models is substantially less computationally intensive than finite element approaches based on computational mechanics or fiber hinges, but they cannot model local buckling. Most of these models also do not address low-cycle fatigue and fracture, although some have been linked to subroutines tracking cycles and/or yielding excursions against predicted life.

First formulated were phenomenological models constructed of empirical functions and coefficients that needed to be calibrated on experiment-specific data to replicate the various stages of behavior (e.g., Higginbotham and Hanson 1976; Ikeda et al. 1984; Jain et al. 1977, 1978; Jain and Goel 1978; Maison and Popov 1980). Later developments favored models that relied on physical theory to characterize the various branches of the hysteresis loops as well as the transitions from any branch to possible others during the loading history. Physical theory models are intended to predict the behavior of any brace from knowledge of member geometry and material properties (e.g., Dicleli and Calik 2008; Gugerli and Goel 1982; Ikeda and Mahin 1984; Jin and El-Tawil 2003; Nonaka 1987, 1989; Soroushian and Alawa 1990; Zayas et al. 1981), although some of these models neglect to account for Baushinger effects (which can significantly impact the shape of the hysteresis curves) or use complex empirical coefficients to model this effect. Although physical models generally only consist of two elastic members and a plastic hinge, they can reasonably capture brace axial hysteretic behavior (and in some cases out-of-plane deformations), as illustrated in Figure 9.24 for the Dicleli and Calik (2008) model.

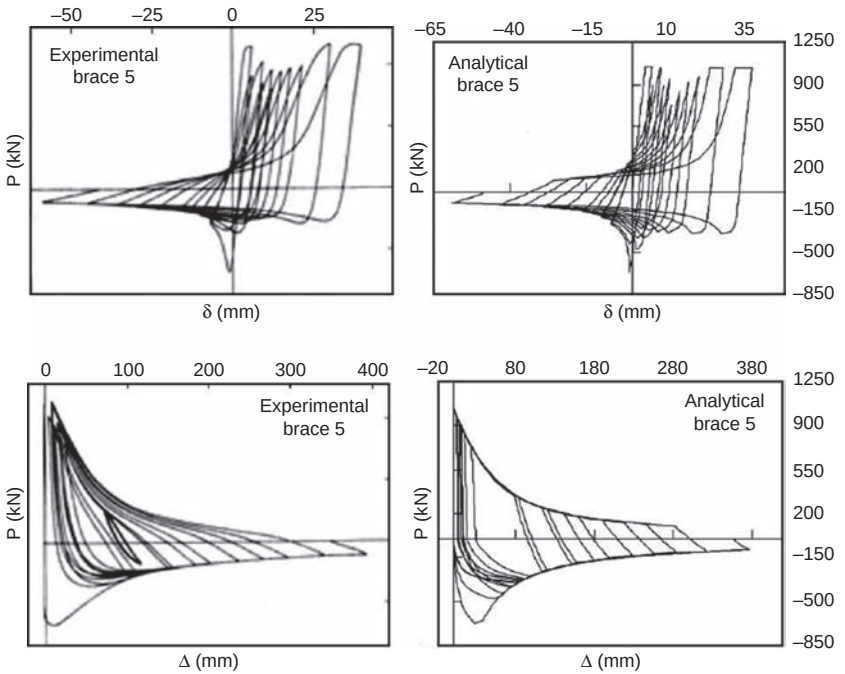

Figure 9.24 Sample results obtained using a Physical Theory Model. (*Courtesy of Murat Dicleli, Department of Civil Engineering, Middle East Technical University, Ankara, Turkey.*)

9.3 Hysteretic Behavior and Design of Concentrically Braced Frames

9.3.1 System Configuration and General Issues

9.3.1.1 Capacity Design and Analysis

Figure 9.2 shows frame configurations permitted or prohibited by AISC 341. Any of the permitted configurations can be designed to perform in a ductile and stable manner during earthquakes. However, a successful design, irrespective of configuration, must recognize and account for the redistribution of forces within the structural system, as braces buckle in compression, yield in tension, and lose compression strength upon larger drifts and during repeated loadings. Explicit recognition of this important redistribution is relatively recent in design codes and standards. Braced frames designed in the absence of such enforced capacity design principles may exhibit an erratic behavior during severe earthquakes due to possible beam and column buckling or connection failures.

Although most contemporary codified design requirements have embraced capacity design principles that are generally applicable for any frame configuration, many codes and standards still treat V- and inverted V-braced frames with separate requirements, in recognition of their unique characteristics as a result of the unbalanced forces applied to their beams during brace yielding and buckling (Section 9.3.3). Such a differentiation is therefore kept in the organization of this section.

Braces are the first elements designed in a concentrically braced frame. The forces to consider for their design are typically obtained from an elastic analysis, but their behavior is highly nonlinear due to brace buckling and yielding, as described in Section 9.2. Braces are the designated energy dissipating mechanisms for this type of structural system. Yielding and buckling of braces typically develop at drifts of 0.3 to 0.5%, and postbuckling axial deformations of braces can reach up to 20 times their yield deformation. Section 9.2 has outlined the desirable features of braces to ensure they can reach such deformations and survive severe earthquakes without premature brace fractures. These important requirements limiting member slenderness and width-to-thickness ratios are not repeated in this section, but are mandatory given that brace rupture can lead to excessive demands on beams and columns and possible collapse. However, issues related to determination of the effective length of brace, not previously addressed, is presented in Section 9.3.2.

Having designed the braces, their strengths dictate the demands on the remaining components of the structural systems. These demands on beams, columns, connections and other parts, are reviewed in details below, building on the information presented in the previous sections rather than repeating it. These components are designed to remain elastic, and the following discussion focuses on the determination of demands for the design of these structural elements, one exception being that, in many instances, ductile behavior of the brace gusset connectors is also essential to achieve satisfactory, as described in a later section.

Note that nonlinear inelastic analysis of braced frames assuming pin connections at the intersection of all members (as done in truss analysis) will unavoidably predict concentration of damage in a single level of the braced frame, because such an idealized model provides no means for yielding to spread to other levels, as shown by the example of Section 6.3.1. This is a consequence of the postbuckling degradation of compression strength and further aggravated by the absence of significant strain hardening in the braces. However, results from such simplified models disagree with field observations following earthquakes that demonstrate the spreading of yielding and buckling along building height. This is because the pin connections model fails to recognize the key role played by all columns (including those not part of the SCBF) to distribute forces along the height of

buildings. MacRae et al. (2004, 2010) provided a "continuous column concept" and procedure to estimate the likely drift concentration in frames of different heights, which may in turn be used to estimate the column stiffness required to achieve the desired performance. Extrapolating this concept, Wada et al. (2009) proposed rocking rigid walls (pinned at their base) that were effectively implemented in a building to evenly distribute energy dissipation along building height.

Therefore, as a minimum, the continuity of the braced-frame columns must be modeled. Likewise, for tension-only structures, CSA S16 requires every column in the building to be fully continuous over the building height to prevent concentration of inelastic demand in a single story.

9.3.1.2 Brace Layouts for Balanced Lateral Strengths

Energy dissipation by tension yielding of braces is more reliable than by buckling of braces in compression, even for braces of low slenderness and compactness. Consequently, to ensure a minimum of structural redundancy and a good balance of energy dissipation between compression and tension members, structural layouts that predominantly depend on the compression resistance of braces (rather than their tension resistance) must be avoided in an earthquake-resistant design perspective. Examples of unacceptable braced-frame layouts are shown in Figure 9.25, along with recommended alternatives. Four braces in compression and only one brace in tension resist the load applied on the five-bay braced frame shown in Figure 9.25a. The four braces in the braced-core of Figure 9.25c are all in compression when resisting the torsional moment resulting from seismically induced inertial force acting at the center of mass (for simplicity, columns resisting only gravity loads are not shown in that figure). Better designs are shown in Figs. 9.25b and 9.25d for each of those cases, respectively.

Seismic design codes prevent the use of nonbalanced structural layouts by requiring that braces along a given structural line be deployed such that at least 30% but no more than 70% of the total lateral horizontal force acting along that line is resisted by tension braces (which is equivalent to making the same requirement for compression braces). Note that although the wording of such clauses would not cover the case shown in Figure 9.25c, the intent of the clauses would. Codes typically waive this requirement if nearly elastic response is expected during earthquakes (which AISC 341 approximates with a special "amplified seismic load" condition described later).

This requirement has sometimes been interpreted by considering a balance of member strengths rather than design forces. For frames having the same number of compression and tension braces, and designed for slenderness limits of $4\sqrt{E/F_y}$, this distinction was less

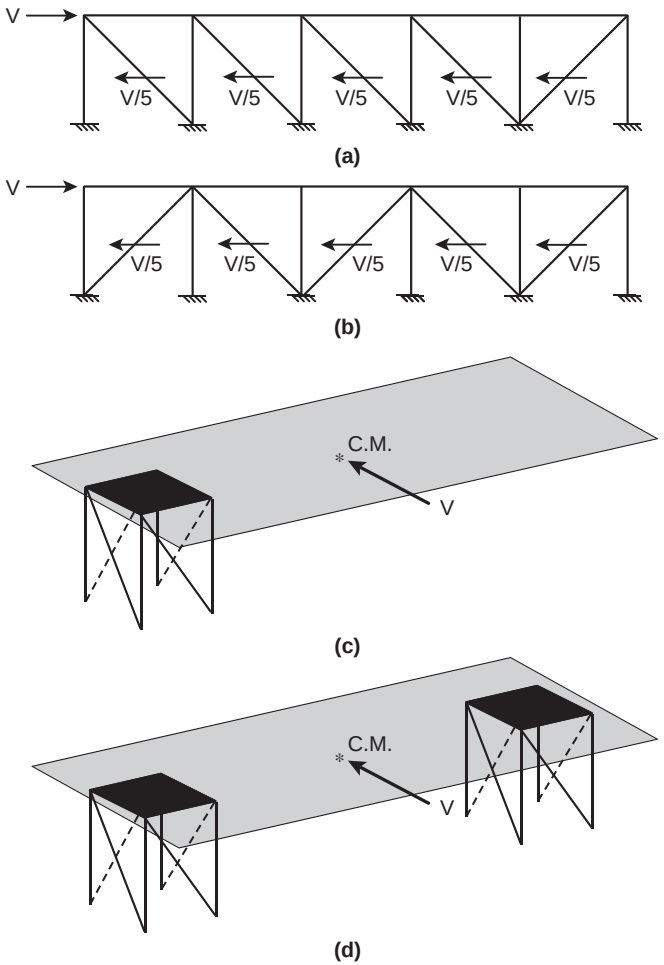

Figure 9.25 Brace layouts to ensure balanced lateral strength: (a and c) unacceptable layouts; (b and d) acceptable alternative layouts.

significant (i.e., for $F_y = 50$ ksi, the slenderness limit becomes 98, and the compression strength of a brace for that slenderness is half of the tension strength, the compression brace thus providing 33% of the braced frame strength). However, the clause refers to 30% and 70% of the lateral horizontal force based on the elastic analysis force distribution between the tension and compression members, irrespective of member strengths (i.e., for the same two-brace frame example, this force distribution is 50% and 50% as the compression brace is designed to resist half of the applied force).

Given that CSA-S16-09 allows tension-only systems in some circumstances, recognizing that no lateral force is applied to the

compression braces that are neglected in the corresponding elastic analysis, the same intent is achieved by requiring instead that the "ratio of the sum of the horizontal components of the factored tensile brace resistances in opposite directions is between 0.75 and 1.33."

9.3.1.3 Impact of Design Approach on System Overstrength

The design approach adopted for braced frames can have a significant impact on their behavior. In most seismic regions, it is a standard practice to use elastic analysis to determine brace forces, which imply equal forces in the tension and compression braces when an equal number of compression and tension braces (of same area and length) resist the horizontal shear force at a given story. Brace area is determined by compression strength, and the corresponding tension strength is a consequence of this chosen area. Given that the buckling stress of a compression member decreases as a function of KL/r, the area needed to resist a given compression force increases for more slender members, and so does the corresponding brace tension yield strength.

When braces having greater KL/r values are used in concentrically braced frames, because of the resulting greater difference in tension and compression strengths, greater system overstrength is possible, as shown in Figure 9.26 (Tremblay 2003). Figure 9.26a shows brace compression strength as a function of slenderness, per CSA S16 design equations (similar curves would be obtained per other design specifications), and the corresponding degraded compression strength after displacement cycles at a specified ductility demand level. Figure 9.26b shows the corresponding tension strength, given that brace area is determined from the compression force, and therefore increases as a function of member slenderness. The sum of brace tension and degraded compression strengths, except in the approximate range of $25 < KL/r < 75$ where a slight decrease in system strength is observed, shows a net gain in overstrength for progressively more slender members (Figure 9.26c). Tremblay (2003) demonstrated that this overstrength can have a definite positive impact on achieving more stable braced frame response.

For comparison, in a tension-only design approach, braces are sized based on their tension strength alone (giving the flatline in Figure 9.26b), their compression strength being neglected. In this case, for the sum of the strengths (Figure 9.26c), the actual strength of the compression brace would provide system overstrength at low member slenderness, and progressively decreasing overstrength as slenderness increases. However, such an overstrength would be rare in practice, because the tension-only design approach typically leads to highly slender braces such as rod or flat bars.

9.3.1.4 Collector Forces versus Forces from Above

Beyond resisting gravity loads, some beams in braced frame buildings must also be designed to serve as collector elements, to transfer the

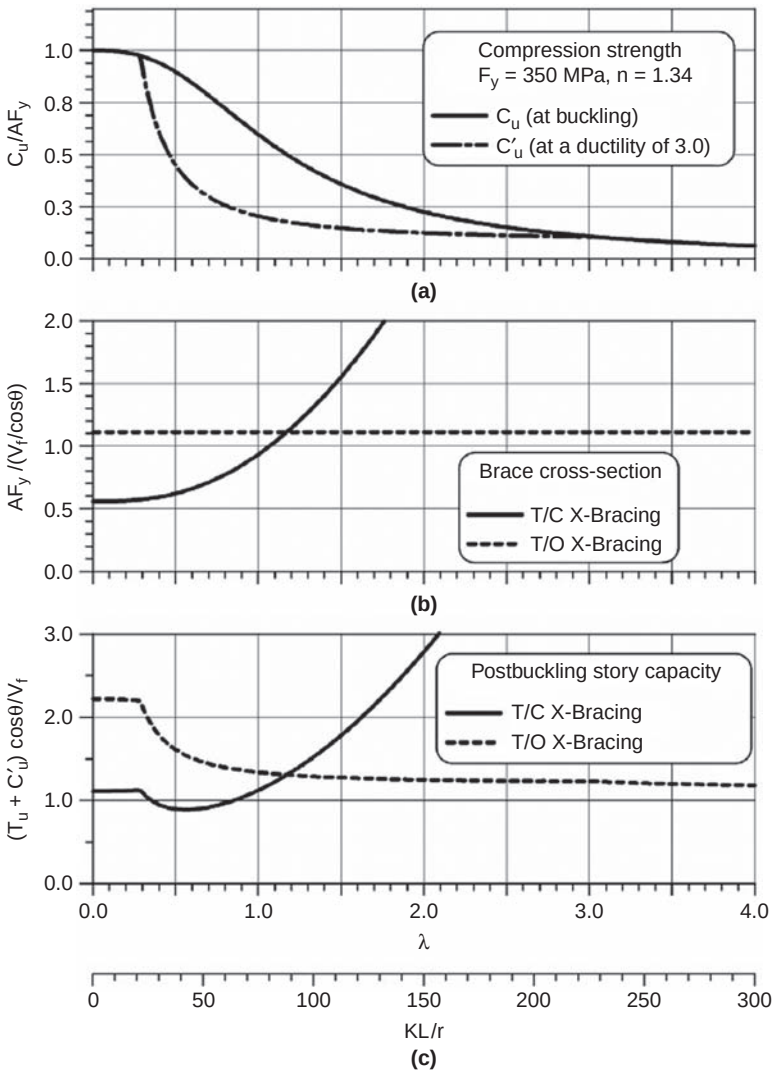

Figure 9.26 Comparison of strengths for design based on compression strength (T/C) versus tension-only assumption (T/O): (a) compression strength and degraded postbuckling compression strength as a function of brace area; (b) brace area as a function of lateral design force; (c) sum of brace strengths as a function of lateral design force. (*Tremblay 2003, copyright © American Institute of Steel Construction. Reprinted with permission. All rights reserved.*)

seismic inertial forces from the floor slabs into the braced bays, and in some case to facilitate load redistribution between different braced bays. Failure of these collector beams or their connections, preventing the transfer of seismic forces to the vertical lateral force-resisting system, could compromise the response of the entire building.

In the early days of seismic design, this transfer of inertial forces to the braced frames was assumed to be implicitly achieved without special detailing, whereas it is now recognized that ensuring integrity of a complete load path for the seismic inertial forces in the horizontal plane often requires that collector beams (a.k.a. drag struts or ties) be designed if to perform as intended. Per capacity design principles, the load path provided by collectors must remain elastic to ensure full development of the vertical braced frame's plastic mechanisms, which for braced frames must account for changes in load paths due to strength degradation of the compression braces (as illustrated later). Griffis and Patel (2006) and ATC (1999) provide general information and typical load paths for the design of collectors. Rogers and Tremblay (2010) provide similar information for steel roof deck diaphragms, including a ductile diaphragm alternative approach.

9.3.2 Brace Design

Typically, brace design is governed by compression strength (the limited applications of tension-only design permitted by CSA-S16 being a notable exception), which is a function of the slenderness KL/r. AISC 360 outlines standard procedures to determine the effective length factor, K, to size the braces, and higher values can be conservatively used if in the presence of uncertainties (L being typically taken as the distance from the intersecting axes of structural members in the analysis models). However, using capacity design principles to assess the demands imparted by the buckling braces on their connections and other structural elements, knowledge of the actual effective length is important, and conservatism dictates the use of lower K values.

Recommended K factors for braced frames subjected to cycles of inelastic deformations depend on brace configurations (whether braces cross or not between levels), in-plane versus out-of-plane buckling, brace connection types, and even brace cross-sectional types.

Beyond selection of appropriate K factors, seismic design issues for braces are limited to selection of structural members that meet the specified width-to-thickness ratio limits and member slenderness limits. Member properties tables only including members that meet these limits are available to expedite design (e.g., AISC 2006). Note that problems of excessive slenderness, when encountered during design, can be resolved by changing the brace configurations instead of using bigger braces (e.g., changing from X-bracing to inverted-V bracing in a particular story or bay).

9.3.2.1 Inelastic Cyclic Out-of-Plane Buckling

Early studies on the elastic behavior of X-braced frames subjected to noncyclic load showed that the tension brace can provide some resistance against *out-of-plane* buckling of the compression brace and justified the use of a value of K less than one for out-of-plane buckling. However, in the perspective of cyclic inelastic response (such as for

seismic design), many engineers believed this assumption to be incorrect, given that both braces are buckled when the braced frame is returned to its original position (i.e., zero lateral frame displacement), after having successively been stretched in tension. Therefore, they recommended that a value K of 1.0 be used for out-of-plane buckling, not relying on the tension brace to provide lateral bracing in seismic applications.

Research on X-braced frames (El-Tayem and Goel 1986 for z-axis buckling of braces, Tremblay et al. 2003 for rectangular HSS) demonstrated that in spite of the above brace slackness at zero frame displacements, with out-of-plane buckling over the entire brace length, the tension brace provides resistance against out-of-plane buckling anew as it reloads at larger frame drifts. For braces connected using single gussets, El-Tayem and Goel recommended use of an effective length of 0.85 times the half diagonal length, whereas Tremblay et al. reported values ranging from 0.83 to 0.90 of L_H, where L_H is defined as the distance between the brace intersection point and the plastic hinge in the gusset (for gusset hinges meeting the $2t_g$ criterion presented in Section 9.3.5).

The above effective length values for buckling modes that include gusset hinging would expectedly vary for different gusset thicknesses, with thicker values progressively approaching full fixity conditions, although such a continuous relationship has not yet been quantified. As one data point, Nakashima and Wakabayashi (1992) reported that analyses for the out-of-plane buckling of X-braced frames with fixed-end braces using KL equal to 0.7 times the half-diagonal length provided a good match with experiment results (note that 0.7 is the theoretical effective length factor for a fix-pin brace). The above results also assume that braces are continuous through their midlength connection point, or reinforced with cover plates (Tremblay et al. 2003) or by other bridging means to provide continuous stiffness across that point when discontinuous braces are used; effective length equations derived for the case of discontinuous braces (Davaran 2001, Moon et al. 2008) are awaiting experimental verification.

Note that although elastic buckling typically develops in both segments of the compressed brace in an X-braced frame, as inelastic buckling develops, plastic hinging first develops in one of the segments; the ensuing degradation of the brace compression strength (Section 9.2.3) results in lower forces in the compression brace, preventing inelastic buckling from developing in the second brace segment. This often reported phenomenon (e.g., El-Tayem and Goel 1986, Lee and Bruneau 2004, Tremblay et al. 2003) is illustrated in Figure 9.27.

For braces spanning freely between columns and beams (e.g., configurations in Figures 9.2a, c, d, and e) and buckling out-of-plane, Astaneh-Asl et al. (1985) showed that an effective length KL of $1.0L_H$

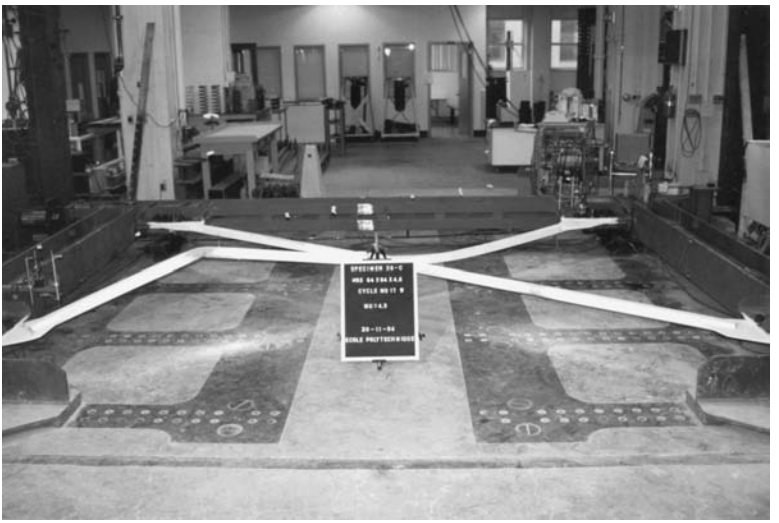

Figure 9.27 Inelastic buckling concentrated in one segment of a brace in an X-braced frame. (*Courtesy of Robert Tremblay, Département des génies civil, géologique et des mines, EcolePolytechnique, Montréal.*)

could be used (for gusset hinges meeting the $2t_g$ criterion presented in Section 9.3.5). Accounting for gusset flexural stiffness, Tremblay et al. 2003 reported values 5% to 12% lower. However, for the alternative elliptical gusset hinging (Section 9.3.5), Lehman et al. (2008) recommended using $K = 1.0$ with the actual brace length.

Finally, it must be recognized that out-of-plane brace buckling is liable to damage architectural finishes close to the braced frame (Figure 9.28). Sabelli and Hohbach (1999), Tremblay et al. (2003), and Shaback and Brown (2003) proposed equations to quantify the magnitude of this out-of-plane deformation.

9.3.2.2 Inelastic Cyclic In-Plane Buckling

For many typical brace connection details, the gussets provide more restraint against in-plane buckling of the braces than out-of-plane buckling; for equal brace slenderness, plastic moment of the gusset plate hinging out-of-plane is less than the plastic moment of the brace hinging to accommodate in-plane buckling of the brace (hinging of the gusset is unlikely in that direction). However, in many instances, in-plane buckling may occur instead of out-of-plane buckling (or be designed to occur, as in-plane buckling is more desirable to prevent damage to adjacent claddings and nonstructural elements).

For braces spanning freely between columns and beams (e.g., configurations in Figures 9.2a, c, d, and e), buckling in-plane and developing plastic hinges in the braces adjacent to the gusset,

(a)

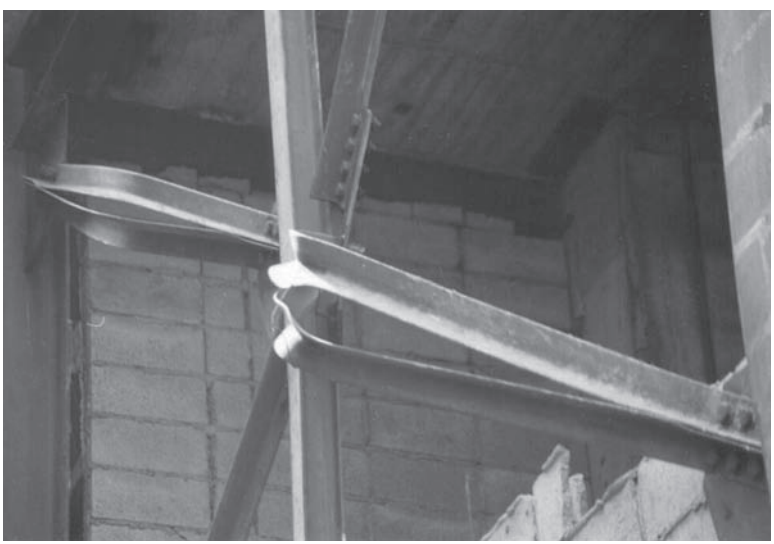

(b)

Figure 9.28 Masonry cladding damaged by out-of-plane buckling of braces: (a) global view; (b) close-up view of *z*-axis buckling of individual braces.

Astaneh-Asl and Goel (1984) recommended a value of KL of $0.5L_H$ (corresponding to fix–fix conditions). Tremblay et al. (2008) recommended a $KL = 0.9L_H$ when using a horizontal "knife-plate" gusset developed specifically to facilitate in-plane buckling (Section 9.3.5), with L_H being the distance between the plastic hinges in the gusset.

Considerably less data exists for in-plane buckling in X-braced frames. A K-value of 0.6 used with half of the full brace length has been recommended for braces developing their plastic moment capacity at their end connections (Nakashima and Wakabayashi 1992, Sabelli and Hohbach 1999).

9.3.2.3 Built-Up Braces

Double-angle braces are frequently used in braced frames, as well as other built-up shapes occasionally. For buckling modes that can impose large shear on stitches, AISC 341 requires the slenderness ratio of individual buckling elements between the stitches to be no greater than the governing slenderness of the built-up member, and that the sum of the shear strengths of the stitches exceeds the tensile strength of each element of the built-up brace. This stricter requirement than what is specified in AISC 360 was formulated based on research results that showed more severe local buckling and premature fracture in such built-up braces subjected to cyclic inelastic deformations. Furthermore, at least two stitches shall be used, with none located in the middle fourth of the brace length; bolted holes where plastic hinges are expected to form in the braces are undesirable given that the higher stresses that would be induced at the net section of such braces would lead to their premature fracture.

Built-up laced brace members of archaic construction fall beyond the scope of AISC 341. Typically, laced built-up compression members were built from angles and channels connected with bars and plates by rivets to form I-shapes and box shapes; single lacings, double lacings, battens, combined lacings and battens, and perforated cover plate configurations have all been used at times. Typical cross-sections and their original design are found in steel design textbooks published at the turn of the century (e.g., Ketchum 1920, Kunz 1915). Research on their ultimate cyclic behavior (Dietrich and Itani 1999; Itani et al. 1998; Lee and Bruneau 2004, 2008a, 2008b; Uang and Kleiser 1997) as well as observed damage following earthquakes (Tremblay et al. 1996) demonstrated the severe seismic vulnerability of laced built-up sections, largely due to their often large width-to-thickness ratios and diverse possible failure modes (which can include lacing buckling and individual component buckling, in addition to all the other issues presented in this chapter). Lee and Bruneau (2004) also proposed equations for their low-cycle fatigue life, based on limited data. The behavior of laced built-up shapes remains complex and some observed behaviors remain unexplained; for example, Lee and Bruneau (2004, 2008a) observed instances of out-of-plane buckling

behavior permanently changing into in-plane buckling after a few cycles of inelastic deformation.

9.3.3 Beam Design

The effect of load redistribution due to brace buckling and yielding should be considered for the design of beams in the braced bays. To ensure ductile frame response, the resultant forces on the beams in the braced bays can be calculated using capacity design principles. Both cases of peak and degraded postbuckling compression strengths must be considered to determine the critical demands on the beams throughout the cyclic response of the frame. This section illustrates how this is accomplished for some typical braced frame configurations; in all cases here, tension and compression forces in braces are both considered positive.

9.3.3.1 V- and Inverted V-Braced Frames Configurations

The impact of unequal compression and tension brace forces on the behavior of V- and inverted V-braced frames has long been recognized (e.g., Khatib et al. 1988). If improperly accounted for, the resulting unbalanced force can negatively impact behavior of the beams, and in-turn lead to undesirable plastic collapse mechanisms. Figure 9.29 illustrates this concept for a simple frame.

In the elastic range, each brace resists half of the lateral load applied. However, once the buckling strength of the compression brace is reached, any additional increase in the lateral load, V, is entirely resisted by the brace in tension. The difference in the vertical component of the forces results in an unbalanced vertical load, P_{un}, applied to the beam at the beam-to-brace intersection point:

$$P_{un-v} = (T - C)\sin\theta \tag{9.7}$$

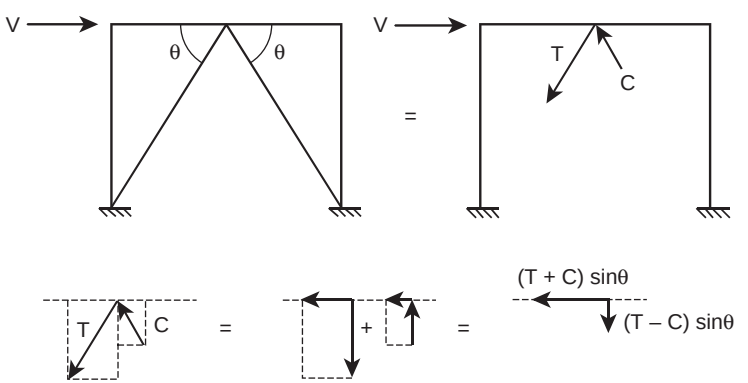

Figure 9.29 Forces acting on beam of inverted V-braced frame due to unbalanced resistance.

where the angle θ is defined in Figure 9.29. Likewise, the axial force in the beam is:

$$P_{un-h} = (T + C)\cos\theta \tag{9.8}$$

The magnitude of the unbalanced force changes as drifts increase and can be calculated taking into account the degraded strength of the brace as a function of drift (as done in Section 6.3.1 with a simplified brace hysteretic behavior).

For expediency, the horizontal unbalanced force used in design is given by Eq. (9.8) considering the tension brace expected yield strength together with the maximum expected buckling strength of the compression brace (i.e., neglecting any brace strength degradation that may have already taken place at the drift at which tension brace yielding occurs). During cyclic inelastic loading, this maximum horizontal force could be reached during the cycle when brace buckling first occurs (i.e., maximum compression strength) followed by tension yielding of the other brace. For given brace areas, the magnitude of this horizontal unbalanced force increases with decreasing brace slenderness, *KL/r*.

The largest vertical unbalanced force is reached when the tension brace has yielded and the compression braced has reached its lowest postbuckling strength. For cyclic loading, this would be the degraded compression strength described in Section 9.2.3. For given brace areas, the magnitude of this vertical unbalanced force increases with increasing brace slenderness, *KL/r*.

Note that although the braces reduce the span of the beam during elastic response, this benefit is lost during inelastic response, with the braces applying a downward pull to the beam. In fact, unless the beam is designed to consider the development of this unbalanced force, it may develop plastic hinging before yielding of the tension brace, with the undesirable resulting plastic collapse mechanism shown in Figure 9.30. Khatib et al. (1988) and others have shown that such beam flexibility and plastic mechanism can cause inelastic deformations

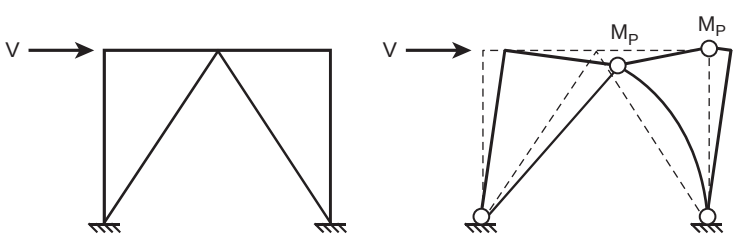

Figure 9.30 Undesirable plastic collapse mechanism of inverted V-braced frame having plastic hinge in beam.

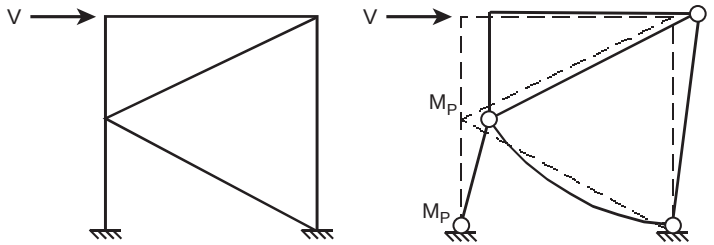

FIGURE 9.31 Plastic collapse mechanism of K-braced frame, with plastic hinge in column.

to concentrate in a single level of a multistory frame, with detrimental consequences.

The above concepts also explain why some braced frame configurations are undesirable in seismic regions. For example, in a K-type braced frame (Figure 9.31), the unequal buckling and tension yielding strengths of the braces would create an unbalanced horizontal load pulling at midheight of the columns, jeopardizing the ability of the structure to resist gravity loads.

The 1992 edition of the AISC Seismic Provisions indirectly attempted to account for the above behavior by requiring compression braces in V-, Inverted V-, and K-braced frames to be designed for a force 50% greater than otherwise calculated. More appropriately, the demands due to such unbalanced forces were first explicitly considered in the 1997 AISC Seismic Provisions, as a special case, for the design of V-type and inverted V-type braced frame—whereas use of K-braced frames became prohibited in SCBFs (but remained permitted in OCBFs of two stories or less, until AISC 341-05).

Consistently with the philosophy introduced in 1997, but affected by the changes outlined in Table 9.1, the AISC 341-10 requires that beams in SCBFs be designed to resist a maximum unbalanced vertical load calculated using the expected yield strength ($R_y F_y A_g$) of the braces in tension, and 30% of the brace buckling strength in compression, expressed as 0.3 times the lesser of $R_y F_y A_g$ and $1.14 F_{cre} A_g$, where F_{cre}, is F_{cr}, determined per AISC 360 Chapter E using expected yield stress $R_y F_y$ in lieu of F_y (note that 1.14 is equal to 1/0.877). As a safeguard in case of plastic hinging in the beam at the point where the braces meet, beams are required to be continuous between columns and capable of resisting their tributary gravity loads together with the above unbalanced vertical load, assuming that the braces provide no support.

Note that the demands on the beams due to the unbalanced load created by the unequal tension and compression strength scan be mitigated by alternating V- and inverted V-braced configurations from story to story to create an X-bracing patterns spanning two

stories at a time, as done in Figure 9.3a. Another strategy, known as the "zipper column" is described in Section 9.4.2.

9.3.3.2 X-Braced Frame Configurations

For any other brace configuration, the same capacity design principles described above are applicable. Arguably implicit in the intent of previous editions, AISC 341-10 for the first time explicitly specified that all parts of an SCBF should be analyzed accordingly, considering a first case in which the braces in compression have reached their expected maximum buckling strength, and another in which they reach their expected postbuckling strength—together with the other braces reaching their expected strength in tension.

For X-braced and split-X-braced configurations, corresponding free-body diagrams are shown in Figure 9.32. Using the first free-body diagram for a beam supported at midlength by the intersecting braces, for a symmetrically loaded frame (i.e., $P_1 = P_2 = P$), the axial load in the beam can be calculated as:

$$\sum F_x = 0 = 2P + (T_{i+1} + C_{i+1}) \cos \theta_{i+1} - (T_i + C_i) \cos \theta_i \qquad (9.9)$$

where the nominal member forces in stories i and $i + 1$ are considered. Similar equilibrium equations could be written for nonsymmetrically loaded frames (i.e., $P_1 \neq P_2$). In this case, half of the beam is in compression (P_1) and half in tension (P_2).

Recognizing that braces in adjacent stories may not reach their maximum strengths simultaneously, Redwood and Channagiri (1991)

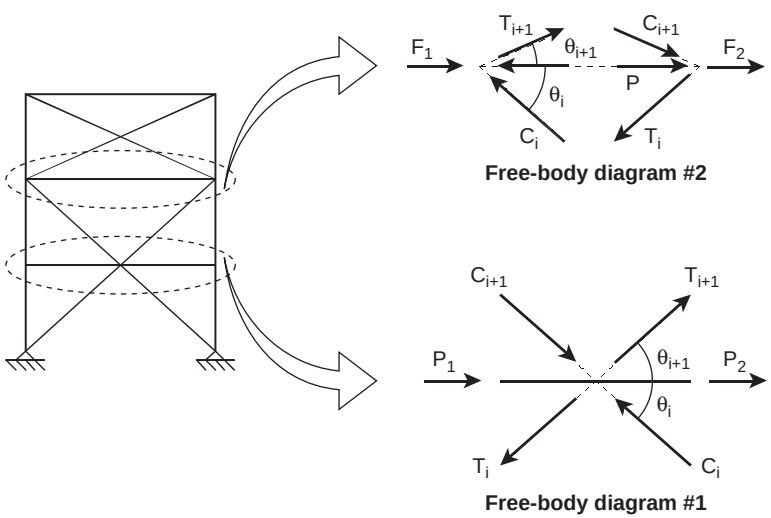

Figure 9.32 Free-body diagrams for calculating beam actions.

suggested that only 75% of the brace strengths in story $i + 1$ be considered for beam design:

$$P = 0.5\,(T_i + C_i)\cos\theta_i - 0.5\,(0.75)(T_{i+1} + C_{i+1})\cos\theta_{i+1} \tag{9.10}$$

Lacerte and Tremblay (2006) suggested that 50% of the brace strengths in story $i + 1$ should be used (instead of 75%) to adequately capture the variations observed in nonlinear inelastic analyses. Note that use of this 75% factor, although aligned with capacity design objectives, is not explicitly required by AISC 341-10.

In the second free-body diagram, the beam spans the full width of the braced bay, and brace buckling and yielding will produce an internal redistribution of forces. Even for the case of earthquake loads symmetrically applied to the frame, this beam acts as a load-transfer member. For a given ratio of F_1/F_2 dictated by the characteristics of the horizontal load path, the axial force in the beam, P, is obtained by solving the following two equations of equilibrium:

$$P = (T_{i+1})\cos\theta_{i+1} - (C_i)\cos\theta_i + F_1 \tag{9.11a}$$

$$P = (T_i)\cos\theta_i - (C_{i+1})\cos\theta_{i+1} - F_2 \tag{9.11b}$$

and consequently,

$$F_1 + F_2 = (T_i + C_i)\cos\theta_i - (T_{i+1} + C_{i+1})\cos\theta_{i+1} \tag{9.11c}$$

where the value of P should be taken as the maximum value calculated using either the expected buckling strength or expected post-buckling strength for the compression braces above and below the beam.

When these axial forces are combined with the moments acting on the beams due to gravity and other seismic actions, the adequacy of the beams can be checked with the standard beam-column design equations.

9.3.3.3 Transfer Beams for Irregular Layout

Although Section 9.3.3 has focused so far on the beams in the braced bays, similar capacity design principles must also be used in other situations to ensure adequate transfer of structural forces, particularly when irregular bracing layouts are encountered. For example, in addition to the forces obtained from elastic analysis, unbalanced horizontal forces due to unequal tension and compression strengths of the braces must be considered to design the transfer beams linking the two incomplete braced frames in Figure 9.33. The worst case demands shall be considered, as both elastic and inelastic behaviors develop at different stages of frame response, and continuity of the load path must be maintained throughout the entire response.

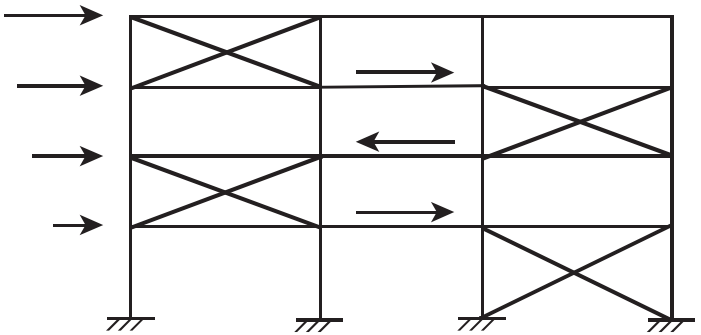

Figure 9.33 Forces in transfer beams between incompletely braced bays.

9.3.4 Column Design

The need to protect columns that resist gravity loads is obvious and recognized. Capacity design provides a reliable approach to calculate the maximum and minimum demands on columns when a complete sway mechanism develops. However, in medium and high rise structures, evidence from inelastic dynamic analyses indicates that brace yielding is not simultaneous at all the stories across the building height, and that using capacity design in those instances can be conservative (also leading to high foundation design forces).

Some of the approaches that have been proposed to estimate column forces are presented here, understanding that results from nonlinear inelastic analysis can be used to provide upper bounds to the values obtained by these methods.

9.3.4.1 Column Forces per Capacity Design

Capacity design remains a safe approach to calculate column forces for design. In spite of its conservatism for taller frames, it is appropriate for low-rise frames and the upper stories of medium- and high-rise buildings where all braces may develop their capacity simultaneously. In a study of inverted V-braced frames of up to 12 stories, Tremblay reported instances of braces simultaneously at their maximum buckling strength over the entire building height (Tremblay and Robert 2001); instances of braces yielding in tension simultaneously over four consecutive stories were commonly encountered in a later study on braced frames of split-X configuration (e.g., Figure 9.3a configuration) (Lacerte and Tremblay 2006).

Using a capacity design approach, the columns in the braced bay should be designed to remain elastic for gravity load actions acting with the forces delivered by the braces, assuming that the braces achieve their expected tensile strength together with their expected buckling or postbuckling strength (whichever gives the greater column forces, similarly to the approach described for beams).

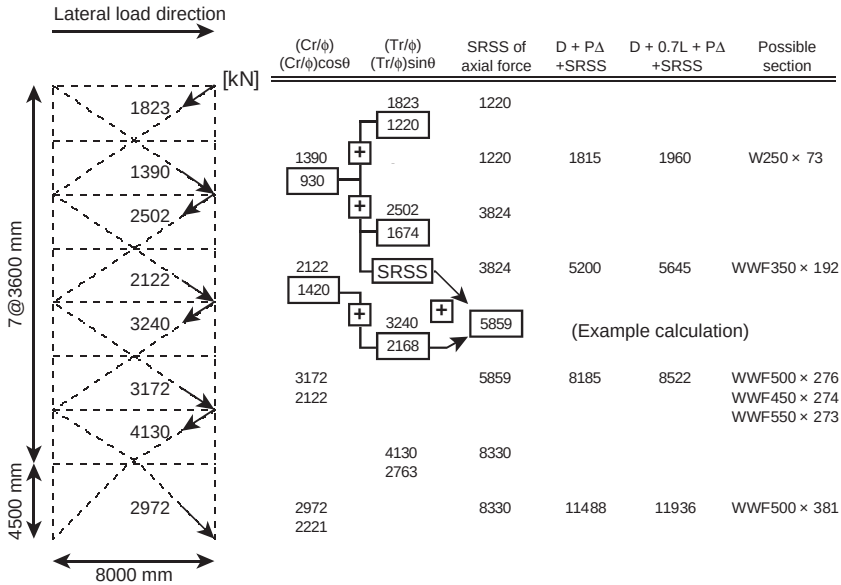

Figure 9.34 SRSS estimates of column forces in an eight-story CBF analyzed by Redwood and Channagiri (1991).

For example, for the frame in Figure 9.34 (as done in Section 6.2.2), maximum axial compression on columns would be obtained by summing the vertical components of the expected tension and compression brace strengths (e.g., that sum, not shown in Figure 9.34, would be 12,297 kN for the first-story column).

Note that in a V- or inverted V-braced frame, the shears at the ends of the beams, due to the unbalanced forces applied in their span, would also add to the demands on the columns.

9.3.4.2 Column Forces per AISC Amplified Load Combination Method

AISC 341-02 introduced an "amplified seismic load" concept to "account for overstrength of members of the Seismic Load Resisting System" to expedite design in specific instances identified by the Seismic Provisions. The approach was expedient, implementing a special load combination for which $\Omega_o E$ was used instead of the earthquake loads, E, in load combinations prescribed by the applicable building code, where Ω_o is a seismic overstrength factor (Chapter 7). Among many uses, this amplified seismic load approach was specified by AISC 341-02 and 341-05 to determine axial forces to consider for the design of columns; these axial forces were also to be considered while neglecting concurrently acting flexural forces resulting

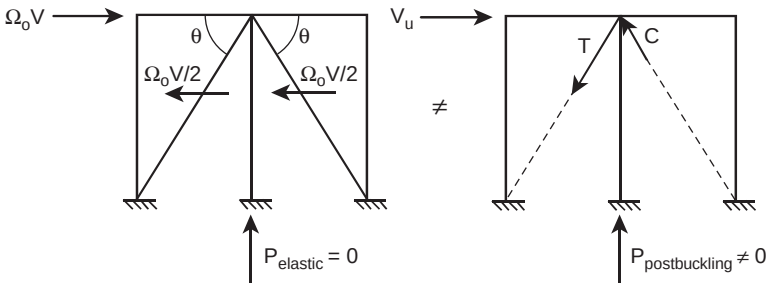

Figure 9.35 Comparison of design forces for a middle column from amplified elastic analysis results and from capacity design principles.

from story drifts. No references were provided to substantiate how this arbitrary procedure could approximate comparable column demands obtained from capacity design procedures or nonlinear time-history analyses.

The frame in Figure 9.35 provide one example of how the amplified seismic load method fails to predict correct appropriate column design forces: results from elastic analysis indicate that each brace resists half of the lateral load applied to the frame, and no force is applied to the middle column, whereas postbuckling analysis using capacity design principles correctly predicts that column to be subjected to compression forces due to the postbuckling behavior of the compression brace.

AISC 341-10 retained the amplified seismic load concept for a number of purposes, in which the effects of horizontal forces including overstrength are defined as E_{mh} (set as equal to $\Omega_o E$ in ASCE-7), but specified that E_{mh} be defined based on capacity design principles in a number of instances. For the design of SCBF columns, beams and connections, AISC 341-10 specifies the use of load combinations using the amplified seismic load in which E_{mh} shall be taken as the larger force determined from "(1) an analysis in which all braces are assumed to resist forces corresponding to their expected strength in compression or in tension, and (2) an analysis in which all braces in tension are assumed to resist forces corresponding to their expected strength and all braces in compression are assumed to resist their expected postbuckling strength"—effectively implementing capacity design principles.

As an upper bound, column forces obtained from that AISC 341-10 procedure need not exceed the values that would be obtained either from a nonlinear analysis, or from an elastic analysis using the amplified seismic loads applied on a model of the structure with all of its compression braces removed, that latter exception being only appropriate in those instances where the postbuckling columns

compression strength case gives the more critical column demands (e.g., as in Figure 9.35). Considering that $0.3P_n$ in compression corresponds to only 4% and 15% of AF_y when $KL/r = 200$ and 100, respectively, elastic analysis of a CBF frame omitting the compression braces from the model is expedient and could give conservative column forces in those cases (provided that these analysis results also give forces in the tension braces equal to their yield strengths). For cases where the maximum compression strength of the braces gives more critical column demands (e.g., in an inverted V-braced frame), omitting the compression braces from the analysis would erroneously ignore the forces applied by the compression braces on the columns.

For design expediency, AISC 341-10 also allows columns to be designed for these axial forces while neglecting concurrently acting flexural forces resulting from story drifts (unless these moments are due to loads applied to the columns between story levels). This is not rigorously correct, because variation of up to 0.025 rad in interstory drifts at adjacent levels, which develop as a consequence of the brace inelastic behavior and subjects the columns to significant flexure (MacRae et al. 2004, Richards 2009, Sabelli 2001). Tests by Newell and Uang (2008) demonstrated the ability of heavy W14 columns of standard story-height length and having width-to-thickness ratios in compliance with AISC 341, to achieve drift capacities of 0.07 to 0.09 rad while withstanding axial force demands of up to 75% of their nominal axial yield strength, corresponding to plastic rotation capacities of approximately 15 to 25 times the member yield rotation. This suggests that heavy SCBF columns may be forgiving to the simplification permitted by AISC; future research may help determine the range over which these findings can be generalized.

9.3.4.3 Column Forces per Obsolete SRSS Method

Redwood and Channagiri (1991) proposed a square-root-sum-of-the-squares (SRSS) method to reduce demands on columns accounting for the fact that yielding does not develop at all stories simultaneously. The method sums the expected tension and compression brace forces of the first two braces above the column at the story under consideration, with an SRSS combination of the forces coming from the other braces at the stories above. The approach is illustrated for an eight-story CBF in Figure 9.34. For example, at the fourth floor, the use of the SRSS procedure results in a design axial force of 5859 kN, rather than the design axial force of 7412 kN that is obtained through capacity design procedures.

However, for a number of reasons, the method has been found to be unconservative when verified against the results from nonlinear time history analyses using some of the substantially stronger ground motion time history records that have become customarily used since 1991 (Lacerte and Tremblay 2006). Therefore, the SRSS method is presented here for completeness of historical perspective, but is not

recommended for use anymore. A hybrid approach, considering the sum of forces from capacity design over a set number of stories, together with a SRSS combination of the forces from the other stories above, has not been proposed at this time.

9.3.4.4 Lateral Forces and Inelastic Rotation at Brace Point Between Floor Levels

Small accidental eccentricities in the loads applied to a beam by braces can distort it in a manner similar to what is shown in Figure 9.36. Similar torsional behavior was also experimentally observed by Schachter and Reinhorn (2007). To prevent beam instability at the braces connection point, beams in SCBFs and OCBFs must be laterally braced at their point of intersection with the braces, or alternatively be demonstrated to have sufficient out-of-plane strength and stiffness to ensure their stability. AISC 360 (Appendix A) specifies the required strength and stiffness of lateral braces.

9.3.5 Connection Design

Bolted or welded gussets are frequently used to connect braces to beams and columns in braced frames. Braces of large cross-section are sometimes directly welded to the beams and columns. Capacity design principles dictate the design of all other connections in the braced frame, considering the worst combined demands of braces tension and compression strengths, as described earlier.

Figure 9.36 Inelastic rotation at brace connection point in absence of lateral bracing.

All connections in a concentrically braced frame should be designed to be stronger than the members they connect, allowing the bracing members to yield and buckle per the intended plastic mechanism. Consequently, to accommodate the inelastic cyclic response that typically develops during a severe earthquake, connections must be designed to resist the expected tensile strength of the braces ($= R_y A F_y$), and, as a separate condition, resist the maximum compression strength of the brace acting together with the moment that develops at the flexural plastic hinge.

Note that when gussets are used, flexural hinging at the connection may develop in the gusset itself, or alternatively in the brace itself, in which case the gusset must be able to elastically resist the expected plastic moment of the brace magnified to account for some strain hardening (i.e., typically $1.1 R_y M_p$ of the brace) acting simultaneously with a force equal to the maximum compressive brace strength. Net section fracture of the brace (e.g., Figures 9.37a to c), gusset buckling (e.g., Figure 9.37e), and weld failures (e.g., Figure 9.37d) are examples of undesirable failure modes; plates welded to increase brace thickness at a brace net section, and gusset stiffeners (Figure 9.38), are possible strategies to prevent such failures. Similar capacity design procedures are then used to size the design the welded or bolted parts of the connection details.

Typically, when braces buckle in the plane of their gusset, the gusset is designed to be stronger than the hinging brace. However, when braces buckle outside the plane of the gusset, plastic hinging of the gusset is preferred, because the gusset thickness required to develop hinging in the brace in that case would be substantial, and because the out-of-plane buckling behavior of braces having thicker gusset is not necessarily more ductile (Roeder et al. 2009); hinges in rectangular HSS braces have a lower low-cycle fatigue life than hinges in solid gusset plates.

To allow a plastic hinge to form in a gusset plate without excessive local straining of that plate, the commentary to AISC 341 recommends that the brace terminates at a point on the gusset such that it provides a free length between the end of the brace and the assumed line of restraint on the gusset perpendicular to the brace. Per the recommendations of Astaneh et al. (1982, 1986), the minimum recommended free length is equal to two times the gusset plate thickness (Figure 9.39), but kept short enough to preclude gusset buckling. Typical gussets sized in compliance with this recommendation are shown in Figure 9.40.

To reduce the sometimes large gusset plates that result from application of that recommendation, which can also induce local yield deformations in the beam and column, Lehman et al. (2008) proposed an alternative gusset yield pattern following an elliptical yield line path. Experimental and analytical work demonstrated that

(a)

(b)

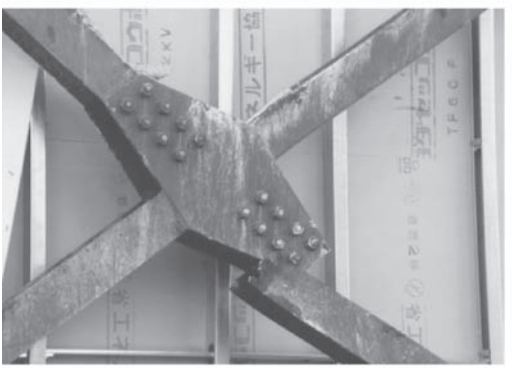

(c)

(d)

(e)

Figure 9.37 Undesirable failure modes in concentrically braces frames: (a) net section fracture of flat-bar brace; (b) global view of same building; (c) net section fracture of W-shape brace; (d) beam weld fracture; (e) gusset buckling and fracture.

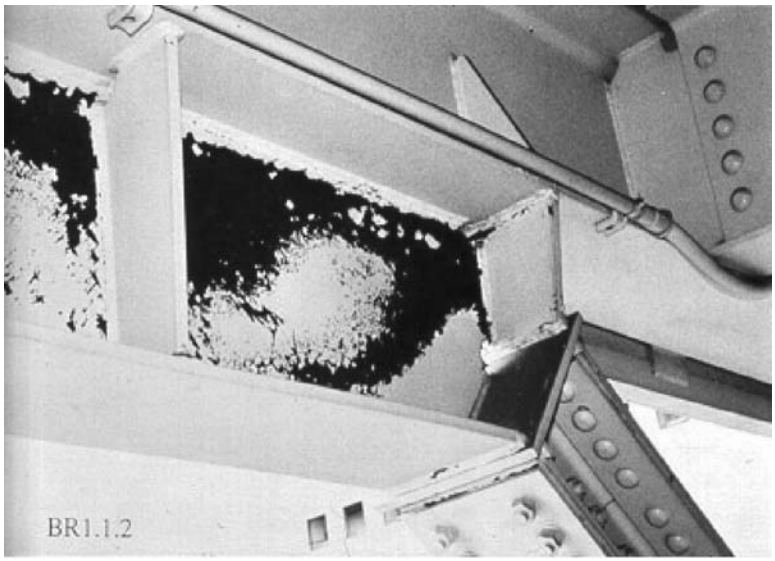

Figure 9.38 Stiffened gusset showing evidence of ductile yielding. (*Courtesy of M. Nakashima, Disaster Prevention Research Institute, University of Kyoto, Japan.*)

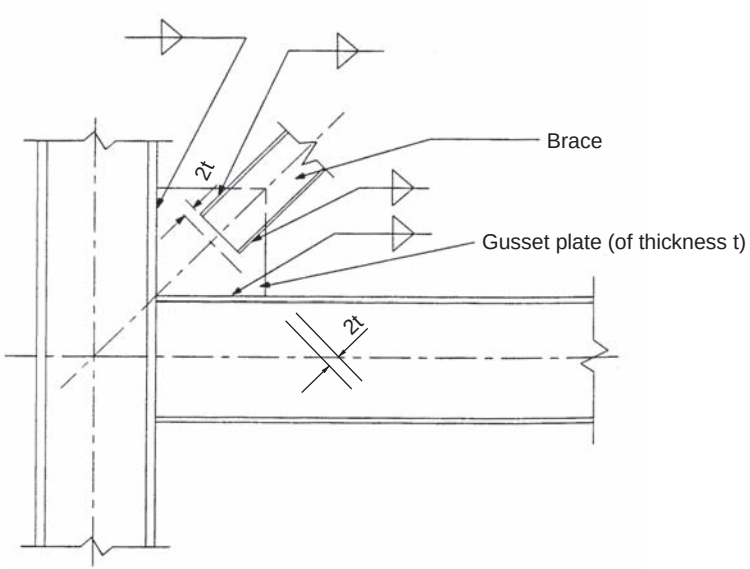

Figure 9.39 Brace-to-gusset plate requirements for out-of-plane buckling of braces (*AISC 1995*).

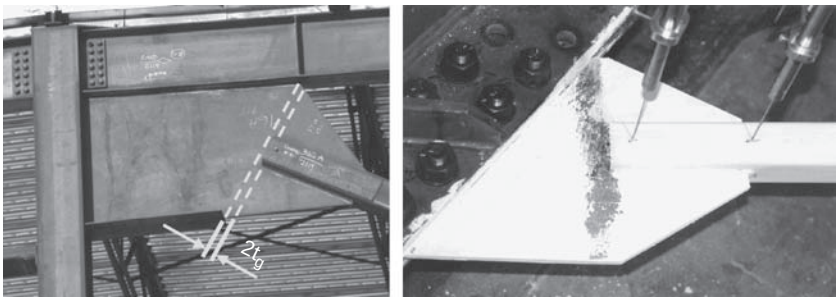

Figure 9.40 Gussets with recommended free length: (a) implementation in a steel structure; (b) evidence of plastic hinging (revealed by flaked plate) during testing. (*Courtesy of Robert Tremblay, Département des génies civil, géologique et des mines, EcolePolytechnique, Montréal.*)

optimal performance was achieved with a clearance width of six to eight times the gusset thickness (Figure 9.41).

Kiland and Sabelli (2006) presented a gusset detail for which a concentric stiffener that strengthens a corner gusset against out-of-plane buckling is extended and connected to the brace. The stiffener plate is provided with a free length that permits its plastic hinging, and oriented to facilitate in-plane buckling of the brace. Experimental results (Lehman et al. 2010, Tremblay et al. 2008) demonstrated satisfactory gusset inelastic behavior (Figure 9.42). By analogy with the gusset detail shown in Figure 9.40, a minimum free length equal to twice the thickness of the knife-edge is recommended.

Beyond the above requirements, gussets are designed per the requirements of AISC 360. However, note that when excessive gussets sizes are obtained (Figure 9.43—although the design assumptions and circumstances that led to those strange and unusually large gussets are unknown), the designer should consider braces directly welded to the frame (i.e., without gussets) or steel plate shear walls (Chapter 12) as more cost-effective options.

Finally, note that proprietary braces and connections have also been developed as options to conventional brace connection details. Manufacturers of these systems should be consulted to obtain information on their cyclic inelastic performance and failure modes, as well as forces to consider for capacity design purposes.

9.3.6 Other Issues

Capacity design principles are applicable for the design of all components within the braced frame, but also to which the frame connects, particularly when the failure mode of these components is not ductile. Failure of base connections (Figure 9.44) or of structural elements where truss members connect (Figure 9.45) will negate all efforts invested to ensure ductile behavior of the structural system.

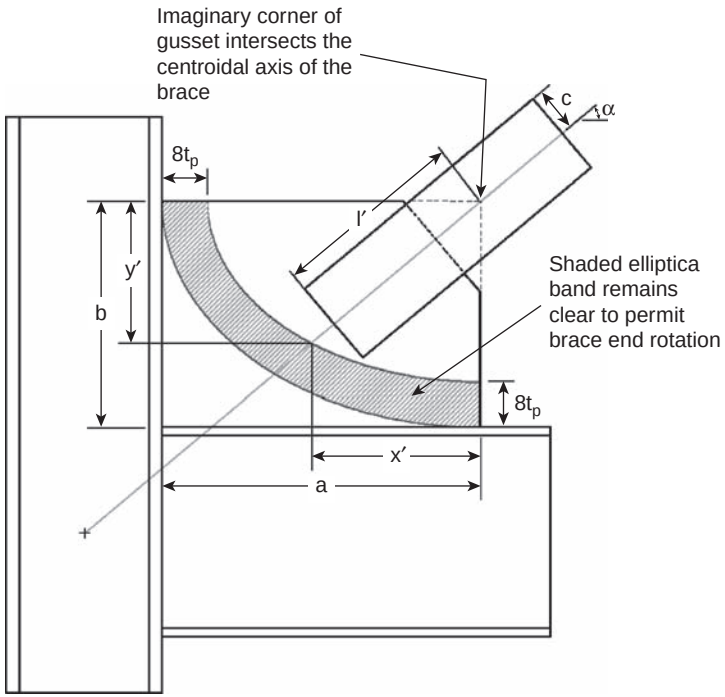

(a)

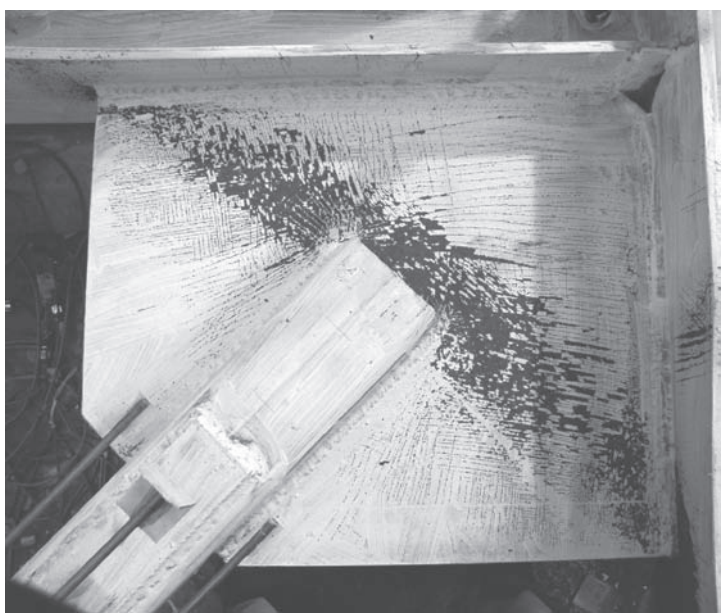

(b)

Figure 9.41 Alternative elliptical yield line concept for gusset design: (a) concept; (b) yielding pattern on correspondingly designed gusset. (*Courtesy of Charles Roeder, Department of Civil and Environmental Engineering, University of Washington.*)

Figure 9.42 Ductile gusset for in plane hinging. (*Courtesy of Charles Roeder, Department of Civil and Environmental Engineering, University of Washington.*)

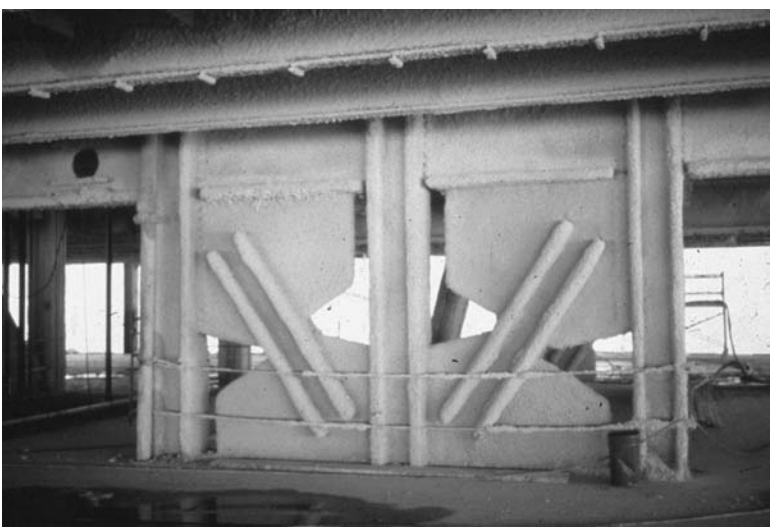

Figure 9.43 Disproportionate gusset plate sizes. (*Courtesy of J. Keith Ritchie, Canada.*)

Particular attention must be paid to column splice details. AISC only permits complete penetration groove welds in welded column splices because partial penetration groove welds perform poorly under cyclic loading (Bruneau and Mahin 1990). AISC 341 also requires that column splices be designed to develop at least 50% of the lesser

Figure 9.44 Example of failed column base connection.

Figure 9.45 Failed brace anchorage.

available flexural strength of the connected members, and a shear strength equal to $\Sigma M_{pc}/H_c$ where ΣM_{pc} is the sum of the nominal plastic flexural strengths, $F_{yc}Z_c$, of the columns above and below the splice, and H_c is the clear height of the column between beam connections. This is consistent with observations that columns can be subjected to large moments due to differences in interstory drifts during brace buckling and yielding (see Section 9.3.4).

9.4 Other Concentric Braced-Frame Systems

Although CBFs are one of the oldest structural systems, as described in Section 9.1, many innovative concepts have been proposed to enhance energy dissipation and seismic performance, building on the general principles and knowledge presented earlier. A few of these are briefly summarized in this section.

9.4.1 Special Truss Moment Frames (STMF)

Goel and Itani (1994) proposed a Special Truss Moment Frame (STMF) concept to resist earthquakes by dissipating seismic energy in specially detailed ductile truss elements. It is intended as a solution based on capacity design principles for long-span moment frames where trusses must be used instead of regular W-shape beams. STMFs have a well-defined middle special segment detailed to exhibit stable hysteretic behavior while undergoing large inelastic deformations, whereas the parts of the truss outside of that special segment are designed to remain elastic (Figure 9.46). In the X-diagonal configuration of the special segment, the braces are detailed to dissipate energy by elongation in tension (following principles similar to CBFs) in addition to plastic hinging of the top and bottom chords of the truss. In a Vierendeel configuration of the special ductile segment, the braces are removed over the segment, and the top and bottom chords of the truss provide the energy dissipation by developing plastic hinges. AISC 341 specifies minimum requirements for their design, whereas detailed design guidance and examples are presented by Goel et al. (1998), and Chao and Goel (2008a, 2008b).

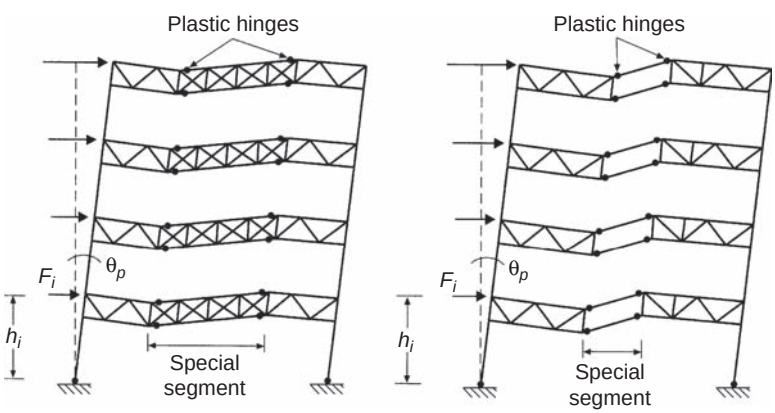

Figure 9.46 Yield mechanism in STMF. (*Courtesy of S. Goel, Department of Civil and Environmental Engineering, University of Michigan.*)

9.4.2 Zipper Frames

Khatib et al. (1988) proposed the zipper-frame concept as a way to better distribute energy dissipation across the height of CBFs and prevent concentration of energy dissipation in a single story. The concept consists of using a vertical member spanning the height of the frame, except for the first story, and linking the beams at their brace connection points. The original design intent was to spread the unbalanced vertical forces created by unequal tension and compression strengths of the braces to all of the beams, thus mitigating the loss of story strength that would otherwise develop when compression strength degradation of the braces occurs in a particular story. In the case of flexible beams developing significant vertical deformations or weak beams developing plastic hinges under the unbalanced loads, tying all the brace-to-beam intersection points together also forces the compression braces over the entire frame height to buckle simultaneously, and thereby better distribute the energy dissipation over the height of the building. Whittaker et al. (1990) reported that simultaneous brace buckling over the height of a building produces a single-degree-of-freedom mechanism, resulting in a more uniform distribution of damage over the height of the building. Nonlinear time-history analysis by Khatib et al. (1988) demonstrated this for zipper frames, with more uniform distribution of inelastic response over frame height than for other brace configurations.

Analyses by Tremblay and Tirca (2003) indicated dynamic instability of zipper frames when subjected to severe near-field and subduction earthquake ground motions, but more importantly reported that zipper struts along the frame height transferred the unbalanced vertical forces up or down in a complex manner. This makes their design per capacity design principles problematic. To provide a more systematic load path, Leon et al. (2003) proposed a "suspended zipper frame" in which the top level braces are designed to behave as an elastic "hat truss" to prevent overall collapse. Information on design recommendations and experimental validations of the concept (Figure 9.47) are presented by Yang et al. (2008a, 2008b) and Schachter and Reinhorn (2007). Note that AISC 341 provides no specific design requirements for zipper frame systems, but refers to the system in its commentary.

9.5 Design Example

The following section illustrates the design of a Special Concentrically Braced Frame (SCBF). The design applies the requirements of ASCE 7 (2010) and AISC 341 (2010). The example is not intended to be a complete illustration of the application of all design requirements. Rather, it is intended to illustrate key analysis and proportioning techniques that are intended ensure ductile response of the structure.

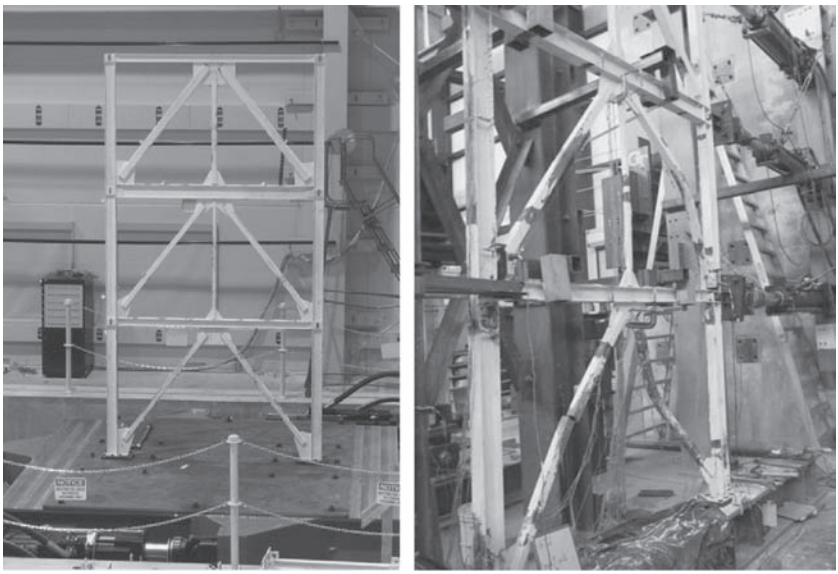

(a) (b)

Figure 9.47 Zipper frame tests: (a) shake table test specimen (*Courtesy of Andrei Reinhorn, Department of Civil, Structural, and Environmental Engineering, University at Buffalo.*); (b) static test specimen. (*Courtesy of C.S. Yang, and R.T. Leon, Department of Civil and Environmental Engineering Georgia Tech.*)

9.5.1 Building Description and Loading

The example building is identical to the one used in Chapter 8 (Special Moment Frames); more detailed seismicity and building information is included in that example. The difference in this case is that Special Concentrically Braced Frames are used. The system seismic design parameters are shown in Table 9.2.

The typical plan is shown in Figure 9.48 and the typical frame elevation is shown in Figure 9.49.

Based on the seismic-design data, a generic seismic response spectrum is constructed in accordance with ASCE 7. Because there is only

R	6
I	1.0
C_d	5
Ω_o	2

Table 9.2 Seismic Design Data

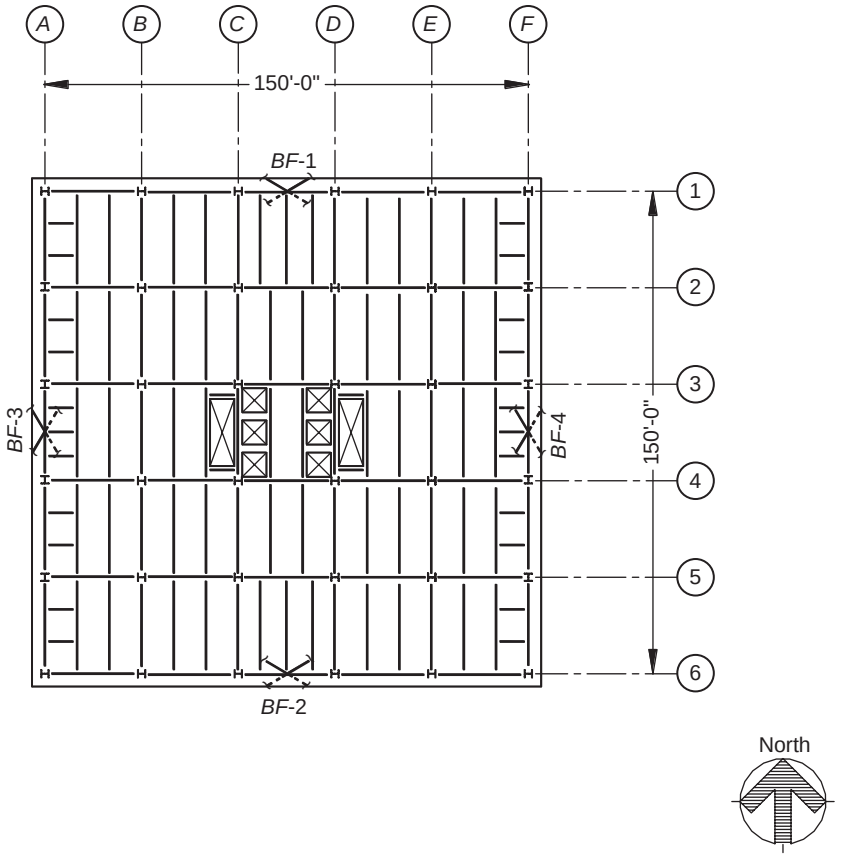

Figure 9.48 Typical floor plan.

one braced bay on each side of the structure, the design shear at every story must be multiplied by a redundancy factor ρ equal to 1.3.

9.5.2 Global Requirements

The structure must be designed to provide both adequate strength and adequate stiffness. Typically strength requirements will govern the design of lower buildings, whereas taller buildings will be controlled by drift. The threshold height is dependent on many factors, including the shape of the response spectrum, the analytical procedure used, and the braced bay configurations and proportions.

Where strength considerations govern, the design process is fairly straightforward: the braced-frame members (beams, columns, and braces) are designed to provide adequate strength, then the columns and beams in the bay are redesigned to preclude their failure when

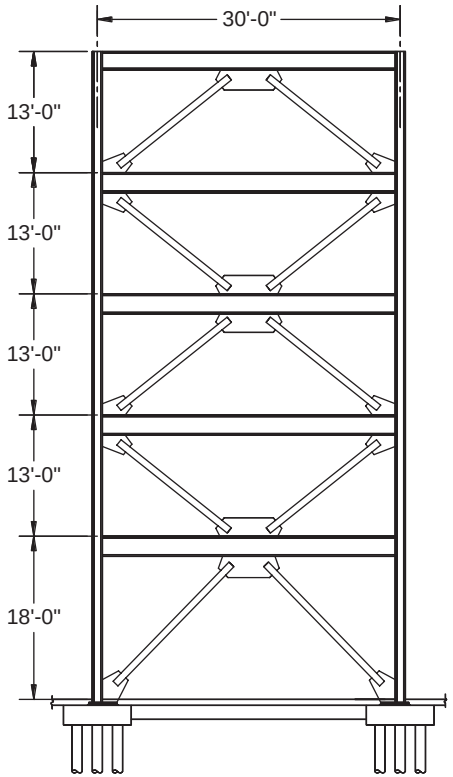

Figure 9.49 Typical frame elevation.

subjected to the forces corresponding to fully yielded and strain-hardened braces. A reanalysis may be performed to confirm that the required brace strength has not been increased because of an increase in frame stiffness (due to change of period on the response spectra when member forces are obtained from dynamic analysis).

Where drift is the governing concern, the process requires more iterations. Any increase in brace strength will in turn impose larger forces on beams and columns when the braces yield. Thus, any stiffening of the frame should be done with the required strength proportioning of the different components (brace, beam, and column) in mind.

9.5.3 Basis of Design

The design of SCBFs is based on the expectation of a global yield mechanism in which braces yield in tension and buckle in compression and plastic hinges form at the column bases. Where frame beams are connected rigidly to columns, hinging in the beam or column is

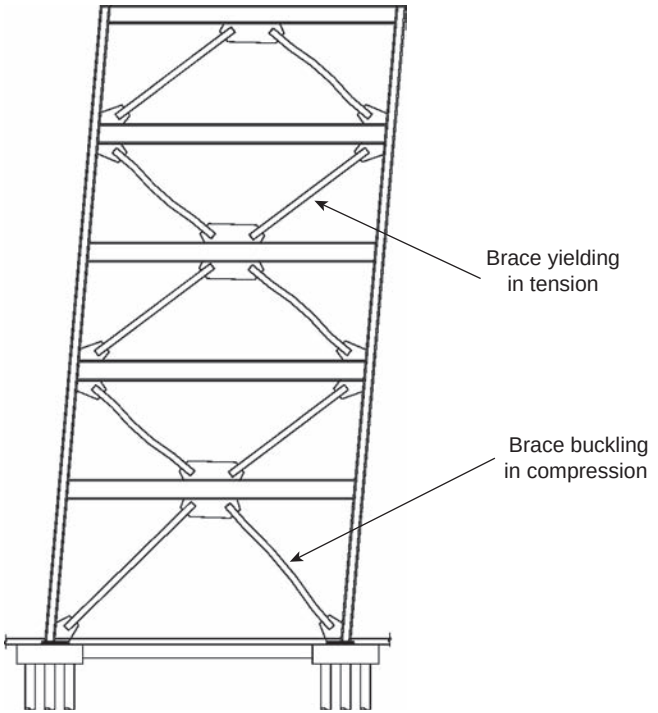

Figure 9.50 Anticipated mechanism.

also anticipated. Otherwise, large relative rotations must be accommodated in the beam-to-column connections. Figure 9.50 shows this mechanism.

Because brace buckling entails loss of strength and stiffness, SCBFs are subject to dramatic force redistributions. To determine maximum design forces, the anticipated mechanism is considered twice: once with maximum brace buckling forces, and again with braces having a reduced, postbuckling strength.

For purposes of these plastic mechanism analyses, the following brace strengths are used:
For the brace in tension:

$$T = R_y F_y A_g \tag{9.12}$$

where A_g is the gross area of the brace.

For the brace in compression (at its maximum force):

$$C_{max} = 1.14 F_{cr} A_g \tag{9.13a}$$

where F_{cr} is the critical buckling stress utilizing a yield strength of $R_y F_y$.

The value of 1.14 corrects for the factor of 0.877 used in AISC 360 equations for flexural buckling strength to account for out-of-straightness effects.

For the brace in compression (at its postbuckled, residual strength):

$$C_{min} = 0.3F_{cr}A_g \tag{9.13b}$$

An elastic analysis is used for preliminary design. Subsequently, two plastic mechanism analyses are performed, with brace forces as described above, to determine maximum forces that beams and columns within the frame must resist. The sizes of these elements are increased based on these forces. The adequacy of the revised design is reconfirmed with another elastic analysis. It is possible that more than one iteration is required to establish a design that satisfies both sets of requirements: those checked in the elastic analysis (member strength adequacy for the design base shear; drift control), and those checked in the plastic mechanism analyses (beam and column strength at the limit state).

The elastic analysis procedure used in this example is a linear Modal Response Spectrum (MRS) analysis. This is typically advantageous due to the reduction in design forces. ASCE 7 permits for this method and the reduction in overturning moment that typically results from this approach compared with the vertical force distribution prescribed by the Equivalent Lateral Force procedure of ASCE 7.

9.5.4 Preliminary Brace Sizing

Based on the results of the elastic analysis, brace sizes are obtained. Table 9.3 shows these sizes, along with their expected strengths in tension and compression as described above.

9.5.5 Plastic Mechanism Analysis

Two plastic mechanism analyses are performed on the frame. These are intended to capture both axial forces corresponding to brace inelastic action and flexural forces at the beams intersected by braces along their length. Although it is anticipated that these brace forces correspond to large drifts, and that columns may develop significant flexural forces at these drifts (due to fixity at beams or varying story drifts), these analyses are not intended to determine such flexural forces. Indeed, it is permitted to neglect them, under the assumption that limited flexural yielding in the column may be tolerated as long as overall buckling is precluded.

For purposes of member design it is sufficient to model the frame with the brace forces corresponding to each mechanism and with zero lateral drift.

Mechanism 1 combines the expected brace tension strength [Eq. (9.12)] with the maximum compression force [Eq. (9.13a)]. Braces are considered to be in compression or tension based on the

Level	Brace Size	Expected Tension Strength $R_yF_yA_g$ (kips)	Expected Compression Strength $1.14F_{cr}A_g$ (kips)	Residual Compression Strength $0.3F_{cr}A_g$ (kips)
Fifth Floor	HSS 6.625 × .312	267.50	142.09	36.43
Fourth Floor	HSS 7 × .500	441.21	246.81	62.98
Third Floor	HSS 8.625 × .500	549.78	396.16	98.79
Second Floor	HSS 9.625 × .500	619.08	489.97	121.15
First Floor	HSS 10 × .625	794.64	561.36	140.24

TABLE 9.3 Brace Sizes and Expected Strength

first mode displacement. That is, all of those sloping in one direction are considered to be in tension, and those sloping the opposite direction in compression. This assumption can be reversed for the analysis of asymmetric conditions. Note that these forces were derived considering simultaneous yielding of braces in adjacent stories; see Section 9.3.3.2 for a discussion of adjustments to this assumption that have been proposed.

Mechanism 2 combines the expected brace tension strength [Eq. (9.12)] with the residual compression force [Eq. (9.13b)]. The same assumptions regarding compression and tension are used.

Figure 9.51 shows the frame elevation used for both mechanism analyses. Note that the forces acting at each level to produce equilibrium with this plastic mechanism are different than those calculated from elastic analysis; in many cases, they will be much lower than the collector design forces calculated, taking into account the localized effects of higher modes. Modeling of these reactions with springs on both sides of the frame can be used to reflect the anticipated distribution of collector forces.

9.5.6 Capacity Design of Beam

As seen in Figure 9.51, the forces in the plastic mechanisms can impose both flexural and axial forces in each of the beams. The forces can be substantial, especially in the postbuckled mechanism in which the beam provides the majority of the resistance counterbalancing the forces corresponding to the capacity of the braces in tension.

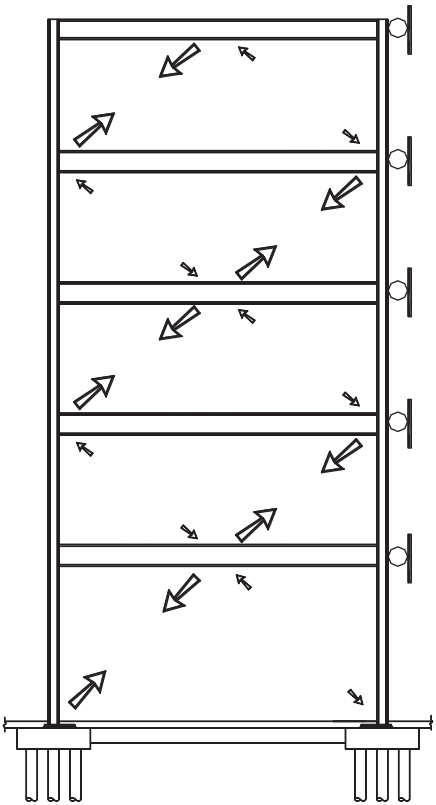

Figure 9.51 Mechanism analysis models.

The seismic axial force in the beam at the second floor is calculated based on the difference in the capacity above and below as follows:

$$F_{i+1} = V_i - V_{i+1} \tag{9.14}$$

$$V_i = (R_y F_y A_{g(i)} + 0.3 F_{cr} A_{g(i)}) \cos(\theta_i) \tag{9.15}$$

$$V_2 = 565.25 \text{ kips}$$

$$V_1 = 603.27 \text{ kips}$$

$$F_2 = 38.02 \text{ kips}$$

where F_{i+1} is the total force entering into the frame (corresponding to the plastic mechanism) at level i+1 and V_i is the shear strength (corresponding to the plastic mechanism) at level i.

For simplicity the force is assumed to enter into the frame as two equal forces, one at each column. The axial force in the beam can thus

be determined from static equilibrium, with the postbuckling strength case giving the larger axial (and flexural) forces in this case:

$$P_u = \frac{1}{2}(R_y F_y A_{g(1)} + 0.3F_{cr}A_{g(1)})\cos(\theta_1) - (R_y F_y A_{g(2)} + 0.3F_{cr}A_{g(2)})\cos(\theta_2) \tag{9.16}$$

$$P_u = 19.01 \text{ kips}$$

Beam flexural forces are similarly calculated based on the high tension strength and low postbuckled strength of the braces. The vertical force acting downwards on the second-floor beam is:

$$R_u = (R_y F_y A_{g(1)} - 0.3F_{cr}A_{g(1)})\sin(\theta_1) - (R_y F_y A_{g(2)} - 0.3F_{cr}A_{g(2)})\sin(\theta_2) \tag{9.17}$$

$$R_u = 175.97 \text{ kips}$$

These forces are combined with gravity shears and moments in the design of the beam. Assuming a fixed-end beam (and adequate fixity in the column and adjacent beam):

$$M_u = \frac{175.97 \text{ kips} \times 30 \text{ ft}}{8} + 0.7 \text{ kips/ft} \times \frac{(30 \text{ ft})^2}{12} = 712 \text{ kip-ft}$$

A W24 × 76 is sufficient for the combined axial and flexural forces. Note that this large size is due to the change in beam slope from the first to the second level and the change in brace size. Note also that the slab braces the section against lateral-torsional buckling. It also braces against lateral buckling, but not against torsional buckling, which will govern the axial strength.

9.5.7 Capacity Design of Column

A similar approach can be taken with the column, determining maximum forces acting on it from brace expected strengths. Thus, for the column in compression, the seismic axial force for mechanism 1 for this configuration can be calculated as:

$$P_{E_i} = \sum_{i+1}^{n}(1.14F_{cr}A_{g_x})\sin\theta_x + \sum_{i}^{n}\frac{1}{2}(R_y F_y A_{g_x} - 1.14F_{cr}A_{g_x})\sin\theta_x \tag{9.18}$$

The subtractive part of the second term, which represents the beam shear reaction due to the slightly unbalanced vertical force, is minor and is often neglected in the two-story X configuration. Note that the braces do not impart their loads to the column at the same level in all configurations. Care should be taken to ensure that the loads are determined consistently with the configuration used. Free-body diagrams, such as shown in Figure 9.52, are helpful; these should include the beam (and the shear imposed on it by the braces).

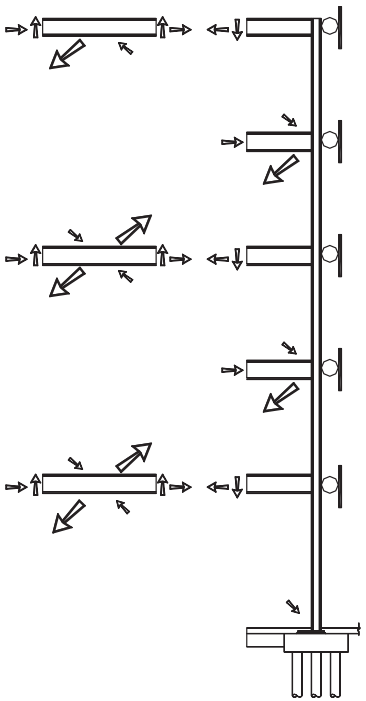

Figure 9.52 Free-body diagrams illustrating forces acting on column.

Note that in this configuration, the brace in compression at the first floor does not contribute to the column compression, as it connects at the base. Also, note that in mechanism 2 column axial forces will be significantly less than those from mechanism 1 for this bracing configuration.

Equation (9.18) can be conservatively simplified to:

$$P_{E_i} = \sum_i^n \frac{1}{2}(R_y F_y A_{g_x} + 1.14 F_{cr} A_{g_x}) \sin(\theta_x) \tag{9.19}$$

Thus the seismic axial force in the first-floor column can be calculated as:

$$P_E = 1553.22 \text{ kips}$$

If braces of moderate slenderness are used $(KL/r \leq \sqrt[4]{E/F_y})$ the column design can be simplified. The seismic component of the axial force need not exceed:

$$P_E \; \Omega_o E \tag{9.20}$$

where E is determined from an elastic analysis.

This seismic force is combined with gravity forces for a total load of 1850 kips. The column is designed for an effective length of $KL = 1 \times 18$ ft = 18 ft. A W14 × 176 section may be used.

Although it is in violation of values obtained from free-body diagrams, when designing in compliance to AISC-341-10, for reasons described earlier in this chapter, column flexural forces due to drift are not combined with these mechanism-based axial forces for design of the column. This would not necessarily be the case for design accomplished per other codes or standards.

9.5.8 Iterative Analysis and Proportioning

The capacity design of columns and beams inevitably leads to stiffening of the structure, altering its dynamic properties and possibly increasing the required design base shear. At least one more iteration of analysis is required to ensure compliance with the required base-shear strength. If brace sizes are increased, the beams and columns must be reassessed and another iteration becomes necessary. Otherwise, the capacity design of the beam and columns ensures that they are adequate to resist forces generated by brace yielding.

9.5.9 Connection Design

As discussed earlier, the design of an SCBF anticipates brace behavior that includes

- Tensile yielding
- The development of high compression forces
- Buckling

The first two behaviors are straight forward force requirements. Brace connections are designed for these maximum forces (which are presented in Table 9.3). Design for the higher tension governs most of the connection limit states. The limit states of web crippling (e.g., of a beam web adjacent to a connection gusset plate) and of gusset-plate buckling need only be evaluated for the expected compression strength of the brace, typically somewhat lower than the expected tension strength.

The third behavior requires a connection configured to maintain its integrity even as the brace buckles and undergoes inelastic rotation, typically out-of-the plane of the frame. No calculations are involved in evaluating this requirement. The designer simply selects a brace connection type that has demonstrated this capacity. See Figures 9.39, 9.40, and 9.41 for examples.

9.5.10 Completion of Design

Several items remain to complete the design. These include

- Brace connections
- Column splices
- Base plates
- Foundations
- Diaphragms, chords, and collectors

Although each one of these items is necessary and important, the execution is similar to that of many other components of a building design.

9.5.11 Additional Consideration: Gravity Bias in Seismic Systems

Earthquakes generally impose cyclic accelerations on structures. As these accelerations are not sustained in any single direction, moderate ductility demands in these structures do not generally result in uncontrolled displacements; buildings subject to large inelastic demands undergo inelastic drift in opposite directions at different times during the earthquake, and may be left with a residual drift after the earthquake. Typically, these residual drifts tend to be significantly lower than maximum drifts, but can be substantial at times, particularly for earthquakes excitations having large energy pulses (as observed in some accelerograms recorded near fault ruptures).

As demonstrated throughout this book, because seismic accelerations may act on a seismic system in either direction, seismic systems are conceived, tested, and designed with the expectation of cyclic demands. In real conditions, members of the seismic load-resisting systems tend to have some gravity forces present before any seismic loads are applied. However, such gravity forces tend to have a negligible effect on the yield strength of the system; they act similarly to residual stresses, causing slightly earlier yielding and rounding the transition from elastic to inelastic behavior. If the gravity forces are shared between yielding members ("fuses") and nonyielding members, the gravity forces are shed from the fuses as they yield and are transferred to the other members.

For all seismic systems, it is anticipated that nonfuse members will be designed to support the entire gravity force without reliance on the yielding fuse. For example, a moment-frame beam acting as a transfer girder should be designed to support the gravity forces as a simple-span member. Under cyclic yielding the initial fixed-end moments will "shake down" (see Section 4.5). The fuse (the plastic hinge zone of the beam) will ultimately resist only seismic moments,

whereas the nonfuse portion (the rest of the beam span) will resist the entire gravity moment.

Another example of this is the V-braced (or inverted V-braced) frame, discussed in Section 9.3.3.1, in which the beam is designed for the full gravity load (in conjunction with forces imposed by the braces), regardless of the fact that an elastic analysis of the structure shows little of the force resisted in beam flexure. If the gravity forces are accounted for in the design of braces under compression in an SCBF, buckling will occur at the same lateral drift as for a similar system without gravity forces in the braces. The larger braces constitute a source of overstrength for the fully yielded structure. The degree of overstrength is a function of the ratio of gravity force to seismic force in the member.

Special consideration is required when gravity forces cannot be shed and the members of the seismic load resisting system must continue to resist them during (and after) an earthquake. Under such conditions much less structural ductility can be tolerated and both inelastic drift and inelastic member deformation may accumulate much more than in a conventional system.

Consider the structure shown in Figure 9.53. The gravity loads are resisted by a cantilever system whose back span is the braced frame at the top level. This cantilever imposes a lateral force couple on the structure, pulling to the left at the top and pushing to the right at the next level down. The brace at that level is under compression due to the gravity load. At some level of lateral force to the left, the brace will reach its elastic limit and inelastic deformation will occur. Lateral forces to the right, however, must be far greater to cause inelastic deformation; they must first overcome the gravity force and then reach the strength of the brace. Thus, there is effectively a high overstrength in one direction.

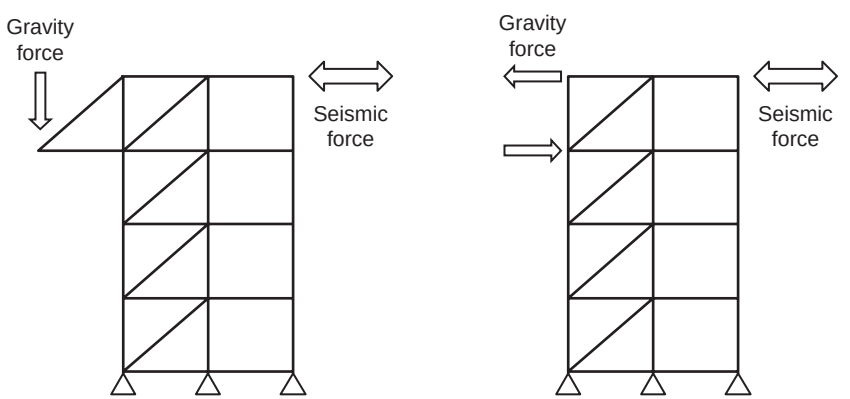

Figure 9.53 Structure with gravity bias.

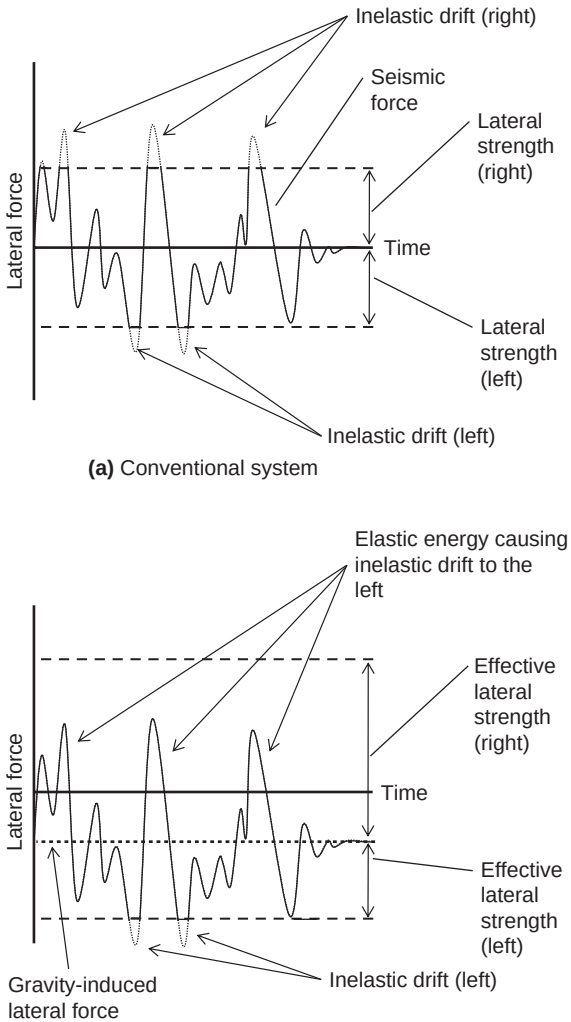

Figure 9.54 Effect of gravity bias on effective lateral strength and ductility demands.

Figure 9.54 conceptually shows the consequences of this bias. The time history response shown in Figure 9.54a is for a conventional structural system having no gravity bias; Figure 9.54b is for a similar system with gravity bias.

In the conventional system, the available strength is measured from zero lateral force. In this system, there are inelastic deformations both to the left and to the right; although these do not return the

structure to zero displacement, there is significant cancellation of opposing inelastic drifts.

With gravity bias, the total system strength is effectively increased due to the design for the combined effects of gravity-induced and seismic lateral forces. The effective lateral strength can be defined as the difference between the gravity-induced lateral force and the total lateral strength; this quantity is presumably adequate in the critical direction (to the left in Figure 9.53) and much larger than necessary in the opposite direction (to the right). There are two consequences to this difference in effective strength. First, the additional overstrength in the strong direction, if sufficiently high, can prevent or dramatically reduce inelastic drift in that direction. This precludes any beneficial cancellation of inelastic drifts in opposite directions. Second, the peaks of seismic force pushing the structure to the right are stored as elastic energy, which, when released, result in additional inelastic deformations to the left. In conjunction these two effects cause a rapid accumulation of inelastic drift in the weaker direction. The structure is said to "walk" in that direction under strong cyclic motion. This effect is similar to what would happen in a braced frame having single diagonal braces, which have very different tension and compression behavior, as is discussed in Section 9.3.1.2.

9.6 Self-Study Problems

Problem 9.1 Design the members of the single-story concentrically braced frame shown below for the given loads:

(a) Perform a nonseismic design, that is, select the lightest members that satisfy the AISC 360 requirements for the factored loads.
(b) Perform a seismic design, that is, select the lightest members that satisfy the AISC 341 requirements for Special Concentrically Braced Frames.
(c) Comment on the differences between the designs and explain their causes.

For both designs

- Use square HSS Sections with A500 Gr. B (F_y = 46 ksi) for the braces.
- Use W-shapes with A992 Gr. 50 (F_y = 50 ksi) for the beam and columns.
- Assume pin-ended braces and beam and that the beam is continuous between the columns.
- Consider the beam unbraced laterally over its entire length.
- The columns are laterally braced at their tops.
- When using available design aids, to reference the sections, page numbers, and edition of the design aids used.
- Loads shown are unfactored and the lateral loads shown are seismic loads already reduced for the appropriate R value. Only consider the $1.2D + 0.5L + 1.0E$ load combination.

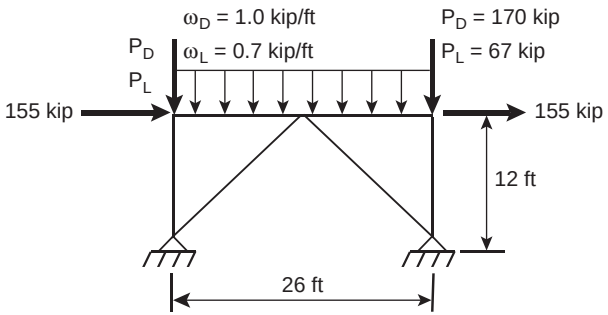

Problem 9.2 For the braced-frame structure shown here, only answer the following specific targeted questions:

(1) For each of the three cases below, calculate the axial force that will be used to design member A-B, and indicate if it is a tension or compression force.

(a) When that force is obtained using the AISC 341 Amplified Seismic Load approach, assuming that the *overstrength factor*, Ω_o, prescribed in the applicable building code is 2.0 in this case

(b) When that force is obtained by a *true capacity design approach* consistent with the AISC 341 requirements when the diagonal braces are A500 Grade B HSS 6.000×0.312 members

(c) When that force is obtained by a true capacity design approach consistent with the AISC 341 requirements when the diagonal braces are Buckling Restrained Braces (BRBs) (see Chapter 11). For this problem, consider the core of the BRBs' diagonal braces to be A36 steel plates of area equal to 2 in^2. For this purpose, also use a strain-hardening adjustment factor, ω, equal to 1.4, and a compression strength adjustment factor, β, equal to 1.1. Note: Knowledge presented in Chapter 11 is pre-requisite to completing this part (c).

(2) For the SCBF problem in (1.b) above, calculate the member slenderness and compactness of the HSS 6.000×0.312. Calculate these values explicitly, rather than using use precalculated or tabulated values of slenderness and compactness. Then, indicate if the HSS 6.000×0.312 is admissible to be used as a brace in an SCBF, in accordance with AISC 341.

Also note that all members are pin–pin in this frame.

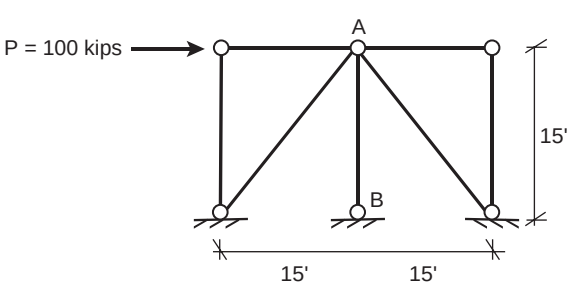

Problem 9.3 The SCBF shown is subjected to a vertical seismic excitation. Braces are HSS 9.625 × 0.50 members of ASTM A500 Grade 42 steel.

(a) Indicate if the HSS braces are acceptable for this SCBF application, and explain why.
(b) Assuming that the HSS braces are acceptable for this SCBF application, calculate what would be the maximum pull-out force to consider for the anchorage at Point A per capacity design approach using the strengths specified by AISC 341.

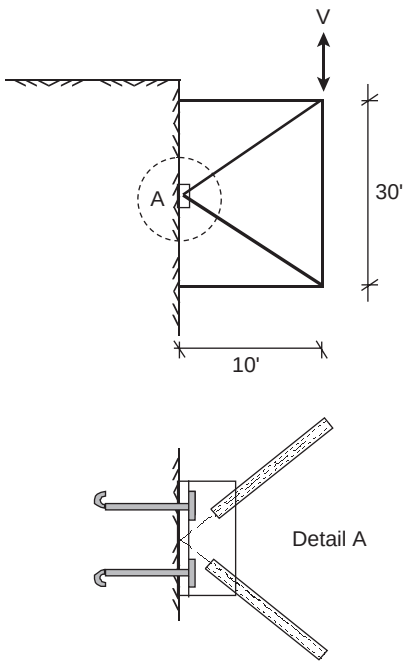

Problem 9.4 For the Special Concentrically Braced Frame (SCBF) shown:

(a) Design the lightest Round HSS (ASTM A500) that can resist the applied factored load shown and that comply with AISC 341.
(b) Design the beam in compliance with AISC 341.

There are no gravity loads acting on the beam. Optionally, the connections and columns could also be designed.

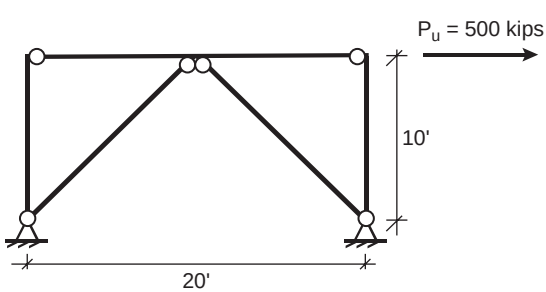

Problem 9.5 For the two-story SCBF located on design lines ② or ③ only, and shown in the figures, for the governing load combination:

(a) Design the braces below the 2nd level (i.e., the braces at the first floor).
(b) Design the girder at the 2nd level (i.e., the lower beam, not the roof beam) assuming $L_b = 15$ ft.
(c) Design the column below the 2nd level (i.e., columns at the first floor).
(d) Check the drifts at the 2nd level considering both shear and flexural drift components.
(e) Indicate what are the values of R, C_d, and Ω_o to consider for the design of this SCBF.

The specified (unfactored) gravity loads are

Roof:	DL = 60 psf	LL = 40 psf
2nd Floor:	DL = 60 psf	LL = 70 psf

Unfactored lateral loads acting on the frames have been obtained from seismic analysis of this building.

Life load reduction factors and wind loads are neglected. All members are assumed pin-ended (K = 1.0). Use W-shape columns and beams (Grade 50), and HSS shapes for braces (Grade 46).

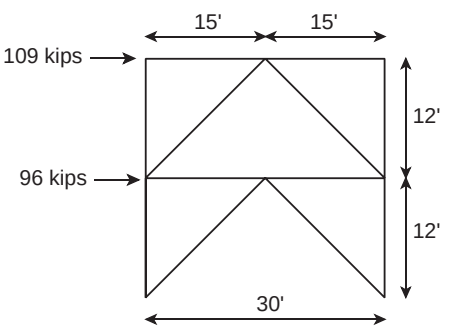

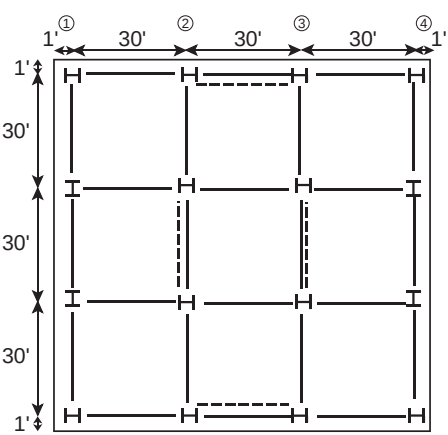

Problem 9.6 The single-story SCBF shown is subjected to an externally applied 100 kips seismic ultimate lateral load F_u (divided into two equal 50 kips load as shown in the figure). Gravity loads are neglected in this problem. For that frame:

(a) Determine if the W10 × 45 diagonal braces have adequate strength and meet the requirements of AISC 341.
(b) Using the W10 × 45 braces [assuming they are acceptable, irrespectively of the answer in part (a) above], check whether a W36 × 260 continuous girder can satisfy the capacity design requirements of AISC 341. Assume $L_b = 7.5'$ and $C_b = 1.0$ here.
(c) Using the capacity design requirements of AISC 341, size the lightest W10 column section meeting all specified requirements. Use brace and girder sizes from (a) and (b) above.
(d) Assuming W10 × 45 braces, design the discontinuous horizontal struts and zipper column in the second figure using the most economical W10 sections for each, on the basis of meeting the requirements of capacity design.

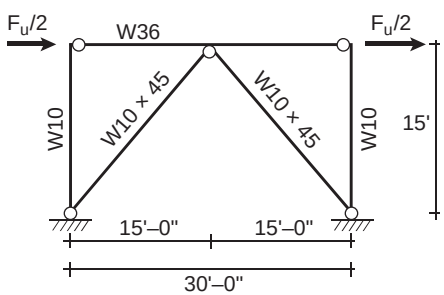

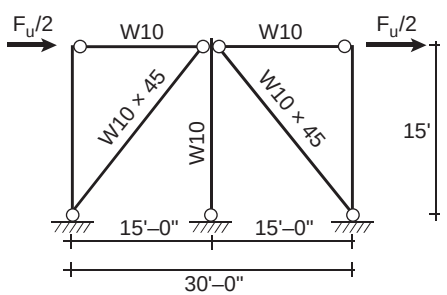

Problem 9.7 Find the maximum lateral load, *V*, which can be applied on the single-story STMF shown below. Provide a solution, first for the case when the X-diagonals are not present (Vierendeel), second for the case when ½-inch × 3/8-inch flat bar braces are used. It is not required in this problem to verify that the rest of the frame remains elastic. Also calculate M_p of the top and bottom chords of this STMF in the special segment (SS) region.

For this frame, all members are Grade 50 steel and

- Exterior columns are W18 × 86.
- Vertical truss members outside of the S.S. are 2L 2½ × 2½ × 3/16.
- Diagonal truss members outside of the S.S. are2L 3 × 3 × 5/16.
- Each of the top and bottom chords outside of the S.S. consists of 2L 3 × 3 × 5/16.
- Each of the top and bottom chords outside of the S.S. consists of 2L 2½ × 2½ × 3/8.

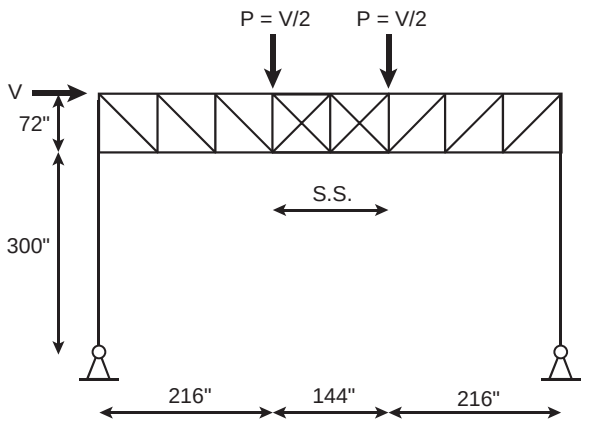

Problem 9.8 (Project-Type Problems)

(1) Write a computer program to develop the axial force versus moment (P-M) interaction diagram of any doubly symmetric beam-column, taking into account buckling of the member with formation of a plastic hinge at its midlength. Compare results from this program with codified design equations and explain the reasons for the observed differences.

(2) Review the exact analytical equations that describe the inelastic cyclic behavior of axially loaded members and provide some numerical examples for slender, intermediate, and stocky members. Examples should be by hand calculations (as much as reasonably possible).

References

AIJ. 1995. *Reconnaissance report on damage to steel building structures observed from the 1995 Hyogoken-Nanbu Earthquake*, Nakashima, M., and Bruneau, M., editors for English Edition. Osaka: Architectural Institute of Japan.

AISC. 1992. *Seismic Provisions for Structural Steel Buildings*. Chicago: American Institute of Steel Construction.

AISC. 1993. *Load and Resistance Factor Design Specification for Structural Steel Buildings.* Chicago: American Institute of Steel Construction.

AISC. 1997. *Seismic Provisions for Structural Steel Buildings*. Chicago: American Institute of Steel Construction.

AISC. 2002. S*eismic Provisions for Structural Steel Buildings ANSI/AISC 341-02.* Chicago: American Institute of Steel Construction.
AISC. 2005. *Seismic Provisions for Structural Steel Buildings ANSI/AISC 341-05.* Chicago: American Institute of Steel Construction.
AISC. 2006. *Seismic Design Manual*. Chicago: American Institute of Steel Construction.
AISC. 2010a. *Seismic Provisions for Structural Steel Buildings ANSI/AISC 341-10.* Chicago: American Institute of Steel Construction.
AISC. 2010b. *Specification for Structural Steel Buildings ANSI/AISC 360-10*. Chicago: American Institute of Steel Construction.
AISC. 2011. *Manual of Steel Construction*, 14th ed. Chicago: American Institute of Steel Construction.
Archambault, M.-H., Tremblay, R., and Filiatrault, A. 1995. "Étude du Comportement Séismiquedes Contreventements Ductilesen X avec Profilés Tubulairesen Acier." *Rapport Technique EPM GCS; 95-09,* Department of Civil Engineering, ÉcolePolytechnique, Montréal. p. 346.
Astaneh-Asl, A., Goel, S. C., and Hanson, R. D. 1982. "Cyclic Behavior of Double Angle Bracing Members with End Gusset Plates," *Report No. UMEE 82R7. A*ugust. Ann Arbor, MI: Department of Civil Engineering, University of Michigan.
Astaneh-Asl, A., and Goel, S. C. 1984. "Cyclic In-Plane Buckling of Double-Angle Bracing." *Journal of Structural Engineering, ASCE,* vol. 110, no. 9, 2036–2055.
Astaneh-Asl, A., Goel, S. C., and Hanson, R. D. 1985. "Cyclic Out-of-Plane Buckling of Double-Angle Bracing." *Journal of Structural Engineering, ASCE,* vol. 111, no. 5, 1135–1153.
Astaneh-Asl, A., Goel, S. C., and Hanson, R. D. 1986. "Earthquake-resistant Design of Double Angle Bracing." *Engineering Journal, AISC,* vol. 23, no. 4, pp. 133–147.
ATC. 1999. *ATC-48 Built to Resist Earthquakes, The Path to Quality Seismic Design and Construction: Building Safety and Earthquakes, Part D: The Seismic Load Path.* Redwood City, CA: Applied Technology Council, p. 4.
Bennett, D. 2009. *The Creation of Bridges*. Secaucus, NJ: Chartwell Books, p. 232.
Black, R. G., Wenger, W. A., and Popov, E. P. 1980. "Inelastic Buckling of Steel Struts Under Cyclic Load Reversal," *Report No. UCB/EERC-80/40.* Berkeley: Earthquake Engineering Research Center, University of California.
Bonneville, D., and Bartoletti, S. 1996. "Case Study 2.3: Concentric Braced Frame, Lankershim Boulevard, North Hollywood." *1994 Northridge Earthquake; Building Case Studies Project; Proposition 122: Product 3.2, SSC 94-06,* Seismic Safety Commission State of California, pp. 305–324.
Brockenbrough, R. L. 2002. "AISC Rehabilitation and Retrofit Guide—A Reference for Historic Shapes and Specifications." *Design Guide 15*. Chicago: American Institute of Construction.
Broderick, B. M., Goggins, J., and Elghazouli, A. Y. 2005. "Cyclic Performance of Steel and Composite Bracing Members." *Journal of Constructional Steel Research,* vol. 61, no. 4, 493–514.
Bruneau, M., and Mahin, S. A. 1990. "Ultimate Behavior of Heavy Steel Section Welded Splices and Design Implications." *Journal of Structural Engineering, ASCE,* vol. 116, no. 18, 2214–2235.
BSSC. 1995. "NEHRP (National Earthquake Hazards Reduction Program) Recommended Provisions for the Development of Seismic Regulations for New Buildings," *Report FEMA 222A.* Washington, D. C.: Building Seismic Safety Council, Federal Emergency Management Agency.
Carstensen, G., and Gildemeister C. 1918. *New York Crystal Palace–Illustrated Description of the Buildings*. New York: Riker, Thorne and Co. Publishers, p. 106.
Chao, S. H., and Goel, S. C. 2008a. "Performance-Based Plastic Design of Special Truss Moment Frames." *AISC Engineering Journal,* vol. 45, no. 2, 127–150.
Chao, S. H., and Goel, S. C. 2008b. *Performance-Based Plastic Design: Earthquake-Resistant Steel Structures*. Country Club Hills, IL: International Code Council Publications, p. 261.

CISC. 2010. *Handbook of Steel Construction*, 10th ed. Willowdale, Ont: Canadian Institute of Steel Construction.
CSA. 1994. "Limit States Design of Steel Structures." *CAN/CSA-S16.1.* Rexdale, Ont: Canadian Standard Association.
CSA. 2001. "Limit States Design of Steel Structures." *CAN/CSA-S16-01.* Rexdale, Ont: Canadian Standard Association.
CSA. 2009. "Limit States Design of Steel Structures."*CAN/CSA-S16-09.* Mississauga, Ont: Canadian Standard Association.
Davaran, A. 2001. "Effective Length Factor for Discontinuous X-Bracing Systems." *Journal of Structural Engineering, ASCE,* vol. 127, no. 2, 106–112.
DeLony, E. 1992. *Landmark American Bridges.* New York: American Society of Civil Engineers, p. 152.
Dicleli, M., and Calik, E. E. 2008. "Physical Theory Hysteretic Model for Steel Braces." *Journal of Structural Engineering, ASCE,* vol. 134, no. 7, 1215–1228.
Dietrich, A. M., and Itani, A. M. 1999. "Cyclic Behavior of Built-up and Perforated Steel Members on the San Francisco–Oakland Bay Bridge." *Report No. CCEER 99-9,* June. Reno: Center for Civil Engineering Earthquake Research, University of Nevada.
Elchalakani, M., Zhao, Z. L., and Grzebieta, R. 2003. "Tests on Cold-Formed Circular Tubular Braces under Cyclic Axial Loading." *Journal of Structural Engineering, ASCE,* vol. 129, no. 4, 507–514.
El-Tayem, A. A., and Goel, S. C. 1986. "Effective Length Factor for the Design of X-bracing Systems." *AISC Engineering Journal,* vol. 23, no. 1, 41–45.
Fell, B. V., Kanvinde, A. M., Deierlein, G. G., Myers, A. M., and Fu, X. 2006. "Buckling and fracture of concentric braces under inelastic cyclic loading." *SteelTIPS*. Moraga, CA: Structural Steel Educational Council.
Fell, B. V., Kanvinde, A. M., Deierlein, G. G., and Myers, A. T. 2009. "Experimental Investigation of Inelastic Cyclic Buckling and Fracture of Steel Braces." *Journal of Structural Engineering, ASCE,* vol. 135, no. 1, 19–32.
Friedman, D. 1995. *Historical Building Construction: Design, Materials, and Technology.* New York: W. W. Norton & Company, p. 450.
Goel, S. C., and Itani, A. M. 1994. "Seismic-Resistant Special Truss-Moment Frames." *Journal of Structural Engineering*, ASCE, vol. 120, no. 6, 1781–1797.
Goel, S. C., and Lee, S. 1992. "A Fracture Criterion for Concrete-Filled Tubular Bracing Members Under Cyclic Loading." *Proceedings of the 1992 ASCE Structures Congress*, pp. 922–925. Reston, VA: ASCE.
Griffis, L. G., and Patel, V. B. 2006. AISC Steel Design after College, http://www.aisc.org/assets/0/424/426/430/d73a3653-5bfb-4af0-aab9-8fe6f06dfacf.pdf
Griggs, Jr, F. E. 2009. "Preservation and Restoration of 19th Century Cast and Wrought Iron Bridges." *ASCE Practice Periodical on Structural Design and Construction,* vol. 14, no. 4, 159–175.
Gugerli, H., and Goel, S. C. 1982. "Inelastic Cyclic Behavior of Steel Bracing Members." *Report No. UMEE 82R1*. Ann Arbor, MI: Department of Civil Engineering, University of Michigan.
Hassan, O. F., and Goel, S. C. 1991. "Modeling of Bracing Members and Seismic Behavior of Concentrically Braced Steel Structures." *Report No. UMCE 91-1*, January. Ann Arbor, MI: Department of Civil Engineering, University of Michigan.
Higginbotham, A. B., and Hanson, R. 1976. "Axial hysteretic behavior of steel members." *Journal of the Structural Division*, vol. 102, no. 7, 1365–1381.
Huang, Y., and Mahin S. A. 2010. "Simulating the Inelastic Seismic Behavior of Steel Braced Frames Including the Effects of Low-Cycle Fatigue." *Pacific Earthquake Engineering Research Center Report No. PEER 2010/104,* Berkeley: University of California. p. 186.
ICBO. 1994. *Uniform Building Code*. Whittier, CA: International Conference of Building Officials.
Ikeda, K., and Mahin, S. A. 1984. "A Refined Physical Theory Model for Predicting the Seismic Behavior of Braced Frames." *Report No. UCB/EERC-84/12.* Berkeley: Earthquake Engineering Research Center, University of California.

Ikeda, K., Mahin, S. A., and Dermitzakis, S. N. 1984. "Phenomenological Modeling of Steel Braces under Cyclic Loading." *Report No. UCB/EERC-84/09*. Berkeley: Earthquake Engineering Research Center, University of California.

Itani, A. M., Vesco, T. D., and Dietrich, A. M. 1998. "Cyclic Behavior of As-Built Laced Members with End Gusset Plates on the San Francisco–Oakland Bay Bridge." *Report No. CCEER 98-01,* March. Reno:Center for Civil Engineering Earthquake Research, University of Nevada.

Jain, A. K., and Goel, S. C. 1978. "Hysteresis Models for Steel Members Subjected to Cyclic Buckling or Cyclic End Moments and Buckling." *UMEE Rep. No. 78R6*, Ann Arbor, MI: University of Michigan.

Jain, A. K., Goel, S. C., and Hanson, R. D. 1977. "Static and Dynamic Hysteresis Behavior of Steel Tubular Members with Welded Gusset Plates." *Report No. UMEE 77R3*, June. Ann Arbor, MI: Department of Civil Engineering, University of Michigan.

Jain, A. K., Goel, S. C., and Hanson, R. D. 1978. "Hysteresis Behavior of Bracing Members and Seismic Response of Braced Frames with Different Proportions." *Report No. UMEE 78R3,* July. Ann Arbor: Department of Civil Engineering, University of Michigan.

Jin, J., and El-Tawil, S. 2003. "Inelastic cyclic model for steel braces." *Journal of Engineering Mechanics, ASCE*, vol. 129, no. 5, 548–557.

Kanvinde, A. M., and Deierlein, G. G. 2007. "A Cyclic Void Growth Model to Assess Ductile Fracute in Structural Steels due to Ultra Low Cycle Fatigue." *Journal of Engineering Mechanics, ASCE*,vol. 133, no. 6, 701–712.

Ketchum, M. S. 1918. *Structural Engineers' Handbook,* 2nd ed. New York: McGraw-Hill Co.

Ketchum, M. S. 1920. *The Design of Highway Bridges of Steel, Timber and Concrete*. New York: McGraw-Hill Co.

Khatib, I. F., Mahin, S. A., and Pister, K. S. 1988. "Seismic Behavior of Concentrically Braced Steel Frames." *Report No. UCB/EERC-88/01.* Berkeley: Earthquake Engineering Research Center, University of California.

Kiland, J. P., and Sabelli, R. 2006. *IBC Structural/Seismic Design Manual Volume 3: Building Design Examples for Steel and Concrete.* Washington, D.C.: International Code Council.

Kunz, F. C. 1915. *Design of Steel Bridges; Theory and Practice for use of Civil Engineers and Students.* New York: McGraw-Hill Co.

Lacerte, M., and Tremblay, R. 2006. "Making use of brace overstrength to improve the seismic response of multistory split-X concentrically braced steel frames." *Canadian Journal of Civil Engineering,* vol. 33, no. 8, 1005–1021.

Lee, K., and Bruneau, M. 2002. "Review of Energy Dissipation of Compression Members in Concentrically Braced Frames." *Technical Report MCEER-02-0005,* 216 pp. Buffalo, NY:Multidisciplinary Center for Earthquake Engineering Research, State University of New York at Buffalo.

Lee, K., and Bruneau, M. 2004. "Seismic Vulnerability Evaluation of Axially Loaded Steel Built-up Laced Members." *Technical Report MCEER-04-0007,* 279 pp. Buffalo, NY: Multidisciplinary Center for Earthquake Engineering Research, State University of New York at Buffalo.

Lee, K., and Bruneau, M. 2005. "Energy Dissipation of Compression Members in Concentrically Braced Frames:Review of Experimental Data." *Journal of Structural Engineering, ASCE,* vol. 131, no. 4, 552–559.

Lee, K., and Bruneau, M. 2008a. "Seismic Vulnerability Evaluation of Axially Loaded Steel Built-up Laced Members - I: Experimental Results." *Earthquake Engineering and Engineering Vibrations Journal*, vol. 7, no. 2, 113–124.

Lee, K., and Bruneau, M. 2008b. "Seismic Vulnerability Evaluation of Axially Loaded Steel Built-Up Laced Members - II: Evaluations." *Earthquake Engineering and Engineering Vibrations Journal,* vol. 7, no. 2, 125–136.

Lee, S., and Goel, S. C. 1987. "Seismic Behavior of Hollow and Concrete-Filled Square Tubular Bracing Members," *Report No. UMEE 87-11*, December. Ann Arbor, MI: Department of Civil Engineering, University of Michigan.

Lehman, D., Lumpkin, E., Hsiao, P. C., Roeder, C., Tsai, K. C., Wu, A. C., Wei, C. Y., and Tsai, C. 2010. "Cyclic Response of Three-Story Full-Scale Concentrically Braced Frame System." *Proceedings of 9th U.S. National and 10th Canadian Conference on Earthquake Engineering,* Toronto.

Lehman, D. E., Roeder, C. W., Herman, D., Johnson, S., and Kotulka, B. 2008. "Improved seismic performance of gusset plate connections." *Journal of Structural Engineering, ASCE,* vol. 134, no. 6, 890–901.

Leon, R. T., and Yang, C. S. 2003. "Special inverted-V-Braced frames with Suspended Zipper Struts." *Proceedings of International Workshop on Steel and Concrete Composite Construction, National Center for Research on Earthquake Engineering,* Taipei.

Liu, Z., and Goel, S. C. 1987. "Investigation of Concrete-Filled Steel Tubes under Cyclic Bending and Buckling." *Report No. UMCE 87-3.* Ann Arbor: Department of Civil Engineering, University of Michigan.

Liu, Z., and Goel, S. C. 1988."Cyclic Load Behavior of Concrete-Filled Tubular Braces." *Journal of the Structural Division*, *ASCE*,vol. 114, no. 7,1488–1506.

MacRae, G. 2010. "The Development and Use of the Continuous Column Concept."*Joint Proceedings of the 7th International Conference on Urban Earthquake Engineering (7CUEE) & 5th International Conference on Earthquake Engineering (5ICEE),* Tokyo.

MacRae, G. A., Kimura, Y, and Roeder, C. 2004. "Effect of Column Stiffness on Braced Frame Seismic Behavior." *Journal of the Structural Division*, *ASCE*, vol. 130, no. 3, 381–391.Maison, B., and Popov, E. P. 1980."Cyclic Response Prediction for Braced Steel Frames." *Journal of the Structural Division*, *ASCE*, vol. 106, no. 7, 1401–1416.

Moon, J., Yoon, K. Y., Han, T. S., and Lee, H. E. 2008. "Out-of-Plane Buckling and Design of X-Bracing Systems with Discontinuous Diagonals," *Journal of Constructional Steel Research,* vol. 64, no. 3, 285–294.

Nakashima, M., and Wakabayashi, M. 1992. "Analysis and Design of Steel Braces and Braced Frames in Building Structures." *Stability and Ductility of Steel Structures under Cyclic Loading.* Fukumoto, Y. and Lee, G. C., editors. Boca Raton: CRC Press, pp. 309–321.

Newell, J. D., and Uang, C. M. 2008. "Cyclic Behavior of Steel Wide-Flange Columns Subjected to Large Drift."*Journal of Structural Engineering, ASCE,* vol. 134, no. 8, 1334–1342.

Nonaka, T. 1987. "Formulation of Inelastic Bar under Repeated Axial and Thermal Loadings." *Journal of Engineering Mechanics*, *ASCE*, vol. 113, no. 11, 1647–1664.

Nonaka, T. 1989. "Elastic-Plastic Bar under Changes in Temperature and Axial Load." *Journal of Structural Engineering*, *ASCE*, vol. 115, no. 12, 3059–3075.

Popov, E. P., and Black, R. G. 1981. "Steel Struts under Severe Cyclic Loadings." *Journal of the Structural Division*, *ASCE*. vol. 107, no. ST9, 1857–1881.

Redwood, R. G., and Channagiri, V. S. 1991. "Earthquake-Resistant Design of Concentrically Braced Steel Frames." *Canadian Journal of Civil Engineering*, vol. 18, no. 5, 839–850.

Richards, P. W. 2009. "Seismic Column Demands in Ductile Braced Frames," *Journal of Structural Engineering, ASCE,* vol. 135, no. 1, 33–41.

Roeder, C. W., Lehman, D. E., Clark, K., Powell, J., Yoo, J. -H., Tsai, K. -C., Lin, C. -H., and Wei, C. -Y. 2010. "Influence of gusset plate connections and braces on the seismic performance of X-braced frames." *Earthquake Engineering & Structural Dynamics,* n/a. doi: 10.1002/eqe.1024.

Roeder, C. W., Lehman, D. E., Lumpkin, E., and Hsiao, P. C. 2009. "Seismic Evaluation and Rehabilitation of Concentrically Braced Frames," *ATC/SEI Conference on Improving the Seismic Performance of Existing Buildings and Other Structures,* pp. 777–788.

Rogers, C., and Tremblay, R. 2010. "Impact of Diaphragm Behavior on the Seismic Design of Low-Rise Steel Buildings," *AISC Engineering Journal,* vol. 47, no. 1, 21–36.

Sabelli, R. 2001. "Research on improving the Design and Analysis of Earthquake Resistant Braces Frames," *2000 NEHRP Fellowship in Earthquake Hazard Reduction,*

Final Report to FEMA and EERI. Oakland, CA: Earthquake Engineering Research Institute.

Sabelli, R., and Hohbach, D. 1999. "Design of Cross-Braced Frames for Predictable Buckling Behavior." *Journal of Structural Engineering, ASCE,* vol. 125, no. 2, 163–168.

Schachter, M., and Reinhorn, A. M. 2007. "Three-Dimensional Modeling of Inelastic Buckling in Frame Structures." *Report MCEER-07-0016*. Buffalo, NY: Multidisciplinary Center for Earthquake Engineering Research, State University of New York at Buffalo.

SEAOC. 1978, 1990, 1996. *Tentative Lateral Force Requirements*. Seismology Committee, Structural Engineers Association of California. Sacramento/San Francisco/Los Angeles: CA.

Shaback, B., and Brown, T. 2003. "Behavior of square hollow structural steel braces with end connections under reversed cyclic axial loading." *Canadian Journal of Civil Engineering,* vol. 30, 745–753.

Soroushian, P., and Alawa, M. S. 1990. "Hysteretic modeling of steel struts: Refined physical theory approach." *Journal of Structural Engineering, ASCE,* vol. 116, no. 10, 2903–2916.

Tang, X., and Goel, S. C. 1987. "Seismic Analysis and Design Considerations of Braced Steel Structures." *Report No. UMCE 87-4.* June. Ann Arbor, MI: Department of Civil Engineering, University of Michigan.

Tang, X., and Goel, S. C. 1989. "Brace Fractures and Analysis of Phase I Structures," *Journal of Structural Engineering, ASCE*, vol. 102, no. 8, 1960–1976.

Tremblay, R. 2002. "Inelastic Seismic Response of Bracing Members." *Journal of Constructional of Steel Research,* vol. 58, 665–701.

Tremblay, R. 2003. "Achieving a Stable Inelastic Seismic Response for Multi-Story Concentrically Braced Steel Frames." *Engineering Journal,* vol. 40, no. 2, 111–129.

Tremblay, R. 2008. "Influence of brace slenderness on the fracture life of rectangular tubular steel bracing members subjected to seismic inelastic loading." *Proceedings of ASCE/SEI Structures Congress,* Vancouver.

Tremblay, R., Archambault, M. H., and Filiatrault, A. 2003. "Seismic Performance of Concentrically Braced Steel Frames made with Rectangular Hollow Bracing Members." *Journal of Structural Engineering, ASCE,* vol. 129, no. 12, 1626–1636.

Tremblay, R., Bruneau, M., Nakashima, M., Prion, H. G. L., Filiatrault, M., and DeVall, R. 1996. "Seismic Design of Steel Buildings: Lessons from the 1995 Hyogo-ken Nanbu Earthquake." *Canadian Journal of Civil Engineering,* vol. 23, no. 3, 757–770.

Tremblay, R., and Filiatrault, A. 1996. "Seismic Impact Loading in Inelastic Tension-Only Concentrically Braced Steel Frames: Myth or Reality?" *Earthquake Engineering and Structural Dynamics,* vol. 25, no. 12, 1373–1389.

Tremblay, R., Haddad, M., Martinez, G., Richard, J., and Moffatt, K. 2008. "Inelastic Cyclic Testing of Large Size Steel Bracing Members." *Paper No.05-05-0071, Proceedings 14th Word Conference on Earthquake Engineering,* Beijing.

Tremblay, R., and Robert, N. 2001. "Seismic Performance of Low- and Medium-Rise Chevron Braced Steel Frames," *Canadian Journal of Civil Engineering,* vol. 28, no. 4, 699–714.

Tremblay, R., Timler, P., Bruneau, M., and Filiatrault, A. 1995. "Performance of Steel Structures during the January 17, 1994, Northridge Earthquake." *Canadian Journal of Civil Engineering,* vol. 22, no. 2, 338–360.

Tremblay, R., and Tirca, L. 2003. "Behavior and Design of Multistory Zipper Concentrically Braced Steel Frames for the Mitigation of Soft Story Response." *Proceedings of 4th International Conference on Behavior of Steel Structures in Seismic Areas (STESSA).* Naples, Italy. pp. 471–477.

Uang, C. M., and Bertero, V. V. 1986. "Earthquake Simulation Tests and Associated Studies of a 0.3-Scale Model of a Six-Story Concentrically Braced Steel Structure." *Report No. UCB/EERC-86/10.* Berkeley: Earthquake Engineering Research Center, University of California.

Uang, C. M., and Kleiser, M. 1997. "Cyclic Performance of As-Built Latticed Members for the San Francisco-Oakland Bay Bridge," *Report No. SSRP-97/01,* June. La Jolla, California: Division of Structural Engineering, University of California, San Diego.

Uriz, P., Filippou, F. C., and Mahin, S. A. 2007. "Model for cycle inelastic buckling of steel braces." *Journal of Structural Engineering, ASCE*, vol. 134, no. 4, 619–628.

Uriz, P., and Mahin, S. A. 2008. "Toward earthquake-resistant design of concentrically braced steel-frame structures." *Pacific Earthquake Engineering Research Center Report No. PEER 2008/08*, Berkeley: University of California. p. 401.

Wada, A., Qu, Z., Ito, H., Motoyui, S., Sakata, H., and Kasai, K. 2009. "Seismic Retrofit Using Rocking Walls and Steel Dampers." *ATC/SEI Conference on Improving the Seismic Performance of Existing Buildings and Other Structures,* San Francisco.

Whittaker, A. S., Uang, C. M., and Bertero, V. V. 1990. "An Experimental Study of the Behavior of Dual Steel Systems." *Report No. UCB/EERC-88/14.* Berkeley: Earthquake Engineering Research Center, University of California.

Yang, C. S., Leon, R. T., and DesRoches, R. 2008a. "Design and Behavior of Zipper-Braced Frames." *Engineering Structures,* vol. 30, no. 4, 1092–1100.

Yang, C. S., Leon, R. T., and DesRoches, R. 2008b. "Cyclic Behavior of Zipper-Braced Frames." *Earthquake Spectra,* vol. 26, no. 2, 561–582

Yoo, J. H., Roeder, C. W., and Lehman, D. E. 2008. "Analytical Performance Simulation of Special Concentrically Braced Frames," *Journal of Structural Engineering, ASCE,* vol. 134, no. 6, 881–889.

Zayas, A. Z., Shing, P. B., Mahin, S. A., and Popov, E. P. 1981. "Inelastic Structural Modeling of Braced Offshore Platforms for Seismic Loading." *Report No. UCB/EERC-81/04.* Berkeley: Earthquake Engineering Research Center, University of California.

Zhao, X. L., Grzebieta, R., and Lee, C. 2002. "Void-filled Cold-formed Rectangular Hollow Section Braces Subjected to Large Deformation Cyclic Axial Loading." *Journal of Structural Engineering, ASCE,* vol. 128, no. 6, 746–753.

CHAPTER 10
Design of Ductile Eccentrically Braced Frames

10.1 Introduction

10.1.1 Historical Development

Although a properly designed and constructed steel moment frame can behave in a ductile manner, it was shown in Chapter 8 that the substantial lateral flexibility of moment frames is such that their design is often governed by code-required story drift limits. Special concentrically braced frames, on the other hand, have a large lateral stiffness, but their energy dissipation capacity is hindered by brace buckling. In the early 1970s, a new steel system called the eccentrically braced frame (EBF) was proposed in Japan (Fujimoto et al. 1972, Tanabashi et al. 1974). The EBF combines the advantages of both high elastic stiffness and high ductility at large story drifts. This type of framing system dissipates seismic energy by controlled shear or flexural yielding in a small segment of the beams called links.

In the United Sates, the EBF system was first studied by Roeder and Popov (1978). In the 1980s, numerous studies on link behavior provided insight into the cyclic response of EBFs (Engelhardt and Popov 1989; Hjemstad and Popov 1983, 1984; Kasai and Popov 1986a, 1986b; Malley and Popov 1984; Manheim and Popov 1983; Ricles and Popov 1989). Experimental verifications of EBF response at the system level were also conducted in the mid- to late-1980s (Roeder et al. 1987, Whittaker et al. 1989, Yang 1985). These studies led to the development of design provisions in the 1988 Uniform Building Code and later in AISC 341 (AISC 2010).

Further studies were conducted in the past two decades, including full-scale testing of large-size links for not only building but also bridge applications (Dusicka and Itani 2002, McDaniel et al. 2003, Sarraf and Bruneau 2004, Zahrai and Bruneau 1999). Recent research on links has also extended from I-shaped rolled links to built-up sections including I-shaped sections, boxed sections (Berman and Bruneau 2008b), and double C sections (Mansour et al. 2008). With increasing emphasis on performance-based design, the concept of replaceable links has also been explored (Dusicka and Lewis 2010, Mansour et al. 2008, Ramadan and Ghobarah 1995, Stratan et al. 2003).

10.1.2 General Behavior and Plastic Mechanism

An eccentrically braced frame is a framing system in which the axial forces induced in the braces are transferred either to a column or another brace through shear and bending in a small segment of the beam. Typical EBF geometries are shown in Figure 10.1. Architecturally, EBF also provides more freedom for door opening than CBF. The critical beam segment is called a "link" and is designated by a length, *e*, in the figure. Links in EBFs act as structural fuses to dissipate the earthquake-induced energy in a building in a stable manner. In practical applications, the horizontal links have been commonly used; see

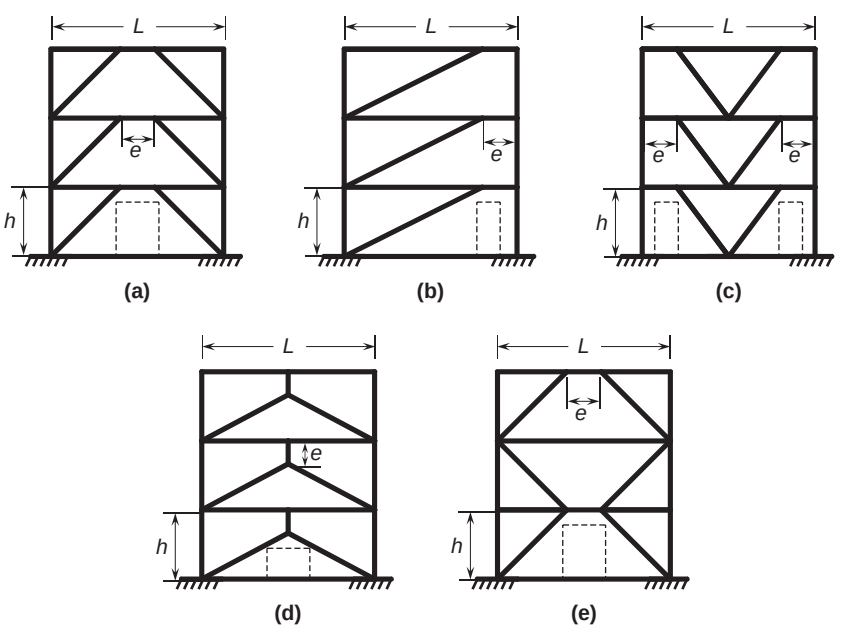

Figure 10.1 Typical EBF configurations.

(a) EBF with interior links **(b)** EBF with exterior links

Figure 10.2 Examples of EBF construction.

Figure 10.2 for two examples. Figure 10.1e shows an EBF where a link does not exist in every floor. The links in Figure 10.1d are oriented vertically; therefore, unlike all the other configurations, they are not integral with the beams.

Links in Figures 10.1b and c are connected to the columns. It has been shown in Chapter 8 that beam-to-column moment connections are vulnerable to brittle fracture. As it will be shown later, link-to-column moment connection is subjected to both high moment and high shear, making it even more vulnerable to brittle fracture. For this reason, it is highly desirable that these two configurations be avoided.

10.1.3 Design Philosophy

Figure 10.3 shows the desirable plastic mechanism of EBF. Yielding of the links, shown cross-hatched, occurs along the height of the frame. The remaining part of the structure is then designed to remain essentially elastic. A comparison of the expected plastic mechanism between SCBF and EBF is shown in Figure 10.4. In a SCBF, braces are designed and detailed as structural fuses. For an EBF, however, links need to be properly designed and detailed to have adequate strength and ductility. All the other structural components (beam segments outside of the links, braces, columns, and connections) are proportioned following the capacity design principles to remain essentially elastic during the design earthquake.

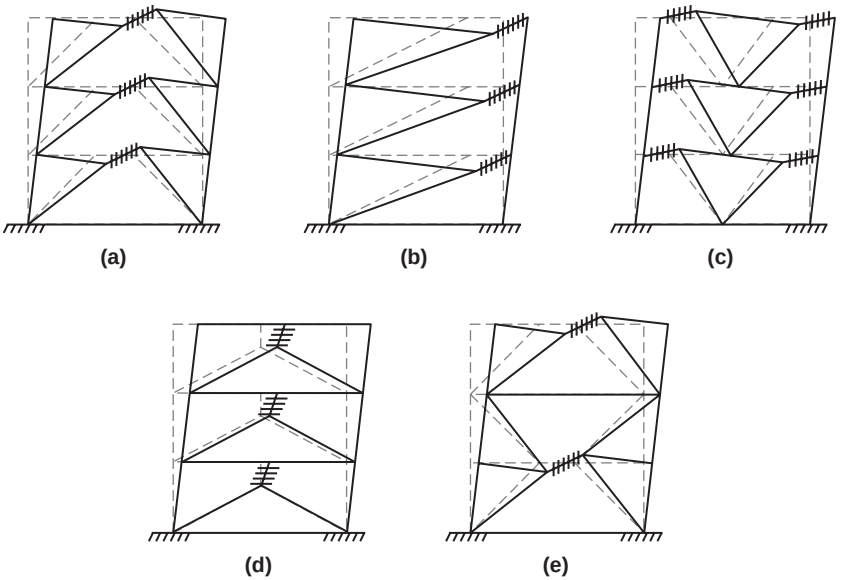

Figure 10.3 Yield mechanism of EBF.

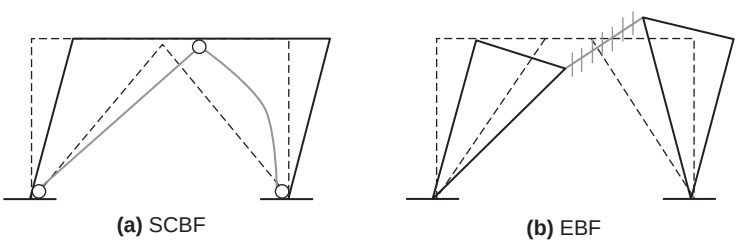

Figure 10.4 Expected deformed configuration of SCBF and EBF.

10.2 Link Behavior

10.2.1 Stiffened and Unstiffened Links

Figure 10.5 shows two I-shaped links that were tested cyclically (Malley and Popov 1983). For the specimen that did not have stiffeners, web local buckling due to shear would occur early. Such local buckling could be delayed by adding transverse stiffeners. When the stiffeners were sufficiently close, Figure 10.5b shows the formation of diagonal tension field in the subpanels. Continued large displacement cycling finally caused material tearing in the links. For the unstiffened link, tearing usually took place near the

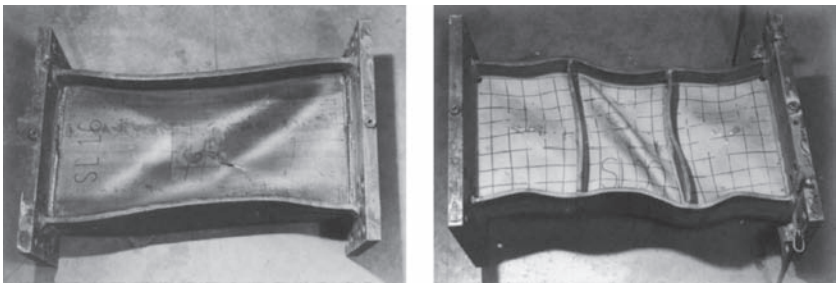

(a) Unstiffened link (W18 × 60) **(b)** Stiffened link (W18 × 40)

FIGURE 10.5 Unstiffened versus stiffened link. (*Malley and Popov 1983, with permission from EERC, University of California, Berkeley.)*

center of the web region due to material fatigue from severe web curvature reversals.

The effect of adding stiffeners to stiffen the link can be better demonstrated by comparing the cyclic response of two links of identical size, one without and the other with three stiffeners (Hjelmstad and Popov 1983). Figure 10.6 shows that not only the shear strength but also the energy dissipation capacity are significantly improved with the addition of web stiffeners.

10.2.2 Critical Length for Shear Yielding

Figure 10.7 shows the free-body diagram of a link. Ignoring the effects of axial force and the interaction between moment and shear in the link, flexural hinges form at two ends of the link when both M_a and M_b reach the plastic moment, M_p. A shear hinge is said to form when

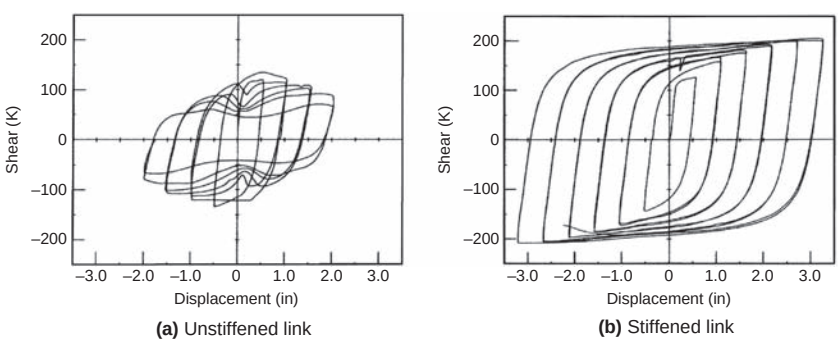

FIGURE 10.6 Cyclic response of unstiffened and stiffened W18 × 40 links, $e = 28$ in. (*Hjelmstad and Popov 1983, with permission from EERC, University of California, Berkeley*.)

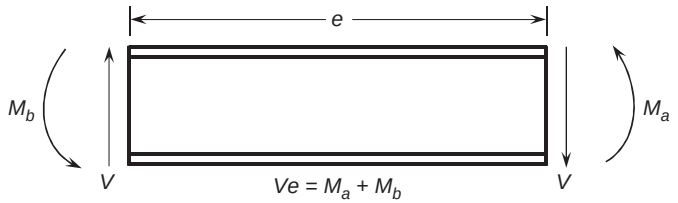

Figure 10.7 Link deformation and free-body diagram.

the shear reaches V_p. The plastic moment and shear capacities are respectively computed as follows:

$$M_p = F_y Z \tag{10.1a}$$

$$V_p = \tau_y A_{lw} \tag{10.1b}$$

where the link web area, A_{lw}, is equal to $(d - 2t_f)t_w$ and $2(d - 2t_f)t_w$ for I-shaped and built-up box sections, respectively. The yield shear stress, τ_y, is taken as $0.6F_y$ and $0.55F_y$ in AISC 341 (AISC 2010) and CSA S16 (CSA 2009), respectively. A balanced yielding condition corresponds to the simultaneous formation of flexural hinges and a shear hinge. The corresponding link length is

$$e_0 = \frac{2M_p}{V_p} \tag{10.2}$$

In a short link ($e \le e_0$), a shear hinge will form. When $e > e_0$, a flexural (or moment) hinge forms at both ends of the link, and the corresponding shear force is

$$V = \frac{2M_p}{e} \tag{10.3}$$

Based on plastic theory, Eq. (10.2) can be modified slightly to include the effect of interaction between M and V. Nevertheless, experimental results (see Figure 10.8) indicated that the interaction is weak and that such interaction can be ignored (Kasai and Popov 1986b).

Test results also showed that a properly stiffened short link can strain harden and develop a shear strength equal to $1.5V_p$. For example, Figure 10.6b shows the link shear strength reached 200 kips, but Eq. (10.1b) gives a V_p value of 126 kips based on a measured web yield stress of 39.5 ksi. The end moments of a link that has yielded in shear can continue to increase due to this strain hardening and, therefore, flexural hinges can develop. To avoid high bending strains that

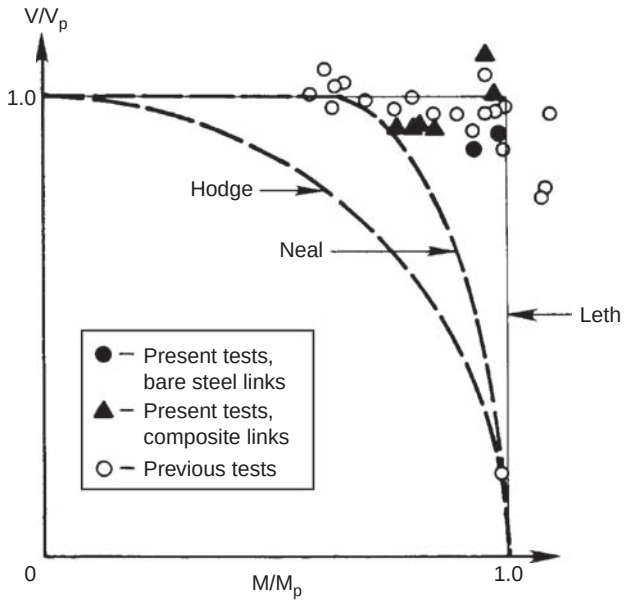

Figure 10.8 M-V interaction of links. (*Ricles and Popov 1987, with permission from EERC, University of California, Berkeley.*)

may lead to severe flange buckling or to failure of link flange-to-column welds, these end moments are limited to $1.2M_p$, and the maximum length, e_0, in Eq. (10.2) for a shear link is modified as follows (Kasai and Popov 1986b):

$$e_0 = \frac{2(1.2M_p)}{1.5V_p} = \frac{1.6M_p}{V_p} \tag{10.4}$$

10.2.3 Classifications of Links and Link Deformation Capacity

Experimental results have shown that the inelastic deformation capacity of an EBF can be greatly reduced when long links ($e > e_0$) are used. Following the above logic, it can be shown that flexural hinges dominate the link response when e is larger than $2.6M_p/V_p$. (If the moment at flexural hinges reaches $1.2M_p$, the corresponding shear for a link with a length of $2.6M_p/V_p$ is $0.92V_p$.) In the transition region where $1.6M_p/V_p < e < 2.6M_p/V_p$, the link undergoes simultaneous shear and flexural yielding (Engelhardt and Popov 1989). Figure 10.9 classifies links in EBFs; for design purpose a link is classified as either a short or shear link (developing only shear yielding), a long or moment link (developing only flexural yielding), or an intermediate link (developing both shear and flexural yielding).

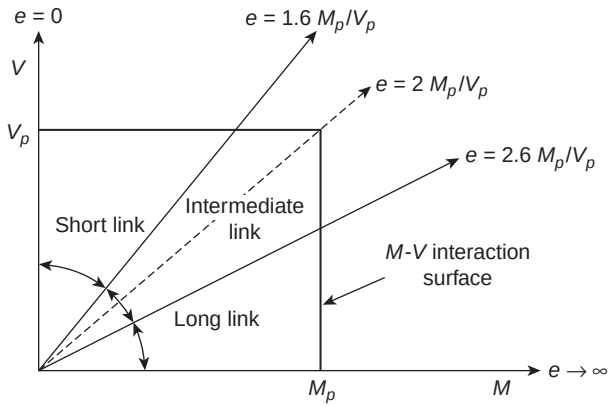

Figure 10.9 Classification of links.

The effect of link length on the failure mode and deformation capacity is demonstrated in Figure 10.10 (Okazaki et al. 2004). Figure 10.10a shows that the closely spaced stiffeners are effective in preventing shear buckling of a short link. Relatively uniform shear yielding in the web occurred along the entire link length, thus producing a large deformation capacity. On the other hand, Figure 10.10c depicts the behavior of a long link ($e \geq 2.6M_p/V_p$), where flexural buckling occurred primarily in the form of flange local buckling. The deformation capacity is very limited as the link web did not yield along its length and contribute any plastic deformation. Figure 10.10b demonstrates the behavior of an intermediate link ($1.6M_p/V_p < e < 2.6M_p/V_p$). Both shear and flexure are dominating in this case, where the plastic deformation was contributed by flexure buckling in the flanges and web shear buckling in the end panels.

The plastic mechanism in Figure 10.3 shows that the links are subjected to an inelastic rotation angle, γ_p, at the ends of the links. This link rotation angle is the plastic rotation angle between the link and the portion of the beam outside of the link. The links need to have a sufficient deformation capacity to accommodate this deformation demand. Testing shows that a link's inelastic rotation capacity is dependent on the link's length—the shorter the length, the larger the rotation capacity (Kasai and Popov 1986a). To develop a large rotation capacity, closely spaced intermediate stiffeners are needed. The allowable link deformation capacity, γ_a, as given by AISC 341 is shown in Figure 10.11.

10.2.4 Link Transverse Stiffener

Once shear buckling occurs in a stiffened link, tearing along the perimeter of the link panes due to stress concentration created by the buckled web may cause significant strength degradation. For

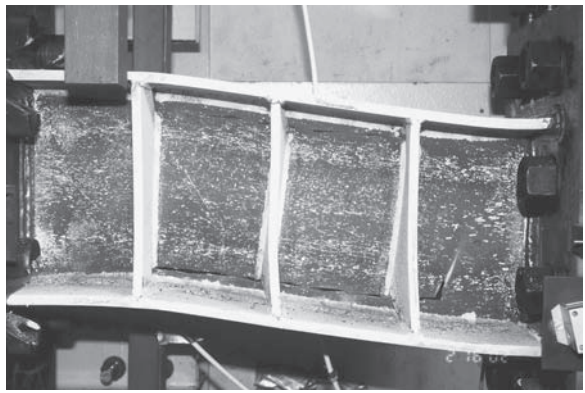

(a) Short link

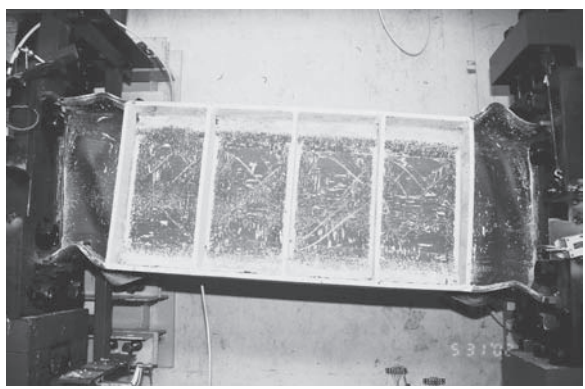

(b) Intermediate link

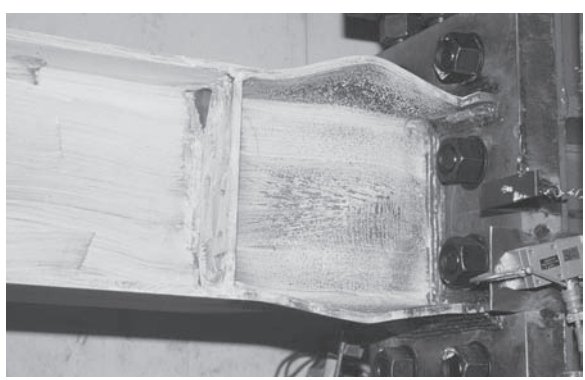

(c) Long link

FIGURE 10.10 Link failure modes. (*Courtesy of M.D. Engelhardt, Dept. of Civil Engineering, University of Texas, Austin.*)

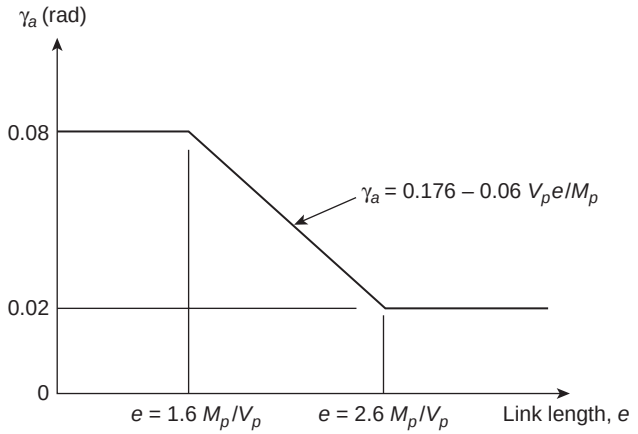

Figure 10.11 Allowable link rotation angles.

practical applications, allowing the link to behave in the postbuckling region can also result in hazardous lateral-torsional buckling problem. Therefore, it is appropriate to consider web buckling as the shear link design ultimate limit state (Kasai and Popov 1986a).

Figure 10.12 shows the typical hysteretic loop envelopes of a short link under cyclic loading. Depending on the loading history used for testing, the link deformation capacity, γ_u, at shear buckling can be very different. For example, the value of γ_u for a link under monotonic loading can be about twice that of the same link under symmetrically cyclic loading. Based on test data, Kasai and Popov (1986a)

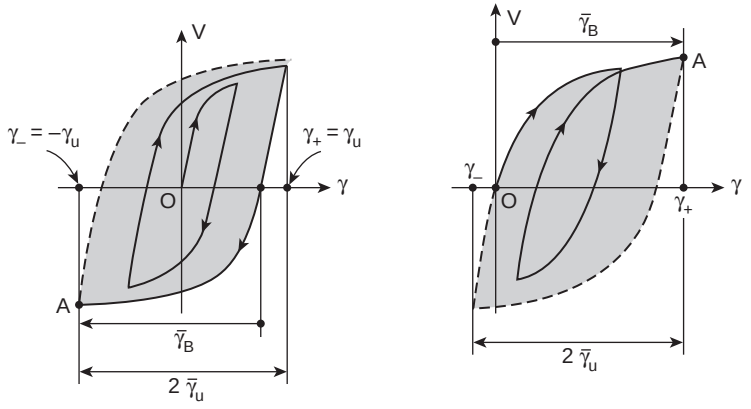

(a) Symmetric loading **(b)** Non-symmetric loading

Figure 10.12 Buckling hysteretic loop envelopes for shear link. (*Kasai and Popov 1986a, with permission from EERC, University of California, Berkeley.*)

observed that the link buckling deformation capacity, $\bar{\gamma}_B$, shown in Figure 10.12 is a more reliable parameter for predicting the cyclic web buckling under different loading histories. $\bar{\gamma}_B$ is defined as the link deformation measured from the farthest point of zero shear when shear buckling occurs (labeled as point "A" in Figure 10.12). Based on a cyclic plastic theory, the following simple expression was derived and correlated well with the test data of A36 steel links:

$$\bar{\gamma}_B = 8.7 K_s \left(\frac{t_w}{b}\right)^2 \tag{10.5}$$

where b is the web panel height, and K_s, which is a function of the panel aspect ratio, is an elastic plate buckling coefficient. For design purposes, a conservative approximation of the above equation for the range of γ_u from 0.03 to 0.09 rad can be established:

$$\frac{a}{t_w} + \frac{1}{5}\frac{d}{t_w} = C_B \tag{10.6}$$

where a = stiffener spacing; d = link depth; and C_B = 56, 38, and 29, respectively, for γ_u = 0.03, 0.06, and 0.09 rad. For other values of γ_u, C_B can be linearly interpolated. In deriving the above equation, it was assumed that the stiffener spacing is no larger than the link depth.

10.2.5 Effect of Axial Force

The presence of an axial force in a link reduces not only its flexural and shear capacities but also its inelastic deformation capacity (Kasai and Popov 1986b, Ghobarah and Ramadan 1990). When the axial force, P_u, exceeds 15% of the yield force, P_y(= $A_g F_y$), the *P-M* interaction equation in Eq. (3.25) can be used to compute the reduced plastic moment, M_{pa}:

$$M_{pa} = 1.18 M_p \left(1 - \frac{P_u}{P_y}\right) = \frac{M_p}{0.85}\left(1 - \frac{P_u}{P_y}\right) \tag{10.7}$$

Based on the von Mises yield criterion in Eq. (3.29), the reduced shear capacity is

$$V_{pa} = V_p \sqrt{1 - \left(\frac{P_u}{P_y}\right)^2} \tag{10.8}$$

Defining the normalized axial force ratio ρ′ as

$$\rho' = \frac{P_u / P_y}{V_u / V_y} = \left(\frac{P_u}{V_u}\right)\left(\frac{A_g}{0.6 A_{lw}}\right) \tag{10.9}$$

and replacing M_p and V_p in Eq. (10.2) by M_{pa} and V_{pa}, the reduced value of e_0 when $\rho' \geq 0.5$ can be approximated as follows (Kasai and Popov 1986b):

$$e_0 = \frac{1.6M_p}{V_p}(1.15 - 0.3\rho') \tag{10.10}$$

The correction is unnecessary if $\rho' \leq 0.5$, in which case AISC 341 requires that the link length shall not exceed that given by Eq. (10.4).

10.2.6 Effect of Concrete Slab

Research conducted on composite links showed that composite action can significantly increase the link shear capacity during the first cycles of large inelastic deformations (Ricles and Popov 1989). However, composite action deteriorates rapidly in subsequent cycles due to local concrete floor damage at both ends of the link. The research also showed that the composite slab cannot be used as lateral bracing for the links. Because links are also a protected zone where shear stud connectors cannot be used, AISC 341 ignores the effect of composite action in link design.

10.2.7 Link Overstrength

The overstrength of a link is defined as the ratio between the maximum shear developed in the link and the V_{na} value, where V_{na}, the link shear strength, is the smaller of V_p or $2M_p/e$ calculated based on the actual yield stress. In deriving Eq. (10.4), it was assumed that the link will strain harden and develop a shear strength of $1.5V_p$. Recent testing conducted by Okazaki et al. (2005) confirmed this assumption, wherein the average I-shaped link overstrength was 1.41 for short links (see Figure 10.13). The overstrength tended to be lower for longer links.

Note from Figure 10.13 that a few data points from Dusicka and Itani (2002) and McDaniel et al. (2003) show very high overstrength values. These data were based on cyclic testing of large-size, I-shaped built-up shear links for bridge applications. Unlike typical rolled sections, these built-up sections have large flange area-to-web area ratios. Such high overstrength, which is not reflected in AISC 341, can be detrimental from the capacity design point of view because it may overload the other part of the structure if not properly considered in design. The higher shear overstrength of these links is mainly due to the participation of flanges in resisting shear. Manheim and Popov (1983) and Richards (2004) have recommended procedures to account for this additional strength. The concept behind these procedures is to treat each flange as a fix-ended beam. The shear resisted by each flange

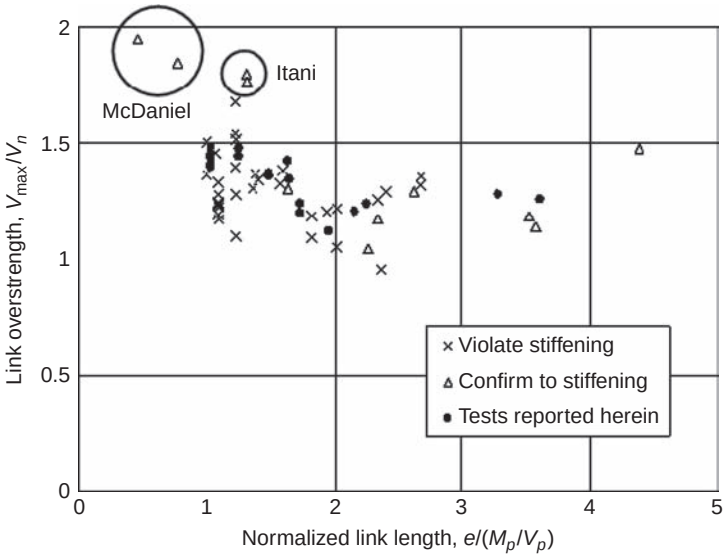

Figure 10.13 Link overstrength. (*Courtesy of M.D. Engelhardt, Dept. of Civil Engineering, University of Texas, Austin.*)

corresponds to that when the plastic moment of the flange, reduced to account for the axial force effect in the flange, is developed.

10.2.8 Qualification Test and Loading Protocol Effect

When an EBF configuration requires one end of the link to be connected to the column, AISC 341 requires that the link-to-column connection be tested by a specified cyclic loading sequence such that the connection can sustain the maximum link rotation based on the length of the link (Figure 10.11). In a testing program to evaluate some types of link-to-column connections, Okazaki et al. (2004, 2005) originally based it on the loading sequence specified in the 2002 edition of AISC 341 (AISC 2002). Test results revealed that some properly designed link specimens did not meet the code-specified rotation capacity. Furthermore, unexpected fracture pattern in the web was also observed (Figure 10.14). A subsequent analytical study concluded by Richards and Uang (2006) showed that the loading protocol used was too severe when compared with those used by researchers in the 1980s. A new loading protocol that simulated a more realistic deformation demand of the links during earthquake excitations expected in North America was then developed and adopted in the subsequent editions of AISC 341 (AISC 2005). Figure 10.15 compares both cyclic loading sequences. Testing with the revised loading sequence showed that the link specimens

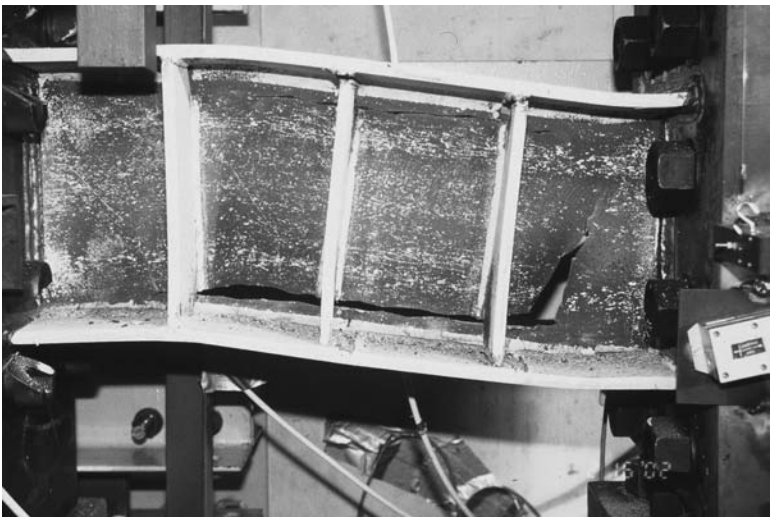

Figure 10.14 Link fracture in the web. (*Courtesy of M.D. Engelhardt, Dept. of Civil Engineering, University of Texas, Austin.*)

earlier considered by Okazaki et al. (2005) were able to deliver the code-specified rotation capacity.

10.3 EBF Lateral Stiffness and Strength

10.3.1 Elastic Stiffness

The variations of the lateral stiffness of a simple EBF with respect to the link length is shown in Figure 10.16 (Hjelmstad and Popov 1984). Note that e/L ratios of 0.0 and 1.0 correspond to a concentrically braced frame and a moment frame, respectively. The figure shows the advantage of using a short link for drift control.

10.3.2 Link Required Rotation

Consider the plastic mechanism of an interior link configuration shown in Figure 10.17a. Applying simple plastic theory, the kinematics of the plastic mechanism requires that

$$\gamma_p = \frac{L}{e}\theta_p \tag{10.11}$$

where θ_p is the plastic story drift angle (or plastic story drift ratio), and γ_p is the plastic deformation demand of the link. The expression shows that γ_p increases rapidly as the link length is reduced. Because

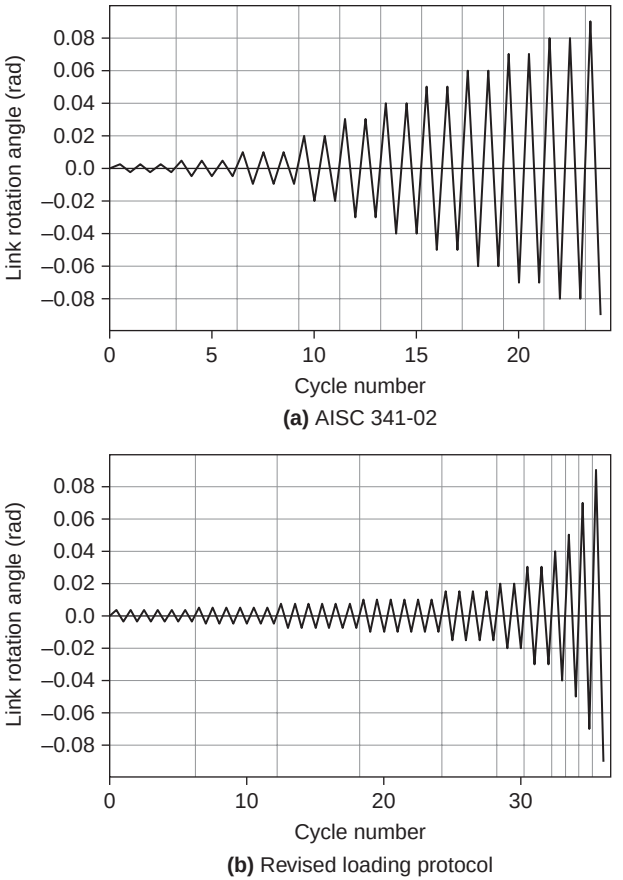

Figure 10.15 AISC link test loading sequence. (*Richards and Uang 2006.*)

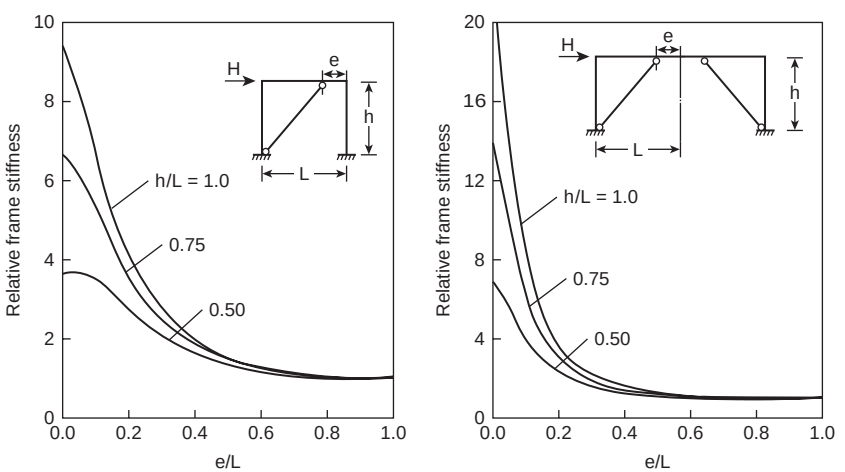

Figure 10.16 Variations of lateral stiffness with respect to *e/L* for two simple EBFs. (*Hjelmstad and Popov 1994, with permission from EERC, University of California, Berkeley.*)

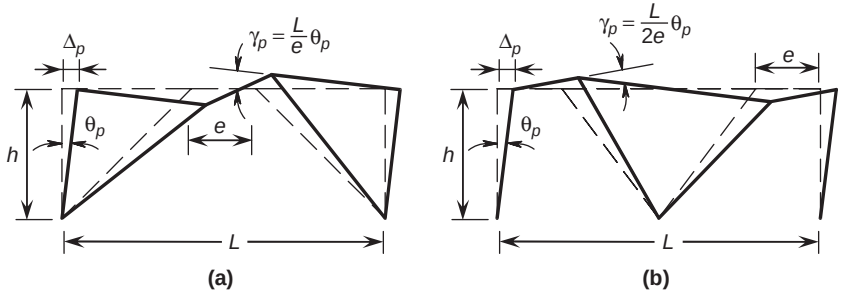

Figure 10.17 Link rotation demand.

the elastic component of the total drift angle is generally small, the plastic story drift angle, θ_p, can be conservatively estimated as the total story drift divided by the story height, h:

$$\theta_p \approx \frac{\Delta_s}{h} = \frac{C_d \Delta_e}{h} \tag{10.12}$$

where Δ_e is the story drift produced by the prescribed design earthquake force, and C_d (= 4) is the deflection amplification factor. To ensure that the deformation capacity of the link given in Figure 10.11 is not exceeded, Eq. (10.11) leads to a lower limit on the link length. Note that the kink that forms between the link and the beam outside the link also implies damage of the concrete slab at the ends of the link.

10.3.3 Plastic Analysis and Ultimate Frame Strength

Unless architectural considerations dictate otherwise, a short link is usually used so that the link will yield primarily in shear and forms a shear plastic hinge. The lateral strength of the EBF then can be calculated conveniently using simple plastic theory. Assuming that the link behaves in an elastic-perfectly plastic manner, the lateral strength, P_u, of the simple one-story split V-shaped EBF frame can be computed by equating the external work to the internal work:

$$W_E = P_u(h\theta_p) \tag{10.13a}$$

$$W_I = \int_0^e V_p \gamma_p dx = eV_p\gamma_p \tag{10.13b}$$

where V_p is the shear strength of the link. Substituting Eq. (10.11) into Eq. (10.13b), the resulting ultimate strength of the EBF frame is

$$P_u = \frac{V_p L}{h} \tag{10.14}$$

As long as the link yields in shear, the above equation shows that the ultimate strength is independent of the link length.

The simple plastic theory can also be applied to multistory frames (Kasai and Popov 1985). For example, consider the three-story EBF shown in Figure 10.3b. Assume a lateral load pattern with the applied load at the *i*-th floor designed as P_i. The span of the frame is L, and the height from the base to each floor is h_i. With the assumed yield mechanism, the scale load factor, α, producing the yield mechanism can be computed by equating the external and interior works.

$$W_E = \sum_{i=1}^{3} \alpha P_i h_i \theta_p \tag{10.15a}$$

$$W_I = \sum_{i=1}^{3} \int_0^e V_{pi} \gamma_p dx = e\gamma_p \sum_{i=1}^{3} V_{pi} \tag{10.15b}$$

$$\alpha = \frac{e\gamma_p \sum_{i=1}^{3} V_{pi}}{\sum_{i=1}^{3} P_i h_i} \tag{10.16}$$

where V_{pi} is the plastic shear strength of the link at the *i*th floor. The above calculation ignores the gravity load. If a uniformly distributed gravity load is applied to each floor, an additional external work corresponding to the assumed yield mechanism needs to be added to W_E. For the yield mechanism in Figure 10.3a, however, the external work produced by the uniform gravity load is zero due to the symmetry of the frame.

The above examples assume a short link such that a shear plastic hinge in the form of uniform yielding along the length of the link forms. For intermediate and long links, flexure and shear dominate the link strength. The ultimate strength of the frame then decreases with an increase in link length. Figure 10.18 illustrates the strength variations (Kasai and Popov 1985). This figure also indicates that the ultimate strength of an EBF with short links is significantly larger than that of a moment frame (i.e., $e/L = 1.0$).

Note from the yield mechanisms shown in Figure 10.3 that only one end of each diagonal brace is connected eccentrically to the beam to create a yielding link (the so-called active link), whereas the other end of the brace is concentrically, or in practice sometimes nearly concentrically, connected to the beam and column centerlines. Next consider two EBF configurations in Figure 10.19. Case (a) contains three active links. In Case (b), however, the braces are connected to the beams eccentrically at both the top and bottom ends. It appears at first glance that the latter case is desirable as it contains more links. But it has been shown that not all the links are fully effective (Kasai

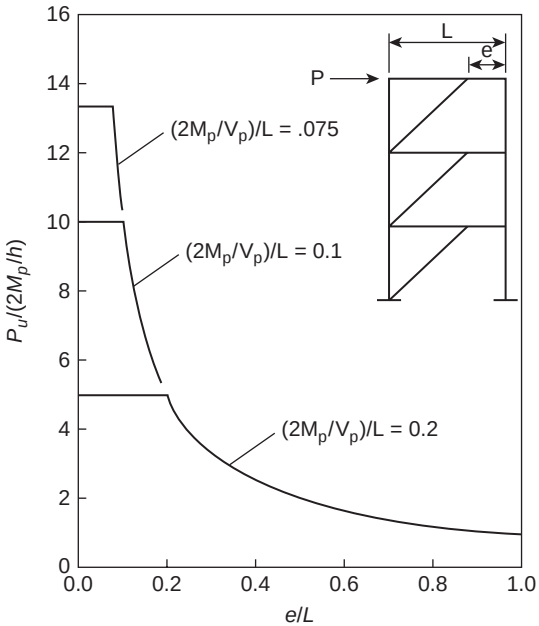

Figure 10.18 Variations of EBF ultimate strength with *e/L*. (*Kasai and Popov 1985, with permission from EERC, University of California, Berkeley.*)

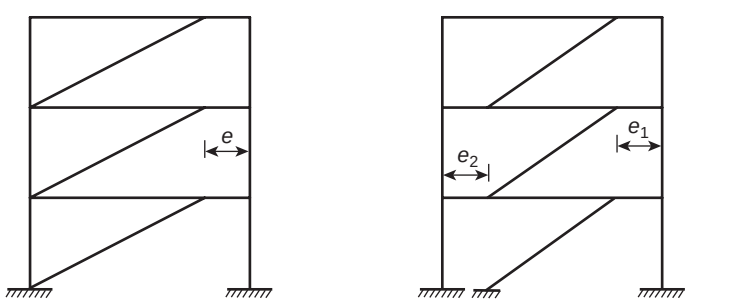

(a) EBF with active links **(b)** EBF with active and inactive links

Figure 10.19 EBF configurations with active and inactive links.

and Popov 1985). If the upper link has design shear strength significantly lower than that of the link in the story below, the upper link will deform inelastically and limit the force that can be developed in the brace and to the lower link. Under such circumstances, the upper link is called an active link and the bottom link is called an inactive link. Because it is difficult to design all links to be active and all the links need to be detailed and fabricated as if they are active anyway, EBF configurations that contain inactive links are not economical and are not recommended.

10.4 Ductility Design

10.4.1 Sizing of Links

Links in an EBF are designated as structural fuses and are sized for code-specified design seismic forces. So the member sizes are to be selected based on the basic seismic load combinations. It is highly desirable that the actual web area is equal to the required web area, or, if not possible, only slightly larger. In AISC 341-02, the I-shaped link sections need to be seismically compact, i.e., the width-thicknesses for both flange and web local buckling limit states need to satisfy the requirement of highly ductile members. But the stringent flange local buckling requirement ($b_f/2t_f \le 0.30\sqrt{E/F_y}$) often requires a heavier section with a larger web area. Overdesigning links is not desirable from the capacity design point of view because it has a direct impact on the design of braces, columns, and beams outside the links. Because the moments at the ends of a shear link are not expected to be high, based on both analytical study (Richards and Uang 2005) and experimental verification (Okazaki et al. 2005), the limit of $b_f/2t_f$ has been relaxed from $0.30\sqrt{E/F_y}$ to $0.38\sqrt{E/F_y}$.

The required link rotation as computed from Eq. (10.11) also cannot be larger than the allowable rotation capacity (see Figure 10.11).

10.4.2 Link Detailing

10.4.2.1 I-Shaped Links

Full-depth web stiffeners must be placed symmetrically on both sides of the link web at the diagonal brace ends of the link. These end stiffeners are required to have a combined width not less than $(b_f - 2t_w)$ and a thickness not less than $0.75t_w$ or 3/8 in, whichever is larger. The origin of this thickness requirement is described in Section 10.4.2.3.

The link needs to be stiffened in order to delay the onset of web buckling and to prevent flange local buckling. The stiffening requirement is dependent on the length of link. For a shear link with $e \le 1.6M_p/V_p$, a relationship among the link web deformation angle, γ_p, the web panel aspect ratio as well as the beam web slenderness ratio was developed (Kasai and Popov 1986a). Based on Eq. (10.6), the link stiffener spacing can be rewritten as follows:

$$a = C_B t_w - \frac{d}{5} \tag{10.17}$$

These C_B values were slightly modified and adopted in AISC 341 as follows:

(1) When $e \le 1.6M_p/V_p$, intermediate stiffeners are needed per Eq. (10.17), but the coefficient C_B is a function of the

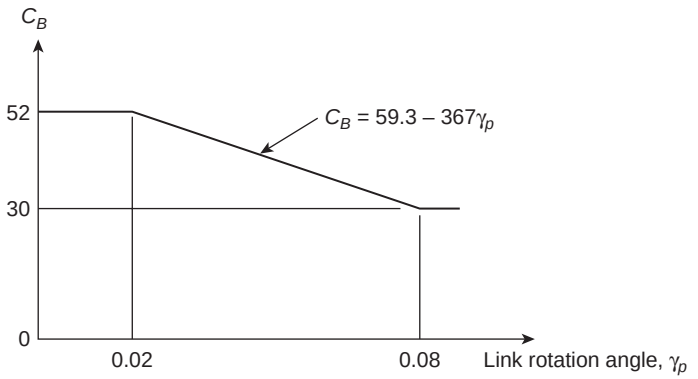

Figure 10.20 Variation of C_B.

deformation demand; the relationship between C_B and γ_p implied by AISC 341 is shown in Figure 10.20.

(2) When $2.6M_p/V_p \le e \le 5M_p/V_p$, intermediate stiffeners shall be provided at a distance $1.5b_f$ from each end of the link to control flange local buckling.

(3) When $1.6M_p/V_p \le e \le 2.6M_p/V_p$, intermediate stiffeners satisfying the requirements of both Cases 1 and 2 are needed.

(4) When $e > 5M_p/V_p$, intermediate stiffeners are not required.

Intermediate link web stiffeners must be of full depth. Although two-sided stiffeners are required at the end of the link where the diagonal brace intersects the link, intermediate stiffeners placed on one side of the link web are sufficient for links of depth less than 25 in. In links of depth less than 25 in the thickness of one-sided stiffeners is specified to be no less than t_w or 3/8 in (10 mm), whichever is larger. Fillet welds connecting a link stiffener to the link web shall have design strength to resist a force of $A_{st}F_y$, where A_{st} is the stiffener area. The design strength of fillet welds fastening the stiffener to the flanges shall be adequate to resist a force of $A_{st}F_y/4$.

In the testing of large-size built-up shear links, brittle fracture in the web was observed (McDaniel et al. 2003). The fracture initiated from a flange-web-intermediate stiffener junction where the region was highly restrained due to welding. An analysis of the failure showed that the cause was a stress concentration at the end of the stiffener vertical welds because the stiffener was terminated too close to the flange-to-web groove weld. It was recommended that the stiffener vertical welds be terminated from the flange-to-web weld by a minimum distance of $3t_w$. In another testing program, fracture in the web initiating from the ends of stiffener vertical welds was also

observed (Figure 10.14). To delay the onset of link web fracture, Okazaki et al. (2005) suggested that the stiffener welds be terminated a distance of $5t_w$ from the k-line in the rolled section.

10.4.2.2 Built-Up Box Links

When eccentrically braced frames are desirable in locations where lateral bracing of the link cannot be achieved (such as between two elevator cores, or along the facade of building atriums), links with built-up box sections could be used, as such built-up box cross-sections are not susceptible to lateral-torsional buckling. Eccentrically braced frames having such links and without lateral bracing of the link beam performed in a ductile manner during experiments, provided the specified section compactness requirements were met (Berman and Bruneau 2007, 2008a, 2008b). Note that HSS sections cannot be used for such links, due to concerns about their low cycle fatigue life under large inelastic deformations (see Chapter 9).

However, recognizing that extremely tall and narrow boxes can experience lateral-torsional buckling (i.e., buckle about their weak axis), design provisions require that the links of built-up box sections be sized such that $I_y > 0.67I_x$, where I_y is the link's moment of inertia about an axis in the plane of the EBF, and I_x is the moment of inertia about an axis perpendicular to that plane. Furthermore, simultaneously with the other forces acting on the link beams, a lateral load acting at the brace-to-beam points and perpendicularly to the frame plane must be considered conservatively, together with a corresponding out-of-plane stiffness requirement, to further prevent weak or laterally flexible link as well as to ensure adequate lateral restraint to the brace.

Berman and Bruneau (2005) derived relationships setting the maximum spacing of stiffeners for shear yielding links (i.e., $e \le 1.6M_p/V_p$) of built-up box sections as $20t_w - (d - 2t_f)/8$ to develop a link rotation angle of 0.08 rad, and $37t_w - (d - 2t_f)/8$ for a corresponding 0.02 rad limit. However, as experimental and finite element simulations only validated the closer stiffener spacing required for the 0.08 rad link rotation angle; that value is required for all links until further data becomes available.

Berman and Bruneau (2006, 2007, 2008a) showed the importance of providing intermediate web stiffeners for shear yielding built-up box section links with h/t_w greater than $0.64\sqrt{E/F_y}$ and less than or equal to $1.67\sqrt{E/F_y}$. For shear links with h/t_w less than or equal to $0.64\sqrt{E/F_y}$, intermediate web stiffeners are not required because they have no effect on flange buckling (which is the controlling limit state in that case). Nor are they required for links of lengths exceeding $1.6M_p/V_p$, because local buckling of both webs and flanges in flexure dominates link strength degradation in that instance; for that reason, the width-to-thickness of web and flanges in those long links is limited to $0.64\sqrt{E/F_y}$.

External intermediate stiffeners, as in Figure 10.21, were considered in the experimental and analytical work of Berman and Bruneau (2006, 2008a, 2008b); these were welded to both the webs and the flanges. However, because such stiffeners have no benefit on flange buckling, AISC 341 and CSA S16 do not require them to be connected to the flange. This suggests that intermediate stiffeners could be fabricated inside the built-up box section (which may be desirable for

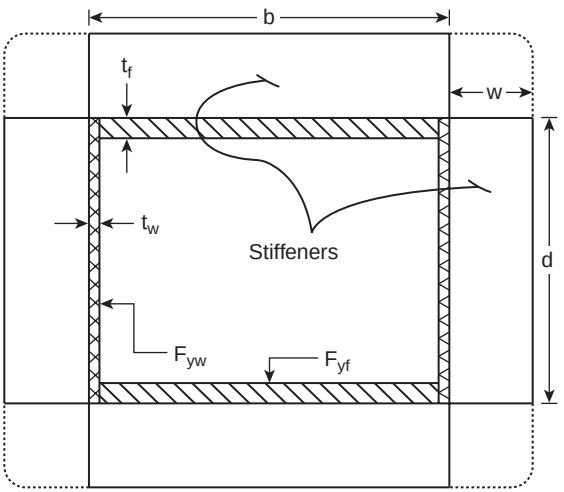

(a)

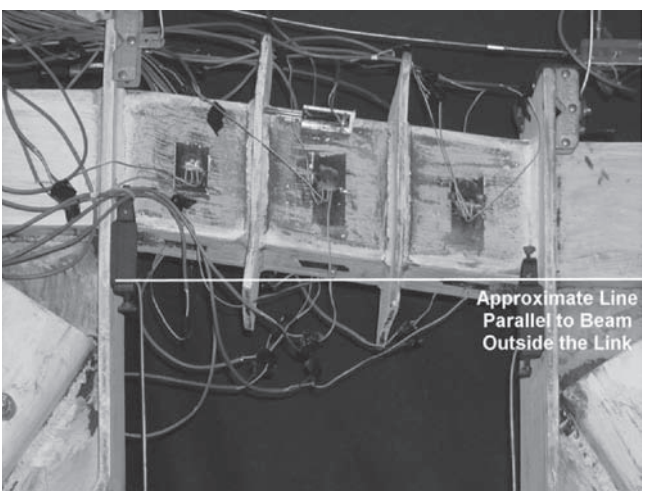

(b)

Figure 10.21 (a) Generic built-up box cross-section with exterior stiffeners; (b) deformed Link at 0.123 rads rotation. (*Berman and Bruneau 2005; Courtesy of MCEER, University at Buffalo.*)

architectural appeal or other reasons). Note that equations prescribing the minimum required areas and inertia for intermediate stiffeners for I-shaped sections have been derived without considering connection to the flanges (Bleich 1952, Malley and Popov 1984, Salmon et al. 2009), but web stiffeners were found to provide stability to the flanges in I-shaped links (Malley and Popov 1984); this is not the case in built-up box cross-sections.

Finally, for capacity design purposes, note that tested built-up box cross-section links (Berman and Bruneau 2005) have strain hardened 11% more in strength than wide flange links (Richards 2004); correspondingly, braces, beams (outside the link), and columns must be designed for such proportionally larger forces.

10.4.2.3 Origin of Code Specified Stiffener Thickness Requirements

The axial force in intermediate stiffeners was obtained by Malley and Popov (1984) from a free-body diagram considering a diagonal tension field developing in the beam's web. Setting this force to $A_{st}F_{yst}$, and solving for A_{st}, conservatively assuming that a one-sided intermediate web stiffener carries that entire force alone, gives

$$A_{st} = \frac{F_{uw}t_w a}{0.828F_{yst}}\left[1 - \frac{a/h}{\sqrt{1+(a/h)^2}}\right] \tag{10.18}$$

where A_{st} = minimum cross-sectional area of one stiffener, F_{uw} = specified minimum tensile strength of link web, t_w = thickness of one link web, h = clear height of link web, a = spacing of intermediate web stiffeners, and F_{yst} = specified minimum yield strength of stiffener. A slightly more liberal value is obtained if accounting for part of the beam web to work together with the stiffener to resist the axial force. Malley and Popov suggested a contributing beam web area of $t_w b_f/2$. For comparison, ANSI/AISC 360-05 assumed $18t_w^2$ for stiffeners; note that requirements for A_{st} were eliminated in AISC 360-10.

Malley and Popov (1984) also suggested a required minimum inertia of intermediate stiffeners. Starting from the equation derived by Bleich (1952) for plates with simply supported edges free to rotate (adopted in AISC 360), the required stiffness for intermediate stiffeners is

$$I_{st} \geq jat_w^3 \tag{10.19}$$

where

$$j \geq \frac{2.5}{(a/h)^2} - 2.0 > 0.5 \tag{10.20}$$

Malley and Popov suggested using an alternative equation for plates with edges fixed against rotation, and conservatively magnifying the requirements from this equation by 4 to arbitrarily keeping the stiffeners straight in the postbuckling inelastic range.

$$j \geq \frac{5.9}{(a/h)^2} - 2.9 \tag{10.21}$$

An example in Malley and Popov (1984) showed that, for a ratio (h/a) of 1.9, a 0.412-inch-thick intermediate stiffener would have been required for a W18 × 50 shear link (which was then rounded up to ½-inch accounting for available plate thicknesses). For the same W18 × 50 shear link, for a ratio (h/a) of 3 (i.e., approximately 50% more closely spaced stiffeners), a 0.72-inch-thick stiffener would be required per Malley and Popov's equation. The corresponding stiffener thicknesses for this same W18 × 50 example, but calculated instead per the AISC 360-05 equation, would be 0.16 in and 0.3 in, respectively, for the two different stiffener spacing considered above. Note that the requirement for thicker stiffeners at closer spacing is a consequence of the assumptions used in the derivation of this equation, namely, that transverse stiffeners be rigid enough to cause a buckling node to form along the line of the stiffener, irrespective of whether or not a tension field action is expected.

Implementation in AISC 341-10 led to the simplified requirements outlined in Section 10.4.2.1, combined with the AISC 360 requirements for standard design. Application of these AISC requirements would result in the use of a 0.375 in stiffener for the above W18 × 50 shear link example, which is significantly less than required by the Malley and Popov equation, irrespectively of stiffener spacing. Nonetheless, EBFs detailed per the AISC 341 (with 3/8-inch-thick stiffeners) have performed well in the past, suggesting that the Malley and Popov equations for sizing intermediate stiffener are too conservative.

10.4.3 Lateral Bracing of Link

To ensure stable hysteresis, an I-shaped link must be laterally braced at each end to avoid out-of-plane twisting (Hjelmstad and Lee 1989, Engelhardt and Popov 1992). Lateral bracing also stabilizes the eccentric bracing and the beam segment outside the link. The concrete slab alone cannot be relied upon to provide lateral bracing (Ricles and Popov 1989). Therefore, AISC 341 requires that both top and bottom flanges of the I-shaped link beam be braced at link ends. Bracing should have an available strength and stiffness as required for expected plastic hinge locations for highly ductile members. Lateral bracing at link ends is not required for box link due to its inherent torsional rigidity. But the moment of inertia, I_y, about an axis in the plane of the EBF shall be larger than $0.67I_x$.

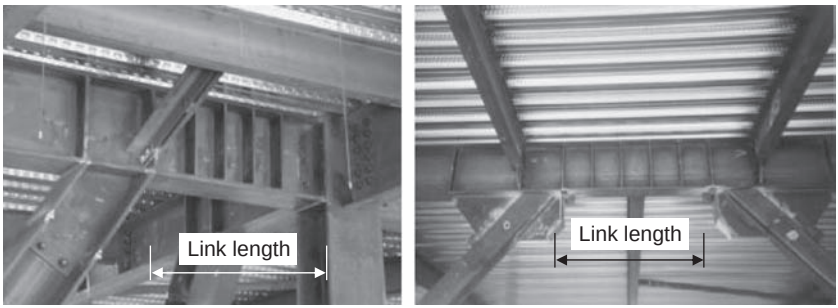

(a) Exterior link **(b)** Interior link

FIGURE 10.22 Lateral bracing of links.

Figure 10.22 shows two examples of the link lateral bracing; the link length, e, is also shown. Because AISC 341 specifies that lateral bracing be placed at the ends of the link, to be effective the two lateral bracings in Figure 10.22b should be placed further inward.

10.5 Capacity Design of Other Structural Components

10.5.1 General

Figure 10.23 shows the typical internal force distribution of the link, brace, and beam outside the link of two popular EBF configurations. The nominal shear strength of the link, V_n, is determined as follows:

$$V_n = \min\left\{V_p, \frac{2M_p}{e}\right\} \tag{10.22}$$

All other elements (beam segments outside the link, braces, columns, and connections) are then designed for the forces generated by the actual (i.e., expected) capacity of the links rather than the code-specified design seismic forces. That is, these elements are to be designed to resist the loads developed by the fully yielded and strain-hardened links. The capacity design concept requires that the computation of the link strength not only be based on the expected yield stress of the steel but also includes the consideration of strain hardening. The link shear strength is adjusted upward first by the material overstrength factor, R_y, and then by a cyclic hardening factor, ω:

$$V_l = \omega(R_y V_n) \tag{10.23}$$

The value of ω, to be explained below, varies with the member type.

10.5.2 Internal Force Distribution

When a yield mechanism is formed, the EBF no longer responds in the elastic range and the internal force distribution like that shown in Figure 10.23 cannot be obtained from an elastic analysis. With the adjusted link shear strength, V_l, known, however, it is possible to establish the internal seismic forces by hand calculations. A procedure to calculate the internal forces for the EBF frame in Figure 10.23a is summarized below.

(1) Drawn the free-body diagrams (see Figure 10.24).

(2) The link bends in reverse curvature. Assuming the inflection point is at midspan, the link end moment is

$$M_l = \left(\frac{e}{2}\right) V_l \tag{10.24}$$

where V_l is the adjusted link shear strength.

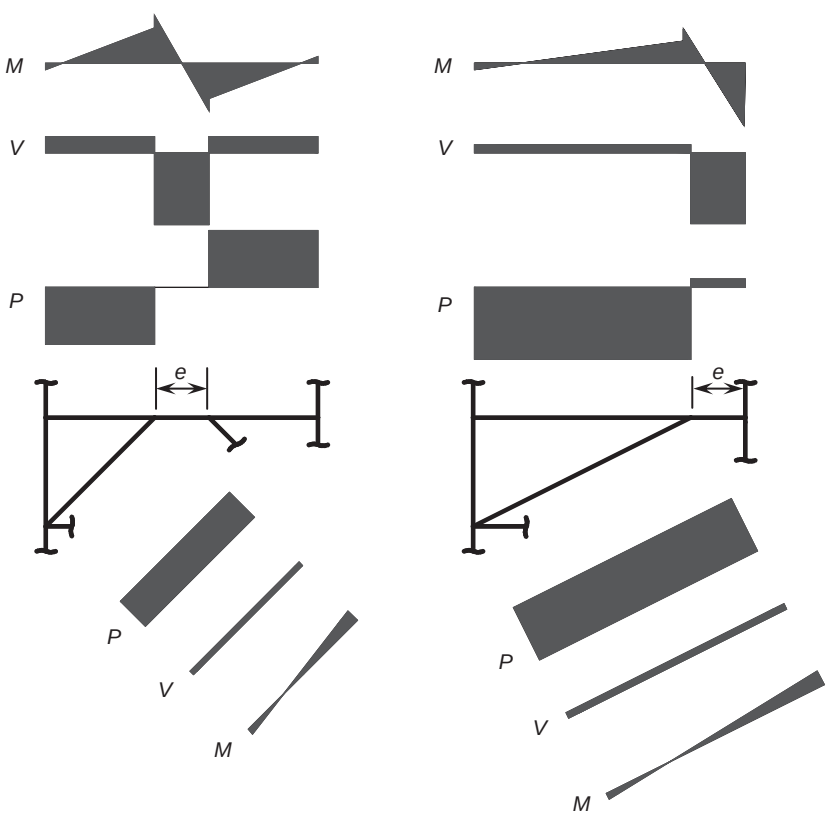

Figure 10.23 Typical internal force distributions.

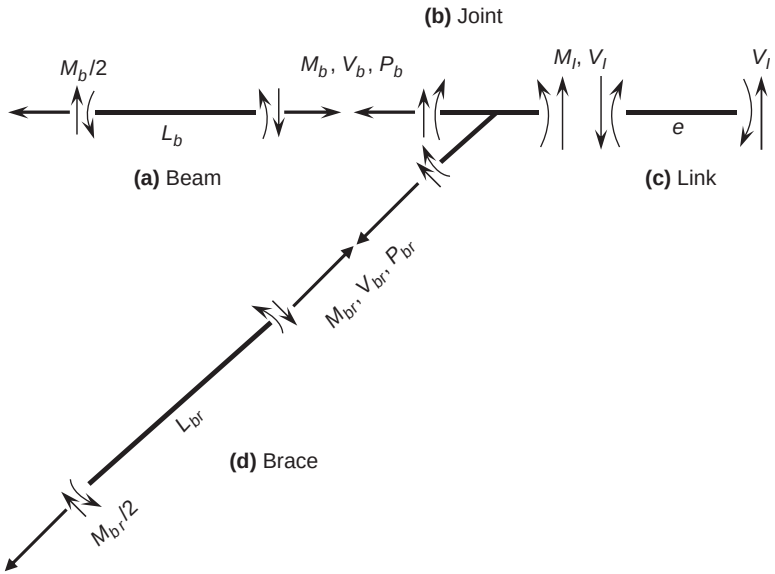

Figure 10.24 Free-body diagrams of link, beam, joint, and brace.

(3) Referring to the joint free-body diagram in Figure 10.24b, the link end moment is resisted by the beam and the brace. The distribution to each member is based on the relative flexural stiffness. When the far-end connections of both the beam and brace are fully restrained, the end moments in the beam and brace are

$$M_b = \left(\frac{I_b / L_b}{I_b / L_b + I_{br} / L_{br}} \right) M_l \tag{10.25a}$$

$$M_{br} = \left(\frac{I_{br} / L_{br}}{I_b / L_b + I_{br} / L_{br}} \right) M_l \tag{10.25b}$$

Half of the beam end moment is carried over to the other end. The beam shear, V_b, then can be calculated by statics:

$$V_b = \frac{1.5 M_b}{L} \tag{10.26}$$

(4) Consider the vertical equilibrium of the joint free-body. The link and the beam shear acting on the free-body is mainly balanced by the vertical component of the brace axial force. (The contribution from the brace shear force is usually small and

can be ignored in preliminary design.) Therefore, the brace axial force is

$$P_{br} = \frac{V_l + V_b}{\sin\theta} \tag{10.27}$$

where θ is the inclination angle of the brace. The above equation shows that the ratio of the brace axial force to the link shear force is controlled primarily by the geometry of the EBF and is not affected by link yielding.

(5) Consider the horizontal equilibrium of the joint free-body. The horizontal component of the brace axial force needs to be balanced by the axial force in the beam.

$$P_b = P_{br}\cos\theta = \frac{V_l + V_b}{\tan\theta} \tag{10.28}$$

Thus, the required deign forces in the beam and brace are determined.

10.5.3 Diagonal Braces

Diagonal brace is often connected to the link beam by fully restrained moment connection such that it can participate in resisting a portion of the link moment, thus reducing the moment in the beam outside of the link. In such case, the brace needs to be designed as a beam-column. Equation (10.27) also shows that the brace axial force increases as the inclination angle of the brace is reduced. So it is desirable that the angle be kept above, say, 40°.

For brace design, AISC 341 requires that the cyclic strain-hardening factor, ω, in Eq. (10.23) be taken as 1.25 for I-shaped links and 1.4 for boxed links. Note from Section 10.2.2 that cyclic testing of I-shaped links showed that the cyclic strain-hardening factor can reach 1.4 to 1.5. For economic reasons, however, a lower value of 1.25 was chosen by AISC. The justification follows. First, the material overstrength factor, R_y, for the link is already used in Eq. (10.23) to compute the required seismic force in the brace, yet the material overstrength of the brace is not considered for the calculation of its design strength. In fact, a resistance factor, ϕ, is used to compute the brace deign strength. When the effect of both material overstrength (conservatively taken as 1.1) and resistance factor (= 0.9) are considered, the effective cyclic strain-hardening factor would have been 1.53 (= 1.1/0.8 × 1.25), which matches well with the AISC implicitly assumed ω value of 1.5. In situations where a much significant strain hardening would occur (e.g., when built-up I-shaped links with thick flanges are used), it is prudent to use a larger ω value.

Because diagonal braces in an EBF are designed to remain elastic while allowing the links to deform inelastically, many of

the ductility-related design provisions for braces in the SCBF system intended to permit stable cyclic buckling of braces are not needed in EBF. But AISC 341 still requires the braces to be treated as moderately ductile members for the section compactness requirement.

10.5.4 Beams Outside of Link

For all except Case (d) in Figure 10.1, the beam segment and the link are a single continuous wide flange or built-up box member. For Cases (a) and (b), the beam(s) outside the link is subjected to both high moment and high axial force (see Figure 10.23). Therefore, these beams need to be designed as a beam-column. Designing these beams is challenging in EBF design, so it is desirable to reduce both moment and axial force demand in the beam. To reduce the beam end moment, a short link can be used to reduce e in Eq. (10.24). Connecting the brace to the link beam by fully restrained moment connection also helps [Eq. (10.25a)]. To limit the beam axial force to a manageable level, the inclination angle of the brace should not be too small [Eq. (10.28)].

Because experience shows that design of the beam segment outside of the link can be problematic, to facilitate EBF design AISC 341 specifies an even lower ω value (= 1.1) for beam design; this value is 88% of the value (= 1.25) used for brace design. This relaxation is justified because, first of all, testing showed that limited yielding in the beam will not be detrimental to EBF performance, as long as stability of the beam is assured (Engelhardt and Popov 1989). Furthermore, it is assumed that the composite floor slab, which is generally ignored in computing the beam strength, will also participate in resisting the bending moment and axial force. With this background information in mind, the designer is cautioned to use a larger ω value in situations such as when the floor slab is not present or when built-up I-shaped links are used. Because AISC 341 implicitly assumes that the beam may experience limited yielding, beams should satisfy the width-thickness limitations for moderately ductile members.

To further facilitate the design of beams outside of the link when, as shown in Figure 10.1 with the exception of Case (d), a single continuous member is used for both the link and the beam at each floor level. AISC 341 allows the engineer to use the expected yield stress, R_yF_y, to compute the beam design strength. This is because any increase in yield strength in the link is also present in the beam segment.

Based on the discussion presented so far, it is obvious that the beam required design force and the link design strength are highly coupled when the same member is used for both the link and the beam segment, Figure 10.1d shows one exception when the links are oriented vertically. In this case the beam strength has to be based on F_y, not R_yF_y. This configuration is attractive when it is desirable that

the gravity load-carrying capacity of the entire beam is not impaired by the yielding or buckling of the link (Fehling et al. 1992). This type of EBF configuration has also been shown to be effective for the seismic rehabilitation of not only steel but also reinforced concrete frames (Perera et al. 2004).

Because high axial force in the beam tends to cause difficulty in beam design, one way to bypass this problem is to use an EBF configuration like that shown in Figure 10.1e. In this case, the lateral loads are mainly transmitted downward to the base through the diagonal braces (Engelhardt and Popov 1989). But because the links do not exist in every floor, larger link sections are needed, and the redundancy for seismic resistance is also reduced.

10.5.5 Columns

Using a capacity design approach, columns in braced bays must have a sufficient strength to resist the sum of gravity-load actions and the moments and axial forces generated by the adjusted shear strength of the link. This procedure assumes that all links will yield and reach their maximum strengths simultaneously. Nevertheless, available multistory EBF test results showed that this preferred yielding mechanism is difficult to develop. For example, shaking table testing of a reduced-scale, six-story EBF building showed that links in the bottom two stories dissipated most of the energy (Whittaker et al. 1989). Therefore, this design procedure may be appropriate for low-rise buildings and the upper stories of medium- and high-rise buildings but may be too conservative in other instances. For this reason, AISC 341 allows the columns to be designed for a seismic effect corresponding to that when all the links reach the adjusted link strength [Eq. (10.23)] with ω equal to 1.1 ($= 0.88 \times 1.25$). But an ω value of 1.25 still needs to be used when the number of stories is less than 3. Column members should also satisfy the width-thickness limitations for highly ductile members.

10.5.6 Connections

10.5.6.1 Diagonal Brace Connections

It was shown in Chapter 9 that diagonal brace connections in an SCBF need to be designed for the expected tensile and compressive strengths of the brace because the brace serves as the structural fuse. The gusset plate is also detailed to accommodate inelastic rotation due to brace buckling. Nevertheless, these stringent requirements are not needed for brace connections in an EBF because links, not braces, are structural fuses. The brace connection only needs to be designed for the same forces as the brace.

Figure 10.25a shows the detail of a diagonal brace-to-beam connection used in a full-scale, six-story EBF building tested at BRI, Japan

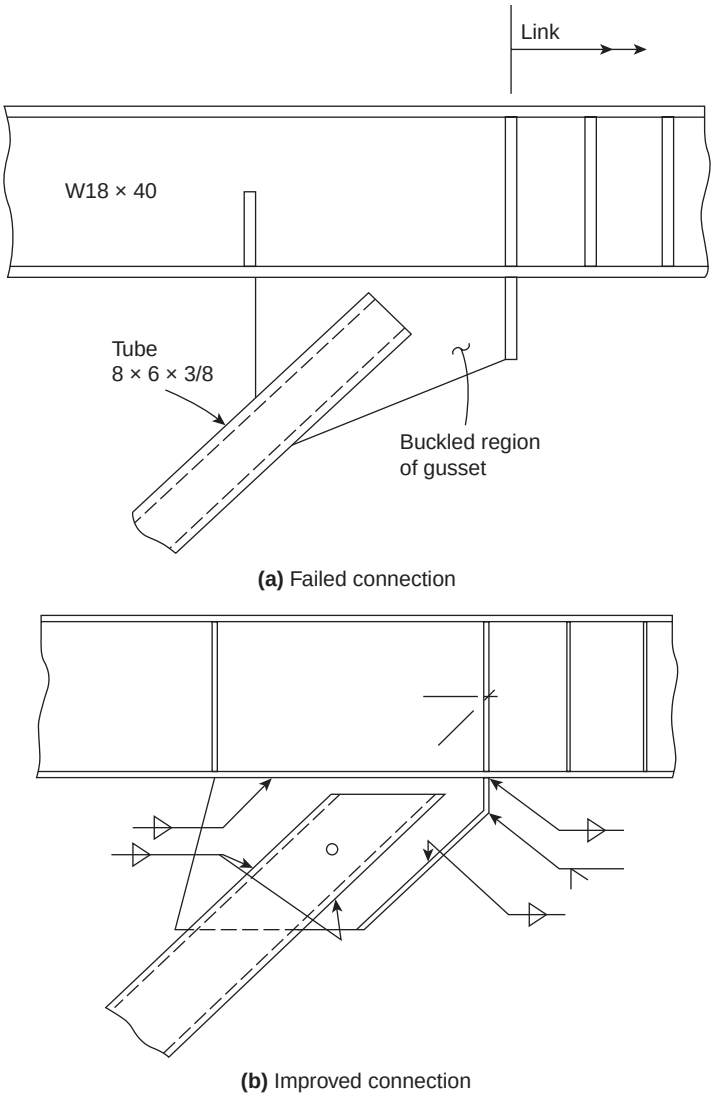

Figure 10.25 Brace-to-beam gusset connection. (*Courtesy of M.D. Engelhardt, Dept. of Civil Engineering, University of Texas, Austin.*)

(Roeder et al. 1987). The gusset plate buckled when the link end was subjected to a large negative bending moment. An improved detail in Figure 10.25b shows that not only the free edge of the gusset is stiffened but also the brace end is extended further toward the beam (Engelhardt and Popov 1989). See Figure 10.22b for one example in real application.

Fully restrained moment connection is needed if the diagonal brace is designed to carry a portion of the link end moment. Complete-joint-penetration groove welds, especially in the brace flanges, are generally used. Figure 10.22a shows one such example; note the designer opted to shop weld the brace-to-beam connection to avoid overhead welding in the field, and the brace was field spliced.

The design of beam-to-column connection for the end of the brace opposite the link is the same as that of SCBF.

10.5.6.2 Link-to-Column Connections

When an EBF configuration with exterior links is used, fully restrained moment connections are needed to connect the link to the column. Based on cyclic testing of pre-Northridge style I-shaped link-to-column moment connections conducted before 1994 (Malley and Popov 1984, Engelhardt and Popov 1989), it was observed that a fully welded moment-resisting connection with complete-joint-penetration groove welds in the flanges and a web connection capable of developing a shear capacity of the link performed better than a similar connection but with a bolted web connection where bolt slippage could occur. As shown in the next paragraph, however, the former connection detail is still not reliable based on testing conducted after 1994. The performance was even inferior when the link was connected to the weak-axis of the W-shaped column. A similar problem also exists when the I-shaped link is connected to a built-up box column (Tsai and Young 1991).

Okazaki et al. (2006) explored the potential of using four types of link-to-column connections with improved welds and details originally developed for post-Northridge SMF moment connections. Cyclic testing showed that the majority of test specimens, including those with welded flange-weld web connections, failed by fracture of the link flanges near the groove welds. The performance depended strongly on the link length, with the inelastic link rotation capacity decreasing significantly with an increase in the link length. Because the test results suggested that premature failure of the link flange is a concern for both short and longer links, one option that is permitted by AISC 341 is to reinforce the link near the column end. See Figure 10.26 for one example that utilizes a welded haunch; the corresponding length of the link is also shown.

Although AISC does not provide any prequalified link-to-column moment connections to date, further study by Okazaki et al. (2009) showed two promising connection details. The first one, which is suitable for shop welding and column-tree type of erection procedure, involves the use of all-around fillet welds to connect the link flanges and web to the column. See Figure 10.27 for the detail. It is suggested that the size of the fillet weld be equal to 1.5 times the thickness of the link flange or web. To avoid introducing undercuts or weld defects at the link-flange edges, which are a common location

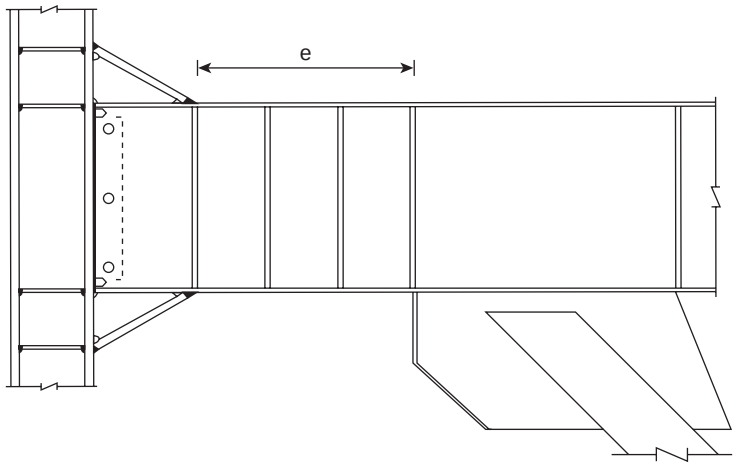

Figure 10.26 Example of reinforced link-to-column connection. (*Copyright © American Institute of Steel Construction. Reprinted with permission. All rights reserved.*)

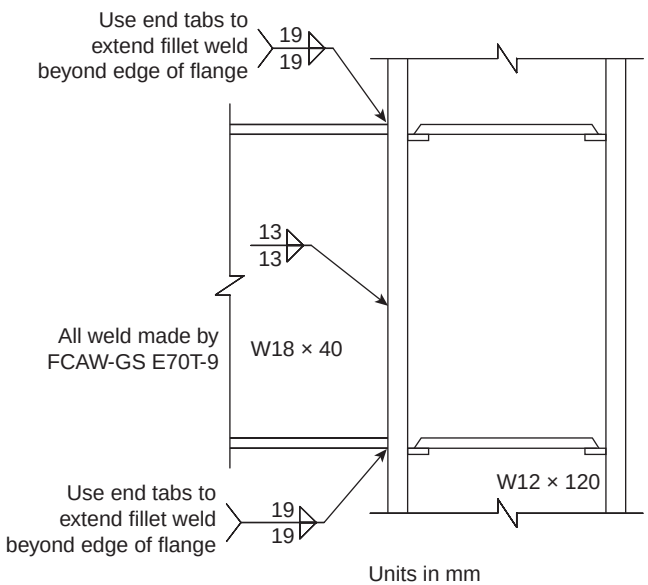

Figure 10.27 All-around fillet welded link-to-column connection. (*Courtesy of M.D. Engelhardt, Dept. of Civil Engineering, University of Texas, Austin.*)

for fracture initiation, it is important to use weld tabs to run-off the fillet welds beyond the edge of the link flange.

The second promising connection type is suitable for field welding and erection procedure, and the detail is shown in Figure 10.28a.

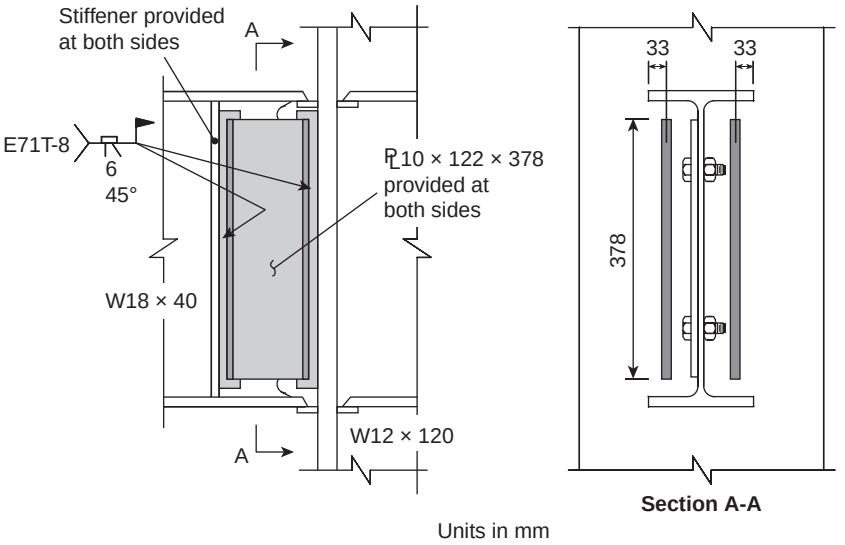

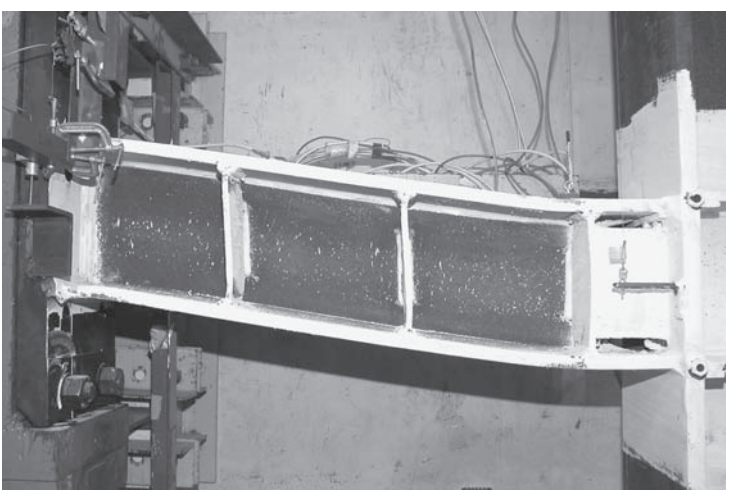

(b)

Figure 10.28 Link-to-column connection reinforced with supplemental web stiffeners. (*Courtesy of M.D. Engelhardt, Dept. of Civil Engineering, University of Texas, Austin.*)

It requires a pair of supplemental stiffeners to reinforce the first link web panel next to the column, with these stiffeners oriented parallel to the link web but offset from the link web but a short distance. To avoid welding to the link flanges, these stiffeners are of partial height. Each stiffener is welded to the column flange and the first link web stiffener by either groove or fillet weld. Figure 10.28b shows that the

reinforcement is effective in preventing fracture at the link-to-column connection. The thickness of the supplemental stiffeners is selected such that the nominal plastic moment of the reinforced segment is larger than the expected link end moment.

When an exterior link is used, an elastic analysis would show that the moment at the column end is generally larger than that at the brace end, i.e., the inflection point is not at the midspan of the link. When the link is not too short, however, end moment equalization would occur due to redistribution of the moments at higher deformation levels, and Eq. (10.24) is still valid (Kasai and Popov 1986b). For link shorter than $1.6M_p/V_p$, the link shear will reach $\omega R_y V_p$, and the following end moments should be assumed in design (AISC 341-10):

$$M_{\text{column end}} = R_y M_p \tag{10.29a}$$

$$M_{\text{brace end}} = e(\omega R_y V_p - R_y M_p) \geq 0.75 R_y M_p \tag{10.29b}$$

where $\omega = 1.25$.

10.6 Design Example

The following section illustrates the design of an eccentrically braced frame. The design applies the requirements of ASCE 7 (2010) and AISC 341 (2010). The example is not intended to be a complete illustration of the application of all design requirements. Rather, it is intended to illustrate key analysis and proportioning techniques that are intended ensure ductile response of the structure.

10.6.1 Building Description and Loading

The example building is nearly identical to the one used in Chapter 8 (Special Moment Frames); more detailed seismicity and building information is included in that example. The difference in this case is that eccentrically braced frames are used and only one bay of braced frames is provided at the perimeter framing lines in each orthogonal direction. The seismic design parameters are shown in Table 10.1.

The typical plan is shown in Figure 10.29 and the typical frame elevation is shown in Figure 10.30.

R	8
I	1.0
C_d	4
Ω_o	2

Table 10.1 Seismic Design Parameters

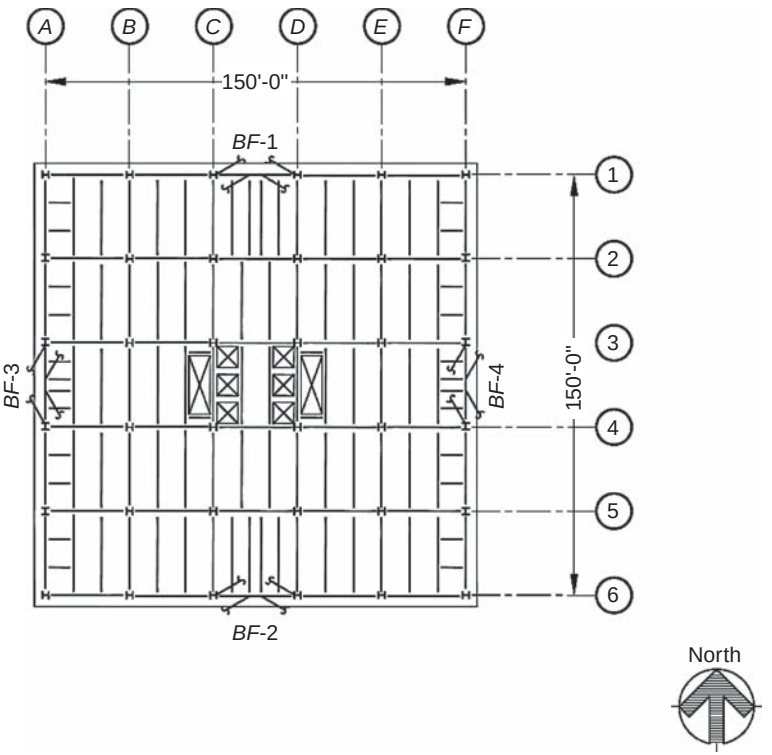

Figure 10.29 Typical floor plan.

Based on the seismic design data a generic seismic response spectrum is constructed in accordance with ASCE 7. Because there is only one braced bay on each side of the structure, the design shear at every story must be multiplied by a redundancy factor ρ equal to 1.3.

10.6.2 Global Requirements

The structure must be designed to provide both adequate strength and adequate stiffness. Typically strength requirements will govern the design of lower buildings, whereas taller buildings will be controlled by drift. The threshold height is dependent on many factors, including the shape of the response spectrum, the analytical procedure used, and the braced bay configurations and proportions.

Where strength considerations govern the design process is fairly straightforward: the braced frames are designed to provide adequate strength, then the columns, braces, and beams outside the link are redesigned to preclude their failure when subjected to the forces corresponding to fully yielded and strain-hardened links. A reanalysis may be performed to confirm that the required brace strength has not

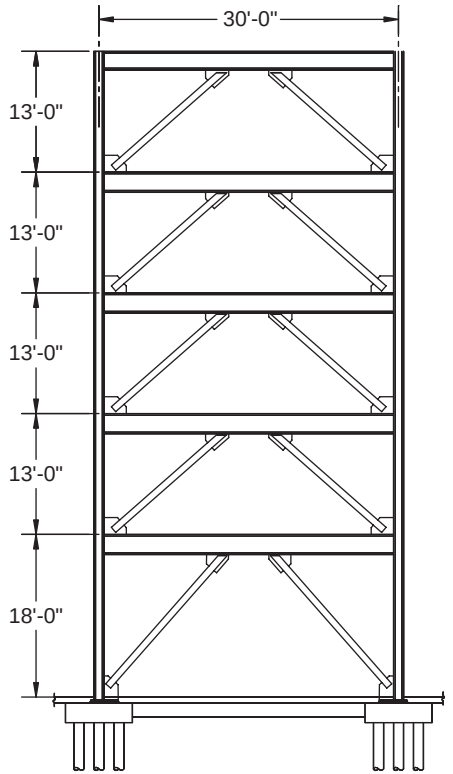

Figure 10.30 Typical frame elevation.

been increased due to an increase in frame stiffness (due to change of period on the response spectra when member forces are obtained from dynamic analysis).

Where drift is the governing concern the process requires more iteration. Any increase in link strength will impose larger forces on beams and columns when the link yields. Thus, any stiffening of the frame should be done with the required strength proportioning in mind.

Link rotation demands are also checked using the design story drift and compared with permissible maxima derived from link testing.

10.6.3 Basis of Design

The design of EBF is based on the expectation of a global yield mechanism in which links yield in shear, flexure, or a combination of the two, and plastic hinges form at the column bases. Where frame beams are connected rigidly to columns, hinging in the beam or column is also anticipated. Otherwise, large rotations must be accommodated in the beam-to-column connections. In this case, pinned beam-to-column connections are used. Figure 10.31 shows this mechanism.

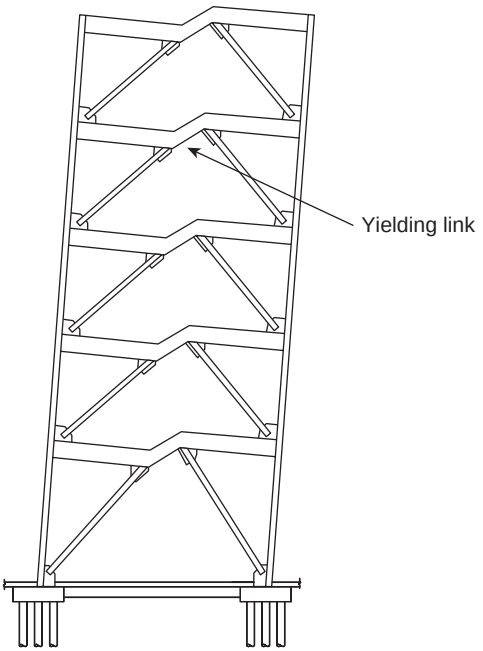

Figure 10.31 Anticipated mechanism.

The value of the link beam shear in this mechanism is adjusted for both material overstrength and strain hardening. For shear-governed, I-shaped links, this quantity is taken as

$$V_{link} = 1.25R_y F_y (0.6A_{lw}) \tag{10.30}$$

where A_{lw} is the area of the web excluding the flanges and V_{link} is the adjusted shear strength of the link, including material overstrength and strain hardening.

10.6.4 Sizing of Links

To start the preliminary design, the following steps are taken:

- Determination of base shear
- Vertical distribution of forces
- Horizontal distribution of forces to frames

These steps are not illustrated in this example.

For preliminary design purposes the frame shear can be assumed to be resisted entirely by the link and braces. Figure 10.32 shows a free-body diagram of half the frame.

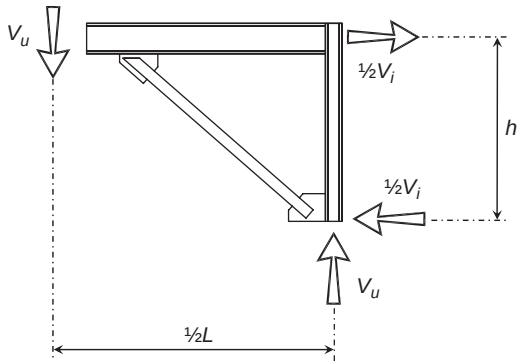

Figure 10.32 Free-body diagram showing link shear and frame shear.

Thus, the link shear in this configuration can be assumed to be

$$V_u = \frac{V_i h}{L} \tag{10.31}$$

where h is the story-to-story height, L is the bay width, and V_i is the shear resisted in the frame at level "i." Required link strengths thus obtained are shown in Table 10.2.

Links may be governed by shear or by flexure. Generally, shear-governed links are more ductile, and the engineer may elect to provide such links. To ensure shear-governed links, link beam sizes are selected based on their plastic shear capacity, and the link length is limited in order to limit the moment that can develop. Thus the link beams will be selected based on their shear strength:

$$\phi(0.6A_{lw}F_y) \geq V_u \tag{10.32}$$

where ϕ is 0.90, A_{lw} is the area of the web excluding flanges, and V_u is the required shear strength of the link. Preliminary link beam sizes are presented in Table 10.3.

Level	Frame Shear (kips)	Required Link Strength (kips)
Roof	201.0	87.1
Fifth Floor	361.4	156.6
Fourth Floor	477.0	206.7
Third Floor	551.5	239.0
Second Floor	589.7	353.8

Table 10.2 Preliminary Required Link Strengths

Level	Beam Size
Roof	W14 × 26
Fifth Floor	W18 × 46
Fourth Floor	W21 × 57
Third Floor	W21 × 73
Second Floor	W27 × 114

Table 10.3 Preliminary Link Beam Sizes

Next, to ensure shear-governed links, the link length is limited based on the ratio of its shear to flexural strength. The theoretical dividing line between shear-governed and flexure-governed links is a length of:

$$e = \frac{2M_p}{V_p} \tag{10.33}$$

where e is the clear link length from edge of connection to edge of connection; M_p is the link flexural strength, ZF_y; and V_p is the link shear strength, $0.6F_y A_w$.

Link lengths in this example are set at three quarters of this limiting value (i.e., $1.5M_p/V_p$). This is a design decision intended to guarantee shear-governed links; other approaches are acceptable. Note that the horizontal distance between the intersections of the brace centerlines (henceforth designated as x) with the beam centerline is not necessarily equal to the eccentricity, e. For preliminary design, it will be taken as equal, and the actual dimension will be substituted after members are selected and the brace-to-beam connection is configured. These link lengths, initially equal to the workpoint-to-workpoint eccentricities, x, are shown in Table 10.4.

Again, selection of such short link lengths ensures a shear-governed link. Thus, link flexure need not be checked. If link axial

Level	Workpoint Eccentricity, x (in)
Roof	30.2
Fifth Floor	37.3
Fourth Floor	40.2
Third Floor	47.9
Second Floor	59.1

Table 10.4 Workpoint Eccentricities

forces exceed 15% of AF_y, both the shear and flexural strengths are reduced and must be compared with the required strengths. In this example link axial forces are low, to the extent that such capacity reductions are not applicable.

Preliminary column and beam sizes can be determined based on the link beam sizes selected. Forces corresponding to the expected strain-hardened link strength are used to calculate maximum axial forces in both the beams and columns. Drift-induced flexural forces in the columns are neglected, as allowed by Section F3.3 of AISC 341. (This would not necessarily be the case for design accomplished per other codes or standards.) This permits a straightforward procedure for deriving design forces. The practical result of neglecting these flexural forces is that some flexural yielding is likely to occur at the design story drift. For this reason, highly ductile members are required for columns and moderately ductile members are required for beams within the eccentrically braced frames.

To derive the column and beam forces the expected strain-hardened link strengths are calculated using Eq. (10.30). The resulting values are presented in Table 10.5.

The mechanism shown in Figure 10.33 results in these forces being generated in the link. An analysis model may be constructed to calculate the corresponding forces in columns, braces, and beams, or free-body diagrams may be used. This example uses the latter approach. This latter approach is reasonable when pin-ended members are used; otherwise, it is somewhat cumbersome and possibly inaccurate to trace the expected strain-hardened link forces through each frame using free-body diagrams alone.

Figure 10.33 shows the model of the anticipated mechanism for the alternate computer analysis model approach.

The free-body diagram method employed in this example is to cut each link at the center, where the moment is taken to be zero, and impose a force there equal to the adjusted link shear strength. Corresponding column, brace, and beam forces are obtained. Figure 10.34 shows a free-body diagram of half the frame at the second floor, and Figure 10.35 shows a free-body diagram of half the beam within that frame along with associated axial shear and moment diagrams.

Level	V_{link} (kips)
Roof	137.4
Fifth Floor	250.8
Fourth Floor	330.8
Third Floor	370.1
Second Floor	598.2

Table 10.5 Adjusted Link Strengths

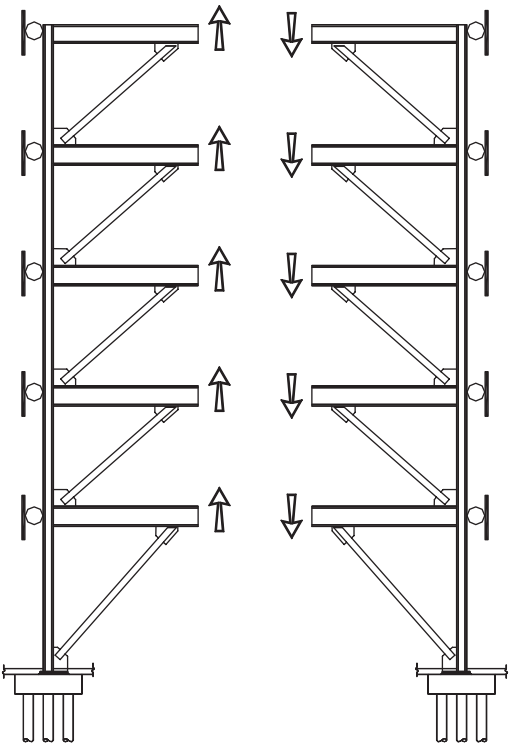

Figure 10.33 Mechanism analysis model.

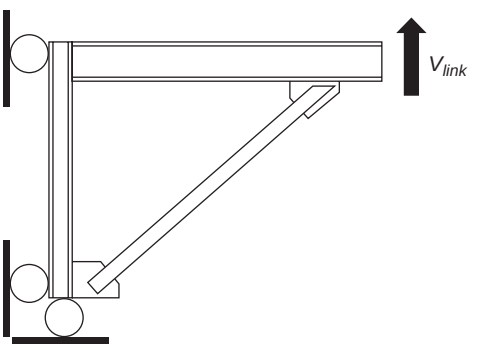

Figure 10.34 Half-frame free-body diagram.

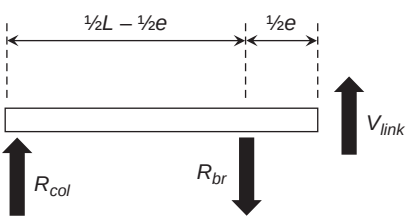

Figure 10.35 Beam free-body diagram.

The vertical seismic force in the brace at each level can be determined from the beam shear diagram, and the brace axial force can then be calculated using simple trigonometry.

$$R_{br} = V_{link}\left(\frac{L}{L-x}\right) = V_{link}\left(1+\frac{x}{2a}\right) \tag{10.34}$$

$$E_{br} = \frac{R_{br}}{\sin\theta} \tag{10.35}$$

where a is the distance from the brace/beam intersection to the column centerline, R_{br} is the vertical force in the brace corresponding to the adjusted link shear strength, E_{br} is the axial design force in the brace due to earthquake load effects, L is length of the braced bay, x is distance between brace centerline intersections with beam centerline (preliminarily taken equal to link length e), and θ is the brace angle from the horizontal.

At the second floor beam the reaction at the first floor braces is:

$$R_{br} = 598.2\left(\frac{360}{360-59.1}\right) = 715.7 \text{ kips}$$

The first floor braces seismic force is:

$$E_{br} = \frac{715.7 \text{ kips}}{\sin(55.1°)} = 872.2 \text{ kips}$$

The brace and its connections are designed to resist these forces in combination with gravity forces prescribed by ASCE 7. Preliminary brace sizes are shown in Table 10.6.

The column force from the link is determined similarly:

$$R_{col} = V_{link}\left(\frac{x}{2a}\right) = V_{link}\left(\frac{x}{L-x}\right) \tag{10.36}$$

Level	Brace Size
Fifth Floor	W14 × 43
Fourth Floor	W14 × 61
Third Floor	W14 × 68
Second Floor	W14 × 74
First Floor	W14 × 109

Table 10.6 Preliminary Brace Sizes

where R_{col} is the beam vertical reaction at the column corresponding to the adjusted link shear strength. Note that this force is directed upward, whereas the reaction at the brace acts downwards.

The first-floor upward force on the column from the second-floor link is:

$$R_{col} = 5.98.2\left(\frac{59.1}{360-59.1}\right) = 117.6 \text{ kips}$$

Simultaneously, the downward column force resulting from the overturning of the levels above is determined from the adjusted link strengths at those levels:

$$P_i = V_{link(i)}$$

Thus, the total first-floor column seismic axial force is:

$$E_1 = \sum_3^{roof} V_{link(i)} - V_{link(2)} \frac{x}{L-x} \tag{10.37}$$

$$E_1 = 137.4 + 250.8 + 330.8 + 370.1 - 117.6 \ = 971.5 \text{ kips}$$

Note that because this column receives force from at least three links, Section F3.3 of AISC 341 permits the seismic force to be reduced using a factor of 0.88 to represent the diminished likelihood of simultaneous strain hardening in the links to the degree assumed by the 1.25 factor. Thus,

$$E_1' = 0.88(971.5) = 854.9 \text{ kips}$$

These earthquake forces are combined with a proportion of the gravity forces using the following load combinations:

$$R_u = (1.2 + 0.2S_{DS})D + 0.5L + E \tag{10.38}$$

$$R_u = (0.9 - 0.2S_{DS})D - E \tag{10.39}$$

In this example the columns are only spliced once, four feet above the third floor. Preliminary column sizes are shown in Table 10.7. These are designed considering only the axial force and using the full story height with $K = 1.0$.

	Size
Upper Column	W14 × 68
Lower Column	W14 × 132

Table 10.7 Preliminary Column Sizes

The beams are in turn checked for the combined axial and flexural forces coming from the link. It is generally advantageous to utilize the brace to resist a portion of the link end moment and thus reduce flexural demands on the beam outside the link. The portion resisted by the brace can be determined based on the relative flexural stiffness of the beam outside the link and the brace (which depends on the moment of inertia, true length, and degree of fixity at the far end of each member), using either hand or computer methods. However, the simplified analysis used in this example does not account for such relief of flexural demands on the beam outside the link by any fixity provided at the brace-to-beam connection.

Figure 10.23 shows the moment and axial force diagrams of the beam. The moment from the link can be calculated as

$$M = V_{link}\frac{x}{2} \tag{10.40}$$

The beam axial force in this configuration is one half of the frame shear V_i at this level. This value can be calculated by rearranging Eq. (10.31) as follows:

$$P = \frac{1}{2}V_i = \frac{1}{2}V_{link}\left(\frac{L}{h}\right) \tag{10.41}$$

Note that AISC 341 permits a reduction from link capacity-based forces by applying a factor of 0.88 to the design forces for the beam outside the link. This factor has a different purpose from that in column design. In beam design, it represents tolerance of some yielding in the beam outside the link, consistent with successful test specimens in both design and observations of behavior.

$$M' = 0.88M = 0.88V_{link}\left(\frac{x}{2}\right) \tag{10.42}$$

$$M' = (0.88)598.2\left(\frac{591}{2}\right) = 15,564 \text{ kip-in}$$

$$P' = 0.88P = (088)\frac{1}{2}V_{link}\left(\frac{L}{h}\right) \tag{10.43}$$

$$P' = (0.88)\frac{1}{2}598.2\left(\frac{360}{216}\right) = 438.65 \text{ kips}$$

These forces are added to the flexural forces due to gravity and the vertical component of seismic load. The beam is checked for the

combined effects of axial and flexural forces, with its axial capacity typically governed by torsional buckling between the orthogonal framing (assuming buckling about the weak axis is precluded by restraint provided by the deck). The second-order P-δ effect of the axial load on the flexural demand on the beam is typically minor (or nil) because of the shape of the moment diagram.

Note that if the beam is inadequate, increasing its size also increases the link strength and thus the demands on the rest of the frame (including the beam outside the link). Alternate strategies to address inadequacy of the beam include

- Local strengthening of the beam outside the link with reinforcing cover plates. Detailing of the force transfer in and out of these plates requires careful attention.
- Reduction of the eccentricity between brace centerline intersections with the beam centerline (this also reduces the link length).
- Using a rigid brace-to-beam connection to draw some of the moment into the brace (see equations in Section 10.5.2).
- Reducing or eliminating the beam axial-force demands through an alternative frame configuration, as done for example with the frame shown in Figure 10.36 (after

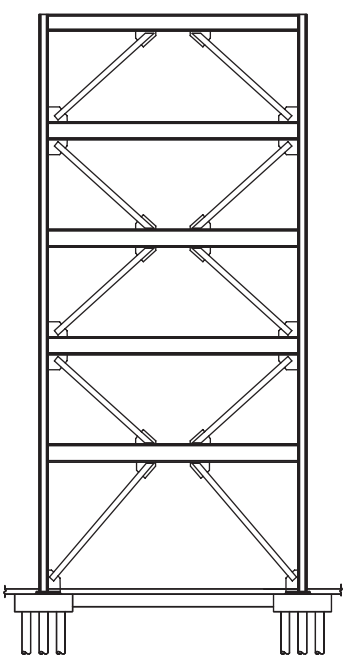

Figure 10.36 Alternate frame configuration.

Engelhardt and Popov 1989). This particular configuration would cause a large increase in link shear at the second and fourth floors, while eliminating links at the third and fifth floor. The axial force demands on the beams outside the links would be reduced dramatically at the second and fourth floors, as all of the frame shear is transferred between braces at different levels entirely within the beam-to-column connections.

Note that in the beam under consideration (for the original frame configuration assumed in this example), the combined effects calculated above using standard *P-M* interaction equations result in an excessive demand on the beam outside the link. Nevertheless, the beam size is not be revised on the basis on the above simple analysis. Instead, to reduce the flexural demand on the beams outside the link, rigidity of the brace-to-beam connections will be taken into account. In other words, a more rigorous analysis will be employed to determine the distribution of link end moment between the beam and the brace. Should the resulting combined flexural and axial demands in the beam outside the link still exceed the member's strength, use of a built-up member with a similar web but heavier flanges would then be the solution.

Using the preliminary member sizes above, a three-dimensional computer model is constructed. A modal response spectrum analysis is performed on this model using the design response spectrum. Interstory drifts are compared with the allowable drift, and the adequacy of the link member sizes is verified.

Optimization is possible at this stage because an analysis may show that some of the frame shear can be carried in the columns, allowing smaller link sizes (relative to those selected on the basis of the preliminary analysis) to be used at some levels. This reduces the resulting mechanism-based forces in beams and columns, and thus the required sizes of those members. Such downsizing is relatively straightforward for the braces and columns, but necessitates much greater attention for the beam when it is the same member as the link (which is typically the case). Reducing the demand on the beam outside the link by changing beam sizes will also reduce its capacity.

Additionally, in this case, the brace-to-beam connection is fixed in order to draw more of the moment from the strain-hardened link into the brace rather than into the beam outside the link. The division of this total moment between the brace and the beam outside the link is determined based on their relative flexural stiffness, and so it is necessary to examine the effect of reducing the brace size on the beam outside the link. Final member sizes selected, after due consideration of all the above matters, are shown in Table 10.8.

Level	Brace	Level	Beam	Link Length, *e* (in)		Column
Fifth Floor	W18 × 55	Roof	W12 × 35	24.1	Upper Column	W14 × 68
Fourth Floor	W21 × 68	Fifth Floor	W16 × 45	26.1		
Third Floor	W21 × 93	Fourth Floor	W18 × 60	31.7		
Second Floor	W21 × 101	Third Floor	W18 × 71	31.9	Lower Column	W14 × 132
First Floor	W21 × 111	Second Floor	W21 × 122	53.4		

Table 10.8 Final Member Sizes

10.6.5 Final Link Design Check

At this point member sizes have been selected and are considered final. As mentioned earlier, a reanalysis to check drift and confirm the design forces is performed after any change in member size.

With final member sizes determined, the true link dimension, *e*, may be distinguished from the frame centerline offset dimension *x*. Here, the design uses a brace-to-beam connection with direct flange-to-flange welds (connections with gussets make it possible for *e* to equal *x*). The dimension *x* represents the distance between the intersection points of the brace centerlines with beam centerline. The dimension *e* represents the distance between the brace connections. Figure 10.37 shows both dimensions.

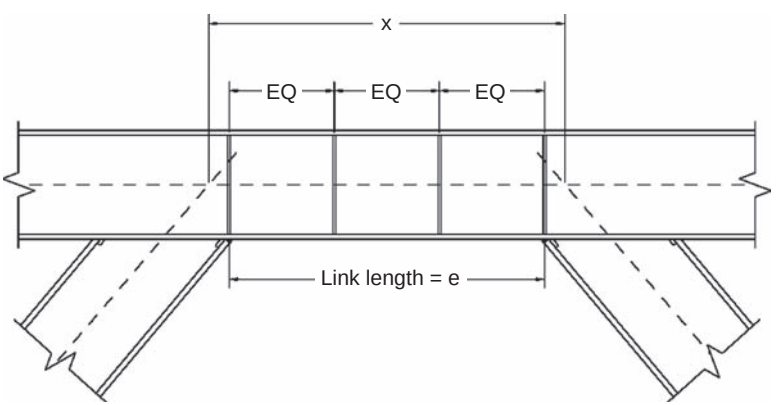

Figure 10.37 Link dimensions.

The link length e can be calculated as follows:

$$e = x + \frac{d_{beam}}{\tan\theta} - \frac{d_{brace}}{\sin\theta} \tag{10.44}$$

where d_{beam} is the beam member depth and d_{brace} is the brace member depth.

Link dimensions are given in Table 10.9. The link length, e, is compared with the ratio of moment capacity, M_p, to shear capacity, V_p. A ratio of 1.6 or lower indicates a shear-governed link; a ratio above indicates a flexure-governed link. The comparison is also used for certain detailing requirements, as illustrated in Section 10.6.7.

If the link is shear-governed, the required link shear strength from the analysis is appropriate for design of the link. If the link is governed by flexure, the required flexural strength from the analysis may not be appropriate if x is significantly different from e (this is why the design procedure for EBF in Section F3 of AISC 341 has flexural strength converted to equivalent shear strength.) The true required flexural strength should be calculated at the end of the link rather than at the centerline intersection. It may be determined from the required shear strength:

$$M_u = \frac{V_u e}{2} \tag{10.45}$$

Level	Brace	Level	Beam	x (in)	Link length e (in)	$\frac{e}{M_p/V_P}$
Fifth Floor	W18 × 55	Roof	W12 × 35	37.23	24.12	0.97
Fourth Floor	W21 × 68	Fifth Floor	W16 × 45	39.84	26.13	0.98
Third Floor	W21 × 93	Fourth Floor	W18 × 60	44.08	31.77	1.08
Second Floor	W21 × 101	Third Floor	W18 × 71	43.68	31.96	1.10
First Floor	W21 × 111	Second Floor	W21 × 122	64.67	53.46	1.24

Note that because deep braces are used, the link length e is shorter than the eccentricity x.

TABLE 10.9 Final Link Design

Use of this required flexural strength is equivalent to the AISC 341 formulation of the shear strength of a flexure-governed link (ASIC 341 Equation F3-7):

$$V_n = \frac{2M_p}{e} \tag{10.46}$$

In this case all links are shear governed and the results of the analysis may be used to design the link beams without adjustment for the true eccentricity, e.

For both shear-governed and flexure-governed links, the analysis gives the appropriate moments in the beam outside the link (at the force level under consideration). That is, the flexural forces in the beam outside the link relate to the centerline dimension, x, whereas the flexural forces in the link relate to the link length, e. Determination of the flexural forces corresponding to the strain-hardened link shear [Eq. (10.30)] requires special treatment as illustrated in Figure 10.35.

10.6.6 Link Rotation

The system parameters for EBF are based on tests that have shown stable, ductile behavior within certain ranges of link rotation. The seismic design provisions for EBF accordingly limit the expected link rotations to values based on these ranges. For shear-governed links with $e \le 1.6M_p/V_p$, the permissible inelastic rotation angle is 0.08 rad. The link inelastic rotation is estimated using the design story drift. The design story drift calculated by amplifying the results of an elastic analysis is a very rough estimate of actual expected drifts. The inelastic drift can be calculated as

$$\Delta_{in} = \Delta - \Delta_e \tag{10.47}$$

$$\Delta = C_d \Delta_e \tag{10.48}$$

$$\Delta_{in} = (C_d - 1)\Delta_e \tag{10.49}$$

where C_d is the deflection amplification factor, which is equal to 4 for eccentrically braced frames; Δ is the design story drift; Δ_e is the drift from an elastic analysis using the prescribed base shear; and Δ_{in} is the inelastic drift.

At the second floor:

$$\Delta_{in} = (4 - 1)0.326 = 0.979 \text{ in}$$

The inelastic portion of the drift is assumed to be entirely due to link rotation. This rotation is calculated based on kinematics as shown in Figure 10.17.

$$\gamma_p = \frac{\Delta_{in}}{h}\left(\frac{L}{e}\right) \tag{10.50}$$

For the current example:

$$\gamma_p = \frac{0.979}{216}\left(\frac{360}{53.46}\right) = 0.03 \text{ rad}$$

indicating that the link rotation is well below the permissible limit. At the upper stories the link inelastic rotation angle reaches as high as 0.07 rad, i.e., still below the 0.08 rad limit for shear-governed links.

When the link rotation is excessive, the building may be stiffened to reduce the drift. This can be done by increasing the column and brace size, increasing the link beam size, or decreasing the link length.

Increasing the column and brace size is straightforward, although generally these elements are not a major source of flexibility. (For taller frames, columns do contribute significant flexibility. Although it is possible to reduce the calculated link rotations by increasing the column size, it is unclear whether such a change would have an effect on the actual link rotations.) Increasing the link beam size will impose larger forces on the braces and columns. Reducing the link length will reduce drift, but also the amplification of drift into link rotation; nevertheless it is often a viable approach.

10.6.7 Link Detailing

The link requires special detailing to withstand the expected link rotations and shear deformations without flange or web buckling. Full-depth stiffeners are required on both sides of the web at each end of the link. AISC 341 has prescriptive thickness and welding requirements for these stiffeners. In addition they may be designed to transfer brace forces into the beam web. This connection design is not illustrated in this example.

These link-end stiffeners are also the location of required lateral bracing. In accordance with AISC-360-10, these braces should be designed such that

$$P_u = \frac{0.06\ R_y Z F_y}{h_o} \tag{10.51}$$

$$\beta_{br} = \frac{1}{\phi}\left(\frac{10\ M_r C_d}{L_b h_o}\right) \tag{10.52}$$

where P_u is the required strength of the lateral bracing; β_{br} is the required stiffness of the lateral bracing; and where, for the link at the second floor

$$h_o = d - t_f$$

$$h_o = 21.7 - 0.96 = 20.7 \text{ in}$$

Note that L_b should be taken to be L_q, the maximum unbraced length corresponding to the flexural demand, M_r, which is taken to be the expected flexural strength in this application. Thus, the length L_q may be assumed to be equal to the limiting length L_p.

$$M_r = M_u = R_y Z F_y \tag{10.53}$$

$$M_r = 1.1(307)(50) = 16{,}885 \text{ kip-in}$$

$$C_d = 1.0$$

$$\phi = 0.75$$

$$P_{br} = \frac{[0.06(1.1)(307 \text{ in}^3)(50)]}{(20.7 \text{ in})} = 48.8 \text{ kips}$$

$$\beta_{br} = \frac{[10(16{,}885)(1.0)]}{[0.75(123.6)(20.7)]} = 87.8 \text{ kips/in}$$

For short links with $e \le 1.6M_p/V_p$, intermediate stiffeners are required. The spacing is a function of the predicted link rotation angle:

$$s \le \left[59.3 - 22\left(\frac{\gamma_p}{0.06}\right)\right] t_w - \frac{d}{5} \tag{10.54}$$

where d is the link depth; t_w is the link web thickness; s is the stiffener spacing; and γ_p is the plastic link rotation angle, not to be taken less than 0.02.

$$s \le \left[59.3 - 22\left(\frac{0.03}{0.06}\right)\right] 0.06 - \frac{21.7}{5} = 24.5 \text{ in}$$

These stiffeners may be on one side of the web for beams less than 25-inch deep, as all the beams in this example are. AISC 341 has prescriptive thickness requirements for these stiffeners. It also has prescriptive welding requirements for connecting the stiffeners to the beam. Figure 10.38 shows the second-floor link beam, as a typical result for this example.

10.6.8 Completion of Design

Several items remain to complete the design. These include

- Brace connections. These would be designed to resist the same forces as the braces themselves. See Eq. (10.34) for the derivation of the brace seismic force.
- Column splices
- Base plates

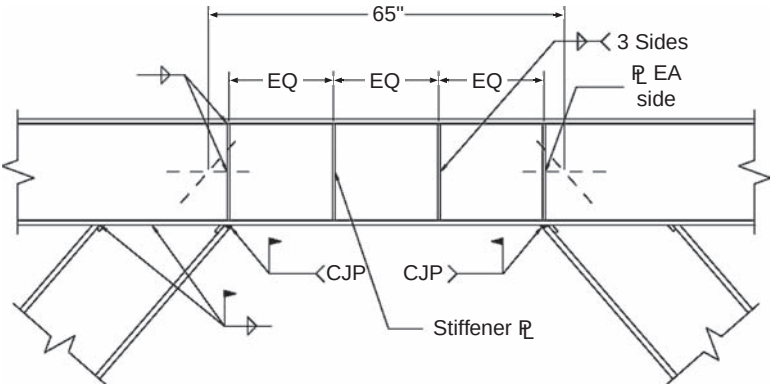

Figure 10.38 Second-floor link beam.

- Foundations
- Diaphragms, chords, and collectors

Although each one of these items is necessary and important, their execution is similar to that of many other components of a building design.

10.7 Self-Study Problems

Problem 10.1 Design the members of the single-story eccentrically braced frame shown below such that it satisfies AISC 341. Loads shown are unfactored and seismic loads are already reduced by the appropriate R value. Only consider the $1.2D + 0.5L + 1.0E$ load combination.

(a) Perform a nonseismic design, i.e., select the lightest members that satisfy the AISC 360 requirements for the factored loads.
(b) Perform a seismic design, i.e., select the lightest members that satisfy the AISC 341 requirements for EBFs. Include a check of the maximum link rotation angle from analysis, amplified per ASCE 7 with $I = 1.0$, versus the maximum rotation allowed by AISC 341. Also include the design of the link stiffeners per AISC 341 and the required design forces for link lateral bracing.
(c) Comment on the differences between the designs and explain their causes.

For both designs:

- Use square HSS sections with A500 Gr. B ($F_y = 46$ ksi) for the braces.
- Use W-shapes with A992 ($F_y = 50$ ksi) for the beam and columns.
- A structural analysis computer programs may be used, provided all force diagrams necessary for design are provided. In this case, to get forces on members outside of the link, an additional load case would

be necessary, with seismic loads amplified to account for the expected strength of the link and its strain hardening, per AISC 341. Hand methods of structural analysis are also acceptable (i.e., using relative stiffnesses to determine the moment into the brace and beam-outside-the-link).

- Assume the braces and beams are pin-connected to the column.
- Assume the braces are rigidly connected to the beam.
- The columns are laterally braced at their tops.
- The beam is laterally braced at the ends of the link and at the intersection with the columns.
- If using available design aids, reference all appropriate sections, page numbers, and edition of the design aids used.

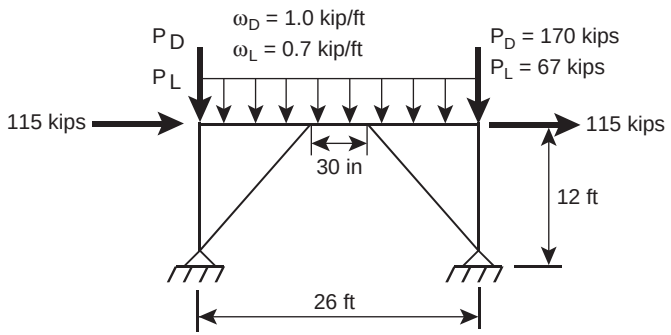

Problem 10.2 For the eccentrically braced frame structure shown here, only answer the following specific targeted questions:

(1) Determine if the link has adequate shear and flexural strengths to resist the applied loads. Check both values, even if one of the two strengths is found to be insufficient.
(2) Determine the exact value of the maximum link rotation angle (at the design story drift) that is permitted by the AISC 341 for a link of that specific length.

Consider that the W18 × 71 beam is continuous between the columns, but pinned at the column faces. The braces are pin-pin and the columns are simply supported at their bases.

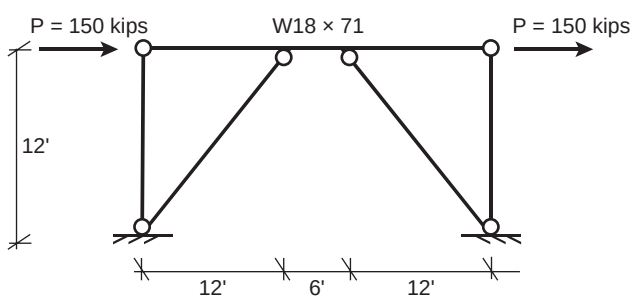

Problem 10.3 For the single-story EBF shown in the figure to this problem:

(a) Determine if a W14 × 48 link beam has adequate strength to resist the externally applied 100 kips seismic ultimate lateral load F_u (divided into two equal 50 kips load as shown in the figure following).
(b) Indicate whether the same W14 × 48 link beam meets the appropriate compactness requirements for the intended purpose.
(c) Assuming that an elastic computer analysis of this frame gives a drift $\delta_e = 0.129$ in, determine the expected corresponding plastic link rotation angle. Assume $C_d = 4.0$ and $I = 1.0$.
(d) Using capacity design, determine if the W14 × 48 beam outside of the link has adequate strength for the expected combination of axial and bending forces in that member. Assume an unbraced length of beam outside the link of 6ft 0 in.
(e) Indicate whether the W14 × 48 beam outside of the link meets the appropriate compactness requirements for the intended purpose.
(f) Using capacity design, size the diagonal braces using the most economical W10 shape.
(g) Indicate whether the braces sized in part (f) above meets the appropriate compactness requirements for the intended purpose.

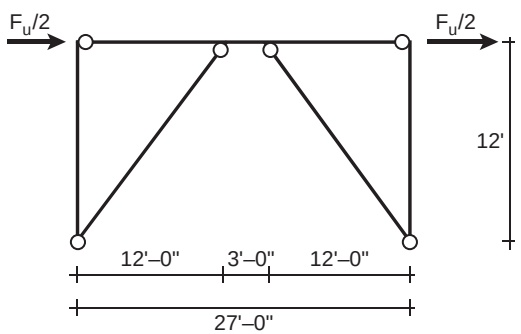

Problem 10.4 An explosion destroyed the middle column of a two-story two-bay steel frame. The dotted line in the figure below shows where that column used to be before the explosion. The rest of the frame, minus its central column, remained intact after the explosion. At the time of the explosion, that frame was only subjected to three point loads, each of magnitude P (no other gravity loads or lateral loads were applied at that time). In particular, there are no uniformly distributed loads applied to this frame.

This two-bay two-story steel frame was designed with an eccentrically braced frame on the second story, and special moment resisting frame on the first story.

Part I Calculate the maximum load, P, that can be resisted by this frame after the explosion. For simplicity, assume that the braces of the EBF and columns of the frame are infinitely strong and rigid. Also assume in this Part I that the W24 × 76 beam is of constant cross-section and able to develop its plastic moment at the face of the columns (i.e., no need to consider special SMRF connections in this *Part I*).

Part II

(a) Design a beam with an RBS detail in compliance with the AISC 341 that would allow the frame to resist the same load, *P*, as in *Part I* after the explosion. In this problem:
- Select an appropriate geometry for the RBS and location of the RBS along the beam length.
- Provide the maximum reduction in flange width permitted by AISC 341.
- Only consider possible W24 beams.
- Clearly show all appropriate free-body diagrams relevant to the calculations.
- Use a table to summarize the important values needed in this design, showing a logical process to search for the lightest possible W24 beam that would satisfy the problem statement.

(b) For the solution in Part (a), check whether the moment at face of column is acceptable.

(c) Check whether the beam selected in Part (a) meets the specified limits for this prequalified connection.

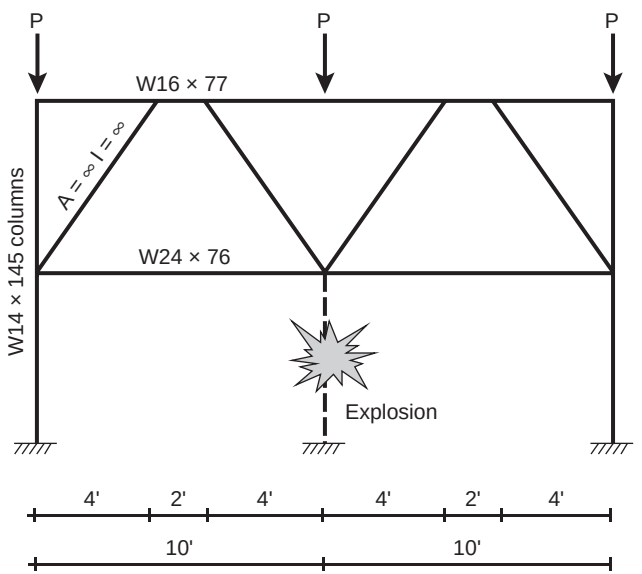

References

AISC. 2002, 2005, 2010. *Seismic Provisions for Structural Steel Buildings, ANSI/AISC 341.* Chicago: American Institute of Steel Construction.

AISC. 2010. *Specification for Structural Steel Buildings, ANSI/AISC 360-10.* Chicago: American Institute of Steel Construction.

Berman, J., and Bruneau, M. 2005. "Approaches for the Seismic Retrofit of Braced Steel Bridge Piers and Proof-of-Concept Testing of an Eccentrically Braced Frame with Tubular Link." *Technical Report MCEER-05-0004.* Buffalo,

NY: Multidisciplinary Center for Earthquake Engineering Research., State University of New York at Buffalo.
Berman, J., and Bruneau, M. 2006. "Further Development of Tubular Eccentrically Braced Frame Links for the Seismic Retrofit of Braced Steel Truss Bridge Piers." *Technical Report MCEER-06-0006.* Buffalo, NY: Multidisciplinary Center for Earthquake Engineering Research, State University of New York at Buffalo.
Berman, J., and Bruneau, M. 2007. "Experimental and Analytical Investigation of Tubular Links for Eccentrically Braced Frames." *Engineering Structures,* vol. 29, no. 8, 1929–1938.
Berman, J., and Bruneau, M. 2008a. "Tubular Links for Eccentrically Braced Frames, I: Finite Element Parametric Study." *Journal of Structural Engineering, ASCE,* vol. 134, no. 5, 692–701.
Berman, J., and Bruneau, M. 2008b. "Tubular Links for Eccentrically Braced Frames, II: Experimental Verification." *Journal of Structural Engineering, ASCE,* vol. 134, no. 5, 702–712.
Bleich, F. 1952. "Buckling Strength of Metal Structures," *Engineering Societies Monographs.* New York: McGraw Hill.
CSA. 2009. "Limit States Design of Steel Structures," *CAN/CSA-S16-*09. Mississauga, Ont: Canadian Standard Association.
Dusicka, P., and Itani, A. M. 2002. "Behavior of Built-up Shear Links under Large Cyclic Deformations," *Proc., Annual Meeting, Structural Stability Research Council*.
Dusicka, P., and Lewis, G. R. 2010. "Investigation Of Replaceable Sacrificial Steel Links," *Proc., 9th U.S. National and 10th Canadian Conference on Earthquake Engineering.,* Paper No. 1659.
Engelhardt, M. D., and Popov, E. P. 1989. "On Design of Eccentrically Braced Frames." *Earthquake Spectra, EERI,* vol. 5, no. 3, 495–511.
Engelhardt, M. D., and Popov, E. P. 1992. "Experimental Performance of Long Links in Eccentrically Braced Frames." *Journal of Structural Engineering, ASCE,* vol. 118, no. 11, 3067–3088.
Fehling, E., Pauli, W., and Bouwkamp, J. G. 1992. "Use of Vertical Shear-Links in Eccentrically Braced Frames," *Proc., 10th World Conference on Earthquake Engineering* ,Madrid, vol. 8, 4475–4479, IAEE.
Fujimoto, M., Aoyagi, T., Ukai, K., Wada, A., and Saito, K. 1972. "Structural Characteristics of Eccentric K-Braced Frames." *Trans.AIJ*, no. 195, 39–49, May.
Ghobarah A., and Ramadan, T. 1990. "Effect of axial forces on the performance of links in eccentrically braced frames." *Engineering Structures,* vol. 12, no. 2, 106–113.
Hjelmstad, K. D., and Lee, S. G. 1989. "Lateral Buckling of Beams in Eccentrically Braced Frames." *Journal of Constructional Steel Research, ASCE,* vol. 14, no. 4, 251–272.
Hjelmstad, K. D., and Popov, E. P. 1983. "Cyclic Behavior and Design of Link Beams." *Journal of Structural Engineering, ASCE,* vol. 109, no. 10, 2387–2403.
Hjelmstad, K. D., and Popov, E. P. 1984. "Characteristics of Eccentrically Braced Frames." *Journal of Structural Engineering, ASCE,* vol. 110, no. 2, 340–353.
Kasai, K., and Popov, E. P. 1985. "On Seismic Design of Eccentrically Braced Frames," *Proceedings of the 8th World Conference on Earthquake Engineering,* vol. 5, 387–394, IAEE.
Kasai, K., and Popov, E. P. 1986a. "Cyclic Web Buckling Control for Shear Link Beams." *Journal of Structural Engineering, ASCE,* vol. 112, no. 3, 505–523.
Kasai, K., and Popov, E. P. 1986b. "General Behavior of WF Steel Shear Link Beams." *Journal of Structural Engineering, ASCE,* vol. 112, no. 2, 362–382.
Malley, J. O., and Popov, E. P. 1983. "Design Considerations for Shear Links in Eccentrically Braced Frames." *Report EERC-83/24.* Berkeley: Earthquake Engineering Research Center, University of California.
Malley, J. O., and Popov, E. P. 1984. "Shear Links in Eccentrically Braced Frames." *Journal of Structural Engineering, ASCE,* vol. 110, no. 9, 2275–2295,
Manheim, D. N., and Popov, E. P. 1983. "Plastic Shear Hinges in Steel Frames." *Journal of Structural Engineering, ASCE,* vol. 109, no. 10, 2404–2419.

Mansour, N., Shen, Y., Christopoulos, C., and Tremblay, R. 2008. "Experimental Evaluation of Nonlinear Replaceable Links in Eccentrically Braced Frames and Moment Resisting Frames." *Proceedings of the 14th World Conference on Earthquake Engineering,* IAEE.

McDaniel, C. C. Uang, C. M., and Seible, F. 2003. "Cyclic Testing of Built-up Steel Shear Links for the New Bay Bridge." *Journal of Structural Engineering, ASCE,* vol. 129, no. 6, 801–809.

Okazaki, T., Arce, G., Ryu, H.-C., and Engelhardt, M. D. 2004. "Recent Research on Link Performance in Steel Eccentrically Braced Frames." *Proceedings of the 13th World Conference on Earthquake Engineering,* IAEE.

Okazaki, T., Arce, G., Ryu, H.-C., and Engelhardt, M. D. 2005. "Experimental Study of Local Buckling, Overstrength, and Fracture of Links in Eccentrically Braced Frames." *Journal of Structural Engineering, ASCE,* vol. 131, no. 10, 1526–1535.

Okazaki, T., Engelhardt, M. D., Drolias, A., Schell, E., and Uang, C. M. 2009. "Experimental Investigation of Link-to-Column Connections in Eccentrically Braced Frames." *Journal of Constructional Steel Research, ASCE,* vol. 65, no. 7, 1401–1412.

Okazaki, T., Engelhardt, M. D., Nakashima, M., and Suita, S. 2006. "Experimental Performance of Link-to-Column Connections in Eccentrically Braced Frames." *Journal of Structural Engineering, ASCE,* vol. 132, no. 8, 1201–1211.

Perera, R., Gomez, S., and Alarcon, E. 2004. "Experimental and Analytical Study of Masonry Infill Reinforced Concrete Frames Retrofitted with Steel Braces." *Journal of Structural Engineering, ASCE,* vol. 130, no. 12, 2032–2039.

Ramadan, T., and Ghobarah, A. 1995. "Behaviour of Bolted Link-Column Joints in Eccentrically Braced Frames." *Canadian Journal of Civil Engineering,* vol. 22, no. 4, 745–754.

Richards, P. 2004. "Cyclic Stability and Capacity Design of Steel Eccentrically Braced Frames." Ph.D. Dissertation, University of California, San Diego.

Richards, P. W., and Uang, C. M. 2005. "Effect of Flange Width-Thickness Ratio on Eccentrically Braced Frames Link Cyclic Rotation Capacity." *Journal of Structural Engineering, ASCE,* vol. 131, no. 10, 1546–1552.

Richards, P. W., and Uang, C. M. 2006. "Testing Protocol for Short Links in Eccentrically Braced Frames." *Journal of Structural Engineering, ASCE,* vol. 132, no. 8, 1183–1191.

Ricles, J. M., and Popov, E. P. 1989. "Composite Action in Eccentrically Braced Frames." *Journal of Structural Engineering, ASCE,* vol. 115, no. 8, 2046–2065.

Roeder, C. W., and Popov, E. P. 1978. "Eccentrically Braced Steel Frames for Earthquakes." *Journal of the Structural Division, ASCE,* vol. 104, no. ST3, 391–411.

Roeder, C. W., Foutch, D. A., and Goel, S. C. 1987."Seismic Testing of Full-Scale Steel Building–Part II." *Journal of Structural Engineering, ASCE,* vol. 113, no. 11, 2130–2145.

Salmon, C. G., Johnson, J. E., and Malhas, F. A. 2009. *Steel Structures: Design and Behavior,* 5th edition. New York: Prentice Hall.

Sarraf, M., and Bruneau, M. 2004. "Performance Tests Of Innovative Ductile Steel Retrofitted Deck-Truss Bridges." *Proceedings of the 13th World Conference on Earthquake Engineering,* IAEE.

Stratan, A., Dubina, D., and Dinu, F. 2003. "Control of Global Performance of Seismic Resistant EBF with Removable Link," *Proceedings of 4th International Conference on Behavior of Steel Structures in Seismic Areas (STESSA).* Naples, Italy. pp. 455–461.

Tanabashi, R., Naneta, K., and Ishida, T. 1974. "On the Rigidity and Ductility of Steel Bracing Assemblage," *Proceedings of the 5th World Conference on Earthquake Engineering,* Rome, IAEE. vol. 1, 834–840.

Tsai, K. C., and Young, Y. F. 1991. "A study of large EBF subassemblages with link-to-box column connection," *Proceedings of the Pacific Conference on Earthquake Engineering,* pp. 69–80.

Whittaker, A. S., Uang, C.-M., and Bertero, V. V. 1989. "Seismic Testing of Eccentrically Braced Dual Steel Frames." *Earthquake Spectra, EERI,* vol. 5, no. 2, 429–449.

Yang, M.-S. 1985. "Shaking Table Studies of an Eccentrically Braced Steel Structure," *Proceedings of the 8th World Conference on Earthquake Engineering*, San Francisco, IAEE, vol. 4, 257–264.

Zahrai, S. M., and Bruneau, M. 1999. "Cyclic testing of ductile end diaphragms for slab-on-girder steel bridges." *Journal of Structural Engineering, ASCE,* vol. 125, no. 9, 987–996.

This page intentionally left blank